Standards and Codes of Practice in Medical Radiation Dosimetry

Proceedings of an International Symposium, Vienna, 25–28 November 2002

Vol. 1

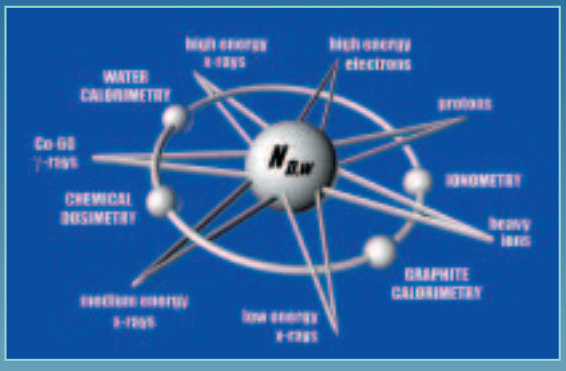

IAEA ESTRO ISRO

STANDARDS AND CODES OF PRACTICE IN MEDICAL RADIATION DOSIMETRY

VOLUME 1

ALL BLANK PAGES HAVE BEEN

RETAINED INTENTIONALLY

IN THIS WEB VERSION.

BLANK

PROCEEDINGS SERIES

STANDARDS AND CODES OF PRACTICE IN MEDICAL RADIATION DOSIMETRY

PROCEEDINGS OF AN INTERNATIONAL SYMPOSIUM
HELD IN VIENNA, AUSTRIA,
25–28 NOVEMBER 2002,
ORGANIZED BY
THE INTERNATIONAL ATOMIC ENERGY AGENCY,
CO-SPONSORED BY THE EUROPEAN COMMISSION
(DIRECTORATE-GENERAL ENVIRONMENT),
THE EUROPEAN SOCIETY
FOR THERAPEUTIC RADIOLOGY AND ONCOLOGY,
THE INTERNATIONAL ORGANIZATION FOR MEDICAL PHYSICS
AND THE PAN AMERICAN HEALTH ORGANIZATION,
AND IN CO-OPERATION WITH
THE AMERICAN ASSOCIATION OF PHYSICISTS IN MEDICINE,
THE EUROPEAN FEDERATION OF ORGANISATIONS
FOR MEDICAL PHYSICS,
THE INTERNATIONAL COMMISSION ON RADIATION UNITS
AND MEASUREMENTS,
THE INTERNATIONAL SOCIETY FOR RADIATION ONCOLOGY
AND THE WORLD HEALTH ORGANIZATION

In two volumes

VOLUME 1

INTERNATIONAL ATOMIC ENERGY AGENCY
VIENNA, 2003

IAEA Library Cataloguing in Publication Data

International Symposium on Standards and Codes of Practice in Medical Radiation Dosimetry (2002 : Vienna, Austria)

Standards and codes of practice in medical radiation dosimetry : proceedings of an international symposium held in Vienna, Austria, 25–28 November 2002 / organized by the International Atomic Energy Agency ; co-sponsored by the European Commission, Directorate-General Environment...[et al.]. In 2 vols. — Vienna: The Agency, 2003.

2 v. ; 24 cm. — (Proceedings series, ISSN 0074–1884)

Contents : v. 1.

STI/PUB/1153

ISBN 92–0–111403–6

Includes bibliographical references.

1. Radiology, Medical — Congresses. 2. Radiation dosimetry — Standards — Congresses. I. International Atomic Energy Agency. II. Series: Proceedings series (International Atomic Energy Agency).

IAEAL 03–00338

Printed by the IAEA in Austria
December 2003
STI/PUB/1153

FOREWORD

In technologically advanced societies, there are many applications and processes that employ ionizing radiation. In order to use radiation safely and effectively, it is necessary to be able to measure radiation properly. Dosimetry is the science of radiation measurement. Knowledge of dosimetry enables nuclear technology to be applied to meet the needs of society. Medical radiation dosimetry deals with those applications in which patients are irradiated for either diagnosis or therapy.

These Proceedings present a refereed selection of papers that were presented at the International Symposium on Standards and Codes of Practice in Medical Radiation Dosimetry, held in Vienna from 25 to 28 November 2002. Over 250 scientists from 62 countries attended the meeting, at which 140 presentations were delivered covering a broad range of topics in medical radiation dosimetry.

Since the last IAEA meeting on dosimetry (Measurement Assurance in Dosimetry, held in Vienna from 24 to 27 May 1993), three major activities have affected progress in medical radiation dosimetry. Firstly, in terms of measurement technology, much work has gone into perfecting calorimetric methods for the determination of absorbed dose to water, and so one entire session of the symposium was devoted to that topic. Secondly, since several primary standards dosimetry laboratories have developed the capability to provide instrument calibrations based on their newly refined standards of absorbed dose to water, the IAEA and other organizations developed new dosimetry codes of practice using these standards. In the opening session, one talk focused on the development of dosimetry codes of practice, in particular the international code of practice published by the IAEA in Technical Reports Series No. 398, Absorbed Dose Determination in External Beam Radiotherapy. The third major activity in dosimetry relates to the mutual recognition arrangement (MRA) of the Comité international des poids et mesures, which was signed by the laboratories, including the IAEA's, responsible for metrology in the field of ionizing radiation standards. One of the talks in the opening session dealt with the MRA explicitly, but several of the sessions on comparisons were motivated by the need to establish degrees of equivalence between the dosimetry standards of different laboratories. The new standards, the dosimetry protocols that use them and the MRA, which encourages comparisons, have together raised dosimetry to a new level.

Of course, the requirement for accuracy in dosimetry is driven primarily by the demands for cancer therapy — too low a dose leaves the patient to die from cancer and too high a dose may result in a dramatic increase in complication rates. An overt attempt was made during the symposium to highlight the

link between accuracy in dosimetry and cancer therapy. For example, a plenary session focused on the impending crisis in cancer management, and regular scientific sessions dealt with clinical radiotherapy dosimetry and with radiotherapy dosimetry auditing. In addition, scientific sessions were dedicated to dosimetry issues in brachytherapy, proton and hadron therapy and diagnostic radiology. One session was devoted to nuclear medicine, in an attempt to bridge the gap between the experts who measure radioactivity and those who deal with quality assurance in nuclear medicine.

The symposium programme comprised 14 scientific sessions, and at the end of each session there was a brief discussion arising from the material that had been presented. During these discussions, participants were encouraged to suggest recommendations that would provide guidance to everyone concerned with the field of dosimetry. Session 15 contains the list of the participants' recommendations as summarized by the Chair of the session, P.J. Allisy-Roberts of the Bureau international des poids et mesures. Many institutions and organizations have since incorporated elements of these recommendations into their own work plans. In addition, a meeting of symposium participants was held at the IAEA in July 2003 in order to draw up a plan of action in response to the recommendations. This action plan is available from the IAEA in a separate document entitled International Action Plan on Medical Radiation Dosimetry.

The IAEA would like to thank the Programme Committee and the co-sponsoring and collaborating organizations. Special thanks are due to the session Chairs and Co-chairs who, in advance of the symposium, acted as referees and editors of the material for their sessions in addition to preparing their own presentations. Their exceptional contribution increased the level of scientific interaction, thereby enhancing the success of the symposium. Owing to the important changes taking place in the field of dosimetry, participants would like to see the medical physics community hold the next meeting on medical radiation dosimetry in six years' time (2008).

EDITORIAL NOTE

The Proceedings have been edited by the editorial staff of the IAEA to the extent considered necessary for the reader's assistance. The views expressed remain, however, the responsibility of the named authors or participants. In addition, the views are not necessarily those of the governments of the nominating Member States or of the nominating organizations.

Although great care has been taken to maintain the accuracy of information contained in this publication, neither the IAEA nor its Member States assume any responsibility for consequences which may arise from its use.

The use of particular designations of countries or territories does not imply any judgement by the publisher, the IAEA, as to the legal status of such countries or territories, of their authorities and institutions or of the delimitation of their boundaries.

The mention of names of specific companies or products (whether or not indicated as registered) does not imply any intention to infringe proprietary rights, nor should it be construed as an endorsement or recommendation on the part of the IAEA.

The authors are responsible for having obtained the necessary permission for the IAEA to reproduce, translate or use material from sources already protected by copyrights.

Material prepared by authors who are in contractual relation with governments is copyrighted by the IAEA, as publisher, only to the extent permitted by the appropriate national regulations.

BLANK

CONTENTS OF VOLUME 1

Poster presentation

AIR KERMA AND ABSORBED DOSE TO WATER STANDARDS FOR PHOTONS (Session 3)

Poster presentation

MEETING THE NEEDS (Session 4)

DOSIMETRY PROTOCOLS AND COMPARISONS — I (Session 5)

DOSIMETRY PROTOCOLS AND COMPARISONS — II (Session 6)

Poster presentations

DOSIMETRY ISSUES FOR DIAGNOSTIC RADIOLOGY (Session 7)

POSTERS ON DIAGNOSTIC RADIOLOGY (Session 8a)

POSTERS ON DOSIMETRY PROTOCOLS AND COMPARISONS (Session 8b)

BLANK

EXECUTIVE SUMMARY

The International Symposium on Standards and Codes of Practice in Medical Radiation Dosimetry was organized by the IAEA and held in Vienna from 25 to 28 November 2002 to foster exchange of information and highlight recent advances in research in this field. Over 250 scientists from 62 Member States attended the symposium, at which 140 presentations were delivered covering a broad range of topics in medical radiation dosimetry. A refereed selection of papers presented at the symposium forms the core of these Proceedings.

A key issue addressed by the symposium was knowledge of the accuracy of radiation doses delivered to patients, which is essential for the safe and effective diagnosis and treatment of disease. Such accuracy in dose measurement is an integral part of a comprehensive quality assurance programme to ensure that the technology is used properly and has the intended effect on patients.

A special plenary session entitled Meeting the Needs focused attention on the impending crisis in cancer management. A speaker from the International Agency for Research on Cancer indicated that cancer incidence within developing countries is expected to increase by 50% within the next decade, primarily due to population ageing. In the discussion following this special session, representatives of the manufacturers participating in the equipment exhibition held as part of the symposium, as well as speakers and delegates, tried to identify appropriate and affordable technologies and to define possible roles for the IAEA to help in transferring equipment and developing the local expertise required to meet the needs arising from this crisis.

Recommendations from the symposium sessions were presented for discussion and approval by participants in the final session, which was chaired by P.J. Allisy-Roberts of the Bureau international des poids et mesures. All the recommendations are listed in Session 15, Conclusions and Recommendations. Although many of the recommendations concern the scientific community, some are directed to governments and industry, as these affect the practical application of nuclear technology in the health care sector in both developing and developed countries. Several themes appear consistently throughout the various recommendations, such as the importance of education and training required for health care workers to diagnose and treat patients safely and effectively. In addition, the symposium recognized that:

(a) Appropriate and affordable equipment is required to meet the needs of developing countries in particular, with manufacturers as partners in the process of technology transfer;

(b) It is essential for treatment methodologies to be supported by infrastructural services in medical physics, including diagnostic radiology;
(c) Programmes in quality control and assurance should provide the necessary auditing tools to demonstrate the safe and effective application of nuclear technology for patients.

Explicitly within the field of medical radiation dosimetry, the symposium made recommendations:

(1) For the further development of physical standards;
(2) For performance comparisons and participation in audits by end users and primary and secondary standards dosimetry laboratories in the subfields of nuclear medicine, brachytherapy, proton therapy and clinical dosimetry.

There are recommendations for primary and secondary standards dosimetry laboratories:

(i) To develop further their absorbed dose to water standards and air kerma standards;
(ii) To refine the assessment of the uncertainties on the physical standards;
(iii) To participate in comparison exercises in order to build confidence in their measurement capabilities.

A recommendation was made to enhance the application of the IAEA's dosimetry code of practice for external beam radiotherapy, TRS 398, and to complete the development of a new dosimetry code of practice for diagnostic radiology.

A Technical Meeting was convened at the IAEA in mid-2003 to prepare an action plan, International Action Plan on Medical Radiation Dosimetry, in response to the recommendations of the symposium. Many laboratories have found the recommendations particularly useful in defining their individual work plans.

OPENING SESSION

(Session 1)

Chair

K.R. SHORTT
IAEA

Co-Chair

A. MEGHZIFENE
IAEA

Rapporteur

G. IBBOTT
United States of America

BLANK

OPENING ADDRESS

W. Burkart
Deputy Director General,
Department of Nuclear Sciences and Applications,
International Atomic Energy Agency, Vienna

I am very pleased to welcome you to Vienna and to this International Symposium on Standards and Codes of Practice in Medical Radiation Dosimetry.

May I also say how pleased I am to see such a large number of delegates here: 335 delegates have registered, representing 77 countries and 10 international organizations. I am sure that this high level of interest truly reflects the important role of dosimetry in medicine.

You have a challenging programme this week, thanks to the scientific committee. The time and effort that was spent to help create this programme will, I am sure, be well rewarded.

I would add that each of the co-sponsoring and co-operating organizations is represented on the Scientific Committee. We appreciate the financial support provided by our co-sponsoring organizations, namely the European Commission, the European Society for Therapeutic Radiology and Oncology, the International Organization for Medical Physics and the Pan American Health Organization.

Since the last IAEA sponsored symposium on dosimetry in 1993 there have been several new developments. I would like to mention two of them.

In today's first scientific session, P.J. Allisy-Roberts, from the Bureau international des poids et mesures, will provide an overview of the mutual recognition arrangement (MRA). The IAEA is a signatory to the MRA because of the important role that it plays in disseminating radiation measurement standards to our Member States. The IAEA is committed to helping Member States link their radiation metrology standards to those of the International Metrology System — the SI from Le Système International.

An important event in 2000 was the publication of the dosimetry code of practice in Technical Reports Series No. 398. This publication and other similar codes of practice have brought greater simplicity to dosimetry as a result of defining a protocol based on direct calibration in terms of absorbed dose standards. P. Andreo will summarize this later, and the two sessions tomorrow morning will focus attention on the results of the implementation of these new codes of practice.

Of course, there have been new scientific developments in dosimetry standards themselves, and the sessions before and after lunch today will highlight that work.

The core of the IAEA's programme in dosimetry has two components. One is the dissemination of radiation measurement standards, and the other involves verification of the accuracy of the standards at the user's level in a hospital. Two sessions are devoted to this topic, including a poster session that focuses on national auditing networks within various Member States.

There are many other interesting sessions in the symposium programme. In particular I note the session on nuclear medicine dosimetry, which looks at the radiation metrology links between dosimetry and nuclear medicine. This has, until now, focused exclusively on determining radioactivity content, but with little emphasis on dosimetry.

I also draw your attention to a special plenary session entitled Meeting the Needs, which will take place at the end of today. The purpose of this session is to heighten awareness of the impending crisis in cancer management in developing countries. It will focus attention on solutions in terms of technology transfer and human resources development, taking into account the economic and medical infrastructure and the treatment of human disease.

We are grateful to the ten companies whose voluntary contributions were used to fund the speakers to attend this special session. Without their financial commitment this session would not take place. It is a relatively new feature of IAEA meetings to have this level of interaction between industry, the IAEA and Member States, and so I urge delegates to visit the exhibits and learn about the new equipment, in order to have a better idea of what manufacturers now have to offer.

Concerning the sessions in general, we request that you make recommendations at the time of each session summary. Scientific meetings take place all too often with little proactive attempt to create an impact on the strategic direction of the field. It is in the recommendations that you will have the chance to point to and influence our future work. Where are the gaps in our knowledge of the field? What should the priorities be? Please make your recommendations as broad as possible, but still within the confines of dosimetry. I may also add that the recommendations do not have to be restricted to the work of the IAEA. Where there are generic issues we will incorporate those that fall within our mandate into our planning cycle. Other issues will be identified as a challenge to those in the field. I wish you success in this important exercise.

Finally, I would like to turn to the issue of the Proceedings of the symposium. On your behalf I would like to thank the session Chairs and the referees and staff who reviewed the papers. They reflect the importance and scientific quality of the symposium.

In conclusion, I am sure that you will have a stimulating and interesting meeting. Vienna has a long and distinguished history of both the arts and sciences. This symposium continues these traditions. Please use this symposium

to interact with each other to the full in this unique environment and exchange your experience and ideas for the future. I wish you success and look forward to meeting you during the course of the week.

BLANK

OPENING ADDRESS

A. Wambersie
International Commission on Radiation Units and Measurements

Thank you for giving me the opportunity to say a few words on behalf of all organizations co-sponsoring or collaborating with this important symposium.

The European Commission, European Society for Therapeutic Radiology and Oncology, International Organization for Medical Physics, Pan American Health Organization, American Association of Physicists in Medicine, European Federation of Organisations for Medical Physics, International Society for Radiation Oncology, World Health Organization, and, of course, my own organization, the International Commission on Radiation Units and Measurements (ICRU), do appreciate to have been invited to participate actively in this symposium and want to express their sincere thanks to the organizers.

We welcome all delegates, and we know that many of them have carefully prepared a contribution.

Scanning the programme, I see several topics that are of broad interest for all the co-sponsoring and collaborating organizations, and to all those who are working in the different fields in which radiation is used.

In the sessions dealing with primary standards, absorbed dose in water and kerma in air, different approaches and opinions will be expressed and, in particular, the discussion on uncertainties will be of great interest. One of the issues is to build a bridge and evaluate conversion between:

— Quantities that can be measured, in perfectly controlled conditions and with great accuracy, at the standards laboratories;
— Quantities that are related to the biological effects and/or risks and that therefore are important in radiation therapy and protection.

When dealing with dosimetry for medical applications, the goal of the irradiation must always be kept in mind.

In cancer radiation therapy — because cancer is always a life threatening disease — the priority, the most important duty, is to provide the patient with the optimal treatment available, which should be applied following the best code of practice.

This implies the collaboration of the health care workers involved in cancer therapy: the radiation oncologists (physicians), medical physicists and radiographers–technicians who are responsible — as a team — for the safe and

effective treatment of the patient. In many countries there is a need for a sufficient number of well qualified and trained experts in each of these categories. The plenary session, Meeting the Needs, should help to remind us of the link between the needs (medical and social), the technology (technological aspects) and the people (teams) involved in the treatments.

From a dosimetry point of view, there is evidence that a difference in absorbed dose of 5% can be detected clinically, at least in some situations (dose at the reference point in treatments with curative intent). This number (5%) provides the frame of the dosimetric requirements in cancer therapy and illustrates the challenge for medical physicists.

Perhaps more important is uniformity in dosimetry; that is, agreement on common dosimetry protocols. This is especially true for centres participating in collaborative multi-centre studies or clinical trials.

Accuracy in quantities and unit definitions, as well as in the quantitative evaluation of all parameters that could influence biological effects, is a prerequisite for the significance of any clinical trial.

In diagnostic radiology the issues are, of course, not the same as in cancer therapy, especially as far as the required dosimetric accuracy is concerned. The main objective of diagnostic radiology is (should be) to reach the appropriate diagnosis, the most complete and reliable set of information in order to answer a clinical question, in the frame of a given medical situation.

The technique should thus be orientated mainly towards diagnostic efficiency. Of course, any unjustified irradiation should be avoided. Any improvement in dosimetry will bring a benefit for patients in general and will increase the confidence in all radiation protection studies (e.g. dose–effect relationships, especially at low dose).

Although a lower accuracy on dose is often tolerated in diagnostic radiology, compared with therapy, the quantities that are measured, or intended to be measured, should be clearly and carefully reported.

Several sessions of the meeting will approach the issues of quantities (units), calibration, dosimetric protocols and more technical aspects.

As Chairman of the ICRU I am particularly pleased to see that the focus of this International Symposium on Standards and Codes of Practice in Medical Radiation Dosimetry is very closely aligned with the general objectives and achievements of the ICRU.

As you all know, the ICRU has been involved since its creation in 1925 (i.e. more than 75 years ago) in developing sets of quantities, and units for these quantities, in the different fields in which ionizing radiation is applied. The ICRU is not only involved in quantities and units, it also recommends measurement procedures and physical data (numerical values) for the quantities, in a continuous effort to assure and to improve uniformity in measuring and reporting.

Many of the themes of this symposium are part of the ICRU's current programme.

In this respect I am pleased to inform you that an ICRU report on dosimetric procedures in diagnostic radiology is ready to go to the printer. Besides dosimetric procedures, the report recommends definitions (and even symbols) to facilitate the exchange of information.

Finally, nuclear medicine raises specific and complex dosimetric issues that will also be dealt with in this symposium. In particular, the heterogeneous distribution of radionuclides in tissue results in heterogeneous dose distribution at the microscopic level. Even the concept of absorbed dose may show limitations in some nuclear medicine applications. ICRU Report 67, which appeared in 2002, provides some approaches to that problem.

In summary, the list of topics announced in the programme appears to be comprehensive and touches on the major issues.

As an international meeting of this size, focusing on radiation dosimetry, is a fairly rare event, all co-sponsoring organizations recognize it as a special privilege to be invited to participate and to collaborate. I am sure that this symposium will offer opportunities and trigger several new activities within these organizations; it is certainly the case as far as the ICRU is concerned.

On behalf of all organizations co-sponsoring and collaborating in this symposium, I wish you all an interesting, fruitful and enjoyable meeting.

BLANK

MUTUAL RECOGNITION ARRANGEMENT AND PRIMARY STANDARD DOSIMETRY COMPARISONS

P.J. ALLISY-ROBERTS, D.T. BURNS
Bureau international des poids et mesures,
Sèvres
E-mail: allisy-roberts@bipm.org

Abstract

In 1999 the majority of the Member States of the Metre Convention signed an arrangement for the mutual recognition of national measurement standards and of calibration and measurement capabilities (CMCs). Part of this mutual recognition arrangement involves an open access database of CMCs that in turn needs to be supported by comparisons of national standards. The paper outlines the mutual recognition arrangement, gives some details of the comparisons of national primary standards in the field of dosimetry and shows how these can support the claims for the CMCs in the key comparison database.

1. MUTUAL RECOGNITION ARRANGEMENT

The mutual recognition arrangement (MRA) [1] was set up in 1999 by the Comité international des poids et mesures (CIPM) as a formal system whereby the national metrology institutes (NMIs) of Member States of the Metre Convention and the Associate States and Economies of the General Conference of Weights and Measures (CGPM) could recognize the calibration and measurement capabilities (CMCs) of all signatories as being equivalent. Indeed, the metrological objectives of the MRA are to establish degrees of equivalence for national measurement standards, to recognize the CMCs of the NMIs and to provide a system of traceability to the international system of units (SI).

The MRA has a main body of text that forms the detailed arrangement; associated with this is a technical supplement that describes the process of establishing degrees of equivalence. The MRA also has a set of appendices, A to F, that contains the practical details and is kept up to date in the key comparison database (KCDB) held on the web site of the Bureau international des poids et mesures (BIPM). Appendix A lists all the signatories to the MRA and includes some institutes that are not NMIs but that have been designated by the Member States of the Metre Convention as holding particular national measurement standards. In the field of ionizing radiation, designation is

especially important, as many national standards are held in specialist institutes associated with the atomic energy authority in a Member State. Secondary standards dosimetry laboratories not currently listed as designated laboratories for their country are encouraged to apply to their NMI for such designation. In addition to the Member States of the Metre Convention and the Associate States and Economies of the CGPM, two international organizations have signed the MRA, one of which is the IAEA. The signatories are given in date of signature order followed by alphabetical order.

Appendix B of the KCDB contains all the details of the many key comparisons that have been made or that are in progress. Once each comparison has been completed and the report has been published, a direct link to the report is given and the results are presented to demonstrate the degrees of equivalence of the NMIs. The KCDB is updated on a daily basis to incorporate the latest information and updates. A complete list of the key comparisons is given in appendix D and the guidelines for running CIPM key comparisons are given in appendix F.

Appendix C of the KCDB lists all the CMCs that have been declared by the NMIs for each of the metrology fields in which they offer measurement services. Indeed, the IAEA Dosimetry Laboratory was one of the first laboratories to have their CMCs in radiation dosimetry published in the KCDB. As part of their declaration, each NMI has to demonstrate that it has a quality system in place, or being put in place, that conforms with the requirements of the International Organization for Standardization (ISO) published in ISO 17025. This demonstration may be made through a formal accreditation body or through self-declaration with peer review, for example by another NMI. Both the IAEA and the BIPM are following the latter scheme, although the BIPM provides calibrations only to NMIs or designated institutes. The CIPM has decided that the deadline for the implementation of a quality system is the end of 2003. The full process of the declaration of CMCs is discussed below.

As CMCs are many and varied in each field, it is not possible to have key comparisons to cover every area. Nevertheless, CMC claims need to be supported by the NMI's participation in a relevant comparison. Consequently, the regional metrology organizations (RMOs) organize supplementary comparisons of calibration capabilities to provide the necessary support for their members. Indeed, as the MRA is an arrangement that covers the world, the RMOs co-operate with each other over the review of CMCs; this is supervised by a joint committee of the RMOs and the BIPM, known as the JCRB. The terms of reference of the JCRB are given in appendix E.

Each NMI is responsible for ensuring that their CMCs in appendix C are consistent with any new results and equivalences published in appendix B. In

the event of any discrepancy, the NMI must either withdraw its discrepant CMC entry or increase the relevant uncertainty of the CMC to cover this difference. A working group of the JCRB in each field monitors the consistency of the CMCs with the relevant comparison results. For example, the RMO Working Group on Ionizing Radiation CMCs consists of the RMO Technical Co-ordinators in this field and is scheduled to meet in the autumn of 2003 at the BIPM.

The MRA itself and all the related documents are available for downloading from the BIPM's web site at http://www.bipm.org. The JCRB part of the web site is particularly rich in practical information, such as the:

(a) Procedure for CMC entry into appendix C;
(b) Timetable for submission of CMCs;
(c) Procedure for modifying CMCs;
(d) BIPM's instructions for creating CMC Excel files;
(e) Instructions for uncertainty matrices in CMC files;
(f) Classification of services for ionizing radiation CMCs.

2. TYPES OF COMPARISON

Comparisons may be organized on behalf of the CIPM by the BIPM or by the consultative committees, such as the Consultative Committee for Ionizing Radiation (CCRI). These are almost exclusively key comparisons that by definition will lead to degrees of equivalence for the participating NMIs. Indeed, the decision as to what constitutes a key comparison in a particular field is solely that of the consultative committee. As mentioned earlier, the RMOs may also organize comparisons. These may either be key comparisons that will extend the participation of a CIPM key comparison to other Member States in the region, or they may be supplementary comparisons specifically to support CMCs.

The comparisons organized by the BIPM are normally the BIPM ongoing series of comparisons in key areas for the NMIs with the highest technical competence. The comparisons are against the BIPM's stable standards, such as the quantum based standards, the standards of air kerma and absorbed dose to water and the International Reference System (SIR) for activity measurements. These BIPM standards form the basis of the key comparison reference value (KCRV) against which the degrees of equivalence are established for the NMIs that participate.

The CIPM key comparisons organized by the consultative committees are again for the NMIs with the highest technical competence in the key areas. The comparison will often use high level transfer standards for the measurements and will run to an agreed time schedule, not usually longer than 18 months.

These key comparisons also lead to a KCRV unless they can instead be linked directly to the BIPM's KCRV. The degrees of equivalence will be related to the relevant KCRV.

The protocol for the key comparison will include the participants, the transfer standards and the pattern for their circulation, transport, handling, insurance, customs clearance details, start date, detailed timetable and contingencies in the event of problems. It will also include technical information on the use of the transfer standards, instructions on reporting the results and advice on the estimation of uncertainties. Each participant has to declare the traceability of its own standard to the SI.

Once the measurements have been completed, the results for each NMI must be reported to the pilot laboratory. Each report must include an uncertainty budget for the result to be valid. Having received the results, the pilot laboratory may identify that an NMI has submitted a result that appears to be discrepant. This could be indicated, for example, by a value that is more than three standard uncertainties away from the expected result. In such a case, the NMI is given the opportunity to check for any numerical error that it might have made, without knowing in which direction its result lies with respect to the other results. Once it declares its final value, the pilot laboratory produces a Draft A report of all the results, which remains confidential to the participants. Any subsequent changes or removals of results may only be made with the agreement of all the participants and if there is a sound scientific basis to do so, for example an identifiable problem with the transfer standard.

When the participants have agreed with the results in the Draft A report, the pilot laboratory produces a Draft B version, which may also include the KCRV and the proposed degrees of equivalence. This report is circulated to the participants and also to the consultative committee, or to a key comparisons working group (KCWG) of the consultative committee. At this stage the participants may publish their own results independently, if the other participants are in agreement.

The KCRV is that of the BIPM standard for the ongoing key comparisons, and is normally the weighted mean of the comparison results of a CIPM key comparison that involves the use of one or more transfer standards. The KCRV has an uncertainty associated with it that is usually the uncertainty of the weighted mean.

The degree of equivalence of each laboratory, i, with respect to the reference value, x_R, is given by a pair of numbers, $D_i = (x_i - x_R)$, and U_i, its expanded uncertainty ($k = 2$), both expressed in the same units. The expanded uncertainty is given as twice the square root of the variance:

$$U_i = 2\sqrt{[(1 - 2/n)u_i^2 + (1/n^2)\Sigma u_i^2]}$$

where n is the number of laboratories and each laboratory, i, has contributed to the KCRV, x_R.

The degree of equivalence between two laboratories, i and j, is given by a pair of numbers, $D_{ij} = D_i - D_j = (x_i - x_j)$, and U_{ij}, its expanded uncertainty ($k = 2$), both expressed in the same units.

The approximation $U_{ij} \sim 2\sqrt{(u_i^2 + u_j^2)}$ is often used if there are no obvious correlations between the results of the two laboratories.

There are many examples of published comparisons in the KCDB that show the matrices and graphs of degrees of equivalence. To be published, the Draft B report must be approved by the consultative committee. The process can be quite rapid if the participants and the KCWG have already approved the contents and the degrees of equivalence. Once agreed, the Draft B report becomes the final report, and the results and degrees of equivalence may be published in appendix B of the KCDB. If an RMO key comparison has taken place, the final report may include links to the CIPM key comparison through the linking laboratories that have taken part in both comparisons. The RMO key comparison may have been published separately but may not include a KCRV nor the degrees of equivalence, as these will be linked to the corresponding CIPM key comparison.

The publication route for the final report will depend on the degree of original content and on the wider significance of the comparison. It may be published as a BIPM or NMI report if it is a BIPM ongoing comparison with a single NMI, or it may be published in Metrologia or another appropriate scientific journal if there is significant new scientific content. Normally, the final report of a CIPM or RMO key or supplementary comparison will be published in the Metrologia Technical Supplement, which is published electronically by Institute of Physics Publishing on the internet and is freely available by visiting the BIPM web site. In this case, the final report may be quite long, containing many important details that will provide a complete record of the comparison for the future. Obviously, such a report may not be appropriate for another scientific journal.

The comparisons organized by an RMO are open to any RMO member or invited institute with the appropriate technical competence. Participants may also be from another RMO if this is thought to be useful. An important aspect is that for an RMO key comparison there must be at least two linking NMIs participating in the corresponding CIPM key comparison to enable a robust link to be established by the KCWG. Only those NMIs participating in the CIPM key comparison may have their results included in the KCRV. An RMO key comparison may extend the degrees of equivalence in appendix B of the KCDB to the other participants. However, only those participants that are signatory to the MRA may have their results included in the KCDB.

Supplementary comparisons to support CMC entries that are organized by the RMO will normally follow the same procedures as for a key comparison, but they do not have a KCRV or degrees of equivalence in the KCDB. Although the report of the comparison may be published in the Metrologia Technical Supplement if the consultative committee is in agreement, the results of the comparison are not actually published in the KCDB.

The procedure for the organization of an RMO key comparison is straightforward but must be followed to enable the results to be included as appropriate. The RMO technical committee or working group develops the comparison protocol following the Guidelines for CIPM Key Comparisons and the protocol for the corresponding CIPM key comparison. There must be adequate participation of linking NMIs to enable the link to be made in a robust way, and the protocol must be reviewed and approved by the consultative committee KCWG or by the consultative committee itself.

Occasionally an NMI is not ready to participate at the time scheduled for a comparison but wishes to participate at a later date. This is possible if another NMI that has participated is willing to undertake a subsequent bilateral comparison. The link to the original comparison is then made through the single, linking NMI. Such a procedure may also be followed in the event that an NMI has unsatisfactory results in the original comparison because of some problem associated with the transfer standard. Sometimes, only two NMIs have the capability to undertake a particular type of calibration, and they may wish to make a bilateral comparison to demonstrate their capability to support their CMCs. All of these cases are valid reasons to undertake bilateral comparisons. However, these comparisons must be registered in advance with the consultative committee and approved in format and content before they may be entered into appendix B of the KCDB. The results, except for bilateral comparisons linked to a key comparison, will not be published in the KCDB degrees of equivalence.

3. IONIZING RADIATION DOSIMETRY KEY COMPARISONS

Currently there are four BIPM ongoing key comparisons in the field of ionizing radiation dosimetry. Each has a unique identifier in the KCDB, such as BIPM.RI(I)-K1 for air kerma in ^{60}Co radiation beams. Although this particular comparison has been ongoing for many years and the results of each comparison at the BIPM are published and available on the BIPM web site, the final report containing the degrees of equivalence for each participant NMI has not yet been approved. This is because there is debate currently over the methods used to obtain the values and the uncertainties associated with the

effects of the graphite wall of cavity standards, and debate also on the axial non-uniformity correction factors.

The comparisons of X ray air kerma in low energy and medium energy beams (BIPM.RI(I)-K2 and BIPM.RI(I)-K3, respectively) have also been published individually but not yet collectively because of the calculations in recent years concerning the electron loss and photon scatter correction factors. In addition, a new fluorescence correction factor has been calculated, arising from the argon content of air. This is particularly important for low energy X ray beams. It is expected that once the CCRI Section I on dosimetry (CCRI(I)) has approved the values for these various correction factors for the BIPM standards, in May 2003, the degrees of equivalence will be published for all the NMIs together with an indication as to whether their own standards have newly calculated correction factors for these effects.

The fourth dosimetry comparison is that for absorbed dose to water in ^{60}Co gamma beams, known as BIPM.RI(I)-K4. Some 12 NMIs have primary standards for absorbed dose to water, although two of these have only compared their standards with that of the BIPM quite recently. Again, each comparison is published individually, and the collective report to demonstrate the degrees of equivalence of each NMI should be published once all the participants have approved this final report.

Although some graphs and matrices were presented as examples, they have not been reproduced in this paper, as a consensus has not yet been reached on the values to be published. It is anticipated that once the CCRI(I) has agreed the various correction factors and uncertainties for the degrees of equivalence, the results of all the comparisons will be openly available in appendix B in the autumn of 2003.

In addition to these ongoing BIPM key comparisons, the CCRI(I) has launched a key comparison for the dissemination of primary standards for absorbed dose to water, through the calibration of secondary standard chambers. This comparison, identified as CCRI(I)-K4, has taken more than two years, but nine primary standards laboratories have participated and the Draft A report of the comparison is being drafted. The results indicate that the primary laboratories are disseminating their primary standards for absorbed dose to water well within their quoted uncertainties. This comparison will make it easier for RMOs to link the corresponding comparisons that they are running. At the moment, only the Asia Pacific Metrology Programme (APMP) has registered a key comparison, APMP.RI(I)-K4, which will be linked to the CCRI(I) key comparison in due course. The APMP is also running an X ray comparison for medium energy beams, APMP.RI(I)-K3.

The procedure for RMOs to initiate a dosimetry key comparison is quite straightforward. As dosimetry key comparisons are determined by the

CCRI(I), an RMO can only run a key comparison if a CIPM dosimetry key comparison already exists; otherwise it can run a supplementary comparison. It is normally the RMO technical committee or working group that decides whether a corresponding dosimetry key comparison should be undertaken. If this decision is taken, the proposal should be registered in the KCDB using the appropriate comparison status form, available from the CCRI's Executive Secretary. The details that are registered include a description of the comparison, the proposed start date, the participant NMIs and the pilot laboratory. This status form is updated periodically by the pilot laboratory as the comparison proceeds, and it is through this mechanism that the KCDB is kept up to date.

One of the main functions of RMO dosimetry comparisons is to support the CMCs of their members. As the number of key comparisons is deliberately limited and each CMC has to be supported by participation in a comparison, many calibration capabilities are supported by supplementary comparisons rather than key comparisons. The RMOs are responsible for running as many supplementary comparisons as deemed necessary. These might be for quantities in radiation protection, such as personal dose equivalent, or for energies not covered by key comparisons, such as the ISO narrow series, or for dose levels that are not normally subject to a key comparison, such as kGy doses used in sterilization processes. A status form should also be completed for any supplementary comparison.

4. CONCLUSION

A description of the MRA has been given together with the procedures to participate in comparisons. There are currently 21 NMIs involved in dosimetry key comparisons. The results of these key comparisons are not yet published in the MRA KCDB, as agreement needs to be reached on the method to determine the correction factors used for the different types of primary standard. Once this is done and the CCRI(I) has approved the outcome, the degrees of equivalence for each NMI can be computed and the results published, probably by the end of 2003.

As soon as the results of these CIPM key comparisons are available in the KCDB, any corresponding RMO key comparisons may be linked through jointly participating NMIs. The RMOs running supplementary comparisons can publish their reports in the KCDB and thus demonstrate the traceability of their members' CMCs to the SI.

ACKNOWLEDGEMENT

The authors wish to express their thanks to C. Thomas, the manager of the KCDB.

REFERENCE

[1] Mutual Recognition of National Measurement Standards and of Calibration and Measurement Certificates Issued by National Metrology Institutes, Comité international des poids et mesures, Sèvres (1999).

BLANK

ROLE OF THE IAEA CODES OF PRACTICE IN THE RADIATION DOSIMETRY DISSEMINATION CHAIN

P. ANDREO
Medical Radiation Physics,
Stockholm University–Karolinska Institute,
Stockholm, Sweden
E-mail: pedro.andreo@ks.se

Abstract

For the past three decades the IAEA has published codes of practice for external beam radiotherapy dosimetry. Their most important aspect, compared with national dosimetry protocols, is that the IAEA has developed dosimetry recommendations both for metrology institutions and for hospitals in developing and industrialized countries, thereby covering most of the links in the radiation dosimetry dissemination chain. The IAEA codes of practice have become standards against which most other dosimetry protocols are compared, and today they are some of the most commonly used citations in the radiation dosimetry scientific literature. The role played by the IAEA codes of practice, notably by Technical Reports Series No. 277, as the precursor of Technical Reports Series No. 398, has been to promote the development of radiation dosimetry at different levels, linking the various components of the dosimetry chain from the standards laboratory to the delivery of radiotherapy treatments and the radiation protection of the patient.

1. INTRODUCTION

The task of a code of practice (CoP) or protocol for radiation dosimetry is to provide users with consistent procedures and data for the determination of the absorbed dose to a medium in reference conditions (beam or source calibration). It is based on the use of a dosimeter calibration factor provided by a standards laboratory, which ensures traceability to the International Measurement System for radiation metrology. CoPs have mainly been addressed to external beam radiotherapy, for which the absorbed dose to water is determined, and these will be the focus of this paper (see Fig. 1). Other areas, such as the dosimetry of brachytherapy sources and diagnostic radiology, are important, but fall outside the scope of this paper.

For more than 30 years, but especially since the publication in 1987 of the IAEA CoP for radiotherapy dosimetry in Technical Reports Series No. 277 (TRS 277) [1], the IAEA has played a leading role in supporting the

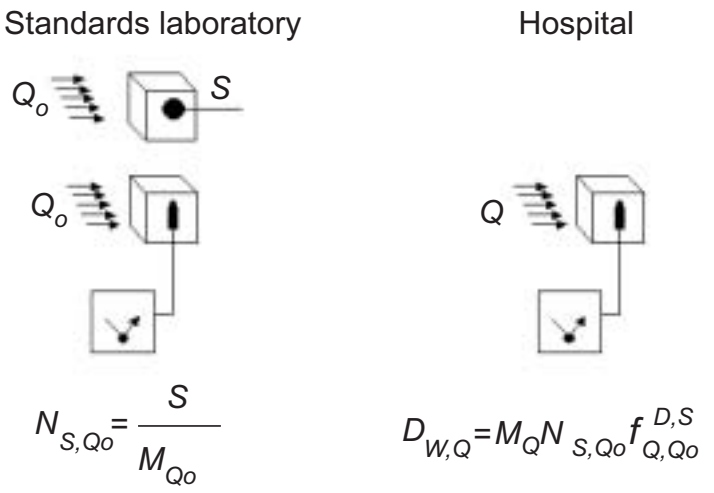

FIG. 1. The basis of a general CoP. At the standards laboratory an ionization chamber is provided with a calibration factor in terms of the radiation quantity, S, in a beam of quality Q_o, $N_{S,Qo}$. The chamber is subsequently placed at the reference depth in water in the hospital's beam, of quality Q, and the dose to water determined in accordance with the equation shown on the right hand side. M_Q is the instrument reading in the user's beam, suitably corrected to the reference conditions for which $N_{S,Qo}$ is valid; f is any overall factor necessary to convert from the calibration quantity, S, at the calibration quality, Q_o, to dose, D, at the user's quality, Q.

international community with recommended procedures for the calibration of radiotherapy beams. Some aspects of this support have gone beyond the classical development and publication of a dosimetry protocol (cf. most national dosimetry recommendations), because, in addition, the IAEA has linked CoPs to its multiple activities in the fields of radiation metrology, clinical radiotherapy and radiation protection. The IAEA CoPs have also become standards against which most other dosimetry protocols are compared, and today they are some of the most common citations in the radiation dosimetry scientific literature.

It is the purpose of this paper to provide a historical perspective of the role played by the IAEA in publishing international CoPs and disseminating radiation standards to ensure the traceability of the radiation dosimetry chain. The various IAEA CoPs will be summarized first, emphasizing the main aspects of their development and formalisms. This will be followed by a description of the establishment of the IAEA/World Health Organization (WHO) network of secondary standards dosimetry laboratories (SSDLs) and a

discussion of key issues that link the various components of the dosimetry chain to the delivery of a radiotherapy treatment and the radiation protection of the patient.

2. DEVELOPMENT OF IAEA CoPs

2.1. TRS 110 (1970) and the pre-TRS 277 age

More than 30 years ago the IAEA, on behalf of the IAEA, Pan American Health Organization (PAHO) and WHO, published its first CoP for radiotherapy dosimetry, TRS 110 [2]. The publication of this CoP preceded the creation of the network of SSDLs, but was linked to it. TRS 110 was aimed at dosimetry for kilovoltage X rays, ^{60}Co and ^{137}Cs radiotherapy in developing countries, and was based on roentgens and rads. Readers of historical publications will still find many interesting practical recommendations, such as quality assurance procedures that recommend taking radiographs of the ionization chambers to check that the internal electrode construction has not moved, and procedures for the determination of the uncertainty of a measurement. By way of an anecdote, TRS 110 was the first and only IAEA CoP that included the name of the author on its cover, J.B. Massey, recognizing that the IAEA acted solely as a publisher of the report.

For the following almost 20 years the IAEA dosimetry activities focused on the development of the SSDL network [3]. During this long period there were no updates of TRS 110 or new IAEA CoPs published, although generations of national dosimetry protocols emerged. The absence of IAEA recommendations favoured the arbitrary use of such national protocols, mostly issued in the United Kingdom and United States of America, with the results that multiple protocols were used within a given country and that there were no practical links between medical physics departments and SSDLs, except for detector calibrations.

2.2. TRS 277 (1987 and 1997)

The publication in 1987 of the TRS 277 CoP [1] established a quantum leap with regard to the IAEA's role in harmonizing international radiotherapy dosimetry. A new generation of N_K based national protocols had emerged in the early 1980s, and the authors of TRS 277 were chosen from among the authors of those national protocols. The goal was to develop an international CoP that included the best aspects of each national protocol, avoiding known imperfections and a lack of consistency in the data. TRS 277 was addressed to

both medical physicists and SSDLs worldwide, establishing consistency at all levels of the dosimetry chain. Several industrialized countries adopted it, thus helping to end the common perception that IAEA recommendations were addressed solely to developing countries. Interestingly enough, in some other industrialized countries TRS 277 was seen as a competitor to the national protocol rather than as an update (even if this national protocol was one of the 'parents' of this new CoP, which was often referred to as a 'cosmetic change').

Owing to its wide dissemination, TRS 277 became the standard protocol against which the others were compared. Its data were included in practically all the dosimetry recommendations published since 1986, following the avalanche of national protocols[1], and many investigations have used modified national dosimetry protocols that incorporate TRS 277 data. The CoP has been translated into many different languages, even if the only non-English version formally released by the IAEA has been in Spanish.

As in all N_K based protocols, in TRS 277 the determination of the absorbed dose to water at a reference depth in a phantom is accomplished in a two step process. In the first step, a chamber factor in terms of the absorbed dose to the cavity air, N_D, is derived:

$$N_{D,\mathrm{air}} = N_K(1-g)k_{\mathrm{att}}k_m k_{\mathrm{cel}} \tag{1}$$

where the meaning of the factors g, k_{att} and k_m and their values for a large set of ionization chambers are given in TRS 277. In the second step, at the user's beam quality, Q, the absorbed dose to water, $D_{w,Q}$, at a point in a phantom at which the effective point of measurement of the chamber is positioned, is obtained from the dose to the cavity air using the Bragg–Gray principle:

$$D_{w,Q}(P_{\mathrm{eff}}) = M_Q(P_{\mathrm{eff}})N_D(s_{w,\mathrm{air}})_Q\, p_Q \tag{2}$$

---

[1] The development of so many different national protocols in the late 1980s was usually justified in terms of the 'idiosyncrasies of each country'. There was a broad consensus on the data included in most protocols for the stopping power ratios and different correction factors, and most protocols yielded almost exactly the same absorbed dose. One can therefore wonder why so many protocols were needed. The reality is that sometimes each group of protocol authors introduced small details in the recommended procedures to perform a given step, yielding discrepancies up to several per cent in D_w for certain conditions. Tired of keeping track of those 'small details', this author sometimes feels certain nostalgia for the period when everybody followed, say, International Commission on Radiation Units and Measurements Report 14 or 21. Unfortunately, a similar trend can be discerned today for absorbed dose to water protocols.

where $M_Q(P_{eff})$ is the dosimeter reading at the user's beam quality, Q, corrected for pressure, temperature, recombination and polarity; $s_{w,air}$ is the stopping power ratio water to air at the beam quality Q; p_Q is the perturbation factor of the ionization chamber for in-phantom measurements at the beam quality Q; and P_{eff} is the effective point of measurement of the chamber, shifted from the chamber centre towards the source. Note that the use of $M_Q(P_{eff})$ means that the reading of the detector (caused by interactions in its entire volume) is assigned to the point P_{eff}. Employing the notation in common use today, for high energy photon and electron beams the perturbation factor, p_Q, can be written as:

$$p_Q = (p_{cav} p_{wall} p_{cel\text{-}gbl})_Q \quad (3)$$

where p_{cav} corrects for the electron fluence perturbation, p_{wall} corrects for chamber wall effects and $p_{cel\text{-}gbl}$ accounts for the effect of the metallic central electrode in cylindrical ionization chambers, both during the chamber calibration in air and during user in-phantom measurements, hence the explicit notation $p_{cel\text{-}gbl}$, as given in TRS 381, indicating that this is a global factor (originally denoted by p_{cel} in TRS 277).

Like any other protocol, TRS 277 had imperfections. It did not provide details for the calibration and use of plane-parallel chambers and, for these chambers, all perturbation factors were assumed to be unity. Furthermore, some of the correction factors had been included without a proper verification, and they turned out to be erroneous. A second edition of TRS 277 was published in 1997, which corrected the errors [4]. Among these were some perturbation correction factors in kilovoltage X rays, a field in which TRS 277 has triggered numerous scientific developments, and also in high energy photon and electron beams. Changes in the shift of the effective point of measurement of cylindrical ionization chambers were introduced, harmonizing the value for all megavoltage photon beams to $0.6r_{cyl}$, where r_{cyl} is the radius of the air cavity of a cylindrical chamber. More important numerically was the update of the values for the global perturbation factor, $p_{cel\text{-}gbl}$, as the newly recommended values were half of those given in 1987. This introduced noticeable changes in the dose determination, mainly for electron beams, as this factor entered into the cross-calibration procedure for plane-parallel chambers.

2.3. TRS 381 (1997)

A major limitation of TRS 277 was the lack of detailed procedures for dosimetry based on the use of plane-parallel ionization chambers, and TRS 277 was complemented in 1997 by TRS 381 [5] to rectify this limitation. Furthermore, being released in a period of dynamic changes, when new

standards were being developed, TRS 381 served as a bridge between N_K and $N_{D,w}$ based CoPs.

The purpose of TRS 381 was also to update the formalism of TRS 277 so that the new trends for calibrating chambers in terms of absorbed dose to water, $N_{D,w}$, would be consistent with the existing N_K procedures. Equation (1) for the chamber factor was replaced by:

$$N_{D,\text{air}} = N_K(1 - g)k_{\text{att}}k_m k_{\text{cel}} \tag{4}$$

where the subscript 'air' was included in N_D to specify without ambiguity that it refers to the absorbed dose to the air of the chamber cavity. The factor k_{cel} takes into account the non-air equivalence of the central electrode of a cylindrical ionization chamber only during the chamber calibration in terms of air kerma at ^{60}Co. As an alternative to the use of the effective point of measurement of the chamber, TRS 381 introduced the use of a chamber displacement perturbation factor, p_{dis}. In this case the reference point of the detector is taken to be at the cylindrical chamber centre, and Eq. (2) was replaced by:

$$D_{w,Q}(\text{ch centre}) = M_Q(\text{ch centre})N_{D,\text{air}}(s_{w,\text{air}})_Q p_Q \tag{5}$$

and Eq. (3) for the perturbation factor was replaced by:

$$p_Q = (p_{\text{cav}}p_{\text{dis}}p_{\text{wall}}p_{\text{cel}})_Q \tag{6}$$

where, in addition to the use of p_{dis}, the factor p_{cel} corrects for the effect of a metallic central electrode during in-phantom measurements at the user's beam quality.

TRS 381 provided details for cross-calibrating plane-parallel chambers in high energy electron beams as well as in ^{60}Co. Simpler procedures than those in TRS 277 were included for the determination of energy related parameters, together with new stopping power ratios, procedures for measurements in plastic phantoms, etc. Most importantly, up to date perturbation factors were provided for a variety of plane-parallel ionization chambers. This resulted in considerable changes in electron beam dosimetry, notably for chambers without an appropriate guard zone.

2.4. TRS 398 (2000)

The most recent international CoP for radiotherapy dosimetry, TRS 398 [6], is based on standards of absorbed dose to water, following the development

of these standards during the past decade. To establish uniformity in the dosimetry of the various radiation beam types used in radiotherapy, the formalism was extended to encompass kilovoltage X rays, ^{60}Co gamma rays, high energy photons, electrons, protons and heavy ions, which is reflected in the picture on its cover. As was the case for TRS 110 30 years ago, the new CoP is sponsored by several international organizations, this time the European Society for Therapeutic Radiology and Oncology (ESTRO), IAEA, PAHO and WHO. Less than two years after its publication, TRS 398 has become the protocol to be used in many countries, both at the SSDLs and in hospitals, so that its role in the dosimetry chain is already well established.

TRS 398 includes the various ionization chamber calibration possibilities available in different national standards laboratories, from ^{60}Co gamma rays to direct calibrations in high energy photon and electron beams. The options available, together with specific recommendations in each case, are summarized in the CoP. The so called beam quality factor, k_Q, together with an $N_{D,w}$ chamber calibration in ^{60}Co, forms the common basis for reference radiotherapy dosimetry.

In TRS 398 the absorbed dose to water at the reference depth z_{ref} in water for a user's beam of quality Q and in the absence of the chamber is given by:

$$D_{w,Q} = M_Q N_{D,w,Qo} k_{Q,Qo} \tag{7}$$

where $N_{D,w,Qo}$ is the calibration factor in terms of absorbed dose to water of the dosimeter provided by the standards laboratory at a reference beam quality Q_o, M_Q is the reading of the dosimeter in the user's beam corrected to the reference values of temperature, pressure, polarity and recombination for which the calibration factor is valid and $k_{Q,Qo}$ is the beam quality factor, which corrects for the difference between the reference beam quality, Q_o, and the actual user quality, Q. $k_{Q,Qo}$ is equal to unity when Q_o and Q are the same.

The beam quality correction factor, $k_{Q,Qo}$, is defined as the ratio, at the qualities Q and Q_o, of the calibration factors in terms of absorbed dose to water of the dosimeter:

$$k_{Q,Qo} = \frac{N_{D,w,Q}}{N_{D,w,Qo}} \tag{8}$$

The most common reference quality, Q_o, used for the calibration of ionization chambers is ^{60}Co gamma radiation, in which case the symbols $N_{D,w}$ and k_Q are used. Ideally, the beam quality correction factor should be measured directly for each chamber at the same quality as the user's clinical beam. However, this is not feasible in most standards laboratories. For users without access to specific $N_{D,w,Q}$ calibrations obtained experimentally, TRS 398

provides k_Q factors calculated theoretically using the Bragg–Gray theory (except in the case of kilovoltage X rays). It is emphasized that experimentally derived and calculated k_Q factors generally agree better than those suggested by the uncertainties estimated for each method [7, 8]. The main advantage of using a chamber calibration factor at ^{60}Co, $N_{D,w}$, together with directly measured values of beam quality correction factors, k_Q, for that particular chamber at other beam qualities, is that the individual chamber response at various beam qualities is intrinsically taken into account. In contrast, the calculated values of k_Q have an uncertainty larger than that for experimentally determined values and inevitably ignore chamber to chamber variations in response as a function of energy–beam quality within a given chamber type.

The parallelism between the $N_{D,w}$ and the N_K–$N_{D,\mathrm{air}}$ formalisms can be established by comparing Eqs (5) and (7) for the same reference beam quality, Q_o. For the absorbed dose to water, $D_{w,Qo}$, determined at the same reference depth, it follows that:

$$N_{D,w,Qo} = N_{D,\mathrm{air}}(s_{w,\mathrm{air}})_{Qo}\, p_{Qo} \tag{9}$$

where Q_o usually refers to ^{60}Co gamma rays. The assumed constancy in $N_{D,\mathrm{air}}$ (following that of W/e) allows this relation to extend to any reference quality.

It is important to note that the basic data and beam quality indices used in TRS 398 are consistent with those in TRS 277 (2nd edition) and TRS 381 (see Ref. [9]). The probable changes in absorbed dose determination in reference conditions for high energy photon and electron beams are therefore mostly caused by differences due to the use of the new type of standards [10].

3. IAEA/WHO NETWORK OF SSDLs

It is well known that the International Measurement System for radiation metrology constitutes a framework for ensuring traceability in radiation dosimetry, where calibrated detectors that are traceable to the primary standards at the Bureau international des poids et mesures (BIPM) and primary standards dosimetry laboratories (PSDLs) are disseminated to users (see Fig. 2). The main role of an SSDL is to bridge the gap between the PSDLs (and the BIPM) and the users of ionizing radiation.

After a difficult start [11], a network of SSDLs was established in 1976 as a joint project by the IAEA and the WHO. By 2001 [12] the network included 73 laboratories and six SSDL national organizations in 61 IAEA Member States, of which more than half are in developing countries. The SSDL network also

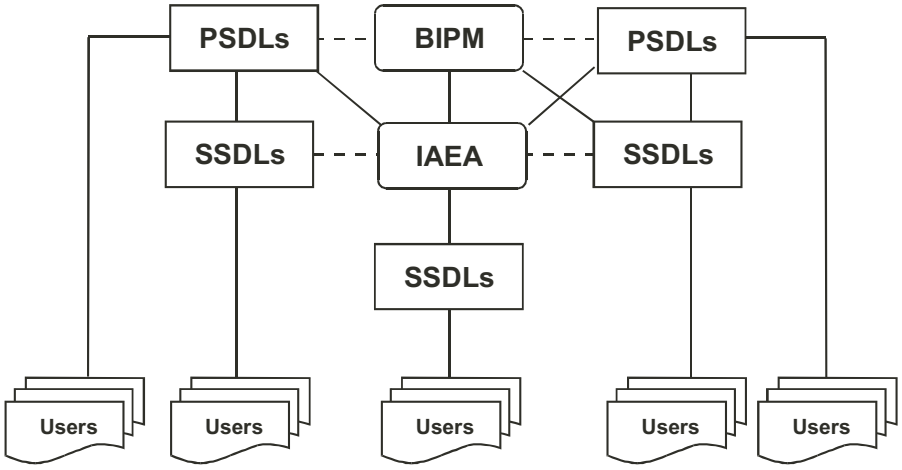

FIG. 2. The International Measurement System for radiation metrology, where the traceability of user reference detectors to primary standards is achieved either by direct calibration at a PSDL or, more commonly, at an SSDL with a direct link to the BIPM, a PSDL or the IAEA/WHO network of SSDLs. The dashed lines indicate comparisons of primary and secondary standards.

includes 20 affiliated members, among them the BIPM, several national PSDLs, the International Commission on Radiation Units and Measurements and other international organizations that provide support to the network.

One of the principal goals of the SSDL network in the field of radiotherapy dosimetry is to guarantee that the dose delivered to patients undergoing radiotherapy treatment is within internationally accepted levels of accuracy. This is accomplished by disseminating traceable calibrations, emphasizing the participation of the SSDLs in quality assurance programmes and assisting, if needed, in performing the calibration of radiotherapy equipment in hospitals using the IAEA CoPs. In addition, in some countries the SSDLs have played the important role of compensating for the lack of qualified medical physicists, which in fact was one of the main reasons for the creation of the network. The balance between radiation metrology and medical physics has now shifted towards the radiation metrology area, and the IAEA recommends that SSDLs should not perform the duties of medical physicists, except in dire situations [13].

The IAEA verifies that the services provided by the SSDL member laboratories follow internationally accepted metrological standards (including

traceability for radiation protection instruments). The first step in this process is the dissemination of dosimeter calibrations from the BIPM or PSDLs through the IAEA to the SSDLs. This is complemented by follow-up programmes and dose quality audits, implemented by the IAEA for the SSDLs to guarantee that the standards disseminated to users are kept within the levels of accuracy required by the International Measurement System.

4. CONCLUDING REMARKS ON THE LINKS IN THE DOSIMETRY CHAIN

The role of the IAEA CoPs in the radiation dosimetry dissemination chain was intrinsically defined in relation to the development of the SSDL network, as the suggestion for developing the first CoP was made during the initial discussions to create the SSDLs, held in 1967 [11]. Thus right from an early stage the need to improve radiotherapy dosimetry was linked to the dissemination chain provided by the SSDLs. Interestingly enough, the need to improve the quality of clinical dosimetry in developing countries had been demonstrated by the IAEA/WHO postal thermoluminescence dosimetry (TLD) service, which historically preceded the development of the SSDL network and the first CoP. The various links in the dissemination chain were therefore established by the IAEA during the 1970s.

It could be thought that the above initial paving of the way would make the rest obvious, but the reality was somewhat different. Firstly, TRS 110 and the creation of the first SSDLs were clearly addressed to the specific needs of developing countries. This did not cause much interest in the rest of the radiotherapy community, contributing to the separation between industrialized and developing countries. Secondly, and perhaps most importantly, the lack of qualified medical physicists in many countries led the SSDL staff effectively to take on their role, in a manner that sometimes turned out to be detrimental to the development of medical physics in such countries. Many hospitals found it more convenient, economically speaking, to purchase the services provided by the national SSDL than to hire physicists or even to promote their education. This induced a separation between SSDLs and medical physicists in some countries that proved to be negative for the two communities. The result was that some of the links of the chain were weakened. This situation persisted for almost 20 years.

As already mentioned, the impact of TRS 277 following its publication in 1987 changed the IAEA's role in harmonizing radiotherapy dosimetry. TRS 277 was addressed to both medical physicists and SSDLs, and this was a major breakthrough. It was not a CoP based on old dosimetry practices; on the

contrary, it incorporated the trends implemented in the new generation of dosimetry protocols and included the most up to date numerical data. This favoured its adoption by physicists and SSDLs in several industrialized countries, ending the gap between dosimetry in developing countries and that in industrialized countries. Comparisons between TRS 277 and many other protocols followed, published in scientific journals, which attracted yet more users. Even some PSDLs contributed to its experimental verification. It was probably the first time ever that a CoP was used at all levels of dosimetry, establishing homogeneity at all levels of the dosimetry chain around the world. From the point of view of the IAEA, TRS 277 has probably been one of its most widely spread publications, becoming one of its 'best sellers'. The international links were thus well established, and the links also included aspects related to the radiation protection of the radiotherapy patient, as the use of the CoP was recommended by the international Basic Safety Standards [14].

The wide dissemination of TRS 277 was partly due to the numerous training courses organized both by the IAEA and by the countries adopting the CoP, attended by SSDL staff and hospital physicists, at which interaction between the two communities was encouraged. Another contributor to the success of TRS 277 has been the IAEA/WHO TLD service, the strongest link of the IAEA to clinical dosimetry, as soon after its publication the CoP became the standard method of the dosimetry done by and disseminated by the IAEA. SSDLs and national quality audit services supported by the IAEA have followed the same trend.

The diffusion of TRS 381 has not been as widespread as that of TRS 277, probably because there are fewer clinical electron beams than high energy photon beams, especially in developing countries. It has also lacked the necessary interest and support of national organizations in industrialized countries, and its implementation has been carried out practically on an individual, hospital by hospital, basis. A major consequence is that many hospitals continue performing electron dosimetry based on TRS 277, which is a practice to be strongly discouraged.

With regard to TRS 398, the newest IAEA CoP, the expectations are very high. It was developed in close collaboration with PSDLs and at a time when major developments are being made in the field of standards of absorbed dose to water. Its adoption by the services provided by the IAEA has already made it a common tool in the SSDL network and in their support to end users, and numerous courses on it have already been organized, while many others are planned. Its role in the radiation dosimetry dissemination chain is clearly established. The IAEA strategy follows the guidelines developed around TRS 277, from which many lessons were learned. The number of hospital users

basing their clinical dosimetry on $N_{D,w}$ calibrations is still small, but the time that has elapsed since it was published is relatively short. That TRS 398 has been published in collaboration with several other international organizations will surely contribute to it gradually replacing TRS 277, certainly by those users who have access to the new type of calibrations.

REFERENCES

[1] INTERNATIONAL ATOMIC ENERGY AGENCY, Absorbed Dose Determination in Photon and Electron Beams, Technical Reports Series No. 277, IAEA, Vienna (1987).

[2] INTERNATIONAL ATOMIC ENERGY AGENCY, Manual of Dosimetry in Radiotherapy, Technical Reports Series No. 110, IAEA, Vienna (1970).

[3] INTERNATIONAL ATOMIC ENERGY AGENCY, Secondary Standard Dosimetry Laboratories: Development and Trends, IAEA, Vienna (1985).

[4] INTERNATIONAL ATOMIC ENERGY AGENCY, Absorbed Dose Determination in Photon and Electron Beams, 2nd edition, Technical Reports Series No. 277, IAEA, Vienna (1997).

[5] INTERNATIONAL ATOMIC ENERGY AGENCY, The Use of Plane Parallel Ionization Chambers in High Energy Electron and Photon Beams, Technical Reports Series No. 381, IAEA, Vienna (1997).

[6] INTERNATIONAL ATOMIC ENERGY AGENCY, Absorbed Dose Determination in External Beam Radiotherapy, Technical Reports Series No. 398, IAEA, Vienna (2000).

[7] ANDREO, P., A comparison between calculated and experimental k_Q photon beam quality correction factors, Phys. Med. Biol. **45** (2000) L25–L38.

[8] ANDREO, P., WESTERMARK, M., McEWEN, M.R., DuSAUTOY, A., THOMAS, R., "Electron beam dosimetry in TRS-398: Theoretical vs experimental k_{Q,Q_o} values: Influence on D_w of the various plane-parallel chamber calibration modalities", IAEA-CN-96-31P, paper presented at Int. Symp. on Standards and Codes of Practice in Medical Radiation Dosimetry, Vienna, 2002.

[9] ANDREO, P., BURNS, D.T., HUQ, M.S., "Review of the data in the international Code of Practice IAEA TRS-398 (2000). Comparison with other dosimetry protocols", Recent Developments in Accurate Radiation Dosimetry (Proc. Int. Workshop Montreal, 2001) (SEUNTJENS, J.P., MOBIT, P.N., Eds), Medical Physics Publishing, Madison, WI (2002).

[10] ANDREO, P., et al., Protocols for the dosimetry of high-energy photon and electron beams: A comparison of the IAEA TRS-398 and previous international Codes of Practice, Phys. Med. Biol. **47** (2002) 3033–3053.

[11] EISENLOHR, H.H., The secondary standard dosimetry laboratories (SSDL) story, SSDL Newsletter No. 42 (2000) 4–11.

[12] MEGHZIFENE, A., et al., IAEA Dosimetry and Medical Radiation Physics Subprogramme Report on Activities, 1999–2000, Rep. CCRI(I)/01-08, Bureau international des poids et mesures, Sèvres (2001).

[13] INTERNATIONAL ATOMIC ENERGY AGENCY, SSDL Network Charter, IAEA, Vienna (1999).

[14] FOOD AND AGRICULTURE ORGANIZATION OF THE UNITED NATIONS, INTERNATIONAL ATOMIC ENERGY AGENCY, INTERNATIONAL LABOUR ORGANISATION, OECD NUCLEAR ENERGY AGENCY, PAN AMERICAN HEALTH ORGANIZATION, WORLD HEALTH ORGANIZATION, International Basic Safety Standards for Protection against Ionizing Radiation and for the Safety of Radiation Sources, Safety Series No. 115, IAEA, Vienna (1996).

BLANK

ABSORBED DOSE STANDARDS AND CALORIMETRY

(Session 2)

Chair

A.R. DuSAUTOY
United Kingdom

Co-Chair

J. SEUNTJENS
Canada

Rapporteur

M.R. McEWEN
United Kingdom

BLANK

REVIEW OF CALORIMETER BASED ABSORBED DOSE TO WATER STANDARDS

J.P. SEUNTJENS
Medical Physics Unit, McGill University,
Montreal, Canada
E-mail: jseuntjens@medphys.mcgill.ca

A.R. DuSAUTOY
National Physical Laboratory,
Teddington, United Kingdom

Abstract

The paper reviews state of the art water and graphite calorimetry as the bases for current absorbed dose to water determination in photon and electron beams. The fundamentals of the methods are reviewed, with the goal of discussing comparatively some of the current uncertainty estimates associated with both techniques.

1. INTRODUCTION

The major techniques currently in use at standards laboratories for the realization of absorbed dose to water can be grouped into three distinct classes: (1) ionization chamber based absorbed dose standards; (2) absorbed dose standards based on the total absorption of low energy electron radiation in a ferrous solution; and (3) absorbed dose calorimeter based standards. Of these three methods, at least in principle, the latter method is considered the most direct, since an absorbed dose calorimeter calibration can be entirely based on the realization of quantities (e.g. electrical power and temperature) that do not require a field of ionizing radiation. In contrast, method (1) relies on the knowledge of the product of W_{air} and a ratio of average restricted collision stopping powers and method (2) relies on an accurate transfer of absorbed dose from a calibration quality to a different radiation quality and hence both these methods do require the use of a field of ionizing radiation for their calibration.

Much new work on absorbed dose calorimetry has been performed since the reviews on radiometric calorimetry of Gunn [1, 2], the calorimetry chapter of Domen [3] and the more recent review paper on water calorimetry by Ross and Klassen [4]. In this context the attention of the reader is drawn to the proceedings of the series of dedicated calorimetry workshops held approximately every five years, initiated at the National Research Council

(NRC) in Ottawa [5] and continued at the National Physical Laboratory (NPL) in the United Kingdom [6, 7], with the next workshop being planned to take place in Australia in 2003, as well as to the calorimetry discussion group on the Internet (http://groups.yahoo.com/group/calorimetry). Because of the role of water and graphite calorimetry in state of the art absorbed dose standards, this brief review concentrates on the basis of these techniques in a comparative way, with the emphasis on advances in both areas since the previous IAEA Symposium on Measurement Assurance in Dosimetry [8].

Absorbed dose calorimetry is based on the underlying assumption that energy imparted by ionizing radiation ultimately appears as a temperature rise. There are, however, examples of situations in which this non-trivial assumption is not fulfilled, such as endothermicity resulting from the energy required to displace atoms in the solid from which the calorimeter is constructed [9], or exothermicity associated with chemical reactions in water [10, 11]. If the assumption of complete energy conversion is fulfilled, or if any discrepancy is well understood and taken into account, the calorimeter can be viewed as the most fundamental and absolute method of the available techniques for the measurement of absorbed dose.

The major absorber materials used for calorimetry in radiation dosimetry have traditionally been tissue equivalent plastics or graphite. Water calorimeters are, however, increasingly being developed and used as primary standards for absorbed dose. The variety of the types of absorbed dose to water standards in use at standards laboratories has been viewed as a distinct advantage for the robustness of the absorbed dose calibration system compared with the air kerma calibration system, which is based entirely on graphite walled chambers. Since graphite and water calorimeters play a pivotal role in the absorbed dose standards, this paper reviews comparatively the concepts, construction, correction factors and uncertainties of water and graphite calorimeters in an attempt to shed light on the uniqueness of each technique.

2. ABSORBED DOSE WATER CALORIMETRY

Various water calorimeters have been designed and built in the past 20 years; these range from small agitated water calorimeters [12] designed to investigate the heat defect in water, to open stagnant water calorimeters and large volume sealed water calorimeters [13, 14]. This paper concentrates on the currently most widespread version of the water calorimeter, the calorimeters derived from the (generation 2) Domen type sealed water calorimeter [15], in which the temperature rise is measured inside a vessel containing highly purified

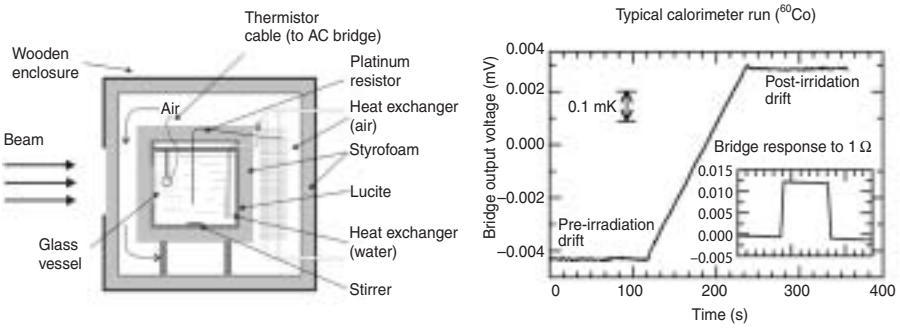

FIG. 1. (a) Schematic drawing of the NRC sealed water calorimeter. Shown are the phantom with a temperature stabilized enclosure, the cylindrical vessel with thermistor probes and auxiliary equipment for monitoring and controlling water temperature. (b) Typical sealed water calorimeter run in a ^{60}Co beam. Inset: response of bridge circuitry to a change of 1 Ω in bridge balancing resistance. (Adapted from Ref. [16].)

water that in turn is positioned inside a large (30 cm × 30 cm × 30 cm) stagnant water phantom. The purity of the water system used in water calorimetry has been proven to be of major significance in the understanding and control of the heat defect. Figure 1 shows the NRC sealed water calorimeter operated at 4ºC as well as a typical ^{60}Co run as an example of such a calorimeter.

Two types of vessel set-up are currently used in stagnant sealed water calorimetry. The first type is the traditional set-up in which the vessel and temperature probes are concentric, with the cylinder axis perpendicular to the beam axis and a diameter of between 3 cm and 7 cm. An alternative type is a set-up in which a flat, large diameter (10 cm or more) cylindrical vessel is used with the axis coinciding with the beam axis and temperature probes pointing inwards, perpendicular to the vessel axis and beam axis. Recent reports on operating water calorimeter absorbed dose standards have been given by the United States standards laboratory (the National Institute of Standards and Technology (NIST)), the Canadian standards laboratory (the NRC), the Belgian standards laboratory (the University of Ghent, Belgium), the German standards laboratory (the Physikalisch-Technische Bundesanstalt (PTB)), the Dutch standards laboratory (the Nederlands Meetinstituut (NMi)) and the Swiss standards laboratory (the Swiss Federal Office of Metrology and Accreditation (METAS)) [15, 17–21].

2.1. Methodology and measurement technology

Advantage is taken in stagnant water calorimetry of the low thermal diffusivity of water, a feature that ensures the preservation of the temperature profile that results from the dose distribution present in the calorimeter after irradiation. Hence, in stagnant water calorimeters a temperature rise, ΔT_w, is measured at a point, and multiplication with the specific heat capacity of water, c_w, leads almost immediately to the quantity of absorbed dose to water.

In practice, however, the accurate determination of absorbed dose to water is complicated by issues that can be categorized as either (1) fundamental effects or (2) technical issues. Fundamental effects are those that potentially compromise the validity of the specific heat capacity applied in the dose measurement. Technical issues are those that complicate a correct measurement of the temperature rise of the calorimeter medium (i.e. water). Both issues are usually treated as correction factors in the dose equation and are detailed later in this section.

The generic equation for absorbed dose to water using a water calorimeter has the following form:

$$D_w = c_{w,p}\Delta T k_{\mathrm{hd}} k_{\mathrm{ht}} k_p k_{\mathrm{dd}} k_{\rho} \tag{1}$$

where

$c_{w,p}$ is the specific heat capacity of water at constant pressure;
k_{hd} is the correction for the heat defect, h (i.e. equal to $1/(1 - h)$, where h represents the heat defect defined later in this paper);
ΔT is the measured thermistor temperature rise;
k_{ht} is a general heat transfer correction factor, which can result from conductive and/or convective modes of heat transfer;
k_p is a perturbation correction factor to account for the absorption and scattering of radiation due to the presence of non-water materials;
k_{dd} is a dose profile correction factor that corrects the measured dose to the dose at the reference point;
k_{ρ} is a density correction factor to account for the difference in density between the calorimeter operation temperature and the temperature at which another detector (such as an ionization chamber) is calibrated.

It should be noted that, since the measurement of the temperature rise in current calorimeters requires a significant time span, the temporal dependence of the effects and the procedure used to analyse a calorimeter run are important in assessing the values of the factors. This issue will be expanded upon in the relevant parts of this paper.

Currently all sealed water calorimeters operated at standards laboratories make use of thermistors to measure the temperature rise. Since the temperature rise (not the temperature) must be measured in absolute terms, thermistors are calibrated relative to reference temperature standards; this is performed over a much wider temperature span than used during calorimeter operation, to allow for optimal accuracy in the readout of the standard thermometer. One usually also takes care of the fact that the thermistor power dissipation during thermistor calibration and during irradiation runs is accounted for using appropriate corrections. Based on the temperature–resistance relation for thermistors, $R = R_0\exp(\beta(1/T - 1/T_0))$, where R_0 is the bead resistance at the reference temperature, T_0, the material constant, β, can be determined. When the material constant is assumed to be temperature independent, it is important to devise the measurement of resistance versus temperature in a symmetric temperature span around the operating temperature of the calorimeter.

Once the thermistors' material constants have been determined, a temperature rise can be measured as $\Delta T = S^{-1}(\Delta R/R)$, with S being the thermistor sensitivity given as $S = \beta T^{-2}$. The degree of long term stability of thermistors contributes to the accuracy of a calorimeter dose determination. To verify the response of the entire bridge set-up during calorimeter operation, the balancing resistor is changed by a precisely known resistance and the change in bridge output voltage is measured. This procedure checks the constancy of the amplifier gain of the detection circuitry. To track potential changes in the thermistor material constant, in principle measurements of resistance versus temperature should be performed, but this is not always practicable once the calorimeter is operating. An indirect way of detecting a change in thermistor characteristics is to track the bridge settings as a function of calorimeter operating temperature, since a change in the thermistor material constant is usually associated with a change in its reference resistance [15]. The overall experience with thermistors shows that their long term stability for the measurement of temperature rise has been excellent [16, 17, 22].

DC as well as AC bridges have been successfully used for the measurement of the resistance change during calorimeter operation [15, 23]. In most cases water calorimeters are operated using a pair of thermistors, which improves the signal to noise ratio by roughly 40%. DC bridges have the advantage of being simple, but tend to be slightly more electrically noisy than their AC counterparts [24].

2.2. Heat defect

The concept of heat defect is used to quantify the difference between energy absorbed, E_a, and energy appearing as heat, E_h; the effect can be defined as:

$$h = \frac{E_a - E_h}{E_a} \tag{2}$$

The heat defect is positive for endothermic processes and negative for exothermic processes in the calorimeter. The poor understanding of the heat defect in water has long been one of the main reasons for the limited viability of water calorimetry as the basis for an absorbed dose to water standard. Various effects can contribute to a heat defect in water, although, at low linear energy transfer, seminal experimental and numerical work at the NRC [10–12] shows that the heat defect is almost entirely due to radiation induced chemical reactions. Qualitatively, Refs [10, 11] show that impurities present in water can serve as scavengers for reactive species such as the hydroxyl radicals created in the radiolysis of water and, after completion of the chemical reactions involved, this process may lead to distortion of the energy balance and hence to a non-zero heat defect. If, however, all impurities are consumed as calorimeter irradiation progresses, the system will tend to a steady state condition for which a zero heat defect is potentially achieved. In general, for unknown levels of organic impurities, a non-zero heat defect exists that is dependent on the accumulated dose, the dose rate and the temporal history of the irradiations applied to the calorimeter.

There are essentially two approaches used to operate a water calorimeter: (1) attempting to achieve a steady state condition for which a zero heat defect is expected; (2) controlling the amount of impurities in the system, calculating the heat defect by a computer simulation of the radiolysis of water and studying the energy balance associated with the creation and removal of products. The former approach has the advantage that it is not dependent on model calculations and their associated uncertainties. These latter uncertainties are due to uncertainties in primary radiation chemical yields, reaction rate constants, the temperature dependence of these quantities, the history of calorimeter operation, the accumulated dose and the dose rate. However, trace impurities present in the system may invalidate the attainment of a steady state and, because of inevitable leaks in valves or probe bushings, this may occur at levels not trivial to observe. The latter approach has the advantage of a system being immune to trace impurities; however, the absorbed dose now requires a heat defect correction, the uncertainty of which depends on all the mentioned contributions. One school of thought therefore considers the most prudent mode of operating a water calorimeter to be to use and check the consistency of the relative response of a variety of systems and to evaluate the uncertainty on the heat defect based on this consistency (e.g. Refs [10, 11, 16, 17]). Following this work, a 1σ uncertainty on the heat defect of 0.3% has been given based on the use of the pure (hypoxic) water system, the H_2 saturated water

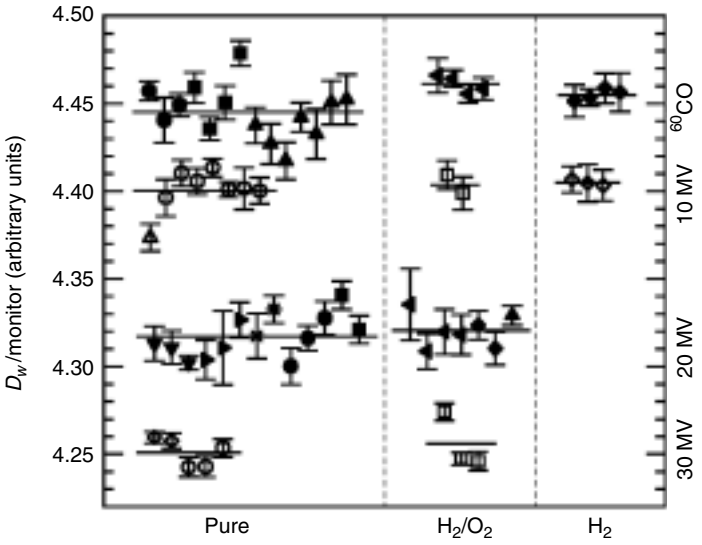

FIG. 2. Relative response of the NRC sealed water calorimeter in high energy photon beams for three different chemical systems. Each datum point corresponds to an average of 10–15 calorimeter runs. The different symbols indicate a different vessel fill. These data are part of a larger set used to assess the uncertainty of 0.3% on the heat defect. (Adapted from Ref. [17].)

system and the 43/57 H_2/O_2 saturated water system with a calculated exothermicity of around –2.4%. In extensive numerical and experimental studies of the latter system, Klassen [25] has addressed the effect of the operating temperature on the primary radiation chemical yields and the reaction rate constants, including the temporal effect on the extrapolation procedure used for run analysis. These effects lead to a slight difference in average exothermicity of the 43/57 H_2/O_2 saturated system (i.e. –2.2% at 4°C and –2.5% at 22°C [17]). Figure 2 shows the relative response of the NRC sealed water calorimeter as a function of the chemical system used for four different photon energies. The consistency of this extensive set of calorimeter data provided part of the background for the choice of the uncertainty on the heat defect.

An alternative approach, followed, for example, at the PTB [19], is to base the determination of absorbed dose on the H_2 saturated system, which theoretically tends to a zero heat defect relatively independent of impurity concentration as soon as all traces of oxygen have been removed from the system. This condition is verified by studying the relative response at several

stages after the preparation of a new fill that contains a well known trace concentration of oxygen. The behaviour of the idealized steady state condition that follows after the initial trace concentrations of oxygen have been consumed depends on how well oxygen can be prevented from leaking back into the system and how well response changes caused by this process can be detected given a limited short term precision. It is therefore possible that the uncertainty on a zero heat defect would be different from zero. With the increasing number of sealed water calorimeters in operation, the assessment and recommendation of a generic value for the type B uncertainty on the heat defect correction would probably be reasonable.

2.3. Heat transfer

Heat transfer in water calorimeters occurs as a result of various sources, all of which lead to non-uniformity in the temperature distribution and hence to heat loss or gain. There are two major sources of excess heat in a water calorimeter: (1) non-water materials, such as the glass vessel, and thermistor probes with a heat capacity significantly lower than and radiation absorption characteristics significantly different from the water; and (2) electrical power dissipation in the thermistors. The instantaneous temperature rise in non-water materials, ΔT_{nw}, is related to the temperature rise, ΔT_w, in water by the equation:

$$\Delta T_{\mathrm{nw}} = \Delta T_w \frac{c_w}{c_{\mathrm{nw}}} \frac{D_{\mathrm{nw}}}{D_w} \tag{3}$$

where c_w and c_{nw} are the specific heat capacities and D_w and D_{nw} the absorbed doses in water and non-water materials, respectively. This excess temperature gives rise to heat flow in the calorimeter. Note that this temperature rise depends on the ratio of absorbed dose in non-water materials to absorbed dose in water, which is why heat loss corrections from this source are slightly beam quality dependent.

Secondly, the absorbed dose distribution in general is not uniform, and this also gives rise to temperature non-uniformities and hence heat transfer. Since the temperature profiles are directly associated with absorbed dose profiles in the calorimeter, this source of heat transfer also introduces a beam quality dependence of the correction factor that potentially can be large for electron beams.

The significant modes through which a water calorimeter tends back to thermal equilibrium are conduction and convection; radiative heat loss is of no importance for the temperature differences generated here. Whereas

initial work with water calorimeters was mainly at room temperature, almost all current water calorimeters at standards laboratories are operated at 4ºC, at which point the density of water is maximal and the driving force for convective motion is absent. The method by which heat transfer is taken into account depends on the technique used for the measurement of the temperature rise in the calorimeter. The traditional method used in calorimetry is fitting and extrapolating the pre-irradiation drift and post-irradiation temperature drift curves to the mid-run point, calculating the difference in bridge signal from these data and converting this signal to a temperature difference using the thermistor calibration data (sensitivity S). This procedure provides an approximate correction for heat loss, as the heat loss is proportional to the temperature difference between two bodies and the proportionality factor — sometimes referred to as the heat modulus or heat transfer coefficient — is a constant over the time frame of the measurement (see below). Correction factors usually used in water calorimetry are factors in addition to this standard extrapolation correction procedure.

The conductive and convective modes of heat transfer in water calorimetry are addressed in more detail in the following sections.

2.3.1. Conductive heat transfer

The heat transport equation with conduction as the only mode of heat transfer is given by:

$$\rho c \frac{\partial T}{\partial t} = \nabla \cdot (k \nabla T) + \rho \dot{D} \tag{4}$$

where

ρ is the mass density and c the specific heat capacity of the medium;
T is the temperature;
t is the time;
k is the thermal conductivity;
$\dot{D}$ is the apparent local absorbed dose rate.

The apparent local absorbed dose rate could possibly include a heat defect, if it can be estimated. An example of this is the effect of the exothermicity of organic impurity contaminated water outside the calorimeter detection vessel. The values of the density, thermal conductivity, specific heat capacity and temperature are location dependent. Equation (4) is involved in evaluating the

effects of non-water materials (through the rate of temperature change given by equations of the same type as Eq. (3)) and the effects of the non-uniformity of the dose profile on the temperature drift curves through the shape of the relative dose profile in the calorimeter. A first important observation can be made from this equation. The excess temperature, defined as the true temperature minus the ideal temperature, for an irradiation of duration Δt, can be written as:

$$T_{\text{real}} - T_{\text{ideal}} = \int_0^{\Delta t} \left(\frac{\partial T}{\partial t} - \frac{\dot{D}}{c}\right) \mathrm{d}t' = \int_0^{\Delta t} \nabla \cdot (k \nabla T)\, \mathrm{d}t' \tag{5}$$

The right hand side of Eq. (5) shows that, for a given value of Δt, this temperature offset is independent of the irradiation dose rate or the accumulated dose. This means that if conduction is the only significant mode of heat transfer, use can be made of calculated excess heat curves describing, for each irradiation time, the post-irradiation thermal behaviour, and these only depend on the non-uniformity of the relative dose profile and/or on the properties and geometry of the non-water material.

Figure 3 shows a typical example of excess temperature curves due to non-water materials, in this case expressed as the ratio of the real temperature

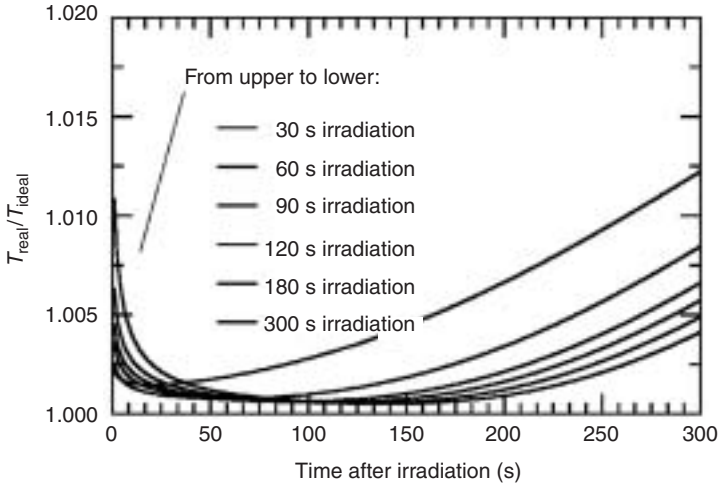

FIG. 3. Excess temperature as a function of time after ^{60}Co irradiation of the calorimeter for irradiation times between 30 s and 300 s. The glass vessel has a diameter of 6.15 cm, a wall thickness of 1.05 mm and two probes with a diameter of 0.5 mm. (Adapted from Ref. [16].)

at the point of measurement and the ideal temperature in the absence of non-water materials as a function of time after the end of an irradiation started under ideal thermal conditions. The curves shown are for a concentric probe (0.5 mm diameter) and glass vessel (diameter of 6.15 cm, wall thickness of 1.05 mm) arrangement and for a number of irradiation times. The excess temperature due to the thermistor probe excess heat drops directly after the end of the irradiation, to increase again minutes after the end of the irradiation, due to heat coming in from the vessel wall. Expressed as a correction on a backward extrapolation to the mid-run point, corrections can be derived for the effects of the probes and the vessel. For this geometry the corrections are of the order of 0.2% [18], but depend critically on the probe and the glass vessel diameter. Increasing the vessel diameter drastically decreases the effect of excess temperature from the vessel wall, such that for diameters of 8 cm and more it can be virtually ignored. More recent work has extended this calculation model to a sequence of irradiations, with the goal of studying the extrapolated correction for runs that start from realistic thermal conditions, as opposed to perfect thermal equilibrium. An important result is that estimated excess heat corrections derived from ideal initial thermal conditions deviate significantly from excess heat corrections derived from subsequent runs, as for the first run the pre-drift extrapolation is based on a (perhaps unrealistic) zero thermal drift situation. The accuracy of the calculation models depends on the thermal history of the calorimeter in a realistic experiment, and experimental work has shown that, within uncertainties, calculated excess heat curves due to vessel excess heat agree with measured excess heat curves [26, 27]. An experimental verification of the temperature drift at the beginning or just after the end of an irradiation run is complicated by an increased thermistor response due to transient effects [16, 17]. It has been hypothesized that this might be due to electron–hole pairs created in the thermistors, of which a significant fraction could have been separated in the electric field created by the voltage drop over the thermistor bead (typically 0.4 V) [27]. Experiments with excessive dose rates have shown that this effect disappears within 20–30 s after the beginning or end of the irradiation, which is of little importance if irradiation times and post-irradiation drifts can be made significantly long [16].

Heat transfer calculations have also been made to assess the effects of the non-uniformity of dose profiles and the effects due to excess heat arising from exothermicity in the volume of water outside the sealed calorimeter vessel. Various calculations have shown that profile non-uniformity corrections are small for kilovoltage and megavoltage X ray beams [18, 23, 26, 27], but could be significant for the lower energy end of clinical electron beams [16]. One way of dealing with this problem is to reduce drastically the irradiation time and consequently increase the dose rate; however, then a thorough understanding

of the thermistor probe excess heat and transient response is required in order to avoid systematic effects on the measured dose.

To combine the different effects leading to heat loss, for simplicity use is often made of additivity of excess temperature or multiplicativity of correction factors for heat loss. It has been shown that for sealed water calorimeters the combined corrections for heat loss are limited to a few tenths of a per cent and uncertainty estimates vary from 0.06% to a few tenths of a per cent [17, 27].

2.3.2. Convective heat transfer

Almost all sealed water calorimeters operated at standards laboratories currently utilize, through different means, an operation temperature of around 4°C, at which point, for water, the coefficient of volumetric expansion is zero and the driving force for convection is absent. The early open water calorimeters and the NIST sealed water calorimeter were operated at room temperature, and various design and operating features in the latter calorimeter reduced the effects of convective motion on the measured dose [28]. An extensive experimental and numerical analysis of the effect of natural convection on the NRC sealed water calorimeter has shown that if the calorimeter, with a vessel diameter of 6.7 cm, is operated at room temperature, the measured dose is affected by convective motion inside and outside the detection vessel. Effects were shown of about 1% and up to 3% for photon and electron beams, respectively [29]. Convection in a vessel of this diameter was shown to affect the temperature drift curves without the display of a clear onset point. The study also retrospectively puts the 3.5% excess response (usually attributed to an uncontrolled heat defect), as well as the thermistor power dependence of the response of early open water calorimeters, in another perspective [29]. For the NIST sealed water calorimeter, which is currently operated at 22°C, experimental studies have shown that the overall effect of convection was fortuitously small [28]. The calculations for the NIST calorimeter confirm this observation [29].

2.4. Other correction factors

The profile uniformity correction factor, k_{dd}, corrects for the effect of the difference in dose at the points of measurement of the thermistor probes versus the dose at the reference point. The correction factor for scattering and absorption of radiation in the vessel wall accounts for the change in dose at the centre of the vessel due to the absorption and scattering of radiation in the vessel wall. Experimental determination of each of these correction factors requires relative measurements with small volume ionization chambers or

diodes. The magnitude of the latter factor depends on the vessel wall thickness, diameter and beam energy. For water calorimeters operated at 4°C the difference in water density between the operation temperature and the temperature at which the dosimeter is calibrated gives rise to a minor correction factor. The various reports in the literature (e.g. Ref. [17]) and in these Proceedings (e.g. Ref. [19]) illustrate the magnitude of these correction factors.

2.5. Application areas of water calorimeter based dose standards

Equally or even more important than serving as reliable absorbed dose standards, water calorimeters have been involved in extensive measurements of ionization chamber beam quality conversion factors for absorbed dose based protocols. The body of experimental data on water calorimetry based absorbed dose beam quality conversion factors is quite respectable for photon beams [30–32], and is increasing, with several new measurements being reported in these Proceedings [20, 21]. An important conclusion from these measurements is that type average data on ionization chamber beam quality correction factors are in agreement with absorbed dose protocol (calculated) data within 0.5% [31, 32]. This extensive body of data is not yet available for electron beam dosimetry, and new work based on second generation water calorimeters that presents data for beam quality conversion factors would be remarkably useful.

2.6. Uncertainties

Table I summarizes a typical uncertainty budget for the NRC water calorimeter based absorbed dose to water standard in high energy photon beams, as reported in Ref. [17].

The NRC uncertainty estimates on thermistor calibration and conductive heat loss are thought of as being of a fairly conservative nature. With the more recent work showing excellent long term constancy of the thermistor material constants and with the experimental verification of the calculated heat loss models [26, 27, 29], the uncertainties on these factors can probably be reduced, as is indicated by the uncertainty estimates (in parentheses) on similar quantities from other reports [19, 27]. New work on absorbed dose measurements in electron beams needs to be done to study sealed water calorimeter performance and heat transfer in these beams.

It is therefore safe to state that for high energy photon beams two remaining effects now dominate water calorimeter absorbed dose uncertainty estimates: device precision (or measurement reproducibility) and uncertainty on the heat defect. While the former source of uncertainty will remain an issue

TABLE I. UNCERTAINTY BUDGET (%) OF THE NRC SEALED WATER CALORIMETER IN HIGH ENERGY PHOTON BEAMS

Quantity	Type A	Type B
Thermistor calibration	—	0.20 (0.06)
Repeatability	0.15	—
Specific heat capacity	—	0.05
Conduction heat loss correction	—	0.15 (0.08)
Field perturbation correction	—	0.02 (0.05)
Profile uniformity	—	0.02
Positioning	—	0.10 (0.06)
Water density	—	0.02
Heat defect	—	0.30 (0.0)
Quadratic summation	0.15	0.41
Combined relative standard uncertainty in D_w	0.43	

Note: The numbers in parentheses present uncertainty estimates on the same quantities from alternative reports (e.g. Refs [19, 27]).

with current measurement technology, there is considerable variation in heat defect uncertainty estimates, with a general decreasing trend in uncertainty as more research on water calorimeters is carried out. Provocatively, this uncertainty has been set to zero in the PTB water calorimeter absorbed dose standard, which is operated using the H_2 saturated system that, in an ideal world, reaches a steady state with zero heat defect. The claim is made that the effect of traces of oxygen at the level of a few tenths of a per cent can be observed accurately in the time frame required to gain sufficient precision [19]. Since all sealed water calorimeters operate under the same general restrictions regarding vessel preparation and water purity, it would probably be wise to adopt a generally accepted consensus uncertainty estimate on the heat defect for the water calorimeters used for standards dosimetry worldwide.

3. ABSORBED DOSE GRAPHITE CALORIMETRY

Graphite calorimeters as the bases for national absorbed dose to water standards have been around for a much longer period than water calorimeters, since issues such as heat defect and convection were assumed to be absent. In addition, the specific heat capacity of graphite is roughly a factor of six lower

than that of water, giving rise to a signal to noise ratio increase of the same magnitude over water calorimetry. Within the framework of fundamental versus technical complications discussed in the section on water calorimetry, only technical complications are involved in graphite calorimetry. These were the main reasons for the International Commission on Radiation Units and Measurements [33] to propose graphite as the recommended calorimetric material. However, to arrive at the desired quantity of absorbed dose to water a conversion procedure is required. Furthermore, the effect of vacuum gaps in photon beams was not assessed numerically until the late 1980s.

Different types of graphite calorimeter have been constructed and are in operation at several standards laboratories. Reference [34] summarizes and puts into context the history of graphite calorimetry at the NPL. Reports on the graphite calorimeter systems of the Laboratoire national Henri Becquerel (LNHB, France), the Australian Radiation Protection and Nuclear Safety Agency (ARPANSA), the NMi and the Italian standards laboratory (the Agency for New Technologies, Energy and the Environment (ENEA)) have recently been published [35–38]. These Proceedings also contain three reports on currently operated graphite calorimeter systems [39–41].

3.1. Methodology and measurement technology

Graphite calorimeters are multibody systems with which, using thermistors, the average temperature rise is measured in a central body or core that is thermally isolated from its surrounding bodies (jackets) by vacuum or air gaps. For guidance on the discussion of graphite calorimeters, a schematic drawing of a frequently used calorimeter type (i.e. the Domen type [42] graphite calorimeter) is shown in Fig. 4. A significant operational difference between this calorimeter type and the water calorimeter system is the fact that the graphite calorimeter can be calibrated by dissipating a known amount of electrical energy in its bodies and measuring the corresponding temperature rise. This capability of being able to determine electrically the specific heat capacity of the absorber is by far the most frequently used method of calibration, although graphite calorimeters have been built for which the specific heat capacity of the core is measured separately against thermometer standards [43, 44].

There are three major modes of operation in solid body calorimetry: (1) the quasi-adiabatic mode, in which the core and the jacket temperature are raised at the same rate so as to minimize heat loss from the core; (2) the heat loss compensated mode, in which the heat loss from the core is quantified by summing the core and jacket signals [42]; and (3) the isothermal mode, in which the heat loss from the core is kept constant and the temperature drift is zero

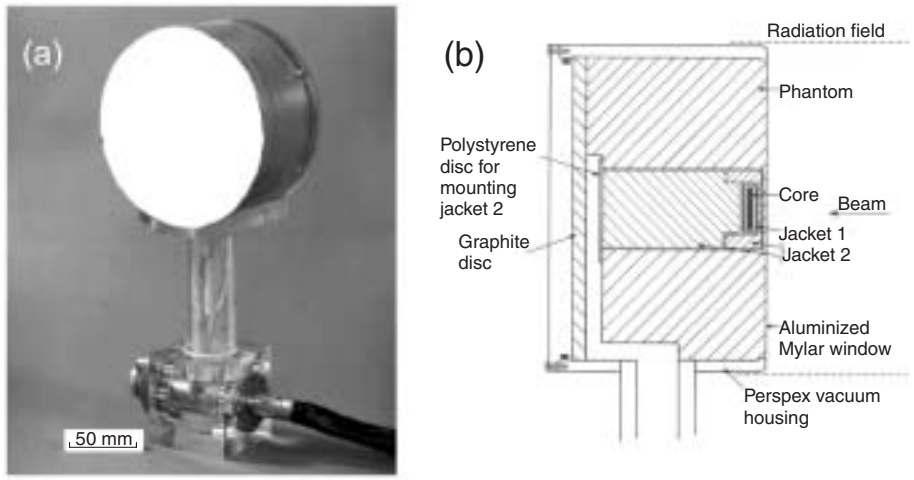

FIG. 4. (a) NPL Domen type, high energy photon beam absorbed dose calorimeter. (b) Schematic drawing of the main components of the NPL high energy photon beam graphite calorimeter.

[45, 46]. In the Domen type calorimeter [42] the masses and heat capacities of the core and first jacket are made approximately equal, which gives rise to a significant simplification in the calibration of the calorimeter. During irradiation with a broad field both the core and first jacket receive approximately the same dose and undergo the same temperature rise, which leads, from the perspective of the core, to quasi-adiabatic conditions. In the calibration mode, electrical energy is dissipated only in the central core, but the temperature changes of the core and first jacket are summed (in the heat loss compensated mode). Reference [42] proves that if the power dissipations are the same in each of the cases $T_{c,\mathrm{irr}} = T_{c,\mathrm{cal}} + T_{j,\mathrm{cal}}$, where $T_{c,\mathrm{irr}}$ represents the core temperature in the quasi-adiabatic mode and $T_{c,\mathrm{cal}}$ and $T_{j,\mathrm{cal}}$ the core and jacket temperatures, respectively, in the heat loss compensated mode.

Since graphite is an efficient conductor, the temperature variations from a point to a point within a calorimeter body are small. Recently, however, the effect on the core of temporal dependence of the uniformity of the temperature profile within a calorimeter body during electrical calibration on the heat transport in the graphite calorimeter has been investigated and is reflected in the uncertainty budget of the NPL photon beam primary standard [47]. If it is accepted that these effects can be ignored, the general thermal behaviour of the system can be relatively easily modelled once the heat transfer coefficients between the different bodies as well as the specific heat capacities of the bodies have been determined.

A generic expression for the absorbed dose to graphite can be written as:

$$D_g = N_e \Delta V_c^{\text{irr}} k_{\text{gap}} \tag{6}$$

where N_e represents the electrically determined calorimeter calibration factor (in Gy/V) and ΔV_c^{irr} the calorimeter bridge output signal obtained during an irradiation (in V), corrected for non-linearities of the measuring system, including the thermistors, for the temperature dependence of the specific heat capacity of graphite and for heat loss. k_{gap} is the calorimeter gap correction factor that accounts for the change in absorbed dose to the core due to the presence of the gap. The electrical calibration factor is derived from:

$$N_e = \frac{E_c}{m_c \Delta V_c^{\text{cal}}} \tag{7}$$

where E_c is the electrically dissipated energy in the central body during a calibration experiment corrected for electrical losses (in wiring, etc.). m_c is the mass of the core, corrected for the fact that foreign materials (such as the measuring thermistors and glue) have different heat capacities and radiation absorption characteristics than pure graphite and hence influence the effective thermal properties of the core. ΔV_c^{cal} is the bridge output signal obtained during an electrical calibration experiment, corrected for non-linearities of the measuring system, including the thermistors, for the temperature dependence of the specific heat capacity of graphite and for heat loss. In order to account for possible differences in amplifier sensitivity between electrical calibration and irradiation, calibration runs need to be corrected to the same bridge reference conditions as irradiation runs for the electrical calibration to be valid.

Beyond technical difficulties in properly evaluating all electrical corrections in both calibration and irradiation experiments, which are similar for each mode of operation (heat loss compensated, quasi-adiabatic or isothermal), the heat loss correction for graphite calorimetry does depend on the mode of operation and has been the subject of significant research.

3.2. Heat transfer

3.2.1. Heat transfer coefficients and thermal system parameters

Given the fact that convection is a negligible mode of heat loss in an evacuated graphite calorimeter, the main modes of heat transfer are through

conduction and radiation. In evacuated calorimeters vacuum gaps reduce direct heat loss through conduction from one body to another body; however, the plastic (often polystyrene) supports of the core in the jacket and the jacket in the shield, as well as the electrical wiring, lead to conductive heat transfer from one body to another. Heat transport through conduction follows an equation of the form:

$$\frac{\mathrm{d}Q}{\mathrm{d}t} = -K\Delta T \tag{8}$$

where Q represents the energy transferred, ΔT the temperature difference between two bodies in the calorimeter and K a heat transfer coefficient that takes the form kA/d, where k is the conductivity of the medium in between the two surfaces, A is the surface area and d is the gap width. For low pressures between the gaps, individual air molecules travelling between the surfaces of the bodies are also directly responsible for heat transfer, and the heat transfer coefficient as a result of this process is proportional to the gas pressure. At 7×10^{-3} Pa the heat transfer coefficient between the core and the jacket in a Domen type graphite calorimeter is of the order of 4×10^{-6} W/K.

Radiative heat loss between two completely concentric bodies is governed by Stefan's law, is proportional to the difference of the fourth power of the temperatures of the bodies and depends on the surface areas and emissivities of the bodies. For absorbed dose calorimetry, in which the calorimeter bodies are different in temperature by no more than 0.1 K, heat loss through radiation can be approximated using the same type of equation as Eq. (8), since the temperature difference is much lower than the average temperature of the two bodies. Radiative heat loss is reduced by providing the inside surfaces of the jacket and shield with aluminized Mylar, for which the emissivity is 0.1. This leads, for the core and jacket in a typical Domen type graphite calorimeter, to values for K of 6×10^{-4} W/K.

From the previous discussion it is clear that for sufficiently small temperature differences both modes of heat transfer follow Eq. (8), with values of K for Domen type graphite calorimeters between 8×10^{-4} W/K and 1.1×10^{-3} W/K between the core and jacket and similar values for the other bodies. Hence, the complete heat transport in a three body calorimeter (relative to a zero surround or medium (m) temperature and assuming no temperature gradients within bodies) can be described as:

$$C_c \frac{dT_c}{dt} = P_c + K_{c,j}(T_j - T_c)$$

$$C_j \frac{dT_j}{dt} = P_j - K_{c,j}(T_j - T_c) + K_{j,s}(T_s - T_j)$$

$$C_s \frac{dT_s}{dt} = P_s - K_{j,s}(T_s - T_j) + K_{s,m}T_s \quad (9)$$

where C_i, T_i and P_i are the heat capacities, temperature and powers, respectively, of the core (c), jacket (j) or shield (s) and $K_{i,j}$ are the heat transfer coefficients between the core and jacket, jacket and shield and shield and surround (medium, m). These system parameters, together with the masses of the calorimeter bodies determined at the construction of the calorimeter, allow for the accurate calculation of temperature drift curves as a result of powers dissipated in the bodies through ionizing radiation or electrical calibration. Accurate knowledge of the system parameters also allows automated thermal control of the calorimeter and ease of operation in the isothermal mode [46].

3.2.2. Heat loss corrections

The heat transferred during an irradiation time interval Δt from or to the core of a calorimeter, for example, is given by:

$$K_{c,j} \int_0^{\Delta t} \left[T_j(t) - T_c(t) \right] dt \quad (10)$$

The rate of temperature change in the core after an irradiation experiment is:

$$\left(\frac{dT_c}{dt} \right)_{t=\Delta t} = \frac{K_{c,j}}{C_c} \left[T_j(\Delta t) - T_c(\Delta t) \right] \quad (11)$$

The true temperature rise, T_c, without heat loss can be measured as a linear backward extrapolation of the slope of the post-irradiation drift curve at the end of the irradiation to a point at time, t_{ex}, if, at this time point, the extrapolated temperature equals the ideal temperature (without heat loss):

$$T_c(\Delta t) - \frac{K_{c,j}}{C_c} \int_0^{\Delta t} \left[T_j(t) - T_c(t) \right] dt \equiv \frac{P_c}{C_c} \Delta t = T_c(\Delta t) - (\Delta t - t_{ex}) \left(\frac{dT_c}{dt} \right) (\Delta t)$$

$$= T_c(\Delta t) - (\Delta t - t_{ex}) \frac{K_{c,j}}{C_c} [T_j(\Delta t) - T_c(\Delta t)] \quad (12)$$

This means that the extrapolation time, t_{ex}, must satisfy:

$$\int_0^{\Delta t} \left[T_j(t) - T_c(t) \right] \mathrm{d}t = (\Delta t - t_{ex})[T_j(\Delta t) - T_c(\Delta t)] \tag{13}$$

Evaluation of the extrapolation time can be performed by integrating the set of heat loss equations (Eq. (9)) using the numerical values of the system parameters for a given set of power dissipations and then solving, using the calculated drift functions (Eq. (13)) for t_{ex}. Note that the absolute magnitudes of the power dissipations (i.e. the dose rates) are not required for this purpose; only their magnitude relative to each other. From Eq. (13) it is also clear that, only in the case of a linear increase in temperature as a function of time, the extrapolation time is given by $t_{ex} = \Delta t/2$. In irradiation experiments this linearity is not necessarily preserved, since heat loss occurs from the jacket to the outer calorimeter bodies. Determination of the extrapolation time therefore becomes important for long irradiation times.

With the knowledge of the system parameters, heat loss corrections from the core in an irradiation experiment can be calculated as:

$$k_c^{\mathrm{irr}} = 1 - \frac{K_{c,j}}{T_c(\Delta t) C_c} \int_0^{\Delta t} \left[T_j(t) - T_c(t) \right] \mathrm{d}t \tag{14}$$

A similar equation can be derived for the heat loss correction during a heat loss compensated calibration experiment.

Finally, it should be noted that the validity of calculated heat loss corrections is coupled to the accuracy of Eq. (9) to describe the system. Firstly, contrary to the situation in an irradiation experiment, during a calibration experiment heat is dissipated at discrete points in a calorimeter body (e.g. the core) and the transport of heat within the complete calorimeter body is assumed to be immediate. Secondly, the presence of additional heat transfer paths, for example between the core and shield by electrical wiring, could introduce additional heat loss terms in the description of the core temperature. These would have to be taken into account in the evaluation of the heat loss correction factors.

3.3. Gap effect corrections

Until the late 1980s the influence of the gap effect in graphite calorimetry for photon beams was largely ignored. Owen and DuSautoy [48] used a flat ionization chamber simulating the core to measure the effect for the NPL photon beam calorimeter. Boutillon [49] was the first to estimate, using only

photon transport and correlated sampling Monte Carlo calculations, the gap corrections in a ^{60}Co beam. Boutillon's definition of the gap correction was the ratio of the dose in the absence of the gap to the dose in the presence of the gap, the centre of the core being at a constant distance from the source and the actual thickness of graphite in front of the core being the same in both cases. Boutillon's work shows that vacuum gaps in a calorimeter lead to a decrease in dose to the core, the magnitude of which depends on the width, height and position of the gap, as well as on the dimensions of the core and on field size. Figure 5 summarizes the corrections for four gap types in a Domen type calorimeter as a function of depth in graphite for the specific conditions outlined.

Using more advanced Monte Carlo calculations including electron transport and using measurements, standards laboratories operating graphite

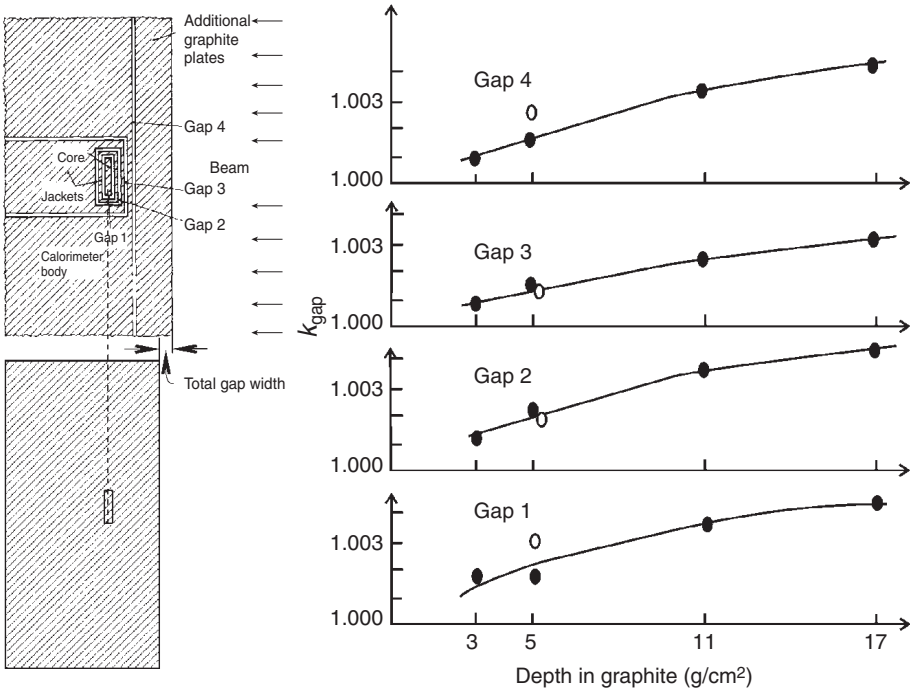

FIG. 5. Gap effect corrections for four different gap types in a graphite calorimeter. Left: designation of the gap types; right: gap effect correction factors as a function of depth for a calorimeter irradiated in a ^{60}Co beam. The closed bullets represent calculated data from Ref. [49]; the open bullets represent measured data from Ref. [48] (with modifications from Ref. [49]).

calorimeters have extended this work to their own calorimeter gap and beam arrangements and energies [36, 50]. The reader is warned to verify carefully the experimental set-ups under which the gap corrections are specified, in order to make valid comparisons.

Gap effect corrections in a Domen type graphite calorimeter were measured by Cottens [51] at $d_{\max}$ in graphite in 12, 20 and 30 MeV electron beams and shown to be as large as 0.8%, with uncertainties of around 0.2%. Since standards laboratories have mainly concentrated on the development of absorbed dose to water standards for photon beams, more up to date information on gap effect corrections in electron beams is lacking.

3.4. Other corrections

Current graphite calorimeter systems operated at standards laboratories require numerous correction factors, such as for differences in depth between the measuring and reference depth and the non-uniformity of the dose distribution over the core. These corrections strongly depend on the peculiarities of the calorimeter system in question and the reader is therefore referred to individual reports for details (e.g. Refs [36, 50]).

3.5. Dose conversion methods

In photon beams two methods are usually used to convert absorbed dose measured in graphite to absorbed dose in water. The first method makes use of the relationship between collision kerma in two media:

$$D_w = D_g \frac{K_{\text{coll},w}\beta_w}{K_{\text{coll},g}\beta_g} = D_g(\psi)_g^w \left(\frac{\bar{\mu}_{\text{en}}}{\rho}\right)_g^w (\beta)_g^w \tag{15}$$

where $(\beta)_g^w$ represents the ratio of the quotient of dose to collision kerma for water to graphite at the respective measurement points, $(\Psi)_g^w$ the ratio of the photon energy fluences from water to graphite at the respective measurement points and $(\bar{\mu}_{\text{en}}/\rho)_g^w$ the ratio of average mass energy absorption coefficients for water to graphite at the respective measurement points. The photon fluence scaling theorem simplifies the evaluation of the ratio of the energy fluences of water to graphite. If Compton scattering is the predominant mode of interaction and all dimensions, including measurement depth, phantom size, field size and source to surface distance, are scaled by the inverse of the electron densities of the two materials, the ratio of energy fluences is given by the inverse square law. Corrections are applied for the fact that the photon

source is not a point source, for air attenuation and for the presence of pair production, bremsstrahlung and annihilation as interaction modes. Monte Carlo simulations provide a direct verification of this method provided that the interaction coefficient data are accurate. More details on the scaling method can be found in Refs [52, 53]. A scaling method could also be developed for electron beams; however, the stopping power and electron fluence ratios that would be involved in such a conversion procedure need to be estimated accurately and, as yet, for graphite no recent attempts to this effect have been reported.

In the second method an ionization chamber is used as a transfer instrument to derive dose to water from dose to graphite (e.g. Ref. [52]). In essence the chamber is calibrated in a graphite phantom representation of the calorimeter and then used for dose measurements in water. Dose at the reference point in water can be derived from dose at the point of measurement in graphite using the equation:

$$D_w = D_g \frac{M_w s_{w,\mathrm{air}} p_{Q,w}}{M_g s_{g,\mathrm{air}} p_{Q,g}} \tag{16}$$

where M_w and M_g represent the corrected ionization chamber reading in water and graphite, respectively, $s_{w,\mathrm{air}}$ and $s_{g,\mathrm{air}}$ the restricted collision mass stopping power ratio water to air and graphite to air, respectively, and $p_{Q,w}$ and $p_{Q,g}$ chamber correction factors at the measurement points in water and graphite, respectively. The accuracy of this method relies less on an absolute knowledge of the interaction data than the previous method, but the challenge lies in the evaluation of the stopping power ratios and the chamber correction factors, which must be known at the respective measurement depths in each of the phantoms. To this end, again, Monte Carlo simulations provide a useful tool. In electron beams, the chamber based dose conversion method has also been used to convert absorbed dose in graphite to absorbed dose to water (e.g. Ref. [54]).

Standards dosimetry laboratories assign a typical uncertainty of the order of 0.19–0.35% to the dose transfer procedures in high energy photon beams [36, 50, 51].

3.6. Uncertainties

Table II shows a summary of the uncertainty budget of the NPL photon absorbed dose standard [55] for the quantity absorbed dose to graphite.

It is immediately clear that the bare measurement precision (reproducibility) of a measurement of temperature rise in a graphite calorimeter is superior to that in water calorimetry; this observation is

TABLE II. UNCERTAINTY BUDGET (%) OF THE NPL GRAPHITE PHOTON CALORIMETER

Quantity	Type A	Type B
Electrical calibration	0.13	0.50*
Repeatability	0.05	—
Core mass	—	0.05
Gap effect correction	—	0.13
Graphite depth	—	0.04
Distance from source	—	0.05
Radial non-uniformity	0.01	0.01
Quadratic summation	0.20	0.54
Combined relative standard uncertainty in D_g	0.56	

Note: The asterisk indicates that, at the NPL, the type B uncertainty on the electrical calibration is currently undergoing a reassessment [47].

confirmed in other reports [36, 50]. Since the measurement technology is the same as with water calorimeters, reasons for this may be the significantly lower specific heat capacity in graphite and the absence of a heat defect and of convection (both could be present locally or temporarily in a sealed water calorimeter). In the situation presented in Table II, the overall uncertainty is dominated by concerns about the validity of the heat loss model used at the NPL in the electrical calibration and by the uncertainty on the gap correction. Other reports on graphite calorimeter performance show a significantly lower overall uncertainty of around 0.24%; this uncertainty is largely dominated by the gap correction only (e.g. Ref. [50]). Combined with an overall uncertainty on the dose transfer from graphite to water of around 0.35%, dose to water can be measured with an uncertainty of between 0.41% and 0.66% in high energy photon beams. The uncertainty estimates on graphite calorimetric absorbed dose determination in electron beams are of a similar order of magnitude [39], with the possible exception of the uncertainty on gap effect corrections, for which only fairly dated studies are available [51].

4. DISCUSSION AND CONCLUSIONS

Each of the calorimeter systems discussed in this paper have simplicities and complexities that are quite distinct and make them, as absorbed dose standards, largely independent of each other. In graphite calorimetry the

complexities are more of a technical and engineering nature; in water calorimetry complexities have been for a long time of a more fundamental nature. The only important similarity between the two techniques is the technology involved in measuring the temperature rise, which is usually based on thermistors. For the interpretation of dosimetry comparisons it might be important to take this correlation into account when directly comparing graphite and water calorimeter standards. In this context it can be mentioned that, at high dose rates, transient thermistor effects have been observed that could conceivably affect extrapolation procedures for very short irradiation times.

The precision of the graphite calorimeter is superior to that of the water calorimeter when operated under the same conditions; however, the gap corrections and the transfer of absorbed dose from graphite to water increase the uncertainty of the former system in establishing the quantity of interest. With more water calorimeter systems being constructed over the past decade, compelling evidence has allowed the reduction of uncertainties on the heat defect, with the most extreme case of a zero uncertainty being reported in these Proceedings [19]. The uncertainty on the heat defect in sealed water calorimetry requires a re-evaluation, with the goal to arrive at a consensus value applicable to all sealed water calorimeters used as absorbed dose standards. Heat transfer in the graphite calorimeter system is governed by system parameters that can be determined without the use of ionizing radiation, and accurate correction procedures have been determined. Some questions have arisen for these calorimeters regarding the accuracy of the heat loss models on the electrical calibration. In water calorimeters operated at 4°C in high energy photon beams the effects of excess heat and profile heat loss through conduction have been modelled and verified experimentally. For high energy photon beams both calorimeter systems arrive at comparable uncertainty estimates. In recent years both calorimeter types have been the basis for a mounting body of data on absorbed dose beam quality conversion factors or absorbed dose calibration factors, both of which are, within uncertainties, in agreement with calculations of these factors based on cavity theory. For those standards laboratories that maintain water as well as graphite calorimeter absorbed dose standards, direct in-house comparisons have and would further consolidate confidence in both systems. Although graphite calorimeters have been developed and extensively used as primary standards in electron beams, this area of application remains to be explored and investigated further with current second generation sealed water calorimeters. Work in this area will also allow much needed experimental values of beam quality conversion factors to be established and may lead to more confidence in the gap corrections and dose conversion procedures from graphite to water for electron beams. In this context recent efforts to develop ‘clinical’

calorimeters suitable for the direct calibration of instruments in clinical beams should be encouraged [20, 41].

Because of their differences, graphite and water calorimeters continue to play a complementary role in absorbed dose to water determination, and they ensure the robustness of the absorbed dose calibration system. It is important that efforts be made at standards laboratories to preserve the experience in both techniques and to keep both systems in operation to maintain this robustness.

ACKNOWLEDGEMENTS

We wish to express sincere gratitude for the body of knowledge and experience in calorimetry that we have been able to access over the years directly and indirectly through interactions and collaborations with our colleagues working in this area, in particular (in arbitrary order) S. Domen, E. Cottens, C. Ross, N. Klassen, K. Shortt, H. Palmans, B. Owen, A. Calverd, B. Burns, M. McEwen, S. Duane, K. Rosser and A. Williams.

J.P. Seuntjens is a research scientist of the National Cancer Institute of Canada, with funds provided by the Canadian Cancer Society. A.R. DuSautoy acknowledges the financial support of the National Measurement System Policy Unit of the United Kingdom Department of Trade and Industry.

K. Stewart is thanked for helpful comments on an early version of the manuscript.

REFERENCES

[1] GUNN, S.R., Radiometric calorimetry: A review, Nucl. Instrum. Methods **85** (1970) 285–312.

[2] GUNN, S.R., Radiometric calorimetry: A review, Nucl. Instrum. Methods **135** (1976) 251–265.

[3] DOMEN, S.R., "Advances in calorimetry for radiation dosimetry", The Dosimetry of Ionizing Radiation, Vol. II (KASE, K.R., BJARNGARD, B.E., ATTIX, F.H., Eds), Academic Press, Orlando, FL (1987).

[4] ROSS, C.K., KLASSEN, N.V., Water calorimetry for radiation dosimetry, Phys. Med. Biol. **44** (1996) 1–29.

[5] ROSS, C.K., KLASSEN, N.V. (Eds), NRC Workshop on Water Calorimetry (Proc. Workshop Ottawa, 1988), Rep. NRC-29637, National Research Council, Ottawa (1988).

[6] Proceedings NPL Workshop on Calorimetry in Radiation Dosimetry, National Physical Laboratory, Teddington, UK (1994).

[7] WILLIAMS, A.J., ROSSER, K.E. (Eds), Recent Advances in Calorimetric Absorbed Dose Standards (Proc. Workshop Teddington, UK, 1999), Rep. CIRM 42, National Physical Laboratory, Teddington, UK (2000).
[8] INTERNATIONAL ATOMIC ENERGY AGENCY, Measurement Assurance in Dosimetry (Proc. Int. Symp. Vienna, 1993), IAEA, Vienna (1994).
[9] FLEMING, D.M., GLASS, W.A., Endothermic processes in tissue-equivalent plastic, Radiat. Res. **37** (1969) 316–322.
[10] KLASSEN, N.V., ROSS, C.K., Absorbed dose calorimetry using various aqueous solutions, Radiat. Phys. Chem. **38** (1991) 95–104.
[11] KLASSEN, N.V., ROSS, C.K., Water calorimetry: The heat defect, J. Res. Natl. Inst. Stand. Technol. **102** (1997) 63–71.
[12] ROSS, C.K., KLASSEN, N.V., SMITH, G.D., The effects of various dissolved gases on the heat defect of water, Med. Phys. **11** (1984) 653–658.
[13] SCHULZ, R.J., WUU, C.S., WEINHOUS, M.S., The direct determination of dose-to-water using a water calorimeter, Med. Phys. **14** (1987) 790–796.
[14] WILLIAMS, A.J., ROSSER, K.E., "Development of the NPL water calorimeter", Recent Advances in Calorimetric Absorbed Dose Standards (Proc. Workshop Teddington, UK, 1999), Rep. CIRM 42 (WILLIAMS, A.J., ROSSER, K.E., Eds), National Physical Laboratory, Teddington, UK (2000) 130–137.
[15] DOMEN, S.R., A sealed water calorimeter for measuring absorbed dose, J. Res. Natl. Inst. Stand. Technol. **99** (1994) 121–141.
[16] SEUNTJENS, J.P., ROSS, C.K., KLASSEN, N.V., SHORTT, K.R., A Status Report on the NRC Sealed Water Calorimeter, Rep. PIRS-0584, National Research Council, Ottawa (1999).
[17] ROSS, C.K., SEUNTJENS, J.P., KLASSEN, N.V., SHORTT, K.R., "The NRC sealed water calorimeter: Correction factors and performance", Recent Advances in Calorimetric Absorbed Dose Standards (Proc. Workshop Teddington, UK, 1999), Rep. CIRM 42 (WILLIAMS, A.J., ROSSER, K.E., Eds), National Physical Laboratory, Teddington, UK (2000) 90–102.
[18] SEUNTJENS, J., PALMANS, H., Correction factors and performance of a 4ºC sealed water calorimeter, Phys. Med. Biol. **44** (1999) 627–646.
[19] KRAUSS, A., "The future Physikalisch-Technische Bundesanstalt primary standard for absorbed dose to water in ^{60}Co radiation", these Proceedings, Vol. 1, pp. 75–82.
[20] PIEKSMA, M., DE PREZ, L.A., VAN DIJK, E., AALBERS, A.H.L., "Measurements of k_Q beam quality correction factors for the NE 2611A chamber in high energy photon beams using the Nederlands Meetinstituut water calorimeter", ibid., Vol. 1, pp. 93–102.
[21] STUCKI, G., MUENCH, W., QUINTEL, H., "The METAS absorbed dose to water calibration service for high energy photon and electron beam radiotherapy", ibid., Vol. 1, pp. 103–113.
[22] MEDIN, J., SEUNTJENS, J., KLASSEN, N., ROSS, C., STUCKI, G., "The OFMET sealed water calorimeter", Recent Advances in Calorimetric Absorbed Dose Standards (Proc. Workshop Teddington, UK, 1999), Rep. CIRM 42

(WILLIAMS, A.J., ROSSER, K.E., Eds), National Physical Laboratory, Teddington, UK (2000) 65–73.

[23] SEUNTJENS, J., THIERENS, H., SCHNEIDER, U., Correction factors for a cylindrical ionization chamber used in medium-energy X-ray beams, Phys. Med. Biol. **38** (1993) 805–832.

[24] WILLIAMS, A.J., ROSSER, K.E., "A comparison of A.C. and D.C. Wheatstone bridges for the purpose of high precision temperature measurement", Recent Advances in Calorimetric Absorbed Dose Standards (Proc. Workshop Teddington, UK, 1999), Rep. CIRM 42 (WILLIAMS, A.J., ROSSER, K.E., Eds), National Physical Laboratory, Teddington, UK (2000) 120–129.

[25] KLASSEN, N.V., personal communication, 1999.

[26] PALMANS, H., "Experimental verification of simulated excess heat effects in the sealed water calorimeter", Recent Advances in Calorimetric Absorbed Dose Standards (Proc. Workshop Teddington, UK, 1999), Rep. CIRM 42 (WILLIAMS, A.J., ROSSER, K.E., Eds), National Physical Laboratory, Teddington, UK (2000) 74–84.

[27] KRAUSS, A., Experimental verification of calculated radiation-induced heat conduction effects in the water absorbed dose calorimeter, Thermochim. Acta **382** (2002) 99–107.

[28] DOMEN, J.K., DOMEN, S.R., Studies of excess heat and convection in a water calorimeter, J. Res. Natl. Inst. Stand. Technol. **106** (2001) 843–856.

[29] SEUNTJENS, J.P., KAWRAKOW, I., ROSS, C.K., "Revisiting convective motion in stagnant water calorimeters operated at room temperature", Recent Advances in Calorimetric Absorbed Dose Standards (Proc. Workshop Teddington, UK, 1999), Rep. CIRM 42 (WILLIAMS, A.J., ROSSER, K.E., Eds), National Physical Laboratory, Teddington, UK (2000) 103–119.

[30] VATNITSKY, S.M., SIEBERS, J.V., MILLER, D.W., Calorimetric determination of absorbed dose to water beam quality correction factor k_Q for high-energy photon beams, Med. Phys. **22** (1995) 1749–1752.

[31] PALMANS, H., MONDELAERS, W., THIERENS, H., Absorbed dose beam quality correction factors k_Q for the NE2571 chamber in a 5 MV and 10 MV photon beam, Phys. Med. Biol. **44** (1999) 647–663.

[32] SEUNTJENS, J.P., ROSS, C.K., SHORTT, K.R., ROGERS, D.W.O., Absorbed-dose beam quality conversion factors for cylindrical chambers in high energy photon beams, Med. Phys. **27** (2000) 2763–2779.

[33] INTERNATIONAL COMMISSION ON RADIATION UNITS AND MEASUREMENTS, Radiation Dosimetry: X-rays and Gamma Rays with Maximum Energies between 0.6 MeV and 50 MeV, Rep. 14, ICRU, Washington, DC (1969).

[34] DuSAUTOY, A.R., McEWEN, M.R., ROSSER, K.E., DUANE, S., NUTBROWN, R.F., "Absorbed dose standards at NPL", Recent Developments in Accurate Radiation Dosimetry (Proc. Int. Workshop Montreal, 2001) (SEUNTJENS, J.P., MOBIT, P.N., Eds), Medical Physics Publishing, Madison, WI (2002) 87–107.

[35] CHAUVENET, B., BALTÈS, D., DELAUNAY, F., Comparison of graphite-to-water absorbed-dose transfers for ^{60}Co photon beams using ionometry and Fricke dosimetry, Phys. Med. Biol. **42** (1997) 2053–2063.

[36] HUNTLEY, R.B., WISE, K.N., BOAS, J.F., "The Australian standard of absorbed dose", Recent Advances in Calorimetric Absorbed Dose Standards (Proc. Workshop Teddington, UK, 1999), Rep. CIRM 42 (WILLIAMS, A.J., ROSSER, K.E., Eds), National Physical Laboratory, Teddington, UK (2000) 37–46.

[37] GRIMBERGEN, T.W.M., VAN DIJK, E., "Absorbed dose measurements at the Netherlands Measurement Institute", Measurement Accuracy in Dosimetry (Proc. Int. Symp. Vienna, 1993), IAEA, Vienna (1994) 35–44.

[38] GUERRA, A.S., LAITANO, R.F., PIMPINELLA, M., Characteristics of the absorbed dose to water standard at ENEA, Phys. Med. Biol. **41** (1996) 657–674.

[39] McEWEN, M.R., DUANE, S., STOKER, I., "Comparison of graphite standard calorimeters in megavoltage photon and electron beams", these Proceedings, Vol. 1, pp. 67–73.

[40] DAURES, J., OSTROWSKY, A., CHAUVENET, B., "Graphite calorimeter: The primary standard of absorbed dose at the Bureau national de métrologie–Laboratoire national Henri Becquerel", ibid., Vol. 1, pp. 83–91.

[41] McEWEN, M.R., DUANE, S., "Portable graphite calorimeter for measuring absorbed dose in the radiotherapy clinic", ibid., Vol. 1, pp. 115–121.

[42] DOMEN, S.R., LAMPERTI, P.J., A heat-loss compensated calorimeter: Theory, design and performance, J. Res. Natl. Bur. Stand. A **78** (1974) 595–610.

[43] SHIPLEY, D.R., DUANE, S., Heat Loss Mechanisms in a Measurement of Specific Heat Capacity of Graphite, Rep. CIRA(EXT)003, National Physical Laboratory, Teddington, UK (1996).

[44] WILLIAMS, A.J., BURNS, D.T., McEWEN, M.R., Measurement of the Specific Heat Capacity of the Electron Beam Graphite Calorimeter, Rep. RSA(EXT)40, National Physical Laboratory, Teddington, UK (1993).

[45] WITZANI, J., DUFTSCHMID, K.E., STRACHOTINSKY, C., LEITNER, A., A graphite absorbed-dose calorimeter in the quasi-isothermal mode of operation, Metrologia **20** (1984) 73–79.

[46] JANSSENS, A., COTTENS, E., PAULSEN, A., POFFIJN, A., Equilibration of a graphite absorbed-dose calorimeter and the quasi-isothermal mode of operation, Metrologia **22** (1986) 265–270.

[47] DUANE, S., personal communication, 2002.

[48] OWEN, B., DuSAUTOY, A.R., Correction for the effect of the gaps around the core of an absorbed-dose graphite calorimeter in high energy photon radiation, Phys. Med. Biol. **36** (1991) 1699–1704.

[49] BOUTILLON, M., Gap correction for the calorimetric measurement of absorbed dose in graphite with a ^{60}Co beam, Phys. Med. Biol. **34** (1989) 1809–1821.

[50] DAURES, J., OSTROWSKY, A., GROSS, P., JEANNOT, J.P., GOURIOU, J., "Calorimetry for absorbed-dose measurements at BNM-LNHB", Recent Advances in Calorimetric Absorbed Dose Standards (Proc. Workshop

Teddington, UK, 1999), Rep. CIRM 42 (WILLIAMS, A.J., ROSSER, K.E., Eds), National Physical Laboratory, Teddington, UK (2000) 15–21.

[51] COTTENS, E., Geabsorbeerde Dosis Kalorimetrie bij Hoge Energie Electronenbundels en Onderzoek van de Ijzersulfaat Dosimeter, PhD Thesis, Univ. Ghent, Belgium (1979).

[52] BURNS, J.E., Absorbed-dose calibration in high-energy photon beams at the National Physical Laboratory: Conversion procedure, Phys. Med. Biol. **39** (1994) 1555–1575.

[53] NUTBROWN, R.F., DUANE, S., SHIPLEY, D.R., THOMAS, R.A.S., Evaluation of Factors to Convert Absorbed Dose Calibrations in Graphite to Water For Mega-voltage Photon Beams, Rep. CIRM 37, National Physical Laboratory, Teddington, UK (2000).

[54] McEWEN, M.R., DuSAUTOY, A.R., WILLIAMS, A.J., The calibration of therapy level electron beam ionization chambers in terms of absorbed dose to water, Phys. Med. Biol. **43** (1998) 2503–2519.

[55] DuSAUTOY, A.R., The U.K. primary standard calorimeter for photon beam absorbed dose measurement, Phys. Med. Biol. **41** (1996) 137–151.

COMPARISON OF GRAPHITE STANDARD CALORIMETERS IN MEGAVOLTAGE PHOTON AND ELECTRON BEAMS

M.R. McEWEN*, S. DUANE, I. STOKER
National Physical Laboratory,
Teddington, United Kingdom
E-mail: simon.duane@npl.co.uk

Abstract

Four different graphite calorimeters are currently in use for megavoltage photon and electron dosimetry at the National Physical Laboratory in the United Kingdom. Their measurements of absorbed dose to graphite have been compared and agree within the uncertainties (typically ±0.5%, 1σ). This level of agreement indicates that no significant, unidentified systematic errors exist in any of the calorimeter designs, and provides a robust basis for the dissemination of absorbed dose measurements.

1. INTRODUCTION

Graphite has been the preferred medium for calorimetry at the National Physical Laboratory (NPL) for many years [1], even though water is often the material most relevant to dosimetry applications. Separate primary standard calorimeters are maintained for high energy photon and electron beams and, after conversion to dose to water, these are disseminated via calibration services to the United Kingdom and worldwide [2, 3]. Various other calorimeters have been developed at the NPL for different applications. The use of more than one primary standard could lead to dosimetric inconsistencies, and so comparisons have been carried out, in both photon and electron beams, of the primary standards with one another and with other calorimeters making absolute measurements of absorbed dose. All uncertainties quoted here are standard (1σ) uncertainties [4].

---

* Present address: National Research Council, Ottawa, Canada.

2. DESCRIPTION OF CALORIMETERS

2.1. The primary standard photon calorimeter

The photon calorimeter is based on the design of Domen and Lamperti [5] and has been described in detail by DuSautoy [6]. Maximum sensitivity is achieved by the use of AC bridges, and thermal isolation is optimized by the use of a vacuum system. The calorimeter is operated in photon beams from ^{60}Co to 20 MV, at dose rates of 0.5 Gy/min and above. Operation in electron beams is possible above 6 MeV at dose rates of 5 Gy/min, and in 16 MeV beams at 1 Gy/min.

2.2. The electron beam primary standard and hi-dose calorimeters

An electron beam calorimeter was first developed for high dose applications in radiation processing and sterilization [7], where the dose rates are greater than 10 kGy/min. This device was operated in 10 MeV beams. The design of the original (referred to here as the hi-dose calorimeter) has been enhanced to enable operation at radiotherapy dose rates down to 5 Gy/min and in electron beams down to 3 MeV [8, 9]. This therapy calorimeter, in which the core thickness has been reduced from 7 mm to 2 mm, is now designated as the NPL's primary standard for electron beam dosimetry, while the original has been retained as a transfer standard for high dose applications. The specific heat capacity of the calorimeter's graphite has been determined in a separate experiment [10], yielding a significant improvement in its uncertainty. The use of a DC bridge and air gaps give adequate sensitivity and isolation from changes in ambient temperature, provided that this is controlled to ±0.2°C.

2.3. Portable graphite calorimeter

A portable calorimeter has been developed at the NPL [11, 12] to enable absolute measurements of absorbed dose in the radiotherapy clinic for photon and electron beams. It is designed for use in high energy photon beams (^{60}Co gamma rays and 4–20 MV X rays) and electron beams (3–25 MeV) at dose rates in the range of 1 Gy/min to 100 Gy/min. Operation at low dose rates is made possible by its active temperature control and by effective screening from electrical interference.

2.4. Previous comparisons

The therapy electron calorimeter was compared with the original hi-dose calorimeter when it was commissioned in 1993, giving a dose ratio (electron/hi-dose) of 1.0010 ± 0.0020 [9]. The photon calorimeter had previously been compared with the original hi-dose electron beam graphite calorimeter [7] in high energy electron beams, giving agreement within the uncertainties (1.0017 ± 0.0034). The photon calorimeter has been compared via transfer standard ionization chambers with the ionometric standard at the Bureau international des poids et mesures, again giving agreement within the uncertainties [6].

3. UNCERTAINTIES

Uncertainties for the various calorimeters are given in Table I. The electron, hi-dose and portable calorimeters have the same uncertainties, provided that the devices are used in the beams and at the doses and dose rates given above. The gap corrections were calculated by Monte Carlo methods, giving maximum values of 0.6% for the photon calorimeter in 4 MV X rays and 0.5% for the electron calorimeter in a 10 MeV beam. The uncertainty for the photon calorimeter is dominated by its electrical calibration, in particular departures from ideal adiabatic operation. During quasi-adiabatic electrical calibration, it is attempted to deliver electrical heating power to the components surrounding the core so as to minimize the amount of heat transferred. It has been found that heat gained by the core from its surroundings (caused by transient

TABLE I. STANDARD UNCERTAINTY COMPONENTS FOR THE NPL CALORIMETERS

Component of uncertainty	Photon		Electron, hi-dose and portable	
	Type A (%)	Type B (%)	Type A (%)	Type B (%)
Analysis method	0.10	0.20	0.21	0.15
Electrical calibration	0.13	0.50	—	—
Thermistor calibration	—	—	0.06	0.05
Specific heat capacity	—	—	—	0.08
Gap correction	0.10	0.17	0.15	0.17
Overall	0.19	0.57	0.26	0.25
Combined	0.60		0.36	

temperature differences) can be of the order of 0.5%, and this is not taken into account in the usual extrapolation back to the mid-heating time. Work continues to resolve this.

4. CALORIMETER COMPARISONS

4.1. Electron primary standard versus hi-dose calorimeter

Although good agreement was obtained some years previously, this comparison was repeated to check long term stability. The calorimeters were operated in an electron beam of energy 16 MeV, and the effect of the different absorber thicknesses was minimized by choosing a measurement depth of 2.2 g/cm^2 and a collimator that minimized the dose gradient in the buildup region. Corrections were applied for axial and radial beam non-uniformity. Measurements were made at a range of dose rates from 18 Gy/min to 90 Gy/min and compared by means of a transmission monitor ionization chamber. The ratios of doses obtained from the two calorimeters at each dose rate are shown in Table II. The doses measured by these two calorimeters remain consistent.

4.2. Photon versus electron primary standard calorimeters

The calorimeters were compared first in a 16 MeV electron beam, at a measurement depth of 2.0 g/cm^2, at a dose rate of around 20 Gy/min, by means of a transmission monitor ionization chamber. A second comparison was carried out in a 10 MV photon beam, at 6 Gy/min. A measurement depth of 5.6

TABLE II. RATIO OF MEASURED DOSES: ELECTRON PRIMARY STANDARD/ HI-DOSE

Dose rate (Gy/min)	Therapy calorimeter/ hi-dose calorimeter
70	1.0017
90	1.0024
18	1.0006
Weighted mean	1.0018 ± 0.0027

g/cm^2 was used (equivalent, in terms of electron density, to 5 g/cm^2 of water) at a source to surface distance of 2 m with a field size of 18 cm diameter. It was not possible to match the backscatter for either case, owing to the much greater size of the photon calorimeter.

Measurements in the 16 MeV beam were carried out over three days, giving values for the ratio of the electron calorimeter/photon calorimeter of 1.0027, 1.0006 and 0.9999. The dose gradient in the buildup region of the depth dose curve was changed on day 3, but without significant effect. The mean value for the ratio (weighted according to the variances) was 1.0004 ± 0.0063. In 10 MV photons the result was 1.0002 ± 0.0066.

4.3. Portable versus primary standard calorimeters

Comparisons were carried out in the three beams at the NPL: ^{60}Co gamma rays, 10 MV photons and 16 MeV electrons. The results of the comparisons are given in Table III, expressed as portable dose over primary standard dose. There are a number of correlated uncertainties (e.g. in the gap effect correction) in these comparisons, which have been removed to give the uncertainties listed.

5. SUMMARY

The agreement between the electron and photon calorimeters is surprisingly good, considering the measurement uncertainties, but depends directly on the photon calorimeter electrical calibration. The overall agreement between all these calorimeters is very reassuring, indicating that there are no significant errors in the realization of absorbed dose at the NPL (Table IV).

TABLE III. RATIO OF MEASURED DOSES: PORTABLE/PHOTON AND PORTABLE/ELECTRON PRIMARY STANDARD

Beam quality	Portable/primary standard	Standard uncertainty (%)
^{60}Co[a]	1.0044	0.63
10 MV X rays[a]	1.0060	0.63
16 MeV electrons[b]	1.0030	0.42

[a] The primary standard for ^{60}Co gamma rays and 10 MV X rays is the photon calorimeter.

[b] The primary standard for 16 MeV electrons is the therapy electron calorimeter.

TABLE IV. SUMMARY OF CALORIMETRIC COMPARISONS CARRIED OUT AT THE NPL

Calorimeter	Portable	Primary electron	Primary photon
Portable	—	—	0.9940[a]
Hi-dose	—	1.0018[b]	—
Primary electron	1.0030[b]	—	0.9998[a]
Primary photon	1.0044[c]	1.0004[b]	—

[a] 10 MV X rays.
[b] 16 MeV electrons.
[c] ^{60}Co.

A water calorimeter is currently under development at the NPL [13], with the long term aim of defining it as the primary standard for both photon and electron beam dosimetry at megavoltage energies. The fact that these comparisons show good agreement between the present standards will simplify the validation of the water calorimeter. It is also intended to use the portable calorimeter as a transfer instrument in international comparisons and thus extend the scope of the work described in this paper.

Having shown that all the graphite calorimeters in use at the NPL are consistent within the measurement uncertainties, we have questioned the need for so many devices. Three of the calorimeters (hi-dose, therapy electron and portable) are very similar in operation, although the hi-dose calorimeter is suitable for energies above 10 MeV and is only maintained so that the therapy calorimeter is not irradiated to high dose levels. Partly based on the result of the comparisons reported in this paper, the hi-dose calorimeter is now designated as a transfer standard, with traceability to the therapy-level primary standard, instead of being a primary standard in its own right. At present, the portable calorimeter performance betters that of the primary standards, although its regular use off-site prevents it being designated as a primary standard. At some point the performance of the photon calorimeter will be significantly improved by the routine use of thermostatic instead of quasi-adiabatic operation, but work towards this is still in progress.

ACKNOWLEDGEMENTS

The authors would like to thank D. Shipley for providing gap effect corrections for the portable calorimeter. The authors would also like to acknowledge the financial support of the National Measurement Policy Unit of the UK Department of Trade and Industry.

REFERENCES

[1] DuSAUTOY, A.R., "NPL calorimetry: The evolution so far", Recent Advances in Calorimetric Absorbed Dose Standards (Proc. Workshop Teddington, UK, 1999), Rep. CIRM 42 (WILLIAMS, A.J., ROSSER, K.E., Eds), National Physical Laboratory, Teddington, UK (2000) 22–27.

[2] ROSSER, K.E., et al., "The NPL absorbed dose to water calibration service for high energy photon beams", Measurement Assurance in Dosimetry (Proc. Int. Symp. Vienna, 1993), IAEA, Vienna (1994) 73–81.

[3] McEWEN, M.R., WILLIAMS, A.J., DuSAUTOY, A.R., Determination of absorbed dose calibration factors for therapy level electron beam ionization chambers, Phys. Med. Biol. **46** (2001) 741–755.

[4] UNITED KINGDOM ACCREDITATION SERVICE, The Expression of Uncertainty and Confidence in Measurement, Rep. M 3003, 1st edn, UKAS, Feltham, UK (1997).

[5] DOMEN, S.R., LAMPERTI, P.J., A heat-loss compensated calorimeter: Theory, design and performance, J. Res. Natl. Bur. Stand. A **78** (1974) 595–610.

[6] DuSAUTOY, A.R., The UK primary standard calorimeter for photon beam absorbed dose measurement, Phys. Med. Biol. **41** (1996) 137–151.

[7] BURNS, D.T., MORRIS, W.T., "A graphite calorimeter for electron beam dosimetry", High Dose Dosimetry for Radiation Processing (Proc. Conf. Vienna, 1990), IAEA, Vienna (1991) 123–136.

[8] BURNS, D.T., McEWEN, M.R., WILLIAMS, A.J., "An NPL absorbed dose calibration service for electron beam radiotherapy", Measurement Accuracy in Dosimetry (Proc. Int. Symp. Vienna, 1993), IAEA, Vienna (1994) 61–71.

[9] McEWEN, M.R., DuSAUTOY, A.R., WILLIAMS, A.J., The calibration of therapy level electron beam ionization chambers in terms of absorbed dose to water, Phys. Med. Biol. **43** (1998) 2503–2519.

[10] WILLIAMS, A.J., BURNS, D.T., McEWEN, M.R., Measurement of the Specific Heat Capacity of the Electron Beam Graphite Calorimeter, Rep. RSA(EXT)40, National Physical Laboratory, Teddington, UK (1993).

[11] McEWEN, M.R., DUANE, S., A portable calorimeter for measuring absorbed dose in the radiotherapy clinic, Phys. Med. Biol. **45** (2000) 3675–3691.

[12] McEWEN, M.R., Development of a Portable Graphite Calorimeter for Measuring Absorbed Dose in the Radiotherapy Clinic, PhD Thesis, Univ. Surrey (2002).

[13] WILLIAMS, A.J., ROSSER, K.E., "Development of the NPL water calorimeter", Recent Advances in Calorimetric Absorbed Dose Standards (Proc. Workshop Teddington, UK, 1999), Rep. CIRM 42 (WILLIAMS, A.J., ROSSER, K.E., Eds), National Physical Laboratory, Teddington, UK (2000) 130–137.

BLANK

THE FUTURE PHYSIKALISCH-TECHNISCHE BUNDESANSTALT PRIMARY STANDARD FOR ABSORBED DOSE TO WATER IN ^{60}Co RADIATION

A. KRAUSS
Physikalisch-Technische Bundesanstalt,
Braunschweig, Germany
E-mail: Achim.Krauss@ptb.de

Abstract

A detector vessel with plane-parallel geometry is used in the Physikalisch-Technische Bundesanstalt water calorimeter. The paper presents some of the operating methods for the calorimeter and discusses the consideration of influence quantities and correction factors and the contributions to the uncertainty budget for the determination of absorbed dose to water in ^{60}Co radiation. The calorimeter will be used as the primary standard after the installation of a new ^{60}Co source.

1. INTRODUCTION

A water calorimeter is being established at the Physikalisch-Technische Bundesanstalt (PTB) as a primary standard for realizing the unit of gray (Gy) for absorbed dose to water, D_w, in ^{60}Co gamma radiation. The calorimetric determination of D_w is based on the measurement of the radiation induced temperature rise at a point in a water phantom. To achieve high accuracy measurements, several influence quantities and corrections must be investigated in detail, preferably both by experimental investigations and by model calculations.

A short description of the basic components and the operating methods for the PTB water calorimeter is given in this paper, and information is given on how to consider the heat defect and some correction factors, which have to be multiplied by the measured temperature increase in order to achieve D_w. Additionally, the standard measurement uncertainty budget so far analysed for the calorimetric determination of D_w in ^{60}Co radiation under reference conditions is presented.

2. WATER CALORIMETER

2.1. Equipment

The PTB water calorimeter is based on the design proposed by Domen [1], which today is used for most water calorimeters [2]. It consists of a water filled cubic phantom of 30 cm edge length made of 1 cm thick polymethylmethacrylate (PMMA) walls. The horizontally directed radiation enters the phantom through a 3 mm thick PMMA window. The phantom is thermally insulated by an 8 cm thick layer of expanded polystyrene and is placed in a wooden container with an edge length of about 100 cm, in which active temperature stabilization is realized. To avoid convection inside the water phantom, the calorimeter is operated at a water temperature of 4°C.

The radiation induced temperature increase is measured inside a thin walled plane-parallel glass cylinder, in which two thin cone shaped glass pipettes of 110 mm length and 0.5 mm outside diameter are mounted opposite each other and perpendicular to the cylinder axis. The tip of each pipette contains a thermistor sensor 0.25 mm in diameter (Fig. 1). The geometry of the detector cylinder, the axis of which coincides with the direction of the radiation, has been chosen to allow for the proper modelling of heat transfer effects in the water calorimeter. The dimensions of the cylinder, which are measured and certified by the manufacturer, are 95 mm outside diameter and 41.5 mm outside length, with a wall thickness of 2.5 mm and 0.75 mm for the cylinder wall and for the flat front and rear walls, respectively.

To control the heat defect of the calorimeter [3, 4], the glass cylinder is filled with high purity water (resistivity 18 MΩ·cm, 5 ppb total organic compound (TOC)) saturated with hydrogen and a small amount of oxygen [5]. The concentration ratio of H_2 and O_2 is chosen so that the system reaches the sta-

FIG. 1. (a) A thermistor pipette of the detector. (b) The small thermistor fixed in epoxy at the tip of the pipette. A thin glass rod seals this pipette version. In a different version (not shown) the thermistor is embedded in a massive glass rod 8 mm long.

tionary state condition (i.e. with zero heat defect) of the pure H_2 system after a pre-irradiation dose of less than 100 Gy. During the pre-irradiation period the measured heat defect as a function of absorbed dose serves as a rough quality check for the detector preparation procedure. The cleaning and filling procedures of the glass cylinder are similar to those described by Domen [1].

The thermistor sensors of the calorimetric detector are connected to two opposing arms of a DC powered, double shielded resistance bridge. This consists of calibrated high precision resistors, offering a temperature coefficient of less than 1 ppm/°C. At a water temperature of 4°C the thermistors have a resistance of about 11 kΩ and a power dissipation of about 12 μW. During irradiation a Keithley 1801 nanovolt preamplifier combined with a Keithley 2001 digital multimeter records the out of balance voltage of the bridge. This bridge circuit offers a signal to noise ratio of about 250 for an irradiation time of 2 min at a dose rate of 1 Gy/min. All instruments used for measurements with the water calorimeter are covered by the quality assurance system of the PTB.

2.2. Calibration

The radiation induced temperature rise is determined from the measured voltage change in the bridge circuit by calibration of the resistance bridge and of the thermistors. The bridge calibration (including the Keithley multimeter) is carried out by switching a calibrated 3 MΩ resistance in parallel with calibrated 700, 1000 or 1300 Ω resistances and measuring the resulting voltage changes. By this method the bridge is calibrated with a relative standard uncertainty of less than 0.1%.

The calibration of the two thermistors is performed before they are mounted inside the glass cylinder of the detector, but is carried out inside the water phantom of the calorimeter using the same equipment as for the irradiation measurements. The water temperature in the calorimeter is changed in steps of about 0.2°C in the temperature range between 1°C and 7°C and measured with a calibrated Pt-25 thermometer. The corresponding balancing resistances of the bridge and the voltage across each arm of the resistance bridge are recorded for each temperature. The calibration factor of a thermistor, which is defined as the ratio of relative resistance to temperature change, is determined by a linear fit to the data ln R versus $1/T$, where ln R is the natural logarithm of the thermistor resistance and T is the absolute temperature of the thermistor. Repeated calibrations of the same thermistors as well as the analysis of the uncertainty budget for the calibration procedure lead to a relative standard uncertainty of about 0.06% for this method.

3. HEAT DEFECT, CORRECTIONS AND UNCERTAINTY BUDGET

3.1. Heat defect

Model calculations of the radiolysis of water predict a stationary state (i.e. zero heat defect) for water saturated with hydrogen [3]. As the hydrogen scavenges reactive OH radicals, this system should be somewhat insensitive to organic impurities in the water, although it is sensitive to oxygen contamination. In the PTB water calorimeter the H_2 system is used (after pre-irradiation of a newly prepared detector) and shows a stable response within about 0.1% for different measurement periods (partly using new detectors) over a dose range of more than 1.5 kGy (Fig. 2). Between successive measurement periods with the same detector, the detector is removed from the calorimeter and stored in dark surroundings. Within the measurement uncertainty no changes in the response of the detector were observed when the measurements were continued.

Although this does not directly prove that the heat defect is zero in the PTB water calorimeter, it seems to be unlikely that impurities with an initial

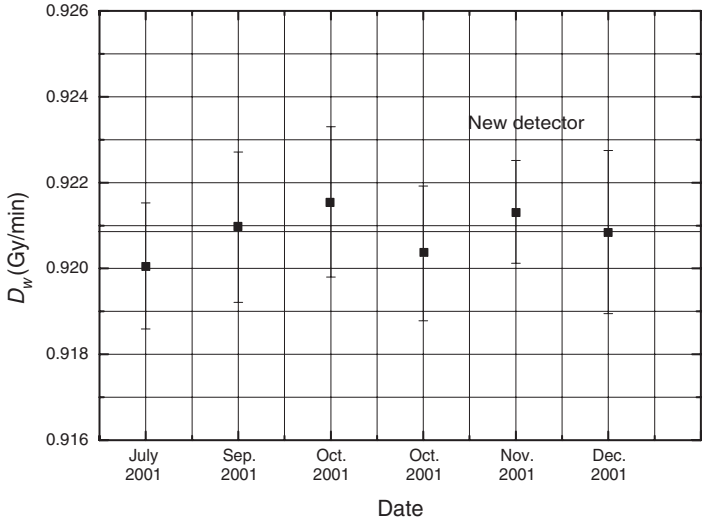

FIG. 2. Results of six experiments conducted in 2001 with the PTB water calorimeter using the H_2 system and two different detectors. Shown are the mean values of the measured dose rate (corrected for ^{60}Co decay to 1 January 1993), including their standard deviations. The solid line indicates the mean value of all experiments.

concentration of about 5×10^{-7} M (following from the TOC level of the high purity water [4]) should produce a stable non-zero heat defect. However, assuming a steady leakage of impurities, for example oxygen, a stable heat defect could occur. Model calculations for the H_2 system with a steady O_2 leakage of 6×10^{-10} M/min show an exothermal heat defect of about 0.2% for irradiations of 2 min at a dose rate of 1 Gy/min. In this case the O_2 leakage is just balanced by the radiation induced O_2 consumption, but a longer interruption of the experiment, for example for two days, would increase the heat defect to several per cent for the following irradiations. This would be clearly visible in the experiment.

It is therefore concluded that the radiation chemistry in the PTB water calorimeter can be based upon the model calculations for the radiolysis and that the heat defect is zero, as predicted by the model. This model prediction is independent of the individual reaction rates of the chemical reactions. The uncertainty of the heat defect is therefore taken to be zero.

3.2. Heat conduction effects

The well defined plane-parallel geometry of the detector cylinder allows heat conduction effects due to irradiation of the detector materials to be accurately determined by three dimensional finite element calculations. Good agreement was found between the calculated heat conduction effects, assuming a uniform ^{60}Co radiation dose profile inside the water phantom, and experimental data [6]. Separate simulations have been performed for heat conduction effects caused by the depth dose profile and by the lateral dose profile of the ^{60}Co radiation.

As the result of a single calorimetric measurement is determined from linear extrapolations of the pre- and post-irradiation drift curves to the mid-run position, the corresponding correction factor, k_C, for the heat conduction effects strongly depends on the time intervals chosen for the extrapolations. Furthermore, for successive irradiations, the correction factors are different and depend on the time between the irradiations. For example, for a series of measurements with pre-drifts, post-drifts and irradiations of 120 s each, the calculated correction factors are $k_C = 1.0009$ for the first and $k_C = 0.9983$ for the second measurement [6]. Taking possible variations of the cylinder geometry and variations in the number of elements used for the finite element calculations into account, an uncertainty for the correction factors of about 0.06% is estimated.

3.3. Perturbation effect

The detector of the water calorimeter perturbs the ^{60}Co radiation field at the point of measurement compared with when the detector is not in place. With the aid of a dummy glass cylinder with a small opening in the cylinder wall for placing a National Physical Laboratory (NPL) ionization chamber inside, the correction for the perturbation effect can be determined as the ratio of the ionization chamber reading without and with the glass cylinder present. In this way the correction factor, k_P, was measured to be 1.0013 ± 0.0005. By simulating the photon transport through the water phantom of the calorimeter by Monte Carlo calculation, the experimental result could be confirmed by the calculated result of 1.0010 ± 0.00003.

3.4. Uncertainty budget

The water calorimeter will be used as the PTB's primary standard for absorbed dose to water in ^{60}Co radiation. The concluding measurements will be performed after the installation of a new ^{60}Co source with a higher dose rate at the PTB irradiation facility. Most of the measurement procedures for the calorimeter, including their uncertainties, have been analysed [7]. The contributions to the uncertainty for the determination of D_w are shown in Table I and are partly explained in the relevant sections of this paper. The uncertainties specified for the positioning of the calorimeter result from measured distance variations of smaller than 0.1 mm for both the source to surface distance (SSD) and the measuring depth of the detector and taking into account dose rate gradients of about 0.2% mm^{-1} and 0.5% mm^{-1}, respectively.

However, some contributions caused by heat conduction, such as the effect of the lateral and depth dose profile, have to be newly analysed using the measured dose profiles taken at the new ^{60}Co source as input for the corresponding finite element calculations. The preliminary uncertainties stated for these effects are estimated from calculations using different finite element models and theoretical dose profiles. Furthermore, as the water calorimeter does not exactly comply with the geometry of the reference conditions for dose measurements in ^{60}Co radiation, this transfer will be made using ionization chambers. The corresponding measurements still have to be performed.

4. CONCLUSIONS

The PTB water calorimeter with a plane-parallel detector is ready for operation. As almost all measurement procedures and correction factors have

TABLE I. UNCERTAINTY BUDGET FOR THE DETERMINATION OF D_w IN ^{60}Co RADIATION UNDER REFERENCE CONDITIONS

Quantity	Uncertainty (%)
Thermistor calibration	0.06
Bridge calibration	0.1
Voltage change	0.1[a]
Positioning	
SSD	0.02
Detector	0.05
Heat conduction effects	
Detector material	0.06
Depth dose profile	0.04[b]
Lateral dose profile	0.04[b]
Heat defect	0
Perturbation effect	0.05
Reference field	0.10[b]
Standard measurement uncertainty (k = 1)	0.21

[a] Depends on the number of measurements.
[b] To be analysed for measurements with the new ^{60}Co source.

been analysed, the preliminary uncertainty budget for the determination of D_w can be summarized. After the installation of a new ^{60}Co source the water calorimeter will be established as the new PTB primary standard for absorbed dose to water in ^{60}Co radiation.

REFERENCES

[1] DOMEN, S.R., A sealed water calorimeter for measuring absorbed dose, J. Res. Natl. Inst. Stand. Technol. **99** (1994) 121.
[2] WILLIAMS, A.J., ROSSER, K.E. (Eds), Recent Advances in Calorimetric Absorbed Dose Standards (Proc. Workshop Teddington, UK, 1999), Rep. CIRM 42, National Physical Laboratory, Teddington, UK (2000).
[3] KLASSEN, N.V., ROSS, C.K., Absorbed dose calorimetry using various aqueous solutions, Radiat. Phys. Chem. **38** (1991) 95–104.
[4] KLASSEN, N.V., ROSS, C.K., Water calorimetry: The heat defect, J. Res. Natl. Inst. Stand. Technol. **102** (1997) 63–74.

[5] KRAUSS, A., ROOS, M., Heat conduction, convection and radiolysis of the H_2/O_2 system in the water absorbed dose calorimeter, Thermochim. Acta **310** (1998) 53–60.

[6] KRAUSS, A., Experimental verification of calculated radiation-induced heat conduction effects in the water absorbed dose calorimeter, Thermochim. Acta **382** (2002) 99–107.

[7] INTERNATIONAL ORGANIZATION FOR STANDARDIZATION, Guide to the Expression of Uncertainty in Measurement, ISO, Geneva (1993).

GRAPHITE CALORIMETER: THE PRIMARY STANDARD OF ABSORBED DOSE AT THE BUREAU NATIONAL DE MÉTROLOGIE—LABORATOIRE NATIONAL HENRI BECQUEREL

J. DAURES, A. OSTROWSKY, B. CHAUVENET
Bureau national de métrologie—Laboratoire national Henri Becquerel,
Gif-sur-Yvette, France
E-mail: josiane.daures@cea.fr

Abstract

The graphite calorimeter is the standard for absorbed dose to water at the Bureau national de métrologie—Laboratoire national Henri Becquerel. The transfer from absorbed dose to graphite to absorbed dose to water is performed by means of chemical dosimetry and ionization chamber measurements. The present graphite calorimeter and its characteristics are described. Special attention is given to the thermal feedback of the jacket, which is the main difference from the Domen type calorimeter. The repeatability and reproducibility of the mean absorbed dose in the calorimeter core are presented in detail. As an example, three sets of measurements in 20 MV X rays taken between 1999 and 2002 are presented. The standard deviation is 0.12% for the first set of measurements performed in 1999. For the second and third set of measurements, taken in 2002, the standard deviation is 0.03%. The improvement in the 2002 standard deviation is mainly due to the change of the ionization chamber used for monitoring the linac beam. Some benefit also comes from changes in the thermal control and measuring systems used. The maximum difference between the mean values of the three series is 0.08%. The combined uncertainty on the reference absorbed dose to graphite is analysed. The influence of the irradiation on the sensitivity of the thermistor has been checked. Recent measurements carried out in the 20 MV photon beam prove that there is no significant difference between the simultaneous measurement of irradiation and electrical power dissipation and the sum of these two quantities measured separately. This confirms previous measurements in ^{60}Co beams. It is not possible to perform this type of measurement with the water calorimeter because electrical calibration is not feasible.

1. INTRODUCTION

The Bureau national de métrologie–Laboratoire national Henri Becquerel (BNM–LNHB) is responsible for ionizing radiation standards in

France and has developed and maintained calorimetry techniques since 1970. Water is the reference medium for gamma rays, X rays and electron beams used for radiotherapy. Graphite and water have close atomic numbers, and several graphite calorimeters have been constructed in the laboratory, along with A150 tissue equivalent plastic calorimeters for neutron and proton therapy beams. Both types are portable, allowing measurements in ^{60}Co beams or in the user's neutron and proton beams. The photon beam standards in terms of absorbed dose to water are currently derived from this graphite calorimeter standard [1].

2. GRAPHITE CALORIMETER

The graphite calorimeter currently in operation at the BNM–LNHB is known as GR8 (it is the eighth graphite calorimeter constructed in the laboratory) and presents some major differences compared with the Domen type calorimeter [2]. The active control of the jacket temperature by thermal feedback reduces heat losses by reducing the core–jacket temperature difference, and hence heat loss compensation is not necessary. The shield is thermally controlled at a constant temperature by means of a PID (proportional integral derivative) regulator.

2.1. Principle

The calorimetry technique consists of measuring ΔE, the mean energy imparted by ionizing radiation and converted into heat, Q, in an element of known mass, m. The ratio Q/m is related to absorbed dose, $\Delta E/m$. No dosimetric radiometrological parameters (such as W/e or G) are needed, and therefore a good uncertainty can be achieved. Nevertheless, the thermal yield or the heat defect, r_{th}, has to be known. As graphite is a pure element, it has no heat defect. The value of r_{th} is taken as unity for the beam qualities considered, but it has to be taken into account in the uncertainty analysis. The mean absorbed dose, $\overline{D}$, to the core of mass m is given by the ratio of Q/m divided by r_{th}. A temperature probe is embedded in the core of the calorimeter; a thermistor is used as the probe, owing to its high sensitivity and low mass.

The electrical calibration does not require knowledge of the specific heat of the core and of the thermistor sensitivity. A known quantity of heat, Q_{el}, is deposited by electrically heating the core, producing a reading, L_{el}, of the thermistor. The calibration factor, F, is the quotient of the two quantities. No dosimetric quantities are involved, only electrical quantities (current and voltage), which are measurable with a very good accuracy.

$$F = \frac{Q_{el}}{L_{el}} \tag{1}$$

If thermal conditions during electrical calibration and radiation measurement are similar, the mean absorbed dose in the core is given by the following equation for any reading, L, of the thermistor:

$$\overline{D} = \frac{FL}{m}\frac{1}{r_{th}} \tag{2}$$

The reference absorbed dose, D, in a homogeneous phantom at the point corresponding to the centre of the core can be determined from Eq. (3):

$$D = \frac{FL}{m}\frac{1}{r_{th}}\prod_i ki \tag{3}$$

Correction factors have to be applied for vacuum gaps, impurities, thermal yield, calorimeter–phantom density difference, dose gradients in the core, etc.

2.2. Calorimeter design

The core is a flat cylinder with a thickness of 3 mm and a diameter of 16 mm. In order to achieve high thermal stability of the core, two graphite intermediate bodies are necessary: the jacket and the shield. The jacket and the shield, which are 2 mm thick, are cylindrically shaped boxes, symmetrical to the midplane of the core. The three bodies are inserted into a large graphite cylindrical block (18 cm in diameter, 10 cm thick), which gives the external shape. These three bodies are kept in position by three silk threads and are glued to the block. The surfaces (except for the core, because of impurities) are covered with a thin aluminized Mylar foil to limit radiative heat transfers. The gaps between each of the bodies and the block are evacuated to reduce thermal transfers. The dimensions of these gaps are close to 1 mm along the axis and about 2 mm perpendicular to the axis. All calorimetric measurements are performed in a graphite phantom (of dimensions 30 cm × 30 cm × 20 cm). A diagram of the GR8 calorimeter is shown in Ref. [3].

2.3. Temperature control with jacket thermal feedback

The sensitivity of the graphite calorimeter is about 1.4 mK/Gy. Typical dose rates in ^{60}Co beams are about 0.5 Gy/min to 1 Gy/min and between 2 Gy/min and 4 Gy/min for accelerator beams, which leads to temperature increase rates of 1 mK/min to 6 mK/min. The temperature drift of the core before and after irradiations, however, has to be stable to within a few μK/min.

Stability is achieved by taking several steps. When the room temperature is regulated at better than about 1 K the calorimeter works without block regulation. When this room temperature stability cannot be achieved the phantom containing the calorimeter can be regulated. The shield temperature is kept constant at about two degrees above the mean room temperature. The jacket temperature is controlled in order to carefully follow the core temperature. One thermistor is embedded in the core and another one is embedded in the shield, forming two opposite arms of a DC Wheatstone bridge. If the output voltage of the bridge diverges from zero, a PID regulator sends to the eight heating thermistors of the jacket a modified power to keep the core–jacket temperature difference as small as possible. This temperature difference is so small that thermal transfers are negligible or at least constant. The calorimeter can therefore be operated in a quasi-adiabatic mode without heat loss compensation techniques. The power dissipated by the jacket feedback rises with irradiations and electrical calibrations. When not in use the thermal feedback is stopped, which allows the jacket and the core to stabilize close to the shield assigned temperature. Equation (3) assumes that the thermal conditions during electrical calibration and irradiation are equivalent. During electrical calibration the core and the jacket rise in temperature in the same way as under irradiation, due to the jacket thermal feedback. An additional electrical power proportional to the jacket–core mass ratio is sent to the jacket to avoid PID oscillations at the beginning and the end of electrical calibrations.

2.4. Measuring system and electrical calibration

The temperature rise in the core is measured by means of a very small thermistor glass covered pearl Fenwall GB38j14. All the thermistors employed are of the same type. The mass of the thermistors is about 0.5 mg, with a diameter close to 0.35 mm, and their temperature coefficient is close to 3.8×10^{-2} K^{-1}. The resistance value at 25°C is 8 kΩ. A very precise DC Wheatstone bridge measures the relative variation of the thermistor resistance, L. The bridge voltage is measured using a Keithley 181 nanovoltmeter. The bridge is unbalanced during

irradiation or electrical calibration. Two ohmic calibrations of the bridge (V/Ω) are performed at the beginning of each measurement by introducing and removing in the other arm a known resistor. A system of parallel resistors is now used to reduce the influence of contact resistors, which might partially explain the improvement of the recent statistics of measurements discussed in Section 4. During electrical calibrations, four thermistors embedded in the core are used to dissipate by the Joule effect the heat quantity, Q_{el}, involved in Eq. (1). This quantity is accurately determined by measuring the voltage and the current across the set of thermistors.

3. EFFECT OF IRRADIATION ON THE THERMISTOR RESPONSE

The reliability of the thermistor response under irradiation is a recurrent question in the field of dosimetry by calorimetry. Previous measurements in the BNM–LNHB ^{60}Co beam have shown no significant effect regarding the uncertainties. It was decided to repeat these experiments in a higher quality photon beam. An opportunity occurred during recent calorimetric measurements in the 20 MV BNM–LNHB medical linac photon beam (Section 4).

3.1. Method

Three types of measurement were successively performed: electrical calibration, irradiation and an electrical calibration simultaneously applied to an irradiation. For the third measurement, the global effect, *G,* is measured by using Eq. (2). Its electrical component, *E,* can be determined from the electrical power measurement, the time interval and the mass of the core; its irradiation component, *I,* can be determined from the second measurement and the monitor charge. The influence of irradiation on the thermistor is determined by the ratio $G/(E + I)$.

3.2. Results

The ratio $G/(E + I)$ has a mean value in the 20 MV BNM–LNHB medical linac photon beam of 0.9998, with a standard deviation of 0.014%. A more exhaustive study of this influence factor should be performed in other high quality photon and electron beams. The results will be of great interest, since they could be extrapolated for water calorimetry, for which such a determination is not possible.

4. CALORIMETER PERFORMANCE IN THE BNM–LNHB MEDICAL LINAC PHOTON BEAMS

The BNM–LNHB linac is a Saturne 43 type radiotherapy machine manufactured by General Electric Medical Systems. The use of its targets and conical flattening filters produces X ray beams that are heavily filtered compared with some research accelerators, whose lightly filtered X ray beams depart from clinical beams.

Under these conditions $TPR_{20,10}$ can be used without restriction to compare the beam quality of the reference calibration beams and the user's clinical beams. The classical dual transmission ionization chamber system for beam monitoring is completed by an additional ionization chamber fixed on the slot for wedges positioned after the secondary collimator system. Its ionization current, temperature and pressure are carefully measured.

A thin flat transmission ionization chamber very similar to the inner monitor was used until the end of 1999. The thin aluminized kapton foils used as electrodes tended to vary with climatic conditions, particularly humidity. As an alternative, a PTW 23344 flat ionization chamber with an additional graphite slab was fixed just on the outside of the primary beam.

The electrode axis is parallel to the beam axis. A 2 mm thick graphite slab covering the entrance surface of the chamber has improved the stability of the monitoring.

4.1. Repeatability

The standard graphite calorimeter is used to calibrate the NE 2571 reference ionization chamber in the graphite phantom. The day starts with an hour long ionometric measurement. The ionization chamber is then replaced by the calorimeter and is centred at the same point in the graphite phantom. A typical series consists of two electrical calibrations, followed by five calorimetric measurements and another electrical calibration. At the end of the day one more ionometric measurement is performed. Ionometric and calorimetric measurements are normalized to the monitor chamber reading corrected for temperature and pressure changes. The difference between these two ionometric measurements is generally less than 0.05%. The mean value is used to determine the calibration factor of the NE 2571 reference chamber. An example of the measurement repeatability is presented in Table I and Fig. 1.

4.2. Reproducibility

Despite several changes in the measurement assembly and methodology, the calibration factor of the chamber only varies by 0.08% over a three-year period. This measurement quality is to the performances of the GR8 graphite calorimeter but also to the stability of the ionization chamber, the accelerator and the beam monitoring system.

TABLE I. CALIBRATION FACTOR OF THE NE 2571 STANDARD GRAPHITE CHAMBER IN THE BNM–LNHB 20 MV BEAM

	Measurement series			
	1999	2002 series 1	2002 series 2	Whole of 2002
Measurement number	16	19	16	35
Calibration factor (Gy/C)	3.8692×10^7	3.8722×10^7	3.8702×10^7	3.8713×10^7
Standard deviation (%)	0.116	0.026	0.031	0.038
Standard deviation of the mean (%)	0.029	0.006	0.007	0.006

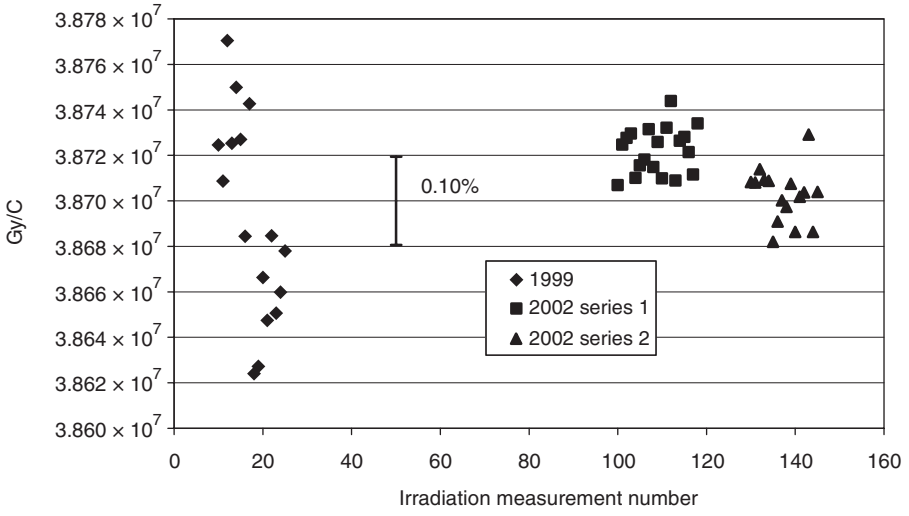

FIG. 1. Mean absorbed dose in the graphite calorimeter core divided by the reference ionization chamber charge.

For lower energy beams of the accelerator the standard deviation is a little higher (i.e. 0.04% and 0.06% for 12 MV and 6 MV, respectively). The maximum differences over three years are always less than 0.1%.

4.3. Non-uniformity absorbed dose correction

The determination of the absorbed dose in graphite at the reference point requires knowledge of the dose gradient in the core. In a ^{60}Co beam the correction is very small and independent of the machine. With linacs the correction is generally higher, depending on the machine and the beam energy. The conical flattening filters are adequate for radiotherapy purposes. Nevertheless, in the metrology field the residual radial heterogeneity has to be accounted for. The correction to be applied in calorimetry can reach 0.4% in the BNM–LNHB 20 MV beam.

4.4. Uncertainty analysis

The main correction comes from the vacuum gaps. Monte Carlo calculations (EGS4 and PENELOPE) and experimental determination by means of a small EDE Scanditronix silicon diode agree on the value of the gap correction factor within 0.1%. The standard uncertainty on this term is estimated to be 0.15% [3]. The mass of impurities in the core (i.e. the thermistors, glue and silk threads) is less than 1%. This correction is small but its contribution to the relative uncertainty is estimated as 0.1%. The thermal yield, whose value is essentially unity, is nevertheless associated with an estimated uncertainty of 0.1%. The overall one standard deviation uncertainties on the graphite absorbed dose standards are 0.24% and 0.27% for ^{60}Co and X rays, respectively. The overall one standard deviation uncertainties of the absorbed to water standards derived from the graphite calorimeter standard are 0.35% and 0.57% for ^{60}Co and X rays, respectively.

5. CONCLUSIONS

The original thermal feedback on the jacket allows the graphite calorimeter to work in a quasi-adiabatic mode, as the core–jacket thermal temperature gradients can be kept very low. This technique might explain the good statistical quality of the measurements. In the BNM–LNHB Saturne 43 GEMS linac the improvement of the measurement repeatability can be attributed to the

new monitoring system for the beam. Considering the performance described above, even though a transfer procedure is needed to obtain the absorbed dose to water, the graphite calorimeter standard is still competitive as compared with direct measurements by water calorimetry.

ACKNOWLEDGEMENTS

The authors would like to thank F. Delaunay for his constant support and valuable discussions and D. Cutarella and E. Leroy for their contribution to the ionometric measurements.

REFERENCES

[1] CHAUVENET, B., BALTES, D., DELAUNAY, F., Comparison of graphite to water absorbed-dose transfers for ^{60}Co photon beams using ionometry and Fricke dosimetry, Phys. Med. Biol. **42** (1997) 2053–2063.

[2] DOMEN, S.R., LAMPERTI, P.J., A heat-loss-compensated calorimeter: Theory, design and performance, J. Res. Natl. Bur. Stand. A **78** (1974) 595–610.

[3] DAURES, J., OSTROWSKY, A., GROSS, P., JEANNOT, J.P., GOURIOU, J., "Calorimetry for absorbed-dose measurements at BNM-LNHB", Recent Advances in Calorimetric Absorbed Dose Standards (Proc. Workshop Teddington, UK, 1999), Rep. CIRM 42 (WILLIAMS, A.J., ROSSER, K.E., Eds), National Physical Laboratory, Teddington, UK (2000) 15–21.

BLANK

MEASUREMENTS OF k_Q BEAM QUALITY CORRECTION FACTORS FOR THE NE 2611A CHAMBER IN HIGH ENERGY PHOTON BEAMS USING THE NEDERLANDS MEETINSTITUUT WATER CALORIMETER

M. PIEKSMA, L.A. DE PREZ, E. VAN DIJK, A.H.L. AALBERS
Nederlands Meetinstituut,
Utrecht, Netherlands
E-mail: mpieksma@nmi.nl

Abstract

Measurements of absorbed dose to water rates were performed with the Nederlands Meetinstituut (NMi) water calorimeter at the Bureau national de métrologie–Laboratoire national Henri Becquerel with a Saturne 43 accelerator for 6, 12 and 20 MV photon beams. A set of five NE 2611A chambers was calibrated against the water calorimeter at all three energies. Correction factors were measured for polarity and recombination effects, and for attenuation by the glass detection vessel. Beam quality correction factors, k_Q, obtained as the ratio of the calibration factors for the high energy photon beams, and the calibration factors for the NMi ^{60}Co beam, agree very well with values published in the literature, and with generic k_Q factors presented by the American Association of Physicists in Medicine Task Group 51 and by the IAEA.

1. INTRODUCTION

Recent protocols for clinical reference dosimetry in external high energy photon and electron beam radiotherapy published by the American Association of Physicists in Medicine (AAPM) [1] and the IAEA [2] are no longer based on calibrations in terms of air kerma, but have instead adopted absorbed dose to water as the calibration quantity. In accordance with these new protocols, forthcoming revised NCS (Nederlandse Commissie voor Stralingsdosimetrie) protocols for the dosimetry of high energy photon and electron beams will also be based on absorbed dose to water. For this reason, and because the most direct way to determine the absorbed dose to water is by employing a sealed water type calorimeter [3, 4], the national standards laboratory of the Netherlands (the Nederlands Meetinstituut (NMi)) is presently developing a water calorimeter as a new standard for absorbed dose to water for high energy photon beams.

Part of the forthcoming NCS protocols will be a table of experimentally determined k_Q beam quality correction factors for the photon beam qualities and dosimetric equipment (graphite ionization chambers) most commonly encountered in Dutch and Belgian clinical practice. These k_Q factors will be measured in situ at selected institutes, using the NMi water calorimeter.

As a preparatory step, a reference set of k_Q factors was measured for the NE 2611A ionization chamber for three high energy photon beams available at the French national standards laboratory (the Bureau national de métrologie–Laboratoire national Henri Becquerel (BNM–LNHB)). The nominal accelerator energies used were 6, 12 and 20 MV.

2. MATERIALS AND METHODS

2.1. NMi water calorimeter

The NMi water calorimeter is of the sealed water type [3–6], in which the temperature rise due to irradiation by high energy photons is measured inside a well defined volume of water enclosed by a sealed, thin walled glass vessel. The quality of the water is carefully controlled by purifying the water and by saturating it with various gases.

The water calorimeter is compact and transportable, weighs 60 kg when empty, and has outer dimensions of only 60 cm × 60 cm × 70 cm. The dimensions of the water phantom are a standard 30 cm × 30 cm × 30 cm. A small spacing between the inner and outer polystyrene foam insulation boxes encloses a copper heat exchange system. The six copper walls are connected in parallel, which helps to reduce temperature gradients inside the water phantom. Cooling is performed by a computer controlled Lauda RC6 CP water cooling thermostat, which uses two PT100 thermometers (one mounted on one of the copper walls and one mounted inside the water phantom) to monitor the calorimeter temperature. A built-in magnetic stirrer can be used to reduce temperature drifts due to conduction. A cold finger placed inside the water phantom can be switched into the cooling circuit to reduce the time needed to cool from room temperature to 4°C (the point at which water has its maximum density and convective motion is avoided).

The NMi water calorimeter can be used in both horizontal and vertical beams; a horizontal geometry was used at the BNM–LNHB. In this configuration the photon beam enters through a window consisting of 100 mm of polystyrene foam and 3.24 mm of Perspex.

2.2. Temperature measurement

2.2.1. Thermistor probe properties

Temperature changes due to irradiating the water in the calorimeter are monitored by means of two thermistor probes. These probes are mounted in a sealed glass detection vessel filled with high purity water. The probes are made of glass of diameter 0.55 ± 0.05 mm and are spaced 10 mm apart. The detection vessel has an outer diameter of 73 mm, a length of about 100 mm and a wall thickness of 0.73 ± 0.03 mm. The thermistor probes are calibrated against NMi SPRT (standard platinum resistance thermometer) temperature standards in the range of 0°C to +8°C. At 4°C the probes have nominal resistances of 20 kΩ and sensitivities of about 4%/°C. The temperature dependence of the thermistor resistances is given by:

$$\frac{1}{T} = a + b \ln R + c \ln^2 R \qquad (1)$$

Using Eq. (1) the sensitivity of a thermistor probe, which is defined as $S \equiv (\mathrm{d}R/\mathrm{d}T)/R$ [4], can be written as $S = -\beta/T^2$, with $\beta = 1/(b + 2c \ln R)$. The quadratic term in Eq. (1) accounts for the fact that the material constant, β, can in fact be slightly temperature dependent.

Two thermistor probes, labelled 2B and 7B, were calibrated against the NMi primary temperature standard. Numerical values for *a*, *b* and *c* were obtained from the calibration data as well as the excess temperature rise per unit power dissipated in the probes, Φ. These values are given in Table I, together with values for β at 4°C. From repeated calibrations of the thermistor

TABLE I. CONSTANTS THAT CHARACTERIZE THERMISTOR PROBES 2B AND 7B

	2B	7B
a	1.04728×10^{-3}	1.04105×10^{-3}
b	2.11482×10^{-4}	2.16727×10^{-4}
c	4.69593×10^{-6}	4.34638×10^{-6}
β	3282.2 K^{-1}	3304.1 K^{-1}
Φ	1.30 mK/μW	1.05 mK/μW

Note: For each probe, numerical values are listed for the parameters *a, b* and *c* in Eq. (1), for the material parameter β (at 4°C) and for the excess temperature rise per unit power (Φ).

probes it was found that the uncertainty in β is 0.03%, which adds directly to the total uncertainty budget for absorbed dose determinations.

2.2.2. Temperature measurement with a parallel circuit

The two thermistor probes are connected in parallel in order that their effective resistance can be measured on the sensitive 10 kΩ scale of a high precision (8.5 digit) digital multimeter (DMM) (HP3458A). Assuming that during an irradiation run the ratio of resistances R_{2B}/R_{7B} is constant (at typical operating temperatures, which range between 3.9°C and 4.1°C, this condition is very well fulfilled), a set of two equations of the type of Eq. (1) can be solved. This procedure yields numerical values for T_{2B}, T_{7B}, R_{2B} and R_{7B}. It is then straightforward to determine the temperature change from the measured resistance change, and to transform this temperature change into absorbed dose, using well known (temperature dependent) literature values for the specific heat capacity of water, C_w [7].

The power dissipated in the thermistor probe beads was 50 μW, and the same power level was used for the temperature calibrations of the probes. During an irradiation the resistance of the thermistor probe changes, and therefore the dissipated power changes. This effect can be corrected for by using the values for Φ given in Table I. A very small correction factor of 1.00001 ± 0.0002 was applied to the measured absorbed dose.

2.3. DMM versus Wheatstone circuit

In earlier experiments with the NMi water calorimeter two AC Wheatstone bridges in combination with two EG&G model 5209 lock-in amplifiers were used to determine resistance changes due to irradiations. However, it became evident that a DMM has many advantages as compared with a Wheatstone circuit. First, the sensitivity of the DMM is more than sufficient for absolute absorbed dose measurements. On the 10 kΩ scale the sensitivity is 1 mΩ, while the total signal is of the order of 250 mΩ. Moreover, the DMM has a better signal to noise ratio for the set-up used, is much less sensitive to ambient (radiofrequency) noise and is much less complex to operate than a Wheatstone circuit. As a result, the standard deviation in the absorbed dose is a factor of 2 better than that of the Wheatstone circuit currently employed by the NMi.

2.4. Water quality

The detection vessel was filled with water prepared by using a high quality water purifying system (Millipore Milli-Q A10) and a bubbling stage to

saturate the water with various gases. The water quality is characterized by the conductivity, σ, and the TOC (total organic compound) value. At a reference temperature of 25°C typical values are σ = 0.055 μS/cm (resistivity = 18.2 MΩ·cm) and TOC = 3 ppb. Downstream of the filling station the water quality was confirmed using a WTW LF330 conductivity meter connected to a LR325/001 conductivity cell.

The gas bubbling stage served to control the heat defect [8]. For the present investigation argon gas was used to saturate the water. Flow rates were controlled by Bronckhorst Hi-Tec flow meters. Flow rates were set at 200 mL/min, flow times being typically 1 h.

2.5. Experimental set-up at the BNM–LNHB

The NMi water calorimeter was aligned with respect to the BNM–LNHB GE Saturne 43 accelerator. A PTW 23344 plane-parallel ionization chamber located directly after the beam collimator, just outside the direct beam, served as a beam monitor. The nominal irradiation time was 60 s. Depending on the energy of the beam, during this time about 2.5–2.8 Gy was deposited at the point of measurement. Data acquisition was started 120 s before the irradiation (pre-drift) and was stopped 120 s after the irradiation (post-drift). Before actual measurements were performed the water calorimeter was preirradiated with at least 50 Gy. The calorimeter signal was then monitored as a function of time, and irradiation runs were sampled only after a stable signal was observed. This procedure ensured a chemical steady state (and thus a constant heat defect) during the measurements.

The beams at the BNM–LNHB were characterized in terms of both $TPR_{20,10}$ and $\%dd(10)_x$. These data are listed in Table II, together with values

TABLE II. BEAM QUALITY INDICES AND EFFECTIVE ATTENUATION COEFFICIENTS, μ_{eff}, FOR THE HIGH ENERGY PHOTON BEAMS USED AT THE BNM–LNHB

Photon beam (MV)	$TPR_{20,10}$	$\%dd(10)_x$	μ_{eff} (cm^2/g)
6	0.678	68.2	0.0222
12	0.751	75.4	0.0261
20	0.784	82.0	0.0348

for the effective attenuation coefficients at a depth of 10 g/cm^2 in water. The latter values are needed to correct for possible deviations from this reference depth.

The ionization chambers used in this investigation were five NE 2611A chambers (serial numbers 116, 117, 118, 119 and 120). These chambers had already been calibrated with respect to absorbed dose to water in the NMi ^{60}Co beam. The same waterproof Perspex sleeve (with a wall thickness of 1 mm) was employed both at the NMi and the BNM–LNHB. The chambers were connected to a Keithley 6517 electrometer. A high voltage of –200 V was applied to the central electrode of the chambers, while the thimble was kept at ground potential.

The following reference conditions apply to the results reported in this paper: SDD (source to detector distance) = 1 m, depth in water = 10 g/cm^2, field size at the thermistor probes = 10 cm × 10 cm, T = 20°C, P = 1013.25 mbar and relative humidity = 0%.

3. RESULTS AND DISCUSSION

Measurements of absorbed dose to water rates were performed using the NMi water calorimeter and the BNM–LNHB Saturne 43 accelerator. Fifty-three irradiation runs were conducted at 6 MV, 52 runs at 12 MV and 48 runs at 20 MV. Linear fits were made to the full pre-drift and to part of the post-drift (the first 10 s were skipped to minimize excess heat effects) of each run, and temperature changes were determined at the midpoint of each run.

The set of five NE 2611A chambers was calibrated against the NMi water calorimeter at all three energies, which was done by positioning the ionization chambers directly inside the water calorimeter phantom (only the glass detection vessel was removed).

3.1. Correction factors

The water calorimeter signal was corrected for the horizontal beam profile (since the two probes were placed 10 mm apart), for attenuation by the glass detection vessel and for deviations from the reference SDD and depth. The measured absorbed dose rates were also corrected for the heat defect (due to chemical reactions) and for excess heat effects (due to the difference in the specific heat capacities of glass and water) [4, 9].

The beam profile correction ranged between –0.1% and +0.4% (with a 1σ uncertainty of 0.1%), depending on the energy of the beam. Correction factors for attenuation by the glass vessel were measured using a waterproof PTW

31002 ionization chamber. This yielded values of 1.0020 ± 0.0003 at 6 MV, 1.0014 ± 0.0001 at 12 MV and 1.0004 ± 0.0002 at 20 MV (1σ uncertainties). For argon saturated water the correction for the heat defect is estimated to be –0.05% [4]. The combined excess heat effects of the glass vessel and probes together with the effect of the finite (10 cm × 10 cm) radiation field were calculated by numerically solving the differential heat flow diffusion equation [4, 9]. For an irradiation time of 60 s a correction of –0.22% was obtained. Estimated uncertainties of 0.2% were assigned to both the heat defect and the total excess heat effect.

The chamber signals were corrected for polarity, recombination, temperature, pressure, humidity and deviations from the reference SDD and depth. Correction factors for polarity, k_{pol}, and recombination, k_{ion}, were determined for all NE 2611A chambers at all three accelerator energies by measuring at both polarities and at half the operating voltage. Expressions recommended in Ref. [2] were used to calculate k_{pol} and k_{ion}. The results are presented in Table III.

3.2. k_Q factors

k_Q factors were derived as the ratio of absorbed dose to water calibration factors for the high energy beams of the BNM–LNHB and those for ^{60}Co gamma radiation, established at the NMi. In Fig. 1 the results are shown as a function of the beam quality index $\%dd(10)_x$, together with literature values of Seuntjens et al. [10] and a generic curve published by the AAPM [1] for NE 2561 chambers (which are virtually identical to NE 2611A chambers). As can been seen in Fig. 1, excellent agreement is found. The maximum discrepancy is 0.5%, which is within the uncertainty of 0.57% (1σ) assigned to the

TABLE III. CORRECTION FACTORS FOR POLARITY AND RECOMBINATION FOR THE NE 2611A CHAMBERS

Chamber	k_{pol}			k_{ion}		
	6 MV	12 MV	20 MV	6 MV	12 MV	20 MV
NE 2611A No. 116	1.0005	1.0001	1.0001	1.0060	1.0075	1.0076
NE 2611A No. 117	1.0001	1.0002	1.0000	1.0055	1.0075	1.0075
NE 2611A No. 118	1.0001	1.0001	1.0000	1.0054	1.0075	1.0075
NE 2611A No. 119	1.0001	1.0003	1.0000	1.0055	1.0077	1.0074
NE 2611A No. 120	1.0002	1.0001	1.0000	1.0055	1.0075	1.0074

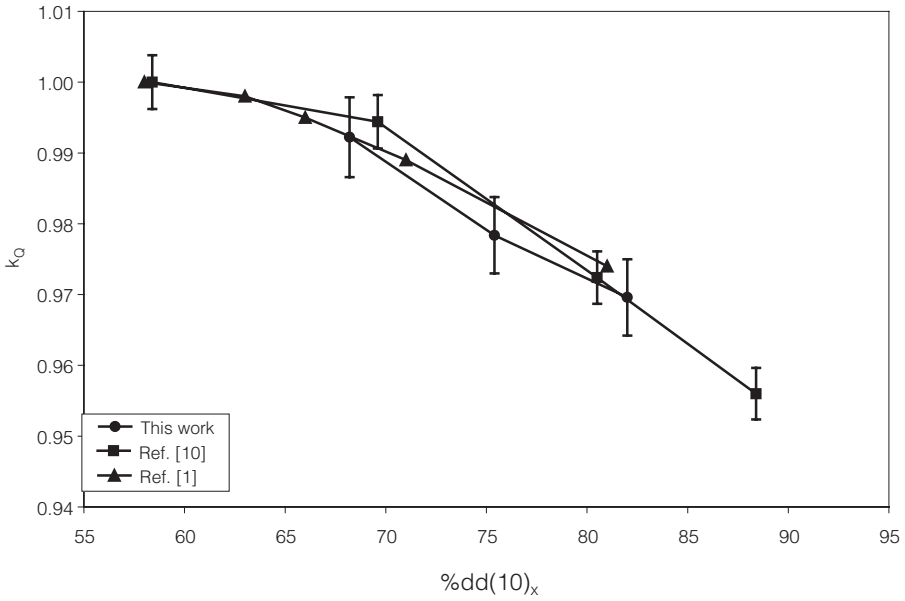

FIG. 1. Absorbed dose beam quality correction factors, k_Q, for the NE 2611A chamber as a function of %dd(10)$_x$. The solid circles represent results obtained in this work, the squares are data from Seuntjens et al. [10] and the triangles represent generic data recommended by the AAPM [1] for the NE 2561 chamber.

presently measured k_Q factors. This uncertainty includes all type A (statistical) and type B (non-statistical) uncertainties associated with the measurements with the NMi water calorimeter and with the NE 2611A chambers. The statistical uncertainty for the calorimeter measurements ranged between 0.16% and 0.20%, while the statistical uncertainty for charge measurements with the NE 2611A chambers was less than 0.06%. The statistical uncertainty for the k_Q factors derived from chamber to chamber variations ranged between 0.09% and 0.12% (1σ uncertainty in the mean).

If $TPR_{20,10}$ is used as the beam quality index, then very good agreement (also within 0.3%) is obtained from a comparison with generic data recommended by the IAEA [2] for both the NE 2611A and the NE 2561 chambers.

4. CONCLUSIONS

The NMi water calorimeter was used in the 6, 12 and 20 MV photon beams available at the BNM–LNHB from a Saturne 43 accelerator to measure absorbed dose to water rates. A set of five NE 2611A chambers was calibrated

inside the phantom of the water calorimeter directly against the water calorimeter at these three energies. Correction factors were measured for attenuation by the glass vessel and for polarity and recombination effects at all three accelerator energies. The k_Q factors obtained agreed very well with literature values. The NMi water calorimeter will be used in a clinical measurement programme in the Netherlands and Belgium to establish generic k_Q factors for several types of graphite walled ionization chamber. These factors will be tabulated in the revised NCS protocols for the clinical dosimetry of high energy photon beams.

ACKNOWLEDGEMENTS

The authors would like to sincerely thank their colleagues A. Ostrowsky, D. Cutarella and F. Delaunay for their generous hospitality and assistance with the experiments during two visits to the BNM–LNHB, Commissariat à l'énergie atomique, Saclay, France, in February and August 2002.

REFERENCES

[1] AMERICAN ASSOCIATION OF PHYSICISTS IN MEDICINE, AAPM's TG-51 protocol for clinical reference dosimetry of high-energy photon and electron beams, Med. Phys. **26** (1999) 1847–1870.

[2] INTERNATIONAL ATOMIC ENERGY AGENCY, Absorbed Dose Determination in External Beam Radiotherapy, Technical Reports Series No. 398, IAEA, Vienna (2000).

[3] DOMEN, S.R., A sealed water calorimeter for measuring absorbed dose, J. Res. Natl. Inst. Stand. Technol. **99** (1994) 121–141.

[4] SEUNTJENS, J., PALMANS, H., Correction factors and performance of a 4°C sealed water calorimeter, Phys. Med. Biol. **44** (1999) 627–646.

[5] PIEKSMA, M., et al., "The NMi absorbed-dose-to-water calorimeter (A status report)", Recent Advances in Calorimetric Absorbed Dose Standards (Proc. Workshop Teddington, UK, 1999), Rep. CIRM 42 (WILLIAMS, A.J., ROSSER, K.E., Eds), National Physical Laboratory, Teddington, UK (2000) 85–89.

[6] PIEKSMA, M., et al., "The NMi water calorimeter", Recent Developments in Accurate Radiation Dosimetry (Proc. Int. Workshop Montreal, 2001) (SEUNTJENS, J.P., MOBIT, P.N., Eds), Medical Physics Publishing, Madison, WI (2002) 108–119.

[7] LIDE, D.R. (Ed.), Handbook of Chemistry and Physics, 73rd edn, CRC Press, London (1992) 6–10.

[8] KLASSEN, N.V., ROSS, C.K., Water calorimetry: The heat defect, J. Res. Natl. Inst. Stand. Technol. **102** (1997) 63–74.

[9] PALMANS, H., "Experimental verification of simulated excess heat effects in the sealed water calorimeter", Recent Advances in Calorimetric Absorbed Dose Standards (Proc. Workshop Teddington, UK, 1999), Rep. CIRM 42 (WILLIAMS, A.J., ROSSER, K.E., Eds), National Physical Laboratory, Teddington, UK (2000) 74–84.

[10] SEUNTJENS, J.P., et al., Absorbed-dose beam quality correction factors for cylindrical chambers in high-energy photon beams, Med. Phys. **27** (2000) 2763–2779.

THE METAS ABSORBED DOSE TO WATER CALIBRATION SERVICE FOR HIGH ENERGY PHOTON AND ELECTRON BEAM RADIOTHERAPY

G. STUCKI, W. MUENCH, H. QUINTEL
Swiss Federal Office of Metrology and Accreditation (METAS),
Bern-Wabern, Switzerland
E-mail: gerhard.stucki@metas.admin.ch

Abstract

The Swiss Federal Office of Metrology and Accreditation (METAS) provides an absorbed dose to water calibration service for reference dosimeters. The calibration service uses ^{60}Co gamma radiation, ten high energy photon beam qualities between $TPR_{20,10}$ = 0.639 and 0.802 and ten electron beam qualities between R_{50} = 1.75 g/cm^2 and 8.54 g/cm^2.

The METAS absorbed dose calibration service for high energy photons is based on a primary standard sealed water calorimeter used to calibrate several METAS NE 2611A and NE 2571A type ionization chamber working standards in terms of absorbed dose to water in the energy range of ^{60}Co to $TPR_{20,10}$ = 0.802. The users' reference dosimeters are compared with the working standards to give calibration factors in absorbed dose to water with an uncertainty of 1.0% for ^{60}Co radiation and 1.4% for higher energies (coverage factor k = 2). The calibration service was launched in 1997. The calibration factors measured by METAS have been compared with those derived from the IAEA Technical Reports Series No. 398 (TRS 398) code of practice and from Recommendations No. 4 of the Swiss Society of Radiobiology and Medical Physics (SSRMP). The comparisons showed a maximum difference of 1.2% for the NE 2561A and NE 2571A chambers. At ^{60}Co gamma radiation the METAS primary standard of absorbed dose to water was bilaterally compared with the primary standards of the Bureau international des poids et mesures. The standards were in agreement within the comparison uncertainties.

The METAS absorbed dose calibration service for high energy electron beams is based on a primary standard chemical dosimeter. A monoenergetic electron beam of known particle energy and beam charge is totally absorbed in Fricke solution. The experiment was carried out in the energy range of 5.3 MeV to 22.4 MeV, which allows the determination of the response of the Fricke dosimeter. Finally, the users' dosimeters are compared with the METAS working standards. The overall uncertainty in the calibration factor of a user's dosimeter is 2% (coverage factor k = 2). The calibration factors measured by METAS have been compared with those derived from TRS 398 and from Recommendations No. 4 of the SSRMP. The comparison showed a maximum difference of 1.2% and 2.5%, respectively, for the NACP-02 chamber.

1. INTRODUCTION

The Swiss Federal Office of Metrology and Accreditation (METAS) develops and maintains primary standards for absorbed dose to water and provides calibration services for reference dosimeter systems used in radiotherapy centres.

In 1997 METAS launched a calibration service for reference dosimetry systems in terms of absorbed dose to water for ^{60}Co gamma radiation and high energy photon beams between $TPR_{20,10} = 0.639$ and $TPR_{20,10} = 0.802$. Since 2001 this service has been based on a primary standard sealed water calorimeter.

In 2002 METAS launched a corresponding service for reference dosimetry systems in terms of absorbed dose to water for high energy electron beams between $R_{50} = 1.75$ g/cm^2 and $R_{50} = 8.54$ g/cm^2. This service is based on a primary standard chemical dosimeter.

A 22 MeV microtron accelerator with a conventional treatment head, which produces clinical beams, is used as a radiation source for both high energy photon and electron beams.

The user reference dosimetry systems are calibrated in terms of absorbed dose to water at those radiation qualities at which they are applied in the therapy centres. The calibration procedure complies with the new IAEA Technical Reports Series No. 398 (TRS 398) code of practice [1] and the new Recommendations No. 8 and No. 10 of the Swiss Society of Radiobiology and Medical Physics (SSRMP) [2, 3].

The METAS calibration factors in terms of absorbed dose to water per unit charge or per unit electrometer reading refer to an air temperature of 20°C, an air pressure of 101 325 Pa and a relative humidity of 50% as reference conditions.

2. ABSORBED DOSE TO WATER CALIBRATION SERVICE FOR HIGH ENERGY PHOTON BEAMS

2.1. General procedure

The calibration procedure has two stages:

(a) The primary standard sealed water calorimeter is used to calibrate the working standards of NE 2611A and NE 2571 type ionization chambers in a water phantom in terms of absorbed dose to water for ten radiation qualities.

(b) The users' reference dosimetry systems are compared with the METAS working standards in a water phantom for the radiation qualities selected by the users from the same ten radiation qualities.

The measurements are carried out with the detector centre at a reference depth in water of 5 g/cm^2 for ^{60}Co and 10 g/cm^2 for high energy photon beams above ^{60}Co, at a field size of 10 cm × 10 cm at the detector centre. The source detector distance is 100 cm.

The radiation quality is specified by the tissue–phantom ratio $TPR_{20,10}$, which is the ratio of the dose measurements at depths of 20 g/cm^2 and 10 g/cm^2 in water for a constant source to detector distance of 100 cm.

2.2. Calibration of working standard against the METAS primary standard

The METAS primary standard is a sealed water calorimeter following the design of the National Research Council of Canada's calorimeter [4]. The relation between the absorbed dose to water, D_w, and the temperature rise of the water, ΔT_w, is given by:

$$D_w = \Delta T_w c_w k \tag{1}$$

where c_w is the specific heat capacity of water and k is a product of several correction factors described in detail in Ref. [4]. The water calorimeter is operated at 4°C to reduce the problem associated with convective heat transfer. The temperature rise is sensed by two thermistor probes in one arm of an AC bridge circuit.

The main corrections to the calorimeter measurements are for the effects of conductive and convective heat transfer, the effects of perturbations of the radiation field by the glass vessel and probes and the heat defect of water [4, 5].

For ^{60}Co radiation the calorimeter is used to determine directly the dose rate at the reference depth. Each working standard is placed in turn in the calorimeter water tank and calibrated against the sealed water calorimeter. These measurements with the working standards are made at 20°C. The calibration factor, $N_{D,w,\mathrm{Co}}$, of a working standard under reference conditions is then given by:

$$N_{D,w,\mathrm{Co}} = \frac{D_w}{M_Q} \tag{2}$$

where M_Q is the dosimeter reading, corrected to reference conditions and for recombination losses.

For high energy photon beams the working standards are indirectly compared with the calorimeter by means of two ionization chambers used as a monitor. The monitor chambers are mounted in the water phantom of the calorimeter, behind the calorimeter vessel or the working standard, respectively, and operated at 4°C or 20°C, respectively. The calibration factor, $N_{D,w,Q}$, of a working standard under reference conditions is then given by:

$$N_{D,w,Q} = \frac{D_w}{M_Q} \frac{M_{\mathrm{WS}}}{M_C} f_{4,20} \tag{3}$$

where M_{WS} is the monitor reading when measuring with the working standard and M_C is the monitor reading when measuring with the calorimeter. The factor $f_{4,20}$ corrects for any difference in the monitor response at 4°C and 20°C, respectively.

2.3. Calibration of a reference dosimeter in terms of absorbed dose to water

The user reference dosimetry systems are compared with the working standards in a cubic water phantom with 60 cm sides. Ionization chambers that are not waterproof are provided with a close-fitting Perspex sleeve with a wall thickness of typically 1 mm.

The METAS certificate states the absorbed dose to water calibration factors as a function of radiation quality with an uncertainty of 1.4% (k = 2) for high energy photon beams and 1% for ^{60}Co gamma rays.

2.4. Comparison of the METAS calibration factors with those from the Bureau international des poids et mesures and with those derived from TRS 398 and from SSRMP Recommendations No. 4

The METAS primary standard of absorbed dose to water was bilaterally compared at ^{60}Co gamma radiation with the primary standards of the Bureau international des poids et mesures. The standards were in agreement within 0.1% [6].

The METAS absorbed dose to water calibration factors for the NE 2611A and NE 2571A chambers were compared with factors derived from SSRMP Recommendations No. 4 [7] (these recommendations were superseded by Recommendations No. 8 [2] in 2000, as far as photon beam dosimetry is concerned) and from TRS 398 [1]. The latter derives the calibration factors from the ^{60}Co absorbed dose calibration of the chamber, together with a calculated

k_Q factor, listed in table 14 of Ref. [1], whereas the former uses an air kerma calibration at ^{60}Co together with a calculated chamber type dependent conversion factor (table C1 of Ref. [7]).

Figures 1 and 2 show the absorbed dose to water calibration factors as a function of beam quality for an individual chamber of type NE 2611A and NE 2571A, respectively. The uncertainties associated with the METAS calibration factors are indicated as uncertainty bars (coverage factor k = 1). For the NE 2611A chamber the METAS calibration factors agree within 0.6% with the factors derived from TRS 398, whereas the factors derived from SSRMP Recommendations No. 4 are lower than the METAS factors by 0.3% to 1.2% for high energy photon beams, depending on beam quality.

For the NE 2571A chamber the METAS calibration factors agree within 0.9% with the factors derived from TRS 398, whereas the factors derived from SSRMP Recommendations No. 4 are lower than the METAS factors by up to 0.8%.

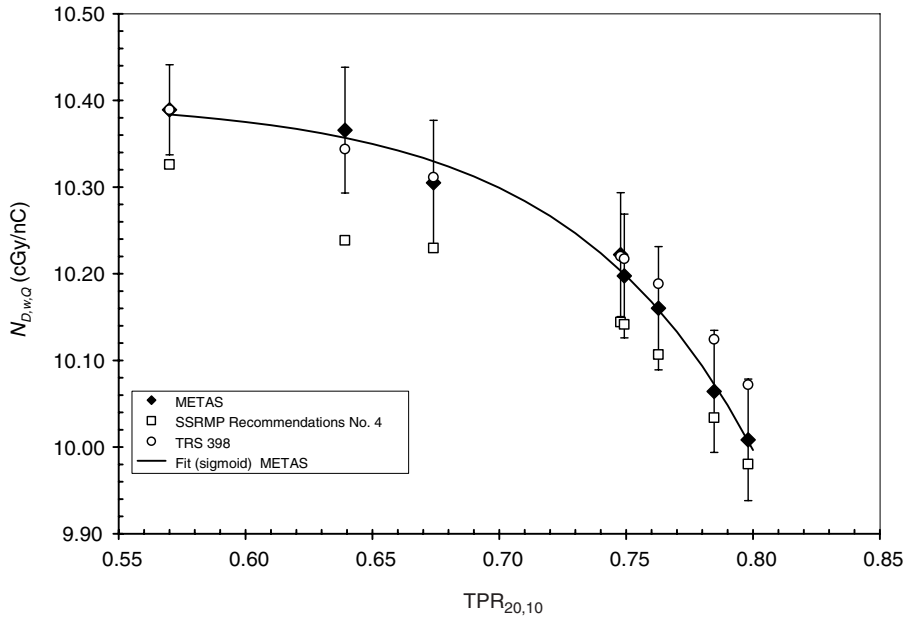

FIG. 1. Type NE 2611A (serial number 127) chamber calibration factors: comparison of METAS with the SSRMP Recommendations No. 4 and TRS 398 codes of practice.

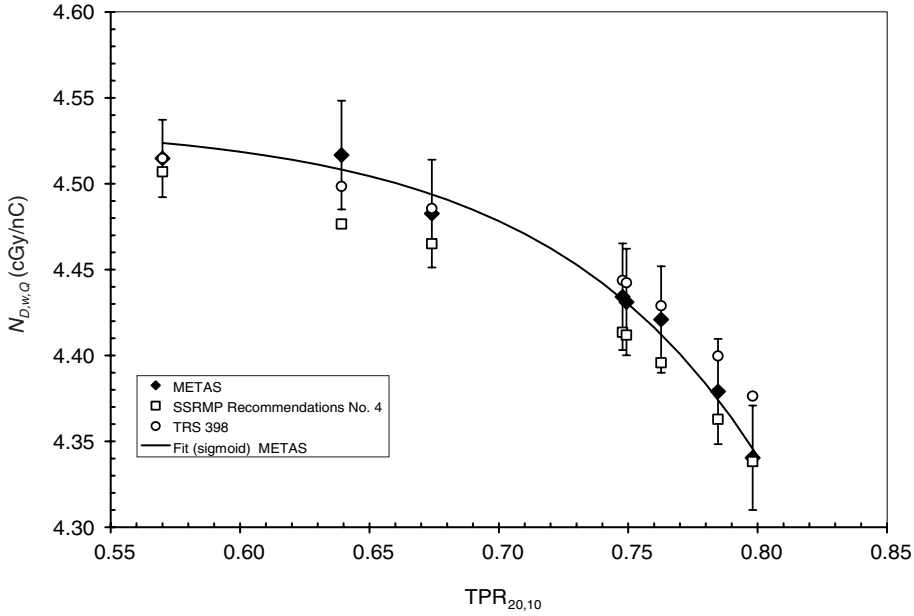

FIG. 2. Type NE 2571A (serial number 2690) chamber calibration factors: comparison of METAS with the SSRMP Recommendations No. 4 and TRS 398 codes of practice.

3. ABSORBED DOSE TO WATER CALIBRATION SERVICE FOR HIGH ENERGY ELECTRON BEAMS

3.1. General procedure

The calibration procedure has three stages:

(a) The primary standard is used to calibrate a chemical dosimeter (ferrous ammonium sulphate) in terms of absorbed dose to Fricke solution for ten radiation qualities.
(b) The chemical dosimeter is used to calibrate several working standards (plane-parallel ionization chambers of type NACP-02) in terms of absorbed dose to water for ten radiation qualities.
(c) Users' reference dosimetry systems are compared with the METAS working standards in a water phantom for the radiation qualities selected by the user from the same ten radiation qualities.

For electron beams the half-value depth in water, R_{50}, is used as beam quality specifier. This is the depth in water (in g/cm^2) at which the absorbed

dose is 50% of its value at the absorbed dose maximum, measured with a constant source to surface distance of 100 cm and at a field size of 15 cm × 15 cm at the phantom surface.

The measurements for stages (b) and (c) are carried out with the detector centre at the reference depth in water, z_{ref}, given by:

$$z_{ref} = 0.6R_{50} - 0.1 \text{ g/cm}^2 \quad (4)$$

where R_{50} is in g/cm^2.

3.2. Calibration of the chemical dosimeter against the METAS primary standard

The METAS primary standard is a chemical dosimeter, the response of which is determined by a total absorption experiment. A monoenergetic electron beam of known particle energy, E_e, and known total number of electrons, N, is fully absorbed in a vessel containing Fricke solution of a given mass, m.

The electron energy is measured using a magnetic spectrometer, and the total number of absorbed electrons is determined by means of an inductive beam charge monitor. This experiment is similar to the one described by Feist [8], but extended to an energy range from 5.3 MeV to 22.4 MeV (which allows the determination of the response of the Fricke solution in that energy range).

The absorbed dose to the Fricke solution, D_F, is given by:

$$D_F = \frac{E_e N}{m} f_T \quad (5)$$

where f_T is a product of several corrections factors. The main correction factors are for losses due to bremsstrahlung, reabsorption of bremsstrahlung, backscattering of electrons and energy losses in the exit and entrance foils. These factors were determined by Monte Carlo calculations [9].

The Fricke dosimeter is an aqueous solution of ferrous ions in 0.4M H_2SO_4. Ionizing radiation converts ferrous ions, Fe^{2+}, into ferric ions, Fe^{3+}, with a radiation yield proportional to the absorbed dose. The increase in the concentration of Fe^{3+}, compared with the concentration in the unirradiated solution, is determined by measuring the change in the optical density, ΔA_T, at 304 nm using an ultraviolet spectrometer. The absorbed dose to the Fricke solution is then given by:

$$D_F = \frac{\Delta A_T}{\varepsilon G \rho l_T} \quad (6)$$

where

- ε is the extinction coefficient of Fe^{3+} minus the extinction coefficient of Fe^{2+} at 304 nm;
- G is the radiation yield of Fe^{3+};
- ρ is the density of the Fricke solution;
- l_T is the optical path length of the readout cell.

Combining Eqs (5) and (6) the calibration factor $\Delta A_T/\varepsilon G$ of the Fricke solution can be determined:

$$\frac{\Delta A_T}{\varepsilon G} = \rho l_T \frac{E_e N}{m} f_T \tag{7}$$

This calibration factor is measured for different beam energies in the range from 5.3 MeV to 22.4 MeV. Within the experimental uncertainty the factor $1/\varepsilon G$ does not depend on the particle energy.

3.3. Transfer from the chemical dosimeter to the working standards

The thus calibrated Fricke solution is filled into small vessels made of polyethylene with a volume of 30 mm × 40 mm × 2 mm, which are placed in turn in a cubic water phantom with sides of 60 cm at the reference depth and compared with the plane-parallel chamber at each radiation quality. The calibration factor, $N_{D,w,Q}$, of a working standard under reference conditions is then given by:

$$N_{D,w,Q} = \frac{\Delta A_B}{\Delta A_T} \frac{l_T}{l_B} \frac{1}{M_Q} \frac{E_e N}{m} f_T f_e \tag{8}$$

where

- ΔA_B is the change of the optical density due to the irradiation in the water phantom;
- M_Q is the dosimeter reading, corrected to reference conditions and for recombination losses;
- l_B is the optical path length of the readout cell;
- f_e is the general Fricke to water dose conversion factor derived from Ref. [10].

3.4. Calibration of a reference dosimeter in terms of absorbed dose to water

The user reference dosimetry system is calibrated against a working standard in a cubic water phantom with sides of 60 cm. Only well guarded plane-parallel ionization chambers are accepted for calibration.

The METAS certificate states the absorbed dose to water calibration factors for electron beams as a function of radiation quality with an uncertainty of 2% ($k = 2$).

3.5. Comparison of the METAS calibration factors with those derived from TRS 398 and from SSRMP Recommendations No. 4

The METAS absorbed dose to water calibration factors for the NACP-02 chamber were compared with factors derived from SSRMP Recommendations No. 4 [7] (these recommendations were superseded by Recommendations No. 10 [3] in 2002, as far as electron beam dosimetry is concerned) and from TRS 398 [1]. The latter derives the calibration factors from the ^{60}Co absorbed dose calibration of the chamber, together with a calculated k_Q factor, listed in table 18 of Ref. [1], whereas the former uses an air kerma calibration at ^{60}Co together with a calculated chamber type dependent conversion factor and calculated stopping power ratios (tables C2–C4 of Ref. [7]).

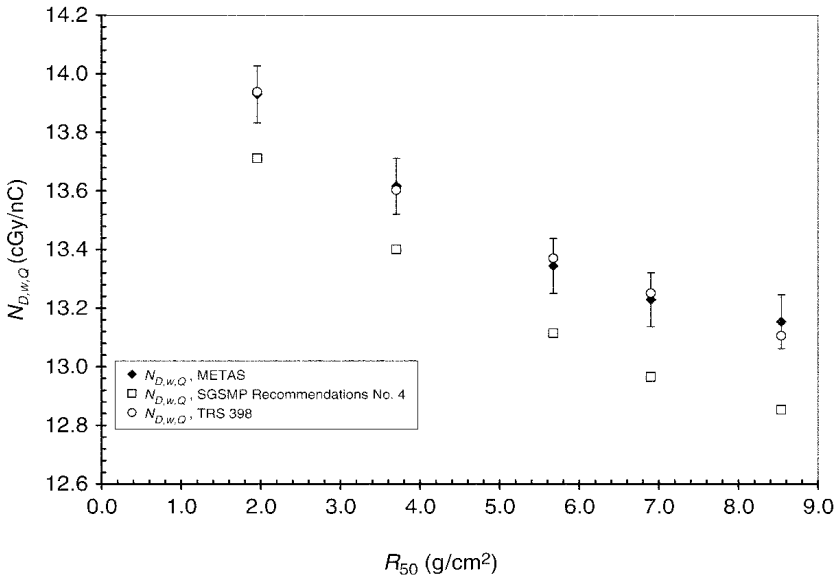

FIG. 3. Calibration factors of chamber NACP-02, (serial number 6905): comparison of METAS with the SSRMP Recommendations No. 4 and TRS 398 codes of practice.

Figure 3 shows the absorbed dose to water calibration factors as a function of beam quality for an individual chamber of type NACP-02. The uncertainties associated with the METAS calibration factors are indicated as uncertainty bars (coverage factor $k = 1$). For the NACP-02 chamber type the METAS calibration factors agree within 1.2% with the factors derived from TRS 398. Some individual chambers show a very good agreement (see Fig. 3). The factors derived from SSRMP Recommendations No. 4 are lower than the METAS factors by 1.5% to 2.5%, depending on beam quality.

4. CONCLUSIONS

The METAS absorbed dose to water calibration service for high energy photon and electron beams is the basis of SSRMP Recommendations No. 8 and No. 10 [2, 3], which superseded Recommendations No. 4. The agreement between the METAS calibration factors and those derived from TRS 398 is within 1.2%, which is within the claimed uncertainties of 1.4% for photon beams and 2% for electron beams.

REFERENCES

[1] INTERNATIONAL ATOMIC ENERGY AGENCY, Absorbed Dose Determination in External Beam Radiotherapy, Technical Reports Series No. 398, IAEA, Vienna (2000).

[2] SWISS SOCIETY OF RADIOBIOLOGY AND MEDICAL PHYSICS, High-energy Photon Beam Therapy Dosimetry with Ionisation Chambers, Recommendations No. 8, SSRMP, Bern (2000).

[3] SWISS SOCIETY OF RADIOBIOLOGY AND MEDICAL PHYSICS, High-energy Electron Beam Therapy Dosimetry with Ionisation Chambers, Recommendations No. 10, SSRMP, Bern (2002).

[4] MEDIN, J., SEUNTJENS, J., KLASSEN, N., ROSS, C.K., STUCKI, G., "The OFMET sealed water calorimeter", Recent Advances in Calorimetric Absorbed Dose Standards (Proc. Workshop Teddington, UK, 1999), Rep. CIRM 42 (WILLIAMS, A.J., ROSSER, K.E., Eds), National Physical Laboratory, Teddington, UK (2000) 65–73.

[5] ROSS, C.K., SEUNTJENS, J.P., KLASSEN, N.V., SHORTT, K.R., "The NRC sealed water calorimeter: Correction factors and performance", ibid., pp. 90–102.

[6] ALLISY-ROBERTS, P., BURNS, D., STUCKI, G., Comparison of the Standards of Absorbed Dose to Water of the METAS, Switzerland and the BIPM for ^{60}Co γ Rays, Rep. BIPM-03/02, Bureau international des poids et mesures, Sèvres (2003).

[7] SWISS SOCIETY OF RADIOBIOLOGY AND MEDICAL PHYSICS, Dosimetry of High Energy Photon and Electron Beams, Recommendations No. 4, Rev. 1992, SSRMP, Bern (1992).
[8] FEIST, H., Determination of absorbed dose to water for high energy photons and electrons by total absorption of electrons in ferrous sulphate solution, Phys. Med. Biol. **37** (1982) 1937–1947.
[9] KAWRAKOW, I., National Research Council, Canada, personal communication, 1999.
[10] MA CHANG MING, NAHUM, A.E., Correction factors for Fricke dosimetry in high-energy electron beams, Phys. Med. Biol. **38** (1993) 423–438.

BLANK

PORTABLE GRAPHITE CALORIMETER FOR MEASURING ABSORBED DOSE IN THE RADIOTHERAPY CLINIC

M.R. McEWEN*, S. DUANE
National Physical Laboratory,
Teddington, United Kingdom
E-mail: mrmcewen@irs.phy.nrc.ca

Abstract

The paper describes a robust and portable calorimeter for use in radiotherapy photon and electron beams. The system consists of the calorimeter itself, means for thermal isolation and temperature control, and a temperature measurement system. The calorimeter is capable of measuring a dose of 1 Gy at dose rates as low as 1.5 Gy/min, with a measurement uncertainty of 0.4% (1 standard deviation). Measurements in a clinical linac beam indicated that there is no significant error in the transfer of ionization chamber calibrations from the National Physical Laboratory to the radiotherapy clinic.

1. INTRODUCTION

A portable calorimeter has been developed at the National Physical Laboratory (NPL) that is designed to measure absorbed dose to water directly in radiotherapy facilities for high energy photon and electron beams. The calorimeter has been built, and the design is described in Ref. [1]. The main purpose of this calorimeter is to investigate the transfer of the calibration of an ionization chamber from the standards laboratory to the clinic. If the beam used to calibrate the ionization chamber is different from that in the radiotherapy clinic, the calibration factor used may not be applicable. By measuring absorbed dose directly in the user's radiation beam any errors in the use of ionization chambers can be identified and investigated.

The calorimeter is constructed from graphite using a solid surrounding body to provide the required temperature control and a DC bridge based temperature measurement system. The temperature control system can typically maintain the temperature of the calorimeter core to within ±0.1 mK over

* Present address: National Research Council, Ottawa, Canada.

several hours. The temperature measurement system for determining the dose has a resolution of 3 μK, and operation at dose rates as low as 1 Gy/min has been achieved.

2. VALIDATION

2.1. Investigation of influence quantities

Prior to the comparison of the calorimeter with the NPL primary standards of absorbed dose, an in-depth investigation was carried out into possible influence quantities, including dose, dose rate and temperature dependence. No significant effect was observed at the 0.1% level. Correction factors were also derived for the effect of air gaps, scatter and attenuation effects and beam uniformity. The 1 mm air gap around the core perturbs the incident beam, affecting the dose measured in the core. The correction is dependent on energy and modality and was determined from Monte Carlo calculations (see Ref. [1] for more details). Scatter and attenuation corrections are required because the calorimeter is not a homogeneous system — around the basic calorimeter body is a temperature control body, which both attenuates the primary beam and introduces sidescatter and backscatter. More detail on these corrections is given in Ref. [2].

2.2. Performance of the calorimeter

Three formal comparisons were carried out in the three available NPL beams — ^{60}Co, linac photons and linac electrons. The values for the noise level, standard deviation and standard uncertainty on the dose measured by the calorimeter are summarized in Table I. The standard uncertainties given in Table I are for a single day's irradiations. As part of the testing in the ^{60}Co

TABLE I. SUMMARY OF CALORIMETER PERFORMANCE

	^{60}Co	10 MV X rays	16 MeV electrons
RMS[a] noise level (μK)	7.7	6.2	6.9
Dose delivered (Gy)	1.1	1.6	2.4
Standard deviation	±0.80%	±0.46%	±0.30%
Standard uncertainty	±0.20%	±0.10%	±0.11%

[a] RMS: root mean square.

beam, the calorimeter was removed from the irradiation room and then replaced two days later. There was no significant difference in the dose rate measured on different days. This indicates that both the construction and operation are robust, which is essential for use in a radiotherapy clinic.

2.3. Uncertainties

The uncertainty budget for calibrating an ionization chamber in terms of dose to graphite using the portable calorimeter is given in Table II. This gives a combined uncertainty in the calibration of a chamber in terms of dose to graphite of ±0.37%. The standard uncertainty on the dose measurement is approaching that of the primary standard photon calorimeter and is better than the electron primary standard.

2.4. Discussion of results of comparison with primary standards

The results of the comparisons are given in Table III, expressed as the dose determined by the portable calorimeter divided by that determined by the primary standard.

There are a number of common uncertainties in these comparisons, which have been removed to give the uncertainty values shown in Table III. The first point to note is that the agreement between the portable calorimeter and the primary standards is within the uncertainties, indicating that there are no significant errors in the operation of the portable calorimeter. However, the fact

TABLE II. PORTABLE CALORIMETER UNCERTAINTIES

Component of uncertainty	Standard uncertainties (%)	
	Type A	Type B
Calorimeter dose measurement (typical)	0.15	
Thermistor calibration		0.10
Specific heat capacity		0.08
Analysis method	0.14	0.10
Chamber reading	0.04	0.10
Correction factors (beam uniformity, scatter, etc.)	0.13	0.20
Overall	0.25	0.27

TABLE III. RESULTS OF COMPARISONS OF THE PORTABLE CALORIMETER WITH THE NPL PRIMARY STANDARDS

Beam quality	Dose ratio (portable/primary)	Standard uncertainty (%)
^{60}Co	1.0044	0.63
10 MV X rays	1.0060	0.63
16 MeV electrons	1.0030	0.42

that all three values of the ratio are greater than unity indicates that some effect may not have been taken into account properly. Over recent years it has become apparent that there is a potential problem with the electrical calibration in the NPL photon calorimeter, and initial measurements indicate that the photon calorimeter currently underestimates the dose by around 0.4%. The comparisons described in this paper are part of a wider investigation of calorimetric standards at the NPL, the full details of which are given in Ref. [3].

2.5. Derivation of dose conversion factors in a clinical photon beam

In radiotherapy dosimetry the quantity of interest is absorbed dose to water. Factors are therefore required to convert the absorbed dose measured by the calorimeter from graphite to water. Measurements were carried out in two clinical photon beams (6 MV and 10 MV) from a Philips SL 15 linac to evaluate the water–graphite conversion factors; this work is described in detail in Ref. [4]. The factors derived for the SL 15 were in very good agreement with those obtained for the NPL linac, indicating that there is no significant difference between the NPL photon beams and those from a clinical linac.

3. CALORIMETER MEASUREMENTS IN A RADIOTHERAPY CLINIC

3.1. Measurements

The measurements were carried out at St Bartholomew's Hospital in London. The linac used for these measurements was a Varian 6EX producing 6 MV X rays at a dose rate of 6 Gy/min. A source to surface distance of 1000 mm was used with a field size of 10 cm × 10 cm. The measurement depth was 5.6 g/cm of graphite, the scaled depth equivalent to 5 cm of water. Ionization chamber

measurements were made in a graphite phantom the same size as the calorimeter. Although the linac is of a different type from that used in the water–graphite scaling work, it was assumed that there were no significant differences in the photon spectrum between a Varian and Philips linac.

It was found that there was significant noise pickup on the calorimeter signal, as shown in Fig. 1. This was present on both sensing channels, and was therefore due to some external source of noise (presumably the linac). It was not possible to isolate the effect in the limited time available.

The performance of the calorimeter is summarized in Table IV, and compared with data obtained at the NPL.

The RMS noise level is around twice that for measurements made at the NPL, which is reflected in the larger standard deviation for the same dose rate. However, the standard uncertainty is low enough to enable a comparison of chamber and calorimeter doses. This is due, in part, to the robustness of the algorithms used to determine the radiation induced temperature rise.

Once the calorimeter measurements had been completed, the chamber phantom was set up with the same source to surface distance, and a series of measurements was carried out to determine the dose via the ionization chamber together with the various corrections (e.g. scatter, attenuation and recombination).

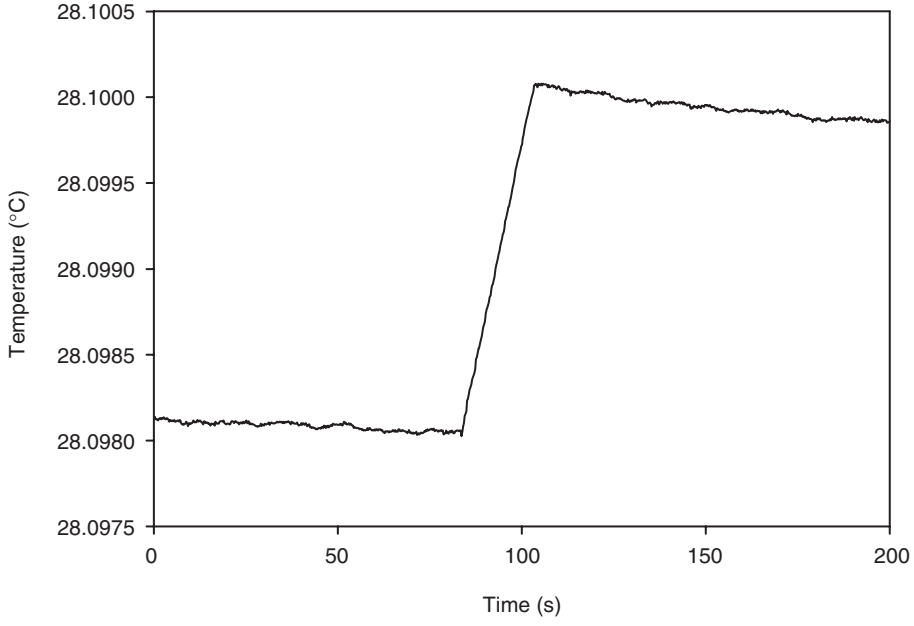

FIG. 1. Typical calorimeter run in a clinical 6 MV beam.

3.2. Discussion of results

Using a graphite calibration factor for the chamber (derived from comparison with the photon primary standard at the NPL), the output factors for the calorimeter and chamber were compared. The ratio of the doses measured by the calorimeter and chamber was determined to be 1.0068, with an overall standard uncertainty estimated to be ±0.71%. It is also useful to compare the calorimeter/chamber ratio with the values obtained in NPL beams (see Table V), as such a comparison removes the uncertainty due to the primary standard calorimeter.

The overall standard uncertainty on each ratio is estimated to be ±0.46%, and the agreement between the measurements is therefore very good. Although this is only a single measurement, it indicates that there is no significant uncertainty introduced by the transfer of the chamber calibration from the NPL to the clinic. As noted above, it is thought that the primary standard photon calorimeter underreads by ≈0.3%, which, if confirmed, will improve the level of agreement (and reduce the overall uncertainty).

TABLE IV. COMPARISON OF CALORIMETER PERFORMANCE AT A CLINIC AND THE NPL

	St Bartholomew's Hospital	NPL
Modality	6 MV X rays	10 MV X rays
RMS noise level (μK)	12.8	6.2
Dose delivered (Gy)	1.5	1.6
Standard deviation	±0.90%	±0.46%
Standard uncertainty	±0.25%	±0.10%

TABLE V. COMPARISON OF CALORIMETER/CHAMBER DOSES FOR VARIOUS BEAMS

Modality	Calorimeter dose/ chamber dose
^{60}Co (NPL)	1.0044
10 MV X rays (NPL)	1.0060
6 MV X rays (St Bartholomew's Hospital)	1.0068

4. CONCLUSION

A portable calorimeter has been developed that is designed to measure absorbed dose in radiotherapy facilities. A thorough validation of the portable calorimeter has been successfully carried out, and a comparison with the NPL primary standards gave agreement within the measurement uncertainties. The overall standard uncertainty in the calibration of an ionization chamber in terms of absorbed dose to graphite is estimated to be 0.37%, a value very similar to the primary standard calorimeters.

The first use of the calorimeter in a radiotherapy clinic has highlighted the reasons calorimetry in such facilities is rarely attempted: the combination of a lack of time and an environment unsuited to making low noise electrical measurements means that it is a significant challenge to achieve a measurement uncertainty better than 0.5%. The investigation at the radiotherapy clinic, comparing the portable calorimeter with an ionization chamber traceable to the NPL primary standard photon calorimeter, gave a dose ratio of 1.0068 (standard uncertainty of 0.71%). This result indicates that, for this particular accelerator, there is no significant uncertainty introduced by the transfer of the chamber calibration from the NPL to the clinic. Further measurements in a range of clinical beams are required to confirm this result.

ACKNOWLEDGEMENTS

This work was funded as part of the United Kingdom National Measurement System, Ionising Radiation Metrology Programme, by the National Measurement System Policy Unit of the United Kingdom Department of Trade and Industry. The authors would like to thank R. Thomas for assisting in the external testing and E. McCauley for providing access to the St Bartholomew's Hospital's linac to carry out the measurements.

REFERENCES

[1] McEWEN, M.R., DUANE, S., A portable calorimeter for measuring absorbed dose in the radiotherapy clinic, Phys. Med. Biol. **45** (2000) 3675–3691.

[2] McEWEN, M.R., DUANE, S., The NPL Portable Graphite Calorimeter, National Physical Laboratory, Teddington, UK (in press).

[3] McEWEN, M.R., DUANE, S., STOKER, I., "Comparison of graphite standard calorimeters in megavoltage photon and electron beams", these Proceedings, Vol. 1, pp. 67–73.

[4] NUTBROWN, R.F., McEWEN, M.R., THOMAS, R.A.S., DUANE, S., SHIPLEY, D.R., Comparison of conversion factors for x-ray beams from a Philips SL15 and the NPL linear accelerator, Phys. Med. Biol. **46** (2001) N245–N252.

BLANK

AIR KERMA AND ABSORBED DOSE TO WATER STANDARDS FOR PHOTONS

(Session 3)

Chair

I. CSETE
Hungary

Co-Chair

L. BÜERMANN
Germany

Rapporteur

M.R. McEWEN
United Kingdom

BLANK

RECENT DEVELOPMENTS AND CURRENT STATUS OF AIR KERMA STANDARDS

L. BÜERMANN
Physikalisch-Technische Bundesanstalt,
Braunschweig, Germany
E-mail: ludwig.bueermann@ptb.de

I. CSETE
Országos Mérésügyi Hivatal,
Budapest, Hungary

Abstract

The current status of air kerma standards for kilovoltage X rays and for ^{137}Cs and ^{60}Co gamma radiation maintained at primary standards dosimetry laboratories is reviewed using results of the bilateral key comparisons between the air kerma standards of the Bureau international des poids et mesures (BIPM) and those of national metrology institutes. Owing to the re-evaluation of k_{wall} and k_{an}, which are the correction factors for wall effects and axial beam non-uniformity for cavity ionization chambers, respectively, a significant increase of about 0.8% in the realization of the gray for air kerma in both ^{137}Cs and ^{60}Co fields is to be expected. A consistent set of free air chamber correction factors for electron loss, photon scatter, fluorescence and bremsstrahlung was calculated at the BIPM using state of the art Monte Carlo methods for all free air chamber standards in use worldwide. Consistent use of this set by all national metrology institutes would further improve the degree of equivalence of free air chamber standards.

1. INTRODUCTION

Primary standards dosimetry laboratories (PSDLs) usually maintain air kerma standards for kilovoltage X rays (10–300 kV) and for ^{137}Cs and ^{60}Co gamma radiation. Free air chambers (FACs) and cavity ionization chambers are used as primary air kerma standards for kilovoltage X rays and for ^{137}Cs and ^{60}Co gamma radiation, respectively. The majority of the national metrology institutes (NMIs) have signed the mutual recognition arrangement (MRA) [1] on national measurement standards and on calibration and measurement certificates issued by NMIs. The MRA has been available for signing since 14 October 1999. In accordance with the MRA, the signatories participate in Comité international des poids et mesures key comparisons carried out by the Consultative Committees or the Bureau international des poids et mesures (BIPM), which determine the key comparison reference value (KCRV). The

degree of equivalence of a national measurement standard is expressed quantitatively in terms of its deviation from the KCRV and the uncertainty of this deviation. The Consultative Committee for Ionizing Radiation (CCRI(I)) currently provides for air kerma standards three types of key comparison and one supplementary comparison. The air kerma key comparisons are organized on a bilateral basis between the air kerma standards of the BIPM and those of the participating NMIs. The radiations used are low energy (10–50 kV) and medium energy (100–250 kV) X ray beams and ^{137}Cs and ^{60}Co gamma radiation. The participation of NMIs in the relevant key comparison within a period of ten years is a requirement for their own data to be entitled to be included in the key comparison database (KCDB) for air kerma. In keeping with the long standing method of presenting the data, the CCRI(I) took the decision at its meeting in 1999 [2] to use the air kerma rate determined by the BIPM as the KCRV. This is why the BIPM air kerma standards are of particular importance.

As the air kerma key comparisons have been conducted on an ongoing basis since 1966 for low energy X rays and since 1975 for medium energy X rays and ^{60}Co gamma radiation, the results provide an invaluable database, which can be regarded as an indicator of the status of the air kerma standards operated worldwide. Consequently, this database and the NMI reports at the CCRI(I) meetings, which take place every two years, were used as an essential source of information for this paper. In accordance with the different techniques used to measure the air kerma of kilovoltage X rays and ^{137}Cs and ^{60}Co gamma radiation, this paper is divided into two main parts, one dealing with the current status and new developments of FACs and the other with those of cavity ionization chambers.

2. CURRENT STATUS AND NEW DEVELOPMENTS OF FREE AIR CHAMBER STANDARDS

All PSDLs employ FACs for the realization of the unit of air kerma in kilovoltage X ray beams. Plane-parallel and cylindrical types of different designs are in use. A review of the characteristics and design of FACs has been given by Wyckoff and Attix [3]. For a FAC standard of measuring volume V, the air kerma rate is determined by the relation:

$$\dot{K} = \frac{I}{\rho_{\text{air}} V} \frac{W_{\text{air}}}{e} \frac{1}{1 - g_{\text{air}}} k_h k_s k_d k_a k_{\text{sc}} k_e k_l k_p k_{\text{other}} \qquad (1)$$

where ρ_{air} is the density of air under reference conditions (usually T = 293.15 K, P = 101 325 Pa and h = 50%), I is the ionization current under these conditions,

W_{air} [4] is the mean energy expended by an electron to produce an ion pair in dry air, e is the elementary charge, g_{air} is the mean fraction of the initial electron energy lost by bremsstrahlung production in air and k_i is a correction factor to be applied to the standard. k_h corrects for dependencies on the air humidity, k_s for ion recombination losses, k_d for electrical field distortions, k_a for the attenuation of the photon beam in the air column lying between the defining reference plane of the aperture and the centre of the collecting volume, k_{sc} for ionization increase due to scattered photons, k_e for ionization losses caused by secondary electrons impinging on the electrodes, k_l for photon transmission through the edges of the diaphragm, k_p for photon transmission through the chamber housing and k_{other} stands for other corrections that are specific to particular chamber types or have not been taken into consideration up to now.

The air kerma determined by the BIPM is used as the KCRV and is therefore of particular importance. Values for the physical constants and correction factors used by the BIPM in the determination of the air kerma rate for low and medium energy X rays, and their estimated relative standard uncertainties, are given in Ref. [5]. The relative standard uncertainties associated with the realization of the gray for the quantity air kerma of low and medium energy X rays at the BIPM are 0.20% and 0.22%, respectively. The main component is the relative uncertainty of W_{air}/e, which is 0.15% [4]. Comparisons of BIPM and NMI standards for low energy X rays are usually made directly (i.e. by successively measuring the air kerma rate in the BIPM beam with the two standards). Five different radiation qualities with tube potentials of between 10 kV and 50 kV [5] are used. Comparisons of standards for medium energy X rays are usually made indirectly (i.e. by employing a transfer chamber, which may explain the slightly higher uncertainty of the comparison results of this kind). Four different radiation qualities with tube potentials of between 100 kV and 250 kV [5] are used. Taking into account correlations of uncertainty components between different standards, the relative standard uncertainties in $R_{K,NMI}$, which is the air kerma rate ratio measured with the NMI and BIPM standards, are typically as low as 0.25% and 0.30%. Air kerma comparisons have been made between the standards of the BIPM and of several member States of the Metre Convention that maintain primary standards of this kind. Figure 1 shows the current status of the comparison results for low and medium energy X rays. The values are taken from the relevant BIPM reports, some of which are available on the BIPM web site but are not referenced in this paper separately. The majority of the results lie within the typical expanded uncertainty claimed for the ratio $R_{K,NMI}$, indicated in the figures as dotted lines. Although the results in general are inconspicuous, there are some new developments that will further improve the

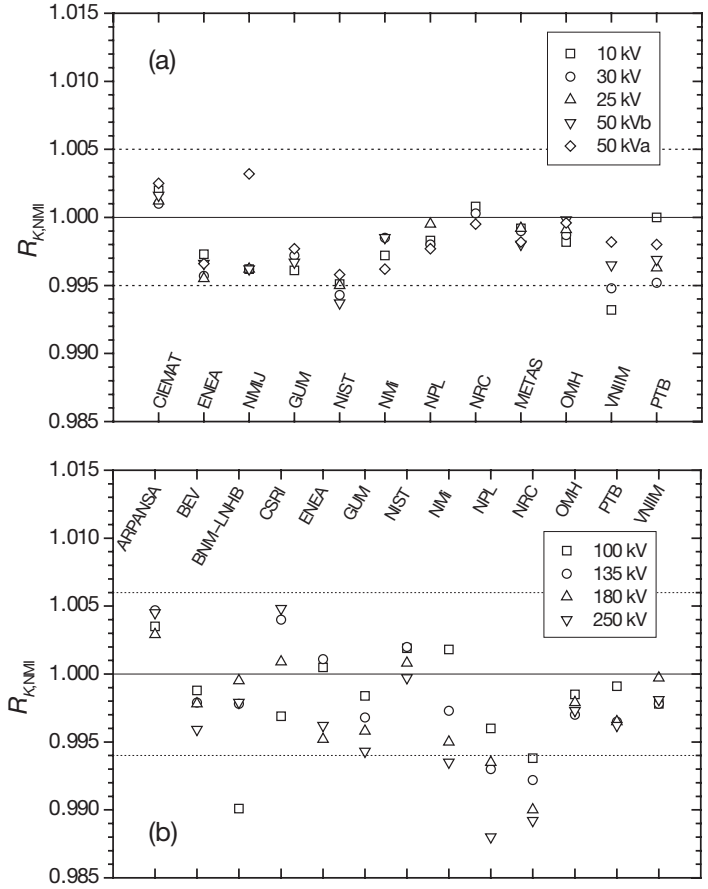

FIG. 1. Results of BIPM low (a) and medium (b) energy X ray comparisons, expressed as the ratio of the air kerma rate determined with the standard of the NMI to that determined with the BIPM standard.

consistency of the results of FAC standards. Achieving the high level of uncertainty requires an accurate evaluation of correction factors. In 1998 Grimbergen et al. [6] described a new method for the determination of X ray quality dependent correction factors for FACs. For the FAC used at the Nederlands Meetinstituut (NMi) they calculated the correction factors for electron loss, k_e, scatter inside the chamber, k_{sc}, and transmission through the diaphragm and front wall, k_{tr}, as a function of monoenergetic photons using Monte Carlo methods. Correction factors for X ray qualities were obtained as the mean of the measured distribution of the air kerma with respect to energy weighted with the calculated correction factors for monoenergetic radiation. It

is the great advantage of this new method that the correction factors need to be calculated as a function of energy only once; when new X ray qualities are introduced or when new X ray facilities are installed it is sufficient to measure the X ray spectra, and the time consuming determination of correction factors is no longer necessary.

This advantage is of importance in view of the increasing number of reference X ray qualities used in diagnostic radiology, radiotherapy and radiation protection (e.g. at the Physikalisch-Technische Bundesanstalt (PTB) about 90 different X ray qualities are in use). In addition, new correction factors obtained by improvement in FAC modelling can easily be introduced. For instance, the PTB has applied the new method for the re-evaluation of the correction factors of its parallel-plate and cylindrical FAC standards using the EGS4 Monte Carlo code [7]. The newly calculated correction factors were first introduced when the PTB compared its standards with the BIPM and Országos Mérésügyi Hivatal (OMH) in 1999 [8–10]. In particular, the PTB correction factor, k_{sc}, included not only the effect of scattered photons but also that of fluorescence photons emitted after photoelectric absorption by argon and subsequently absorbed in the collecting volume. The inclusion of such effects is necessary, as by definition fluorescence photons are not part of the kerma. This contribution had not been considered before for any FAC. In dependence on the dimension of the collecting volume, the correction for this effect can be significant (from 0.2% to 0.5%) for low energy X ray beams. The correction factor k_{sh}, which is specific to the PTB's cylindrical FAC design and corrects for the shadow effect of the central collector, was also calculated with the EGS4 code. Results for k_{sc} and k_{sh} are shown in Fig. 2.

Burns [11, 12] calculated FAC correction factors for electron loss, photon scatter, fluorescence and bremsstrahlung for the BIPM standards and for all other FAC standards worldwide. This set of correction factors is intended for use by all NMIs maintaining FAC standards, and, if they agree, significant improvements in consistency can be expected. At the 15th Meeting of the CCRI(I) it was agreed that the BIPM will implement these new results for its standards before publication in appendix B to the MRA, and that the NMIs will notify the CCRI(I) through the BIPM when similar corrections are included in their standards [13].

3. CURRENT STATUS AND NEW DEVELOPMENTS OF CAVITY IONIZATION CHAMBER STANDARDS

All PSDLs employ graphite cavity ionization chambers to realize the unit of air kerma for ^{137}Cs and ^{60}Co gamma radiation. Cylindrical, pancake,

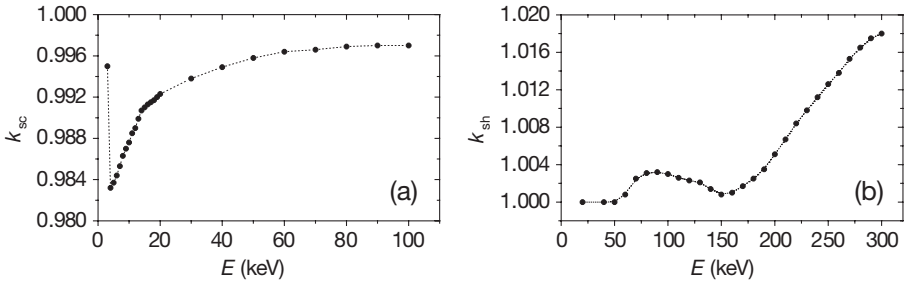

FIG. 2. Correction factors (a) k_{sc} and (b) k_{sh}, calculated with the EGS4 Monte Carlo code, as a function of the energy of the incident photon beam. k_{sc} corrects for ionization gain caused by scattered photons in the collecting volume of the PTB parallel-plate FAC PK100. In particular, k_{sc} contains contributions from fluorescent photons preferentially emitted by argon atoms in the air. At 3 keV only Rayleigh and Compton scattered photons are present, whereas at 4 keV, in addition, 3.2 keV argon K fluorescence photons contribute, which explains the drop-off in the curve. k_{sh} corrects for the shadow effect of the central electrode of the cylindrical PTB FAC. The photon beam enters the chamber with its axis 4.5 cm below the central electrode. The central electrode has a diameter of 7.5 mm and secondary electrons can impinge on the electrode, leading to a loss of ionization in the collecting volume. Below 50 keV the range of the secondary electrons is less than 4.5 cm and k_{sh} = 1. Above 50 keV some photoelectrons reach the central electrode, leading to an increase until the photoelectric interactions are less probable and Compton interactions begin to dominate. As the Compton electrons have less energy than the photoelectrons, k_{sc} first decreases until it rises again due to the increasing energy of the Compton electrons.

spherical and ovoid type chambers of different designs and measuring volumes are in use. According to the Spencer–Attix relationship, for a parallel beam of photons the air kerma rate, $\dot{K}_{\text{air}}$, at the reference point of a graphite cavity ionization chamber in the absence of the chamber is given by:

$$\dot{K}_{\text{air}} = \frac{W_{\text{air}}}{e}\frac{I}{\rho_{\text{air}} V}\frac{1}{1-\bar{g}}\left(\frac{\bar{\mu}_{\text{en}}}{\rho}\right)_{\text{ac}} \bar{s}_{\text{ca}}\, k_h k_s k_{\text{st}} k_{\text{at}} k_{\text{sc}} k_{\text{cep}} k_{\text{an}} k_{\text{rn}} k_{\text{other}} \qquad (2)$$

where ρ_{air} is the density of air under reference conditions, I is the ionization current under these conditions, W_{air} is the mean energy expended by an electron to produce an ion pair in air, e is the elementary charge, $\bar{g}$ is the mean fraction of energy lost due to bremsstrahlung, $(\bar{\mu}_{\text{en}}/\rho)_{\text{ac}}$ is the ratio of air to graphite of the mean mass energy absorption coefficients, $\bar{s}_{\text{ca}}$ is the ratio graphite to air of the mean restricted mass stopping powers and k_i is a correction factor to be applied to the standard. k_h corrects for dependencies on

the air humidity, k_s for ion recombination losses, k_{st} for chamber stem scattering, k_{at} and k_{sc} for the attenuation and scattering of photons in the chamber wall, k_{cep} for the mean origin of electrons, k_{an} and k_{rn} for the axial and radial non-uniformity of the beam and k_{other} stands for other corrections that are specific to special chamber types or that have not been taken into consideration up to now. The product $k_{at}k_{sc}k_{cep}$ is often summarized as k_{wall}, the correction factor for wall effects.

The air kerma determined by the BIPM is used as the KCRV and is therefore of particular importance. Values of the physical constants and correction factors used in the BIPM determination of the air kerma rate for ^{137}Cs and ^{60}Co gamma radiation, and their estimated relative standard uncertainties, are given in Ref. [5]. The relative standard uncertainties associated with the realization of the gray for the quantity air kerma for ^{137}Cs and ^{60}Co gamma radiation at the BIPM are 0.24% and 0.17%, respectively. Taking into account correlations of uncertainty components between different standards (usually the physical constants entering Eq. (2) and k_h) the relative standard uncertainties in $R_{K,NMI}$, which is the air kerma rate ratio measured with the NMI and BIPM standards in the same radiation field, are typically as low as 0.3% and 0.2%, respectively. Air kerma rate comparisons for ^{137}Cs and ^{60}Co gamma radiation have been made between standards of the BIPM and those of several member States of the Metre Convention that maintain primary standards of this kind.

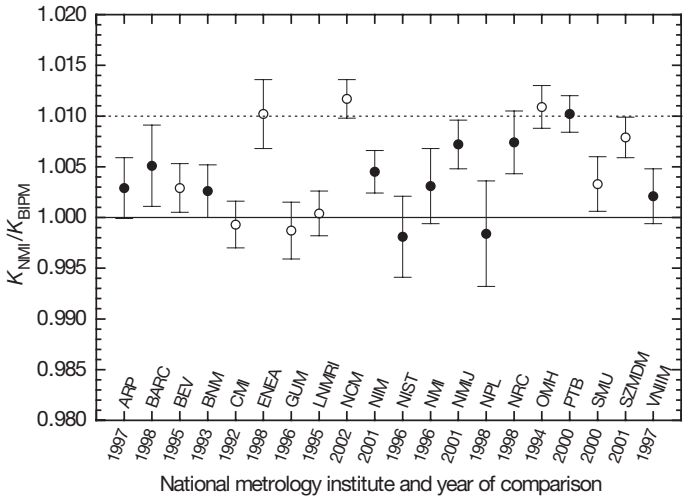

FIG. 3. Results of the BIPM ^{60}Co gamma radiation comparison, expressed as the ratio of the air kerma rate determined with the standard of the NMI to that determined with the BIPM standard. The open symbols indicate that the standard used by the NMI is of the CCO1 design.

Figure 3 shows the current status of the comparison results for ^{60}Co gamma radiation of 20 different NMIs. The values are taken from the relevant BIPM reports, some of which are available on the BIPM web site but are not referenced in this paper separately. The value of the National Research Council of Canada includes the most recent results published in Ref. [14]. There appear to be two groups of results, each of which in itself is inconspicuous within the estimated uncertainties but different from each other by about 1%. This deviation is highly significant, because it is about five times the standard uncertainty of the comparison. The reason for this discrepancy is that different methods are used for the determination of the correction factors k_{wall} and k_{an}. The group with the higher values has re-evaluated k_{wall} and k_{an} by Monte Carlo calculations in accordance with methods developed by Bielajew and Rogers (Ref. [15] and references therein) and Rogers and Treurniet [16].

Because of their particular importance for the current status of air kerma standards based on cavity chambers, it is justified to deal with the correction factors k_{wall} and k_{an} in more detail. The traditional way to determine k_{wall} is to measure the ionization current as a function of wall thickness, which is varied by adding layers of wall material to all sides of the chamber and then extrapolating the measured curve to zero wall thickness. The value obtained is assumed to account for the effects of the attenuation and scattering of photons in the wall, often written as $k_{\mathrm{at}}k_{\mathrm{sc}}$, which must, however, be multiplied by a calculated value of k_{cep}, which shifts the extrapolation point from zero to a mean wall thickness associated with the centre of electron production. Note that from this definition it follows that k_{cep} is less than 1 as long as the chamber response decreases with increasing wall thickness. The alternative is to calculate k_{wall} directly by Monte Carlo methods using an approach described by Rogers and Bielajew [17]. The principle of this approach is illustrated in Fig. 4.

The following equations become evident from Fig. 4:

$$k_{\mathrm{at}} = \frac{\sum_i E_{i,0} e^{\mu_i s_i}}{\sum_i E_{i,0}} \tag{3}$$

$$k_{\mathrm{sc}} = \frac{\sum_i E_{i,0}}{\sum_i (E_{i,0} + E_{i,1})} \tag{4}$$

In Eq. (3) the energy $E_{i,0}$, deposited by electrons generated from the ith primary photon interaction, is weighted with $e^{\mu_i s_i}$, where μ_i is the linear attenuation coefficient and s_i is the photon path length in the wall material to the first interaction point. The weighted sum is the total energy that would be

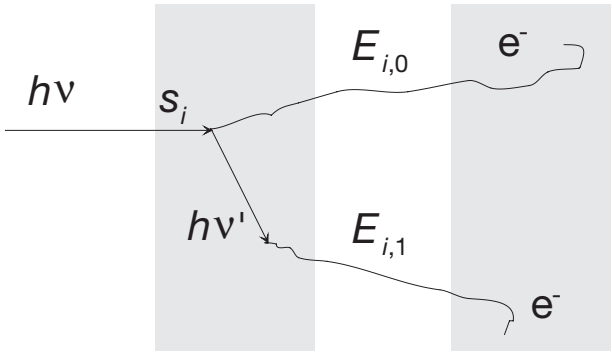

FIG. 4. A photon of energy hν enters the wall of a cavity chamber. After a path of length s_i, the first interaction occurs, producing a scattered photon of energy hν′ and an electron that travels through the cavity and deposits the energy, $E_{i,0}$, in the gas. The scattered photon interacts within the wall and produces an electron that travels through the cavity, thereby depositing the energy, $E_{i,1}$, in the gas.

deposited in the cavity gas by electrons if there was no photon attenuation in the chamber wall. The correction factor for photon attenuation in the wall is the weighted sum divided by the total energy deposited in the cavity by electrons of the first generation when photons are attenuated in the wall. The correction factor for the increase in deposited energy in the cavity gas due to electrons generated by scattered photons in the wall is the total energy deposited in the cavity by electrons of the first generation divided by the sum of the total energies deposited in the cavity by electrons of the first generation and those of all higher generations, expressed in Eq. (4). From Eq. (3) it is obvious that the factor k_{cep} is included in the calculation of k_{at}. The calculated values of k_{wall} differ significantly from those obtained by the extrapolation method [16]. For instance, k_{wall} of the cylindrical cavity chamber of the CCO1 design, which is the standard mostly used for comparison with the BIPM (see Fig. 3), equals 1.022 if calculated and 1.013 if determined by the extrapolation method. The difference is more than four times the standard uncertainty currently estimated for the determination of the quantity of air kerma with cavity chambers.

A controversial discussion about the correction factor k_{an} was triggered in 1990 by Bielajew [18, 19], who presented an analytical theory of the point source non-uniformity correction factor, k_{pn}, for thick walled ionization chambers in photon beams. To avoid any confusion about the correction factors k_{an}, k_{rn} and k_{pn} it is instructive to review their meaning. The following description was adopted from the introduction of Bielajew's paper:

> "When a detector is placed in the field of a radiation source, the point at which the radiation field is being measured is uncertain, owing to the finite size of the detector. In the realm of exposure and air kerma measurement performed in standards laboratories, one usually assumes that the 'point of measurement' is at the geometric centre of the chamber and the corrections for the departure in ion chamber response from the inverse-square law is accounted for by the 'axial' and 'radial' non-uniformity correction factors, k_{an} and k_{rn}, respectively. The axial factor is a correction for the non-uniformity of the photon field along the line from the source through the cavity centre while the radial factor accounts for non-uniformity in the transverse direction. The radial correction also accounts for the transverse field non-uniformity due to finite-size source effects and scatter from the collimator and room."

The latter complicates comparison of k_{an} and k_{rn} with the point source non-uniformity correction factor k_{pn}, as defined in the analytical theory of Bielajew, which is based on the assumption of an ideal point source. Certainly k_{pn} contains all of k_{an} and a portion of k_{rn}. In practice, the transverse field non-uniformity distribution with respect to the associated centre is measured with small ionization chambers, and k_{rn} of standard cavity chambers is calculated based on the measured distribution. In contrast, k_{an} is calculated using different theoretical models, which yield inconsistent results, since generally there are two divergent views as to how such a correction is to be applied.

Rogers et al. [16] calculated k_{pn} by the Monte Carlo method as:

$$k_{pn} = \frac{D_{gas}^{parallel} k_{wall}^{parallel}}{D_{gas}^{point} k_{wall}^{point}} \tag{5}$$

where D_{gas} is the calculated dose to the cavity gas per incident unit of fluence at the reference point of the chamber for a parallel or point source beam and k_{wall} is the wall correction factor in the same cases. The results obtained were consistent with the previous analytical calculations of Bielajew [19]. If k_{pn} is assumed to be close to the traditional definition of k_{an}, the old k_{an} values should be replaced by the newly calculated k_{pn}, and k_{rn} should be applied in the traditional way. In accordance with this concept, there are significant changes in k_{an}, of up to 0.94% in the most extreme case [16].

For more than ten years there has been an intense discussion [15–20] on the validity of the calculated k_{wall} and k_{an} values, which has led to the current unsatisfactory situation reflected in Fig. 3. Rogers and Treurniet [16] reported new results of k_{wall} and k_{an} correction factors calculated by improved Monte Carlo techniques for a wider range of primary standard cavity chambers and

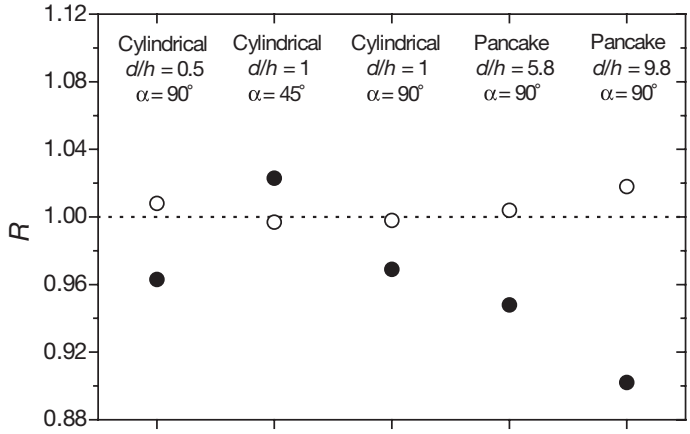

FIG. 5. Ratios $R = (I(\alpha)k_{wall}(\alpha))/(I(0°)k_{wall}(0°))$ of the ionization currents of differently shaped cavity chambers corrected for wall effects at different angles, α, of radiation incidence in a ^{60}Co field and the values obtained at normal incidence, $\alpha = 0°$. d/h is the ratio of the inner diameter and height of the chamber. For consistent correction factors, k_{wall}, the ratios should be close to 1. This is the case for the calculated values, R_{calc} (open symbols). In contrast, the ratios obtained with the extrapolation method, R_{extr} (solid symbols), display substantial deviations from 1.

extended to both ^{60}Co and ^{137}Cs radiation. It was demonstrated that the Monte Carlo calculations were capable of reproducing the measured relative response of a cavity chamber as a function of the wall thickness to well within 0.2%. Application of the new correction factors to the BIPM chamber and different cavity chambers used by NMIs as primary standards increased the mean value of the measured air kerma rate by about 0.8% for both ^{137}Cs and ^{60}Co beams. However, the variation between standards had slightly increased and consequently the results were not suitable for giving experimental evidence of the validity of the calculations. At the 15th Meeting of the CCRI(I), Büermann et al. [21] presented a collaborative work of the PTB and the OMH, in which experimental tests of calculated versus extrapolated wall corrections provided clear evidence that the calculated wall corrections produced consistent agreement using four differently shaped cavity chambers at various, unusual orientations, whereas wall corrections obtained by extrapolation produce highly discrepant results (see Fig. 5).

Csete et al. [22] reported on the results of a recent direct comparison of the primary standards of the PTB and the OMH, in which close agreement was found for both ^{137}Cs and ^{60}Co radiation using k_{wall} and k_{an} correction factors calculated with the EGSnrc code [23]. In particular, one of the chambers

involved in the comparison (PTB-HRK-3) was a pancake type chamber similar to the design of the BIPM pancake type standard chamber, and the OMH standard ND1005 was of the same design as the CCO1 standards, which are the standards mostly used for comparison with the BIPM (see Fig. 3). The consistency of the results strongly confirms the accuracy of the calculated correction factors applied, which is in contrast to the findings of the work by Boutillon [20]. As a consequence, the OMH declared new values for its standard [24] and began disseminating it, and the PTB followed the OMH's lead, starting on 1 January 2002 [25]. In accordance with these results, all chambers of the CCO1 design in Fig. 3 move towards the upper group. These results were further confirmed by the work carried out at ENEA by Laitano et al. [26], in which the k_{wall} correction of the ENEA CCO1 type standard was determined by various (experimental, analytical and Monte Carlo) methods. As a result, ENEA has adopted the Monte Carlo correction from EGSnrc calculations [16]. Rogers et al. [13] presented results that indicate the insensitivity of the Monte Carlo results for k_{wall} both to details of the electron transport algorithms and to the assumed incident photon spectra. Seltzer [13] presented preliminary k_{wall} values for the (spherical) NIST chambers calculated with the Integrated Tiger Series (ITS) code, which were essentially in agreement with the EGSnrc results published by Rogers et al. [16]. Application of the new correction factors would imply an increase in the NIST determination of the air kerma rate at ^{60}Co gamma radiation of about 0.9% and moves the NIST value in Fig. 3 towards the upper group. Recently, Shortt et al. [27] reported on the effect of the wall thickness on the response of a spherical ionization chamber in a ^{137}Cs beam. They found a non-linear extrapolation curve in agreement with the theoretical prediction by Bielajew [28]. The wall correction factor obtained using non-linear extrapolation was in good agreement with the result obtained by Monte Carlo techniques. This work supports the validity of calculated wall correction factors for spherical chambers.

The BIPM announced a work programme based on Monte Carlo calculations with EGSnrc and with PENELOPE, coupled with experimental measurements. When completed, this work on wall and beam non-uniformity corrections will form the basis for new correction factors for the BIPM standards [13]. Several NMIs are currently re-evaluating k_{wall} and k_{an}, and this in the future may well change the overall picture for the comparison results. The current situation raises problems in connection with the KCDB and the definition of the degree of equivalence of primary standards with the key comparison reference value. In order to find a practical solution, at its 15th Meeting in 2001 the CCRI(I) proposed a procedure, to be finalized before its next meeting in 2003, for entering consistent data into the KCDB.

4. CONCLUSION

Undoubtedly the most important new development is the re-evaluation of several correction factors needed for cavity ionization chamber standards. However, there have also been interesting developments using Monte Carlo techniques and spectrometry for the determination of X ray quality dependent correction factors of FACs. Although the application of consistent correction factors improves the degree of equivalence of the national standards, the further decrease of the uncertainty of air kerma determination needs improvements in the determination of the values for W_{air}, $(\bar{\mu}_{en}/\rho)_{ac}$ and $\bar{s}_{ca}$. The expected increase by about 0.8% in the absolute value for the air kerma rate determination for ^{60}Co gamma radiation may give rise to the question of whether the consistency of measured and calculated ratios of air kerma rate and absorbed dose rate to water for ^{60}Co gamma radiation is affected. Currently, work is in progress at the PTB to measure and calculate this ratio by applying different experimental and theoretical methods.

REFERENCES

[1] Mutual Recognition of National Measurement Standards and of Calibration and Measurement Certificates Issued by National Metrology Institutes, Comité international des poids et mesures, Sèvres (1999).

[2] BUREAU INTERNATIONAL DES POIDS ET MESURES, "Analysis of key comparisons and the role of bilateral and regional comparisons", 16th Mtg Consultative Committee for Ionizing Radiation, BIPM, Sèvres (1999) 146.

[3] WYCKOFF, H.O., ATTIX, F.A., "Design of free-air ionization chambers", National Bureau of Standards Handbook 64, US Government Printing Office, Washington, DC (1957).

[4] BOUTILLON, M., PERROCHE-ROUX, A.-M., Re-evaluation of the W value for electrons in dry air, Phys. Med. Biol. **32** (1987) 213.

[5] BOUTILLON, M., ALLISY-ROBERTS, P.J., BURNS, D.T., Measuring Conditions Used for the Calibration of Ionization Chambers at the BIPM, Rep. BIPM-01/04, Bureau international des poids et mesures, Sèvres (2001).

[6] GRIMBERGEN, T.W.M., VAN DIJKD, E., DE VRIES, W., Correction factors for the NMi free-air ionization chamber for medium-energy X-rays calculated with the Monte Carlo method, Phys. Med. Biol. **43** (1998) 3207–3224.

[7] NELSON, W.R., HIRAYAMA, H., ROGERS, D.W.O., The EGS4 Code System, Rep. SLAC-265, Stanford Linear Accelerator Center, Stanford, CA (1985).

[8] BURNS, D.T., BÜERMANN, L., KRAMER, H.-M., LANGE, B., Comparison of the Air-kerma Standards of the PTB and the BIPM in the Low-energy X-ray Range, Rep. BIPM-01/08, Bureau international des poids et mesures, Sèvres (2001).

[9] BURNS, D.T., BÜERMANN, L., KRAMER, H.-M., LANGE, B., Comparison of the Air-kerma Standards of the PTB and the BIPM in the Medium-energy X-ray Range, Rep. BIPM-02/07, Bureau international des poids et mesures, Sèvres (2002).
[10] CSETE, I., BÜERMANN, L., KRAMER, H.-M., LANGE, B., Comparison of the PTB and OMH Air Kerma Standards for Medium Energy X-rays, Rep. PTB-DOS-35, Physikalisch-Technische Bundesanstalt, Braunschweig (2000).
[11] BURNS, D.T., Consistent Set of Calculated Values for Electron-loss and Photon-scatter Corrections for Parallel-plate Free-air Chambers, Working Doc. CCRI(I)/99-4, Bureau international des poids et mesures, Sèvres (1999).
[12] BURNS, D.T., Free-air Chamber Correction Factors for Electron Loss, Photon Scatter, Fluorescence and Bremsstrahlung, Working Doc. CCRI(I)/01-36 rev, Bureau international des poids et mesures, Sèvres (2001).
[13] BUREAU INTERNATIONAL DES POIDS ET MESURES, "Comparisons of measurement standards (x- and γ-rays)", 17th Mtg Consultative Committee for Ionizing Radiation, BIPM, Sèvres (2001) 167.
[14] ROGERS, D.W.O., KAWRAKOW, I., Monte Carlo calculated correction factors for primary standards of air-kerma, Med. Phys. (in press).
[15] BIELAJEW, A.F., ROGERS, D.W.O., Implications of new correction factors on primary air kerma standards in ^{60}Co beams, Phys. Med. Biol. **37** (1992) 1283–1291.
[16] ROGERS, D.W.O., TREURNIET, J., Monte Carlo Calculated Wall and Axial Non-uniformity Corrections for Primary Standards of Air Kerma, Rep. PIRS-663, National Research Council, Ottawa (1999).
[17] ROGERS, D.W.O., BIELAJEW, A.F., Wall attenuation and scatter corrections for ion chambers: Measurements versus calculations, Phys. Med. Biol. **35** (1990) 1065–1078.
[18] BIELAJEW, A.F., Correction factors for thick-walled ionization chambers in point-source photon beams, Phys. Med. Biol. **35** (1990) 501–516.
[19] BIELAJEW, A.F., An analytical theory of the point-source non-uniformity correction factor for thick-walled ionization chambers in photon beams, Phys. Med. Biol. **35** (1990) 517–538.
[20] BOUTILLON, M., About the Determination of the Wall Correction in Cavity Chambers, Working Doc. CCRI(I)/99-3, Bureau international des poids et mesures, Sèvres (1999).
[21] BÜERMANN, L., KRAMER, H.-M., CSETE, I., Results Supporting Calculated Wall Correction Factors for Cavity Chambers (in preparation).
[22] CSETE, I., BÜERMANN, L., KRAMER, H.-M., Comparison of the PTB and OMH Air Kerma Standards for ^{60}Co and ^{137}Cs Gamma Radiation, Rep. PTB-DOS-40, Physikalisch-Technische Bundesanstalt, Braunschweig (2002).
[23] KAWRAKOW, I., ROGERS, D.W.O., The EGSnrc Code System: Monte Carlo Simulation of Electron and Photon Transport, Rep. PIRS-701, National Research Council, Ottawa (2000).

[24] CSETE, I., New Correction Factors for the OMH Air Kerma Standard for ^{137}Cs and ^{60}Co Radiation, Working Doc. CCRI(I)/01-03, Bureau international des poids et mesures, Sèvres (2001).
[25] KRAMER, H.-M., BÜERMANN, L., AMBROSI, P., Change in the realization of the gray at the PTB, Metrologia **39** (2002) 111–112.
[26] LAITANO, R.F., TONI, M.P., PIMPINELLA, M., BOVI, M., Determination of the k_{wall} correction factor for a cylindrical ionization chamber to measure air-kerma in ^{60}Co gamma beams, Phys. Med. Biol. **47** (2002) 2411–2431.
[27] SHORTT, K.R., et al., The effect of wall thickness on the response of a spherical ionization chamber, Phys. Med. Biol. **47** (2002) 1721–1731.
[28] BIELAJEW, A.F., On the technique of extrapolation to obtain wall correction factors for ion chambers irradiated by photon beams, Med. Phys. **17** (1990) 583–587.

BLANK

CALCULATION OF WALL AND NON-UNIFORMITY CORRECTION FACTORS FOR THE BUREAU INTERNATIONAL DES POIDS ET MESURES AIR KERMA STANDARD FOR ^{60}Co USING THE MONTE CARLO CODE PENELOPE

D.T. BURNS
Bureau international des poids et mesures,
Sèvres
E-mail: dburns@bipm.org

Abstract

Following the installation of a new ^{60}Co facility at the Bureau international des poids et mesures (BIPM), a detailed model of the new source was constructed using the Monte Carlo code PENELOPE. Using this calculated photon spectrum, the wall correction factor, k_{wall}, for the BIPM primary air kerma standard has been re-evaluated. The result k_{wall} = 1.0017 (statistical uncertainty 0.0001) is in close agreement with that obtained using the EGSnrc code and also agrees within the uncertainties with the measured value in use at present. It is argued that the present methods for evaluating the axial non-uniformity correction may be flawed, and preliminary results are presented to support this view. The need to consider electron fluence perturbations is discussed.

1. BACKGROUND

The installation of a new ^{60}Co facility at the Bureau international des poids et mesures (BIPM) has made necessary a re-evaluation of the correction factors for the BIPM primary standard for air kerma in this new beam. This paper describes the Monte Carlo calculation of the correction factors for wall attenuation and scatter, k_{wall}, and axial non-uniformity, k_{an}. Given that almost all the comparable calculations to date have used the EGS code [1, 2], it was considered that using a different code would yield a more robust estimate of the uncertainties. This led to the use of PENELOPE [3].

The BIPM standard is a graphite walled parallel-plate ionization chamber with a central collecting plate [4]. Serial number CH5-1 has been modelled; its graphite density is 1.811 g/cm^2. The chamber dimensions are: external diameter 50.5 mm, front and rear wall thickness each 2.83 mm, air cavity diameter 45 mm, thickness 5.16 mm, graphite collector diameter 41 mm and thickness 1 mm. The collector divides the air cavity into two equal thicknesses (each 2.08 mm). The small support for the collector has not been modelled, nor have the electrical connections and the chamber stem.

1.1. Wall correction

The product of the correction factors k_{att} and k_{sc}, which account for photon attenuation and scattering, respectively, in the walls of cavity ionization chambers, has traditionally been evaluated experimentally using an extrapolation method. This method involves measuring the change in ionization current as additional wall material is added, the resulting data being extrapolated to zero wall thickness. This is known to result in overcorrection, because the electrons giving rise to the ionization current are generated at some mean distance from the inner surface of the wall, and so the effective wall thickness for photon attenuation and scattering is less than the actual thickness. This is compensated for using the correction factor k_{cep} for the centre of electron production. The total wall correction, k_{wall}, is the product $k_{att}k_{sc}k_{cep}$.

The extrapolation method would be expected to work well under the ideal conditions of a parallel photon beam incident on a semi-infinite parallel-plate chamber arrangement. However, it is not clear that the extrapolation method will correctly account for attenuation and scattering in the side wall of a real parallel-plate chamber, nor in the curved wall of spherical and cylindrical standards. It should work best for a parallel-plate chamber of large radius, and the BIPM standard was designed with this in mind. For serial number CH5-1 the values in use for the older ^{60}Co source are k_{att} = 1.0396 (standard uncertainty 0.0004), k_{sc} = 0.9720 (0.0007) and k_{cep} = 0.9922 (0.0001), giving k_{wall} = 1.0026 (0.0008).

Bielajew [5] developed a theory for the wall correction that demonstrates the problems associated with the extrapolation method for certain chamber types. Calculations of k_{wall} have been made using the Monte Carlo codes EGS4 [1] and EGSnrc [2] that support these conclusions [6–8]. Values for k_{wall} have been proposed that, if adopted by each laboratory concerned, would have a significant effect on the results of international comparisons of air kerma primary standards. For the BIPM standard, Rogers and Treurniet [8] calculated the value k_{wall} = 1.0014, which is in moderate agreement with the value in use (the statistical standard uncertainty of the calculated value is less than 0.0001, but no overall uncertainty is given in Ref. [8]).

1.2. Non-uniformity correction

For an ideal point detector and a point source of photons, the detector response with distance should follow the inverse square law. However, for a real detector in a real beam this is not the case. The photon distributions radially and axially differ from those for a point source because of the effects of the finite source size, photon scattering in the source, source containment and

collimator, as well as photon scatter from the room and surrounding materials. The deviation from inverse square behaviour also depends on the size and shape of the detector and on the distance from the source. It is common practice to correct separately for radial and axial non-uniformity effects through the use of the factors k_{rn} and k_{an}, respectively. The factor k_{rn} is generally determined from data acquired by scanning radially with a small ionization chamber. The evaluation of k_{an} is the source of some debate. Bielajew [9] developed a theory for the point source non-uniformity correction factor k_{pn}. This factor is closely related to k_{an}, and the two have generally been used interchangeably.

One interpretation of k_{an} for cavity ionization chambers is in terms of the effective point of measurement. As noted above, the electrons giving rise to the ionization current are generated at some mean distance from the inner surface of the wall, and therefore at some mean distance, Δ, closer to the source than the chamber centre. At this closer distance in a divergent beam the photon fluence is greater and the chamber might be expected to over-read, giving rise to a correction factor of the form:

$$k_{an} = [(d - \Delta)/d]^2 \quad (1)$$

where d is the distance from the source to the chamber centre. This is the basis of the BIPM correction factor, although a more sophisticated model has been used [4] that gives the value $k_{an} = 0.9964$ (0.0007) for a distance, d, of 1 m.

By definition, no non-uniformity correction would be required in a parallel photon field, and the correction factor, k_{pn}, defined in Bielajew [9] may be evaluated as the ratio of the energy deposited in the air cavity by a parallel source to that for a point source, each corrected for attenuation and scatter in the chamber wall. Rogers and Treurniet [8] used the Monte Carlo code EGSnrc [2] to calculate k_{pn} using this method (although they used the terminology k_{an}). For the BIPM standard they obtained $k_{pn} = 1.0024$ (0.0003), which is very different from the BIPM value for k_{an}.

2. MONTE CARLO CALCULATIONS

2.1. Realistic source simulation

The new ^{60}Co source, container, head and collimating jaws were simulated in detail using the PENELOPE geometry code PENGEOM, as shown in Fig. 1. More than 50 components were modelled. The collimator bars and central support (yellow) are of lead, except for the final trimmer bar in each jaw (green), which is of depleted uranium. A steel bar (violet) supports each jaw.

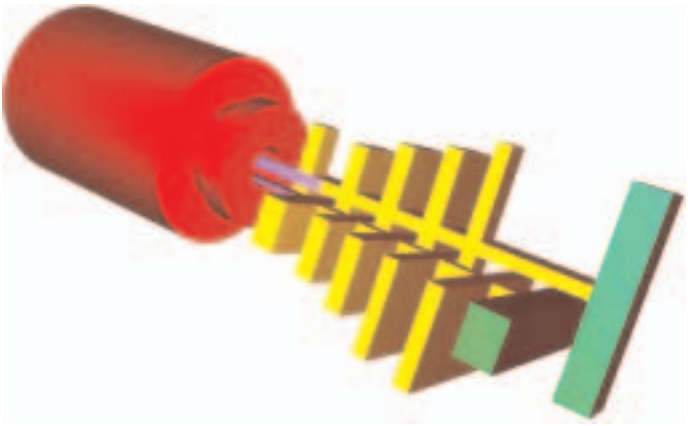

FIG. 1. Model used for the new ^{60}Co source. Only one of each pair of collimating jaws is shown.

The source shielding and primary collimator (red) are of tungsten. Not visible in the figure are the details of the cylindrical source container, which is of stainless steel 23.6 mm in diameter and 37 mm long, with a 1 mm front wall and 3 mm rear wall. The source itself is 20 mm in diameter and 14 mm long, behind which (inside the source container) there is an 11 mm stack of steel discs and an 8 mm air space.

This model was used to create a full phase space file in the plane 90 cm from the source, including information on the type, energy, angle and position of all particles crossing this plane. The photon transport cut-off energy was set to 25 keV. Initial calculations with an electron transport cut-off of 50 keV showed that only 0.5% of the particles in the phase space file were electrons, which could be neglected without loss of accuracy. Raising the electron transport cut-off to 1.25 MeV (i.e. no electron transport) resulted in a speed increase by a factor of more than 20. The resulting neglect of bremsstrahlung reduced the photon energy fluence by only 0.2%, which should have a negligible effect on the results.

Figure 2 shows the normalized distribution of photon number with energy in the phase space plane within a radius of 2.5 cm of the beam axis. A counter was used in PENELOPE to label each particle with its body of origin. In this way the scattered photon contribution from each physical component was identified, as indicated in Fig. 2. The photon scatter component, expressed in terms of energy fluence, is around 21% (compared with around 14% for the older source) and arises mainly from forward-scattering in the source and its container. Only 3% of the photon energy fluence comes from scatter in the collimator.

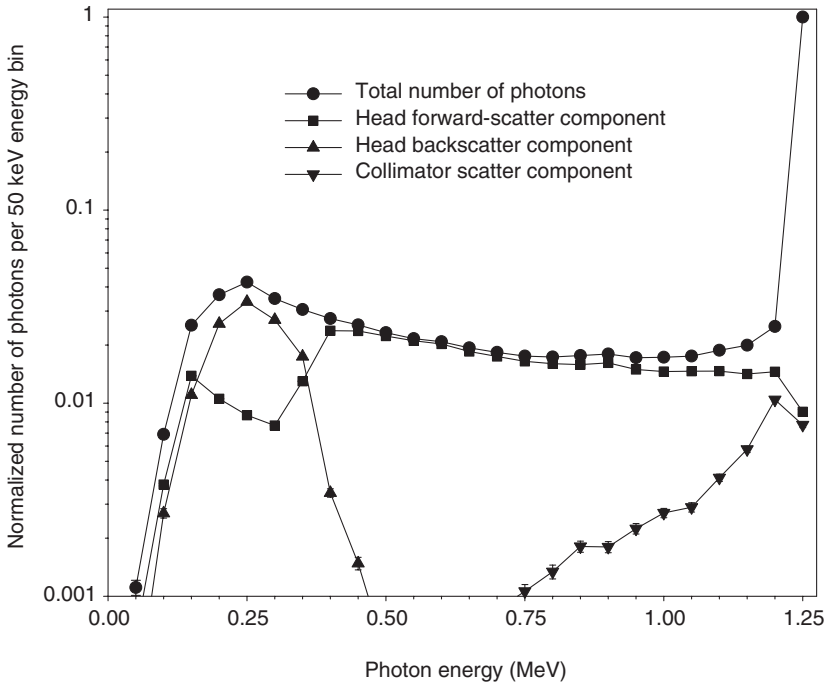

FIG. 2. Distribution of photon number with energy at 90 cm from the source and within 2.5 cm of the beam axis. 10^9 photon histories were required to generate this spectrum of 10^6 photons.

2.2. Method of calculating k_{wall}

The phase space file was used as input to the calculation of k_{wall} for the BIPM standard using the technique of photon regeneration [9]. At the point of interaction of each incident photon in the chamber wall and in the central collector, a new photon is generated that has the same energy and direction as the incident photon. These regenerated photons and their progeny are labelled to allow the separate scoring of energy deposition in the air cavity due to incident, E_{inc}, and regenerated, E_{reg}, photons. The wall attenuation correction is evaluated as:

$$k_{att,MC} = (E_{inc} + E_{reg})/E_{inc} \quad (2)$$

where the subscript MC denotes a calculated value. At the same time, any outgoing scattered photon is also labelled and any subsequent energy deposition scored as E_{sc}. The wall scatter correction is:

$$k_{sc,MC} = E_{inc}/(E_{inc} + E_{sc}) \quad (3)$$

The total wall correction, k_{wall}, is the product $k_{att,MC}k_{sc,MC}$. Note that, by the nature of the calculation, no explicit correction, k_{cep}, is required and only k_{wall} is directly comparable with the measured value. Before making the full calculations, many test calculations were made to optimize the transport parameters. An important finding of this work was the need to match the electron transport cut-off energy in the air cavity to that in the walls and central collector. The calculated energy deposited in the air cavity is extremely sensitive to this matching. For example, for a cut-off energy of 50 keV in the walls and central collector and 10 keV in the air cavity, the energy deposited in the air cavity is underestimated by more than 15%. This may be interpreted in terms of a disturbance of the electron equilibrium at the interface of the air cavity and the front wall.

The final choice for the transport cut-off energy was 10 keV for electrons and 1 keV for photons, in all components. The maximum electron step length was set to 0.1 mm in the cavity and collector, 0.2 mm in the walls and 10 mm in the ambient air. (For the remaining user defined parameters in PENELOPE, the following values were used: C1 = C2 = 0.05, WCC = 10 keV and WCR = –1.)

2.3. Method of calculating k_{an}

It is argued in this paper that the basis of Eq. (1) is flawed because the divergent photon field will give rise to an electron field with the same divergence. Although the Compton process yields an angular distribution of electrons, the mean electron angle is zero with respect to the originating photon. Thus although the higher photon fluence at $(d - \Delta)$ will indeed yield a correspondingly higher electron fluence than at d, the divergence of the electron field will result in an electron fluence at d that reflects the photon fluence at d and not that at $(d - \Delta)$. By implication, the existence of a finite distance Δ between the cavity centre and the mean origin of the electrons giving rise to the energy deposited in the cavity should not in itself result in the need for an axial non-uniformity correction. This point of view was argued by Day [10] as early as 1956.

It is further postulated that the method proposed by Bielajew [9] and used by Rogers and Treurniet [8] to calculate k_{pn} for the BIPM standard may contain a component related to the perturbation of the electron fluence by the air cavity. In particular, if the fluence perturbation is not negligible and is different for point and parallel sources, the resulting value for k_{pn} will include this difference.

In order to test these hypotheses, a procedure is being developed for the BIPM standard that uses a series of chamber models and Monte Carlo calculations to describe, step by step, the entire conversion from the air kerma at the reference point to the mean energy deposited in the air cavity. This results in a self-consistent set of correction factors, including k_{wall}, k_{rn}, k_{an} and a new factor, k_{fl}, which corrects for the perturbation of the electron fluence by the air cavity. The central element of this procedure is an idealized model of the BIPM standard, for which the electron fluence perturbation is negligible and the use of the Bragg–Gray cavity theory justified. The main advantage of this step by step approach is that the electron fluence perturbation is treated explicitly, and effects related to radial and axial non-uniformity are separated from those arising from the fluence perturbation.

3. RESULTS AND DISCUSSION

3.1. Results for k_{wall}

Calculations were made not only for the realistic source model but also for point and parallel monoenergetic sources (of 1.25 MeV) and for point and parallel spectral sources having the same energy spectrum as the realistic model. The results are given in Table I; the statistical standard uncertainty of each value is 0.0001.

The parallel source shows a little more attenuation than the point source, a result that may be related to the fluence perturbation. No difference in scatter is observed for point and parallel sources. The use of a spectrum rather than 1.25 MeV increases attenuation and scatter significantly, resulting in a decrease in k_{wall} of 0.0005. The point spectral result k_{wall} = 1.0015 (0.0001) is in good

TABLE I. RESULTS OF WALL ATTENUATION AND SCATTER CALCULATIONS USING VARIOUS SOURCE MODELS

	$k_{att,MC}$	$k_{sc,MC}$	k_{wall}
Point, 1.25 MeV	1.0290	0.9739	1.0021
Parallel, 1.25 MeV	1.0293	0.9739	1.0026
Point, spectral	1.0320	0.9704	1.0015
Parallel, spectral	1.0326	0.9704	1.0021
Realistic	1.0322	0.9704	1.0017

agreement with the value 1.0014 (0.0001) of Ref. [8], which used this model and demonstrates the consistency of results obtained using PENELOPE and EGSnrc.

The best estimate using the realistic source model is k_{wall} = 1.0017 (0.0001), which, given that the combined standard uncertainty of this value is probably not less than 0.0003, is in reasonable agreement with the value k_{wall} = 1.0026 (0.0008) in use at present.

3.2. Preliminary results for k_{an}

Firstly, the method used by Rogers and Treurniet [8], namely the comparison of energy deposition from point and parallel spectral sources, was repeated for the BIPM standard. This gave the result k_{an} = 1.0020 (0.0004), which is in good agreement with the value 1.0024 (0.0003) of Ref. [8], which again confirms the agreement between PENELOPE and EGSnrc. A second set of calculations was made with the point spectral source model replaced by the realistic source. This comparison of real and parallel spectral sources gave the slightly higher result k_{an} = 1.0031 (0.0005), which is also consistent with Ref. [8] within the statistical uncertainties.

Next, the same real and parallel beam calculations were made using the idealized geometry mentioned in Section 2.3. This gave the lower result k_{an} = 1.0006 (0.0014). Despite the relatively large statistical uncertainty achieved to date, the consistency of this result with unity may indicate that, if electron fluence perturbation effects are removed from the axial non-uniformity calculation (and treated explicitly using k_{fl}), then k_{an} may be close to unity for the BIPM standard, a result that would support the divergence argument of Day [10].

4. CONCLUSIONS

The present results for k_{wall} confirm those of Ref. [8] and give improved confidence in the equivalence of the PENELOPE and EGSnrc codes. However, it should be noted that the results are preliminary, since not all the calculations have used the best choice for the PENELOPE parameters, as noted in Section 2.2. The results for k_{wall} are relatively robust, but those for k_{an} require verification as well as improved statistical uncertainty. Calculations for the electron fluence perturbation correction factor k_{fl} are under way. The overall uncertainties remain to be evaluated.

REFERENCES

[1] NELSON, W.R., HIRAYAMA, H., ROGERS, D.W.O., The EGS4 Code System, Rep. SLAC-265, Stanford Linear Accelerator Center, Stanford, CA (1985).

[2] KAWRAKOW, I., ROGERS, D.W.O., The EGSnrc Code System: Monte Carlo Simulation of Electron and Photon Transport, Rep. PIRS-701, National Research Council, Ottawa (2001).

[3] SALVAT, F., FERNANDEZ-VAREA, J.M., ACOSTA, E., SEMPAU, J., PENELOPE — A Code System for Monte Carlo Simulation of Electron and Photon Transport (Proc. Workshop Issy-les-Moulineaux, France, 2001), OECD, Paris (2001).

[4] BOUTILLON, M., NIATEL, M.T., A study of a graphite cavity chamber for absolute exposure measurements of ^{60}Co gamma rays, Metrologia **9** (1973) 139–146.

[5] BIELAJEW, A.F., On the technique of extrapolation to obtain wall correction factors for ion chambers irradiated by photon beams, Med. Phys. **17** (1990) 583–587.

[6] ROGERS, D.W.O., BIELAJEW, A.F., Wall attenuation and scatter corrections for ion chambers: Measurements versus calculations, Phys. Med. Biol. **35** (1990) 1065–1078.

[7] BIELAJEW, A.F., ROGERS, D.W.O., Implications of new correction factors on primary air kerma standards in ^{60}Co beams, Phys. Med. Biol. **37** (1992) 1283–1291.

[8] ROGERS, D.W.O., TREURNIET, J., Monte Carlo Calculated Wall and Axial Non-uniformity Corrections for Primary Standards of Air Kerma, Rep. PIRS-663, National Research Council, Ottawa (1999).

[9] BIELAJEW, A.F., Correction factors for thick-walled ionization chambers in point-source photon beams, Phys. Med. Biol. **35** (1990) 501–516.

[10] DAY, M.J., The use of the rad in clinical dosage, Br. J. Radiol. **29** (1956) 358–367.

BLANK

MONTE CARLO SIMULATION FOR THE CORRECTION OF CAVITY IONIZATION CHAMBER WALL EFFECTS

T. KUROSAWA, N. TAKATA, Y. KOYAMA
National Metrology Institute of Japan,
National Institute of Advanced Industrial Science and Technology,
Tsukuba, Japan
E-mail: Tadahiro-Kurosawa@aist.go.jp

Abstract

In precise measurements of air kerma with cavity ionization chambers the effects of wall attenuation and scatter are corrected by k_{wall} and that of beam non-uniformity by k_{nu}. These two correction factors were calculated using the EGS4 code. Calculated wall correction factors for two differently sized cylindrical ionization chambers, which were irradiated at an angle of 45° to the central beam axis, essentially agree with those obtained by the extrapolation method.

1. INTRODUCTION

Wall attenuation and scatter correction factors for cavity ionization chambers are used by standards laboratories to establish primary standards for exposure or air kerma in ^{60}Co and ^{137}Cs gamma ray fields. These correction factors are for the photon beam attenuation in the ionization chamber wall and for the scattered photon contribution to the ionization chamber response. Two main approaches are used to determine these correction factors. In the first approach, correction factors are determined by measuring the variation in ionization chamber response as a function of wall thickness in the full buildup region, extrapolating to infer the response at zero wall thickness and then applying a theoretical correction factor to account for the effects of electron transport. The procedure for calculating the corrections for the centre of electron production for cylindrical ionization chambers is less clear. In this paper this method is referred to as the extrapolation method. The second approach uses Monte Carlo calculations to simulate an ionization chamber's response and to extract correction factors. Although the ionization chamber response to photons is extremely sensitive to details of the Monte Carlo simulation, calculated correction factors are much less sensitive. There is agreement in calculated wall correction factors at the 0.2% level between three published reports covering a wide variety of commercial chambers [1–3]. In

addition to problems related to wall corrections, debate has arisen over correction for the effects related to the non-uniformity of the beam or the point of measurement correction. Most standards laboratories use $k_{nu} = 1.000$, but a few major institutes use corrections that differ significantly from unity. Bielajew [4, 5] extended the work of Kondo and Randolph [6] to include anisotropic electron effects within an analytic theory. By using Monte Carlo techniques Bielajew and Rogers [7] confirmed predictions of this theory for the National Research Council of Canada (NRC) and the Bureau international des poids et mesures (BIPM) chambers by running the calculation for weeks.

The EGS4 code [8] has been applied in this paper to calculate these two correction factors. Calculated values were compared with experimental data on chamber response versus wall thickness to estimate their accuracy.

2. CORRECTION FACTORS

The chamber wall correction factors were k_{at}, k_{sc} and k_{CEP}, which correct for photon beam attenuation, scattering in the ionization chamber wall and the depth of the centre of electron production, respectively. The linear approach used in the extrapolation method is shown schematically in Fig. 1. The open symbols demonstrate the normalized signal current of an ionization chamber as a function of wall thickness, and the effects associated with attenuation and the scattering of gamma rays in the wall normalized at zero wall thickness are shown as solid lines. The line passing through the symbols is associated with the product of attenuation and scattering. The inverse of the value for this line becomes the correction $k_{at}k_{sc}$. The product of $k_{at}k_{sc}$ and the signal current is expected to be the imaginary signal current when secondary electron equilibrium is established by the chamber wall but when photon attenuation and scattering are absent. However, the current is overcorrected for photon attenuation because secondary electrons are not produced at the inner surface of the wall but within the wall. This effect is adjusted for overcorrection by multiplying the correction factor, k_{CEP}, obtained from the estimated depth of the centre of secondary electron production and mass attenuation coefficients of wall materials for gamma rays [1].

The procedure for most ionization chambers for calculating corrections for the centre of electron production is unclear because the direction of the gamma ray beam usually differs from the direction of secondary electron transport in the chamber wall. In addition to wall correction problems, Bielajew [4, 5] studied correction for effects associated with beam non-uniformity and the point of measurement in the fields of point sources, extending the analytical theory of Kondo and Randolph [6] to include anisotropic electron effects. He

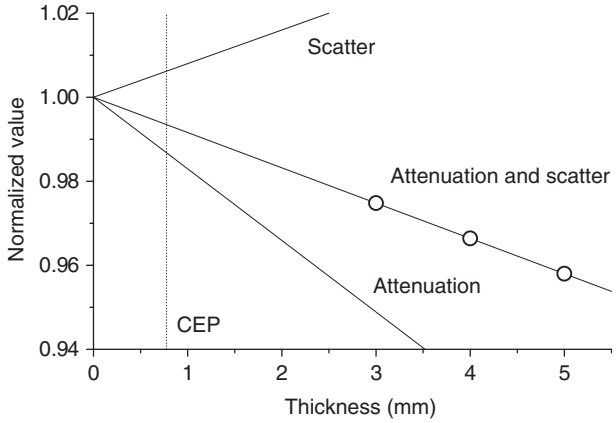

FIG. 1. Schematic diagram of the effects related to attenuation and the scattering of gamma rays in the chamber wall as a function of wall thickness.

found that chamber response does not change linearly with wall thickness, as shown in Fig. 1 [5]. Using Monte Carlo techniques, Bielajew and Rogers [7] confirmed predictions of the theory for the NRC and BIPM chambers by running calculations for weeks. We applied the EGS4 code [8] to our cylindrical ionization chambers to calculate k_{wall} and k_{nu}, in accordance with Eqs (1) and (2), shown below.

3. COMPARISON BETWEEN EXPERIMENTS AND CALCULATIONS

The primary air kerma standard at the National Institute of Advanced Industrial Science and Technology (AIST) for ^{60}Co and ^{137}Cs gamma rays is based on two differently sized cylindrical graphite ionization chambers. One has an inner height and diameter of 50 mm and 40 mm and the other of 19.3 mm and 20 mm, respectively. The graphite used had a density of 1.85 g/cm^3. Measurements were made in ^{60}Co and ^{137}Cs standard fields at the AIST. A chamber was placed in the gamma ray field with the cavity centre at 1 m from the source and with its axis at 45° to the central axis of the beam. Calculation accuracy was estimated by comparing calculated and experimental results for the change of the response with wall thickness. Statistical uncertainties of calculations were less than 0.05%. The ionization current was measured for 3, 4, 5 and 6 mm wall thickness for ^{60}Co gamma rays and 2, 3, 4, 5 and 6 mm for

^{137}Cs gamma rays. We estimated from these data the calculation accuracy to be within 0.1% as compared with the measurements.

4. CALCULATION OF CORRECTION FACTORS

The Monte Carlo calculations were made using the EGS4 code and PRESTA algorithm for electron transport. The value of k_{wall} was determined by:

$$k_{\text{wall}} = \frac{\sum_i r_i^0 e^{+\mu d_i}}{\sum_i (r_i^0 + r_i^1)} \tag{1}$$

where r^0 is the energy deposited in the air cavity by electrons generated by primary photon interaction, r^1 is the energy deposited by electrons generated by second and higher order scattered photons, μ is the linear attenuation coefficient of wall material for primary photons and d the pass length of the photon in the chamber wall from the entry to the first interaction point in the chamber wall.

The value of k_{nu} in the beam of a point source was obtained from the equation:

$$k_{\text{nu}} = \frac{D_{\text{parallel}} k_{\text{wall}}^{\text{parallel}}}{D_{\text{point}} k_{\text{wall}}^{\text{point}}} \tag{2}$$

where D is the energy deposited in the air of the cavity per unit fluence of incident photons at the centre of the chamber and k_{wall} is the wall correction factor for a parallel or point source beam.

5. RESULTS

In January 2001 we took our ionization chambers to the BIPM and measured the air kerma in ^{60}Co and ^{137}Cs gamma ray fields for key comparisons, obtaining values for chamber wall correction factors by both the extrapolation method and Monte Carlo calculations. Table I shows the results obtained for reference points at 1 m from the gamma ray sources. We estimated k_{CEP} = 0.995 in accordance with the method described by Roesch [9]. The extrapolated and calculated results agree within the uncertainties, except the

result for the smaller chamber at ^{137}Cs, for which a difference of 0.28% was obtained. The moderate agreement of the calculated wall corrections with those obtained by the extrapolation method is somewhat surprising. Differences of the order of 1% or more are reported in the literature [7] for cylindrical chambers; these, however, were irradiated with the central beam axis incident at 90° to the chamber axis, in contrast to the 45° used in the work described in this paper.

Table II shows k_{nu} obtained by Monte Carlo calculation in accordance with Eq. (2). The statistical uncertainty of the calculation was 0.1%. The effects due to the non-uniformity of the beam had previously been neglected at the AIST (i.e. $k_{nu} = 1$). Within the statistical uncertainties the calculated values agree with the assumption used previously. Table III shows the values of the product $k_{wall}k_{nu}$. The differences between the values obtained by the Monte Carlo calculations and those used previously are small for both ^{60}Co and ^{137}Cs gamma rays and also for both ionization chambers.

TABLE I. k_{wall} FOR ^{60}Co AND ^{137}Cs GAMMA RAYS OBTAINED BY MONTE CARLO CALCULATION IN ACCORDANCE WITH EQUATION (1) AND BY THE EXTRAPOLATION METHOD FROM MEASUREMENTS AT THE BIPM

Source	Chamber diameter (mm)	k_{wall} (Monte Carlo)	k_{wall} (extrapolated)	Ratio[a]
^{60}Co	20	1.0198	1.0192	1.0006
	40	1.0209	1.0207	1.0002
^{137}Cs	20	1.0166	1.0194	0.9973
	40	1.0192	1.0195	0.9997

[a] The ratio is that of the Monte Carlo results/the extrapolated results.

TABLE II. CORRECTION FACTOR k_{nu} FOR BEAM NON-UNIFORMITY OBTAINED FROM EQUATION (2)

Source	Chamber diameter (mm)	k_{nu} (Monte Carlo)	k_{nu} (used previously)
^{60}Co	20	1.0005	1.0000
	40	1.0008	1.0000
^{137}Cs	20	0.9990	1.0000
	40	0.9983	1.0000

TABLE III. CORRECTION FACTORS $k_{wall}k_{nu}$

Source	Chamber diameter (mm)	$k_{wall}k_{nu}$ (Monte Carlo)	$k_{wall}k_{nu}$ (used previously)	Ratio[a]
^{60}Co	20	1.0203	1.0192	1.0011
	40	1.0217	1.0207	1.0010
^{137}Cs	20	1.0156	1.0194	0.9963
	40	1.0175	1.0195	0.9980

[a] The ratio is that of the Monte Carlo results/the results used previously.

The key comparison result for ^{60}Co beams, expressed as the ratio of the air kerma rate determined with the AIST standard to the BIPM standard in the BIPM radiation field, was 1.0071, with a standard uncertainty of the comparison of 0.0023. Details of the comparison and possible reasons for the significant deviation of both standards can be found in Ref. [10]. The BIPM usually applies the correction factors k_{an} and k_{rn}, which correct separately for the axial and radial non-uniformity of the beam. k_{an} is calculated, whereas k_{rn} is obtained from the measured radial beam profile. In this paper the calculated correction factor k_{nu} was used in accordance with Eq. (2) instead of k_{an} and k_{rn}. This is not entirely precise, because k_{nu} is based on the assumption of a point source, and the effects that are related to the finite size of the source, photon scattering in the source, source containment and collimator, as well as photon scatter from the room and surrounding materials, are ignored in this approach.

6. CONCLUSION

We calculated k_{wall} and k_{nu} for our ionization chambers using the EGS4 Monte Carlo code. Surprisingly, the wall correction factors obtained with the extrapolation method and those calculated with Monte Carlo methods were essentially in agreement. In contrast to this finding, differences of more than 1% have been reported in the literature for cylindrical chambers. A possible reason for this may be the fact that in the work described in this paper the chambers were irradiated with the beam entering the chamber at an angle of 45° to the chamber axis. At this special irradiation geometry the linear extrapolation of the chamber current as a function of wall thickness to zero wall thickness may be justified. Additional work has to be carried out to improve the calculation of the correction factor for the effects associated with beam non-uniformity. In the future the AIST will use calculated k_{wall} and k_{nu} correction factors for its primary standards of air kerma for ^{60}Co and ^{137}Cs gamma rays.

REFERENCES

[1] ROGERS, D.W.O., BIELAJEW, A.F., NAHUM, A.E., Ion chamber response and A_{wall} correction factors in a ^{60}Co beam by Monte Carlo simulation, Phys. Med. Biol. **30** (1985) 429–443.

[2] NATH, R., SCHULZ, R.J., Calculated response and wall correction factors for ionization chambers exposed to ^{60}Co gamma-rays, Med. Phys. **8** (1981) 85–93.

[3] McEWAN, A.C., SMYTH, V.G., Comments on "Calculated response and wall correction factors for ionization chambers exposed to ^{60}Co gamma-rays", Med. Phys. **11** (1984) 216–218.

[4] BIELAJEW, A.F., An analytic theory of the point-source non-uniformity correction factor for thick-walled ionization chambers in photon beams, Phys. Med. Biol. **35** (1990) 517–538.

[5] BIELAJEW, A.F., Correction factors for thick-walled ionization chambers in point-source photon beams, Phys. Med. Biol. **35** (1990) 501–516.

[6] KONDO, S., RANDOLPH, M.L., Effect of finite size of ionization chambers on measurements of small photon sources, Radiat. Res. **13** (1960) 37–60.

[7] BIELAJEW, A.F., ROGERS, D.W.O., Implications of new correction factors on primary air kerma standards in ^{60}Co beams, Phys. Med. Biol. **37** (1992) 1283–1291.

[8] NELSON, W.R., HIRAYAMA, H., ROGERS, D.W.O., The EGS4 Code System, Rep. SLAC-265, Stanford Linear Accelerator Center, Stanford, CA (1985).

[9] ROESCH, W.C., Dose for nonelectronic equilibrium conditions, Radiat. Res. **9** (1958) 399.

[10] ALLISY-ROBERTS, P.J., et al., Comparison of the Standards of Air Kerma of the NMIJ Japan and the BIPM for ^{60}Co γ Rays, Bureau international des poids et mesures, Sèvres (in press).

BLANK

MEASUREMENT OF ABSORBED DOSE TO WATER FOR LOW AND MEDIUM ENERGY X RAYS

H.-M. KRAMER
Physikalisch-Technische Bundesanstalt,
Braunschweig, Germany
E-mail: hans-michael.kramer@ptb.de

Abstract

For low energy and medium energy X rays, that is for tube voltages of up to 100 kV or starting at 100 kV, the dosimetric quantity of interest in the paper is the absorbed dose to water at the surface of a water phantom or at a depth of 2 cm, sometimes 5 cm, in a water phantom, respectively. In the first part of the paper the principal methods by which these quantities can be determined with the aid of calibrated ionization chambers are described. The second part is devoted to an absolute measurement of the absorbed dose to water for medium energy X rays. The method is based on the use of an extrapolation chamber inside a graphite phantom. The steps for converting the electrical charge collected in the measuring volume to the absorbed dose to graphite are outlined, together with the steps leading from absorbed dose to graphite to absorbed dose to water in a water phantom. The method presented is used for determining what is known in X ray dosimetry as the ionization chamber replacement effect.

1. INTRODUCTION

The treatment of superficial or intercavitary malignancies with low and medium energy X rays has regained popularity over the past decade [1]. The number of X ray machines being ordered and installed in North America has increased over recent years [2]. This development puts renewed and increased emphasis on the importance of accurate dosimetry in this energy range. Over the past decade or so an appreciable number of publications dealing with various aspects of dosimetry in X ray beams have appeared [3–14]. Nahum [15] presented a review article on perturbation effects in kilovoltage X ray beams. A number of medium energy X ray dosimetry protocols have been published [2, 16–20], leading to the publication of a comparison between the various protocols [21].

Unlike the case of high energy photon or electron radiation, where the response per unit volume of an ionization chamber can be calculated by means of the cavity theory, the response of a chamber to X radiation cannot be predicted by this theory. Attempts have been made to use water calorimetry to

determine absorbed dose to water directly. The accuracy achievable is limited by the steep dose gradients within the phantom, by the heat defect and its potential energy dependence [22, 23], and by the relatively low dose rate supplied by X ray machines.

For these reasons national metrology laboratories do not employ water calorimetry for dosimetry for X rays. The only realization of the unit of gray for the absorbed dose to water in a water phantom for X rays performed to date by a national metrology institute is an ionometric measurement using an extrapolation chamber in a graphite phantom.

Apart from the introduction and the conclusion, this paper has three sections. An overview of the principles underlying the determination of absorbed dose to water with the aid of calibrated ionization chambers is given in Section 2. The model for evaluating measurements with a graphite extrapolation chamber is presented and the steps for determining absorbed dose to water from such measurements are described in Section 3. Results of the energy dependence of the replacement factor of three ionization chambers are presented in Section 4.

2. DOSIMETRY WITH CALIBRATED IONIZATION CHAMBERS

2.1. Low energy X rays

X rays generated with tube voltages of up to 100 kV are usually termed low energy X rays. In this energy range the absorbed dose to water at the surface of a water phantom, D_w, is obtained from the reading, M, (corrected for deviations from reference temperature and the pressure of the air at the time of measurement) of the ionization chamber irradiated free in air by:

$$D_w = MN_{K_a} B \frac{(\bar{\mu}_{en}/\rho)_w}{(\bar{\mu}_{en}/\rho)_a} k_Q \equiv MN_{K_a} B \left(\frac{\bar{\mu}_{en}}{\rho} \right)_{w,a} k_Q \quad (1)$$

where N_{K_a} is the air kerma calibration factor associated with the reference radiation quality, B is the backscatter factor, $(\bar{\mu}_{en}/\rho)_m$ is the mass energy absorption coefficient of material m averaged over the energy fluence spectrum and k_Q is a correction factor allowing for the difference of the ionization chamber response in the reference and in the user's field. For reasons of simplicity, k_Q is often considered to be a function of the half-value layer only. The double subscript on the right hand side of Eq. (1) denotes the water to air ratio of the mass energy absorption coefficient. There are two possibilities for averaging

over the energy fluence and selecting a matching backscatter factor: (a) the energy fluence of the primary spectrum without backscatter is used, as is the backscatter factor given by the ratio of water kerma in the entrance plane of the water phantom to the water kerma free in air at the same point of measurement; (b) the average is formed over the total energy fluence spectrum, including the contributions from backscattered radiation, in which case the backscatter factor given by the ratio of the air kerma in the entrance plane of the water phantom to the air kerma free in air at that point is used.

Preference should be given to the first alternative, as in this case only one value of the μ_{en} ratio is needed for a given radiation quality, irrespective of the field size. The influence of the field size is covered by the backscatter factor. For the second alternative, both the μ_{en} ratio and the backscatter factor depend, for a given radiation quality, on the field size. Backscatter factors have been determined experimentally [24, 25] and by means of Monte Carlo calculations [26, 27]. Numerical values for the backscatter factor and for the μ_{en} ratio are also given in some of the protocols [2, 16].

2.2. Medium energy X rays

For medium energy X rays absorbed dose to water is determined by measurements at the point of test in a water phantom. Depending on whether the ionization chamber employed is calibrated free in air in terms of air kerma or in terms of absorbed dose to water, the user applies different procedures to obtain the absorbed dose to water. Starting with a chamber calibrated in terms of absorbed dose to water, D_w, the reading, M, of the ionization chamber is converted into D_w by:

$$D_w = MN_{D,w}\Pi k_i \tag{2}$$

where $N_{D,w}$ is the calibration factor in terms of absorbed dose to water. As usual, it relates to reference conditions in view of the influence quantities radiation quality, Q, field size, source to surface distance (SSD), depth inside the water phantom and temperature and atmospheric pressure. If measurements are carried out under conditions that differ from the reference conditions, the influence of the differences is taken into account by the correction factor k_i, where the index i stands for the influence quantity. Reference conditions vary to a certain extent from one protocol to another. A typical set of reference conditions is provided by a field size of 10 cm × 10 cm, a depth inside the phantom of 2 cm, sometimes 5 cm, SSD = 30 cm and the radiation quality stated in the calibration certificate. If the user's radiation quality differs from the reference

radiation quality a beam specifier is used to determine the value of k_Q. The various protocols consistently use the first half-value layer as the primary beam specifier. Secondary specifiers are the X ray tube voltage and the homogeneity coefficient, c_h; that is, the ratio of the first to the second half-value layer.

Starting with an ionization chamber calibrated in terms of air kerma, the absorbed dose to water is derived from the chamber reading in the water phantom by:

$$D_w = MN_{K_a}\left(\frac{\bar{\mu}_{en}}{\rho}\right)_{w,a} p\Pi k_i \tag{3}$$

where the average of the mass energy absorption coefficient is weighted with the energy fluence spectrum at the point of test inside the water phantom (i.e. the radiation hardened with respect to the primary radiation by absorption and softened by scattering). The factor p, which is called the 'replacement factor', takes account of a number of sometimes closely related effects that are associated with the difference between the radiation fields to which the chamber is exposed during calibration free in air and during use inside the water phantom. The following effects have been identified.

(a) The energy and angular distribution in the two fields is different. Of particular importance are differences in the angular distribution. In calibration there is a nearly parallel field, and in the phantom an important fraction of the dose is caused by scattered radiation impinging on the chamber from all directions.
(b) The influence of the chamber stem. In calibration free in air, the part of the stem exposed to the beam contributes to the signal of the chamber by scattering photons in the direction of the sensitive volume. Generally, the stem is of a material with an effective atomic number, Z_{eff}, higher than that of water. Consequently, the stem scatters less than the water it replaces, and for in-phantom measurements the presence of the stem reduces the signal produced in the chamber.
(c) The ionization chamber, which consists of the chamber wall surrounding the cavity, displaces water. In the volume occupied by the cavity this results in a modification of the photon and electron fluence with respect to the situation in the absence of the chamber.

The physics behind the effects listed above is by no means trivial. Within the framework of this work it is impossible to go into all details, and hence the interested reader is referred to the literature [3–5, 7–9, 11, 12, 15, 28].

3. ABSOLUTE DETERMINATION OF ABSORBED DOSE TO WATER

3.1. Potential methods

The problems associated with factor p in Eq. (3) are not encountered when the absorbed dose to water is measured directly in absolute terms; that is, in a measurement of the energy deposited in the volume of interest with a known mass. As mentioned in Section 1, water calorimetry is not a suitable method for the energy region considered in this paper, and hence only some form of ionometric method can be used. Such measurements have been realized by means of an extrapolation chamber inside a graphite phantom [29, 30]. The extrapolation chamber essentially is a guarded parallel-plate chamber of variable depth. The chamber axis coincides with the axis of the incident beam. At the limit of the plate separation, $\Delta x \rightarrow 0$, the absorbed dose to air in the cavity can be converted into absorbed dose to graphite by means of the cavity theory. Owing to limitations in space, only the essential dosimetric steps will be presented in this paper, without giving the full formalism, which is described in detail in Ref. [30].

3.2. The two component model

The first step consists of separating the absorbed dose to air inside the cavity, D_a, into a fraction resulting from the interactions of Compton electrons, D_a^C, and another one resulting from the interactions of photoelectric electrons, D_a^P. When making this distinction, each individual component can be treated by the cavity theory. For the fraction D_a^C there is electronic equilibrium at a graphite to air interface, irrespective of the energy of the incident photon radiation. This follows from the value of the ratio $(\bar{\mu}_{en}(E)/\rho)_{g,a}^C$ of 1.027 at 10 keV, which rapidly drops to 1 with increasing energy. Under conditions of secondary electron equilibrium the absorbed dose to air is identical to the air collision kerma. Consequently, the absorbed dose to air originating from Compton electrons can be converted into the graphite collision kerma by:

$$K_g^C = K_a^C \left(\frac{\bar{\mu}_{en}}{\rho} \right)_{g,a}^C \tag{4}$$

where the notation for the kerma, K, is as for the absorbed dose and the average over the values is taken over the μ_{en} energy fluence spectrum of the photons at the point of measurement. It should be noted that the equivalence of air

and graphite in terms of Compton scattering is the essential reason for choosing graphite as a phantom material. For any material containing hydrogen this equivalence does not exist, which precludes the use of, for instance, an organic substance as a phantom material.

In terms of photoelectric effect, air and graphite are not equivalent; this is due to the strong Z dependence of the photoelectric effect. Owing to the much higher energy of the electrons liberated by photoelectric interactions, the dose to air caused by this fraction can be converted into the dose to graphite by means of the graphite to air ratio of the mass stopping power, $\bar{s}_{g,a}$, averaged over the fluence spectrum of the electrons at the point of measurement; that is, $D_g^P = \bar{s}_{g,a} D_a^P$. In the case of an extrapolation chamber operated at the limit of $\Delta x \to 0$, the treatment of photoelectric electrons by the Bragg–Gray theory is justified, as these electrons lose only a small fraction of their energy in the air gap, even if their energy is in the region of 20 keV to 30 keV. Following the derivation given in Ref. [30], and making use of a minor simplification, the (total) absorbed dose to graphite is obtained by:

$$D_g(\Delta x \to 0) = \frac{\Delta Q}{\rho_a \pi r^2 \Delta x} \frac{\overline{W}}{e} \beta \tag{5}$$

where the product of the first two terms on the right hand side of the equation represents the absorbed dose to air, $\overline{W}$ is the effective W value of air, e is the elementary charge and the factor β converts the absorbed dose to air into that in graphite. β is given by:

$$\beta = \frac{\left(\overline{\mu}_{en}/\rho\right)_g}{\left(\overline{\mu}_{en}/\rho\right)_a^C + \bar{s}_{a,g}\left(\overline{\mu}_{en}/\rho\right)_g^P} \tag{6}$$

This is the result of the two component model originally proposed by Schneider [29].

3.3. From absorbed dose to graphite to absorbed dose to water in a water phantom

The conceptual advantage of an absolute measurement of absorbed dose to graphite with respect to an air kerma measurement free in air lies in the fact that the radiation field inside the graphite phantom contains abundant scattered radiation, as does the radiation field in a water phantom. As is shown in

this section, the absorbed dose to water in a water phantom can be obtained from a measurement of the absorbed dose to graphite in a graphite phantom by means of the following straightforward steps:

(a) Secondary electron equilibrium is established at the depth of measurement in the graphite phantom. As a result, the absorbed dose to graphite and the graphite collision kerma have identical numerical values. The graphite collision kerma is converted into water collision kerma by means of the water to graphite ratio of mass energy absorption coefficients averaged over the energy fluence of the photon spectrum at the point of measurement.
(b) A transfer ionization chamber is calibrated in terms of water collision kerma in the graphite phantom. The chamber walls of the transfer chamber must be thicker than the practical range of the most energetic electrons.
(c) The transfer chamber is positioned in a water phantom, where it measures the water collision kerma. In this step a correction factor potentially necessary for differences in the replacement effect in the two phantom materials has been dispensed with. This simplification is justified as the properties of the radiation fields in terms of primary and scattered radiation are quite similar in the two phantoms. In the energy range considered in this paper and under conditions of secondary electron equilibrium, the numerical values of the water collision kerma and of water absorbed dose are identical.

If the water absorbed dose at the reference point in a water phantom is known, the factor p in Eq. (3) of another ionization chamber can be determined by simply placing an ionization chamber with a known air kerma calibration factor at the reference point and by solving Eq. (3) with respect to p. The values obtained in this way range from about 1.1 at a tube voltage of 100 kV to 1.01 at 280 kV [28]. This is in conflict with other methods for determining the factor p [4, 5, 8, 19, 31], which lead to values of around 1.05 at most.

3.4. Extension of the two component model

It is one of the essential elements of the two component model that the spectrum of primary Compton electrons is identical in terms of total number and spectral distribution, both in air and in graphite. This statement does not, however, mean that the low energy parts of the spectra of the primary electrons are on the whole identical in the two materials. In fact, differences occur at the very low energy end. They are associated with the de-excitation process after

the creation of a K or L shell vacancy as a result of a photoelectric effect or of a Compton scattering event. For the materials considered in this paper, the de-excitation nearly exclusively takes place via an Auger process. In such a process an electron of a higher shell makes a transition to the shell where the vacancy has been created (K or L shell) and thus transfers the energy gained to another electron in a higher shell. This electron escapes with a characteristic energy from the atom that was initially ionized. The energies and transition probabilities are given in Table I.

By means of the stopping powers given in Ref. [3], the practical range of electrons with an energy of 3.1 keV in air at normal pressure and temperature can be estimated to be about 0.2 mm. This means that there is a buildup region in the first 0.2 mm of air adjacent to a graphite to air interface. The extrapolation chamber used in Refs [28–30] allowed the use of plate separations down to 0.2 mm, a value at which buildup is already completed. The effect of the presence of the low energy component on the shape of the extrapolation curve is schematically shown in Fig. 1. The correction factor:

$$k = \frac{\left(\Delta Q / \Delta V\right)_{\text{true}}}{\left(\Delta Q / \Delta V\right)_{\text{exp}}}$$

which takes into account the difference in energy transferred per unit mass to Auger electrons in air and in graphite can be written as:

$$k = \frac{Q_g^{\text{dir}} + Q_g^{\text{deex}}}{Q_g^{\text{dir}} + Q_a^{\text{deex}}} \tag{7}$$

TABLE I. KINETIC ENERGIES, E_{Aug}, AND EMISSION PROBABILITIES, 1 – ω, OF AUGER ELECTRONS ACCORDING TO REF. [32]

Element (transition)	E_{Aug} (eV)	1 – ω
C	272	0.9974
N	390	0.9957
O	512	0.9931
Ar (L–M)	210	0.9985
Ar (K–L)	3100	0.8801

where Q^{dir} denotes the electrical charge created in the measurement volume by electrons liberated as a direct result of Compton or photoelectric interaction in graphite and Q^{deex} denotes the contribution from the Auger electrons emitted in the course of the de-excitation of the atom or molecule after photon interaction. For Q^{deex} the subscripts a and g stand for the materials air and graphite. Speaking in terms of Fig. 1, the factor k takes into account the buildup in the first 0.2 mm of air, which is already completed at the smallest plate separation.

In a somewhat simplified model it can be assumed that the charge contributions in Eq. (7) are proportional to the energy transferred to air by electrons of the corresponding origin. This is equivalent to disregarding a potential energy dependence of the W value. This simplification is made in this paper only to avoid equations that are too long. In the full treatment given in Ref. [30] the energy dependence of the W value is taken into account. Neglecting the energy dependence of the W value, the factor k of Eq. (7) can be approximated by:

$$k \approx \frac{E_{\mathrm{tr},g}^{\mathrm{dir}} + E_{\mathrm{tr},g}^{\mathrm{deex}}}{E_{\mathrm{tr},g}^{\mathrm{dir}} + E_{\mathrm{tr},a}^{\mathrm{deex}}} = \frac{\int \varphi_E(E) E \left(\mu_{\mathrm{en}}/\rho\right)_g \mathrm{d}E}{\int \varphi_E(E) \left\{ (E - E_{\mathrm{Aug},g})(\mu_{\mathrm{en}}/\rho)_g + \sum_i c_i E_{\mathrm{Aug},i} (\mu_{\mathrm{en}}/\rho)_i \right\} \mathrm{d}E} \tag{8}$$

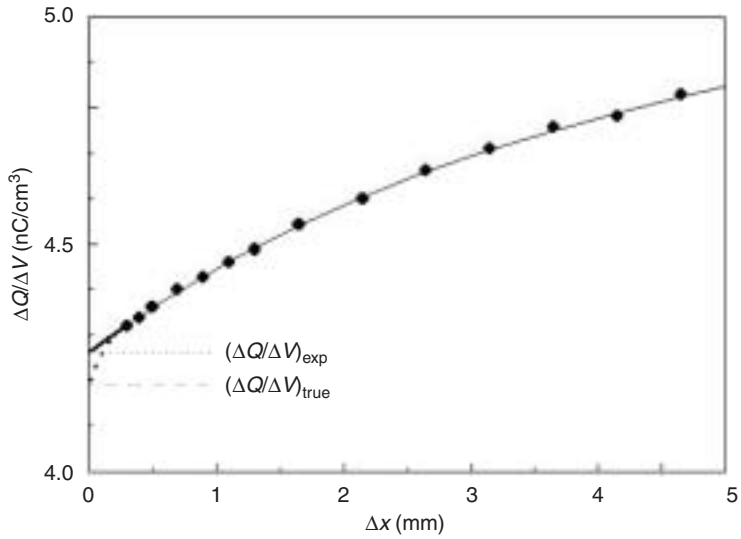

FIG. 1. Example of a differential extrapolation curve (ΔQ/ΔV) versus plate separation obtained for a radiation generated with an X ray tube voltage of 120 kV and a total filtration of 6 mm Al.

where the index i stands for the constituents nitrogen, oxygen and argon, c_i is the fraction by mass of each constituent and E_{Aug} the energy of the Auger electron in graphite or in constituent i (see Table I). For the derivation of Eq. (8) it has been assumed that the fraction of the mass energy absorption coefficient associated with direct interactions and with the de-excitation electrons are given by:

$$\left(\mu_{\mathrm{en}}/\rho\right)^{\mathrm{dir}} = \frac{E - E_{\mathrm{Aug}}}{E}\left(\mu_{\mathrm{en}}/\rho\right)$$

$$\left(\mu_{\mathrm{en}}/\rho\right)^{\mathrm{deex}} = \frac{E_{\mathrm{Aug}}}{E}\left(\mu_{\mathrm{en}}/\rho\right)$$

The result of Eq. (8) is shown in Fig. 2. The squares represent the correction factor, *k,* obtained by integrating over the spectral photon fluence at the point of measurement at a depth of 2 g/cm^2 within the graphite phantom. The energy, *E,* is averaged over the spectral fluence of the incident photon spectra. The primary X ray spectra incident on the phantom are characterized in columns 1 to 4 of Table II.

The last two columns of Table II demonstrate that the effect of Auger electrons is by no means negligible in measurements with a graphite extrapolation chamber, when and if the minimum plate separation is limited to around

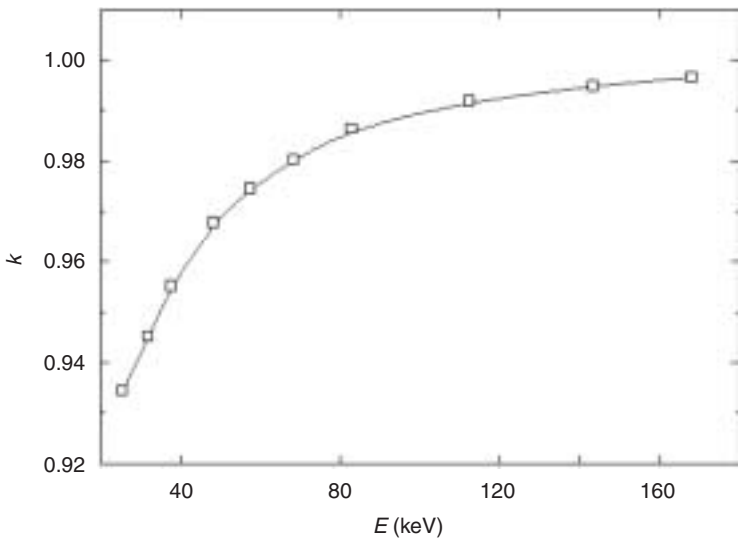

FIG. 2. The effect associated with the Auger electrons on the basis of Eqs (7) and (8) as a function of mean energy of the ten spectra used in Ref. [30].

TABLE II. CHARACTERIZATION OF RADIATION QUALITIES AND VALUES OF k FOR A DEPTH OF 2 g/cm^2 ACCORDING TO EQUATION (8)

Q	Total filtration (mm)	HVL (mm Al)	c_h	k (Eq. (8))	k (Ref. [30])
TW 50	1.0 Al	1.176	0.670	0.934	0.945
TH 50	4.0 Al	2.35	0.804	0.945	0.954
TH 70	4.0 Al	3.18	0.742	0.955	0.962
TH 100	4.0 Al	4.87	0.721	0.968	0.972
TH 120	6.0 Al	6.54	0.764	0.974	0.978
TH 140	9.0 Al	8.51	0.824	0.980	0.983
TH 150	4.0 Al + 0.5 Cu	11.36	0.918	0.986	0.988
TH 200	4.0 Al + 1.15 Cu	14.53	0.945	0.992	0.993
TH 250	4.0 Al + 1.6 Cu	17.01	0.964	0.995	0.995
TH 280	4.0 Al + 3.0 Cu	18.81	0.981	0.997	0.997

Note: The values of k in the last column were obtained by taking the energy dependence of the W value into account [30]. Q in the first column denotes the radiation quality, where the figures stand for the X ray tube voltage in kV. c_h is the homogeneity coefficient (i.e. the ratio of the first to second half-value layer (HVL)).

0.2 mm. The magnitude of the effect increases with decreasing energy. For the softest X radiation a correction greater than 5% is required.

The validity of the extended two component model was tested in a combination of experiments and Monte Carlo calculations. For each of the ten radiation qualities a measurement of the air kerma was performed in the absence of the graphite phantom. These measurements were carried out with the Fasskammer, which is the primary standard of the Physikalisch-Technische Bundesanstalt (PTB) for air kerma for X rays with generating potentials of up to 300 kV. The point of measurement was on the beam axis at the distance at which the phantom surface was positioned.

As a result of this experiment, the quotient of the graphite collision kerma at a depth corresponding to 2 g/cm^2 in the graphite phantom to the air collision kerma in free air (K_g/K_a) was determined. This factor was also calculated by means of the Monte Carlo method. The ratio of the two factors:

$$\frac{\left(K_g/K_a\right)_{\mathrm{MC}}}{\left(K_g/K_a\right)_{\mathrm{exp}}}$$

is denoted by R.

This double ratio gives an indication of the extent to which the absorbed dose to graphite determined experimentally agrees with that determined by Monte Carlo calculations. Ideally, this ratio should have the value 1 for all radiation qualities and for the depths in the phantom examined in Ref. [30] (i.e. 2 g/cm^2 and 5 g/cm^2).

For a depth corresponding to 2 g/cm^2 the ratio R is shown in Fig. 3 as a function of the energy averaged over the photon fluence of the primary spectrum incident on the phantom surface. The square symbols were obtained by evaluating the extrapolation chamber measurements by the two component model (i.e. according to Eq. (5)), while the circles were obtained by multiplying Eq. (5) by the correction factor, k, as given in the last column of Table II. For reasons of clarity, the uncertainty margins, relating to a coverage factor $k = 1$, have been given only for the data presented as circles. At each energy the uncertainty margin of the points of the lower curve is practically the same as for the circles.

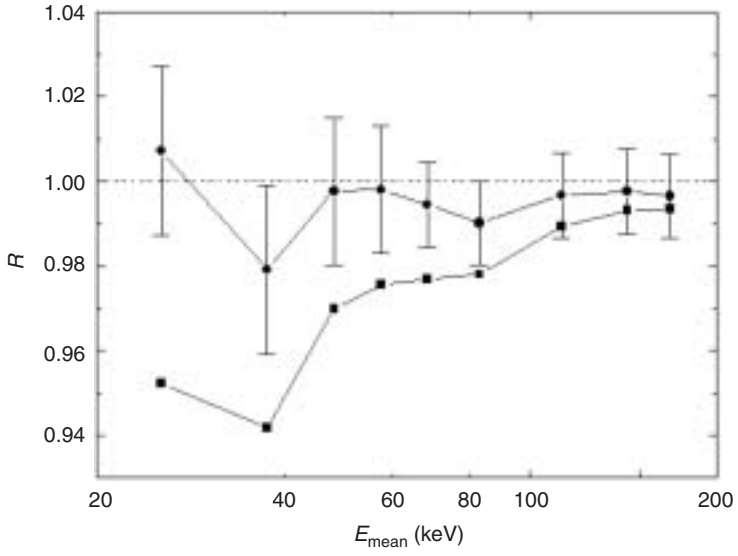

FIG. 3. Ratio R of the Monte Carlo to experimental results of the graphite collision kerma normalized to the air collision kerma at a depth of 2 g/cm^2 as a function of the mean energy of the spectral fluence of the primary photon spectrum.

The uncorrected ratio R (i.e. according to Eq. (5)) decreases significantly from $R \approx 1$ in the upper energy range to around 0.94 in the lower energy range. This behaviour could be expected, as the disequilibrium in the low energy region of the electron spectrum increases in magnitude with increasing dominance of photoelectric interactions; that is, with decreasing mean photon energy.

The minimum at an energy of around 37 keV, corresponding to a tube voltage of 70 kV, is not considered significant. The details of the spectral distribution gain in importance with decreasing tube voltage. For this reason, the uncertainty margins increase with decreasing mean energy.

Taking the effect of Auger electrons into account leads to a very good agreement between the experimental and Monte Carlo results; in particular, a significant overall energy dependence of R no longer exists. Figure 3 demonstrates that the graphite extrapolation chamber in the graphite phantom can be used for reliably determining the absorbed dose to graphite, provided that the effect of the presence of the low energy de-excitation electrons is taken into account.

4. REPLACEMENT FACTOR IN GRAPHITE

Changing the phantom material from water to graphite in Eq. (3) and combining it with Eqs (5) and (6), an expression is obtained for the replacement factor, p, applicable to an ionization chamber used for determining the absorbed dose to graphite by an in-phantom measurement, starting with the calibration free in air, N_{Ka}:

$$p = \left\{ \frac{\Delta Q}{\rho_a \pi r^2 \Delta x} \frac{\overline{W}}{e} \beta k \Big/ M N_{K_a} \left(\frac{\overline{\mu}_{\text{en}}}{\rho} \right)_{g,a} \Pi k_i \right\} \tag{9}$$

With the aid of Eq. (9) the replacement factor, p, was determined for three ionization chambers used as transfer instruments at the PTB. The result for a depth of 2 g/cm^2 is shown in Fig. 4. At low energies the replacement factor is smaller than 1 for all three chambers. This means that the chambers over-respond. This over-response can be explained by the negligible attenuation of the photon irradiation in the chamber cavity compared with that in the undisturbed graphite phantom. This leads to a higher average photon fluence in the cavity than in the same volume of the undisturbed phantom. For a tube voltage of 70 kV, p has a maximum for all three chambers. Depending on the chamber, the values range between about 1.01 and 1.03. With increasing tube voltage the

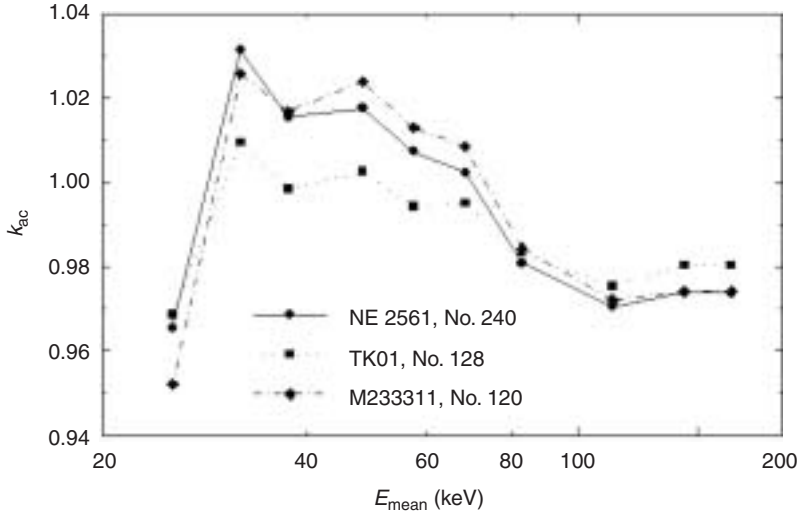

FIG. 4. The variation of the value of the replacement factor p of three different types of ionization chamber as a function of the mean energy of the X ray spectra used.

value of p decreases again. For tube voltages starting at 140 kV the value of the replacement factor of all chambers is below 1 and quite independent of the chamber type.

As the radiation field inside a water phantom is quite similar to that in a graphite phantom, it can be inferred that the replacement factor of the chambers considered in this paper in water will not differ from those found for graphite by more than 1% over the energy range considered in this paper.

5. CONCLUSIONS

For medium energy X rays a graphite extrapolation chamber can be used for determining the absorbed dose to graphite. In a sequence of further steps, eventually the absorbed dose to water in a water phantom is obtained. The evaluation of the measurement with the extrapolation chamber originally proposed by Schneider [29] was refined by considering the distorted electronic equilibrium in an air layer about 0.2 mm thick, adjacent to the graphite to air interface. The electronic equilibrium is distorted because in air a greater fraction of the total energy transfer than in graphite proceeds through Auger electrons. Neglecting this effect in the past led to overestimates of the value of the absorbed dose to graphite and hence also of the absorbed dose to water. This in turn led to unrealistically high values for the replacement factor, of up to 1.1.

By refining the evaluation of the extrapolation chamber measurements in view of the de-excitation electrons, values of the absorbed dose to graphite are obtained that are in good agreement with the Monte Carlo calculations. Replacement factors obtained on the basis of these results range between 0.95 and 1.03 and thus are in agreement with other results published in the literature.

REFERENCES

[1] VERHAEGEN, F., NAHUM, A.E., VAN DE PUTTE, S., NAMITO, Y., Monte Carlo modelling of radiotherapy kV x-ray units, Phys. Med. Biol. **44** (1999) 1767–1789.

[2] MA, C.-M., et al., AAPM protocol for 40–300 kV x-ray beam dosimetry in radiotherapy and radiobiology, Med. Phys. **28** (2001) 868–893.

[3] HARRISON, R.M., Visual demonstration of the displacement effect of an ionization chamber within a phantom at low x-ray energies (<150 keV), Phys. Med. Biol. **38** (1993) 1329–1334.

[4] SEUNTJENS, J., THIERENS, H., SCHNEIDER, U., Correction factors for a cylindrical ionization chamber used in medium-energy X-ray beams, Phys. Med. Biol. **38** (1993) 805–832.

[5] MA, C.-M., "Monte Carlo calculated correction factors for a NE2571 chamber in medium-energy X-ray beams", Measurement Assurance in Dosimetry (Proc. Int. Symp. Vienna, 1993), IAEA, Vienna (1994) 371–381.

[6] NAHUM, A.E., NIGHT, T.R., "Consistent formalism for KV x-ray dosimetry", ibid., pp. 451–459.

[7] SEUNTJENS, J., VERHAEGEN, F., Dependence of overall correction factor of a cylindrical ionization chamber on field size and depth in medium-energy x-ray beams, Med. Phys. **23** (1996) 1789–1796.

[8] MA, C.-M., NAHUM, A.E., Calculations of ion chamber displacement effect corrections for medium-energy X-ray dosimetry, Phys. Med. Biol. **40** (1995) 45–62.

[9] MA, C.-M., NAHUM, A.E., Monte Carlo calculated stem effect corrections for NE2561 and NE2571 chambers in medium-energy x-ray beams, Phys. Med. Biol. **40** (1995) 63–72.

[10] LI, X.A., MA, C.-M., SALHANI, D., Measurement of percentage depth dose and lateral beam profile for kilovoltage X-ray therapy beams, Phys. Med. Biol. **42** (1997) 2561–2568.

[11] MA, C.-M., LI, X.A., SEUNTJENS, J.P., Study of consistency for kilovoltage x-ray beams, Med. Phys. **25** (1998) 2376–2384.

[12] ROSSER, K.E., Investigation of the chamber correction factor (k_{ch}) for the UK secondary standard ionization chamber (NE2561/NE2611) using medium-energy x-rays, Phys. Med. Biol. **43** (1998) 3195–3206.

[13] XIAO, Y., BJÄRNGARD, B., An expression for backscatter factors for ortho voltage x-rays, Phys. Med. Biol. **43** (1998) 1331–1334.

[14] MA, C.-M., SEUNTJENS, J.P., Mass-energy absorption coefficient and backscatter factor ratios for kilovoltage x-ray beams, Phys. Med. Biol. **44** (1999) 131–143.
[15] NAHUM, A.E., Perturbation effects in dosimetry: Part I. Kilovoltage x-rays and electrons, Phys. Med. Biol. **41** (1996) 1531–1580.
[16] INSTITUTION OF PHYSICS AND ENGINEERING IN MEDICINE AND BIOLOGY, The IPEMB code of practice for the determination of absorbed dose for x-rays below 300 kV generating potential (0.035 mm Al–4 mm Cu HVL; 10–300 kV generating potential), Phys. Med. Biol. **41** (1996) 2605–2625.
[17] DEUTSCHES INSTITUT FÜR NORMUNG, Anwendung von Röntgenstrahlen mit Röhrenspannungen von 100 bis 400 kV in der Strahlentherapie, DIN 6809-5, DIN, Berlin (1996).
[18] INTERNATIONAL ATOMIC ENERGY AGENCY, Absorbed Dose Determination in Photon and Electron Beams, 2nd edn, Technical Reports Series No. 277, IAEA, Vienna (1997).
[19] NEDERLANDSE COMMISSIE VOOR STRALINGSDOSIMETRIE, Dosimetry for Low and Medium-energy X-rays: A Code of Practice in Radiotherapy and Radiobiology, Rep. 10, NCS, Delft (1997).
[20] INTERNATIONAL ATOMIC ENERGY AGENCY, Absorbed Dose Determination in External Beam Radiotherapy, Technical Reports Series No. 398, IAEA, Vienna (2000).
[21] PEIXOTO, J.G.P., ANDREO, P., Determination of absorbed dose to water in reference conditions for radiotherapy kilovotage x-rays between 10 and 300 kV: A comparison of the data in the IAEA, IPEMB, DIN and NCS dosimetry protocols, Phys. Med. Biol. **45** (2000) 563–575.
[22] KRAUSS, A., ROOS, M., The heat defect in the water absorbed dose calorimeter, Thermochim. Acta **229** (1993) 125–132.
[23] SELBACH, H.-J., HOHLFELD, K., KRAMER, H.-M., An experimental method for measuring the heat defect of water using total absorption of soft X-rays, Metrologia **29** (1992) 341–347.
[24] KRAMER, H.-M., GROSSWENDT, B., HOHLFELD, K., Experimental determination of the backscatter factor for soft X-rays in water and acrylic glass, Nucl. Instrum. Methods B **9** (1985) 10–19.
[25] KLEVENHAGEN, S.C., Experimentally determined backscatter factors for X-rays generated at voltages between 16 and 140 kV, Phys. Med. Biol. **34** (1989) 1871–1882.
[26] GROSSWENDT, B., Dependence of the photon backscatter factor for water on source-to-phantom distance and irradiation field size, Phys. Med. Biol. **35** (1990) 1233–1245.
[27] GROSSWENDT, B., Dependence of the photon backscatter factor for water on irradiation field size and source-to-phantom distances between 1.5 and 10 cm, Phys. Med. Biol. **38** (1993) 305–310.
[28] SCHNEIDER, U., GROSSWENDT, B., KRAMER, H.-M., "Perturbation correction factor for X-rays between 70 and 280 kV", Dosimetry in Radiotherapy (Proc. Conf. Vienna, 1987), Vol. 1, IAEA, Vienna (1988) 141–148.

[29] SCHNEIDER, U., "A new method for deriving the absorbed dose in phantom material from measured ion dose for X-rays generated at voltages up to 300 kV", Biomedical Dosimetry: Physical Aspects, Instrumentation, Calibration (Proc. Symp. Paris, 1980), IAEA, Vienna (1981) 223–234.

[30] KRAMER, H.-M., GROSSWENDT, B., The role of de-excitation electrons in measurements with graphite extrapolation chambers, Phys. Med. Biol. **47** (2002) 801–822.

[31] ROSSER, K.E., Comparison of Factors Given in ICRU Report 23 and in IAEA TRS 277 for Converting from Exposure/Air Kerma to Absorbed Dose to Water for Medium-energy X-rays, Rep. RSA(EXT)15, National Physical Laboratory, Teddington, UK (1991).

[32] HUBBELL, J.H., et al., Review, bibliography, and tabulation of K, L, and higher atomic shell X-ray fluorescence yields, J. Phys. Chem. Ref. Data **23** (1994) 339–364.

BLANK

EFFECT OF XCOM PHOTOELECTRIC CROSS-SECTIONS ON DOSIMETRIC QUANTITIES CALCULATED WITH EGSnrc

F. HOBEILA, J.P. SEUNTJENS
Medical Physics Unit, McGill University,
Montreal, Canada
E-mail: fadi@medphys.mcgill.ca

Abstract

The work presents a simple implementation of XCOM photoeffect cross-section data in the EGSnrc Monte Carlo code system. The effect of this implementation on the calculation of mass energy absorption coefficients, absorbed dose from point sources and ionization chamber response was investigated. XCOM based photoeffect cross-sections differ from the Storm and Israel data tables by up to 5% for energies larger than 8 keV. This leads to differences in mass energy absorption coefficients (hence collision kerma) of similar magnitude when photoeffect absorption is the predominant photon interaction process. Absorbed doses calculated using EGSnrc for applications in brachytherapy systematically change by up to 2%. EGSnrc calculated ionization chamber response in this energy region is affected by 1%.

1. INTRODUCTION

EGSnrc [1, 2] is a general purpose suite used for the Monte Carlo simulation of the coupled transport of electrons and photons. EGSnrc incorporates significant improvements to its predecessor, EGS4 [3], not only in electron transport but also in low energy photon physics with the simulation of atomic relaxations and bound Compton interactions. EGSnrc uses different approaches to gather the total cross-sections for the various possible photon interactions. Whereas total Compton cross-sections are calculated at run time, the total photoeffect cross-section is interpolated from data stored in a preparation file with a sometimes inadequate energy grid. More importantly, in the standard EGSnrc distribution, these latter data use a data package by Storm and Israel (S&I) [4] that dates back to the early 1970s. Yet, accuracy in low energy photon applications such as brachytherapy (e.g. the dose distribution from ^{125}I) requires up to date low energy photoeffect cross-section data. A simple implementation of the United States National Institute of Standards and Technology (NIST) XCOM based photoeffect cross-sections [5] in EGSnrc and a study of the effect on relevant dosimetric quantities calculated with EGSnrc

(i.e. mass energy absorption coefficients, absorbed dose from point sources and ionization chamber response) is presented in this paper.

2. MATERIALS AND METHODS

2.1. XCOM photoeffect data in EGSnrc

The implementation of new photoeffect data requires modification of the pgs4pepr.dat file that contains these basic data along with pair production cross-sections for elements $Z = 1$ to $Z = 100$. In the standard version of EGSnrc the pgs4pepr.dat file contains photoeffect cross-sections as tabulated by S&I in 1970 [4]. The file is laid out as follows: a header containing information on the number of bins available for each element (maximum is 61 bins/element), a full list of element specific energy grids spanning the 1 keV to 100 MeV range and a list of element specific photoeffect cross-sections. For all elements the photoeffect cross-section values of the pgs4pepr.dat file were updated with the XCOM total photoeffect absorption cross-sections taken from the NIST web version of the XCOM software [6]. The updated pgs4pepr.dat file is named pgs4pepr_xcom.dat.

2.2. Validation

Initial validation of the pgs4pepr_xcom.dat file, which is created semi-automatically, was done by comparing the data file with the original S&I file. The comparison of the two data files resulted in the correction of a small number of duplicate, missing or shifted values. Some of the more dosimetrically important elements, such as carbon, oxygen, hydrogen and lead, were also verified manually. A second validation of the pgs4pepr_xcom.dat file was done using a simple EGSnrc user code named PHOTXsection. PHOTXsection calculates the absorption coefficients of the different photon interactions; that is, coherent (Rayleigh) scattering, incoherent (Klein–Nishina or bound) scattering, photoeffect absorption and pair production. It does so by explicitly simulating the transport of photons on a slab of medium and counting the number of primary photon interactions of a given type. This validation process verifies the overall accuracy of the implemented new data within the data fitting constraints of EGSnrc. This potentially leads to systematic errors, most notably around characteristic energies but also at other energies, depending on the fitting interval defined by the energy boundaries AP and UP in the PEGS4 data preparation package. As shown in Fig. 1(a), the photoeffect cross-sections, as calculated by PHOTXsection using XCOM data, agree within ±1% with the NIST XCOM

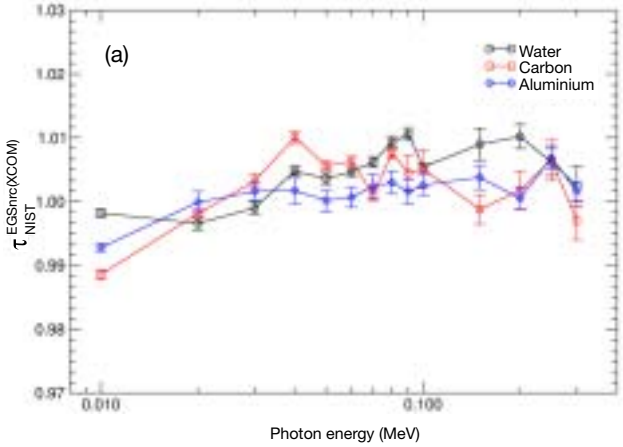

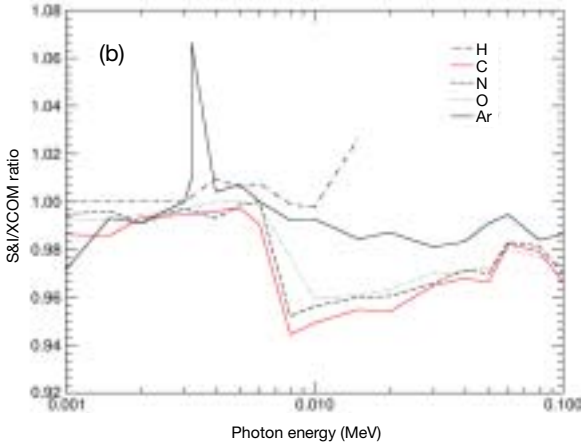

FIG. 1. (a) Ratio of EGSnrc(XCOM) calculated photoeffect cross-sections to NIST database cross-sections. The calculated cross-sections with AP = 1 keV, UP = 2 MeV agree within ±1% with the NIST cross-sections. (b) Ratio of S&I to XCOM photoeffect cross-sections for low Z, dosimetrically important elements. XCOM cross-sections are larger than S&I by up to 5%.

cross-sections for compounds or elements when an interval [AP = 1 keV, UP = 2 MeV] is used. This result slightly improves when an interval [AP = 1 keV, UP = 150 keV] is used.

A comparison of the two photoeffect data sets was undertaken for all 100 elements contained in the data files. Figure 1(b) presents cross-section ratios S&I/XCOM of dosimetrically important low Z elements in an energy range in which photoeffect absorption is an important photon interaction (1–100 keV). This figure shows the XCOM photoeffect cross-sections being systematically larger by up to 5% when compared with the S&I cross-sections for energies higher than 6 keV. This behaviour extends to the 100 elements and over the complete energy range (up to 100 MeV) contained in the data files. For higher Z elements, the increase in cross-section can be as high as 10% when going from an S&I to an XCOM data set. The differences between data sets near absorption edges, as shown by the 3.203 keV argon K edge, can be as high as 6–10%. The ratio curve for hydrogen ends at 10.5 keV, since no cross-section values were contained for higher energies in the S&I pgs4pepr.dat file.

2.3. Dosimetric quantities

2.3.1. Mass energy absorption coefficients

Mass energy transfer and mass energy absorption coefficients were calculated using the XCOM data in EGSnrc. The kerma was obtained by calculating energy deposition by a broad-parallel monoenergetic photon beam in a thin (2 μm) slab of medium of infinite lateral extent. Primary photons were forced to interact in the medium, and electron transport was turned off, resulting in no energy escaping the slab through bremsstrahlung radiation or electron transport, which implies the scoring of kerma. Mass energy absorption coefficients were derived from mass energy transfer coefficients using the relation $\mu_{en}/\rho = (\mu_{tr}/\rho)(1 - \bar{g})$, where $\bar{g}$ is the fraction of the initial energy expanded in radiative interactions upon electrons slowing down in an infinite medium. The $\bar{g}$ value was calculated as the ratio of all the energy radiated by the electrons created from the monoenergetic photons to the energy transferred from the photons to the electrons.

2.3.2. Inverse square corrected radial dose distributions

Point sources emitting very low monoenergetic photons (10–50 keV) were simulated in water using a spherical scoring user code named KERNEL. This user code outputs radial depth dose distributions corrected for the inverse square law fluence reduction.

2.3.3. Calculation of ionization chamber response

Ionization chamber air kerma response, R, is defined as the absorbed dose to the cavity of an ionization chamber, D_{gas}, positioned with its effective point of measurement at a reference point divided by air kerma measured free in air ($K_{free\ air}$) at that same reference point in the absence of the chamber. Response was calculated for a realistic Exradin A11 parallel-plate ionization chamber, for which detailed drawings were obtained from the manufacturer. The chamber mainly consists of C552 air equivalent plastic, in particular the entrance window (1 mm thick) and the collecting plate. Monoenergetic photon point sources of energy 15–200 keV and a source to cavity distance of 100 cm yielding a field radius of 2.2225 cm at the chamber plane were used. The user code CAVRZnrc was used to calculate dose to the gas cavity, D_{gas}. $K_{free\ air}$ at 1 m in air was calculated by determining the photon energy fluence spectrum at the point of measurement using FLURZnrc and by integrating the energy fluence spectrum and mass energy transfer coefficients (from the appropriate data set) over the energy range of the spectrum.

2.4. Other EGSnrc transport parameters

All EGSnrc calculations used the photon transport parameters: AP = PCUT = 1 keV, bound Compton scattering, Rayleigh scattering and atomic relaxations after all photon interactions. Electron transport was simulated by the PRESTA-II algorithm with the parameters: AE = 1 keV, ECUT = 512 keV, photo-electron angular sampling and spin effects. Point source radial dose distribution calculations used the above parameters, while mass energy transfer calculations did not use electron transport and ionization chamber response calculations used electron range rejection as a variance reduction technique.

3. RESULTS AND DISCUSSION

3.1. Mass energy absorption coefficients

Figure 2(a) shows the ratio of mass energy absorption coefficients for air, calculated using EGSnrc, with either the S&I (EGSnrc(S&I)) or the XCOM (EGSnrc(XCOM)) cross-section data sets, and the Hubbell and Seltzer NIST (μ_{en}/ρ) tables [7]. Consistent with the differences in basic photoeffect data, in the 6–100 keV energy range the EGSnrc(S&I) calculated (μ_{en}/ρ) show discrepancies of up to 4% with the NIST database. When using EGSnrc(XCOM), calculated (μ_{en}/ρ) show excellent agreement, within ±0.5% in air and ±1% in

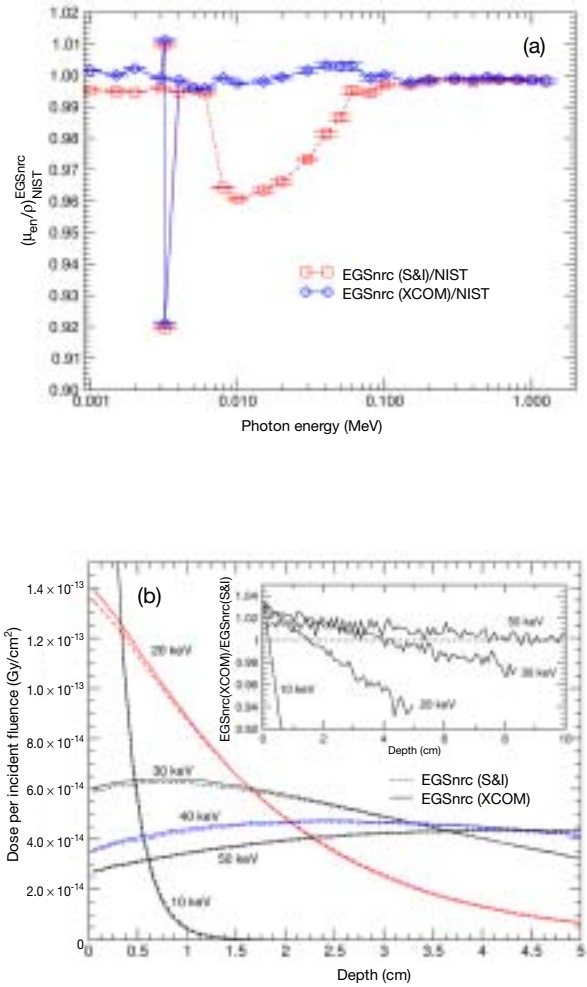

FIG. 2. (a) Comparison of the mass energy absorption coefficients of air calculated using EGSnrc(S&I) and EGSnrc(XCOM) with the NIST database. EGSnrc(S&I) coefficients differ by up to 4% from the NIST data in the 6–100 keV range, while the EGSnrc(XCOM) results are in excellent agreement with the NIST data. (b) Comparison of calculated, inverse square corrected, radial dose curves for monoenergetic point sources in water using EGSnrc(S&I) and EGSnrc(XCOM). Doses calculated near the source with XCOM are 1–3% higher than EGSnrc(S&I) calculated doses.

water (result not shown), with the NIST [7] data over the same energy range. The 3.2 keV peak in Fig. 2(a) is due to EGSnrc interpolation artefacts close to the absorption edge (argon in this case).

3.2. Inverse square corrected dose distributions from point sources

Since low photon energy brachytherapy is a domain for which the implementation of XCOM photoeffect cross-sections in EGSnrc should be beneficial, kernel radial depth dose distributions were calculated and compared using both photoeffect data sets. Monoenergetic point sources immersed in water over a photon energy range of 10 keV to 50 keV using KERNEL were simulated. Figure 2(b) shows the unnormalized calculated radial depth dose distributions. EGSnrc(XCOM) calculated distributions are shown as solid lines, while the dotted lines represent EGSnrc(S&I) distributions. Figure 2(b) demonstrates that EGSnrc(XCOM) calculated doses near the source ($r \sim 0$ cm) are 3% larger for the 10 keV source when compared with the EGSnrc(S&I) doses. This difference decreases down to 1% at 50 keV as Compton scattering interactions become more frequent. This result is explained by the XCOM photoeffect cross-sections being larger than their S&I counterparts, which leads to an increase in photoeffect interactions and in turn to an increase in dose near the source. The larger XCOM cross-sections also lead to a higher attenuation effect, which renders the EGSnrc(XCOM) calculated distributions less penetrating than the EGSnrc(S&I) distributions. This is seen in Fig. 2(b), in which the XCOM and S&I distributions cross-over (see Fig. 2(b), inset).

3.3. Ionization chamber response

For chambers fulfilling Bragg–Gray conditions, ionization chamber response is traditionally calculated using the Spencer–Attix cavity theory. At low photon energies, however, Spencer–Attix cavity theory breaks down and Monte Carlo response calculations constitute an important alternative. Until recently, chamber response calculations using condensed history Monte Carlo systems were inaccurate, due to various approximations in the electron transport physics. Recently, however, the accuracy of EGSnrc calculated response was tested for gas filled cavities under the conditions of the Fano theorem; that is, the cavity being filled with gaseous wall material and attenuation and scattering of the primary beam in the chamber wall being corrected for. In such a test the consistency of the transport was tested, independent of underlying cross-section data, and shown to be in agreement with the Fano theorem [8, 9].

In realistic air filled chambers, however, the air kerma response is also affected, among other factors, by the accuracy of the cross-section data. In this study, in which the focus was on the effect of changing a cross-section data set, we compared EGSnrc(XCOM) and EGSnrc(S&I) calculated ionization chamber responses for the Exradin A11 parallel-plate chamber in 15–200 keV monoenergetic photon beams in air. Figure 3(a) shows the result for a 'pure' Exradin A11 chamber. EGSnrc(XCOM) responses are represented by diamond symbols and a solid line, EGSnrc(S&I) responses are shown by circle symbols and a dotted line. The inset shows the ratio EGSnrc(XCOM)/EGSnrc(S&I) of the calculated responses. EGSnrc(XCOM) calculated responses at the lower energies are up to 1% lower than EGSnrc(S&I) calculated responses. Since the response calculations are executed at very low energies, any trace of high Z impurities in the chamber materials potentially has effects on the chamber response, as the photoeffect cross-sections rapidly increase with Z. We incorporated high Z impurities from materials with Z values ranging from 10 to 82, amounting to 90 μg/g, or 0.01% distributed uniformly in the C552 plastic [9]. Figure 3(b) shows that the response in the presence of high Z impurities is increased by 2% or less at 30–50 kV, and this conclusion is not significantly altered by the data set used: $\text{EGSnrc(XCOM)}_{\text{imp}}$ responses are up to 1% lower than $\text{EGSnrc(S\&I)}_{\text{imp}}$ calculated responses.

4. CONCLUSION

XCOM photoeffect cross-sections were implemented in the EGSnrc Monte Carlo system. We have shown that this implementation modifies EGSnrc calculated results of various low energy dosimetric quantities. Mass energy absorption coefficients calculated using S&I cross-sections show differences of up to 4% compared with the NIST absorption coefficient database, while XCOM calculated mass energy absorption coefficients are in agreement with NIST data [6]. EGSnrc(XCOM) radial depth dose distributions of monoenergetic sources (10–50 keV) in water are less penetrating (by 1–2%) but have a higher dose near the source (1–3%) when compared with EGSnrc(S&I). Ionization chamber responses calculated using XCOM and pure materials are 1% lower than S&I calculated responses, and this conclusion is not modified when a realistic amount of high Z impurities are uniformly present in the chamber's C552 plastic. In order to further improve the use of up to date cross-section data in EGSnrc, the interpolation of data around absorption edges needs to be addressed. Finally, the cross-section data file generated for this study is available from the authors and will be made available for downloading from the EGSnrc web site.

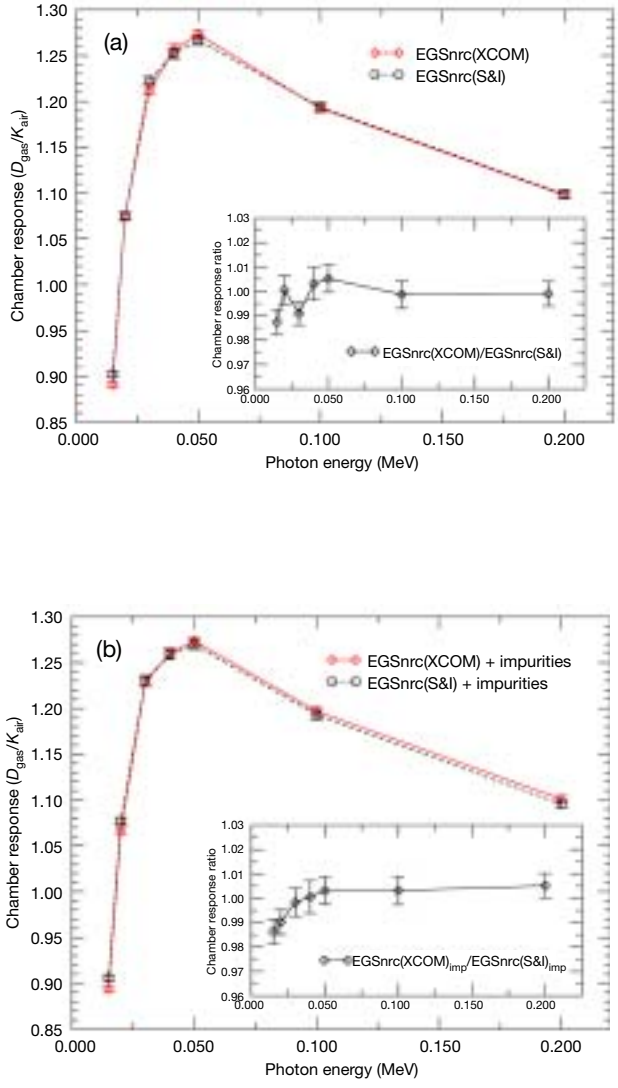

FIG. 3. Ionization chamber response of an Exradin A11 chamber for monoenergetic photon beams calculated using EGSnrc(S&I) and EGSnrc(XCOM). Insert: ratio (XCOM/S&I) of chamber response. (a) For uncontaminated C552 plastic, (b) for C552 plastic in the presence of high Z impurities (90 μg/g).

ACKNOWLEDGEMENTS

This work was partially supported by NSERC (Natural Sciences and Engineering Research Council of Canada) through research grant RG 227800. J.P. Seuntjens is a research scientist of the National Cancer Institute of Canada, with funds provided by the Canadian Cancer Society.

REFERENCES

[1] KAWRAKOW, I., Accurate condensed history Monte Carlo simulation of electron transport. I. EGSnrc, the new EGS4 version, Med. Phys. **27** (2000) 485–498.

[2] KAWRAKOW, I., ROGERS, D.W.O., The EGSnrc Code System: Monte Carlo Simulation of Electron and Photon Transport, Rep. PIRS-701, National Research Council, Ottawa (2001).

[3] NELSON, W.R., HIRAYAMA, H., ROGERS, D.W.O., The EGS4 Code System, Rep. SLAC-265, Stanford Linear Accelerator Center, Stanford, CA (1985).

[4] STORM, E., ISRAEL, H.I., Photon cross sections from 1 keV to 100 MeV for elements Z=1 to Z=100, At. Data Nucl. Data Tables **7** (1970) 565–681.

[5] BERGER, M.J., HUBBELL, J.H., XCOM: Photon Cross-sections on a Personal Computer, Rep. NBSIR 87-3597, National Bureau of Standards, Washington, DC (1987).

[6] BERGER, M.J., HUBBELL, J.H., SELTZER, S.M., COURSEY, J.S., ZUCKER, D.S., XCOM: Photon Cross Section Database (Version 1.2), National Institute of Standards and Technology, Gaithersburg, MD (1999), http://physics.nist.gov/xcom

[7] HUBBELL, J.H., SELTZER, S.M., Tables of X-ray Mass Attenuation Coefficients and Mass Energy-absorption Coefficients 1 keV to 20 MeV for Elements Z=1 to 92 and 48 Additional Substances of Dosimetric Interest, Rep. NISTIR 5632, National Institute of Standards and Technology, Gaithersburg, MD (1995).

[8] KAWRAKOW, I., Accurate condensed history Monte Carlo simulation of electron transport. II. Application to ion chamber response simulations, Med. Phys. **27** (2000) 499–513.

[9] SEUNTJENS, J.P., et al., "Calculated and measured air-kerma response of ionization chambers in low and medium energy photon beams", Recent Developments in Accurate Radiation Dosimetry (Proc. Int. Workshop Montreal, 2001), Medical Physics Publishing, Madison, WI (2002).

MEETING THE NEEDS

(Session 4)

Chair

S. GROTH
IAEA

Co-Chair

K.R. SHORTT
IAEA

Rapporteur

B. VIKRAM
IAEA

BLANK

CANCER EPIDEMIOLOGY IN DEVELOPING COUNTRIES

S.L. WHELAN
International Agency for Research on Cancer,
Lyon
E-mail: whelan@iarc.fr

Abstract

The paper discusses the epidemiology of cancer in developing countries, and focuses in particular on four types of cancer: breast, colorectal, cervical and nasopharyngeal. The demography of developing countries and its effect on the incidence of cancer are also addressed.

1. CANCER BURDEN: INFORMATION SOURCES AND ESTIMATION

The basic measures of cancer occurrence are incidence and mortality. Incidence is the number of new cases diagnosed per year, expressed here as a rate per 100 000 persons per year. This rate is an approximation of the average risk of developing a cancer, and is used to compare the risk of disease between populations and over time. Mortality is the number of deaths occurring per year. In the absence of incidence data, frequency data from hospital or pathology series can give an idea of the relative importance of different cancers in a population. Using data on incidence, mortality, survival and frequency, estimates of the global burden of cancer were prepared for 2000 in GLOBOCAN. The methodology is described in Ref. [1], and estimated national and global numbers and incidence rates cited in this paper are taken from it. In this paper, for the purposes of describing the present and future burden of cancer, incidence data are used.

2. WORLDWIDE INCIDENCE OF CANCER

It is estimated that there were over 10 million new cancer cases worldwide in 2000, 5.4 million of which occurred in developing countries. The developed countries are those in North America and Europe, and Australia, New Zealand and Japan; the developing countries are the remainder. If worldwide incidence is mapped (Fig. 1), the larger burden of all sites of cancer

is in affluent societies, largely owing to tumours associated with smoking and the Western lifestyle (i.e. lung, breast, prostate and colorectal), with dietary factors believed to be of major significance. There is marked geographical variation in the occurrence of the different cancer types.

(a)

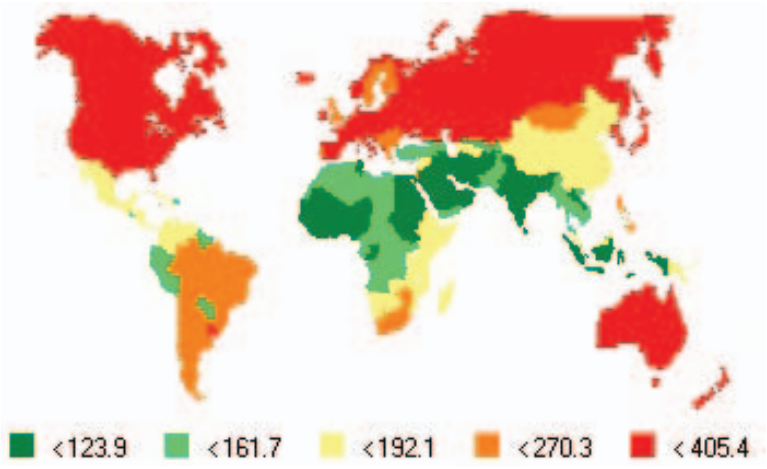

(b)

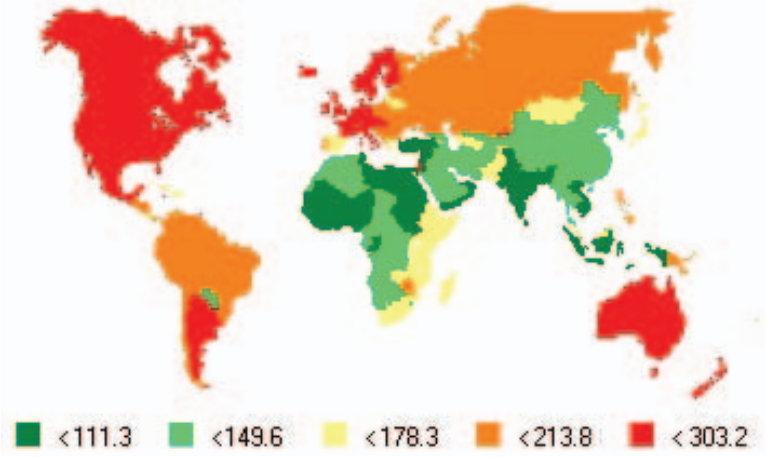

FIG. 1. Male (a) and female (b) worldwide incidence of cancers: all sites.

Figure 2 shows the 12 most frequent cancers for men and women (as number of new cases) in the more developed and less developed regions of the world. Lung cancer is the most common cancer in both, followed by colorectal, breast and prostate in developed countries, and by stomach, breast and liver in developing countries. The risk factors and trends for cancer vary according to area, and up to 25% of tumours in some developing countries are associated

with chronic infections, such as the hepatitis B and C viruses for liver cancer and human papilloma viruses for cervical cancer.

Four sites of cancer are reviewed in more detail, looking at their aetiology and their present and possible future importance in the context of developing countries.

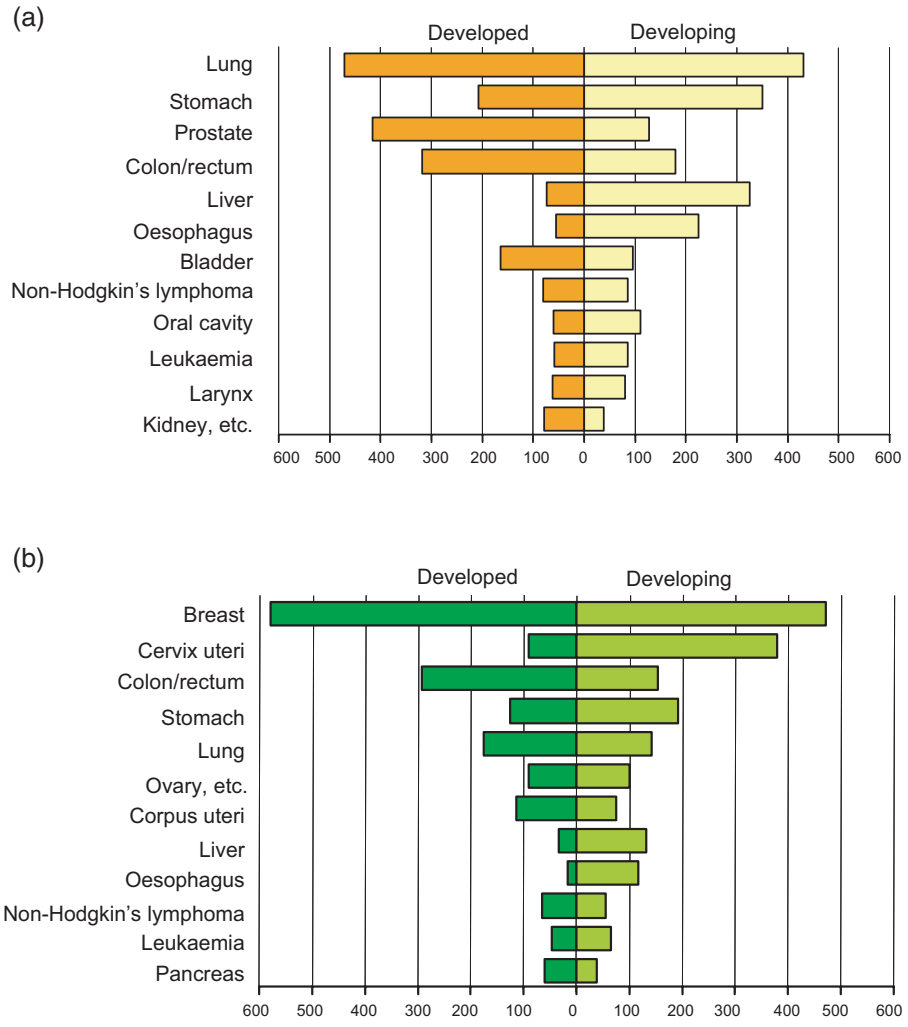

FIG. 2. Number of new cases in 2000 of the 12 most common cancers in (a) males (total of 2 504 000 cases in the developed world and 2 814 000 cases in the developing world) and (b) females (total of 2 176 000 cases in the developed world and 2 562 000 cases in the developing world). Source: Ref. [2].

2.1. Breast cancer

Worldwide, cancer of the breast is by far the most common cancer of women, with an estimated one million new cases in 2000 — 22% of all new cancers in women. More than half the cases are in the industrialized countries; the disease is not yet as common in developing countries, although incidence is increasing. Age standardized incidence rates (ASRs) are 90.4 for North America, 78.2 for western Europe and 82.7 for Australia and New Zealand. High rates are found in the southern part of South America, especially Uruguay, where Montevideo has reported the highest ASR in the world in the latest volume of Cancer Incidence in Five Continents [3] (114.9 per 100 000), and in Argentina, but incidence is low in most African and Asian populations (incidence around 20 per 100 000) (Fig. 3).

Most of the geographical variation observed is probably due to differing environmental and lifestyle exposures. The main risk factors are reproductive and hormonal factors, and risk is increased by early menarche, late menopause, late age at first birth and low parity. The role of diet in breast cancer has to be confirmed, but obesity in postmenopausal women is an important factor [1]. There is a clear association with socioeconomic factors, with women of higher social class being at higher risk [4]. In sub-Saharan Africa the incidence in white women is much higher than in black African women and risk is higher in cities such as Abidjan (Côte d'Ivoire) and Harare (Zimbabwe) than in less urban environments [5].

Incidence rates of breast cancer are increasing in most countries, and the changes are greatest in countries with relatively low rates of incidence of breast cancer. Rises of 1% per year were reported between 1964 and 1985 in Bombay [6] and 2.7% per year in Shanghai between the two time periods 1972–1974 and 1992–1993 [7] (shown in Fig. 4), and 3.6% per year in Singapore between 1968 and 1992 [8]. Cancer registries in China are recording annual increases in incidence of 3–5% [9]. In Ibadan, Nigeria, incidence between 1998 and 1999 was 24.7 per 100 000, compared with 13.7 between 1960 and 1969. In Kampala, Uganda, there has been a significant increase in incidence since the 1960s [10].

While incidence continues to increase, mortality is falling in developed countries as a result of organized mammography screening and improved treatment [11]. The strongest predictive factor for survival after diagnosis is the extent of disease. Screening for breast cancer is expensive, and it is not possible to introduce screening programmes in many developing countries because of technical and financial constraints. The availability and accessibility of diagnostic and treatment services is poor in many developing countries, particularly in sub-Saharan Africa. Women often consult the medical services at a late stage, and breast cancer is not curable once it has metastasized. It is

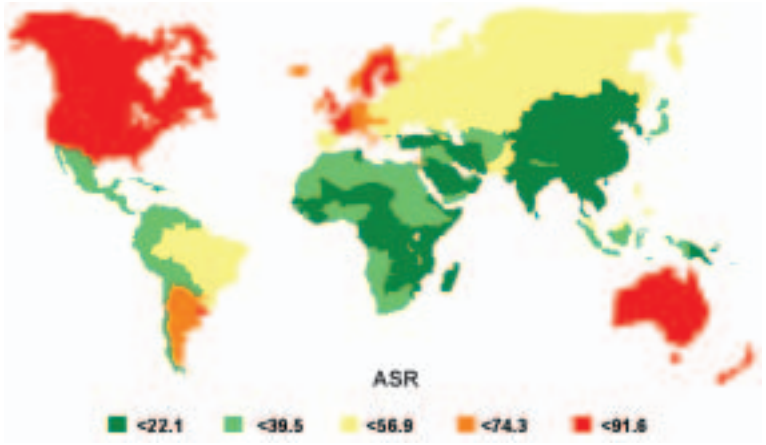

FIG. 3. Incidence of female breast cancer in 2000 (total of 1 050 000 cases).

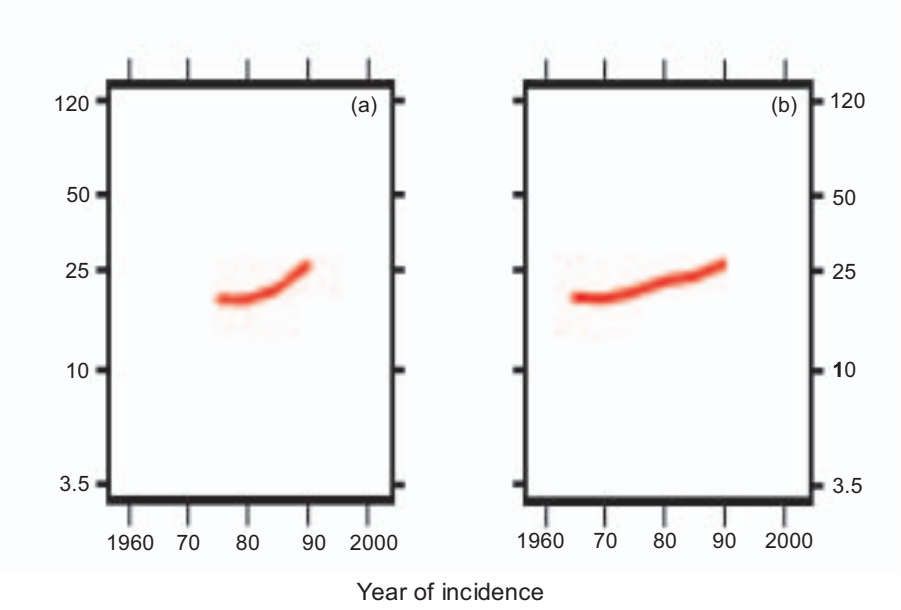

FIG. 4. Female breast cancer incidence ASR in (a) Shanghai and (b) Bombay.

probable that incidence will continue to rise in these countries, but breast cancer already accounts for 18.4% of total cancers in women in developing countries, and it is vital to improve public health education, access to medical services and the availability of chemotherapy and radiotherapy.

2.2. Colorectal cancer

Large bowel cancer occurs predominantly in affluent societies, and is most frequent in North America, western Europe, Australia and New Zealand, and in the southern part of South America (Fig. 5). In 2000 colorectal cancer was estimated to be the fourth most common cancer in the world in both sexes, with an estimated 943 000 cases (9.4% of total cancers). Colorectal cancer comprises 6.2% of cancers in less developed countries.

Temporal changes in countries with high rates have been relatively small, but incidence is increasing in countries of low incidence. Migrant studies show a rapid increase in colorectal cancer incidence when populations move from a low risk area (e.g. Japan) to a high risk area (e.g. the United States of America) [12]. In Israel the age standardized rates in Jewish people born in Europe or the Americas (48.5 in males and 37.5 in females) are substantially greater than in Jewish people born in Africa or Asia (32.7 and 25.0) [3]. The rates for colorectal cancer in black people in the USA now exceed those in white people in several areas [3]. It appears from recent data that risk in the younger age groups in Africa is approaching, and even at times exceeding, that in the USA (Fig. 6) [3].

The increases in incidence in migrant populations point to an environmental causation, probably related to dietary factors, with a possible link to exercise. Epidemiological studies have consistently found a higher risk of colorectal cancer associated with a diet low in vegetables and unrefined plant foods and high in the consumption of red, and particularly processed, meat [11]. In Africa the very low incidence of cancer of the colon and rectum (2.2% of the world's cases in 2000) has frequently been related to the characteristics of the African diet, which is high in cereal and low in animal protein.

Education on healthy diet and lifestyle is important for prevention. Survival following detection and treatment is good and improving in the Western world (62% in the USA, 43% in Europe in the mid-1980s), but lower in developing countries [13].

2.3. Cervical cancer

Cancer of the cervix uteri is the second most common cancer among women worldwide, with an estimated 468 000 new cases and 233 000 deaths in

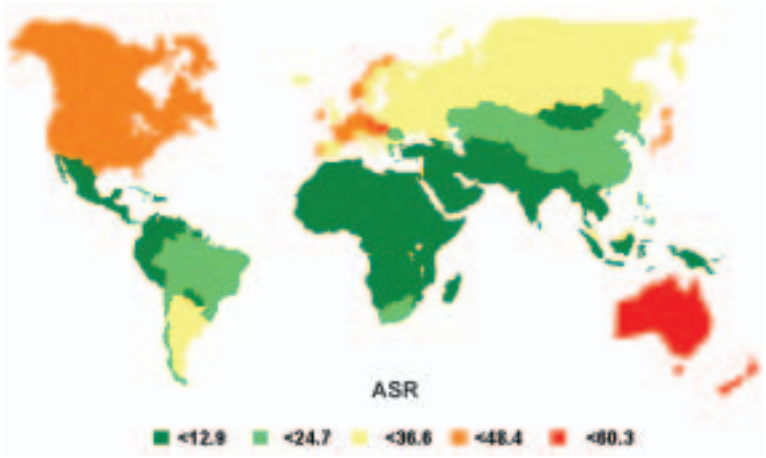

FIG. 5. Male colorectal cancer incidence in 2000.

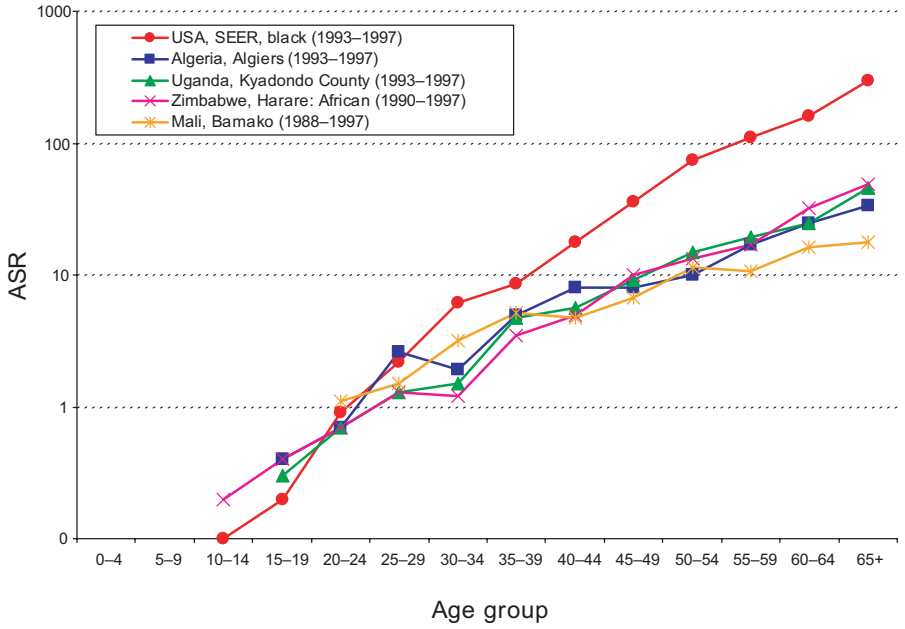

FIG. 6. Incidence of colorectal cancer (both sexes) by age group. SEER: Surveillance, Epidemiology and End Results Program.

2000. Almost 80% of cases occur in developing countries, where it is the most common cancer in women in many regions. The highest incidence rates are found in Latin America and the Caribbean, sub-Saharan Africa (22% of all cancers in females) and South and Southeast Asia (Fig. 7).

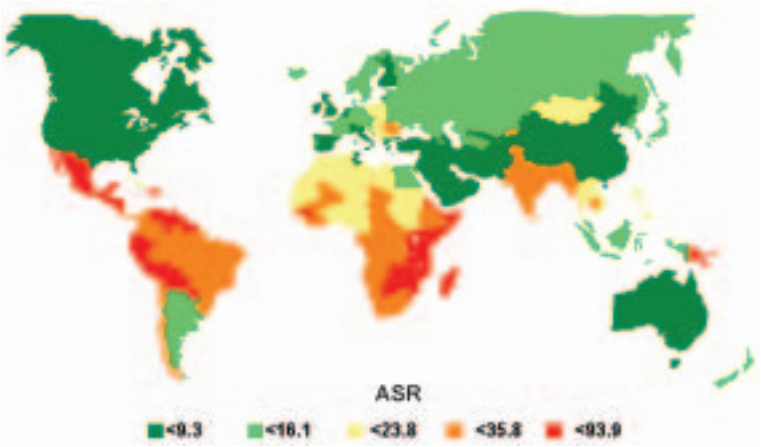

FIG. 7. Incidence of cancer of the cervix uteri in 2000.

Incidence and mortality have fallen steadily over the past 40 years in most Western countries. These declines are mainly related to screening for pre-invasive cancer. In developing countries rates have been relatively stable or show modest declines. There does appear to have been a dramatic decline in incidence in China; for example, in Shanghai the age adjusted incidence of cervical cancer fell from 26.7 per 100 000 to 2.5 between 1972–1974 and 1993–1994 [7]. Such a large decrease cannot be solely the result of screening activities, so there must have been a genuine decrease in exposure to risk factors too. Figures 8 and 9 show trends for selected Asian populations and for an African population.

The main underlying cause of cervical cancer is the human papilloma virus, a common sexually transmitted infection and now considered a 'necessary' initiator. Hormonal factors, such as early age at first birth, use of hormonal contraceptives and high parity, have an influence. Epidemiological studies have shown a consistent association between risk and sexual activity, particularly initiation at an early age and multiple sexual partners, although these may be related to exposure to the human papilloma virus rather than independent risk factors. Other elements related to risk include social class, ethnicity, religion and smoking [20].

It has been noted that estimates of cervical cancer incidence in developing countries are probably lower than actual rates, because many women with cervical cancer do not receive medical care and so are not included in cancer registry data [20]. This is due to a lack of diagnostic facilities and

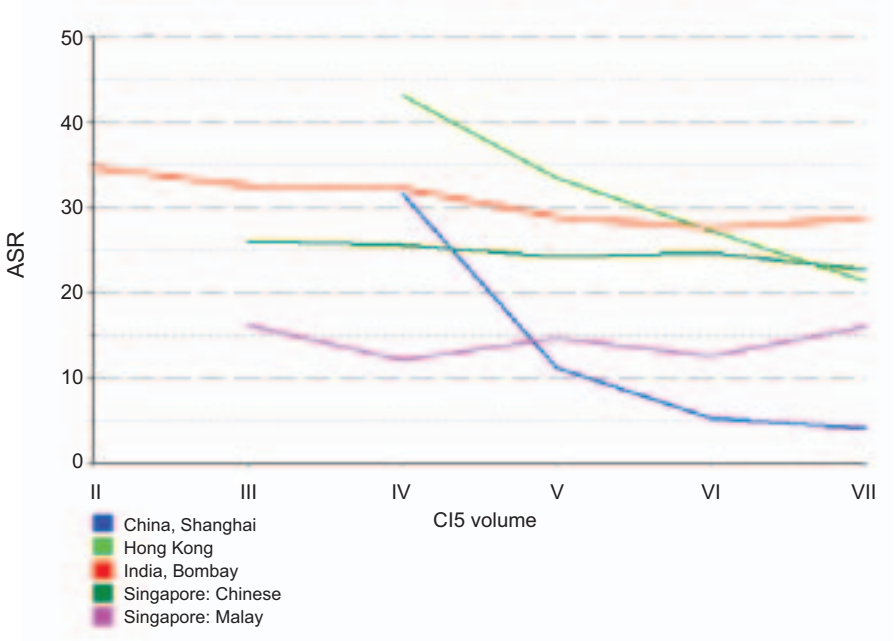

FIG. 8. Trends in incidence of cancer of the cervix uteri in Asia: age 15–74. CI5 volume: Cancer Incidence in Five Continents volume number; II: Ref. [14], III: Ref. [15], IV: Ref. [16], V: Ref. [17], VI: Ref. [18], VII: Ref. [19].

failure to consult medical care providers (particularly on the part of older women, women with late stage illness or women without the resources to pay for diagnosis or treatment).

Cervical cancer prevention has focused on screening using Pap smears. While such screening has been very efficacious in reducing incidence in countries where good quality and population coverage are feasible, in developing countries there is little evidence of success. Screening programmes in Cuba [21] and Costa Rica [22] seem to have had virtually no impact on cervical cancer incidence. Considerable research into the feasibility of using simpler screening methods in developing countries, especially visual inspection following application of dilute acetic acid and Lugol's iodine, is ongoing [23]. Human papilloma virus DNA testing is also being investigated as a screening method for those aged 30 and older.

Screening and treatment of dysplasia are cost effective interventions when compared with expensive treatment of invasive cancer. An effective programme must include health education to inform women about the disease and about how to avoid it. Cervical intraepithelial neoplasms may be treated by local excision, whereas radiotherapy is required for the effective treatment of

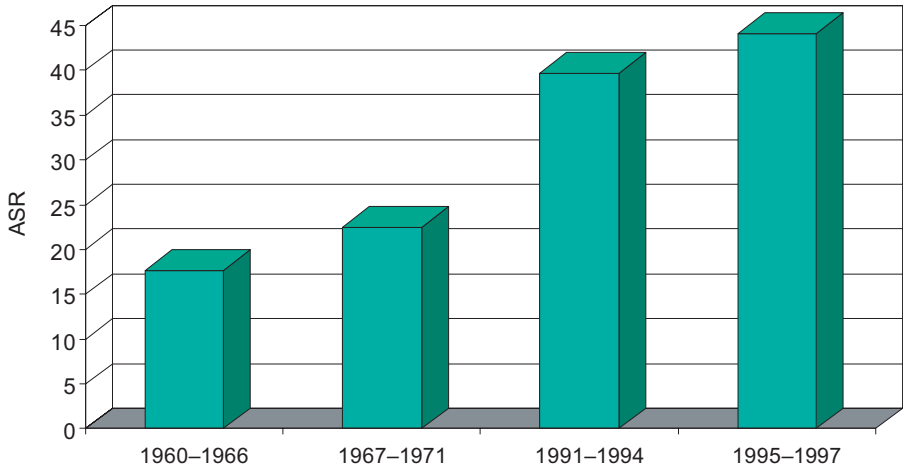

FIG. 9. Trends in incidence of cancer of the cervix uteri in Kampala, Uganda. Source: Ref. [10].

invasive cancer. Many countries in Africa, which has the highest incidence, do not have radiotherapy facilities, and the only solution is for patients to be sent abroad — a solution that is usually too expensive.

2.4. Nasopharyngeal carcinoma

Nasopharyngeal carcinoma (NPC) is a rare malignancy in most parts of the world; ASRs for people of either sex are generally less than 1 per 100 000 persons per year [19], and it comprises only about 0.6% of new cancer cases worldwide. However, incidence is much higher in a few scattered regions, such as the southern provinces of China (Guangdong, Guanxi, Hunan and Fujian) [24], and moderately raised in populations from Southeast Asia [19] and from North Africa, Sudan and Saudi Arabia [25–28] (Figs 10 and 11).

The Epstein–Barr virus (EBV) is now generally accepted to be important in the carcinogenesis of NPC, but infection does not explain the very different geographical and ethnic patterns. In developing countries infection is acquired in childhood, while in developed countries infection is generally delayed until adolescence. The high risk found among Chinese people residing in the southern Chinese provinces is not correlated with the age specific prevalence of EBV infection, found in virtually all Chinese children by the age of five [29]. Intake of several preserved food products, such as Cantonese style salted fish

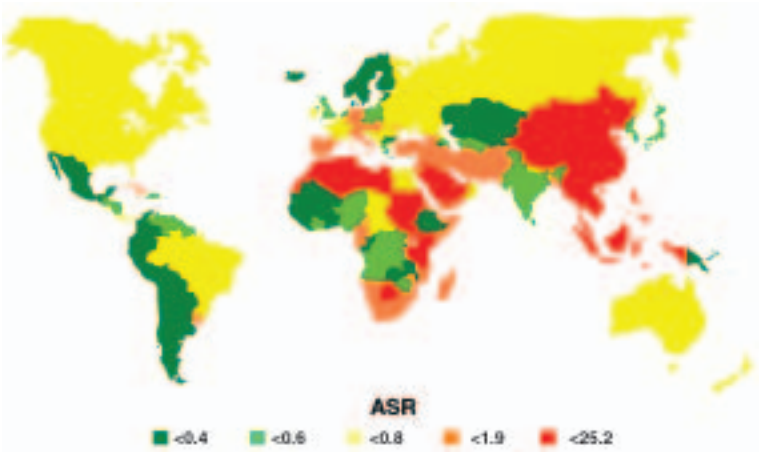

FIG. 10. Incidence of male nasopharyngeal cancer: all ages.

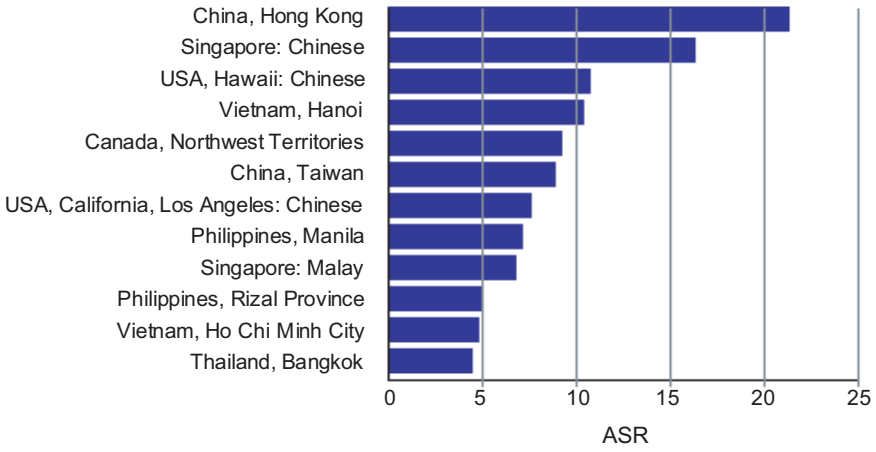

FIG. 11. Incidence of male nasopharyngeal cancer, 1993–1997: all ages.

or Tunisian harissa, has been found to be significantly associated with NPC. Ethnicity–migrant studies demonstrate a role of genetic susceptibility.

A study of data from the Hong Kong cancer registry showed a decline in the ASR from 28.5 from 1980 to 1984 to 20.2 from 1995 to 1999 per 100 000 males, and from 11.2 to 7.8 per 100 000 females, resulting in a total decrease of 29% for males and 30% for females over this 20 year period [30].

Radiotherapy remains the primary treatment modality. This cancer may affect only a small proportion of the world's population, but with an incidence of 21.3 in Hong Kong males, and a mortality rate of 40 for some Chinese populations, the impact within these populations is significant.

3. DEMOGRAPHY

Most developing regions have achieved major reductions in fertility rates in the past 30 years. The exception is sub-Saharan Africa, where rates are still high. The 'epidemiological transition' has occurred, or is occurring, in many developing countries, with a shift from infectious and parasitic diseases to chronic and degenerative diseases. Control of infectious disease and curtailment of family size will result in an increase in proportions of the elderly, and it is estimated that by 2020 one of every six Thais is likely to be aged 60 or older [31]. The world population is expected to increase generally over the next 50 years, but substantially more in less developed countries (by 63%) than in developed countries (Fig. 12).

It is difficult to assess the effect of the acquired immune deficiency syndrome (AIDS) epidemic on demography. In sub-Saharan Africa (accounting for almost two thirds of all human immunodeficiency virus positive persons worldwide), it has been estimated that a total of 21 million person-

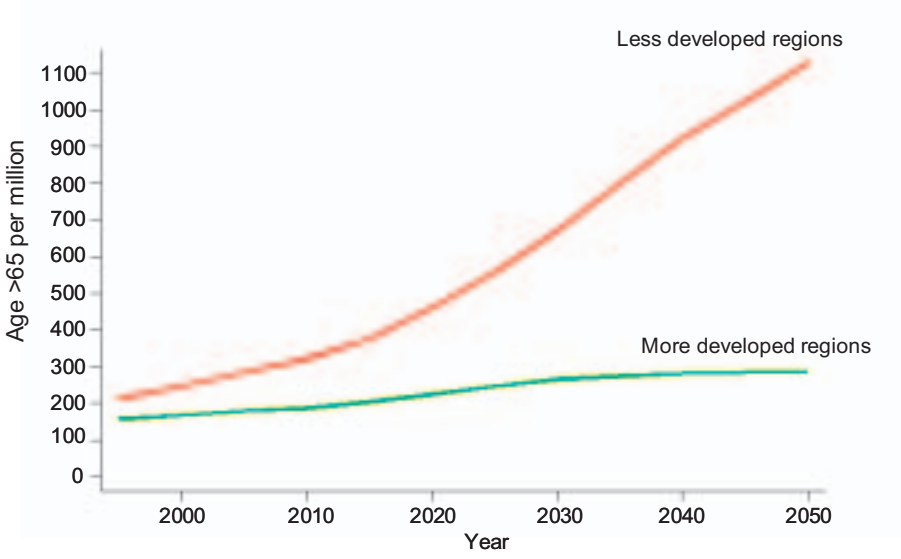

FIG. 12. Projected number of persons aged 65 or over in more developed and less developed regions, 2000–2050. Source: Ref. [32].

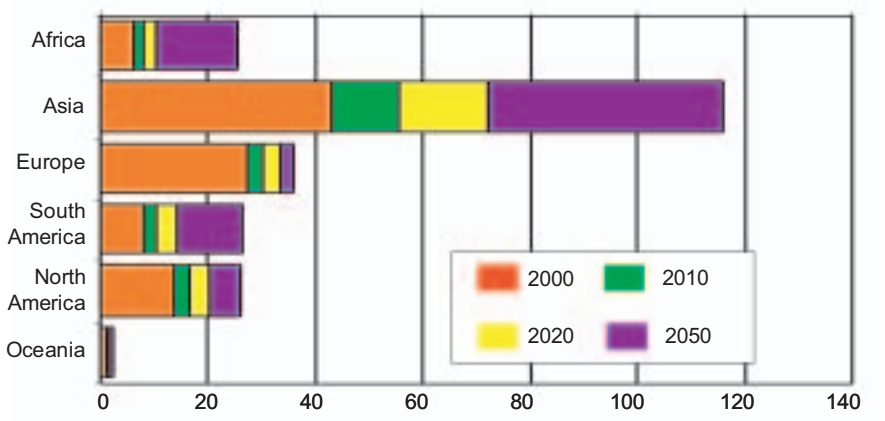

FIG. 13. Increase in cancer numbers (millions) by region.

years of life have been lost to AIDS among women aged 25–64 [33]. The United Nations has estimated life expectancy at birth at 48.3 years in 1995–2000 in the 35 African countries considered 'highly affected', 6.5 years less than it would have been in the absence of AIDS. By 2015 the population of these countries is projected to be 10% less than it would have been without AIDS [34]. While the demographic impact of AIDS remains relatively low outside Africa, prevalence of the disease has been growing rapidly in Asia, Latin America and the Caribbean.

The prediction of future incidence from the data available is not an easy task. Time trend data are based on historical patterns, which are not necessarily a good basis for future projections. For much of the world, and particularly in developing countries, the historical data are not sufficient to permit the modelling of trends in the coming years. Figure 13 presents projected numbers of cases of cancer for 2010, 2020 and 2050 using the GLOBOCAN software and based only on United Nations population projections. The increases do not take known trends into account. Different sources have presented different results, but even if these err on the side of conservatism it is clear that cancer control programmes, to prevent and manage the disease, should already be an imperative for the less affluent countries of the world.

REFERENCES

[1] PARKIN, D.M., BRAY, F.I., DEVESA, S.S., Cancer burden in the year 2000. The global picture, Eur. J. Cancer **37** (2001) S4–S66.

[2] FERLAY, J., BRAY, F., PISANI, P., PARKIN, D.M., GLOBOCAN 2000: Cancer Incidence, Mortality and Prevalence Worldwide, Version 1.0, IARC CancerBase No. 5, IARC Press, Lyon (2001).
[3] PARKIN, D.M., WHELAN, S.L., FERLAY, J., TEPPO, L., THOMAS, D.B. (Eds), Cancer Incidence in Five Continents, Vol. VIII, IARC Scientific Publication No. 155, IARC Press, Lyon (2002).
[4] KOGEVINAS, M., PEARCE, N., SUSSER, M., BOFFETTA, P., Social Inequalities and Cancer, IARC Scientific Publication No. 138, IARC Press, Lyon (1997).
[5] PARKIN, D.M., et al., Cancer in Africa, IARC Scientific Publication No. 153, IARC Press, Lyon (in press).
[6] YEOLE, B.B., JAYANT, K., JUSSAWALLA, D.J., Trends in breast cancer incidence in greater Bombay: An epidemiological assessment, Bull. World Health Organ. **68** (1990) 245–249.
[7] JIN, F., et al., Cancer incidence trends in urban Shanghai, 1972–1994: An update, Int. J. Cancer **83** (1999) 435–440.
[8] SEOW, A., DUFFY, S.W., McGEE, M.A., LEE, J., LEE, H.P., Breast cancer in Singapore: Trends in incidence 1968–1992, Int. J. Epidemiol. **25** (1996) 40–45.
[9] PARKIN, D.M., Global cancer statistics in the year 2000, Lancet Oncol. **2** (2001).
[10] WABINGA, H.R., PARKIN, D.M., WABWIRE-MANGEN, F., NAMBOOZE, S., Trends in cancer incidence in Kyadondo County, Uganda, 1960–1997, Br. J. Cancer **82** (2000) 1585–1592.
[11] STEWART, B.W., KLEIHUES, P., World Cancer Report, IARC Press, Lyon (2003).
[12] SHIMIZU, H., MACK, T.M., ROSS, R.K., HENDERSON, B.B., Cancer of the gastro-intestinal tract among Japanese and white immigrants in Los Angeles County, J. Natl. Cancer Inst. **78** (1987) 223–228.
[13] SANKARANARAYANAN, R., BLACK, R.J., PARKIN, D.M. (Eds), Cancer Survival in Developing Countries, IARC Scientific Publication No. 145, IARC Press, Lyon (1998).
[14] DOLL, R., MUIR, C.S., WATERHOUSE, J.A.H. (Eds), Cancer Incidence in Five Continents, Vol. II, International Union Against Cancer, Geneva (1970).
[15] WATERHOUSE, J.A.H., MUIR, C.S., CORREA, P., POWELL, J. (Eds), Cancer Incidence in Five Continents, Vol. III, IARC Scientific Publication No. 15, IARC Press, Lyon (1976).
[16] WATERHOUSE, J.A.H., MUIR, C.S., SHANMUGARATNAM, K., POWELL, J. (Eds), Cancer Incidence in Five Continents, Vol. IV, IARC Scientific Publication No. 42, IARC Press, Lyon (1982).
[17] MUIR, C.S., WATERHOUSE, J.A.H., MACK, T., POWELL, J., WHELAN, S. (Eds), Cancer Incidence in Five Continents, Vol. V, IARC Scientific Publication No. 88, IARC Press, Lyon (1987).
[18] PARKIN, D.M., MUIR, C.S., WHELAN, S.L., GAO, Y.-T., FERLAY, J., POWELL, J. (Eds), Cancer Incidence in Five Continents, Vol. VI, IARC Scientific Publication No. 120, IARC Press, Lyon (1992).

[19] PARKIN, D.M., WHELAN, S.L., FERLAY, J., RAYMOND, L., YOUNG, J. (Eds), Cancer Incidence in Five Continents, Vol. VII, IARC Scientific Publication No. 143, IARC Press, Lyon (1997).
[20] PROGRAM FOR APPROPRIATE TECHNOLOGY IN HEALTH, Planning Appropriate Cervical Cancer Prevention Programs, 2nd edn, PATH, Seattle, WA (2000).
[21] FERNANDEZ GARROTE, L., LENCE ANTA, J.J., CABEZAS CRUZ, E., ROMERO, T., CAMACHO, R., Evaluation of the cervical cancer control program in Cuba, Bull. Pan Am. Health Organ. **30** (1996) 387–391.
[22] HERRERO, R., et al., Screening for cervical cancer in Latin America: A case-control study, Int. J. Epidemiol. **21** (1992) 1050–1056.
[23] SANKARANARAYANAN, R., "Cervical cancer in developing countries", Trans. R. Soc. Trop. Med. Hyg. **96** (2002) 580–585.
[24] LI, J.-Y., et al., Atlas of Cancer Mortality in the People's Republic of China, China Map Press, Shanghai (1979).
[25] MUIR, C.S., Nasopharyngeal carcinoma in non-Chinese populations with special reference to south-east Asia and Africa, Int. J. Cancer **8** (1971) 351–363.
[26] CAMMOUN, M., VOGT HOERNER, G., MOURALI, N., Tumors of the nasopharynx in Tunisia. An anatomic and clinical study based on 143 cases, Cancer **33** (1974) 184–192.
[27] HIDAYATALLA, A., MALIK MOA, E.L., HADI, A.E., OSMAN, A.A., HUTT, M.S.R., Studies on nasopharyngeal carcinoma in the Sudan. I. Epidemiology and aetiology, Eur. J. Cancer Clin. Oncol. **19** (1983) 705–710.
[28] AL-IDRISSI, H.Y., Head and neck cancer in Saudi Arabia: Retrospective analysis of 65 patients, J. Int. Med. Res. **18** (1990) 515–519.
[29] INTERNATIONAL AGENCY FOR RESEARCH ON CANCER, Epstein–Barr Virus and Kaposi's Sarcoma Herpesvirus/Human Herpesvirus 8, IARC Monographs on the Evaluation of Carcinogenic Risks to Humans, Vol. 70, IARC Press, Lyon (1997).
[30] LEE, A.W., et al., Changing epidemiology of nasopharyngeal carcinoma in Hong Kong over a 20-year period (1980–99): An encouraging reduction in both incidence and mortality, Int. J. Cancer **103** (2003) 680–685.
[31] KINSELLA, K., "Demographic and epidemiologic trends affecting health policy in developing countries", Population Growth and Demographic Structure, United Nations, New York (1999).
[32] UNITED NATIONS, World Population Ageing 1950–2050, United Nations, New York (2002).
[33] YANG, B.H., BRAY, F.I., PARKIN, D.M., SELLORS, J.W., ZHANG, Z.-F., Years of Life Lost from Cervical Cancer Compared with Other Diseases (in preparation).
[34] UNITED NATIONS, World Population Prospects. The 2000 Revision, Vol. II: Sex and Age, United Nations, New York (2001).

BLANK

MEGAVOLTAGE RADIATION THERAPY: MEETING THE TECHNOLOGICAL NEEDS

J. VAN DYK
London Regional Cancer Centre and
University of Western Ontario,
London, Ontario, Canada
E-mail: jake.vandyk@lrcc.on.ca

Abstract

The process of radiation therapy is complex and contains multiple steps, each of which has an impact on the quality of the treatment and on the possible clinical outcome. This treatment process includes diagnosis, patient immobilization, target and normal tissue localization, beam selection, beam shaping, dose calculation, technique optimization, simulation, prescription, treatment verification and, finally, the actual radiation treatment. Depending on the type of disease, it is not necessary that every patient undergo all the steps in the process; however, it is necessary that each step of the process used for a particular patient be carried out with the greatest accuracy. Inaccuracies at any stage of the process will be carried through to subsequent stages and have an impact on clinical outcome. It is therefore important to recognize, when addressing technological needs for megavoltage radiation treatment, that the radiation treatment machine technology should not be considered in isolation from the technologies associated with the other steps of the treatment process. In the purchase of radiation treatment equipment in any country, the following should be considered: (a) the availability and reliability of a country's physical infrastructure; (b) financial considerations; (c) the types and stages of disease most likely to be treated; (d) the number and types of professional staff available to apply the treatment technologies; (e) professional staff training and continuing education resources; (f) the number of patients requiring treatment with the treatment equipment available (i.e. the efficient use of available resources); (g) the treatment planning technologies (e.g. immobilization, imaging and the treatment planning computer) available to prepare the patient for the actual irradiation procedure; (h) the technological considerations of the therapy equipment in the context of the above factors (e.g. ^{60}Co versus linac); (i) the cost of maintenance and local availability of spare parts; (j) perceptions, misperceptions and emotional responses regarding specific technologies; and (k) safety considerations. Identifying the technological needs requires a thorough understanding of the technological capabilities of the treatment technologies available. These capabilities, however, must be placed in the context of the multiple factors listed above.

1. INTRODUCTION

In its simplest form, the purpose of radiation therapy is to irradiate malignant disease to the highest possible dose and, at the same time, to minimize the dose to all other tissues. While there are multiple technological methods available for doing this, the actual radiation treatment needs to be considered in the broader context of the total radiation treatment process. This process contains multiple steps (see column 1 of Table I), each of which has an impact on the quality of the treatment and on the possible clinical outcome. One crucial step in this process is the determination of the location and extent of the disease relative to the adjacent normal tissues. This can be done in a variety of ways, ranging from simple clinical examination to the use of complex three dimensional (3-D) imaging, sometimes aided by contrast agents. As part of this localization process, it is very important that patient immobilization procedures be implemented to ensure that the same patient position will be used during both the planning and the daily treatment stages. With knowledge of the location of the target and critical tissues, decisions can be made about the appropriate beam arrangements to provide adequate tumour coverage while sparing healthy tissues. This beam arrangement may have to be confirmed on a therapy simulator prior to the actual implementation of the radiation treatment. In summary, the treatment process includes diagnosis, patient immobilization, target and normal tissue localization, beam selection, beam shaping, dose calculation, technique optimization, simulation, prescription, treatment verification and, finally, treatment. Depending on the type of disease and the available technologies, it is not necessary that every patient undergo all the steps in the process, nor is the order of the steps always the same; however, it is necessary that each step of the process used for a particular patient be carried out with the greatest accuracy. Inaccuracies at any stage of the process will be carried through to subsequent stages, and may have an impact on the clinical outcome. It is therefore important to recognize, when addressing technological needs for megavoltage radiation treatment, that the radiation treatment machine technology should not be considered in isolation from the technologies associated with the other steps of the treatment process. It makes no sense, for example, to have highly sophisticated linacs capable of 3-D conformal and intensity modulated radiation therapy (IMRT) if there is not a good imaging capability available for accurately defining the extent and location of both tumours and normal tissues.

In the developed countries there has been a struggle for market supremacy between cobalt unit and linac technologies. Organizations that provide development aid have tried to define appropriate technology. For example, the basic requirements for a radiation therapy facility have been defined in an IAEA

TABLE I. STAGES OF THE RADIATION THERAPY PROCESS
(adapted with permission [1])

	Issue	Equipment	Front line staff (support staff)
Diagnosis and clinical evaluation	Tumour pathobiology, staging	Cytology, pathology, imaging, other diagnostic equipment	Radiation oncologist, diagnostic radiologist, other specialists
Therapeutic decisions	Cure or palliation, treatment modalities	None	Radiation oncologist
Patient data and imaging for treatment planning	External and internal contours, CT[a], MR[b], X ray, ultrasound, SPECT[c], PET[d]	Contour taker, diagnostic scanner (CT, MR, nuclear medicine, ultrasound)	Radiation oncologist (radiation therapist[e], dosimetrist, diagnostic technologist, physicist)
Target volume localization	Tumour and normal tissue definition, (image) contouring, image segmentation, margins, field shaping	Computer image display station, contouring software	Radiation oncologist (dosimetrist, radiation therapist, physicist)
Fabrication of treatment aids	Compensators and boluses, immobilization devices, blocks, shields, MLC[f] shaping	Compensator maker, vacuum former for masks, shielding system, MLC	Radiation therapist, mould room technologist, dosimetrist (physicist, radiation oncologist)
Simulation	Virtual simulation and beam display, treatment verification, confirmation of shields	Simulator, CT–simulator, simulator–CT	Radiation oncologist, radiation therapist (dosimetrist, physicist)
Treatment planning	Selection of technique, computation of dose distribution, optimization	Treatment planning system, virtual simulation software	Dosimetrist, physicicst

TABLE I. (cont.)

	Issue	Equipment	Front line staff (support staff)
Treatment	Verification of set-up and portal imaging, verification of equipment performance, dosimetry checks, record keeping	Cobalt-60 machine, linac, brachy-therapy afterloading device, superficial/orthovoltage machine, intensity modulation capability, in vivo dosimetry system	Radiation therapist (dosimetrist, radiation oncologist, physicist)
Patient evaluation during treatment	Treatment tolerance, tumour response	Diagnostic scanner (CT, MR, nuclear medicine, ultrasound)	Radiation oncologist (radiation therapist, nurse)
Patient follow-up	Tumour control, normal tissue response	Diagnostic scanner (CT, MR, nuclear medicine, ultrasound)	Radiation oncologist (nurse)

[a] CT: computed tomography.
[b] MR: magnetic resonance.
[c] SPECT: single photon emission computed tomography.
[d] PET: positron emission tomography.
[e] Radiation therapist: radiation therapy technologist or radiographer.
[f] MLC: multileaf collimator.

Note: This table summarizes the treatment process. A further and very significant effort, especially by physicists, goes into the commissioning, calibrating and quality assurance of the related equipment listed in the table.

report [2], which considered ^{60}Co megavoltage therapy machines but indicated that the IAEA would not consider providing linac technology to developing countries. In 1993 the Pan American Health Organization, along with the World Health Organization and the IAEA, produced a report describing the design requirements for megavoltage X ray machines for cancer treatments in developing countries [3]. Clearly, even within the past decade, there are still different opinions on the benefits (and risks) of ^{60}Co versus linacs for the provision of radiation treatment, especially in the context of developing countries [3–6].

There are a number of complex and interrelated considerations involved when a particular institution in any country makes decisions about the purchase of radiation therapy equipment. These are outlined in the remaining sections of this paper. While the emphasis is on technological considerations, other important issues are summarized to make sure that all factors are considered together and none are handled in isolation.

2. INFRASTRUCTURE

There are tremendous variations around the world in terms of the physical infrastructure required to support equipment used for radiation therapy. One of the basic requirements for operating radiation treatment and related equipment is a constant and stable supply of electricity. In general, linacs also require a sufficient supply of water of good quality and low temperature for cooling. Examining the physical infrastructure should be one of the first and most important actions prior to the purchase of new equipment.

3. ECONOMIC CONSIDERATIONS

While economic considerations are dealt with in detail in a separate paper in these Proceedings [7], the purchasers of radiation therapy equipment are constrained by the financial resources available not only for the purchase of the machine and the construction of the facility but also for the ongoing operating costs, the maintenance costs, the costs of staff training and continuing education, the costs of dosimetry and quality assurance equipment, and eventually the cost of the disposal of the treatment technology once it has completed its useful life. There are a number of situations in which new or used equipment was donated to a developing country but the equipment could not be placed in clinical service, owing either to a lack of spare parts or to a lack of appropriate resources to operate it [6]. Previous analysis has shown that the

purchase of teletherapy machines is directly related to the gross national income per capita [8], and that the significant deficiencies that exist in the availability of radiation therapy equipment are linked to the country's economic status [9].

4. TYPES AND STAGES OF DISEASE

The choice of radiation therapy equipment will be dependent on both the types of disease to be treated and the stage of the disease. Institutions involved in treatments for mostly radical (curative) intent will require different imaging, treatment planning and treatment technologies than those institutions that are treating primarily for palliation. Epidemiological considerations for different regions in the world have been considered in detail [10, 11].

5. PROFESSIONAL STAFF AVAILABILITY

It is very important to recognize the staff support required to commission, operate and maintain radiation therapy and related equipment. It makes little sense to set up a radiation therapy facility if there are no radiation oncologists available to be involved in the patients' care. Similarly, medical physicists and radiation therapists (technologists, radiographers) are required to commission the technologies and to treat the patients. A survey of Latin American countries in 1989 showed that nearly 60% of the centres surveyed had no physicist and did not possess the minimum equipment for dosimetry [12]. Appropriate machine maintenance support is required, either through hired staff or through purchased maintenance contracts. Furthermore, relevant staff training and continuing education are essential, especially for staff who may not have had a complete and thorough professional training or who are applying new technologies for patient treatments without previous experience in the use of that technology.

6. PATIENT THROUGHPUT AND EFFICIENCY

In purchasing new equipment, consideration should be given to the number of patients requiring treatment with the treatment equipment available. For example, in North America there are six high energy radiation therapy machines per one million population, and each machine is used to treat 230 new patients per year [13]. In other parts of the world, such as Africa and

Southeast Asia, there may be only one high energy radiation therapy machine for 20 to 40 million people, and one machine may be used to treat 600 new patients per year [13]. Thus if few staff and few treatment machines are available it will be important to maximize the patient throughput by using equipment that has minimal downtime and sufficient radiation output.

7. TREATMENT PLANNING TECHNOLOGIES

Complex treatment technologies such as linacs with MLCs, which have dynamic treatment capabilities, and the use of intensity modulation require the use of comprehensive patient immobilization procedures and imaging tools (e.g. CT simulation or magnetic resonance imaging (MRI) with image fusion capabilities) for the accurate delineation of the planning target volume and critical organs. If the imaging tools are not available, less complex set-up and treatment procedures are appropriate. Furthermore, radiation treatment planning computer systems are a basic requirement for all radiation therapy centres, whether or not they have sophisticated imaging technologies. These systems come in a wide range of capabilities and can be purchased for basic 2-D treatment planning to complex 3-D image based treatment planning using inverse planning optimization techniques.

8. RADIATION TREATMENT TECHNOLOGIES

The first clinical use of ^{60}Co, on 27 October 1951 in London, Ontario, Canada, was a major entry point into the megavoltage photon era. There is clear evidence that the advent of megavoltage radiation therapy had a major impact on tumour control and patient survival for such diseases as prostate cancer, Hodgkin's disease, head and neck tumours and cancer of the cervix [14]. While there are indications that institutions using advanced technologies have better patient outcomes [15], it has never been directly proved that this is related to the machine energy levels, and could well be due to surrogate issues related to staff training and staff quality, the academic environment and the resources available to institutions having more sophisticated equipment. In the developed world there has evolved a clear preference for the use of multimodality megavoltage accelerators for radiation treatment. In the developing world the issues are not nearly as clear cut and the debate continues with regard to the advantages and disadvantages of ^{60}Co versus linacs. These issues are summarized in Table II [4, 16, 17] and have to some extent been reviewed by others [5, 18]. It is not the intent of this paper to resolve this

TABLE II. COMPARISON ISSUES FOR ^{60}Co TELETHERAPY VERSUS THE USE OF LINACS
(adapted from Refs [4, 16, 17])

	Observation
Radiation beam characteristics	
Penumbra	Dependent on source diameter Dependent on photon energy Dependent on tissue density, especially for higher linac energies Significance depends on uncertainty in target volume definition Significance depends on patient set-up uncertainty Significance depends on organ motion Biological penumbra is always sharper than physical penumbra (i.e. reducing the significance of a larger physical penumbra)
Energy and quality	Cobalt is better for target volumes near the skin surface (e.g. head and neck, breast, brain) Impact of using lower energy can be reduced by the use of multiple fields, arc or rotational techniques
Scattering conditions and dose uniformity	Minor effect for small fields Can be reduced by the use of flattening filters, compensators and clever treatment planning for larger fields
Contour and inhomogeneity corrections	Lack of electronic equilibrium in high energy photon beams in lung yields larger penumbral effects and potential central axis drop in dose Tissue–bone or tissue–prosthesis interface effects cover a larger volume in higher energy photon beams
Dose to bone	Difference is relatively small when considering the photon spectrum at depth for a range of energies
Machine characteristics	
Dose rate	Cobalt has lower uncertainty in dose delivery since it is not dependent on a monitor ionization chamber or a beam steering system
Patient to collimator distance	Larger distance is better for patient set-up Smaller distance reduces penumbra Practically, a compromise between large and small distance

TABLE II. (cont.)

	Observation
Isocentre height	Traditionally smaller on cobalt machines; this is a significant advantage for radiation therapists (technologists), especially in countries in which the therapists are physically smaller
Radioactive source	Virtually monoenergetic for ^{60}Co: simplifies dose calibrations and calculations Reduced beam hardening in attenuators
Service and maintenance issues	Down time substantially less for ^{60}Co: <1% for ^{60}Co; ~3% for 4–6 MV linacs; >5% for multimodality high energy linacs
Safety considerations	
Radiation protection	Source transport issues Source disposal issues Stuck source issues These concerns can be handled with appropriate organization and training Linacs > 10 MeV have increased personnel exposures, owing to residual activity and neutron production Linacs > 10 MeV have increased patient dose equivalent, owing to neutron production
Pacemaker concerns	Substantially reduced concerns on ^{60}Co, owing to the lack of electromagnetic interference
Cost considerations	
Relative annual operating costs, including capital depreciation, building and maintenance costs	Cobalt-60: low energy linac: high energy linac (1:3.2:4.8)
Patient throughput	Differs only by 5–10% compared with linacs with higher dose rates

debate. It is, however, the intent to place the discussion in the context of many of the other factors that need to be considered when purchasing radiation therapy equipment, especially in the developing world.

A significant issue for the developing world is not only the cost of teletherapy equipment but also the maintenance of such equipment. Figure 1 is

taken from a report on the problems of cancer management specifically in anglophone west Africa [19]. These breakdowns extended over very long periods of time (>250 days in some years), although frequently the causes of the breakdowns were due to minor electrical or mechanical problems, which could have been repaired within a few hours in more developed countries with adequate maintenance and engineering services. The machine referred to in Fig. 1 was the only machine available in that region of west Africa for a population of 140 million people. Clearly, this is an extreme example, although it demonstrates the tremendous disparity that exists around the world and that needs to be addressed by institutions acquiring new radiation therapy equipment. The question then is how do we meet the technological needs for

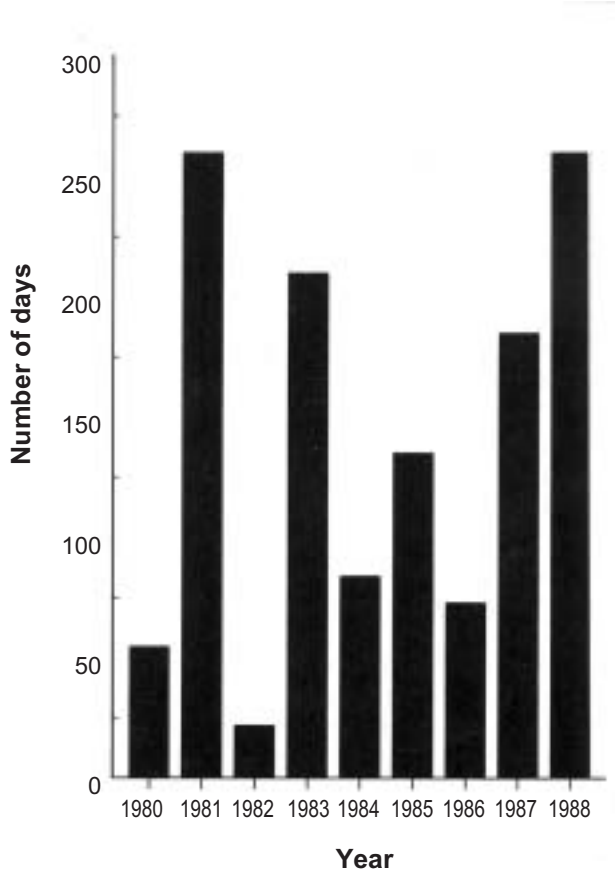

FIG. 1. Breakdown data of a ^{60}Co teletherapy unit in Nigeria from 1980 to 1988. Adapted with permission from Ref. [19].

megavoltage equipment in the developing world? Perhaps one approach is to consider a broad historical review of the technological development of radiation therapy and to see whether historical information can be applied in the context of the developing world.

8.1. Historical development of radiation oncology

The evolution of radiation oncology can be divided into five distinct phases, as summarized in Table III. The first phase occurred between the discovery of X rays in 1895 and the 1940s, when radiation therapy was limited

TABLE III. PHASES OF MAJOR TECHNOLOGICAL DEVELOPMENTS IN RADIATION ONCOLOGY

Phase	Time	Technology	Issues/benefits
1	1895–1940s	100–400 kV X rays	Non-uniform doses to deep seated tumours; skin toxicity; bone toxicity
2	1950s	^{60}Co 4–8 MeV linacs 20–30 MeV betatrons	Megavoltage photons provided skin sparing; improved dose uniformity in the target and reduced doses to normal tissues; increased manual treatment planning
3	1960s–1970s	Multimodality linacs Computerized radiation treatment planning systems Simulators	Increased availability of linacs; increased use of computerized treatment planning; introduction of simulators; increased medical physics human resources to support the technologies; more systematized and comprehensive quality assurance
4	1970s–1980s	CT combined with 3-D treatment planning	Improved targeting; reduced complications; improved dose computations
5	1980s–present	Development of computer controlled dynamic treatments (IMRT) Further improvements in imaging with CT simulators, MRI, PET, PET–CT	Dose escalation with increased probabilities of tumour control and reduced probabilities of normal tissue complications

mainly to lower energy units with 100–400 kV X rays. If any treatment planning took place, it was by using the manual addition of isodose charts. The second phase, beginning in the late 1940s and extending into the 1960s, involved the use of megavoltage photons from ^{60}Co units, low energy (~4–8 MeV) linacs and high energy (~20–30 MeV) betatrons. Treatment planning was on the increase, using primarily manual methods of adding isodose distributions or point calculations for irregular fields. The third phase, during the 1960s and 1970s, at least in the developed world, involved the start of the transition from primarily ^{60}Co treatments to megavoltage linacs combined with the enhanced use of computerized treatment planning systems. This was also the time during which simulators became commercially available. During this phase there was also a significant increase in medical physics human resources to support these sophisticated technologies in the clinical environment, and more systematized and comprehensive quality assurance procedures were implemented. The fourth phase saw the introduction of CT in combination with computer aided 3-D treatment planning. Theoretically, Goitein [20] estimated that CT scanning could improve local control by an average of 6% and improve the probability of survival by an average of 3.5%. Subsequently, multiple studies demonstrated significant changes in treatment plans, comparing plans made without and with the aid of CT scanning [21–23]. The two decades from the 1980s to the present have experienced a revolution in computerized delivery technologies, such that dynamic IMRT is now possible, and a further enhancement of imaging technologies with the use of CT simulation, MR scanning, PET and combined PET–CT allows for the 3-D viewing of targets and critical structures. This allows for higher doses to the target and lower doses to normal tissues. At present, based on the most recent data from the IAEA Directory of Radiotherapy Centres, there are about 4700 linacs and 2400 cobalt units worldwide, while there are 3300 linacs and 440 cobalt units combined in the Group of Seven (G7) countries (i.e. 53% of megavoltage equipment is being used for approximately 11% of the world's population), clearly demonstrating a huge disparity of the equipment available worldwide. These disparities are expected to worsen as a result of the steady change in demographics in developing countries, which predicts that the ageing of their populations will result in a significant increase in the annual incidence of new cancers.

While this brief historical perspective gives a rough overview of how technology evolved, it also provides a perspective on how radiation therapy technology is at present used around the world, since many countries are actually in different time phases of technology implementation based on the descriptors in Table III. For example, some countries have very few megavoltage photon machines, with no treatment planning computers or imaging capabilities. Such countries would be in phase 2 and, with additional

resources, should perhaps seek to escalate to the next phase with the application of treatment planning computers, simulators and possibly CT imaging capabilities. It could be unwise, and potentially unsafe, to aspire directly to phase 5, since their infrastructure (resources, staff, training, maintenance, etc.) may not support this level of transition. It should also be noted that some countries (e.g. India and China) have a large spectrum of facilities available, ranging from a few very well equipped centres to many poorly or underequipped centres, depending on the institution and its location. In such cases the upgrade phasing should be considered on a regional or institutional basis, rather than on a country basis.

9. SUMMARY

There is no simple algorithm to define the technological needs for radiation oncology in any specific country. However, there are general guidelines that need to be acknowledged. These guidelines relate to the major points outlined above. The use of Table III and the historical phases of the evolution of radiation oncology technology should provide institutions in developing countries with a guide for the next reasonably achievable phase in the process of acquiring technology to meet their radiation oncology needs. Radiation therapy equipment purchase and implementation have been, and continue to be, a major long standing problem for developing countries. Most developing countries cannot afford sophisticated equipment. In many instances, if the money were made available through external grants or donations, they still lack the skilled technical personnel to commission the equipment or to maintain the machines in good order, partly due to local constraints, such as power supply fluctuations, and partly due to a lack of resources to find replacement parts or to obtain machine service support (see, for example, Fig. 1) [6, 24].

For developing countries with a relatively low income per capita, ^{60}Co remains the standard for high energy equipment: in general, the more robust and simple, the better [6]. Also, it would be best, as part of the purchase agreement, to arrange for commercial vendors to provide on-site training for preventative maintenance and minor repairs, and for the clinic to have a service contract with the vendor for at least five years [6]. Furthermore, training and continuing education for professional staff need to be part of the long term budget for the proper clinical use of these technologies.

To quote from Durosinmi-Etti [19] of Lagos, Nigeria:

> "Commercial companies should be encouraged to design and produce simple, cheap, rugged, and easily-maintained equipment for such

developing countries. Such equipment should be more mechanical than electrical, and therefore devoid of costly electronic parts, as the power supply in most of these countries is erratic and current fluctuations or blackouts are a common occurrence. Whenever possible, power supply should be provided by battery-operated means."

Of course, this is relevant for countries in transition with a very low income per capita. For countries with higher incomes, decisions will have to be made in accordance with the relevant infrastructure; however, Table III can be used to guide them to the next level of capability. In considering these issues, it is also important to recognize the anticipated future evolution of a particular country's economy and infrastructure. Countries with a good 'prognosis' can anticipate a more rapid evolution than those with a poorer outlook. While an advisory group [3], sponsored by international organizations, has explored the possibility of designing more elementary electrical teletherapy machines, which could have low capital and low operating costs, apparently such a design has not been successful in commercial implementation.

A further consideration for any country in transition is to adopt a broad enough perspective to realize the need to co-ordinate cancer care throughout the entire country or region. For example, providing high quality services and teaching programmes at a reasonable cost can be done best by defining regional centres of excellence or specialization, and equipping them proactively. Large and small centres should be strategically distributed in accordance with the peculiarities of each region or country [12].

In summary, identifying the technological needs for radiation oncology throughout the world requires a thorough understanding of the technological capabilities of the treatment technologies available. These capabilities, however, must be placed in the context of the other essential infrastructure necessary to allow a smooth and safe progression to advanced radiation delivery.

ACKNOWLEDGEMENTS

The author acknowledges fruitful discussions with his colleagues J. Battista, P. Ravindran and T. Kron.

REFERENCES

[1] VAN DYK, J., "Radiation oncology overview", The Modern Technology of Radiation Oncology: A Compendium for Medical Physicists and Radiation Oncologists (VAN DYK, J., Ed.), Medical Physics Publishing, Madison, WI (1999) Ch. 1.

[2] INTERNATIONAL ATOMIC ENERGY AGENCY, Design and Implementation of a Radiotherapy Programme: Clinical, Medical Physics, Radiation Protection and Safety Aspects, IAEA-TECDOC-1040, IAEA, Vienna (1998).
[3] BORRAS, C., STOVALL, J., Design Requirements for Megavoltage X-ray Machines for Cancer Treatment in Developing Countries, Pan American Health Organization, Washington, DC (1993).
[4] VAN DYK, J., BATTISTA, J.J., Cobalt-60: An old modality, a renewed challenge, Curr. Oncol. **3** (1996) 8–17.
[5] RAWLINSON, J.A., "The choice of equipment for external beam radiotherapy", Organization and Training in Radiotherapy for Developing Countries in Africa, IAEA-TECDOC-614, IAEA, Vienna (1991).
[6] MARTIN, W.M., Radiotherapy in developing countries, Br. J. Radiol. Suppl. **24** (1992) 220–224.
[7] LEVIN, C.V., TATSUZAKI, H., "Issues of health economics in the practice of radiotherapy in developing countries", these Proceedings, Vol. 1, pp. 221–230.
[8] LEVIN, C.V., TATSUZAKI, H., Radiotherapy services in countries in transition: Gross national income per capita as a significant factor, Radiother. Oncol. **63** (2002) 147–150.
[9] TATSUZAKI, H., LEVIN, C.V., Quantitative status of resources for radiation therapy in Asia and Pacific region, Radiother. Oncol. **60** (2001) 81–89.
[10] PARKIN, D.M., BRAY, F.I., DEVESA, S.S., Cancer burden in the year 2000. The global picture, Eur. J. Cancer **37** Suppl. 8 (2001) S4–S66.
[11] WHELAN, S.L., FERLAY, J., Cancer Incidence in Five Continents. Age-specific and Standardized Incidence Rates, IARC Scientific Publication No. 120, IARC Press, Lyon (1992) 178–861.
[12] TEIXEIRA, L.C., Situation of radiotherapy in Latin America, Int. J. Radiat. Oncol. Biol. Phys. **19** (1990) 1267–1270.
[13] HANSON, G.P., STJERNSWARD, J., NOFAL, M., DUROSINMI-ETTI, F., An overview of the situation in radiotherapy with emphasis on the developing countries, Int. J. Radiat. Oncol. Biol. Phys. **19** (1990) 1257–1261.
[14] URTASUN, R.C., Does improved depth dose characteristics and treatment planning correlate with a gain in therapeutic results? Evidence from past clinical experience using conventional radiation sources, Int. J. Radiat. Oncol. Biol. Phys. **22** (1992) 235–239.
[15] HANKS, G.E., DIAMOND, J.J., KRAMER, S., The need for complex technology in radiation oncology. Correlations of facility characteristics and structure with outcome, Cancer **55** (1985) 2198–2201.
[16] VAN DYK, J., BATTISTA, J.J., "The cobalt-60 challenge", Co-Efficient Newsletter, MDS Nordion, Ottawa, Vol. 2, No. 1 (2000) 1–2.
[17] BATTISTA, J.J., VAN DYK, J., "Cobalt-60 therapy: Some myths, misconceptions, and misperceptions", Co-Efficient Newsletter, MDS Nordion, Ottawa, Vol. 2, No. 1 (2000) 1–4.
[18] SUIT, H.D., What's the optimum choice?, Int. J. Radiat. Oncol. Biol. Phys. **12** (1986) 1711–1712.

[19] DUROSINMI-ETTI, F.A., An overview of cancer management by radiotherapy in anglophone West Africa, Int. J. Radiat. Oncol. Biol. Phys. **19** (1990) 1263–1266.
[20] GOITEIN, M., The utility of computed tomography in radiation therapy: An estimate of outcome, Int. J. Radiat. Oncol. Biol. Phys. **5** (1979) 1799–1807.
[21] GOITEIN, M., et al., The value of CT scanning in radiation therapy treatment planning: A prospective study, Int. J. Radiat. Oncol. Biol. Phys. **5** (1979) 1787–1798.
[22] VAN DYK, J., BATTISTA, J.J., CUNNINGHAM, J.R., RIDER, W.D., SONTAG, M.R., On the impact of CT scanning on radiotherapy planning, Comput.Tomogr. **4** (1980) 55–65.
[23] PRASAD, S.C., PILEPICH, M.V., PEREZ, C.A., Contribution of CT to quantitative radiation therapy planning, Am. J. Roentgenol. **136** (1981) 123–128.
[24] NOFAL, M., DUROSINMI-ETTI, F., HANSON, G.P., STJERNSWARD, J., Supporting cancer care in the developing countries: Role of IAEA/WHO, Int. J. Radiat. Oncol. Biol. Phys. **19** (1990) 1249–1256.

ISSUES OF HEALTH ECONOMICS IN THE PRACTICE OF RADIOTHERAPY IN DEVELOPING COUNTRIES

C.V. LEVIN, H. TATSUZAKI*
Division of Human Health, International Atomic Energy Agency, Vienna
E-mail: c.v.levin@iaea.org

Abstract

There is a shortfall of radiotherapy facilities, especially in developing countries. The gross national income per capita is identified as a marker for the shortfall of teletherapy equipment. On a microeconomic level, factors influencing the selection of teletherapy and brachytherapy equipment are analysed using activity based costing. These costs relate to equipment costs and local developing country costs of personnel, procedures and clinical practice. The limitation on utilization imposed by personnel shortages is also quantified.

1. INTRODUCTION

There has been a rapid expansion of radiation oncology services in developing countries over the past decade [1, 2]. The question arises of how far, how fast and which technology should be introduced and expanded and yet remain sustainable.

The problem can be reduced to the simple issue of an increasing number of cancer cases (as measured, for example, by the GLOBOCAN database of the International Agency for Research on Cancer), and hence increasing demand for radiotherapy (Fig. 1), in less developed countries, while the current resources for treatment (see the IAEA Directory of Radiotherapy Centres) are at present concentrated in well developed countries (Table I).

By 2015 there will be a shortfall of 10 000 teletherapy machines for providing radiotherapy.

* Present address: National Institute of Radiological Sciences, Chiba-shi, Japan.

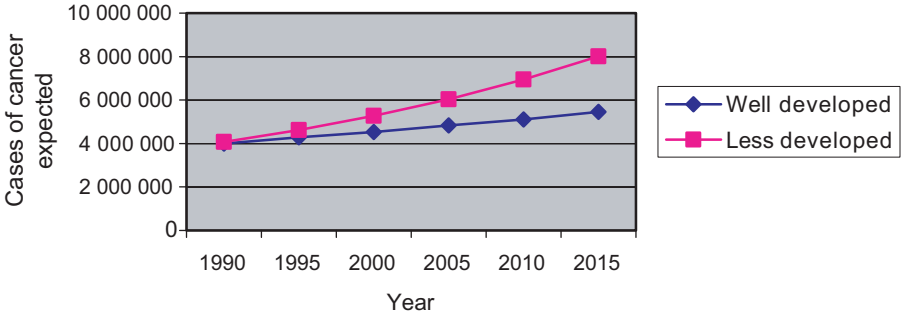

FIG. 1. Cancer cases expected in well developed and less developed countries, 1990–2015.

TABLE I. MEGAVOLTAGE MACHINES IN WELL AND LESS DEVELOPED COUNTRIES

	Less developed countries	Well developed countries
Linacs	671	3802
Cobalt machines	1562	670
Total	2233	4472
Population	5 billion	1.1 billion

2. MACROECONOMICS

A simplistic model, derived from well developed countries, relates the desired amount of megavoltage teletherapy equipment (MEV) and personnel to population, with scant regard to the economic constraints or epidemiological differences [3, 4]. These figures are a culmination of a century of development of this clinical practice in countries with considerable resources and a cancer priority in tertiary health services. However, many countries have inadequate or no radiotherapy services [1], and a jump from this standard to comprehensive services is unrealistic within the existing financial and personnel constraints.

Radiotherapy should be based in a hospital with sound oncology services, including diagnostic, pathology and surgical services. It requires considerable outlay for equipment, building and other infrastructure, and trained personnel. In emerging economies, the process of acquiring radiotherapy is thus a progressive one, starting with basic treatments (teletherapy and

brachytherapy) and clinical quality assurance equipment (imaging, treatment planning and immobilization). An IAEA study [5] shows that the acquisition of teletherapy services, measured in MEV per million population (MEV/mill), is related to the gross national income per capita (GNI/cap), with some regional differences.

It was reasonably postulated that the poorest countries should commence radiotherapy on a small scale, progress with prosperity, then reach a capacity to treat all patients (Fig. 2). This was shown to be valid (Fig. 3) for the 72 developing countries selected. However, the 12 well developed countries analysed tend to continue to acquire equipment to render services more accessible.

Further generalizations can be made on a regional basis. Whereas South and Central America closely follow this pattern, Africa (Fig. 4) consistently has less equipment, while eastern Europe (Fig. 5) has more equipment than expected for their economies.

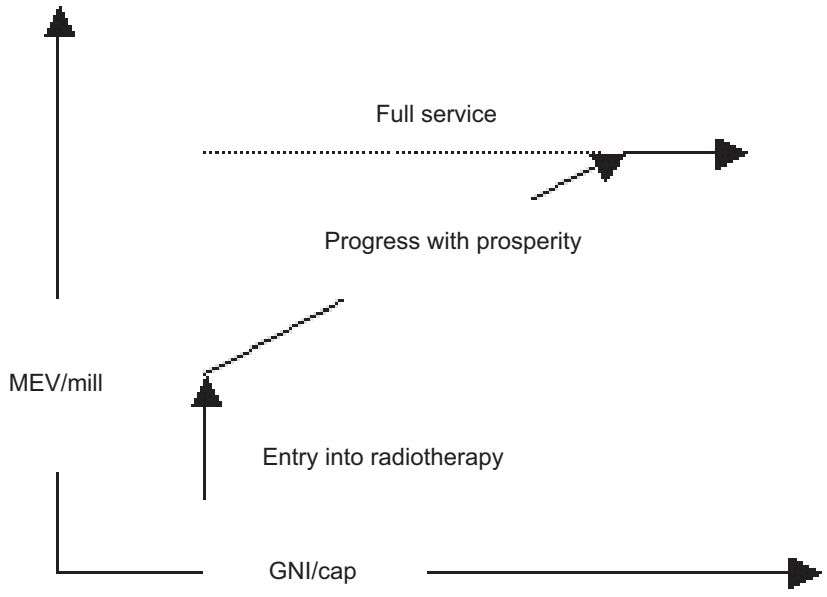

FIG. 2. Hypothesis of the relationship between the acquisition of equipment, expressed as MEV/mill, and GNI/cap.

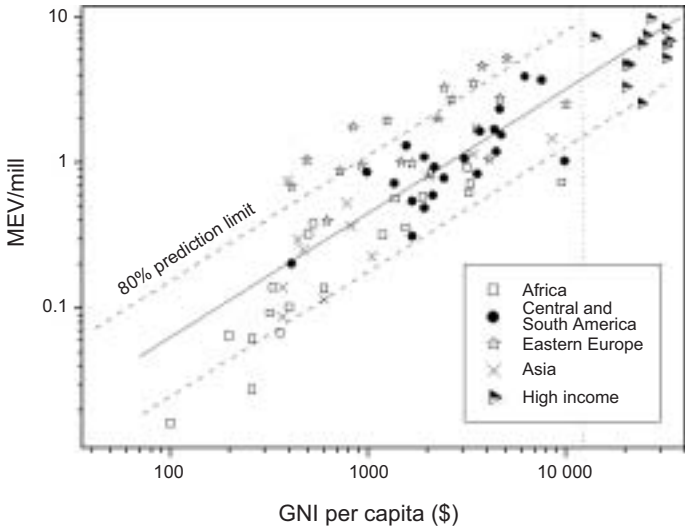

FIG. 3. Results of the plot of equipment (expressed as MEV/mill) against GNI/cap. Well developed countries (high income) were defined as countries with GNI/cap > $12 000.

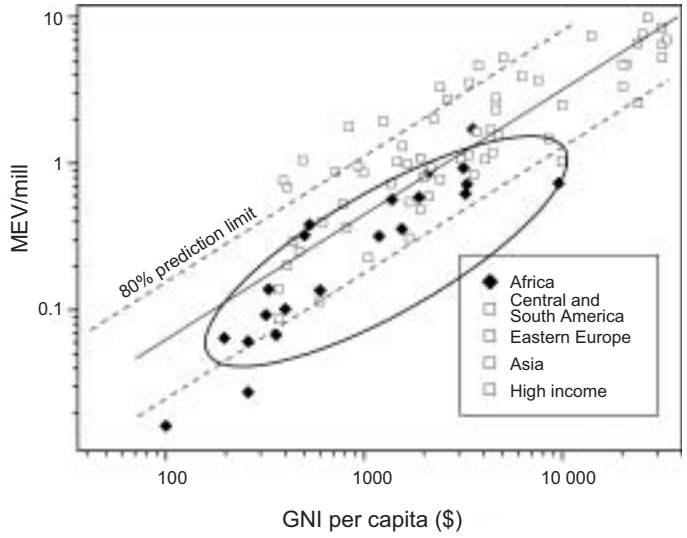

FIG. 4. Africa. MEV/mill for Africa is below the international norms related to GNI/cap.

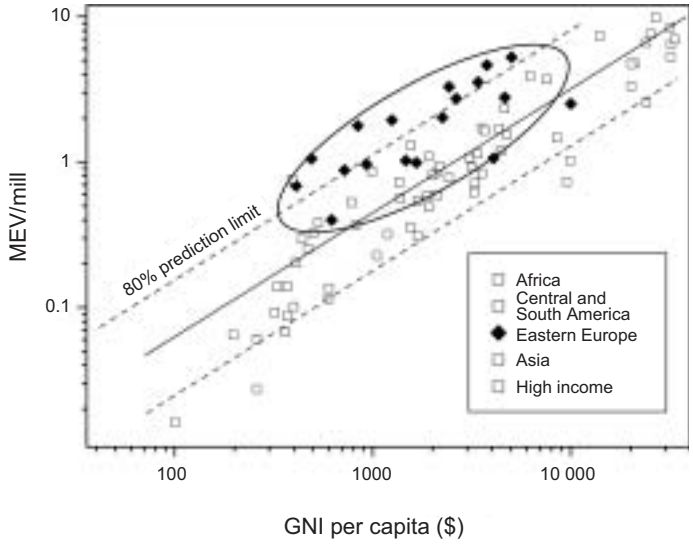

FIG. 5. Eastern Europe. MEV/mill for eastern Europe is above the international norms related to GNI/cap.

3. MICROECONOMICS

Cost effectiveness (rather than cost–benefit) analysis is usually applied to questions regarding health economics [6]. Even the definition of cost creates difficulties. In the evaluation of the cost of radiotherapy in developing countries, the known market prices (the cost to the payer or medical aid rates) cannot be used as a yardstick, as these simply do not exist. In general, the costs are borne by the State — the service provider — and this is the viewpoint taken in this paper.

3.1. Teletherapy

For the first 60 years of the century of radiotherapy, teletherapy was administered by X ray machines modified to deliver high radiation outputs (orthovoltage machines). The technology has rapidly advanced to megavoltages ($E > 1$ MeV) using cobalt machines and, in the 1970s, the introduction of more expensive linacs. The past decade has been characterized by increased integration of tumour imaging by computed tomography and magnetic resonance imaging scanning, and treatment planning to allow

increasingly conformal treatments (treatments covering the tumour to a therapeutic dose, while decreasing the dose volume of normal tissue).

This increasing sophistication has been accompanied by increased costs [7], increased requirements for quality assurance and quality control and the need for trained personnel. The clinical gains between orthovoltage and megavoltage machines were easily demonstrated for larger, deep seated tumours, while increasingly conformal megavoltage treatments result in reduced morbidity and escalating curative doses in smaller, well defined tumours. There has been no evidence to show a clinical difference between orthovoltage, cobalt or low energy linac treatments in the palliative treatment of patients with bone metastases or multiple brain metastases. In the treatment of the pelvis or other broadly defined large volumes, the outcome after treatment with cobalt machines or linacs is similar, except in obese patients, for whom high energy linacs confer an advantage.

The technological advances have occurred predominantly in the management of smaller tumours, which are increasingly seen in well developed countries: the reward of public awareness and early diagnosis using a sophisticated but increasingly costly medical infrastructure.

The cost per patient associated with the administration of teletherapy is comprised predominantly of fixed costs for capital equipment at international prices, but with local building, overhead and personnel costs. The net effect of these factors is that a higher technology equipment cost, for example for a linac, adds little (15%) to the cost of treatment per patient in well developed countries, but can increase costs by a factor of three in developing countries [8]. An example of applying the activity based costing (ABC) model to illustrate the cost of delivering 15 fractions of radiotherapy to a single patient using either a cobalt machine or a linac is shown in Table II. For uniformity, a 10 h working day is taken as standard.

TABLE II. RESULTS OF ABC MODELLING FOR THREE COUNTRIES WITH DIFFERENT ECONOMIES

(*Costs in the USA are used in the ABC model for a high income country, costs in South Africa are used for an intermediate country and costs in Ghana, in parentheses, reflect the ABC costing if a linac were to be installed.)*

	Cobalt therapy costs for 15 fractions ($)	Linac therapy costs for 15 fractions ($)
Ghana	465	(1350)
South Africa	980	1950
USA	4150	4800

As teletherapy has few variable costs, such as the drugs or theatre time associated with chemotherapy and surgery, the cost per patient for teletherapy falls rapidly with increased utilization. These costs per patient fall as the working day extends, to as much as 20 h in some countries [8].

3.2. Brachytherapy

For the treatment of uterine cervical cancers, radium treatment, started a century ago, was replaced by caesium for insertion into cavities adjacent to tumours: brachytherapy. These low dose rate (LDR) insertions under general anaesthesia required two to five days of patient nursing in isolation wards, with severely curtailed visiting and even nursing time. This procedure is rapidly being replaced by 30 min outpatient procedures since the development of high activity but very small iridium sources (micro-high dose rate (mHDR) sources). While this has evident benefits for the patient, it has two major problems: the replacement of costly sources at three month intervals, the need for repeated (as opposed to single) insertions and the attendant need for repeated theatre time for the physician and hence cost to the institution (Table III). At present, the LDR modality is under threat of extinction.

An ABC model has been devised for the different brachytherapy procedures [9]. The results identify the most significant variables influencing the cost per patient treated: total number of patients treated per year, the number of fractions of brachytherapy administered to each patient treated by mHDR, the cost of insertion of the LDR applicator under anaesthesia and the costs incurred in the hospitalization of the patient receiving LDR brachytherapy.

TABLE III. COMPARISON BETWEEN HIGH AND LOW DOSE BRACHYTHERAPY APPLICATIONS

	HDR	LDR
Equipment cost	$$$	$$
Source replacement	Three-monthly ($$$)	No
Procedure duration	30 min	More than three days
Hospital admission	No	Yes ($$$)
Patient capacity	300+	80–100
Multiple applications needed?	Yes, 3–7	No
Anaesthetic needed	No	Yes
Versatility	Gynaecology/oesophagus/bronchus	Mainly gynaecology

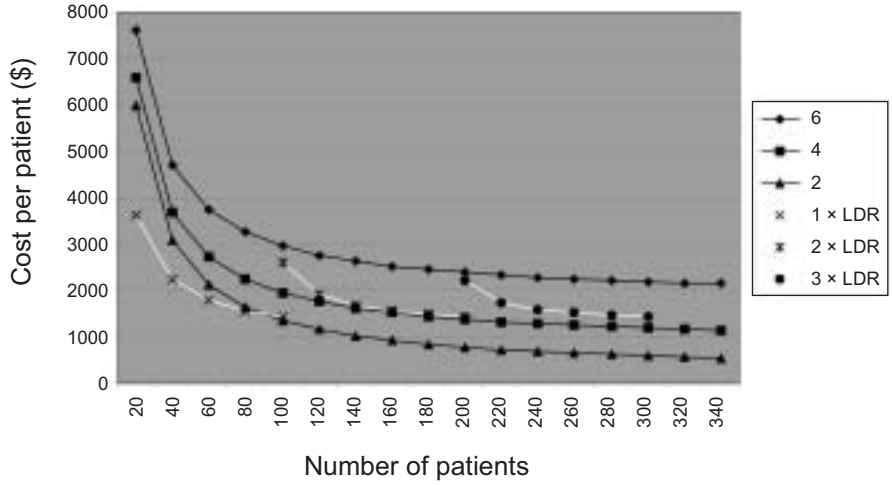

FIG. 6. Cost in dollars per patient treated for differing brachytherapy machines (mHDR and LDR) and different mHDR clinical protocols (six, four or two fractions) versus number of patients within an 8 h working day. This example uses local costs for a country with a GNI/cap of $2000, theatre costs of $250 per procedure and daily nursing costs of $100 per day for pre-admission and the duration of the LDR insertion.

Figure 6 illustrates the initial high cost of using mHDR for a small number of patients. If, however, considerable numbers of patients are treated annually and a small number of fractions is used, then mHDR can be as cost effective as LDR in a developing country.

3.3. Personnel

Machines do not treat patients: this is done by trained personnel. The number of machines and the complexity of the treatments are increasing. Shift work of up to 20 h per day is used to treat the largest number of patients per machine. Yet, overall, the limiting factor in many countries in Asia (Fig. 7) is the shortage of trained radiation oncologists [2]; there is a similar situation in Africa.

The high costs of training in well developed countries plus the loss of trained personnel to these regions represent a significant subsidy paid by countries in transition to support radiotherapy in well developed countries.

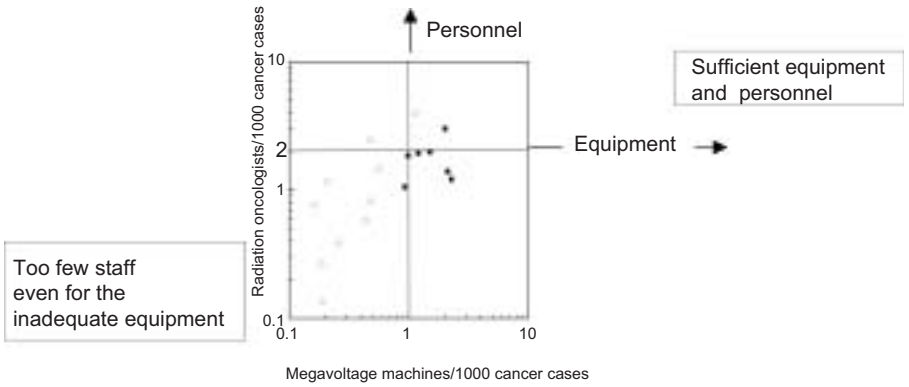

FIG. 7. Relationship between numbers of personnel and megavoltage therapy equipment in the Asia–Pacific region. Less than one megavoltage machine for each 1000 anticipated cancer cases is considered to be inadequate equipment. Less than two radiation oncologists per 1000 anticipated cancer cases is considered to be inadequate personnel.

4. CONCLUSIONS

There is a progressive process in acquiring radiation oncology as regards both the number and the sophistication of the equipment purchased. This expansion of services needs to be accompanied by a national programme of professional education to ensure the full utilization of the equipment for the benefit of cancer patients.

The 'best' equipment is not always the most appropriate equipment, especially when funding is limited.

REFERENCES

[1] LEVIN, C.V., EL-GUEDDARI, B., MEGHZIFENE, A., Radiation therapy in Africa: Distribution and equipment, Radiother. Oncol. **52** (1999) 79–84.

[2] TATSUZAKI, H., LEVIN, C.V., Quantitative status of resources for radiation therapy in Asia and Pacific region, Radiother. Oncol. **60** (2001) 81–89.

[3] INTERNATIONAL ATOMIC ENERGY AGENCY, Design and Implementation of a Radiotherapy Programme: Clinical, Medical Physics, Radiation Protection and Safety Aspects, IAEA-TECDOC-1040, IAEA, Vienna (1998).

[4] INTER-SOCIETY COUNCIL FOR RADIATION ONCOLOGY, Radiation Oncology in Integrated Cancer Management, ACR Publications, Reston, VA (1991).
[5] LEVIN, C.V., TATSUZAKI, H., Radiotherapy services in countries in transition: Gross national income as a significant factor, Radiother. Oncol. **63** (2002) 147–150.
[6] NEYMARK, N., Assessing the economic value of anticancer therapies, Recent Results Cancer Res. **148** (1998).
[7] VAN DER GIESSEN, P.-H., Maintenance costs for cobalt machines and linear accelerators: New machines versus old, Radiother. Oncol. **62** (2002) 349–350.
[8] INTERNATIONAL ATOMIC ENERGY AGENCY, Activity Based Costing of Teletherapy Services: A Predictive Model, IAEA, Vienna (in preparation).
[9] INTERNATIONAL ATOMIC ENERGY AGENCY, Activity Based Costing of Brachytherapy Services: A Predictive Model, IAEA, Vienna (in preparation).

USE OF IMAGING TECHNIQUES IN RADIATION ONCOLOGY

C. BORRÁS, D. RUDDER, P. JIMÉNEZ
Pan American Health Organization,
Washington, D.C.
E-mail: borrasca@paho.org

Abstract

Accurate physical dosimetry is irrelevant for tumour control and minimizing complications in radiation oncology if the tumour volume and sensitive structures are not accurately delineated. The imaging techniques used for this task have evolved markedly since the 1960s. To optimize resources, imaging equipment needs to be tailored to the type of treatment equipment in the facility. To simulate treatments given with ^{60}Co units and/or simple linacs, a simulator may be less expensive than a computed tomography (CT) scanner, but also less useful. With careful protocols to ensure patient position reproducibility and compatible immobilization devices, a CT scanner housed in a diagnostic department may be shared by a therapy department. Mobile digital portal imagers may be the solution to verify treatments. Imaging techniques that offer three dimensional capabilities are essential if the facility wants to install stereotactic surgery, conformal radiation therapy using multileaf collimators, dynamic wedges and/or intensity modulated radiation therapy. Particular attention needs to be given to computerized diagnostic and therapeutic systems that can be linked electronically.

1. INTRODUCTION

Imaging techniques are used in radiation oncology for disease diagnosis, tumour localization and staging, treatment simulation, treatment planning, clinical dosimetry displays, treatment verification and patient follow-up. The following imaging modalities may be used: conventional radiology (X ray units and simulators), X ray computed tomography (CT) (CT scanners), ultrasound, magnetic resonance imaging (MRI) and nuclear medicine (gamma cameras, single photon emission tomography and positron emission tomography (PET)). The type of equipment and its uses have evolved over the years following the technology changes in radiation oncology and in computers.

2. DEVELOPMENTS IN INDUSTRIALIZED COUNTRIES

In the 1960s, when teletherapy was performed with ^{60}Co units, conventional radiology was used for cancer diagnosis and treatment. Gamma cameras helped tumour staging by detecting metastases. Treatment planning consisted of evaluating axial dose distributions, generated either manually or with the recently available computerized treatment planning systems. Anatomical information, including patient contours, was either drawn manually or obtained using a B mode ultrasound unit. Typical examples of the images obtained with these units are shown in Fig. 1. Treatment verification was performed by placing films in the radiation beam, with the patient under treatment.

In the 1970s (Fig. 2) simulators were developed for exclusive use in radiation oncology departments. In the 1980s two dimensional imaging was

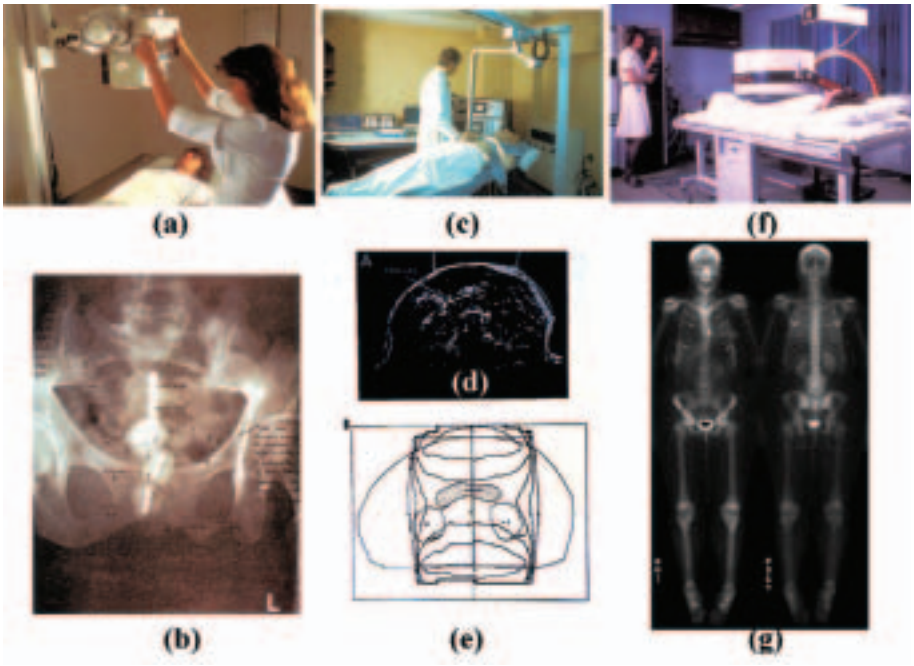

FIG. 1. Examples of diagnostic units used in radiation oncology and the images produced. (a) Conventional diagnostic X ray unit; (b) anteroposterior radiograph of a gynaecological brachytherapy implant for source localization; (c) B mode ultrasound unit; (d) ultrasound scan showing location of pancreatic tumour, spine, kidneys and port margin; (e) computer plotted therapy plan; (f) gamma camera; (g) whole body bone scan.

replaced by three dimensional displays with the incorporation of CT, and in the 1990s of MRI. Ultrasound units were found useful to guide brachytherapy applications, especially in the prostate. Digital portal imagers allowed accurate treatment field verification (Fig. 3). Three dimensional treatment planning systems overlaid isodose distributions on to CT images using software that allowed for automatic anatomical input, surface and volume rendering and dose–volume histograms (Fig. 4). Some incorporated the capability of inverse planning (i.e. once the desired dose distribution is decided, the field size, gantry, collimator and couch angles, etc., can be automatically selected). The 2000s are seeing a change from anatomical to functional imaging with the advent of MRI units capable of spectroscopy at 3 T and with the advent of PET units. According to the United Nations Scientific Committee on the Effects of Atomic Radiation [1], in 1997 there were 70 centres worldwide performing PET examinations. In 2001 combined CT–PET units were introduced in

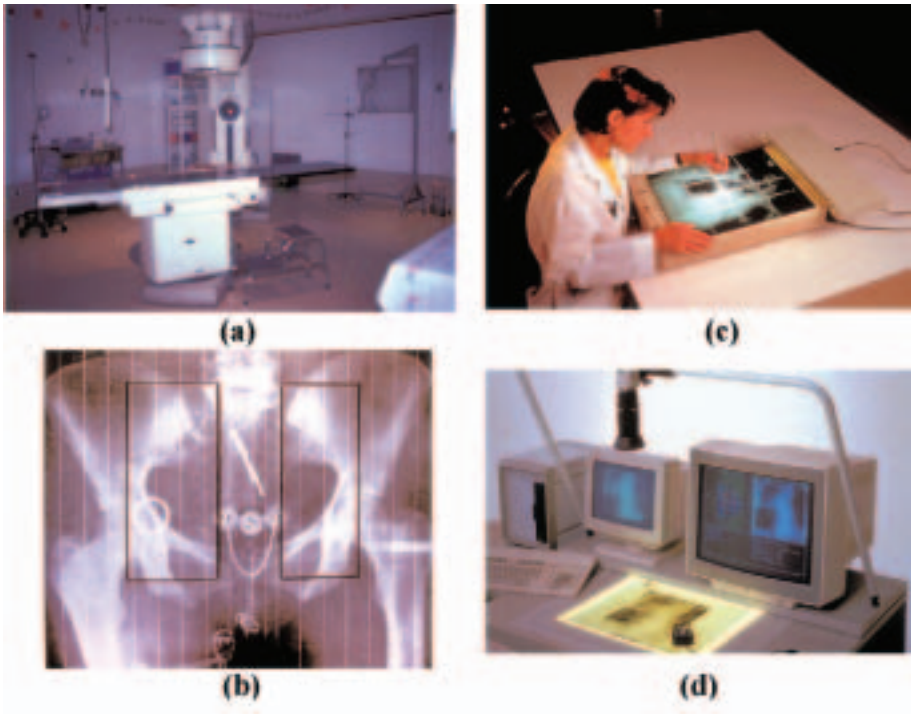

FIG. 2. Simulation of treatment fields. (a) Conventional X ray simulator; (b) simulator film of a brachytherapy implant with superimposed paraortic external beam therapy fields; (c) manual entry of simulator film into the treatment planning system; (d) entry of simulator film into the treatment planning system using a digitizing camera.

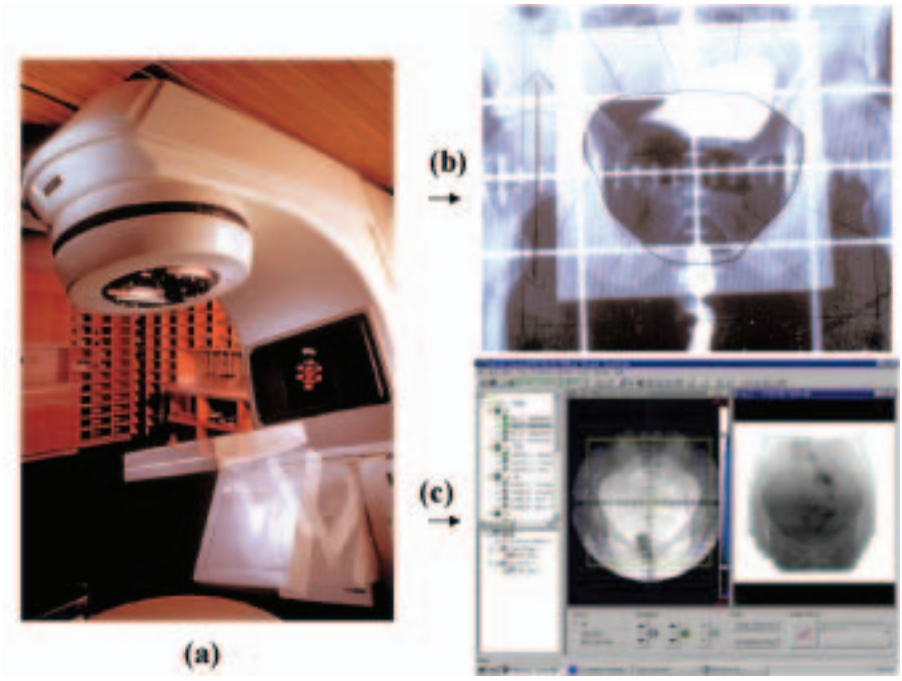

FIG. 3. Portal imaging. (a) Linac equipped with a portal imaging device; (b) portal image versus a simulator film; (c) portal image versus a digitally reconstructed radiograph.

radiotherapy departments. In 2002 a fusion of CT, MRI and PET images became available (Fig. 5). Molecular imaging is being developed.

Data from the United States of America indicate that 39.6 million CT procedures were performed in 2001, a 51% increase from 1998, and about 50% of the CT scanners purchased that year had multislice capability. From data on CT use obtained in 2000 by the Center for Devices and Radiological Health of the US Food and Drug Administration [2], it can be inferred that approximately 4% of all the exams performed are for treatment planning. MRI procedures in 2001 rose to 18 million, with 60% of the MRIs installed having magnets of 1.5 T or greater. At the end of 2002 at least 21 companies provided products for the various stages of the intensity modulated radiation therapy (IMRT) process: imaging equipment for staging, patient immobilization and positioning devices, imaging units for treatment planning, treatment planning systems, post-planning verification devices, and software for treatment verification, quality assurance (QA), patient information and image

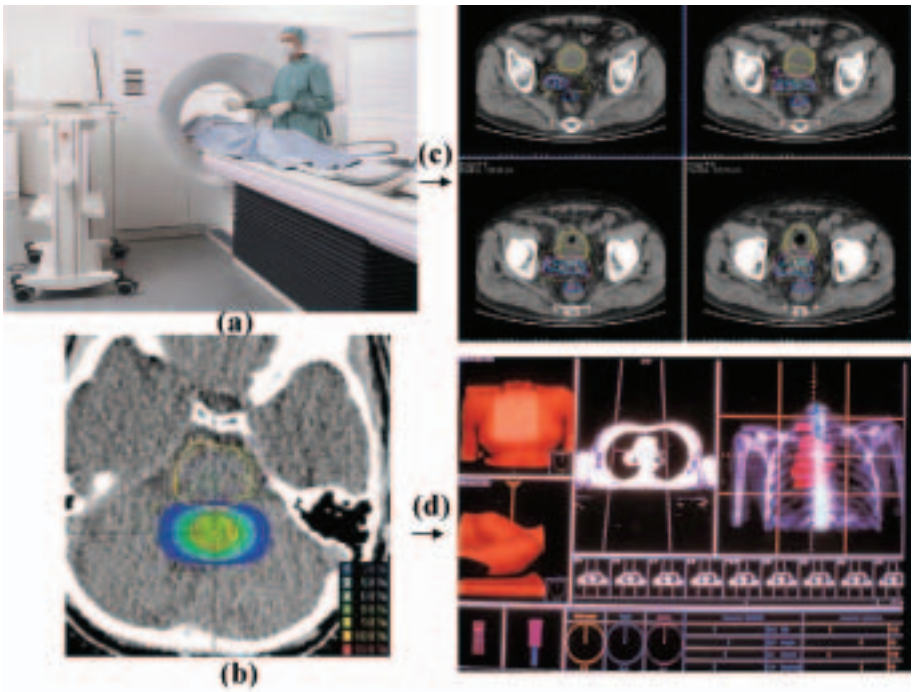

FIG. 4. CT imaging. (a) CT scanner; (b) isodose distribution for a malignant glioma; (c) isodose distributions for a cancer of the prostate treated with a permanent brachytherapy implant; (d) automatic features of a CT scanner based treatment planning system.

management [3]. With some of these products in the million dollar range, equipment and software are outside the reach of developing countries.

3. SITUATION IN DEVELOPING COUNTRIES

The gap in cancer detection and treatment between well developed and developing countries is widening. In part this is due to the fact that resources for health services are distributed differently. In developing countries cancer treatment is mostly carried out in public institutions — which are short of funding and forced to prioritize needs — while advanced diagnostic imaging equipment is bought by private facilities. In response to requests by the Ministries of Health of the Americas, the Pan American Health Organization evaluates radiation oncology departments in their entirety: physical infrastructure, equipment and supplies, human resources, maintenance and

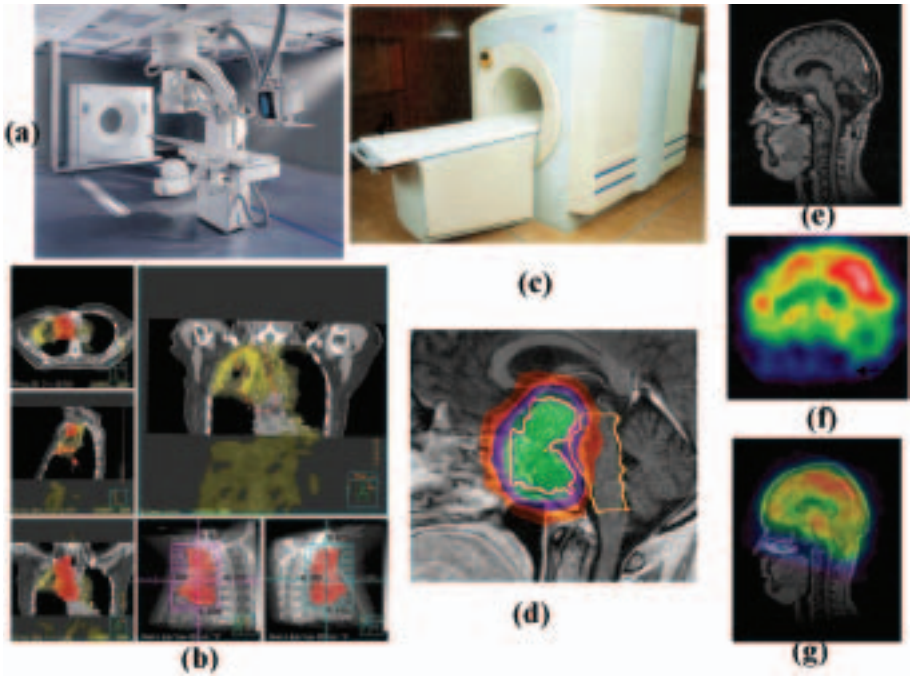

FIG. 5. Fusion images. (a) CT–PET unit; (b) CT–PET fusion images; (c) MRI unit; (d) isodose distribution for a cavum recurrence on an MRI image; (e) MRI image of a brain tumour; (f) PET image of the same brain tumour; (g) MRI–PET fusion image.

quality assurance programmes, and radiation safety. To update existing information on the types and frequencies of imaging units used for radiation oncology, a specific survey was developed and sent to all Latin American medical physicists. The survey forms filled out for cancers of the cervix–endometrium, breast, prostate, head and neck, colon–rectum and oesophagus — the most common cancers in the Latin American and Caribbean countries — are still coming in, but a common picture is emerging. CT may be used for patient diagnosis and treatment follow-up, but rarely for treatment planning and dosimetry. MRI and/or PET, where available (Argentina, Brazil, Chile and Mexico have PET units), are used to diagnose cancer, but not for treatment planning. Owing to the lack of prevention and early detection programmes, cancers are diagnosed at later stages, and tumour extension is mostly evaluated by clinical examination. Often radiation treatments are given for palliative purposes, where an accurate tumour localization in three

dimensions is not critical. Simulators are rare, and other imaging units in radiation oncology departments are non-existent. Treatment planning systems, where available, provide two dimensional displays, rarely overlaid on anatomical structures, except in brachytherapy, in which anatomical information is obtained with anteroposterior and lateral radiographs taken with a conventional X ray unit. Portal films to verify treatment fields are rarely taken, as X ray film is very expensive and the treatment machines have such heavy patient workloads that they cannot be spared for treatment simulation and verification. Furthermore, technicians are poorly trained and many facilities operate without medical physicists to develop adequate protocols to optimize the use of existing equipment.

4. MINIMUM REQUIREMENTS IN DEVELOPING COUNTRIES

The population in developing countries is ageing and cancer incidence is increasing. If radiation oncology is to cure cancers, imaging techniques need to be incorporated. Field sizes may need to be decreased to lower morbidity of healthy tissues, and absorbed doses to the planning treatment volume may need to be increased to achieve better tumour control. In other words, the tumour volume needs to be determined with greater accuracy. As Goitein said in 1982 [4] to justify the use of CT in radiation oncology, cancer is a three dimensional disease.

Owing to financial and educational (lack of trained staff) constraints, resources need to be optimized through careful planning. The imaging equipment has to be tailored to the type of treatment equipment in the facility. To simulate treatments given with ^{60}Co units and/or simple linacs, a simulator may be less expensive than a CT scanner, but less useful. With careful protocols to ensure patient position reproducibility and compatible immobilization devices, a CT scanner housed in a diagnostic department may be shared by a therapy department if appropriate scheduling is agreed upon and the therapy department provides its own technical staff. Mobile digital portal imagers may be the solution to verify treatments. In the long term they should be less expensive than films, chemicals and darkrooms.

Imaging techniques that offer three dimensional capabilities are essential if the facility wants to install stereotactic surgery, conformal radiation therapy using multileaf collimators, dynamic wedges and/or IMRT, which may change the dose rate, gantry angle, couch angle and collimator settings during treatment. Particular attention needs to be given to computerized diagnostic and therapeutic systems that can be linked electronically [5]. Diagnostic images acquired for tumour localization may be fed to the simulator — if these two

processes are not obtained in a CT simulator — from there to the treatment planning system and finally to the accelerator (or vice versa if inverse planning is not performed). To ensure safety, the International Electrotechnical Commission (IEC) has developed standards for imaging and radiotherapy systems that equipment manufacturers adhere to. The IEC has also adopted the DICOM (Digital Image Communication) standard, which facilitates accurate digital data transfer among devices, ensuring compatibility between data from different manufacturers. Owing to the complexity involved when treatment machines are linked, the IEC also has a DICOMRT standard. The problem with these standards is that they do not ensure interoperability, only interconnectivity.

National regulatory agencies, such as the US Food and Drug Administration, have to approve all new medical devices for their efficacy as well as safety prior to their commercial release. The European Union has homologation regulations and standards for good practice manufacturing. National regulatory radiation protection agencies license facilities and/or individuals engaged in practices that involve the use of ionizing radiation. Medical physics organizations, such as the American Association of Physicists in Medicine, develop and publish guidelines and protocols to test equipment performance and implement QA programmes. Here lies the crux of the matter. To test equipment performance specifications and regulatory standards, as well as to develop and implement appropriate QA programmes, medical physicists require comprehensive training covering diagnostic radiology, radiation therapy and nuclear medicine procedures. Hence the challenge in developing countries to successfully acquire and deploy new technologies (such as IMRT) lies not so much in financial limitations but in the lack of sufficient personnel, adequately trained.

REFERENCES

[1] UNITED NATIONS, Sources and Effects of Ionizing radiation (Report to the General Assembly), Vols I and II, Scientific Committee on the Effects of Atomic Radiation (UNSCEAR), UN, New York (2000).

[2] STERN, S.H., "Nationwide evaluation of X ray trends 2000–2001. Survey of patient radiation exposure from computed tomographic examinations in the United States", paper presented at NCRP Symp. on Computed Tomography: Patient Dose, Arlington, VA, 2002.

[3] Intensity modulated radiation therapy product comparison, Imaging Technol. News **42** 5 (2002).

[4] GOITEIN, M., Limitations of two-dimensional treatment planning programs, Med. Phys. **9** (1982) 580–586.

[5] BORRÁS, C., "Automation in precision radiotherapy: From image acquisition to dose computation — Existing and needed standards", paper presented at Int. Conf. on Medical Imaging, Medical Physics, and Precision Radiation Therapy, Guangzhou, China, 1999.

BLANK

DOSIMETRY PROTOCOLS AND COMPARISONS — I

(Session 5)

Chair

V.G. SMYTH
New Zealand

Co-Chair

D.I. THWAITES
European Society for Therapeutic Radiology and Oncology and
International Society for Radiation Oncology

Rapporteur

K.E. ROSSER
United Kingdom

BLANK

EXPERIENCE WITH THE UNITED KINGDOM (IPEM) ABSORBED DOSE TO WATER RADIOTHERAPY DOSIMETRY PROTOCOLS FOR PHOTONS (1990) AND ELECTRONS (2003)

D.I. THWAITES
Western General Hospital, University of Edinburgh,
Edinburgh, United Kingdom
E-mail: dit@holyrood.ed.ac.uk

Abstract

The United Kingdom has been using an absorbed dose to water dosimetry code of practice for megavoltage photon beams, based on the National Physical Laboratory (NPL) graphite calorimeter primary standard, since 1990. The NPL calibration service provides chamber calibration factors in terms of absorbed dose to water directly across a range of beam qualities. More recently, a similar graphite calorimeter primary standard has been developed for electron beam dosimetry, which also provides calibration factors directly for a range of beam qualities. This calibration approach has been piloted, comparing methods and results with those for the earlier air kerma calibration based code of practice. A new electron dosimetry code of practice (IPEM 2003) has been developed, which is about to be brought into use in UK centres. Both direct absorbed dose to water protocols provide a simpler formalism for use in practice and significantly reduced uncertainties compared with previous approaches based on a ^{60}Co air kerma chamber calibration. Statements of dose in a given beam increase by the order of 1% on going over to the new approach.

1. INTRODUCTION

There has been a growing acceptance over the past few years to move from dosimetry protocols based on air kerma calibrations to newer approaches based on direct absorbed dose to water calibrations. The main rationale has been to reduce the inherent uncertainties, but also to simplify the formalism.

United Kingdom radiotherapy centres have been using an absorbed dose to water dosimetry protocol for megavoltage photon beams since the publication of the 1990 code of practice [1] by the Institute of Physical Sciences in Medicine (IPSM, later renamed the Institution of Physics and Engineering in Medicine and Biology (IPEMB), which later still became the Institute of Physics and Engineering in Medicine (IPEM)). This was made possible by, and is based on, the development of the National Physical Laboratory (NPL) graphite calorimeter primary standard, which was set up in 1988 as the basis for

a calibration service that uniquely provided direct absorbed dose to water chamber calibration factors, $N_{D,w}$, for ^{60}Co and also for X ray beams of a quality index (QI) in the range of 0.62 to 0.79 [2, 3]. These calibration factors could be determined directly, as the NPL operates both a ^{60}Co unit and a variable energy linac.

More recently the NPL has developed a similar graphite calorimeter system as a primary standard for electron dose. A calibration service has been introduced that is based on this and is able to provide direct $N_{D,w}$ factors for hospital ionization chambers in electron beams over a range of beam qualities of nominal energy from 4 MeV to 19 MeV [4, 5]. A new UK (IPEM) protocol has been developed for general clinical use, based on this direct service [6].

2. MEGAVOLTAGE PHOTON BEAMS

2.1. The NPL absorbed dose primary standard and chamber calibration procedures

The NPL's primary standard graphite calorimeter and its performance and the transfer from absorbed dose to graphite to absorbed dose to water have been described in detail previously [2, 3]. For convenience, three Nuclear Enterprises NE 2561/2611 ionization chambers are used as 'working standards' (i.e. as transfer instruments for transferring calibrations from the calorimeter). They are regularly calibrated against the calorimeter in a graphite phantom over the available range of beam qualities, showing a good long term stability of approximately 0.1% over 12 years. The doses are then converted from dose to graphite to dose to water. This has been based on scaling theorem and cavity theory approaches, with independent checks using cavity theory and Monte Carlo modelling. Any parameters required are in the form of ratios, water to graphite, which reduces uncertainties. The conversion is estimated to introduce a standard uncertainty of 0.5% to the absorbed dose to water calibration factors.

Hospital ionization chambers are then intercompared with the three transfer instruments in a 1 mm thick Perspex (polymethylmethacrylate (PMMA)) waterproofing sheath in a water phantom, with the centre of the chamber at reference depths of 5 cm (QI ≤ 0.75) or 7 cm (QI > 0.75). When the calibration service was first set up, each chamber was calibrated directly at each beam quality available at the NPL (^{60}Co and seven X ray qualities). The $N_{D,w}$ calibration factors were then given as a function of QI. There were some early problems of nonconsistency between ^{60}Co and megavoltage X rays and of variations of up to 1% in the factors, which were due to a number of small causes, mainly differences in matching filtration and hence spectra for a given value of QI across the quality

range between the primary standards dosimetry laboratory (PSDL) beams and hospital beams. These were resolved by increasing the filtration on the NPL research linac beams to match more closely clinical linac beams. Since then, all aspects of the calibration system have proved very stable, with typical variations in the $N_{D,w}$ versus QI curve for a given chamber at different calibration periods being no more than a few tenths of a per cent. More recently the data from extensive measurements on many chambers of types NE 2561 and NE 2611 (and also for NE 2571) have been analysed and the calibration factors for all beam qualities, Q, have been compared with those for ^{60}Co, taken as a normalizing reference quality, Q_o. This has shown that the quality dependent correction, $k_Q = N_{w,Q}/N_{w,Qo}$, for these chambers does not vary significantly from one chamber to another of the same type. A mean set of experimentally determined k_Q has therefore been taken for each chamber type. The determinations of calibration factors at different qualities are now all taken as independent determinations of $N_{w,Qo}$ (equal to the experimentally determined $N_{w,Q}$ divided by the appropriate value of the experimentally determined k_Q). This means that subsequent chamber calibrations can be based on fewer points. The mean value from all determinations is obtained, and the set of finally reported $N_{D,w}$ is obtained from this mean $N_{w,Qo}$ combined with the accepted set of k_Q. They are presented against the QI in the calibration certificate. The standard uncertainty on the calibration factors provided for a hospital chamber is estimated to be 0.7%.

2.2. IPSM code of practice (1990)

The UK IPSM (now the IPEM) provided a dosimetry protocol in 1990 [1] to utilize this service. This superseded the previous air kerma calibration based protocol. There is therefore now up to 12 years' experience of operating at the hospital level with the absorbed dose to water protocol.

All 65 UK radiotherapy centres have access to one of approximately 55 local standard systems, which are also based on NE 2561/2611 ionization chambers, making the dissemination equipment from the PSDL to the hospital common for all centres. These local 'secondary standard' systems are calibrated at the NPL every three years. Hospital field instruments, commonly NE 2571 Farmer chambers, are calibrated against the local standard systems at least annually. This must be done with both chamber centres at the same reference depths that the NPL $N_{D,w}$ calibration factors were provided for and using the same 1 mm PMMA sheath on the local standard as was used at the time of the NPL calibration. The field instrument calibration is commonly carried out by the simultaneous irradiation of both chambers side by side in a PMMA phantom. The use of a non-water phantom could potentially introduce some small additional uncertainties. However, for cylindrical chambers of similar

diameters and materials, for example NE 2561/2611 and NE 2571 chambers, these are expected to be negligible. The reading from each chamber and electrometer should be corrected for recombination, which will be dependent on the dose per pulse, on the chamber and on the polarizing voltage supplied by the electrometer.

The application of the protocol is very straightforward, and minimizes the introduction of areas of possible error or difference. This has resulted in a very stable consistency of dosimetry between radiotherapy centres at different times and over the range of clinical beam qualities. This has been demonstrated by UK-wide dosimetry intercomparisons, including photon beam calibration audits, organized by the IPEM. The first of these took place in the late 1980s and just into the early 1990s [7], when most centres used the older protocol. It showed the standard deviation (SD) of the distribution of audit measured/stated doses to be 1.5%. The second, in the mid-1990s [8], when almost all centres were using the new protocol, showed an equivalent SD of 1%. While other factors are involved in this improving consistency, one factor has been the implementation of the absorbed dose to water protocol. This close reproducibility of basic calibration dosimetry across the country has continued to be demonstrated by the regular audits carried out in the UK radiotherapy dosimetry audit network [9].

The change in stated dose in moving from the earlier approach based on an air kerma calibration to that based on the direct absorbed dose to water calibration factors is approximately 1%, with the newer protocol providing a greater stated dose in the same beam and conditions.

2.3. Uncertainties in megavoltage photon beam calibration following the UK approach

As stated above, the standard uncertainty on the calibration factors provided by the NPL for a hospital chamber is estimated to be close to 0.7% (comprising the combination of close to 0.2% type A and 0.7% type B). For practical hospital beam calibration using a field instrument, this needs to be combined with the estimated uncertainties for the additional steps involved in the hospital.

An analysis of the uncertainties of clinical beam dose calibration using a field instrument, following various dosimetry approaches, including that based on IPSM 1990 [1], was presented almost ten years ago [10]. It specifically considered the approach based on using the UK direct absorbed dose to water protocol and took into account all steps, including the calibration of the local standard, the calibration of the field instrument and the practical measurements required for beam calibration. It included some estimates of the effects from short term and long term linac monitor stability and also utilized

the results from the UK national dosimetry intercomparison to help to refine the estimates and to compare them with observed variations in the practical implementation and operation of dosimetry protocols and procedures in UK hospitals [7]. It concluded that the combined standard uncertainties in the determination of absorbed dose to water in reference conditions in these circumstances was 1.3% for ^{60}Co and 1.6% for megavoltage X ray beams. It is now possible to update these estimates to take account of the fact that modern linacs are typically more stable in terms of dose per monitor unit and to consider the consequences of the improved results from more recent UK dose audits on estimates of dosimetry uncertainty.

The stability of linacs has improved over the past ten years. Using more recent data on standard uncertainties of dose per monitor unit values and other parameters from analyses of departmental quality control programmes reduces the uncertainty estimate given above for megavoltage X ray beams from 1.6% to 1.1%. This applies to the determination of absorbed dose to water in reference conditions following an absorbed dose to water protocol and using a chamber with a directly determined calibration factor, for example from the NPL calibration service. (If only a ^{60}Co calibration factor is available and k_Q factors are used, the uncertainties will increase to 1.5%, in agreement with the estimate in IAEA Technical Reports Series No. 398 [11].) These are significant reductions compared with air kerma calibration approaches, for which the standard uncertainty has been estimated at 2–2.5% for megavoltage X ray beams [10].

As a comparison with likely variations in the practical application of procedures between different radiotherapy centres, the results from recent UK X ray dosimetry intercomparisons and audits [9] can be considered. In these the dosimetry protocol followed by centres and also that used for the audit measurement system has been the UK approach, based on the NPL X ray calibration service [1]. It should be noted that for intercomparisons in which the audit dosimetry system and the radiotherapy centres audited use the same standards laboratory and the same very closely defined dosimetry code of practice, such as IPSM 1990 [1], the systematic uncertainties in the dosimetry standards and the systematic uncertainties in the calibration factors should be common and should therefore not affect the SD of the distribution of audit results. These results should therefore only reflect the random uncertainties between centres. The SD of the distribution of dose ratios (audit measured/local centre stated) from recent UK megavoltage X ray audits is 1% [8, 9], an improvement from the 1.5% observed in the earlier national study [7]. These values must include some contribution from the random uncertainties in:

(a) The local standard calibration factors (the audit system dosimetry chain and the radiotherapy centre dosimetry chain);
(b) The audit measurements themselves.

If these were accurately known then they could be subtracted in quadrature from the most recent audit SD of 1%, and the remaining figure could be assumed to be all due to practical uncertainties in the departments (equipment and procedures). This could be used as the relevant component in the practical estimate of overall uncertainty in the determination of absorbed dose to water in reference conditions for megavoltage X ray beams. However, while the uncertainty contributions (a) and (b) may be estimated, they are not accurately known. Therefore, as a pessimistic assumption, no subtraction is made from the observed audit SD of 1%. Combining this in quadrature with the uncertainty quoted on the NPL calibration factors thus produces an upper estimate of 1.3% in the determination of absorbed dose to water in reference conditions for megavoltage X ray beams. This can be compared with the estimate of 1.1% given above using best recent data.

3. ELECTRON BEAMS

3.1. Approach based on absorbed dose to water calibrations

Currently UK electron dosimetry is based on an $N_{D,\mathrm{air}}$ approach utilizing an air kerma calibration [12]. However, over recent years the NPL has developed a similar graphite calorimeter primary standard for electron beams [4, 5] as that operated for photon beams [2, 3]. This is the basis of a similar absorbed dose to water calibration service recently set up for electron beams, which again has the almost unique ability to provide direct $N_{D,w}$ calibration factors over a range of electron beams of nominal energy 4–19 MeV. The underlying objective is also similar (i.e. to provide reduced uncertainties for clinical electron beam dosimetry). This is in keeping with the evolution of other recent national and international recommendations [11, 13], although not many standards laboratories can currently provide direct calibrations over a range of beam qualities, as their access is generally limited to ^{60}Co beams only. A new UK (IPEM) protocol has been developed for general clinical use, based on the NPL $N_{D,w}$ electron calibration service [6].

One of the principal advantages of obtaining calibration factors directly in terms of absorbed dose to water over a range of beam qualities, as compared with an air kerma based approach, is that each ionization chamber is directly characterized at each of those beam qualities. All air kerma approaches rely on

characterizing chamber types as a whole (e.g. to determine perturbation correction factors) rather than individual chambers. This general observation applies for both photon and electron beams. However, there are much larger chamber to chamber variations in electron beams than in photon beams, and particularly for some designs of parallel-plate chambers [5]. It is therefore less reliable to assume that all chambers of a given type behave in the same way; this is one source of increased uncertainties for the older approaches. This limitation is still present in applications of absorbed dose to water protocols in which an $N_{D,w}$ factor is provided for only one reference beam quality, commonly ^{60}Co, and theoretically derived or generic experimental beam quality correction factors are then used to move to other beams and qualities.

3.2. The NPL absorbed dose primary standard and chamber calibration procedures

The NPL calibration service for electron beams is based on the primary standard electron beam graphite calorimeter [4] and yields a direct calibration of an ionization chamber in terms of absorbed dose to water. The calibration is a two step process. Firstly, reference ionization chambers (NACP parallel-plate type) are calibrated against the calorimeter in a graphite phantom at specified reference depths for each beam quality. A conversion is then carried out from graphite to water, based on cavity theory, using ratios (water/graphite) of perturbation factors and stopping power ratios (material/air). The users' chambers are then compared with the NPL reference chambers in a water phantom, also at the specified reference depths. This follows a formalism first proposed by Burns et al. [14].

The beam quality is specified directly in terms of $R_{50,D}$ in water, measured from depth dose curves in the normal way in a large enough field to provide in-scatter equilibrium at the central axis, such that $R_{50,D}$ is independent of field size. The $N_{D,w}$ factors are provided as a function of $R_{50,D}$. The calibration factors provided are applicable at the specific reference depths ($0.6R_{50,D} - 0.1$ (cm)) relevant to each beam quality. Chambers and electrometers are calibrated independently, with a full recombination assessment of the chamber.

3.3. Calibration reference depth

For electron beams, where the spectrum is changing with depth, the reference depths must be specified robustly and unambiguously. The chamber calibration factors supplied by the NPL are stated for specific reference depths in water. The absorbed dose calibration of clinical electron beams must be carried out at the same reference depths in water to ensure the close applicability of

the factors; that is, to ensure that the energy spectra, mean energy, etc., are similar at the chamber calibration and then at the beam calibration using that chamber and calibration factor. The reference depths depend on the beam quality specifier, $R_{50,D}$, and follow the suggestion of Burns et al. [15]:

$$z_{\text{ref}} = 0.6R_{50,D} - 0.1 \text{ (cm)}$$

This reference depth has been selected as it gives a significant improvement in consistency between chamber calibration factors for different clinical machines [15], thereby improving accuracy. This is in keeping with the approaches of other recent protocols [11, 13]. For lower quality beams ($R_{50,D} \leq$ 4 cm, $E_o \leq 10$ MeV) the calibration reference point will typically be found to lie at or very close to the depth of dose maximum. However, for higher quality beams this will often not be the case and the calibration reference depth will typically be at a greater depth than the depth of dose maximum. In this case a conversion is required from the reference depth to the depth of dose maximum, since the latter is normally the value required for the normalization of clinical dosimetry systems for treatment planning purposes. However, for a wide range of machines and beams the percentage depth dose conversion required is no more than a few per cent.

3.4. Pilot testing of the new NPL electron calibration service

The NPL, in conjunction with an IPEM working party, has piloted the transfer of this calibration service from the NPL to the clinic [5]. These trials involved 17 UK radiotherapy centres supplying a total of 46 chambers of the NACP, Markus, Roos and Farmer types. Calibration factors were derived from the primary standard calorimeter at seven energies in the nominal energy range 4–19 MeV. Investigations were also carried out into chamber perturbation corrections, polarity effects, ion recombination and repeatability of the calibration process. The instruments were returned to the radiotherapy centres for measurements to be carried out comparing the NPL direct calibration with the 1996 IPEMB air kerma based code of practice [12].

It was found that, in general, all chambers of a particular type (for Farmer, NACP and Roos designs) showed the same energy response within experimental uncertainties, and that polarity and recombination behaviour was also reasonably consistent. Perturbation corrections were obtained and were found to agree well with the standard data used in the IPEMB 1996 code. In particular, no difference was seen between the NACP and Roos chambers. However, it was found that results could be significantly variable for some examples of the Markus chamber.

The results of the comparisons between measuring dose using the approach based on the NPL service providing direct $N_{D,w}$ calibrations and the air kerma based approach embodied in the IPEMB 1996 code of practice show that the stated doses are greater using the new approach. The change in stated dose was no more than 2% for individual chambers of Farmer, NACP and Roos designs, and generally less than 1%. Average changes were close to 1% for the graphite walled Farmer type chambers and close to 0.5% for the NACP and Roos parallel-plate chambers. However, for Markus chambers the results were much more variable chamber to chamber, with a mean difference of around 2%.

3.5. IPEM electron dosimetry code of practice (2003)

Following this, a new UK (IPEM) electron dosimetry protocol has been developed for general clinical use, based on the direct $N_{D,w}$ calibration service [4, 5]. The designated chambers included are the NACP and Roos parallel-plate designs for any energy beam and graphite walled Farmer type chambers for higher energy beams ($R_{50,D} \geq 4$ cm, $E_o \geq 10$ MeV). Based on the observations noted above during the pilot study, the Markus chamber is not recommended as a designated chamber for beam calibration dosimetry. All chamber measurements are to be carried out with the effective points of measurement of the chamber positioned at the point of interest; a $0.6r$ shift for cylindrical chambers, where r is the internal radius of the chamber cavity, and inside the front face of parallel-plate chambers. For parallel-plate chambers, depths of measurement must take into account the equivalent thickness of the front wall. The primary recommendation is to carry out measurements in a water phantom, although guidance is given for other materials for some situations. Any data required are compatible with currently internationally accepted values (and with other international recommendations, such as Ref. [11]) and are given in terms of $R_{50,D}$ as the beam quality specifier. The protocol is necessarily more complex in operation than the equivalent photon protocol. However, it is significantly simpler, with significantly reduced uncertainties, compared with the previous electron protocol.

Procedures are given for:

- The determination of depth doses;
- The determination of absorbed dose at the reference point for beam calibration, using a calibrated designated chamber at the same reference depths as used for chamber calibration, and applying the appropriate $N_{D,w}$ to the corrected chamber reading;

- Relating doses from this point to other points in the beam, in particular converting from the reference point to the depth of dose maximum if the two are not the same;
- The determination of relative output factors for non-reference field sizes and depths;
- The use of other chambers as field instruments, and the required methods to transfer a calibration from a directly calibrated chamber to such a chamber;
- Extension to beam qualities outside the range available at the standards laboratory;
- The use of non-water phantoms.

Appendices cover:

- Practical corrections to the instrument reading;
- Chamber characteristics;
- An outline of the formalism;
- The data required and their sources;
- Uncertainties.

3.6. Uncertainties in electron beam calibration following the new UK approach

Standard uncertainties on the direct absorbed dose to water calibration factors supplied by the NPL are estimated to be approximately 0.75%. Standard uncertainties on the determination of absorbed dose to water at the reference depth in a water phantom are estimated to be approximately 1.1% when following the $N_{D,w}$ protocol. If using a non-water phantom this estimate increases and lies within the range 1.2–1.5%, depending on the phantom material and on whether the reference depth lies at the depth of dose maximum. All the above values are valid for both parallel-plate and Farmer chambers and are estimated on the basis of:

- For the calibration factors, information from the NPL on the uncertainties in its calibration service;
- For the practical procedures in the clinic, using experience from clinical practice in relatively optimal conditions.

These estimated uncertainties are a significant improvement on those quoted for approaches to the determination of electron absorbed dose based on a ^{60}Co air kerma calibration [10, 12], which are generally in the range 2–3%.

As a comparison to likely variations in the practical application of procedures between different radiotherapy centres, the results from the electron dosimetry intercomparison carried out in UK centres from 1994 to 1996 [8] can be considered. This was at a time when the air kerma protocol (IPEMB 1996) was in use in clinics and the audit dosimetry was also conducted using this protocol. The intercomparison showed:

- An SD on the distribution of checks on air kerma calibrations of the local chambers used for electron dosimetry of 1.2–1.3%;
- An SD of 1.8% on the distribution of comparisons of electron dose per monitor unit at the depth of dose maximum in all the beams checked.

Some of the difference in these uncertainties must be associated with the selection of parameters in the air kerma based approach in use at the time and their applicability and the various steps in this approach. Some must also be associated with the audit measurements themselves. However, the pessimistic assumption can be made that all the difference is due to practical procedures. This difference can then be combined with the NPL quoted value for the uncertainty on the $N_{D,w}$ calibration factor values of 0.75%. This then gives an upper estimate of the overall uncertainties on the determination of absorbed dose to water per monitor unit at the depth of dose maximum in a water phantom using the $N_{D,w}$ protocol of approximately 1.4%. This can be compared with the optimal estimate of 1.1% for the $N_{D,w}$ protocol given above.

4. IMPLEMENTATION OF A NEW DOSIMETRY PROTOCOL IN THE RADIOTHERAPY CENTRE

Some recommendations for safe implementation that have been developed from the experience of the introduction of new dosimetry protocols into clinical practice include:

- A detailed assessment of the new code of practice as it applies in the local situation should be carried out; it should be ensured that the protocol is in agreement with the chamber calibration procedures and factors supplied by the standards laboratory in the local standard calibration certificate.
- The theory, formalism, data, etc., should be assessed and an evaluation made of the expected changes for the local beams.
- The new method should be compared with the previous methods used and conformation of the expected changes for the local beams should be obtained.

- Changes should be discussed with physicists elsewhere who have already worked through the process.
- Dose changes should be assessed experimentally, working through the whole process; are the changes as expected?
- Independent checking of methods and results should be utilized, both within the department (e.g. more than one physicist working through the procedures and calibrations independently, using more than one measurement system and independently setting up for measurements) and also ideally by using an external audit or intercomparison before changing practice.
- Expected changes should be discussed with clinicians before changing practice, to evaluate the consequences on prescriptions, departmental data, etc.
- The date of change should be agreed and recorded in local physics and clinical documentation.
- In vivo dosimetry should be used as final verification.

5. CONCLUSIONS

The UK has a relatively long experience of operating an absorbed dose to water protocol for megavoltage photon beams, based on the NPL graphite calorimeter primary standard and calibration service and the IPSM 1990 code of practice [1]. It is currently making the change to a similar approach for electron beam dosimetry [6], based on a new NPL graphite calorimeter and electron calibration service and a newly developed electron dosimetry code of practice. Both calibration services provide $N_{D,w}$ directly over a range of beam qualities, so there is no need to use k_Q factors. This further decreases the uncertainties. The protocols provide a simpler formalism for practical use than previous approaches based on air kerma calibrations, and also significantly reduced uncertainties. They improve consistency chamber to chamber and also between beam modalities and beam qualities. Changes in stated doses are typically 1% for megavoltage photon beams. For electron beams the changes are no more than 2% and typically less than 1%. There is close agreement with the recent AAPM [13] and IAEA [11] approaches.

It is likely that in future absorbed dose primary standards will move from being based on graphite calorimeters to being based on water calorimeters (in which the absorbed dose to water is derived directly in a water phantom), as this is well under development at the NPL.

REFERENCES

[1] INSTITUTE OF PHYSICAL SCIENCES IN MEDICINE, Code of practice for high-energy photon therapy dosimetry based on the NPL absorbed dose calibration service, Phys. Med. Biol. **35** (1990) 1355–1360.

[2] DuSAUTOY, A.R., The UK primary standard calorimeter for photon-beam absorbed dose measurement, Phys. Med. Biol. **41** (1996) 137–151.

[3] BURNS, J.E., Absorbed-dose calibrations in high-energy photon beams at the National Physical Laboratory: Conversion procedure, Phys. Med. Biol. **39** (1994) 1555–1575.

[4] McEWEN, M.R., DuSAUTOY, A.R., WILLIAMS, A.J., The calibration of therapy level electron beam ionization chambers in terms of absorbed dose to water, Phys. Med. Biol. **43** (1998) 2503–2519.

[5] McEWEN, M.R., WILLIAMS, A.J., DuSAUTOY, A.R., Determination of absorbed dose calibration factors for therapy level electron beam ionization chambers, Phys. Med. Biol. **46** (2001) 741–755.

[6] INSTITUTE OF PHYSICS IN ENGINEERING AND MEDICINE, The IPEM code of practice for electron dosimetry for radiotherapy beams of initial energy from 4 to 25 MeV based on an absorbed dose to water calibration, Phys. Med. Biol. **48** (2003) 2929–2970.

[7] THWAITES, D.I., WILLIAMS, J.R., AIRD, E.G., KLEVENHAGEN, S.C., WILLIAMS, P.C., A dosimetric intercomparison of megavoltage photon beams in UK radiotherapy centres, Phys. Med. Biol. **37** (1992) 445–461.

[8] NISBET, A., THWAITES, D.I., A dosimetric intercomparison of electron beams in UK radiotherapy centres, Phys. Med. Biol. **42** (1997) 2393–2409.

[9] THWAITES, D.I., POWLEY, S.K., NISBET, A., ALLAHVERDI, M., "The United Kingdom's radiotherapy dosimetry audit network", these Proceedings, Vol. 2, pp. 183–190.

[10] THWAITES, D.I., "Uncertainties at the end point of the basic dosimetry chain", Measurement Assurance in Dosimetry (Proc. Int. Symp. Vienna, 1993), IAEA, Vienna (1994) 239–255.

[11] INTERNATIONAL ATOMIC ENERGY AGENCY, Absorbed Dose Determination in External Beam Radiotherapy, Technical Reports Series No. 398, IAEA, Vienna (2000).

[12] INSTITUTION OF PHYSICS AND ENGINEERING IN MEDICINE AND BIOLOGY, The IPEMB code of practice for electron dosimetry for radiotherapy beams of initial energy from 2 to 50 MeV based on an air kerma calibration, Phys. Med. Biol. **41** (1996) 2557–2603.

[13] AAPM TASK GROUP 51, AAPM's TG-51 protocol for clinical reference dosimetry of high-energy photon and electron beams, Med. Phys. **26** (1999) 1847–1870.

[14] BURNS, D.T., McEWEN, M.R., WILLIAMS, A.J., "An NPL absorbed dose calibration service for electron beam radiotherapy", Measurement Assurance in Dosimetry (Proc. Int. Symp. Vienna, 1993), IAEA, Vienna (1994) 61–71.

[15] BURNS, D.T., DING, G.X., ROGERS, D.W.O., R_{50} as a beam quality specifier for selecting stopping-power ratios and reference depths for electron dosimetry, Med. Phys. **23** (1996) 383–388.

IMPLEMENTATION OF THE NEW IAEA CODE OF PRACTICE IN BRAZIL

L.N. RODRIGUES*
Laboratory of Instrument Calibration,
Instituto de Pesquisas Energéticas e Nucleares/
Comissão Nacional de Energia Nuclear,
São Paulo

C.N. MELLO DA SILVA
National Laboratory for Metrology of Ionizing Radiation,
Instituto de Radioproteção e Dosimetria/
Comissão Nacional de Energia Nuclear,
Rio de Janeiro

Brazil

E-mail: lnatal@net.ipen.br

Abstract

In order to implement the new IAEA code of practice in Brazil the national calibration laboratories, the National Laboratory for Metrology of Ionizing Radiation and the Laboratory of Instrument Calibration, are calibrating clinical dosimeters in terms of air kerma and absorbed dose to water in a ^{60}Co gamma ray beam. The $N_{D,w}/N_K$ ratios thus obtained are then compared with the literature values; a satisfactory agreement has been found. Additionally, several training courses have been organized for the dissemination of the new formalism among medical physicists. The planned target date for the full implementation of calibration in terms of absorbed dose to water is December 2002, following the same decision of the Nordic countries.

1. INTRODUCTION

The IAEA recently published the final version of a new code of practice based on standards of absorbed dose to water [1]. This will be implemented in Brazil gradually, making the transition from the existing code of practice used in the country, IAEA Technical Reports Series No. 277 (TRS 277) [2], which is based on an air kerma calibration.

* Formerly at the National Laboratory for Metrology of Ionizing Radiation, Brazil.

In both calibration laboratories in Brazil, the National Laboratory for Metrology of Ionizing Radiation and the Laboratory of Instrument Calibration (LNMRI and LCI), in which there is no access to a linac, the approach used is to provide radiotherapy centres with a calibration factor in terms of absorbed dose to water for the ionization chamber at the reference quality ^{60}Co, and with theoretically derived quality correction factors for the appropriate chamber type, which must be applied to other beam qualities.

This paper discusses the investigations carried out to give confidence in the use of the new code of practice and the plans for its implementation.

2. PRELIMINARY INTERCOMPARISONS

In order to implement the new formalism, which is based on absorbed dose to water, a series of intercomparisons has been performed in Brazil since 1997. The first step of its implementation was to analyse the long term stability of four secondary standard chambers used as transfer instruments (NE 2561 chambers) with traceability to the Bureau international des poids et mesures (BIPM) in terms of the quantity of interest. The second step consisted of the calibration of the transfer and reference standards from the LNMRI and LCI in order to evaluate the ratio $N_{D,w}/N_K$ for such chambers. In a preliminary analysis the ratios thus obtained were compared with the values acquired by other laboratories, such as the National Physical Laboratory (NPL) in the United Kingdom and the IAEA Dosimetry Laboratory.

The procedure thus adopted at the LNMRI and LCI was to analyse the ratio between the ^{60}Co calibration factor in terms of absorbed dose to water and the calibration factor in terms of air kerma for the four transfer standards before offering the calibration service in terms of absorbed dose to water to users. Moreover, a series of intercomparisons between these standards was performed in order to establish general chamber behaviour.

The long term stability of the secondary standards was evaluated from their recalibration results and also from intercomparisons performed since 1997 in terms of air kerma and absorbed dose to water. The recalibration of the national standard (the NE 2561 chamber No. 168) at the BIPM shows a variation of ±0.08% on the ratio $N_{D,w}/N_K$ over six years. However, an overall variation of ±0.22% was found for the three remaining secondary standards after their recalibration. The short term stability was measured by the results obtained during the intercomparisons, showing a maximum deviation of 0.18% compared with the response of the national standard in a ^{60}Co beam. The typical procedure established for the intercomparisons consists of the normalization of all measurements to the response of the LNMRI national standard (the NE 2561 chamber No. 168).

The results obtained for these four NE 2561 chambers give an $N_{D,w}/N_K$ ratio of 1.084 ± 0.013 and show a good agreement of –0.7% and –0.5% compared with the ratios obtained by the NPL [3] and IAEA [4], respectively. Since these results demonstrated the validity of such an approach, some clinical dosimeters have since then been calibrated. The ratio $N_{D,w}/N_K$ obtained for the NE 2571 chambers (1.096 ± 0.013) shows an excellent agreement of ±0.3% with the literature values [4–6]. The ratio $N_{D,w}/N_K$ for the PTW N30001 Farmer chambers (1.091 ± 0.013) gives an agreement of +0.3% compared with IAEA values [4]. However, for the NE 2505/3A and NE 2581 chambers ratios of 1.096 ± 0.013 and 1.096 ± 0.013, respectively, were found, which present a larger variation (+1.2%). The $N_{D,w}/N_K$ ratio found for the Exradin A12 chambers was 1.104 ± 0.013. It should be pointed out that the LNMRI participated in a recent intercomparison promoted by the Inter-American Metrology System, which showed an agreement of –0.2% compared with BIPM values for this type of chamber [7]. No reported values have been found in the literature for the Wellhöfer IC 70 (1.095 ± 0.013) or PTW N30013 (1.092 ± 0.013) chambers. The values of N_K and $N_{D,w}$ determined by both the LNMRI and LCI, with the corresponding $N_{D,w}/N_K$ ratios, are given in Table I. The relative uncertainty of the calibration factor N_K is 0.8% (coverage factor $k = 2$) and for $N_{D,w}$ is 0.9% (coverage factor $k = 2$), giving a combined uncertainty of 1.2% (coverage factor $k = 2$) for the ratio $N_{D,w}/N_K$.

3. TRAINING COURSES

The above intercomparisons and the evaluation of the long term stability of the secondary standards took place at the same time as training courses on the new formalism of absorbed dose to water, and in this way the updated knowledge of the laboratory staff was transferred to hospital physicists. These courses have demonstrated their effectiveness for radiotherapy centres in Brazil, since practical lectures and experimental procedures on absorbed dose determination in water are given.

The training courses have been organized at the LNMRI since 1996, and had a total of 165 participants by 2002. In the first year the course was held at a hospital in central Brazil; theoretical aspects of the IAEA protocol (TRS 277) were covered, followed by an intercomparison in terms of absorbed dose to water involving seven hospitals. In 1997, 53 medical physicists attended the course and an intercomparison in terms of absorbed dose to water was performed using the TRS 277 formalism. Participants from 17 hospitals brought their own dosimetry systems, which were compared with the LNMRI secondary standard. The results showed an overall agreement of ±1%, which is the

TABLE I. VALUES OF N_K AND $N_{D,w}$ DETERMINED BY THE LNMRI AND LCI, WITH THE RESPECTIVE $N_{D,w}/N_K$ RATIOS

Hospital	Chamber model	N_K (mGy/division)	$N_{D,w}$ (mGy/division)	$N_{D,w}/N_K$
1	A12	43.12	47.72	1.107
2	A12	43.01	47.34	1.101
3	N23333	9.571	10.43	1.090
4	N30001	49.38	54.17	1.097
5	N30001	48.91	53.01	1.084
6	N30001	10.24	11.19	1.093
7	N30002	48.61	52.97	1.090
8	N30013	47.97	52.74	1.099
9	N30013	48.77	53.19	1.091
10	N30013	49.77	54.06	1.086
11	NE 2505/3A	40.83	44.76	1.096
12	NE 2505/3A	40.73	44.61	1.099
13	NE 2561	93.08	101.7	1.092
14	NE 2561	96.31	103.9	1.078
15	NE 2561	93.14	100.6	1.080
16	NE 2561	93.30	100.6	1.079
17	NE 2561	94.25	103.0	1.093
18	NE 2571	962.0	1046	1.088
19	NE 2571	959.6	1055	1.100
20	NE 2571	42.81	47.01	1.098
21	NE 2571	1048	1149	1.097
22	NE 2571	8.993	9.869	1.097
23	NE 2571	412.0	449.5	1.091
24	NE 2571	714.5	783.6	1.096
25	NE 2571	1017	1113	1.095
26	NE 2571	959.6	1055	1.099
27	NE 2571	405.5	445.3	1.098
28	NE 2571	8.699	9.556	1.098
29	NE 2571	413.9	454.2	1.097
30	NE 2581	1231	1336	1.085
31	NE 2581	965.2	1063	1.102
32	NE 2581	1229	1349	1.097
33	NE 2581	8.773	9.635	1.098
34	NE 2581	934.8	1022	1.094
35	NE 2581	1229	1349	1.097
36	IC 70	44.57	48.47	1.088
37	IC 70	44.50	49.06	1.103

same agreement obtained by the LNMRI in the intercomparison of calibration factors in terms of N_K and $N_{D,w}$ promoted by the IAEA/World Health Organization network of secondary standards dosimetry laboratories (SSDLs) in 1997 [4]. It should be pointed out that larger variations were observed in the first analyses, which were due to mistakes in selecting the appropriate correction factors for the chambers. In the following year an intercomparison was completed with only two hospitals, since the ionization chambers showed some leakage due to their transport to the SSDL in Rio de Janeiro. To avoid such problems it was decided to focus in the subsequent training courses on the experimental practice of the procedure for the determination of absorbed dose to water in a ^{60}Co beam.

In the next courses a practical comparison between N_K and $N_{D,w}$ formalisms was promoted, which demonstrated their advantages and disadvantages. Some changes have recently been introduced, and specific courses on the main chapters of TRS 398 have been organized. The first, held in August 2002, dealt with the code of practice for high energy electron beams and included practical lectures at the hospital that covered the beam quality specification, the calibration of plane-parallel chambers using the cross-calibration procedure and the determination of output factors. The numbers of medical physicists who attended the training courses are shown in Fig. 1.

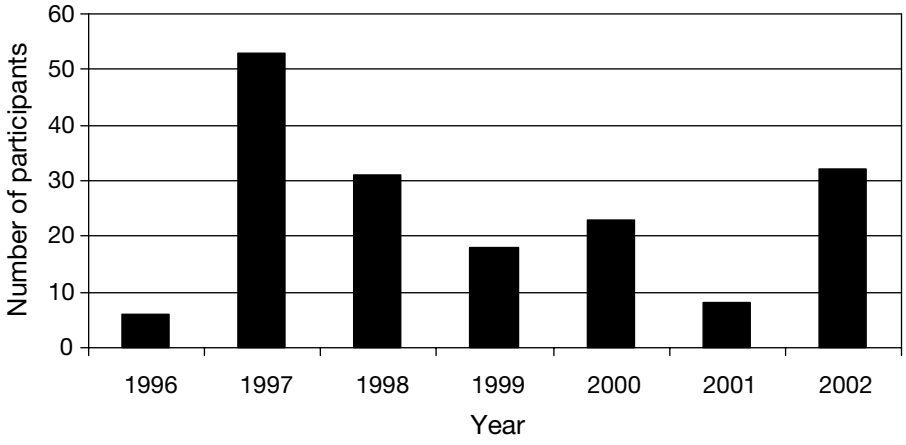

FIG. 1. Number of participants in the training courses organized in order to promote the IAEA codes of practice.

4. CONCLUSION

The method adopted in this investigation and the comparison of the $N_{D,w}/N_K$ ratios with the literature values gives us confidence in the results thus obtained and allows us to provide calibration factors promptly in terms of absorbed dose to water for hospitals in Brazil. The planned target date for the full implementation of calibration in terms of absorbed dose to water is December 2002, following the same decision of the Nordic countries [3].

REFERENCES

[1] INTERNATIONAL ATOMIC ENERGY AGENCY, Absorbed Dose Determination in External Beam Radiotherapy, Technical Reports Series No. 398, IAEA, Vienna (2000).

[2] INTERNATIONAL ATOMIC ENERGY AGENCY, Absorbed Dose Determination in Photon and Electron Beams, 2nd edn, Technical Reports Series No. 277, IAEA, Vienna (1997).

[3] INTERNATIONAL ATOMIC ENERGY AGENCY, Report of a Nordic dosimetry meeting on the implementation of the new international code of practice for radiotherapy dosimetry, TRS-398, SSDL Newsletter No. 45 (2001) 25–27.

[4] MEGHZIFENE, A., CZAP, L., ANDREO, P., Intercomparison of ionization chamber calibration factors in the IAEA/WHO network of SSDLs, SSDL Newsletter No. 38 (1998) 13–19.

[5] SHARPE, P., Progress Report on Radiation Dosimetry at NPL, Working Doc. CCRI(I)/01-21, Bureau international des poids et mesures, Sèvres (2001) 1–7.

[6] KRAMER, H.-M., Informative Progress Report on the Standards for Water Absorbed Dose at PTB, Working Doc. CCRI(I)/01-20, Bureau international des poids et mesures, Sèvres (2001) 1–2.

[7] SHORTT, K., et al., "International dosimetry comparison", paper presented at the 2002 American Association of Physicists in Medicine Meeting, Montreal, 2002.

FINNISH NATIONAL CODE OF PRACTICE FOR THE REFERENCE DOSIMETRY OF RADIATION THERAPY

A. KOSUNEN, P. SIPILÄ, H. JÄRVINEN,
R. PARKKINEN, I. JOKELAINEN
Radiation and Nuclear Safety Authority (STUK),
Helsinki, Finland
E-mail: antti.kosunen@stuk.fi

Abstract

A Finnish national code of practice (CoP) for the reference dosimetry of external beam radiotherapy and brachytherapy has been established. The CoP is to be used as a handbook for the reference dosimetry of the methods of radiotherapy in use in Finland. The CoP covers the dosimetry of high energy photon and electron beams and the dosimetry of low energy X rays for external beam radiotherapy. Implementation of the CoP initiates in Finland dose determinations on the basis of the absorbed dose to water approach. Generally the CoP follows the formalism of IAEA Technical Reports Series No. 398 (TRS 398), but with specific selections of the alternative methods described in TRS 398. The methods in the CoP for brachytherapy dosimetry are based on the use of a well type ionization chamber, in accordance with IAEA-TECDOC-1274. Procedures both for the calibration of a well type ionization chamber and for the measurement of the reference air kerma rate of ^{137}Cs, ^{192}Ir, ^{125}I and ^{103}Pd sources are included. The CoP was prepared by the National Metrology Laboratory for Ionizing Radiation in Finland (the secondary standards dosimetry laboratory of STUK) in close co-operation with Finnish radiotherapy physicists. An overview of the CoP and the specific national features is presented.

1. INTRODUCTION

The main objective in establishing a national code of practice (CoP) for radiation therapy dosimetry in Finland is to maintain consistent practices for reference dosimetry at hospitals as the absorbed dose to water based approach of IAEA Technical Reports Series No. 398 (TRS 398) [1] is implemented. There are nine radiotherapy centres in Finland, which have, for external beam radiotherapy, 18 multienergy and eight single photon linacs, five low energy (<100 kV) conventional X ray units and two X ray units operating below 10 kV (grenz ray equipment). As TRS 398 includes guidance for many radiotherapy modalities not in use in Finland, a condensed 'dosimetry manual' version with practical national features has been found useful.

There are 11 afterloading brachytherapy units in Finland, in which are used ^{137}Cs low dose rate (LDR), ^{125}I LDR and ^{192}Ir high dose rate (HDR) sources. The use of well type ionization chambers for brachytherapy dosimetry has become common practice during recent years. However, the reference air kerma rate used for dose delivery is still based on the calibrations made by the manufacturers of the sources and well type chambers. The CoP is aimed at standardizing the national practice for the calibration of well type ionization chambers and for the determination of the reference air kerma rates of brachytherapy sources.

In addition to achieving accurate dosimetry, the methods recommended in the CoP aim to optimize the use of national resources in Finland. Since the ionization chambers in use in Finnish hospitals are mainly of the same type, it is practical to present the derived calibration factors for the set of linac beam qualities in the calibration certificate issued by a secondary standards dosimetry laboratory (SSDL). Mainly for the same reason, it is possible for an SSDL to perform the cross-calibration of a plane-parallel ionization chamber in the user's linac electron beam, as a service. On this basis, the calibration methods used by the National Metrology Laboratory for Ionizing Radiation in Finland (the SSDL of STUK) have been adjusted to support the methods recommended in the CoP.

Training for the users of the CoP is organized through the annual meetings of Finnish radiotherapy physicists and the SSDL staff and through the regular site visits of the SSDL staff to the hospitals.

2. RECOMMENDATIONS FOR THE REFERENCE DOSIMETRY OF HIGH ENERGY PHOTON AND ELECTRON BEAMS

The recommendations for the reference dosimetry of high energy photon and electron beams are based on TRS 398 [1]. The following modifications and selections of the alternative methods and equipment described in TRS 398 have been made.

2.1. Ionization chambers and phantoms

Currently in Finland only the NE 2571 type of cylindrical ionization chamber is used for the reference dosimetry of high energy photon beams. The water protection sleeves used in these chambers are of a uniform type, with a 1 mm thick polymethylmethacrylate (PMMA) wall. There has been no interest in using alternative types of chamber, as the experience with the NE 2571

type has so far been good. The chamber related data and parameters for this type of chamber only are given in the CoP. Other types of chamber described in TRS 398 may be used, but require chamber parameters taken directly from TRS 398.

Only the NACP type plane-parallel chambers (NACP-01 and NACP-02) have been used for electron beam dosimetry in Finland in recent years. NACP chambers have been found reliable, especially when they are calibrated in an electron beam. However, purchase of NACP chambers from the manufacturer has become difficult, and they may not be available in the future. The Roos type plane-parallel ionization chamber has become an alternative in Finland, mainly because of its similarities in the perturbation behaviour relative to electron beam energy [1, 2]. NACP and Roos chambers are recommended in the CoP for electron beam reference dosimetry. The chamber related data for other types of plane-parallel chamber have to be applied directly from TRS 398.

A water phantom and a vertical beam set-up (with no entrance window in the phantom) are recommended for the determination of both the beam quality specifier and the absorbed dose to water.

2.2. Beam quality specifier

The tissue phantom ratio ($TPR_{20,10}$) is recommended as a primary beam quality specifier for high energy photon beams. As an alternative, the ratio of ionizations at 10 cm and 20 cm depths for a field size of 10 cm × 10 cm and measured with a constant focus to phantom surface distance (SSD) of 100 cm ($J_{10,20}$) can also be used. The relationship between $J_{10,20}$ and $TPR_{20,10}$ is based on the relationship between the dose ratio at 20 cm and 10 cm depths with a constant SSD of 100 cm and a field size of 10 cm × 10 cm ($PDD_{20,10}$) and $TPR_{20,10}$, as described in TRS 398. If $J_{10,20}$ is used as a beam quality specifier the relationship between $J_{10,20}$ and $TPR_{20,10}$ has to be verified experimentally for each photon beam quality. $J_{10,20}$ was selected instead of $PDD_{20,10}$ because the numerical value of $J_{10,20}$, as an inverse number to $PDD_{20,10}$, is not so easily confused with the numerical value of $TPR_{20,10}$. Furthermore, $J_{10,20}$ as a parameter referring to ionization is more straightforward to use.

The half-value depth of electrons determined from the depth ionization distribution ($R_{50,ion}$) is used as a beam quality specifier for electron beam dosimetry. $R_{50,ion}$ was selected because it is a directly measurable, ionization based parameter. The correlation between $R_{50,ion}$ and the calibration correction factor, k_Q, is that described in TRS 398. The half-value depth of electrons determined from the depth dose distribution (R_{50}) is used only as an intermediate parameter between $R_{50,ion}$ and k_Q.

2.3. Calibration of ionization chambers

The ionization chambers used for high energy photon beam dosimetry at the SSDL of STUK are calibrated in a ^{60}Co gamma radiation beam. Individual water sleeves are used for the chambers. The calibration of the chambers for photon dosimetry is performed both for the ionization chamber and for the user's measurement chain (the chamber with the electrometer). The calibrations of the plane-parallel chambers used for electron beam dosimetry are performed in the user's linac electron beams [3]. The IAEA's cross-calibration methodology using an SSDL working standard as a reference instrument is followed for plane-parallel chambers [1, 2]. The plane-parallel chambers for electron beam dosimetry are calibrated as chambers only, without the user's electrometer. The recommended calibration interval for ionization chambers used for high energy photon and electron beam dosimetry is three years. A calibration certificate issued by the SSDL of STUK contains the following information:

(a) The calibration factor of the chamber for absorbed dose to water with the calibration beam quality (N_{Qo}).
(b) The derived calibration factors for a set of user beam qualities (N_Q) relative to beam specifiers (R_{ion} for electrons, $\text{TPR}_{20,10}$ and $J_{10,20}$ for photons). The values of k_Q from TRS 398 used in the derivation are also listed.
(c) The results of the check source and leakage current measurement. The expected value of the check source measurement is presented for a period of three years.
(d) The sensitivity of the user's electrometer relative to the electronics of the SSDL. This is determined in connection with the calibration of photon ionization chambers.
(e) For a plane-parallel chamber used for electron beam dosimetry, the recombination factor and polarity effect at the calibration beam.

To minimize the overall uncertainty of the recombination effects determined by the two voltage method, the same collection voltages as used in the determination of the recombination factor at calibration are recommended for the determination of the recombination factor at the actual dose measurement.

2.4. Beam calibration procedure

2.4.1. Verification of beam performance and determination of beam specifier

The beam performance in respect of the critical parameters must be checked prior to actual dose measurements. Attention is paid to the

reproducibility and repeatability of the monitor system of the linac, to the beam flatness and symmetry and to the depth dose (ionization) characteristics (i.e. the beam quality specifier). Beam flatness and symmetry and the depth ionization characteristics must be measured with the field size used in the beam calibration. The measurements can be performed with an automatic detector scanner system. More detailed guidance on the detectors and the detector set-up when used with a scanner is included in the CoP. All the measured results must be compared with the tolerance and action limits in the quality control of the linac. Experience with linacs in Finland has shown that the TPR can be measured to within about a 0.2–0.5% reproducibility, and the same order of accuracy is expected in measurements of beam flatness and symmetry.

To improve the set-up accuracy of the chamber, the use of a rigid depth gauge is recommended both in the determination of the beam quality specifier and in the actual dose measurement [4].

2.4.2. Verification of dosimeter performance

Verification of dosimeter performance is based on measurements with a check source and the determination of the polarity and recombination effects of the chamber in a linac beam. The check source measurement must be carried out prior to the actual dose determination. The check source result is used only to verify the performance of the dosimeter, not to correct the calibration factor for ambient climatic conditions. Guidance for current measurements and for checking the collecting voltage are also included in the CoP.

Polarity and recombination measurements must be carried out at the reference measurement conditions for the beam calibration for each individual beam quality and dose rate in use. The polarity effect must be measured at least once prior to the first use of the chamber in a linac beam. The recombination correction factor should be determined in connection with each dose determination (see Section 2.4.3). The tolerance limits for polarity and recombination effects in respect of the dosimeter performance are based in the CoP on the International Electrotechnical Commission standard for ionization chambers for radiotherapy [5].

2.4.3. Beam calibration

The delivered dose must be high enough for at least four significant numbers to appear on the display of the electrometer. The repeated readings should be reviewed, preferably as a graph, to ensure the stable performance of the measurement chain. Depending on the repeatability of the monitor system of

the linac, at least three measurements should be made. The minimum to maximum variation of the repeated measurements should be less than 0.5%.

The dose at the reference depth must be determined as described in TRS 398. Typically, a small polarity effect (of less than 0.5%) in a linac beam can occur with the chambers recommended, and so measurements with only one polarity of the collecting potential are required. The recombination correction factor must be determined and applied as described in TRS 398. It is left to the local practice of the hospital to determine the normalization depth of the beam output for treatment planning or calculation purposes.

3. RECOMMENDATIONS FOR THE REFERENCE DOSIMETRY OF LOW ENERGY X RAYS

The calibrations of the plane-parallel chambers for absorbed dose to water with low energy X rays at the SSDL of STUK are based on the use of an air kerma standard ionization chamber. The calibration of the user's chamber is performed on the surface of a PMMA phantom, and the standard absorbed dose is determined in accordance with the measured air kerma value and conversion formalism in TRS 277 [6]. The Bureau international des poids et mesures equivalent X ray qualities are used. The dose determination procedure follows that of TRS 398. A type of guidance for the verification of the dosimeter and beam performance similar to that for the dosimetry of high energy photon and electron beams is also included for low energy X rays in the CoP.

4. RECOMMENDATIONS FOR THE DOSIMETRY OF BRACHYTHERAPY

The recommendations apply to the determination of the reference air kerma rate of ^{137}Cs, ^{192}Ir, ^{125}I and ^{103}Pd radioactive photon sources. The procedures for the calibration of both well type chambers and brachytherapy sources are based on IAEA-TECDOC-1274 [7]. Procedures for dose measurements in a phantom or for quality control measurements are not discussed.

4.1. Well type ionization chambers

Mostly Standard Imaging HDR 1000 Plus well type chambers are used in Finland for brachytherapy dosimetry, although there is one PTW HDR type chamber. The Standard Imaging HDR 1000 Plus chamber is the well type

chamber used by the IAEA, and has been tested with good results by the SSDL of STUK [7–9]. This type of chamber or chambers of similar quality are therefore recommended.

4.2. Calibration of well type chambers for the reference air kerma rate

The SSDL of STUK has two standard well chambers and a ^{137}Cs LDR source available for calibration. The calibration of standard chambers for the reference air kerma rate and for ^{137}Cs, ^{192}Ir, ^{125}I and ^{103}Pd sources is traceable to the University of Wisconsin (an SSDL traceable to the United States National Institute of Standards and Technology). Either the STUK's ^{137}Cs LDR source or short lived ^{192}Ir, ^{125}I or ^{103}Pd LDR sources provided by the user can be used for calibrations of the user's chamber at the SSDL of STUK. For practical and safety reasons the calibrations with the user's HDR sources are performed only at the hospital.

4.3. Calibration of brachytherapy sources by the user

Well type ionization chambers are recommended instead of free in air measurements for the calibration of the user's brachytherapy sources. The verification of the measurement chain and the review of quality control data for the sources and the dosimeter are carried out prior to the source calibration, analogously with that for external beam calibrations. Also, comparisons are made with the reference air kerma rate stated by the manufacturer and with the measurements by the staff of the SSDL. Consistency of 2–3% should be achieved between the various results, otherwise a further investigation of the deviations must be undertaken.

REFERENCES

[1] INTERNATIONAL ATOMIC ENERGY AGENCY, Absorbed Dose Determination in External Beam Radiotherapy, Technical Reports Series No. 398, IAEA, Vienna (2000).

[2] INTERNATIONAL ATOMIC ENERGY AGENCY, The Use of Plane Parallel Ionization Chambers in High Energy Electron and Photon Beams, Technical Reports Series No. 381, IAEA, Vienna (1997).

[3] PARKKINEN, R., et al., Implementation of the IAEA TRS 381 for the electron beam calibration of plane parallel ionization chambers in Finland, Radiother. Oncol. **56** (2000) S199 (abstract).

[4] SIPILÄ, P., et al., Stick out like a sore thumb, Radiother. Oncol. **61** (2001) S89 (abstract).
[5] INTERNATIONAL ELECTROTECHNICAL COMMISSION, Medical Electrical Equipment — Dosimeters with Ionization Chambers as Used in Radiotherapy, Rep. IEC 60731, IEC, Geneva (1997).
[6] INTERNATIONAL ATOMIC ENERGY AGENCY, Absorbed Dose Determination in Photon and Electron Beams, 2nd edn, Technical Reports Series No. 277, IAEA, Vienna (1997).
[7] INTERNATIONAL ATOMIC ENERGY AGENCY, Calibration of Photon and Beta Ray Sources Used in Brachytherapy, IAEA-TECDOC-1274, IAEA, Vienna (2002).
[8] SIPILÄ, P., et al., Practical experiences of using a well chamber, Radiother. Oncol. **56** Suppl. 1 (2000) 199.
[9] TÖLLI, H., SIPILÄ, P., KOSUNEN, A., Comparison of calibration of well type ionization chambers between IAEA and the SSDL of Finland, SSDL Newsletter No. 46 (2002).

UNITED KINGDOM CODE OF PRACTICE FOR KILOVOLTAGE X RAY DOSIMETRY

K.E. ROSSER
National Physical Laboratory, Teddington, United Kingdom

R.J. AUKETT
Department of Clinical Physics and Bioengineering,
Walsgrave NHS Trust, Coventry, United Kingdom

A.G. GREENER
Medical Physics Department, Guy's and St. Thomas' NHS Trust,
London, United Kingdom

R.M. HARRISON
Regional Medical Physics Department, Newcastle General Hospital,
Newcastle upon Tyne, United Kingdom

A.E. NAHUM
Radiation Physics, Radiation Oncology Department,
Fox Chase Cancer Center, Philadelphia, Pennsylvania,
United States of America

The IPEM kV Dosimetry Working Party

E-mail: ker@npl.co.uk

Abstract

The 1996 United Kingdom code of practice (CoP) for kilovoltage X ray dosimetry is based on an ionization chamber that has been calibrated directly in terms of air kerma. The CoP is separated into three distinct energy regions, each with their own dosimetry methods, namely medium, low and very low energy X rays. The Institute of Physics in Engineering and Medicine (IPEM) is about to publish an addendum to this CoP that includes two main changes: firstly, new values of k_{ch} for very low energy X rays will be recommended that differ by a maximum of 7% from the 1996 CoP; secondly, for medium energy X rays, the addendum gives a choice of determining absorbed dose to water at the surface of a water phantom as well as at 2 cm deep in water. The method of determining absorbed dose to water at the surface will be based on that for low energy X ray dosimetry, with values of backscatter factors and the ratio of mass energy absorption coefficients of water to air taken from the American Association of Physicists in Medicine (AAPM) protocol. The paper compares the

IAEA, AAPM, IPEM and Nederlandse Commissie voor Stralingsdosimetrie CoPs for low and medium energy X rays. It is reassuring that the four CoPs agree in their determination of absorbed dose to water within experimental uncertainty.

1. INTRODUCTION

The United Kingdom code of practice (CoP) for kilovoltage (kV) X ray dosimetry [1] is based on an ionization chamber that has been calibrated directly in terms of air kerma and is separated into three distinct energy regions, each with their own dosimetry methods, namely the:

(a) Medium energy X ray region: X rays of half-value layers in the range of 0.5 to 4 mm Cu (generated at tube voltages in the range of 160 kV to 300 kV).
(b) Low energy X ray region: X rays of half-value layers in the region of 1 to 8 mm Al (generated at tube voltages in the range of 50 kV to 160 kV).
(c) Very low energy X rays: X rays of half-value layers in the range of 0.035 to 1 mm Al (X rays generated at tube voltages in the range of 8 kV to 50 kV).

This paper describes an addendum to the 1996 CoP that is due to be published. The addendum will recommend new values of k_{ch} for very low energy X rays and an alternative method of measuring the absorbed dose to water at the surface of a phantom for medium energy X rays. The IAEA [2], American Association of Physicists in Medicine (AAPM) [3], Institute of Physics in Engineering and Medicine (IPEM) [1] and the Nederlandse Commissie voor Stralingsdosimetrie (NCS) [4] CoPs are then be compared for low and medium energy X ray dosimetry.

2. ADDENDUM TO THE IPEM 1996 CoP

2.1. Medium energy CoP

The addendum will give the option of determining the absorbed dose to water either at 2 cm deep in water or at the surface of a phantom, depending on the user's requirements. The surface dose can be determined in a similar manner to that for low energy X rays, assuming that the change in the stem scatter between the calibration and measurement in air is negligible within stated uncertainties. The addendum to the IPEM CoP will adopt values given

in the AAPM CoP [3] for backscatter factors and the ratio of mass energy absorption coefficients of water to air averaged over an in-air spectrum.

2.2. Very low energy CoP

For very low energy X rays the IPEM 1996 CoP recommends that the absorbed dose to water be measured using an air kerma calibrated parallel-plate ionization chamber. If the ionization chamber is on the beam axis, at the surface of a full scatter water phantom, then the absorbed dose to water ($D_{w,z=0}$) is given by:

$$D_{w,z=0} = M_{\mathrm{ph}} N_k k_{\mathrm{ch}} \left[\left(\frac{\bar{\mu}_{\mathrm{en}}}{\rho} \right)_{w/\mathrm{air}} \right]_{z=0,\varphi} \quad (1)$$

where M_{ph} is the instrument reading at the surface of the phantom corrected to standard temperature and pressure, N_k is the air kerma calibration factor, k_{ch} is a factor that accounts for the change in response of the ionization chamber between the calibration in air and measurement at the surface of a full scatter water phantom and $[(\bar{\mu}_{\mathrm{en}}/\rho)_{w/\mathrm{air}}]_{z=0,\varphi}$ is the ratio of mass energy absorption coefficients of water to air averaged over the photon spectrum at the surface of the phantom. The estimated uncertainty (1σ) in the determination of absorbed dose to water at the surface of a water phantom is ±4%.

The main problem with the 1996 CoP is the value recommended for k_{ch}. At the time the CoP was written there was little information available on the values of k_{ch} for very low energy X ray chambers, so the historical practice of assuming a value of unity was endorsed by the CoP.

2.2.1. Value of k_{ch} given in the IPEM addendum

Work by Ipe et al. [5], Greener [6], Perrin et al. [7] and Dieker [8] (adopted in the Deutsches Institut für Normung (DIN) standard [9]) shows that the value of k_{ch} for very low energy X rays differs significantly from unity. The value of k_{ch} was determined in Refs [5–8] for a range of field diameters, source to chamber distances and phantom types. Figure 1 shows that within experimental uncertainty k_{ch} is independent of these factors. It can further be seen from Fig. 1 that the value of k_{ch} for the M23344 and M23342 soft X ray chambers agrees within experimental uncertainty (±3.2% at 1σ quoted by Ipe et al. [5]). The IPEM addendum will therefore recommend one set of values for both chambers to cover most clinical applications.

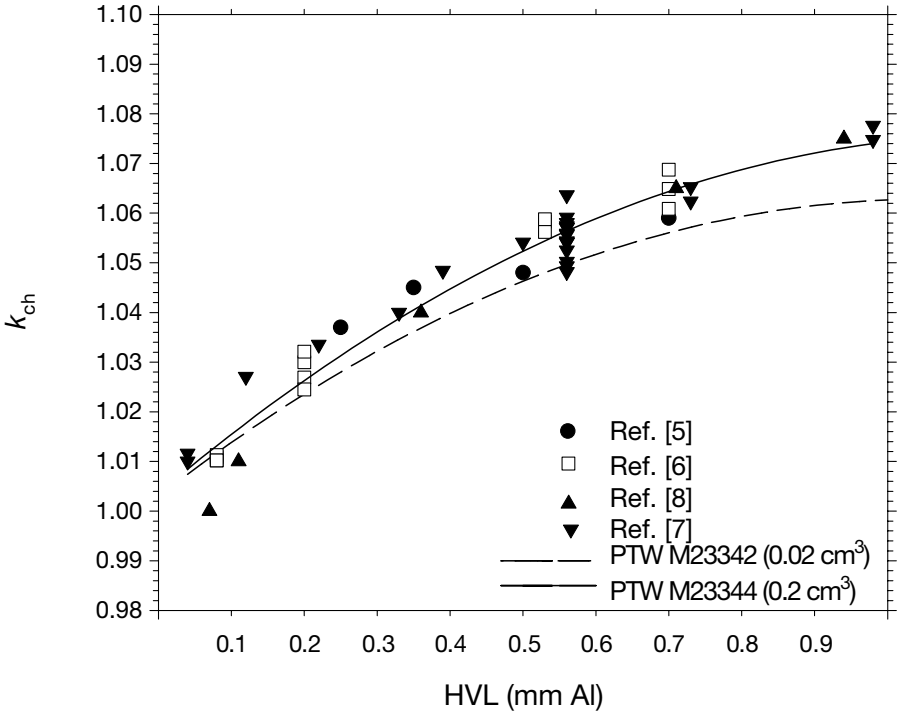

FIG. 1. Comparison of the values of k_{ch} for PTW M23344 and M23342 soft X ray chambers.

2.2.2. Buildup material

There is some debate in the literature about the amount of material required to provide full buildup for low energy X rays. At the time the IPEM CoP [1] was written the amount of material required to provide full buildup was unknown. The CoP therefore recommended that PTW M23344 and PTW M23342 chambers should be used with buildup to bring the wall thickness to at least 8.5 mg/cm^2 (corresponding to the thickness of the epidermis). However, the AAPM [3] CoP states that the wall thickness (including chamber wall) required to provide full buildup at 50 kV is 4 mg/cm^2. This creates a problem for the PTW M23344 and PTW M23342 chambers, as their wall thickness is only 3 mg/cm^2. However, Verhaegen [10] (see Fig. 2) has shown, using the EGSnrc [11] Monte Carlo code with a full X ray spectrum as the input to the code, that full buildup is achieved in water for the wall thickness of the PTW M23344 and PTW M23342 chambers for the highest energies for which this type of chamber would be used. The new IPEM addendum therefore recommends that no additional buildup is required. However, additional

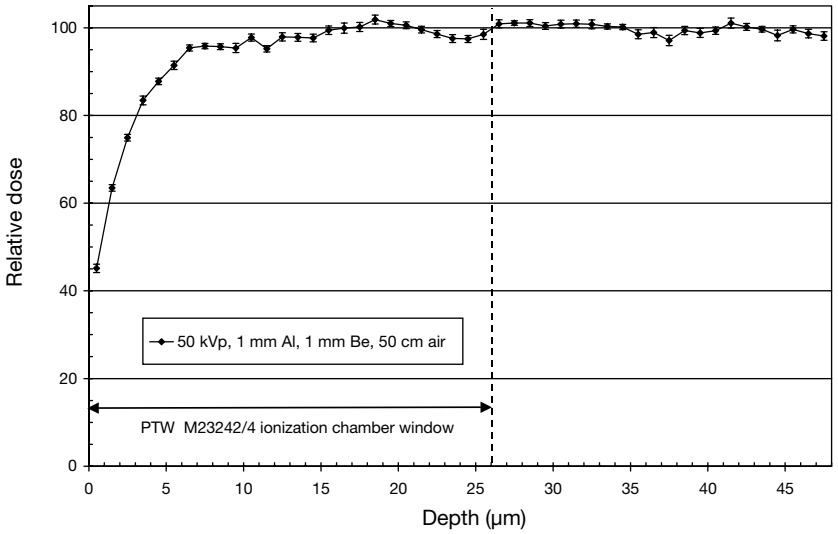

FIG. 2. Depth dose curve in the buildup region for 50 kV X rays (1 mm Al HVL) (taken from Ref. [10]).

buildup maybe required if the number of secondary electrons originating outside the chamber is significant (e.g. in the presence of electron contamination from the applicator).

3. COMPARISON OF THE IPEM CoP WITH THE IAEA, AAPM AND NCS CoPs

It is difficult to compare the CoPs for kV X ray dosimetry, as all the CoPs define the energy limits for low and medium energy differently and, in addition, only the IPEM CoP addresses the problems of very low energy dosimetry. This paper hence compares only in their regions of overlap, and no attempt is made to extrapolate data.

3.1. Low energy X ray dosimetry

Figure 3 shows a comparison of the product $B_w\ [(\bar{\mu}_{en}/\rho)_{w/air}]_{z\,=\,0,\varphi}$ derived using the IAEA [2], IPEM [1], AAPM [3] and NCS [4] CoPs. The comparison was made for a source to surface distance (SSD) of 30 cm and a field diameter of 5 cm at the chamber. All the CoPs use the same procedure to determine absorbed dose to water. It can be seen that the CoPs agree within the estimated uncertainty (±1.5% at 1σ).

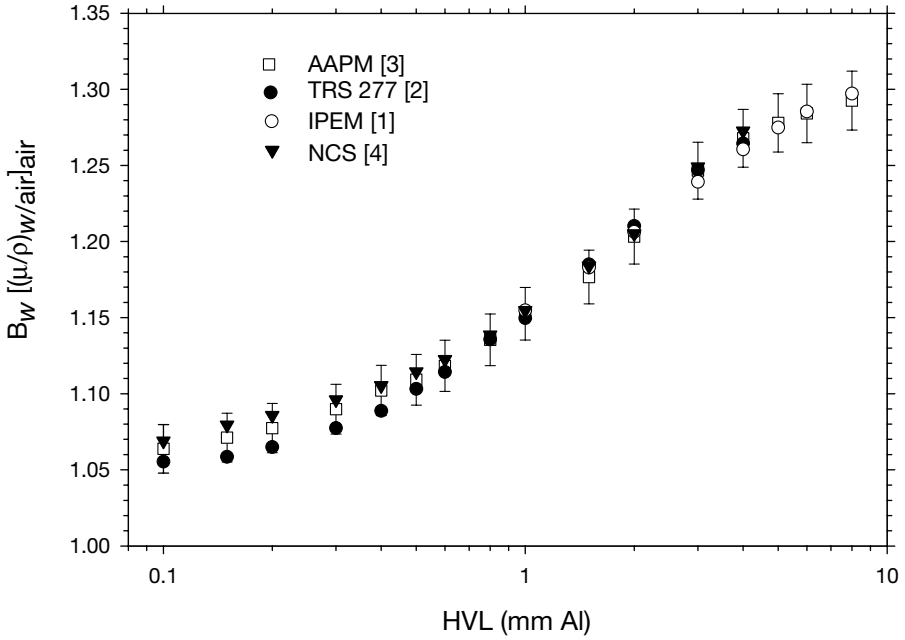

FIG. 3. Comparison of the AAPM, IAEA, IPEM and NCS CoPs for low energy X ray dosimetry, for SSD = 30 cm and a beam diameter of 5 cm at the chamber.

3.2. Medium energy X rays

This comparison is valid for an NE 2561/NE 2611 ionization chamber placed at a depth of 2 cm in water and irradiated with a 10 cm × 10 cm field. The CoPs use similar dosimetry methods to derive absorbed dose to water even though their nomenclature is different. There is a slight difference between the CoPs, however, as the AAPM and NCS CoPs account for the effect of scatter and attenuation due to the waterproof sleeve, whereas the other CoPs do not address this problem. This, however, is a small effect, with a value of 0.995 for the sheath of an NE 2561/NE 2611 chamber (polymethylmethacrylate (PMMA) sheath 1 mm thick). Figure 4 shows a comparison of the product $k_{ch}[(\bar{\mu}_{en}/\rho)_{w/air}]_{z\,=\,0,\varphi}$ (the values for the AAPM and NCS CoPs also include the effect of the waterproof sheath) derived using the IAEA, IPEM, AAPM and NCS CoPs. It can be seen that all the CoPs agree within experimental uncertainty (±3% at 1σ).

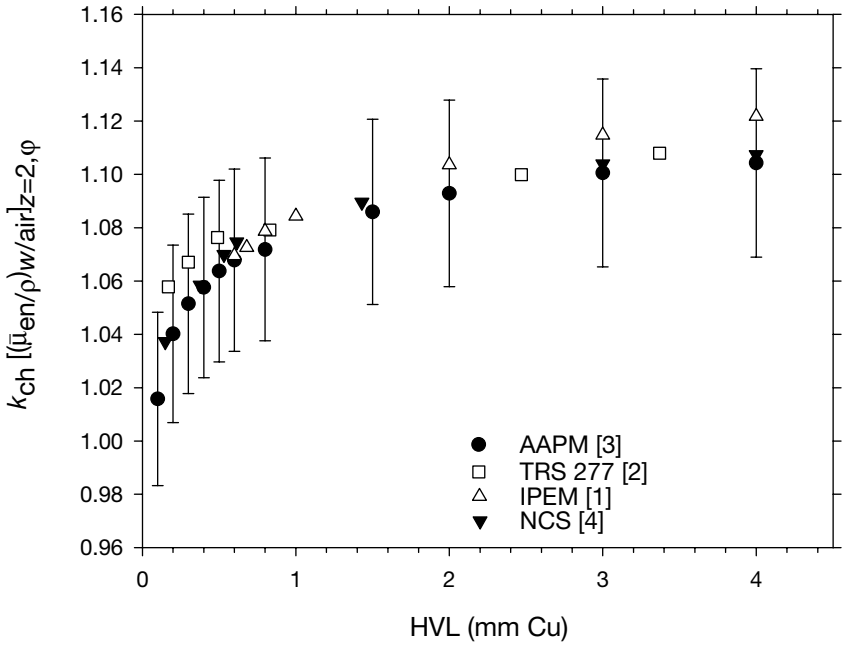

FIG. 4. Comparison of the IAEA, AAPM, IPEM and NCS CoPs for medium energy X rays for an NE 2561/NE 2611 or NE 2571 ionization chamber, for a beam diameter of 10 cm at a depth of 2 cm in water. (The AAPM and NCS CoPs include the effect of a waterproof sheath.)

4. DISCUSSION

Over the past decade there has been a lot of work on kV X ray dosimetry. In 1996 the IPEM published a CoP, and is about to publish an addendum to this CoP. The addendum will include two main changes to the 1996 CoP: firstly, new values of k_{ch} for very low energy X rays will be recommended that differ by a maximum of 7% from the 1996 CoP; secondly, for medium energy X rays the addendum gives a choice of determining absorbed dose to water at the surface of a water phantom as well as at 2 cm deep in water.

It is reassuring when comparing the IPEM, AAPM, IAEA and NCS CoPs that they agree within stated uncertainties for both low and medium energy X ray dosimetry. There is a tendency in modern CoPs to adopt dosimetry methods based on an ionization chamber calibrated directly in terms of absorbed dose to water. For kV X ray dosimetry there are technical difficulties in the realization of the quantity absorbed dose to water; to our knowledge no primary standards laboratory is offering routine calibrations directly in terms of absorbed dose to water. We suggest that rather than recommend a direct

calibration in terms of absorbed dose to water for kV X ray dosimetry, the IAEA Technical Reports Series No. 398 (TRS 398) protocol should be followed by an addendum on the determination of absorbed dose to water based on a chamber calibrated in terms of air kerma.

REFERENCES

[1] INSTITUTION OF PHYSICS AND ENGINEERING IN MEDICINE AND BIOLOGY, The IPEMB code of practice for the determination of absorbed dose to water for x-rays below 300 kV generating potential (0.035 mm Al–4 mm Cu HVL; 10–300 kV generating potential), Phys. Med. Biol. **41** (1996) 2605–2625.

[2] INTERNATIONAL ATOMIC ENERGY AGENCY, Absorbed Dose Determination in Photon and Electron Beams, 2nd edn, Technical Reports Series No. 277, IAEA, Vienna (1997).

[3] AMERICAN ASSOCIATION OF PHYSICISTS IN MEDICINE, AAPM protocol for 40–300 kV x-ray beam dosimetry in radiotherapy and radiobiology, Med. Phys. **28** (2001) 868–893.

[4] NEDERLANDSE COMMISSIE VOOR STRALINGSDOSIMETRIE, Dosimetry of Low and Medium Energy X-rays. A Code of Practice for Use in Radiotherapy and Radiobiology, Rep. 10, NCS, Delft (1997).

[5] IPE, N.E., ROSSER, K.E., MORETTI, C.J., MANNING, J.W., PALMER, M.J., Air kerma calibration factors and chamber correction values for PTW soft X-ray, NACP and Roos ionization chambers at very low X-ray energies, Phys. Med. Biol. **46** (2001) 2107–2117.

[6] GREENER, A.G., Guy's and St. Thomas' NHS Trust, London, personal communication.

[7] PERRIN, B.A., WHITEHURST, P., COOPER, P., HOUNSELL, A.R., The measurement of k_{ch} factors for application with the IPEMB very low energy dosimetry protocol, Phys. Med. Biol. **46** (2001) 1985–1995.

[8] DIEKER, J., "Calibration correction with soft X-ray measurements using a phantom", Medizinische Physik '81 (Proc. 12th Symp.), Vol. 1 (BUNDE, E., Ed.), Dr. Alfred Hüthig Verlag, Heidelberg (1982) 111–116.

[9] DEUTSCHES INSTITUT FÜR NORMUNG, Clinical Dosimetry; Applications of X-rays with Peak Voltages between 10 and 100 kV in Radiotheraphy and Soft Tissue Diagnostics, DIN 6809-4, DIN, Berlin (1988).

[10] VERHEAGEN, F., National Physical Laboratory, Teddington, UK, personal communication.

[11] KAWRAKOW, I., Accurate condensed history Monte Carlo simulation of electron transport, EGSnrc, the new EGS4 version, Med. Phys. **27** (2000) 485–498.

[12] INTERNATIONAL ATOMIC ENERGY AGENCY, Absorbed Dose Determination in External Beam Radiotherapy, Technical Reports Series No. 398, IAEA, Vienna (2000).

NORWEGIAN SYSTEM FOR IMPLEMENTING THE IAEA CODE OF PRACTICE BASED ON ABSORBED DOSE TO WATER

H. BJERKE
Norwegian Radiation Protection Authority,
Østerås, Norway
E-mail: Hans.Bjerke@nrpa.no

Abstract

In 2001 the Nordic secondary standards dosimetry laboratories (SSDLs) recommended the use of absorbed dose to water as the quantity for the calibration standard and code of practice in radiotherapy. The code of practice adopted was IAEA Technical Reports Series No. 398. The Norwegian system for implementation includes the ^{60}Co calibration of SSDL and hospital dosimeters in terms of absorbed dose to water at the Norwegian SSDL and on-site visits to every clinic teaching the new code and performing dose measurements. Comparisons of the Norwegian Radiation Protection Authority ^{60}Co absorbed dose to water calibration at the Finnish SSDL with the French primary standards dosimetry laboratory showed agreement within 0.4%. The on-site visit measuring system compared with the Finnish on-site equipment agreed within 0.6%. The on-site visits were welcomed, and demonstrated the need for external dosimetry audits to improve the local implementation of the code of practice.

1. INTRODUCTION

A Nordic meeting recommended [1] using dosimetry based on absorbed dose to water standards, calibrations and protocols for radiotherapy by 2001: IAEA Technical Reports Series No. 398 (TRS 398) [2] was chosen as the dosimetry protocol. The Norwegian secondary standards dosimetry laboratory (SSDL) at the Norwegian Radiation Protection Authority (NRPA) performed the implementation of the new dosimetry protocol, and a national dosimetry group of medical physicists from hospitals monitored the work. A secondary standard for absorbed dose to water has been calibrated since 1992 at the Bureau international des poids et mesures (BIPM) in a ^{60}Co gamma beam, and calibration in water has been available.

The system for the implementation of dosimetry based on absorbed dose to water standards, calibrations and protocols consisted of:

(a) An NRPA calibration of its own and hospital reference chambers both in air kerma and absorbed dose to water.

(b) Nationwide visits for teaching, training, cross-calibrating in electron beams and the determination of dose according to TRS 277 [3], TRS 381 [4] and TRS 398.
(c) National records being set up for all photon and electron radiotherapy beams containing the dose determined by the previous and new code of practice reported by the medical physicists at the hospitals. This will be historical evidence of the shift between the two dosimetry protocols.
(d) Visits to an SSDL in Finland (the Radiation and Nuclear Safety Authority (STUK)) and the Laboratoire national Henri Becquerel (LNHB) in France to verify the NRPA calibration, measurements and dose determinations.

The system and progress of the implementation was reviewed in an IAEA co-ordinated research project.

2. MATERIALS AND METHOD

Prior to the first visit to the hospitals, three NRPA chambers and one from each hospital were calibrated in a ^{60}Co gamma beam at the NRPA in terms of both quantities, air kerma and absorbed dose to water. The NRPA chambers were of the types NE 2571, NE 2611 and PR-06C. The hospital chambers were of types NE 2571 and Wellhöfer FC65-G (IC 70).

The water phantom for calibration meets the requirements given in TRS 398 for the calibration of ionization chambers in ^{60}Co gamma radiation in standards laboratories. The accuracy of the calibrations was tested in a EUROMET project [5]. For the type of chamber used by the NRPA, the calibration coefficients given by SSDLs traceable to the BIPM were consistent within 0.3% for both N_K and $N_{D,w}$. This shows the level of uncertainties for the NRPA calibrations. The calibration phantom was used on the first site visit to determine the absorbed dose to water based on the air kerma standard in 16 clinical photon beams (see Fig. 1). At the same time, the local medical physicist was asked to measure and determine the photon dose following the same protocol and using local equipment and calculations.

On a visit to STUK in 2001 the whole Norwegian dose determination system for photon beams was compared with the Finnish on-site equipment at the University Hospital of Helsinki (HYKS). Later, in 2002, two of the chambers (the NE 2571 and NE 2611) were sent to the LNHB for calibration in a ^{60}Co gamma beam and three photon beams [6] as a test of the uncertainty in the SSDL ^{60}Co calibration and k_Q values taken from TRS 398.

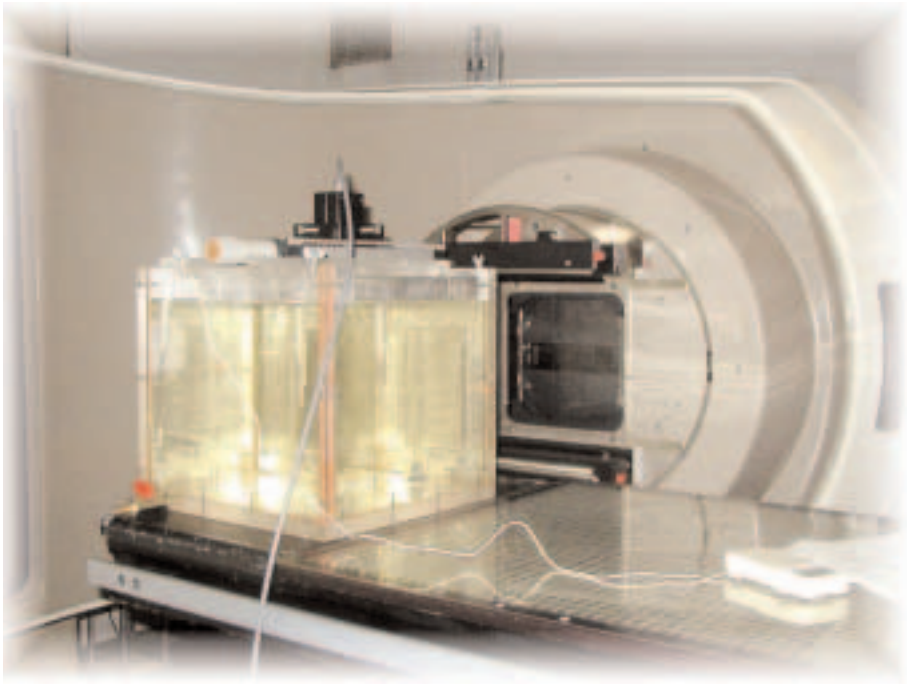

FIG. 1. Calibration phantom for dose determination in photon beams.

The NRPA used waterproof FC65-G and Roos type chambers for the electron measurements. The electron dosimetry could not be performed in the calibration phantom because of the horizontal beam and the 4 mm polymethylmethacrylate (PMMA) window; the large water tanks used for the hospitals' own beam data analysis measurements were therefore used. Setting up the tank was time consuming, and the Bjerke phantom [7] was constructed for cross-calibration and dose determination in electron beams. This phantom was used on the third trip to complete the cross-calibration of local plane-parallel chambers and electron beam dosimetry.

Co-operation with the medical physicists at the hospitals was part of the implementation of the system and was conditional for the SSDL taking on clinical work. The national dosimetry group monitored the work and met every third month.

3. RESULTS AND DISCUSSION

The dose in photon beams was first determined on the basis of TRS 277. The dose was normalized to the local dose determination. Results for all photon

beams in Norway and for the two beams used for quality control for the SSDL's site visit equipment in Finland are given in Fig. 2 (QC1 and QC2). For the 16 photon beams (B1–B16) the deviations between the hospitals' and the SSDL's absorbed dose to water determinations for TRS 277 were in the range of –1.9% to +4.4%. Most of the deviations were explained by the local implementation of TRS 277 and the use of plastic phantoms. The lack of recent calibrations of thermometers, barometers and electrometers caused minor deviations. The reasons for the deviations were found in co-operation between the hospitals and the NRPA, and correcting measures were taken by the hospitals.

Site visit equipment from the NRPA and STUK were compared at HYKS. It can be seen from Fig. 2 that dose determination of the NRPA and STUK in beams QC1 and QC2 agreed within 0.6%. The uncertainty of the NRPA photon determination is stated to be 1.0%, with a coverage factor of 1, and the result of the comparison is within the uncertainty.

The SSDL of Finland and the primary standards dosimetry laboratory (PSDL) of France determined the absorbed dose to water calibration coefficients, $N_{D,w}$, for two chambers of type NE 2571 and NE 2611. Compared with the NRPA calibration, the Finnish calibration in a ^{60}Co beam agreed within 0.3% and the French calibration within 0.4%. The LNHB calibrated the chambers for

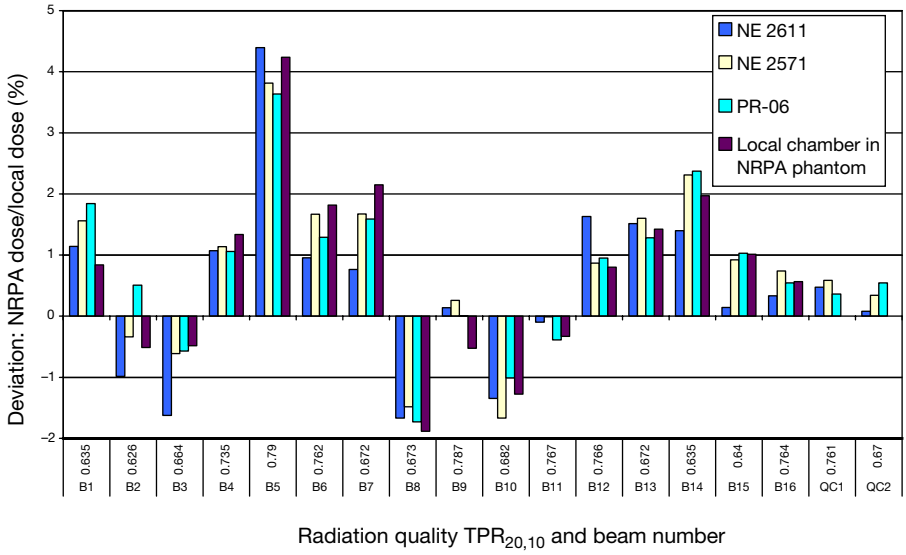

FIG. 2. Deviation (%) of the NRPA dose determination (TRS 277) from the local dose determination (TRS 277) for different photon beam qualities, $TPR_{20,10}$. The baseline is dose measured with local equipment. For QC1 and QC2, STUK dose determination is the baseline. For each B and Q, one pillar represents measurements from one chamber.

photon qualities $TPR_{20,10}$ equal to 0.675, 0.749 and 0.784 [6]. The uncertainties of the absorbed dose to water coefficients were 1.1%, with a coverage factor of 1. The k_Q values from the LNHB for the three qualities were 0.992, 0.980 and 0.970 for NE 2571 No. 3016 and 0.995, 0.982 and 0.972 for NE 2611 No. 153. The deviation in k_Q between these and the theoretical values in TRS 398 are +0.1, +0.4 and +0.4% for NE 2571 and –0.3, –0.2 and –0.2% for NE 2611.

TRS 398 recommends direct measurement of k_Q for a set of beam qualities at a PSDL for a particular chamber. This is the basis of the first and second recommendations given in the implementation chapter. The third recommendation is to use a theoretical k_Q from TRS 398. Our two chambers had k_Q for a set of beam qualities determined by the French PSDL. In Fig. 2 the introduction of k_Q from the LNHB would change the level between the first and second pillars for all B and Q by 0.4–0.6% for all TPRs (i.e. the change of k_Q would decrease the determined dose for NE 2611 and increase it for NE 2571).

By correcting for displacement of the effective point of measurement, p_{dis}, and linking the data in the photon dose worksheet for TRS 398 to the worksheet for TRS 277, it was possible to predict the historical dose shift for all 18 photon qualities (see Fig. 3). The figure shows that the dose in photon beams before 2002, based on TRS 277 and a ^{60}Co air kerma standard and chamber calibration, has been overestimated by 1–1.5% as now determined using TRS 398 and a ^{60}Co absorbed dose to water dosimetry standard and chamber calibration. The medical physicists reported a smaller dose shift. The mean shift in 32 clinical photon beams under TRS 398 reference conditions was +0.9%.

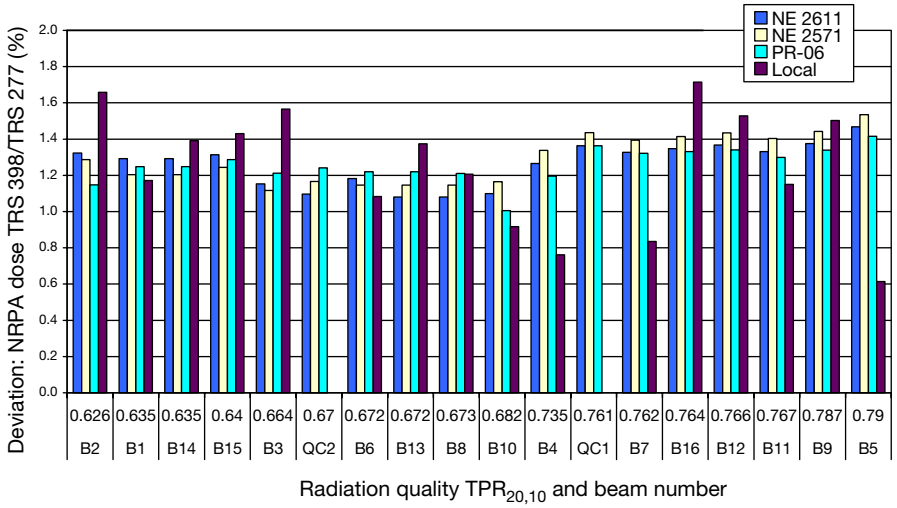

FIG. 3. Theoretical determination of relative dose in an NRPA phantom (TRS 398 dose/TRS 277 dose) given in per cent.

On the second set of visits, this time for electron beams, priority was given to the cross-calibration of the hospital plane-parallel chambers in the highest energy electron beam and measurements of absorbed dose to water in different electron beams in accordance with TRS 398. All linacs were in clinical use, and setting up the local water tanks was time consuming. Local determination of dose was therefore given low priority. This time the absorbed dose was compared with the treatment unit's monitor calibration earlier determined by the hospital.

The results from absorbed dose to water measurements for high energy electron beams are shown in Fig. 4. Compared with TRS 398 dosimetry, the nominal doses given by the linacs were on average overestimated by 0.6% and the dose deviations were –2.3% to +4.6%. The uncertainty of the electron measurements was 1.5%, with a coverage factor of 1.

Cross-calibration of the NRPA Roos chamber was performed at each site to record the stability of the calibration in the electron beams. The standard deviation for the absorbed dose to water coefficient ($N_{D,w}$) corrected to the same electron beam quality was less than 0.3%. The uncertainty in cross-calibration for the Bjerke phantom is stated as 1.5%, with a coverage factor of 1.

4. CONCLUSION

It can be seen from the NRPA dose determinations that in Norway the air kerma standard and TRS 277 have overestimated doses for high energy

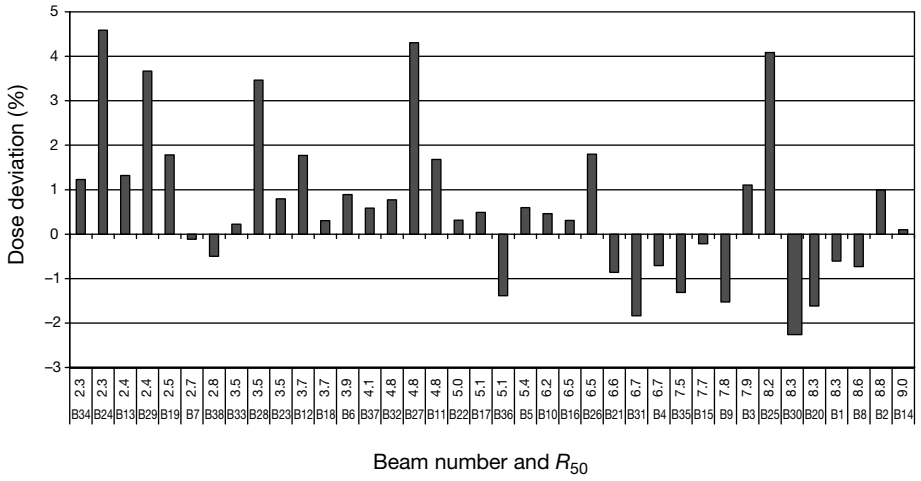

FIG. 4. Deviation (%) of the NRPA dose determination (TRS 398) and 100 monitor units given by the linac (TRS 381) for different electron beams.

photons according to TRS 398 by 1.0–1.5%, while the dose change for electron beams is smaller than the uncertainty. On-site measurements of photon beams following TRS 277 showed high deviations due to the local implementation of the code of practice. If the absorbed dose to water based dosimetry is the correct dosimetry, reports from hospitals show that the air kerma based photon dosimetry has overestimated the dose by 0.9%. No records are available for electron beams from the local medical physicists at the time of writing.

Because the $N_{D,w}$ calibration coefficients are 13% greater than the N_k coefficients, there is a potential for errors if the wrong coefficient is inadvertently used. The system described for implementing the absorbed dose to water standard and code of practice in radiotherapy has disseminated the new approach in a consistent way to all clinics and has minimized any chance of this occurring. Medical physicists in the hospitals welcomed the visits, and clinical dosimetry has been improved. The measurements showed a need for audits to control the local implementation of a code of practice in dosimetry.

The k_Q values for the clinical photon beams were theoretical and taken from TRS 398. Calibrations at the LNHB gave k_Q for two chambers. These chambers are represented in Fig. 2 in the two first pillars for each beam. The factors from different sources deviate at most by 0.4%. The uncertainties in theoretical k_Q are stated as 1.0%, and 0.7% from a PSDL, in table 15 in TRS 398.

ACKNOWLEDGEMENTS

Nordic colleagues and medical physicists at the hospitals in Norway inspired this work. I wish to give special thanks to my co-workers I. Korneliussen and E. Agathe Hult. This research was carried out in co-operation with IAEA Agreement No. 11627.

REFERENCES

[1] JÄRVINEN, H., Report of a Nordic dosimetry meeting on the implementation of the new international code of practice for radiotherapy dosimetry, TRS-398, SSDL Newsletter No. 45 (2001) 25–27.

[2] INTERNATIONAL ATOMIC ENERGY AGENCY, Absorbed Dose Determination in External Beam Radiotherapy, Technical Reports Series No. 398, IAEA, Vienna (2000).

[3] INTERNATIONAL ATOMIC ENERGY AGENCY, Absorbed Dose Determination in Photon and Electron Beams, 2nd edn, Technical Reports Series No. 277, IAEA, Vienna (1997).

[4] INTERNATIONAL ATOMIC ENERGY AGENCY, The Use of Plane Parallel Ionization Chambers in High Energy Photon and Electron Beams, Technical Reports Series No. 381, IAEA, Vienna (1997).

[5] BJERKE, H., et al., Comparison of two methods of therapy level calibration at ^{60}Co gamma beams, Phys. Med. Biol. **43** (1998) 2729–2740.

[6] DELANUAY, F., et al., First Calibration Campaign (02–26 April 2002) in High Energy X-ray Photon Beams for the Development of Techniques at SSDLs for the Dissemination of Absorbed Dose to Water Standards, CRP E2.10.04, Bureau national de métrologie, Gif-sur-Yvette (2002).

[7] BJERKE, H., HULT, E.A., "A water phantom for cross calibration and reference dose determination in high electron and photon beams", IAEA-CN-96/34P, poster presented at Int. Symp. on Standards and Codes of Practice in Medical Radiation Dosimetry, Vienna, 2002.

DOSE DETERMINATION IN ELECTRON BEAMS IN ACCORDANCE WITH TRS 398 USING DIFFERENT IONIZATION CHAMBERS

R.-P. KAPSCH, K. DERIKUM
Physikalisch-Technische Bundesanstalt,
Braunschweig, Germany
E-mail: ralf-peter.kapsch@ptb.de

Abstract

The consistency of absorbed dose measurements in high energy electron beams using ionization chambers of different types and different chambers of the same type is investigated. For two chambers each of types NE 2561, NE 2571 and PTW 23332 the differences between the dose values obtained were determined by experiment. The measurements were performed in electron beams with nominal energies of 10, 16 and 20 MeV. Dose values measured with different chambers of the same type agree to within 0.2%, while values for the absorbed dose measured with different types of chamber deviate by as much as 1.5% (depending on the beam quality).

1. INTRODUCTION

The IAEA code of practice in Technical Reports Series No. 398 (TRS 398) [1] for the determination of absorbed dose in external beam radiotherapy is based on the use of air filled ionization chambers calibrated in a reference beam radiation quality, Q_o. The beam quality correction factor, k_{Q,Q_o}, corrects for the difference between the response of an ionization chamber in the reference beam quality, Q_o, and in the actual user beam quality, Q. When the reference quality is ^{60}Co gamma radiation, this factor is denoted by k_Q. In TRS 398 [1] it is recommended to use measured values for k_Q, when available. If such experimental data are not available, calculated values for k_Q must be used (as described in appendix II of TRS 398 [1]).

The values measured for the absorbed dose should be consistent when different ionization chambers are used in the same radiation beam. This paper investigates the consistency of the determination of absorbed dose in high energy electron beams when ionization chambers of different types and different chambers of the same type are used and k_Q values calculated in accordance with appendix II of TRS 398 [1] are applied.

2. METHOD

We determined beam quality correction factors for different chambers in our electron beams relative to those for a reference chamber of type NE 2561. The reference radiation quality, Q_o, is ^{60}Co radiation.

According to TRS 398 [1], the absorbed dose to water measured with the reference chamber in an electron beam of quality Q is given by:

$$D_{w,Q}^{(\mathrm{ref})} = M_Q^{(\mathrm{ref})} N_{D,w}^{(\mathrm{ref})} k_Q^{(\mathrm{ref})} \tag{1}$$

where k_Q is the beam quality correction factor (calculated in accordance with appendix II of TRS 398 [1]) and the superscript (ref) denotes the chamber used for the measurements.

When the same dose is measured with another ionization chamber, denoted by (x), then the beam quality correction factor to be used with this chamber (in order to obtain the same dose value) can be calculated as:

$$k_Q^{(x),\mathrm{ref}} = \frac{D_{w,Q}^{(\mathrm{ref})}}{M_Q^{(x)} N_{D,w}^{(x)}} = \frac{M_Q^{(\mathrm{ref})} N_{D,w}^{(\mathrm{ref})}}{\mathrm{M}_Q^{(x)} N_{D,w}^{(x)}} k_Q^{(\mathrm{ref})} \tag{2}$$

The superscript (x),ref means that this beam quality correction factor experimentally determined for chamber (x) is based on the dose value measured with chamber (ref) using value $k_Q^{(\mathrm{ref})}$ from TRS 398 [1].

The ratio of the value $k_Q^{(x),\mathrm{ref}}$ obtained experimentally and the value $k_Q^{(x)}$ obtained from TRS 398 [1] is equal to the ratio of the absorbed dose values one would measure with chambers (ref) and (x) using the calculated k_Q values according to TRS 398 [1].

3. EXPERIMENT

The chambers used in this study were two chambers of type NE 2561 (cavity volume 0.33 cm^3, graphite walls, hollow aluminium central electrode) with serial numbers 244 (the reference chamber) and 297, two chambers of type NE 2571 (Farmer design chamber, cavity volume 0.6 cm^3, graphite walls, 1 mm aluminium central electrode) with serial numbers 977 and 2906, and two chambers of type PTW M23332 (cavity volume 0.3 cm^3, polymethylmethacrylate (PMMA) wall with graphite coating, aluminium central electrode) with serial numbers 233 and 272. Further characteristics of these chambers can be found in table 3 of TRS 398 [1]. A Roos type plane-parallel chamber FK6 No. 11 was employed for measuring the depth ionization curves.

The measurements were performed on a Philips SL-75/20 linac at nominal electron energies of 10, 16 and 20 MeV. The repetition rate of the pulsed beams was 25 Hz (for 16 MeV and 20 MeV) or 50 Hz (for 10 MeV), giving a dose rate of 0.5 Gy/min for all beams. The radiation beam was horizontally incident on a water phantom with an entrance window of PMMA 3.15 mm thick. The source to surface distance was 1 m for all measurements, and the field size at the phantom surface was 15 cm × 15 cm, except for the measurement of the depth dose curves, for which it was 20 cm × 20 cm.

A variable, stabilized high voltage supply provided the polarizing voltage. The ionization current was measured with a Keithley 616 electrometer, the output voltage of which was converted into a frequency of pulses, which were counted for a specified time. The number of counts represents the collected charge.

The cylindrical chambers were positioned with the reference point (centre of the cavity volume) at a depth $z_{ref} + 0.5r_{cyl}$, where z_{ref} is the reference depth, in accordance with TRS 398 [1], and r_{cyl} is the cavity radius of the chamber. All readings were normalized to the average reading of two external monitor chambers (Wellhöfer IC 10) positioned inside the water phantom at the same depth as the chamber, but displaced laterally by a distance of 3 cm from the chamber centre. In spite of a variation greater than 2% in the dose rate of the linac during a period of more than 6 h, the reading of chamber NE 2561 No. 244, normalized to the monitor reading, was stable to within 0.03% (standard deviation). Similar results hold for the other chambers used in this study.

The chamber readings were corrected for polarity and incomplete saturation. The correction factor for polarity, k_{pol}, was determined in accordance with equation (12) in TRS 398 [1] from the readings M_+ and M_- obtained at positive and negative polarity of the chamber voltage, respectively. The correction factor for incomplete saturation, k_S, was calculated using the formula developed by Derikum and Roos [2]. For some of the chambers applied in this study and some beam qualities, the validity of this formula was checked by measuring saturation curves (dependence of the inverse reading, $1/M$, on the inverse polarizing voltage, $1/V$), and fitting a straight line to the linear part of this curve. The correction factor, k_S, obtained from this linear fit differs from the calculated value by less than 0.05%.

The ionization chambers employed in this study were calibrated in terms of absorbed dose to water in the ^{60}Co reference field of the Physikalisch-Technische Bundesanstalt (PTB), traceable to the primary standard of absorbed dose to water of the PTB. The repeatability of the calibration factors in successive calibrations is better than 0.05% (standard deviation) for all chambers.

4. RESULTS

4.1. Electron beam qualities

The beam quality is specified by the half-value depth, R_{50}, at which the absorbed dose is 50% of its value at the absorbed dose maximum. It is derived from the half-value of the depth ionization distribution in water, $R_{50,\mathrm{ion}}$, using equation (23) of TRS 398 [1].

For all electron beams, central axis depth ionization curves were measured in the water phantom using a Roos type plane-parallel chamber (FK6 No. 11). The readings of this chamber were corrected for ion recombination and polarity at all depths. The correction factors were derived from a set of representative measurements near the surface, the ionization maximum and the depths corresponding to 90% and 50% of the ionization maximum (as recommended in TRS 398 [1]).

In every electron beam ten depth ionization curves were measured in the backward and forward directions, and $R_{50,\mathrm{ion}}$ was calculated by linear interpolation. The relative standard deviation of the values obtained for $R_{50,\mathrm{ion}}$ was smaller than 0.16% for all beams. The beam qualities are shown in Table I. The reference depth, z_{ref}, for the determination of the absorbed dose to water (also shown in Table I) was calculated using equation (24) of TRS 398 [1]. At this depth the relative dose gradient is less than 0.5%/mm for all beams. Since the uncertainty of positioning the chamber is below 0.1 mm, the dose deviates by less than 0.05% from its value at the reference depth.

After determining the beam qualities, the beam quality correction factors, $k_Q^{(x)}$, were calculated in accordance with appendix II of TRS 398 [1]. The values obtained for $k_Q^{(x)}$ are shown in Table II, together with the values of the various perturbation factors used for the calculation.

TABLE I. SUMMARY OF BEAM QUALITIES AND REFERENCE DEPTHS FOR THE ELECTRON BEAMS INVESTIGATED IN THIS STUDY

Designation of beam	10 MeV	16 MeV	20 MeV
$R_{50,\mathrm{ion}}$ (cm)	4.10	6.45	7.96
R_{50} (cm)	4.16	6.58	8.13
z_{ref} (cm)	2.40	3.85	4.78

TABLE II. SUMMARY OF BEAM QUALITY CORRECTION FACTORS AND VALUES USED FOR THEIR CALCULATION
(according to appendix II of TRS 398 [1])

	^{60}Co	10 MeV	16 MeV	20 MeV
$s_{w,\mathrm{air}}$	1.133	1.0513	1.0305	1.0202
		p_{cav}		
NE 2561	1.0	0.9575	0.9707	0.9769
NE 2571	1.0	0.9633	0.9746	0.9800
M23332	1.0	0.9713	0.9802	0.9844
		p_{dis}		
NE 2561	0.9852	1.0	1.0	1.0
NE 2571	0.9872	1.0	1.0	1.0
M23332	0.9900	1.0	1.0	1.0
		p_{wall}		
NE 2561	0.9902	1.0	1.0	1.0
NE 2571	0.9922	1.0	1.0	1.0
M23332	1.0016	1.0	1.0	1.0
		p_{cel}		
NE 2561	1.0	1.0	1.0	1.0
NE 2571	0.993	0.998	0.998	0.998
M23332	0.993	0.998	0.998	0.998
		$k_Q^{(x)}$		
$k_Q^{(\mathrm{NE\ 2561})}$	—	0.9107	0.9050	0.9016
$k_Q^{(\mathrm{NE\ 2571})}$	—	0.9171	0.9095	0.9054
$k_Q^{(\mathrm{M23332})}$	—	0.9135	0.9036	0.8984

4.2. Experimental beam quality correction factors

According to Eq. (2), the ratio of the chamber readings of the reference chamber (ref) to that of the chamber under test (x) is needed to calculate the experimental beam quality correction factor. In order to verify that the output of the linac was sufficiently stable during the measurements, the reading of the reference chamber (ref) was measured before and after measuring the reading of the chamber under test (x). In all cases, the relative deviation between the two readings of the reference chamber was smaller than 0.05%.

The readings were each obtained as the average of at least ten successive measurements. They were corrected for temperature, pressure, polarity and

recombination, and experimental beam quality correction factors were calculated in accordance with Eq. (2). The results are given in Table III.

Assuming a relative standard uncertainty for the repeatability of the calibration factors of 0.05% (cf. Section 3) and for the chamber readings of 0.1% (including the uncertainty of correction for polarity and recombination), the relative standard uncertainty of the experimentally determined beam quality correction factors is 0.16% (assuming no uncertainty for the theoretical beam quality correction factor of the reference chamber).

5. DISCUSSION

The relative difference between the measured beam quality correction factors of different chambers of the same type is 0.2% at most. This value agrees with the measurement uncertainty of our experimental beam quality correction factors, which is about 0.16% (standard deviation).

The $k_Q^{(x),\mathrm{ref}}$ values measured in relation to chamber NE 2561 No. 244 differ by not more than 0.81% from the values calculated following the approach of appendix II of TRS 398 [1]. However, the relative differences of the values for chambers of type NE 2571 in relation to the values for M23332 chambers are about 1.5% in the 10 MeV beam and about 1% in the 16 MeV and 20 MeV beams. Hence, when applying the beam quality correction factors calculated in

TABLE III. EXPERIMENTAL BEAM QUALITY CORRECTION FACTORS AND RELATIVE DIFFERENCES BETWEEN THEORETICAL (cf. TABLE II) AND EXPERIMENTAL BEAM QUALITY FACTORS

Chamber	$k_Q^{(x),\mathrm{ref}}$			$\frac{k_Q^{(x),\mathrm{ref}} - k_Q^{(x)}}{k_Q^{(x)}} \times 100\%$		
	10 MeV	16 MeV	20 MeV	10 MeV	16 MeV	20 MeV
NE 2561 No. 297	0.9099	0.9036	0.9010	–0.088%	–0.154%	–0.066%
NE 2571 No. 977	0.9106	0.9057	0.9007	–0.709%	–0.418%	–0.519%
NE 2571 No. 2906	0.9114	0.9055	0.9004	–0.622%	–0.440%	–0.552%
M23332 No. 233	0.9209	0.9078	0.9022	0.810%	0.465%	0.423%
M23332 No. 272	0.9208	0.9098	0.9030	0.799%	0.686%	0.512%

accordance with appendix II of TRS 398 [1], the results of dose measurements for the same dose value differ by this amount if these types of chamber are used.

This relative difference is compatible with the relative standard uncertainty of 1.2% stated in TRS 398 [1] for the calculated beam quality correction factors. The measurements show that the beam quality correction factors calculated in accordance with appendix II of TRS 398 [1] do not allow comparisons of dose measurements to agree by better than 1%, even though the ratio of k_Q values can be measured with a relative uncertainty of about 0.2%. If the results of dose measurements obtained with chambers of different types are to differ by not more than 0.2%, the ratio of the corresponding k_Q values must be as given in Table III. This ratio is independent of the absorbed dose standard (e.g. the reference chamber NE 2561 No. 244 or any other primary or secondary standard).

REFERENCES

[1] INTERNATIONAL ATOMIC ENERGY AGENCY, Absorbed Dose Determination in External Beam Radiotherapy, Technical Reports Series No. 398, IAEA, Vienna (2000).

[2] DERIKUM, K., ROOS, M., Measurement of saturation correction factors of thimble-type ionization chambers in pulsed photon beams, Phys. Med. Biol. **38** (1993) 755–763.

BLANK

DOSIMETRY PROTOCOLS AND COMPARISONS — II

(Session 6)

Chair

S.M. VATNITSKY
IAEA

Co-Chair

M. SAIFUL HUQ
United States of America

Rapporteur

K.E. ROSSER
United Kingdom

BLANK

INTERCOMPARISON OF ABSORBED DOSE TO WATER AND AIR KERMA BASED DOSIMETRY PROTOCOLS FOR PHOTON AND ELECTRON BEAMS

M. SAIFUL HUQ
Department of Radiation Oncology,
Kimmel Cancer Center of Jefferson Medical College,
Thomas Jefferson University,
Philadelphia, Pennsylvania, United States of America
E-mail: saiful.huq@mail.tju.edu

P. ANDREO
Medical Radiation Physics,
University of Stockholm–Karolinska Institute,
Stockholm, Sweden

Abstract

In recent years the IAEA and the American Association of Physicists in Medicine (AAPM) have published external beam dosimetry protocols that are based on the use of an ionization chamber calibrated in terms of absorbed dose to water, $N_{D,w}$, in a standards laboratory's reference quality beam. Since the publication of these protocols many comparisons, theoretical as well as experimental, between $N_{D,w}$ based and between $N_{D,w}$ and the former N_K based protocols, have been published. The comparisons of the basic data included in the various IAEA and AAPM protocols show differences within about 1%, except for the case of plane-parallel chambers with an $N_{D,w}$ calibration, which in electron beams reaches up to a 2% difference. Differences sometimes larger than these upper values have, however, been reported in some of the published experimental studies. The paper provides a comprehensive review of the intercomparisons of the different protocols by various authors and discusses the reasons for the discrepancies between them.

1. INTRODUCTION

The major emphasis in primary standards laboratories around the world has shifted recently from standards for air kerma or exposure to those for absorbed dose to water. Following the development of standards of absorbed dose to water and national dosimetry protocols, pioneered by the United Kingdom and Germany more than ten years ago, new dosimetry protocols

based on the use of an ionization chamber calibrated in terms of absorbed dose to water in a ^{60}Co gamma ray beam, $N_{D,w}$, together with theoretical beam quality correction factors, k_Q, have been published in the Russian Federation [1] and in North America [2]. The IAEA has also published a new code of practice [3] that extends the $N_{D,w}$ formalism to all radiation beam types (excluding neutrons) and includes dosimetry recommendations and standardized procedures for low and medium energy X rays, ^{60}Co gamma rays, high energy photons, electrons, protons and heavy ions. It also includes all the various ionization chamber calibration possibilities available in different national standards laboratories, from kilovoltage X rays and ^{60}Co to direct calibrations in high energy photon and electron beams.

Since the publication of these protocols several studies have been devoted to theoretical and experimental comparisons between $N_{D,w}$ based protocols or between $N_{D,w}$ and the former N_K based protocols. The goal of this paper is to provide an overview of these comparisons and provide an insight into the origin of the similarities and differences that exist between $N_{D,w}$ based protocols and between $N_{D,w}$ and N_K based protocols. The formalism for the $N_{D,w}$ and N_K based protocols has been discussed in detail in the comparisons published and consequently will not be repeated here. Readers are invited to consult the original references for details.

2. SUMMARY OF THE COMPARISONS

Summaries of the various studies performing comparisons between these protocols are given in Tables I and II for high energy photons and electrons, respectively. These include, among other parameters, the types of study undertaken and the range of agreement in the determination of absorbed dose between the various protocols. A discussion of some of these studies is given in Section 3.

3. COMPARISON BETWEEN PROTOCOLS

3.1. Comparison between $N_{D,w}$ based protocols

For clinical photon beams, comparison of absorbed doses between the American Association of Physicists in Medicine (AAPM) TG 51 [2] and the IAEA Technical Reports Series No. 398 (TRS 398) [3] protocols is equivalent to comparing the values of k_Q given in the two protocols, since the contribution from corrections for influence quantities is negligible. Results from the

TABLE I. SUMMARY OF THEORETICAL OR EXPERIMENTAL PUBLISHED STUDIES PERFORMING A COMPARISON BETWEEN $N_{D,w}$ BASED PROTOCOLS AND $N_{D,w}$ AND N_K BASED PROTOCOLS FOR PHOTON BEAMS

Protocols compared	Beam quality	Chamber type	Ratio (%) of k_Q or $(s_{w,\text{air}})_Q p_Q$	Ratio (%) of D_w	T or E[a]	Ref.
TG 51/ TRS 398	0.500–0.850	NE 2571, PTW 30001	Within ±0.2, maximum difference of 0.3	—	T	[4, 5]
TG 51/ TRS 398	0.680–0.799	NE 2571, PTW 30001	0 to –0.2	0 to –0.3	E	[4]
TG 51/ TRS 398	0.672–0.776	NE 2571, PTW 30004, Wellhöfer FC65-G	Within 0.3	—	E	[6]
TG 51/ TG 21	^{60}Co, 6 MV, 18 MV	NE 2571, PTW 23333, Capintec PR-06C, Exradin A12	—	0.2 to 1.5	E	[14]
TG 51/ TG 21	0.571–0.771	NE 2571, Capintec PR-06C	—	0.8 to 2.2	E	[15]
TG 51/ TG 21	0.572–0.781	Eleven types (see Ref. [16])	—	Within ±0.6	T	[16]
TG 51/ TG 21	0.683–0.798	NE 2571, PTW 30001	0 to –0.5	0.7 to 1.3	E, T	[17]
TRS 398/ TRS 277	0.672–0.776	NE 2571, PTW 30004, Wellhöfer FC65-G	—	0.2 to 0.6	E	[6]
TG 51/JARP, TG 51/ TRS 277, TG 51/ TRS 398	0.578–0.779	NE 2571, PTW 23333, Capintec PR-06C, Exradin A12	—	0.6 to 2.1, 0.7 to 1.7, within 0.4	T	[19]
TRS 398/ TRS 277	0.620–0.830	NE 2571, NE 2581, PTW 23332, PTW 31003, PTW 30001	Within ±0.2	—	T	[5]

[a] T: theoretical; E: experimental.

Note: The quality of the beams is specified in terms of $TPR_{20,10}$ or MV, as given by the respective authors.

TABLE II. SUMMARY OF THEORETICAL OR EXPERIMENTAL PUBLISHED STUDIES PERFORMING A COMPARISON BETWEEN $N_{D,w}$ BASED PROTOCOLS AND $N_{D,w}$ AND N_K BASED PROTOCOLS FOR ELECTRON BEAMS

Protocols compared	Beam quality range	Chamber type	Ratio (%) of k_Q or $(s_{w,\text{air}})_Q p_Q$	Ratio (%) of D_w	T or E[a]	Ref.
TG 51/ TRS 398	2.4–6.7 cm	NE 2571, PTW 30001, Scanditronix NACP, PTW Markus, Wellhöfer PPC40	Cylindrical chamber, up to 0.4, plane-parallel chamber, up to 2	—	T	[4, 5]
TG 51/ TRS 398	2.4–6.7 cm	NE 2571, PTW 30001, Scanditronix NACP, PTW Markus, Wellhöfer Roos	—	–0.6 to 1.8 ($N_{D,w}$), –0.3 to –0.7 (cross-calibration)	E	[4]
TG 51/ TG 21	9 and 16 MeV	NE 2571, PTW 23333, Capintec PR-06C, Exradin A12	—	1.4 to 2.1	E	[14]
TG 51/ TG 21	2.41–8.02 cm	NACP, Markus, Capintec PR-06C	—	2.4 to 4.9 ($N_{D,w}$), 0.9 to 3.3 (cross-calibration)	E, T	[15]
TG 51/ TG 21	4–20 MeV	Eleven cylindrical and five plane-parallel types (see Ref. [16])	—	—	E	[16]
DIN 6800/ TG 51	1.424–7.457 cm	PTW 30006, PTW Roos, PTW Markus	—	0 to –0.7	E	[7]
TG 51/ TG 21	2.41–6.69 cm	NE 2571, PTW 30001, PTW Markus, NACP Scanditronix, Wellhöfer PPC40, Wellhöfer PPC05	—	0.7 to 2.9 ($N_{D,w}$), 0.8 to 3.2 (cross-calibration)	E	[4]
TG 51/ JARP, TG 51/ TRS 277, TG 51/ TRS 398	3.47–7.88 cm	NE 2571, PTW 23333, Capintec PR-06C, Exradin A12	—	1.5 to 3.8, 0.2 to 1.9, within 0.6	E	[19]

TABLE II. (cont.)

Protocols compared	Beam quality range	Chamber type	Ratio (%) of k_Q or $(s_{w,\mathrm{air}})_Q p_Q$	Ratio (%) of D_w	T or E[a]	Ref.
TRS 398/ TRS 381	2.27–8.13 cm	NACP, PTB Roos, PTW Roos, PTW Markus, Wellhöfer Roos	—	0.9 (cross-calibration), 1.5 ($N_{D,w}$)	E	[20]
TRS 398/ TRS 277	2.27–8.13 cm	NACP, PTB Roos, PTW Roos, PTW Markus, Wellhöfer Roos	—	–0.8 to 1.5 (cross-calibration), 1 to 2 ($N_{D,w}$)	E	[20]
TRS 398/ TRS 381, TRS 398/ TRS 277	About 1–20 cm	NE 2571, PTW 23332, NACP, Markus, Roos	Within ±0.3, 0.5 to 3	—	T	[5]

[a] T: theoretical; E: experimental.
Note: The quality of the beams is specified in terms of R_{50} or nominal energy (MeV), as given by the respective authors.

theoretical comparisons in Refs [4, 5] are shown in Fig. 1 for a PTW 30001 and an NE 2571 chamber. Analyses of the contributions to the observed differences in k_Q show that the water to air stopping power ratios are within ±0.2% for most clinical photon beam qualities (and reach a maximum of 0.45% at around $\mathrm{TPR}_{20,10} = 0.8$, to decrease again). The contribution of the perturbation correction factors is of up to 0.5%. Differences in the beam quality specification between the two protocols[1] contribute a maximum difference of 0.3% in the determination of k_Q (Fig. 1). Experimental comparison between the two protocols shows a maximum difference of 0.3% and 0.2% in the determination of D_w and k_Q, respectively [4]. Similar results have been reported in Ref. [6].

For the denominator of k_Q, at the reference quality of ^{60}Co, the perturbation correction factor, p_{dis}, contributes a difference of about 0.4% for the two chambers and p_{wall} contributes up to 0.3% for the PTW chamber [4].

For cylindrical chambers in electron beams Fig. 2 shows calculated ratios TG 51/TRS 398 of k_Q, as a function of the beam quality, R_{50} [4, 5]. The almost constant differences are explained in terms of the similar values of the quantities in the numerator of k_Q, as the water to air stopping power ratios are identical and

[1] The photon beam quality in TRS 398 is specified by the tissue phantom ratio, $\mathrm{TPR}_{20,10}$, whereas in TG 51 it is specified by the per cent depth dose at 10 cm depth excluding electron contamination, $\%\mathrm{dd}(10)_x$.

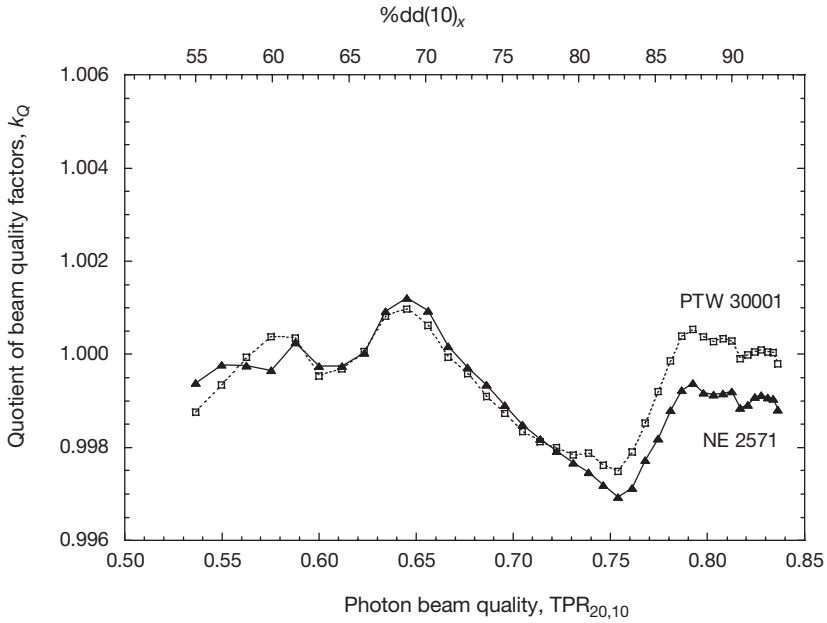

FIG. 1. Quotient TG 51/TRS 398 of the beam quality correction factors, k_Q, for high energy photon beams as a function of the beam quality parameters $TPR_{20,10}$ and $\%dd(10)_x$, for the Farmer type ionization chambers NE 2571 (triangles) and PTW 30001 (squares). (The correspondence between the beam quality parameters is approximate.) Reproduced with permission [4].

the fluence correction perturbation factors are taken from the same experimental data set. However, the different recasting of these perturbation factors as a function of R_{50} in the two protocols yields substantially different values at low electron energies, in a region where the correction reaches its maximum value. This can be seen in the upper curve of Fig. 2, where the filled triangles show quotients of the electron fluence perturbation data. Part of the difference in k_Q is due to the mentioned different values of the quantities at ^{60}Co in the denominator of k_Q.

For plane-parallel chambers in electron beams calculated values of the ratios TG 51/TRS 398 of k_Q, as a function of the electron beam quality, R_{50}, for the Markus, NACP and Roos chambers, are shown in Fig. 3. The dashed line is the quotient that would correspond to the k_Q factors for a Markus chamber calculated with the same electron fluence perturbation correction factor in the two protocols, instead of using the data for each protocol, which are shown as the open triangles labelled "p_{cav} Markus". For the Roos and NACP chambers the nearly constant difference in k_Q is due to the use of the same electron fluence perturbation correction factor (unity) in both protocols, whereas k_Q

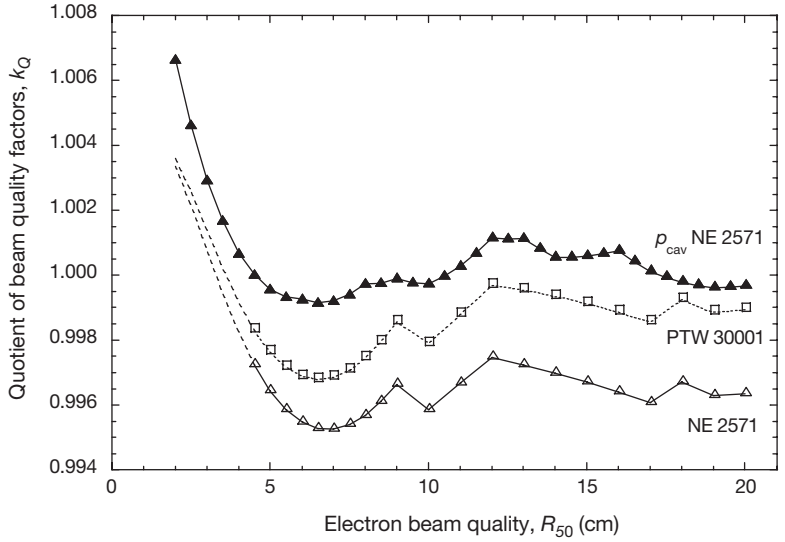

FIG. 2. Quotient TG 51/TRS 398 of k_Q as a function of the electron beam quality R_{50} for the cylindrical (Farmer type) ionization chambers NE 2571 (open triangles) and PTW 30001 (squares). The filled triangles show quotients of the electron fluence perturbation data, approximately the same for the two chambers. Reproduced with permission [4].

differs by up to 0.7% for the two protocols. This gap in k_Q is almost entirely due to the nearly 1% difference in the p_{wall} values for ^{60}Co of the plane-parallel chambers that enter in the denominator of k_Q. For the Markus chamber the difference in p_{cav} compounds this effect, yielding a maximum difference of almost 2% at the lowest energies.

For electron beams, experimental comparisons of absorbed doses to water, D_w, using the TG 51 and TRS 398 protocols, have been made in Ref. [4]. For beam energies between 6 MeV and 18 MeV it was found that the D_w ratio lies between –0.6% and 1.8% when cylindrical and plane-parallel chambers with a direct calibration factor $N_{D,w}$ (in ^{60}Co) were used for measurements. For cross-calibrated plane-parallel chambers the D_w ratios were within 0.4% of each other. The differences in the absorbed dose obtained from the two protocols essentially follow the differences observed between the k_Q values. Reference [7] has reported results of experimental measurements of D_w ratios between the Deutsches Institut für Normung (DIN) [8] and TG 51 in the energy range of 6 MeV to 18 MeV. It was found that the dose difference between the two protocols lies between 0% and –0.7%. This difference was attributed to the use of different water to air stopping power ratios, monoenergetic in DIN 6800-2 and realistic in TG 51, and the correction for the central aluminium central electrode, p_{cel}.

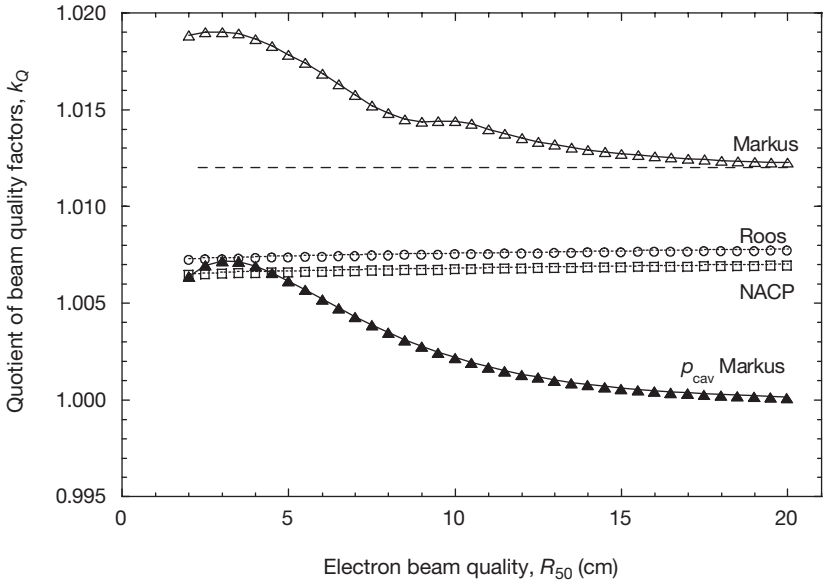

FIG. 3. Quotient TG 51/TRS 398 of k_Q, as a function of R_{50}, for the plane-parallel ionization chambers Markus (triangles), NACP (squares) and Roos (circles). The dashed line would correspond to the k_Q factors of a Markus chamber calculated with the same electron fluence perturbation correction factor in the two protocols, instead of calculating with the protocols data, whose ratios are shown as filled triangles, p_{cav} Markus. Reproduced with permission [4].

3.2. Comparison between $N_{D,w}$ and N_K based protocols

Since the publication of TG 51 and TRS 398 numerous studies comparing these protocols with the air kerma based protocols of TG 21 [9], TRS 277 [10], TRS 381 [11], the Nederlandse Commissie voor Stralingsdosimetrie (NCS) [12] and the Japanese Association of Radiological Physics (JARP) [13] have been published. This section gives a summary of these studies.

References [14–18] show that TG 51 increases D_w by approximately 1% for photon beams and 1–3% for electron beams in comparison with TG 21 when calibration factors are traceable to the United States National Institute of Standards and Technology. References [17, 18] identified that the differences in basic data between TG 21 and TG 51 are about 0.5% for photon beams and about 1% for electron beams. The major factors that contribute to the observed differences between the two protocols are the (a) water to air stopping power ratios, (b) central electrode correction factor, (c) wall correction factor at ^{60}Co, (d) change of standards from N_X to $N_{D,w}$ and (e) differences in measured values of $N_{D,w,Q_{\text{cross}}}$, obtained from the cross-calibration of plane-parallel chambers.

Reference [19] gives calculated ratios of D_w between the Japanese protocol JARP [13], TRS 277 [10], TRS 398 [3] and TG 51 [2] for various Farmer type chambers in photon and electron beams. For photon beams it was found that the TG 51 results were higher by 0.6–2.1% and 0.7–1.7% than those for JARP and TRS 277, respectively, and agreed with TRS 398 to within 0.4%. For electron beams the TG 51 values were slightly higher; that is, 1.5–3.8% and 0.2–1.9% in comparison with JARP and TRS 277, respectively, and agreed with TRS 398 to within 0.6%. The reasons for these discrepancies were analysed by comparing N_{gas} or N_D and a dose conversion factor, F_w.

Reference [6] performed an experimental comparison of TRS 398 [3], TG 51 [2], TRS 277 [10], TG 21 [9] and NCS Report 2 [12] in 6 MV, 15 MV and 18 MV photon beams. It was found that the results obtained with both absorbed dose to water based formalisms resulted in consistent values within 0.3%. Another observation was that there were differences of up to 0.6% between the $N_{D,w}$ based and N_K based formalisms.

Reference [5] analysed the differences in basic data in TRS 398 [3] and former international protocols for photon and electron beams. Except for the factors entering into the determination of the $N_{D,\text{air}}$ chamber factor in TRS 277 [10], the differences in the data between TRS 277 and TRS 398 can be reduced to those of $(s_{w,\text{air}})_Q p_Q$ for high energy photons in the two protocols, as the values for ^{60}Co agree within better than 0.1% for all cylindrical chambers. Ratios of the product $(s_{w,\text{air}})_Q p_Q$ are shown in Fig. 4 for some of the most common cylindrical chambers, as a function of the photon beam quality, $\text{TPR}_{20,10}$. This comparison is based on the data given in the second edition of TRS 277 [10]. It can be seen that for the most common range of clinical qualities the differences are within approximately ±0.2%. Thus for the clinical user a switch from TRS 277 to TRS 398 involves very small changes due to the codes themselves; these will be dominated by the change of primary standard from K_{air} to D_w.

Figure 5 shows the experimental comparison of dose ratios TRS 398/TRS 277 in high energy photon beams for the cylindrical ionization chambers NE 2571 (circles), PTW 30010 (triangles) and PTW 30001 [20]. The upper part of the figure (filled symbols) corresponds to dose determinations based on $N_{D,w}$ calibrations in ^{60}Co. It can be seen that for the most commonly used clinical beam qualities the dose ratios are practically constant and around 1.010; this means that results obtained using TRS 398 will be about 1% larger than those obtained with TRS 277. For the highest energies, in the case of a scanned 50 MV beam the difference is slightly larger. These results correspond to the use of the second edition of TRS 277. The lower part of Fig. 5 (open symbols) corresponds to dose determinations with TRS 398 based on $N_{D,w}$ values calculated from N_K. The differences in this case are almost negligible, with a maximum discrepancy

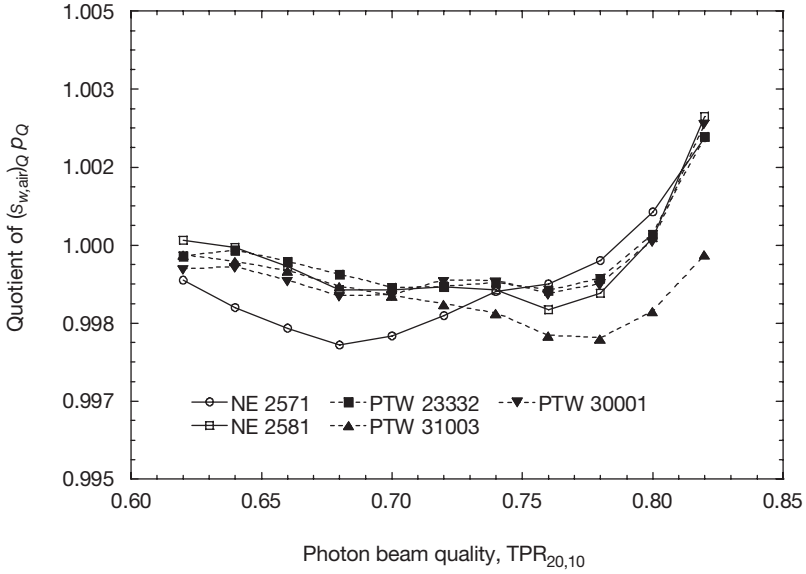

FIG. 4. Quotients TRS 398/TRS 277 of the product $(s_{w,air})_Q p_Q$ for some common NE and PTW cylindrical ionization chambers, as a function of the photon beam quality, $TPR_{20,10}$. The data for TRS 277 are those taken from the second edition of the protocol. Reproduced with permission [5].

of 0.5% for the scanned beam, showing that the differences discussed above are practically due to the new type of standards used for the calibration, and not to the new protocol itself.

Quotients TRS 398/TRS 381 of the product $(s_{w,\mathrm{air}})_Q p_Q$ for electron beams at the relevant reference depths are given in Fig. 6 for cylindrical and plane-parallel ionization chambers as a function of the electron beam quality, R_{50} [5]. The differences are small in all cases, including for Markus chambers, and they are within about ±0.3% in the most commonly used energy range. Ratios are shown by dashed lines for cylindrical chambers below 10 MeV, and differences do not exceed 0.5% in that region. As all perturbation factors for plane-parallel chambers are identical, the curves for the NACP Roos and for the Markus chambers coincide with the quotients of stopping power ratios. Figure 6 also shows the results for cross-calibrated plane-parallel chambers, where it can be seen that the ratio of perturbation factors at the cross-calibration energy, Q_{cross}, shifts the NACP Roos curve upwards by about 0.2%, whereas the Markus curve is shifted downwards by approximately 0.1%. In all cases, for the clinical user a switch from TRS 381 to TRS 398 involves very small changes, which will be dominated by the change from the K_{air} to D_w primary standards.

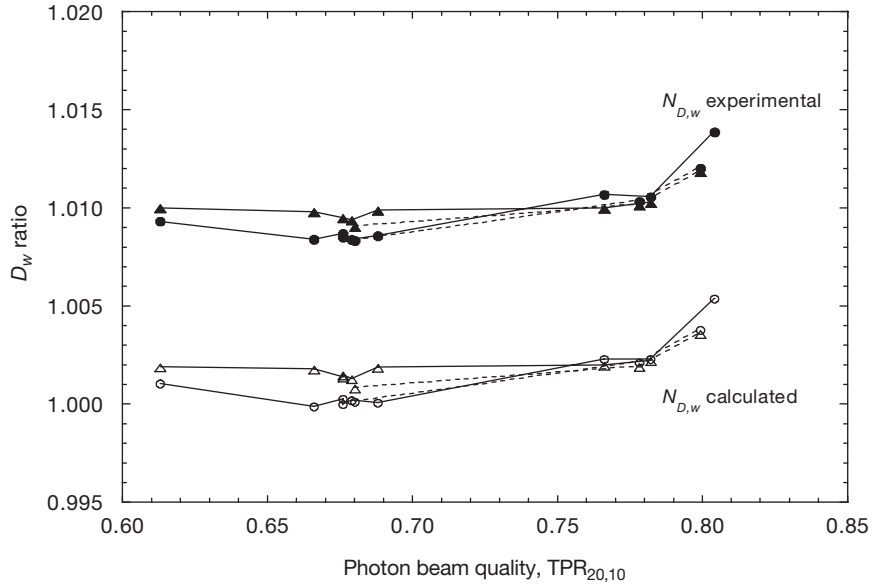

FIG. 5. Experimental comparison of dose ratios TRS 398/TRS 277(2nd edition) in photon beams at the reference depth of 10 cm for cylindrical ionization chambers of the Farmer type NE 2571 (circles) and PTW 30010/30001 (triangles). The upper symbols in each data set correspond to a scanned 50 MV beam. Filled symbols represent dose determinations based on $N_{D,w}$ calibrations in ^{60}Co; open symbols are based on $N_{D,w}$ values calculated from N_K. The average ratios $N_{D,w}/N_{D,w}^{calc}$ are 1.009 and 1.008 for the NE 2571 and PTW 30010, respectively; $N_{D,w}/N_K$ are 1.099 and 1.095. Reproduced with permission [20].

Figure 7 shows the experimental comparison of dose ratios TRS 398/TRS 381 at z_{max} in electron beams for cross-calibrated plane-parallel ionization chambers of the type NACP, PTB Roos, PTW Roos, Wellhöfer Roos and PTW Markus [20]. The almost constancy of the dose ratios shows how close the basic data in the two protocols are. The differences in absorbed dose in the two protocols are of the order of 0.9%, similar to those for photon beams. The similarity of the results obtained with different plane-parallel chambers shows that the cross-calibration procedure yields consistent dose determinations for all chambers, and that chamber to chamber variations of a given type are almost negligible.

4. CONCLUSIONS

Comparison between $N_{D,w}$ and N_K based protocols shows that the differences in absorbed dose between the new and the older protocols are generally

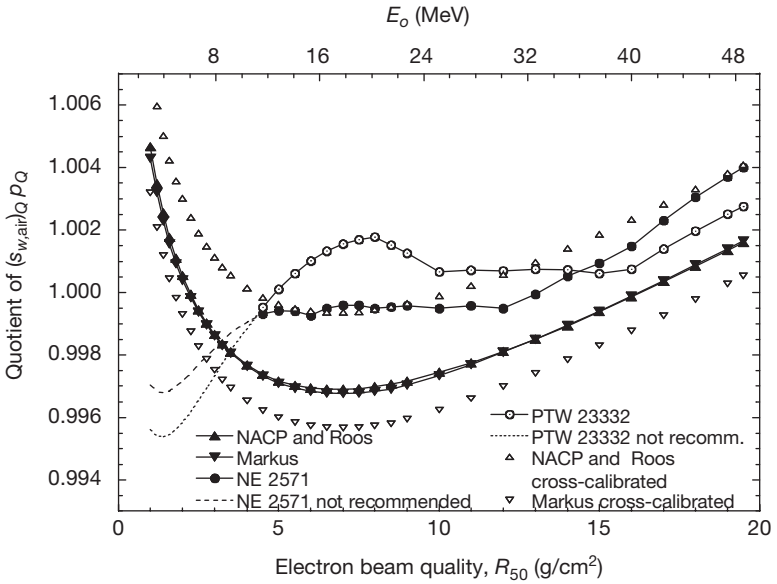

FIG. 6. Quotients TRS 398/TRS 381 of the product $(s_{w,air})_Q p_Q$ for cylindrical and plane-parallel ionization chambers, as a function of the electron beam quality, R_{50}. The curve for the NE 2571 applies to all Farmer type chambers. The open triangles correspond to the quotients of the p_Q cross-corrected product for the plane-parallel chambers in a cross-calibration procedure. Reproduced with permission [5].

small (with a few exceptions) for both photon and electron beams. Since differences are generally small and uncertainties are similar, users could ask "Why change to a new protocol?" Arguments in support of the $N_{D,w}$ based formalism have been provided in Ref. [20], and are summarized as:

(a) There are steps and components in the dosimetry chain the uncertainties of which are very difficult to estimate, such as chamber to chamber differences. The full application of $N_{D,w}$ based procedures is based on specific calibrations of each chamber at the user's beam quality, whereas previous protocols assume that the same data apply to all chambers of a given type.

(b) A possible variation with energy of the quantity W_{air}, the mean energy required to produce a pair of ions in air, has been pointed out (see Ref. [3] and references therein), but no definitive answer has yet been provided. Experimental k_Q values include any possible energy dependence of this quantity.

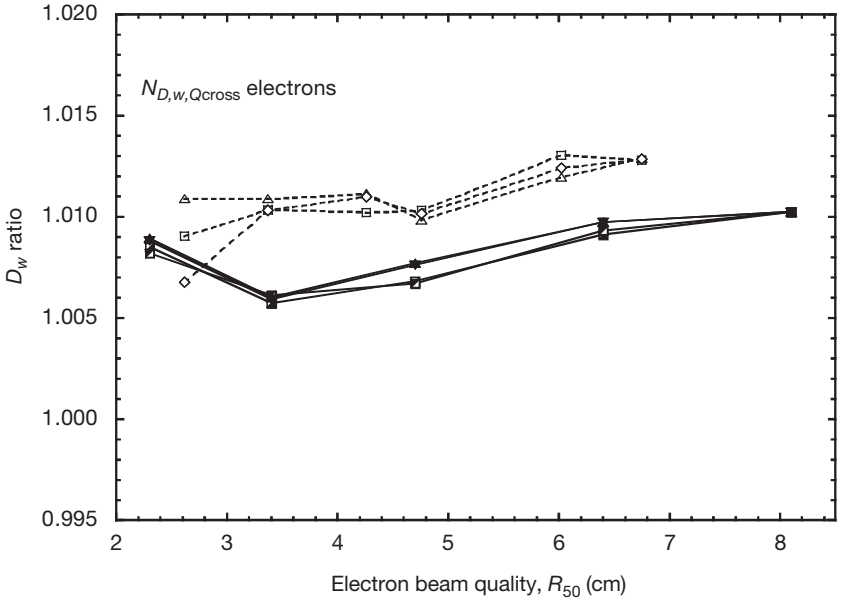

FIG. 7. Experimental comparison of dose ratios TRS 398/TRS 381 in electron beams at the depths of maximum dose for plane-parallel ionization chambers of the type NACP (squares), PTW and Wellhöfer Roos (upward open and filled triangles), PTB Roos (downward triangles), PTW Markus (diamonds). The dose determinations are made with plane-parallel chambers cross-calibrated in a high energy electron beam against Farmer type chambers having $N_{D,w}$ calibrations in ^{60}Co (rightmost data points). Reproduced with permission [20].

(c) The different methods used to determine absorbed dose to water in primary standards laboratories have uncorrelated, or very weakly correlated, uncertainties. This is not the case with air kerma standards, as all are based on the same measuring principle. $N_{D,w}$ based procedures are therefore based on a more robust system of standards.

(d) Several different dosimetry protocols are used today in Europe, which leads to a lack of homogeneity in reference dosimetry (note that this is not the case in the United States of America, for example).

(e) Countries such as the United Kingdom and Germany have based their reference dosimetry on standards of absorbed dose to water for approximately ten years. These countries are major manufacturers of dosimetry equipment, often supplied with $N_{D,w}$ calibrations. Because of this, some European users have already switched to the new formalism, contributing to the lack of homogeneity.

(f) New equipment is available today for which no data exist in the 'old' protocols but which is included in TRS 398.

(g) Implementing an $N_{D,w}$ based protocol implies updating the physicists' knowledge of basic dosimetry and ensures that the most recent scientific developments in dosimetry are incorporated into clinical practice.

REFERENCES

[1] GOSSTANDART, Absorbed Dose Determination in Photon (1–50 MeV) and Electron (5-50 MeV) Radiation Therapy Beams, Standard RD-50-691-89, Gosstandart, Moscow (1990) (in Russian).

[2] AMERICAN ASSOCIATION OF PHYSICISTS IN MEDICINE, AAPM's TG-51 protocol for clinical reference dosimetry of high-energy photon and electron beams, Med. Phys. **26** (1999) 1847–1870.

[3] INTERNATIONAL ATOMIC ENERGY AGENCY, Absorbed Dose Determination in External Beam Radiotherapy, Technical Reports Series No. 398, IAEA, Vienna (2000).

[4] HUQ, M.S., ANDREO, P., SONG, H., Comparison of the IAEA TRS-398 and AAPM TG-51 absorbed dose to water protocols in the dosimetry of high-energy photon and electron beams, Phys. Med. Biol. **46** (2001) 2985–3006.

[5] ANDREO, P., BURNS, D.T., HUQ, M.S., "Review of the data in the international Code of Practice IAEA TRS-398 (2000). Comparison with other dosimetry protocols", Recent Developments in Accurate Radiation Dosimetry (Proc. Int. Workshop Montreal, 2001) (SEUNTJENS, J.P., MOBIT, P.N., Eds), Medical Physics Publishing, Madison, WI (2002) 29.

[6] PALMANS, H., et al., Absorbed dose to water based dosimetry versus air kerma based dosimetry for high-energy photon beams: An experimental study, Phys. Med. Biol. **47** (2002) 421–440.

[7] DOHM, O.S., CHRIST, G., NUSSLIN, F., Electron dosimetry based on the absorbed dose to water concept: A comparison of the AAPM TG-51 and DIN 6800-2 protocols, Med. Phys. **28** (2001) 2258–2264.

[8] DEUTSCHES INSTITUT FÜR NORMUNG, Dosismessverfahren nach der Sondenmethode für Photonen- und Elektronenstrahlung — Teil 2: Ionisationsdosimetrie, DIN 6800-2, DIN, Berlin (1997).

[9] AMERICAN ASSOCIATION OF PHYSICISTS IN MEDICINE, TASK GROUP 21, A protocol for the determination of absorbed dose from high-energy photon and electron beams, Med. Phys. **10** (1983) 741–771.

[10] INTERNATIONAL ATOMIC ENERGY AGENCY, Absorbed Dose Determination in Photon and Electron Beams, 2nd edn, Technical Reports Series No. 277, IAEA, Vienna (1997).

[11] INTERNATIONAL ATOMIC ENERGY AGENCY, The Use of Plane Parallel Ionization Chambers in High Energy Electron and Photon Beams, Technical Reports Series No. 381, IAEA, Vienna (1997).

[12] NEDERLANDSE COMMISSIE VOOR STRALINGSDOSIMETRIE, NCS Code of Practice for the Dosimetry of High-energy Photon Beams, Rep. 2, NCS, Delft (1986).
[13] JAPANESE ASSOCIATION OF RADIOLOGICAL PHYSICS, A Practical Code for the Dosimetry of High-energy Photon and Electron Beams in Radiotherapy, Tsusho-sangyo-kenkyusya, Tokyo (1986) (in Japanese).
[14] CHO, S.H., LOWENSTEIN, J.R., BALTER, P.A., WELLS, N.H., HANSON, W.F., Comparison between TG-51 and TG-21: Calibration of photon and electron beams in water using cylindrical chambers, J. Appl. Clin. Med. Phys. **1** (2000) 108–115.
[15] DING, G.X., CYGLER, J.E., KWOK, C.B., Clinical reference dosimetry: Comparison between AAPM TG-21 and TG-51 protocols, Med. Phys. **27** (2000) 1217–1225.
[16] TAILOR, R.C., HANSON, W.F., Calculated absorbed-dose ratios, TG51/TG21, for most widely used cylindrical and parallel-plate ion chambers over a range of photon and electron energies, Med. Phys. **29** (2002) 1464–1472.
[17] HUQ, M.S., ANDREO, P., Reference dosimetry in clinical high-energy photon beams: Comparison of the AAPM TG-51 and AAPM TG-21 dosimetry protocols, Med. Phys. **28** (2001) 46–54.
[18] HUQ, M.S., SONG, H., ANDREO, P., HOUSER, C.J., Reference dosimetry in clinical high-energy electron beams: Comparison of the AAPM TG-51 and AAPM TG-21 dosimetry protocols, Med. Phys. **28** (2001) 2077–2087.
[19] ARAKI, F., KUBO, H.D., Comparison of high-energy photon and electron dosimetry for various dosimetry protocols, Med. Phys. **29** (2002) 857–868.
[20] ANDREO, P., et al., 2002 protocols for the dosimetry of high-energy photon and electron beams: A comparison of the IAEA TRS-398 and previous international Codes of Practice, Phys. Med. Biol. **47** (2002) 3033–3053.

BLANK

APPLICATION OF TRS 398 USING IONIZATION CHAMBERS CALIBRATED BY PSDLs IN FRANCE AND THE UNITED KINGDOM IN A SERIES OF HIGH ENERGY PHOTON AND ELECTRON BEAMS

I.H. FERREIRA
ESTRO EQUAL Measuring Laboratory, Service de physique,
Institut Gustave-Roussy,
Villejuif, France
E-mail: equal@igr.fr

D. MARRE
Unité de radiophysique et de radioprotection,
Hôpital Henri Mondor,
Créteil, France

M. SAIFUL HUQ
Department of Radiation Oncology,
Kimmel Cancer Center of Jefferson Medical College,
Thomas Jefferson University,
Philadelphia, Pennsylvania, United States of America

A. BRIDIER, A. BEAUDRÉ
Service de physique, Institut Gustave-Roussy,
Villejuif, France

Abstract

Measurements performed at the ESTRO EQUAL Laboratory are now based on the new IAEA code of practice in Technical Reports Series No. 398 (TRS 398). The reference ionization chambers of the EQUAL Laboratory are calibrated by the Bureau national de métrologie–Laboratoire national Henri Becquerel and the National Physical Laboratory primary standards dosimetry laboratories (PSDLs) in terms of absorbed dose to water ($N_{D,w,Q}$) in a series of high energy photon and electron beams. The paper presents the results of two sets of comparisons made in high energy photon and electron beams. These are (a) comparisons between experimental $k_{Q,Qo}$ values provided by the above PSDLs and the theoretical $k_{Q,Qo}$ values obtained from TRS 398 and (b) ratios of absorbed dose to water determined with experimental values of $k_{Q,Qo}$ and $k_{Q,Qo}$ from TRS 398, and with calibration factors in terms of air kerma and calibration factors from TRS 277 for NE 2571,

Wellhöfer IC 70 and NACP chambers. The photon beam qualities investigated were ^{60}Co and high energy photons with $TPR_{20,10}$ values ranging from 0.647 to 0.792; the electron beam qualities range from R_{50} = 1.23 g/cm^2 (4 MeV) to 6.6 g/cm^2 (20 MeV). For the NE 2571 chamber good agreement (<0.1%) was found between the experimental values of k_{Q,Q_o} provided by the PSDLs and the theoretical values obtained from TRS 398. However, for the IC 70 chamber differences of up to 1% were observed between the k_{Q,Q_o} values for $TPR_{20,10}$ values ranging from 0.746 to 0.792 (12–25 MV). These differences lie within the combined standard uncertainty of the primary standards of absorbed dose to water in high energy photon beams and from TRS 398. In electron beams the experimental k_{Q,Q_o} values for the NACP chamber were found to be in good agreement with the theoretical values obtained from TRS 398 for R_{50} values lying between 2.75 g/cm^2 and 6.6 g/cm^2. However, the two sets of k_{Q,Q_o} values were found to differ by 1.7% at R_{50} = 1.23 g/cm^2 (4 MeV) (R_{50} of the reference beam, Q_o, was chosen to be 3.48 g/cm^2). For photon beams the ratios of absorbed dose to water determined with calibration factors in terms of air kerma and calibration factors from TRS 277, and with experimental values of k_{Q,Q_o} and k_{Q,Q_o} from TRS 398, were found to lie between 0.991 and 0.996. The dose ratios for electron beams using TRS 381 (with the cross-calibration technique) and TRS 398 (with experimental k_{Q,Q_o}) were found to lie between 0.994 and 1.000.

1. INTRODUCTION

The European Society for Therapeutic Radiology and Oncology (ESTRO), the World Health Organization (WHO) and the Pan American Health Organization (PAHO) have worked together with the IAEA to develop and introduce the new IAEA code of practice (CoP) in Technical Reports Series No. 398 (TRS 398) [1]. The ESTRO EQUAL Laboratory has noted that a large number of dosimetry protocols and CoPs have been used in Europe for dose calibrations [2, 3]; it also found that about 40% of the European centres audited by it from September 2001 until July 2002 use dosimetry protocols based on standards of absorbed dose to water in photon and electron beams. The ESTRO EQUAL Laboratory has implemented TRS 398 for beam calibrations and has recommended that all participating centres taking part in the EQUAL network use TRS 398 in order to harmonize the reference dosimetry of radiotherapy beams in Europe. This paper compares theoretical (provided by TRS 398) and experimental (obtained from primary standards dosimetry laboratories (PSDLs)) values of beam quality correction factors, k_{Q,Q_o}, for high energy photon and electron beams; it also compares the absorbed doses to water, D_w, determined in high energy photon and electron beams using different IAEA CoPs (i.e. TRS 398 and TRS 277 [4] and TRS 381 [5]).

2. MATERIALS AND METHODS

2.1. Experimental methods

Measurements of absorbed doses were performed using three types of ionization chamber in a ^{60}Co gamma ray beam obtained from a Theratron 780 machine, and in high energy photon and electron beams obtained from a Clinac 2300C/D (Varian) accelerator. These chamber types were an NE 2571 (two chambers), a Wellhöfer IC 70 (new name FC65-G; two chambers) and an NACP-02 (one chamber). The NE 2571 and IC 70 chambers were calibrated in terms of absorbed dose to water at the Bureau national de métrologie—Laboratoire national Henri Becquerel (BNM–LNHB, France) in a series of photon beam qualities, and the NACP-02 chamber was calibrated at the National Physical Laboratory (NPL, United Kingdom) in terms of absorbed dose to water in a series of electron beam qualities. All chambers had an $N_{D,w}$ and N_K calibration at ^{60}Co provided by the BNM–LNHB. The two mentioned PSDLs have very good agreement (<0.2%) between the different standards (i.e. N_K and $N_{D,w}$ calibration factors) [1].

The absorbed dose to water in photon and electron beams was determined from ionization measurements following the procedures described in TRS 277, TRS 381 and TRS 398.

To circumvent the problems associated with instabilities in machine output and monitor response, all measurements were referenced to those of an external reference chamber mounted on the machine head. The external chamber used was an A14 Exradin ionization chamber. All chambers were connected to a Keithley 35040 electrometer. Ionization chamber readings were corrected for temperature (in a water phantom and in air at the level of the monitor chamber), pressure, recombination and polarity effects. The polarity effects were determined from measurements made with positive and negative polarity, and were found to be smaller than 0.1% for all electron beams. The reproducibility of chamber readings in two series of measurements was found to be within 0.1% for the ^{60}Co gamma rays and within 0.2% and 0.3% for the photon and electron beams, respectively.

The absorbed dose to water was determined for photon and electron beams in accordance with the following methods:

(a) For electron beams, absorbed dose to water at the reference depths of TRS 398 using measured k_{Q,Q_o} factors determined by PSDLs; these were compared with absorbed dose to water determined with TRS 381 using cross-calibrated $N_{D,\mathrm{air}}$ for plane-parallel chambers.

(b) For photon beams, the absorbed dose to water at the reference depth of TRS 398 using experimental and theoretical k_{Q,Q_o} factors. Additional comparison was also made between TRS 277 and TRS 398 (using experimental k_{Q,Q_o} factors).

2.2. Monte Carlo calculations

Monte Carlo simulations were performed with the PENELOPE code (PENetration and Energy Loss of Positrons and Electrons) [6] and with the EGS4 code [7]. The main program was based on a correlated sampling method relying on two different geometries to follow the evolution of the tracks and keep score of the relevant quantities.

3. RESULTS AND DISCUSSION

3.1. Comparison between theoretical and experimental k_{Q,Q_o} factors for IC 70 and NE 2571 chambers in high energy photon beams

Tables I and II give the absorbed dose to water calibration factors, $N_{D,w,Q}$, provided by the BNM–LNHB, the photon beam quality correction factors, k_{Q,Q_o}, obtained from TRS 398 and the experimental k_{Q,Q_o} values for the IC 70 and NE 2571 chambers. Both of these chambers were calibrated at the BNM–LNHB in a series of photon beams (i.e. ^{60}Co and high energy photons with $TPR_{20,10}$ values ranging from 0.647 to 0.792), and the k_{Q,Q_o} values were derived from the $N_{D,w,Q}$ values using ^{60}Co as the reference quality beam, Q_o. The BNM–LNHB uses a Fricke dosimeter as a reference standard to calibrate ionization chambers in high energy photon beams. The combined uncertainties for $N_{D,w,Q}$ provided by the BNM–LNHB were ±1.05% (1 standard deviation (SD)) for high energy photon beams and ±0.75% (1 SD) for the ^{60}Co gamma ray beams. The chamber to chamber variation of k_{Q,Q_o} for the NE 2571 and the IC 70 chambers was found to be less than 0.2% and 0.3%, respectively.

For the NE 2571 chamber the k_Q values given by TRS 398 and experimental k_Q factors provided by the BNM–LNHB were found to be in good agreement for the entire range of photon beam qualities investigated (Table I). However, differences of about 0.6–1.0% were observed for the IC 70 chamber for beam qualities with $TPR_{20,10}$ values ranging from 0.647 to 0.784. This difference lies within the combined standard uncertainty of the primary standards of absorbed dose to water in high energy photon beams and TRS 398.

TABLE I. ABSORBED DOSE TO WATER CALIBRATION FACTORS, $N_{D,w,Q}$, EXPERIMENTAL PHOTON BEAM QUALITY CORRECTION FACTORS, k_{Q,Q_o}, PROVIDED BY THE BNM–LNHB AND CALCULATED k_{Q,Q_o} VALUES (TRS 398) (Q_o = ^{60}Co) FOR THE NE 2571 CHAMBER

Nominal energy	$TPR_{20,10}$	$N_{D,w,Q}$ (Gy/nC)	k_{Q,Q_o} (experimental)	k_{Q,Q_o} (TRS 398)	k_{Q,Q_o} (TRS 398)/ k_{Q,Q_o} (experimental)
^{60}Co	—	0.04495	1.000	1.000	1.000
10 MV	0.743	0.04435	0.987	0.986	0.999
18 MV	0.767	0.04406	0.980	0.980	1.000

TABLE II. ABSORBED DOSE TO WATER CALIBRATION FACTORS, EXPERIMENTAL PHOTON BEAM QUALITY CORRECTION FACTORS, k_{Q,Q_o}, FROM THE BNM–LNHB AND CALCULATED k_{Q,Q_o} VALUES (TRS 398) FOR THE WELLHÖFER IC 70 CHAMBER (Q_o = ^{60}Co)

Nominal energy	$TPR_{20,10}$	$N_{D,w,Q}$ (Gy/nC)	k_{Q,Q_o} (experimental)	k_{Q,Q_o} (TRS 398)	k_{Q,Q_o} (TRS 398)/ k_{Q,Q_o} (experimental)
^{60}Co	—	0.04830	1.000	1.000	1.000
4 MV	0.647	0.04783	0.990	0.996	1.006
6 MV	0.675	0.04773	0.988	0.994	1.006
12 MV	0.746	0.04714	0.976	0.984	1.008
20 MV	0.784	0.04656	0.964	0.973	1.009
25 MV	0.792	0.04638	0.960	0.970	1.010

3.2. Comparison between theoretical and experimental k_{Q,Q_o} factors for the NACP chamber in high energy electron beams

The experimental $N_{D,w,Q}$ calibration factors for the NACP chamber, measured at the NPL, are given in Table III as a function of the NPL electron beam

qualities, R_{50}. Also given in Table III are the theoretical values of $k_{Q,Qo}$ for the NACP chamber obtained from TRS 398 and experimentally derived $k_{Q,Qo}$ factors for the NACP chamber. The experimental $k_{Q,Qo}$ factors were derived from the $N_{D,w,Q}$ values by using R_{50} = 3.48 g/cm^2 (E = 10 MeV) as the reference quality beam, Q_o. The combined uncertainties for the NPL electron calibration factors, $N_{D,w,Q}$, was ±0.75% (1 SD).

As can be seen from Table III, the $k_{Q,Qo}$ values given by TRS 398 and the NPL differ by 0.7% to 1.7% for low energy electron beams when R_{50} changes from 1.97 g/cm^2 to 1.23 g/cm^2 (Table III). However, for R_{50} values ranging from 2.75 g/cm^2 to 6.60 g/cm^2, experimental $k_{Q,Qo}$ values agree with the theoretical values to within 0.3%.

When Q_o corresponds to the ^{60}Co beam the measured and calculated $k_{Q,Qo}$ values differ by about 1.6% to 2.0% when R_{50} is between 2.75 g/cm^2 and 5.5 g/cm^2 (Fig. 1). These $k_{Q,Qo}$ from TRS 398 are consistent with the findings of Monte Carlo calculations [8], which show that the theoretical and Monte Carlo calculated $k_{Q,Qo}$ values are similar (Fig. 1). This difference is probably related to the calibration of the NACP chamber at ^{60}Co at the BNM–LNHB and NPL.

TABLE III. ABSORBED DOSE TO WATER CALIBRATION FACTORS, $N_{D,w,Q}$, PROVIDED BY THE NPL, EXPERIMENTAL BEAM QUALITY CORRECTION FACTORS, $k_{Q,Qo}$ (NPL), DERIVED FROM $N_{D,w,Q}$ VALUES AND THEORETICAL $k_{Q,Qo}$ VALUES CALCULATED FROM TRS 398 FOR THE NACP CHAMBER

R_{50} (g/cm^2)	$N_{D,w,Q}$ (Gy/nC) (NPL)	$k_{Q,Qo}$ (experimental)	$k_{Q,Qo}$ (TRS 398) (Q_o = 10 MeV)	$k_{Q,Qo}$ (TRS 398)/ $k_{Q,Qo}$ (experimental)
1.23	0.1542	1.019	1.037	1.017
1.97	0.1534	1.014	1.021	1.007
2.75	0.1523	1.007	1.009	1.002
3.48	0.1513	1.000	1.000	1.000
4.23	0.1500	0.991	0.992	1.001
5.72	0.1481	0.979	0.979	1.000
6.60	0.1467	0.970	0.973	1.003

Note: The experimental and theoretical $k_{Q,Qo}$ values were derived using R_{50} = 3.48 g/cm^2 (E = 10 MeV) as the reference quality beam, Q_o. For the ^{60}Co gamma rays the $N_{D,w}$ was 0.1622 Gy/nC.

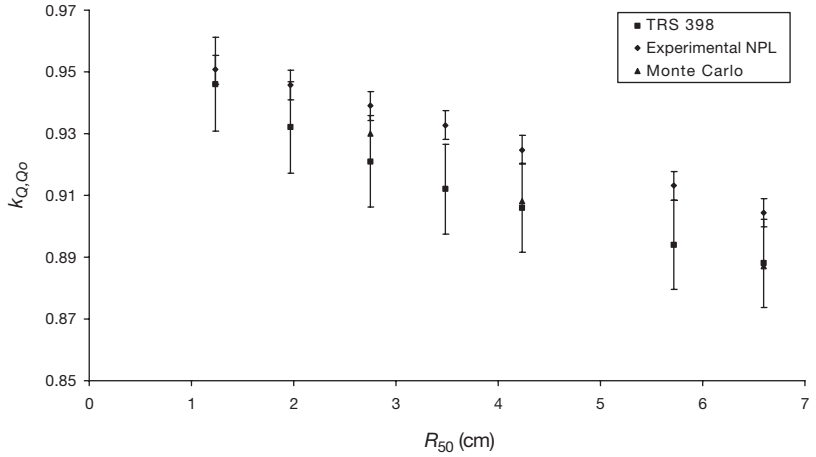

FIG. 1. Monte Carlo results [8], measured (NPL) and calculated (TRS 398) values of the electron beam quality correction factors, k_{Q,Q_o}, for the NACP ionization chamber with $Q_o = {}^{60}Co$. The statistical uncertainties (1 SD) are given.

3.3. Comparison between absorbed dose to water for photon beams using TRS 398 and TRS 277

Ratios of absorbed dose to water, D_w (TRS 277)/D_w (TRS 398 with experimental k_Q), measured following the recommendations of TRS 277 and TRS 398, are given in Table IV for the NE 2571 and IC 70 chambers for various photon beam energies. For TRS 398 the experimental values of k_Q were obtained using ^{60}Co as the reference beam quality, Q_o. The D_w ratios for the NE 2571 chamber were found to lie between 0.991 and 0.993, and those for the

TABLE IV. ABSORBED DOSE TO WATER RATIO USING TRS 277 AND TRS 398 USING EXPERIMENTAL k_Q VALUES FOR THE NE 2571 AND IC 70 CHAMBERS

Nominal energy	$TPR_{20,10}$	D_w (TRS 277)/ D_w (TRS 398 (experimental k_Q)) (NE 2571)	D_w (TRS 277)/ D_w (TRS 398 (experimental k_Q)) (IC 70)
^{60}Co	—	0.991	0.996
6 MV	0.675	0.993	0.991
25 MV	0.792	0.993	0.994

IC 70 chamber between 0.991 and 0.996. These findings are consistent with published results [9].

It should be mentioned that the determination of absorbed dose to water using experimental and theoretical values of $k_{Q,Qo}$, where Q_o = ^{60}Co, is the same as the determination of ratios of the $k_{Q,Qo}$ values (see Section 3.1).

3.4. Comparison between absorbed dose to water for electron beams using TRS 398 and TRS 381: NACP chamber

Table V gives ratios of absorbed dose to water determined with calculated $k_{Q,Qo}$ values (Q_o = ^{60}Co) and $k_{Q,Qo}$ from TRS 398, and with experimental $k_{Q,Qo}$ and $k_{Q,Qo}$ from TRS 398 for an NACP chamber. Also given are the absorbed dose to water ratios determined with the cross-calibration technique and absorbed dose to water ratios from TRS 381, and experimental $k_{Q,Qo}$ and $k_{Q,Qo}$ from TRS 398. Column 3 of Table V gives the ratios of absorbed dose to water determined using TRS 398, but with calculated values of k_Q from TRS 398 (Q_o = ^{60}Co) and measured values of $k_{Q,Qo}$ (R_{50} of the reference beam, Q_o, was chosen to be 3.48 g/cm^2) obtained from the NPL. The dose ratios given in column 4 were obtained using TRS 381, but with the NACP chamber cross-calibrated against a calibrated NE 2571 chamber in a high energy electron beam, and measured values of $k_{Q,Qo}$ (R_{50} of the reference beam, Q_o, was chosen to be 3.48 g/cm^2) obtained from the NPL and $k_{Q,Qo}$ from TRS 398 for dose determination. As can be seen from Table V, when comparisons are made with

TABLE V. ABSORBED DOSE TO WATER RATIO DETERMINED FOLLOWING TRS 398 WITH CALCULATED $k_{Q,Qo}$ VALUES (Q_o = ^{60}Co) AND WITH EXPERIMENTAL $k_{Q,Qo}$ VALUES

(also given are the absorbed dose to water ratios determined with the cross-calibration technique following TRS 381 and with experimental $k_{Q,Qo}$ following TRS 398)

R_{50} (g/cm^2)	Nominal energy	TRS 398 + k_Q calculated with Q_o = ^{60}Co/ TRS 398 (experimental $k_{Q,Qo}$)	TRS 381 + cross-calibration against NE 2571/TRS 398 (experimental $k_{Q,Qo}$)
3.63	9 MeV	0.978	0.999
4.74	12 MeV	0.979	0.994
7.76	18 MeV	0.992	1.000

TRS 381 using the cross-calibration technique, agreement in absorbed doses between TRS 381 and TRS 398 was within 0.6%. However, differences of up to 2.2% were observed when absorbed doses were determined using measured values of k_{Q,Q_o} (obtained from the NPL) and calculated values of k_Q (obtained from TRS 398).

4. CONCLUSIONS

This paper presents results of measurements of absorbed dose to water in high energy photon and electron beams following the recommendations of TRS 398, TRS 381 and TRS 277. Measurements were made using experimental values of k_{Q,Q_o} obtained from two PSDLs (the NPL and BNM–LNHB) in a series of photon and electron beam qualities. For photon beams, agreement in absorbed doses between TRS 398 and TRS 277 was found to be within 1% for the chambers and beam qualities investigated.

For electron beams a maximum difference of about 2% was observed when absorbed doses were determined using an NACP chamber and measured values of k_{Q,Q_o} from the NPL and calculated values of k_Q from TRS 398. In contrast, better agreement (<0.6%) was observed when dose comparisons were made between TRS 381 (with the cross-calibration technique) and TRS 398 (with experimental values of k_{Q,Q_o} obtained from the NPL).

At present, the EQUAL laboratory applies TRS 398 for clinical beam calibration with ionization chambers calibrated in ^{60}Co, photon and electron beams in terms of absorbed dose to water provided by the PSDLs.

REFERENCES

[1] INTERNATIONAL ATOMIC ENERGY AGENCY, Absorbed Dose Determination in External Beam Radiotherapy, Technical Reports Series No. 398, IAEA, Vienna (2000).

[2] FERREIRA, I.H., et al., The ESTRO-EQUAL quality assurance network for photon and electron radiotherapy beams in Germany, Strahlenther. Onkol. **177** (2001) 383–393.

[3] FERREIRA, I.H., et al., "Radiotherapy dosimetry audit: A European programme to improve quality and safety in radiation treatments", Radiological Protection of Patients in Diagnostic and Interventional Radiology, Nuclear Medicine and Radiotherapy (Proc. Int. Conf. Malaga, 2001), IAEA, Vienna (2001) 309–330.

[4] INTERNATIONAL ATOMIC ENERGY AGENCY, Absorbed Dose Determination in Photon and Electron Beams, 2nd edn, Technical Reports Series No. 277, IAEA, Vienna (1997).

[5] INTERNATIONAL ATOMIC ENERGY AGENCY, The Use of Plane Parallel Ionization Chambers in High Energy Electron and Photon Beams, Technical Reports Series No. 381, IAEA, Vienna (1997).

[6] BARO, J., SEMPAU, J., FERNANDEZ-VAREA, J.M., SALVAT, F., PENELOPE: An algorithm for Monte Carlo simulation and energy loss of electrons and positrons in matter, Nucl. Instrum. Methods B **100** (1995) 31–46.

[7] NELSON, W.R., HIRAYAMA, H., ROGERS, D.W.O.,The EGS4 Code System, Rep. SLAC-265, Stanford Linear Accelerator Center, Stanford, CA (1985).

[8] MARRE, D., Evaluation des Perturbations Induites sur la Mesure de la Dose Absorbée avec des Chambres d'Ionisation, des Dosimètres Chimiques et des Dosimètres Thermoluminescents dans des Faisceaux d'Électrons de Haute Energie, PhD Thesis, Toulouse Univ., France (2000).

[9] ANDREO, P., A comparison between calculated and experimental k_Q photon beam quality correction factors, Phys. Med. Biol. **45** (2000) L25–L38.

TESTING OF TRS 398 WITH PHOTONS AND ELECTRONS AT THE GERMAN CANCER RESEARCH CENTRE, HEIDELBERG, GERMANY

G.H. HARTMANN
Department of Medical Physics, German Cancer Research Centre, Heidelberg, Germany
E-mail: g.hartmann@dkfz.de

Abstract

The new IAEA code of practice (CoP) in Technical Reports Series No. 398 was tested within the framework of the IAEA's Co-ordinated Research Project E2 40.09. This test was in particular aimed at determining possible differences between this new international CoP and the German CoP, DIN 6800-2. Four ionization chambers of different types were employed for analysing the measured results. A calibration factor in terms of absorbed dose to water and air kerma was available for each chamber. Calibration factors were obtained by a German secondary standards dosimetry laboratory and by the IAEA. Measurements were performed in ^{60}Co gamma rays and high energy photon and high energy electron beams.

1. INTRODUCTION

This paper focuses on specific differences observed when applying the German Deutsches Institut für Normung (DIN) code of practice (CoP) (DIN 6800-2) [1] and IAEA Technical Reports Series No. 398 (TRS 398) [2]. When testing DIN 6800-2 by comparing the results of measuring absorbed dose in water, possible differences may be attributed to differences in the measuring procedure or differences in the formulas and/or numerical values of the correction factors applied. It is therefore necessary to do both, to compare carefully the formulas and numerical values given in the two CoPs and to perform measurements in accordance with the two CoPs. The comparison of the CoPs is carried out in the following section.

2. DESCRIPTION OF THE DIFFERENCES BETWEEN TRS 398 AND DIN 6800-2

Briefly, DIN 6800-2 is based (as is TRS 398) on a calibration factor of a dosimeter in terms of absorbed dose to water; however, only ^{60}Co gamma

radiation is used as the reference quality. The calibration factor applies for a set of reference conditions, such as the geometrical arrangement, material and dimension of the phantom, and air density. All factors that may lead to a deviation from the reference conditions are called influence quantities, and must be corrected. The departure from ^{60}Co gamma radiation is also treated as an influence quantity. Measurements at other radiation qualities require a correction factor, which is called k_Q for photons and k_E for electrons. According to DIN 6800-2, the general expression for the absorbed dose to water, D_w, in a field of radiation is given by:

$$D_w(P_{\text{eff}}) = kNM$$

where k is the product of the correction factors of all influence quantities, including the beam quality, N is the calibration factor and M is the uncorrected reading of the chamber placed at reference depth. Note that the measuring result always refers to an effective point of measurement in the phantom, P_{eff}, when the chamber is absent.

2.1. Influence factors applying to all radiation types

2.1.1. Pressure, temperature and humidity

The same formula for air pressure and temperature applies in both CoPs. However, DIN 6800-2 states that: "The correction factor according to this formula is not to be applied to dosimeters with open chambers, for which deviations of the air density from the reference air density and changes in the response are taken into account by a check value which has to be determined with a radioactive check source before each measurement." A correction factor for air humidity is not explicitly given; however, the range of the correct operation of an ionization chamber is limited to between 30% and 75% relative humidity.

2.1.2. Polarity effect

The expression used in DIN 6800-2 to correct for the polarity effect in the user's beam includes a correction to be made also for the calibration quality. This difference from TRS 398 is due to the fact that the calibration factor from the secondary standards dosimetry laboratory refers to a specified (routine) polarity without correction.

2.1.3. *Ion recombination*

An approximating formula for pulsed radiation only is given in DIN 6800-2, which may be used for small correction factors (i.e. $k_s < 1.04$):

$$k_s = \frac{(V_1/V_2) - 1}{(V_1/V_2) - (M_1/M_2)}$$

If $1/M$ linearly depends on $1/V$, this formula is exact. TRS 398, however, offers two formulas for this case: (a) a general formula in combination with certain constants and (b) an approximating formula valid for $k_s < 1.03$:

(a) $$k_s = a_0 + a_1\left(\frac{M_1}{M_2}\right) + a_2\left(\frac{M_1}{M_2}\right)^2$$

(b) $$k_s - 1 = \frac{M_1/M_2 - 1}{V_1/V_2 - 1}$$

As long as the correction factor, k_s, remains below 1.03, the largest numerical difference between all three formulas is less than 1–2 tenths of a per cent.

2.1.4. *Displacement for cylindrical chambers*

In TRS 398 the method used for p_{dis} for cylindrical chamber types depends on the radiation modality. In ^{60}Co high energy photon and proton beams the chamber centre is positioned at z_{ref} and values for the displacement correction factor, p_{dis}, are used in the calculation of k_{Q,Q_o}. For electron beams the chamber centre is positioned $0.5r_{\text{cyl}}$ deeper than z_{ref}, where r_{cyl} is the internal radius of the chamber cavity.

In contrast to this procedure, a measurement in accordance with DIN 6800-2 always refers to the effective point of measurement, P_{eff}, which is shifted from the chamber axis towards the radiation source by approximately $0.5r_{\text{cyl}}$. This procedure, however, does not apply in ^{60}Co gamma radiation during measurement and calibration. Because of the different treatment of the displacement effect during the calibration in ^{60}Co and a measurement in a beam of high energy photons and electrons, the calibration factor has always to be applied in combination with a correction factor, k_r, which takes into account the displacement effect in ^{60}Co gamma radiation during the calibration. A good approximation of k_r is given in DIN 6800-2 as $1 + 0.025r_{\text{cyl}}$

(where r_{cyl} is in cm). A displacement correction factor is not included in the calculation of k_Q and k_E.

2.2. Influence factors specific to radiation type

2.2.1. High energy photons

For the measurement of absorbed dose in high energy photons, DIN 6800-2 only allows such cylindrical chambers for which an approval is given by the Physikalisch-Technische Bundesanstalt, whereas TRS 398 more generally recommends the use of cylindrical chambers. In order to obtain the calculated k_Q value, which is given as a function of the beam quality index, the beam quality index has first to be determined. The beam quality index is commonly defined as the tissue phantom ratio, $TPR_{20,10}$. There are different fit formulas to derive this parameter from measured depth dose curves, which, however, yield almost identical results. For certain chambers the beam quality correction factors calculated using the TRS 398 and DIN 6800-2 formalisms can differ by as much as 1%. This is shown in Fig. 1.

2.2.2. High energy electrons

The most important difference between the CoPs is the change of reference depth and the change of beam quality specification, which significantly facilitate the determination of absorbed dose in a high energy electron beam with TRS 398 as compared with DIN 6800-2. Table I shows these parameters in DIN 6800-2 and TRS 398. According to DIN 6800-2, it is a complicated way to finally derive the parameter values needed to calculate the beam

TABLE I. VALUES AND PARAMETERS NEEDED FOR THE DETERMINATION OF REFERENCE DEPTHS AND THE BEAM QUALITY INDEX

	DIN	TRS 398
Reference depth:		
$1 \le \bar{E}_0 < 5$ MeV	Dose maximum	$0.6R_{50} - 0.1$ g/cm^2
$5 \le \bar{E}_0 < 10$ MeV	Dose maximum, minimum 1 cm	
$10 \le \bar{E}_0 < 20$ MeV	Dose maximum, minimum 2 cm	
$20 \le \bar{E}_0 \le 50$ MeV	Dose maximum, minimum 3 cm	
Beam quality index	$\bar{E}_0$, E_0', R_p	R_{50}

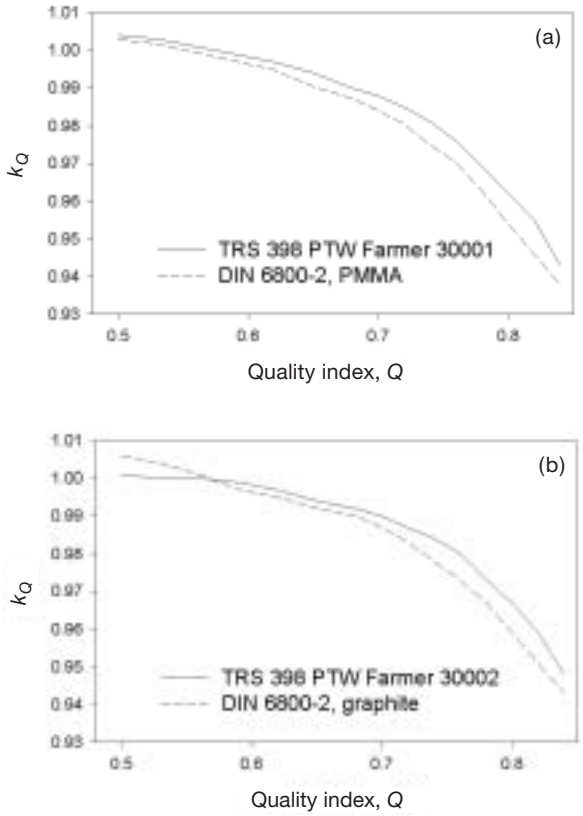

FIG. 1. Beam quality correction factor as a function of the beam quality index for the two PTW chambers, 30001 and 30002, as given in TRS 398 and calculated in accordance with DIN 6800-2.

quality correction factor, k_E. First, the values for R_{50} and R_p have to be measured. Then the mean energy at the phantom surface, $\bar{E}_0$, is derived from R_{50} by:

$$\bar{E}_0 = 0.31 + 2.25R_{50,D} + 0.006R_{50,D}^2$$

At the same time, a substitute initial energy, E_0', is needed to calculate correctly the stopping power ratios in the beam quality correction factor given in DIN 6800-2 as a function of E_0'. This parameter is derived from $\bar{E}_0$ by:

$$E_0' = \bar{E}_0 + f(\bar{E}_0)[R_p - (-0.1129 + 0.5104\bar{E}_0 - 0.0005\bar{E}_0^2)]$$

with:

$$f(\bar{E}_0) = 16 - 0.484\bar{E}_0 + 0.0065\bar{E}_0^2$$

With E_0' and R_p, the practical range, the stopping power ratio needed in k_E is obtained by:

$$\frac{(s_{w,\text{air}})_E}{(s_{w,\text{air}})_{\text{Co}}} = a(E_0')(R_p - z) + b(E_0')$$

where the coefficients a and b again are given as a function of E_0'.

3. MEASUREMENTS

The four ionization chambers listed in Table II were used for the measurements.

Each charge was measured with a Unidos (PTW, Freiburg) electrometer; the reproducibility of the charge measurements was below 0.1%.

3.1. Cobalt-60 gamma radiation

In order to be able to differentiate between various sources for possibly different results, a comparison of absorbed dose in ^{60}Co gamma radiation obtained with four chambers was performed under reference conditions. The results are shown in Table III. In this case, both CoPs are identical. Since the graphite Farmer 30002 chamber is not waterproof, the measurement with this

TABLE II. IONIZATION CHAMBERS USED FOR THE MEASUREMENTS

No.	Ionization chamber type	Serial number	Sensitive volume	$N_{D,w}$ by	N_K by
1	PTW Farmer 30006	0173	Cyl.[a], 0.6 cm^3	DKD[b], Freiburg	DKD, Freiburg
2	PTW Farmer 30002	0209	Cyl., 0.6 cm^3	DKD, Freiburg	DKD, Freiburg
3	PTW Markus M23343	2891	Pp[c], 0.03 cm^3	DKD, Freiburg	IAEA
4	PTW Roos 34001	0094	Pp, 0.10 cm^3	DKD, Freiburg	IAEA

[a] Cyl.: cylindrical chamber.
[b] Deutscher Kalibrierdienst.
[c] Pp: plane-parallel chamber.

TABLE III. ABSORBED DOSE IN ^{60}Co GAMMA RADIATION MEASURED UNDER REFERENCE CONDITIONS WITH DIFFERENT IONIZATION CHAMBERS
(plane parallel chambers may be used for DIN 6800-2)

	D_w in a water phantom (Gy/min)	D_w in RW3 plastic (Gy/min)
PTW Markus M23343	0.2644	—
PTW Roos 34001	0.2642	—
PTW Farmer 30006	0.2625	0.2601
PTW Farmer 30002	0.2648[a]	0.2624
Mean	0.2638 (±0.4%, 1 SD[b])	—

[a] Derived from the measurement in the plastic phantom.
[b] SD: standard deviation.

chamber was performed in a nominal water equivalent plastic phantom. In order to translate this result into an equivalent result in the water phantom, the waterproof Farmer 30006 chamber was also inserted into the plastic phantom. The slightly lower reading of the 30006 chamber under this condition was then inversely applied to the graphite chamber, simulating a virtual measurement with the graphite chamber in the water phantom. The uncertainty due to estimated positioning errors of the chambers of ±0.5 mm amounts to ±0.3%. The results agree entirely within this uncertainty.

3.2. High energy photons

Since cylindrical ionization chambers are recommended for reference dosimetry in clinical high energy photon beams, the comparison of measured absorbed dose in a water phantom was performed only with the waterproof PTW Farmer 30006 chamber. The two available energies of 6 MV and 15 MV were used. The results are summarized in Table IV. Although there is a series of small numerical differences according the two CoPs, the absorbed dose according to DIN 6800-2 is less by only 0.2%.

3.3. High energy electrons

Measurements were performed at 12 MeV and 18 MeV using the plane-parallel PTW Roos 34001 chamber and the waterproof PTW Farmer 30006

TABLE IV. MEASUREMENT RESULTS AT 6 MV AND 15 MV WITH THE PTW FARMER 30006 CHAMBER

	6 MV		15 MV	
Calibration factor (Gy/nC) in ^{60}Co	0.05233		0.05233	
Reference depth (g/cm^2)	5.0		10.0	
Measured charge (nC)	19.057		15.845	
	TRS 398	DIN 6800-2	TRS 398	DIN 6800-2
Product of correction factors (without k_Q)	1.012	1.020	1.014	1.022
$TPR_{20,10}$	0.672	0.671	0.764	0.765
Beam quality correction factor	0.991	0.988	0.973	0.968
Absorbed dose at the 'measuring point'				
TRS 398: at the central axis	1.001		0.818	
DIN 6800-2: at P_{eff}		1.005		0.820
Absorbed dose at the reference depth	1.001	0.998	0.818	0.816
Relative difference (TRS – DIN) (%)	0.2		0.2	

chamber. First a relative depth ionization curve was measured for both energies, then the absolute charge was measured, including all correction factors at a common depth for both CoPs, at 3.0 cm for 12 MeV and at 4.5 cm for 18 MeV. This charge was converted into the charge at the reference depths of TRS 398 and DIN 6800-2. In DIN 6800-2 this was the depth of maximum dose for 12 MeV, and the minimum depth of 2 cm for 18 MeV. Finally, the resultant absorbed dose was converted to that at a common depth. The results are summarized in Tables V and VI.

For both energies, the difference obtained for the absorbed dose at the same depth is about 1% for the Farmer and the Roos chambers. In order to discuss possible reasons for these differences, the calculated quality correction factor, k_Q, for the Roos and the Farmer chambers was considered in more detail. In TRS 398 k_Q is given at the associated reference depth only, whereas in DIN 6800-2 k_E can be derived at a range of depths, including the reference depth of TRS 398. A direct comparison of values can therefore be made at this

TABLE V. MEASUREMENT RESULTS AT 12 MeV AND 18 MeV OBTAINED WITH THE PTW ROOS 34001 CHAMBER WITH A ^{60}Co CALIBRATION FACTOR OF 0.0816 Gy/nC

	12 MeV		18 MeV	
	TRS 398	DIN 6800-2	TRS 398	DIN 6800-2
Beam quality index	4.77[a]	11.2, 13.8[b]	7.5[a]	17.5, 21.0[b]
Reference depth (g/cm^2)	2.8	2.4	4.4	2.0
Measured charge (nC)	13.525	13.663	12.565	13.314
Product of correction factors (without k_Q)	1.030	1.030	1.029	1.029
Beam quality correction factor	0.913	0.898	0.895	0.855
Absorbed dose at the reference depth	1.038	1.031	0.944	0.956
Absorbed dose at equal depth (DIN reference depth)	1.039	1.031	0.965	0.956
Relative difference (TRS – DIN) (%)	+0.8		+0.9	

[a] R_{50} (g/cm^2).
[b] $\overline{E}_0$, E_0' (MeV).

depth. The results are shown in Table VII. Slightly larger values were obtained for the stopping power ratios according to DIN 6800-2. The situation for the perturbation factors is more complex. It appears that TRS 398 offers the available knowledge on the relevant perturbation factor data in a more consistent way, whereas there may be the possibility of an incorrect assessment of the ratio of the perturbation factors when following DIN 6800-2.

4. CONCLUSION

The differences found when following DIN 6800-2 and TRS 398 were very small for high energy photons. A higher difference of up to 1% was obtained for high energy electron beams. It appears that some of the differences in the formalism and in the treatment of the perturbation factors in DIN 6800-2 may be slightly confusing. In particular, TRS 398 treats the available knowledge on perturbation factor data in a more consistent way than DIN 6800-2. In summary, a transition in clinical dosimetry from DIN 6800-2 to TRS 398 would not significantly change the values of absorbed dose under

TABLE VI. MEASUREMENT RESULTS AT 12 MeV AND 18 MeV OBTAINED WITH THE PTW FARMER 30006 CHAMBER WITH A ^{60}Co CALIBRATION FACTOR OF 0.05233 Gy/nC

	12 MeV		18 MeV	
	TRS 398	DIN 6800-2	TRS 398	DIN 6800-2
Beam quality index	4.77[a]	11.2, 13.8[b]	7.5[a]	17.5, 21.0[b]
Reference depth (g/cm^2)	2.8	2.4	4.4	2.0
Measured charge (nC)	21.074	21.158	19.816	20.564
Product of correction factors (without k_Q)	1.019	1.027	1.022	1.030
Beam quality correction factor	0.907	0.891	0.899	0.868
Absorbed dose at the reference depth	1.0192	1.033	0.932	0.962
Absorbed dose at the DIN reference depth	1.020	1.013	0.952	0.962
Relative difference (TRS – DIN) (%)	+0.7		–1.0	

[a] R_{50} (g/cm^2).
[b] $\bar{E}_0$, E_0' (MeV).

TABLE VII. VALUES OF STOPPING POWER RATIO, PERTURBATION FACTOR RATIO, AND k_Q OR k_E AT THE COMMON DEPTH z_{ref} FROM TRS 398

Energy (MeV)	$(s_{w,\text{air}})_{\text{Co}}/(s_{w,\text{air}})_E$		p_E/p_Q				k_Q or k_E			
			Roos		Farmer		Roos		Farmer	
	TRS 398	DIN 6800-2	TRS 398	DIN 6800-2	TRS 398	DIN 6800-2	TRS 398	DIN 6800-2	TRS 398	DIN 6800-2
12	0.923	0.929	0.990	0.974	0.983	0.963	0.913	0.905	0.907	0.895
18	0.904	0.909	0.990	0.974	0.995	0.974	0.895	0.986	0.899	0.886

reference conditions in high energy photons. However, it would have an effect in high energy electrons. For the applicability of DIN 6800-2 this may be considered as a drawback. However, this would be compensated by the fact that TRS 398 represents an internationally consistent CoP that can be applied more easily to any type of radiation.

ACKNOWLEDGEMENT

This work was performed within the framework of the IAEA Co-ordinated Research Project (CRP) E2 40.09.

REFERENCES

[1] DEUTSCHES INSTITUT FÜR NORMUNG, Dosismessverfahren nach der Sondenmethode für Photonen- und Elektronenstrahlung — Teil 2: Ionisationsdosimetrie, DIN 6800-2, DIN, Berlin (1997).

[2] INTERNATIONAL ATOMIC ENERGY AGENCY, Absorbed Dose Determination in External Beam Radiotherapy, Technical Reports Series No. 398, IAEA, Vienna (2000).

BLANK

ABSORBED DOSE CALIBRATION FACTORS FOR PARALLEL-PLATE CHAMBERS IN HIGH ENERGY PHOTON BEAMS

M.R. McEWEN*, S. DUANE, R.A.S. THOMAS
National Physical Laboratory,
Teddington, United Kingdom
E-mail: mrmcewen@irs.phy.nrc.ca

Abstract

A number of NACP and Roos parallel-plate ionization chambers have been calibrated in high energy photon beams in terms of absorbed dose to water to determine their suitability for use in such beams. It was found that chambers of the same type showed similar energy responses at the ±0.4% level, and generic k_Q factors were derived. Several chambers were recalibrated over a period of six months, showing repeatability generally better than 0.5%. Polarity measurements showed unexpected large variations for the correction from one chamber to another, which at present are not understood. Relative wall correction factors for the NACP and Roos chambers were derived and would appear to confirm that the wall correction for the Roos chamber given in IAEA Technical Reports Series No. 381 is too low by 1%. The conclusion from this work is that to maintain the highest accuracy in reference dosimetry, the present practice of using cylindrical chambers for photon beams should be continued.

1. INTRODUCTION

In the dosimetry of high energy photon and electron beams there has been a historical distinction in the types of ionization chamber used. For photon beams cylindrical chambers are the instrument of choice, while parallel-plate chambers are better suited to measurements in electron beams. Ideally one would like to use one chamber for all megavoltage beams, but cylindrical chambers are unsuited to low energy electron beams and there are very few published data for parallel-plate chambers in high energy photon beams [1, 2]. An investigation was therefore carried out in both ^{60}Co and megavoltage photon beams with the aim of deriving calibration factors, investigating chamber to chamber variability and providing much needed information on the use of parallel-plate chambers in high energy X ray beams.

---

* Present address: National Research Council, Ottawa, Canada.

2. METHOD

A set of NE 2561/NE 2611 reference chambers, calibrated against the primary standard graphite calorimeter [3], is used for the dissemination of calibration factors in terms of absorbed dose to water. The parallel-plate chambers were calibrated by comparison with the National Physical Laboratory (NPL) reference chambers in a water phantom. The calibration factor for chamber u at photon beam quality Q is given by:

$$N_{w,Q,u} = N_{w,Q,\mathrm{ref}} \frac{M_{\mathrm{ref}}}{M_u}$$

where $N_{w,Q,\mathrm{ref}}$ is the absorbed dose calibration factor for the reference chamber and M is the chamber reading corrected for temperature, pressure, recombination and polarity.

Two types of parallel-plate chamber were investigated: the NACP-02 and the Roos. Four NACP and three Roos (including one Physikalisch-Technische Bundesanstalt (PTB) prototype chamber) were characterized and, in addition, one NE 2571 Farmer chamber was also calibrated as a check on the procedure used. Measurements were made using the NPL linac in six heavily filtered photon beams with energies in the range of 6 MV to 19 MV (corresponding to values of $\mathrm{TPR}_{20,10}$ in the range of 0.670 to 0.790). In addition, measurements were made in a ^{60}Co beam. Polarity corrections in photon beams are generally taken to be negligible for thimble chambers. However, the lack of data for parallel-plate chambers meant that polarity measurements were made for all photon energies, including ^{60}Co. Sample polarity measurements on a number of thimble chambers were also made. No ion recombination measurements were made, as previous measurements [4] had shown these chamber types to be very consistent in their response. A number of chambers were calibrated several months later to investigate the chamber stability and repeatability of the experimental procedure.

3. UNCERTAINTIES

The uncertainties for the calibration of a parallel-plate chamber in terms of absorbed dose to water are given in Table I. The values in the table are given as standard uncertainties in line with the guidance given by the International Organization for Standardization [5].

When comparing the calibration of one chamber with another (or when comparing two calibrations for the same chamber), the type B uncertainties cancel, resulting in a combined standard uncertainty of ±0.36%.

TABLE I. UNCERTAINTIES IN THE CALIBRATION OF PARALLEL-PLATE CHAMBERS

Component of uncertainty	Type A (%)	Type B (%)
Chamber reading	0.07	—
Chamber repeatability	0.2	—
Reproducibility (positioning)	0.09	—
Polarity correction	0.15[a]	—
Recombination correction	—	0.05
Beam uniformity	0.05	—
Depth correction	—	0.12
Monitor calibration	0.1	—
Calibration of reference chambers	0.2	0.65
Combined uncertainty	0.75[b]	

[a] A typical value for the uncertainty in the polarity correction is given (see below).
[b] The overall uncertainty is applicable to ^{60}Co and megavoltage X ray beams.

4. RESULTS AND DISCUSSION

4.1. Derivation of k_Q factors

Three reference chambers were used to derive calibration factors for the chambers investigated. The variation in the dose measured by the three chambers was less than 0.2% at all energies, which is within the uncertainty in the calibration factor for each chamber. The calibration data for the NE 2571 Farmer chamber were in very good agreement with those obtained previously (generally better than 0.3%), indicating that there was no significant error in the experimental procedure used for the work described in this paper.

For the chambers calibrated several months apart, the repeatability was generally better than 0.5%, and the variations in time appeared to be random. These differences were larger than for thimble chambers, for which we have found stability at better than the 0.3% level over several years. Similar calibration data for parallel-plate chambers in electron beams [4] also showed stability around 0.3%. This would indicate that parallel-plate chambers are sensitive to small variations in the beam quality of linac photon beams, which do not affect thimble chambers.

The calibration data (expressed in terms of the beam quality dependent correction factor, k_Q, defined as in Technical Reports Series No. 398 [6]) are given in Figs 1 and 2.

Calibration factors for the same chamber obtained at different times were treated as independent data sets, as the repeatability data indicated that variations in chamber response are due to the photon beams used. It would appear from these figures that the variations between chambers of the same type are random, and one can therefore define a generic curve for each chamber type, although more chambers are needed to define accurately the calibration curve. There is no apparent difference in energy response between the PTB prototype Roos chamber and the commercial PTW versions. The shapes of the k_Q curves for the NACP and Roos chambers are very similar and the small difference (around 0.3%) at the highest photon energies is within the measurement uncertainties. These k_Q curves are significantly different from those of cylindrical ionization chambers (e.g. Ref. [7]); this is discussed below.

4.2. Polarity correction

The results of the polarity measurements were somewhat confusing. One would expect the correction to be small, and previous measurements in

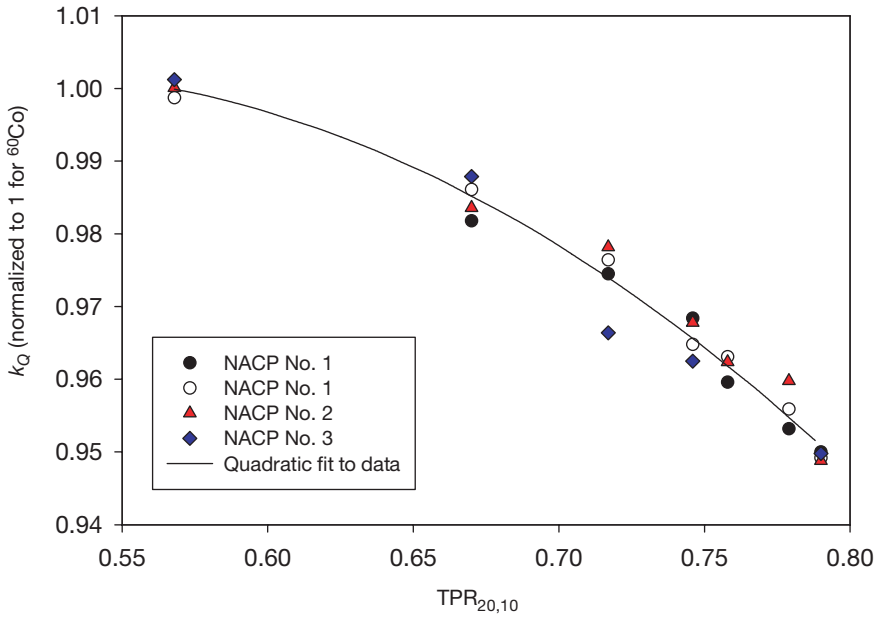

FIG. 1. Experimental k_Q data for the NACP-02 chambers. (The $TPR_{20,10}$ value for ^{60}Co is taken to be 0.568.)

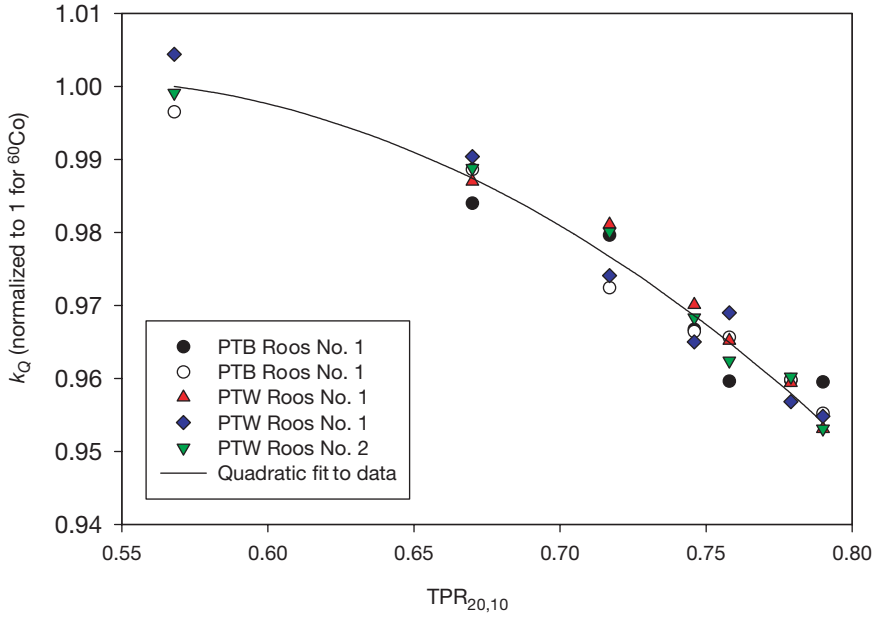

FIG. 2. Experimental k_Q data for the Roos chambers.

electron beams have indicated that there is little variation between chambers of these types. However, some chambers gave unexpectedly large polarity corrections, of up to 0.8%. By contrast, the measured polarity correction for an NE 2611 chamber was less than 0.13% at all energies. The data for the NACP chambers were reasonably consistent, with a correction at all energies around 0.3%. The PTW Roos chambers appeared to be very consistent, and the correction was smaller than for the NACP design (around 0.1%). However, the behaviour of the PTB Roos chamber was significantly different, yielding a large and variable value for the correction. Analysis of the raw data has shown that this is not due to variations in the linac output or lack of time in allowing the chamber to stabilize. Also, it would appear that this unexpected polarity behaviour is a real effect, as one must apply the measured polarity correction in order to obtain consistency between calibrations at different times and between chambers of the same type. The data in Figs 1 and 2 take these polarity corrections into account. The strange behaviour of the PTB Roos chamber may be an isolated case or it may be a function of the construction of the prototype. The number of factors that influence the magnitude of the polarity effect — thickness and surface area of the collecting electrode, measurement depth and photon energy — make it difficult to derive any general conclusions from the data presented in this paper. However, the recommendation always to measure and apply a

polarity correction, as given in most modern codes of practice, is very strongly upheld.

4.3. Wall correction factors in photon beams

Although the aim of this work was to calibrate parallel-plate chambers in terms of absorbed dose to water, it is possible to derive information on the wall correction factor in ^{60}Co and high energy photon beams.

A number of the NACP and Roos chambers were also calibrated in terms of absorbed dose to water in high energy electron beams. It was then possible to determine the difference in the wall correction for the NACP and Roos chambers by taking ratios of calibration factors in ^{60}Co and high energy electrons. Three independent measurements gave mean values of 0.63%, 0.90% and 0.96% (each with a standard uncertainty of ±0.35%). The agreement between these results is within the uncertainties and indicates that the difference in the wall correction is of the order of 0.8%, which is in very good agreement with Palm et al. [8]. Unfortunately, the method used in this work does not realize absolute values for the wall correction. Assuming that the wall correction factor for the NACP is correct, this would seem to confirm that p_{wall} for the Roos chamber given in Technical Reports Series No. 381 [9] is too low, by around 1%. The difference in the k_Q curves for parallel-plate and cylindrical chambers is primarily due to the different perturbation effects of the chamber types. Nystrom et al. [2] give data for the wall correction for the NACP chamber at a number of photon energies. By using the k_Q curve for the NE 2571 chamber as the reference, it is possible to derive the relative change in the wall correction with energy. It was found that these data agreed very well with those of Nystrom and Karlsson [2]. From the data presented in this paper it is difficult to see how the uncertainty on the determination of the wall correction could be reduced, owing to the problems discussed above relating to chamber repeatability and the polarity effect.

5. CONCLUSION

Parallel-plate chambers can be calibrated in terms of absorbed dose to water, but with an uncertainty larger than for thimble chambers. Chamber stability also appears to be worse than that for thimble chambers. Polarity corrections must always be measured and applied, as the polarity effect for a particular chamber is difficult to predict. Relative data on wall correction factors for the Roos and NACP chambers were derived and found to be in good agreement with recent data.

The conclusion from this work is that, to maintain the highest accuracy in reference dosimetry, the present practice of using cylindrical chambers for photon beams and parallel-plate chambers for electron beams should be continued. However, as the response of all thimble chambers is similar, the use of a parallel-plate chamber does provide a semi-independent check on megavoltage photon dosimetry.

ACKNOWLEDGEMENTS

The authors would like to thank R. Nutbrown and K. Rosser for help with the linac measurements and analysis, respectively. The authors would also like to acknowledge the financial support of the National Measurement Policy Unit of the United Kingdom Department of Trade and Industry.

REFERENCES

[1] WITTKAMPER, F.W., AALBERS, A.H.L., MIJNHEER, B., Experimental determination of wall correction factors. Part II: NACP and Markus plane-parallel ionization chambers, Phys. Med. Biol. **37** (1992) 995–1004.

[2] NYSTROM, H., KARLSSON, M., Correction factors applied to plane-parallel ionization chambers, Phys. Med. Biol. **38** (1993) 311–322.

[3] DuSAUTOY, A.R., The UK primary standard calorimeter for photon beam absorbed dose measurement, Phys. Med. Biol. **41** (1996) 137–151.

[4] McEWEN, M.R., WILLIAMS, A.J., DuSAUTOY, A.R., Determination of absorbed dose calibration factors for therapy level electron beam ionization chambers, Phys. Med. Biol. **46** (2001) 741–755.

[5] INTERNATIONAL ORGANIZATION FOR STANDARDIZATION, Guide to the Expression of Uncertainty in Measurement, 2nd edn, ISO, Geneva (1995).

[6] INTERNATIONAL ATOMIC ENERGY AGENCY, Absorbed Dose Determination in External Beam Radiotherapy, Technical Reports Series No. 398, IAEA, Vienna (2000).

[7] ANDREO, P., A comparison between calculated and experimental k_Q photon beam quality correction factors, Phys. Med. Biol. **45** (2000) L25–L38.

[8] PALM, A., MATTSON, O., ANDREO, P., Calibration of plane-parallel chambers and determination of p_{wall} for the NACP and Roos chambers for ^{60}Co γ-ray beams, Phys. Med. Biol. **45** (2000) 971–981.

[9] INTERNATIONAL ATOMIC ENERGY AGENCY, The Use of Plane Parallel Ionization Chambers in High Energy Electron and Photon Beams, Technical Reports Series No. 381, IAEA, Vienna (1997).

BLANK

NOVEL MICRO LIQUID IONIZATION CHAMBER FOR CLINICAL DOSIMETRY

K.J. STEWART, J.P. SEUNTJENS
McGill University Health Centre, Montreal General Hospital,
Montreal, Canada
E-mail: kristins@medphys.mcgill.ca

Abstract

The work investigates the characteristics of two novel liquid ionization chambers currently under development, the MicroLIC and the GLIC-02. The MicroLIC has a nominal sensitive volume of 1.12 mm^3 and is filled with isooctane. The energy response of this chamber was studied by cross-calibrating the MicroLIC against a calibrated Exradin A12 chamber in 6 MV and 18 MV photon beams from a Clinac 21EX. Ion recombination corrections were evaluated using the measured ionization current in Boag's theory for general recombination in gases. Results were compared with previous measurements carried out using another liquid filled chamber (LIC 9902-mix), with a liquid composition of 60% isooctane, 40% tetramethylsilane by weight. The ratio of the average beam quality conversion factors, 18 MV to 6 MV, was 0.982 ± 0.004 for the MicroLIC. This is in reasonable agreement with the ratio of the average beam quality conversion factors for the LIC 9902-mix (1.000 ± 0.003). These values indicate that, compared with gas filled chambers, the MicroLIC has superior energy dependence characteristics. Development of another novel chamber, the GLIC-02, is currently in progress. The properties of this chamber as an air filled detector have been investigated and compared with those of an Exradin A14P planar microchamber for the 6 MV and 18 MV photon beams from a Clinac 21EX. Results indicate that the GLIC-02 has characteristics equivalent to the A14P in terms of calibration factor, ion recombination and energy dependence and is superior in terms of polarity effect.

1. INTRODUCTION

Absorbed dose based protocols [1, 2] recommend the calibration of clinical linacs using air filled ionization chambers for which an absorbed dose to water calibration factor has been established in a ^{60}Co beam. The factor k_Q in these protocols involves the ratio of the mean restricted collision mass stopping power water to air, which is energy dependent. The stopping power ratio water to air varies by 4% for photon beams between ^{60}Co and 20 MV, whereas for electron beams the variation is even larger. For certain insulating liquids, however, the stopping power ratio water to liquid shows very little energy

dependence, making a liquid filled ionization chamber a potentially attractive dosimeter for clinical reference dosimetry. For the dosimetry of non-equilibrium fields (e.g. for small fields or for intensity modulated radiation therapy) air filled devices show significant perturbation effects, and, for these cases, a liquid filled dosimeter is particularly attractive. An additional advantage of using liquid filled chambers is that, owing to the high ionization density in liquids, very small volume detectors will still produce a sufficient signal for accurate measurements. Two guarded liquid ionization chambers currently under development, the MicroLIC and GLIC-02, are investigated in this paper. Ion recombination and energy dependence for the liquid filled MicroLIC are examined and the properties of the air filled GLIC-02 chamber are compared with a commercial chamber of similar volume before the GLIC-02 is filled with liquid.

2. MATERIALS AND METHODS

The linac used in this work was a Varian Clinac 21EX with nominal photon beam energies of 6 MV and 18 MV. Measurements were carried out in a 20 cm × 20 cm × 20 cm RMI Solid Water phantom at 10 cm depth with a 10 cm × 10 cm field at the phantom surface. Absorbed dose was determined using an Exradin A12 (SN 310) chamber with an absorbed dose to water calibration factor for ^{60}Co established at a primary standards laboratory. Corrections were applied for pressure, temperature, polarity and recombination in accordance with the TG 51 [1] protocol, and k_Q values from TG 51 were used along with a correction factor, k_{ph}, to account for differences in the interaction properties of Solid Water versus water. k_{ph} was determined by Seuntjens et al. [3] and was 1.000 and 1.006 for the 6 MV and 18 MV beams, respectively.

2.1. MicroLIC

The MicroLIC was developed using the Exradin A14P (SN 161) planar microchamber, which has a chamber body and electrodes composed of C552 plastic. The A14P was modified to reduce the gap between the cap and collecting electrode to 0.5 mm. The diameter of the collecting electrode was 1.5 mm and the nominal sensitive volume of 1.12 mm^3 was filled with isooctane. The energy response of the MicroLIC was compared with previous results [4] measured using the LIC 9902-mix, a chamber developed by G. Wickman of Umeå University, Sweden. The sensitive volume of the LIC 9902-mix has a diameter of 2.5 mm, thickness of 0.35 mm and is filled with 60% isooctane, 40% tetramethylsilane by weight.

2.1.1. Ion recombination

Johansson et al. [5] investigated general recombination in liquid ionization chambers by applying Boag's theory for gases. This method was initially followed for this work. The chamber response was studied as a function of polarizing voltage between 600 V and 1000 V. The source to surface distance (SSD) was set to 2 m to obtain a low dose per pulse, making general recombination negligible. The lowest pulse repetition frequency (100 MU/min setting) was used to ensure complete charge collection between pulses. The relation between the ionization current and electric field strength was linearly fitted such that $i = (c_1 + c_2 E)\dot{D}$, where i is the ionization current, E is the applied electric field and $\dot{D}$ is the dose rate. The fit constants depend only upon initial recombination and were determined at the low dose rate. Since they were assumed to be dose rate independent, they were used to determine the predicted ionization current in the absence of general recombination at a higher dose rate, which could then be inserted into Boag's formula [5] to determine the general collection efficiency. For this work, however, the predicted current was lower than the measured current, indicating that the Johansson model was inadequate to determine the current in the absence of general recombination. Therefore, for the purpose of this work, the general recombination was estimated using Boag's formula with the measured current.

2.1.2. Energy response

The response of the MicroLIC was measured on two separate days for the 6 MV and 18 MV beams with an SSD of 100 cm. The pulse rate setting was 100 MU/min, to enable complete charge collection between pulses. Measurements were taken with polarizing voltages of ±1000 V to account for polarity effects. The polarity effect in the liquid filled MicroLIC was less than 2% for all measurements, which is significantly less than the 21% polarity effect when the same chamber is filled with air. This difference is due primarily to the significantly larger signal obtained from the liquid filled chamber. Recombination was corrected for as described above.

2.2. GLIC-02

Using the knowledge gained through the work with the MicroLIC and LIC 9902-mix, and in order to address reproducibility issues with the MicroLIC, a new ionization chamber designed for use as a liquid ionization chamber was constructed. This chamber was inspired by some of the design characteristics of the Exradin A14P and is referred to as the GLIC-02 (which

stands for guarded liquid ionization chamber). It is a plane-parallel chamber with its body and electrodes made of C552 plastic and a nominal sensitive volume of 2 mm^3. Before filling the chamber volume with liquid, its characteristics as an air filled device were compared with those of the Exradin A14P (SN 164) chamber, which also has a nominal sensitive volume of 2 mm^3. Each chamber was cross-calibrated against the calibrated Exradin A12 chamber for both the 6 MV and 18 MV beams from the Clinac 21EX. Measurements were taken with polarizing voltages of ±300 V and +150 V, and corrections for polarity and ion recombination were calculated in accordance with the TG 51 protocol. Leakage current was also measured and subtracted from the signal for both chambers.

The response of the air filled GLIC-02 as a function of applied polarizing voltage was also studied. Measurements of chamber response were taken in the current mode for polarizing voltages from 100 V to 300 V in steps of 20 V for both polarities. The polarity effect was calculated for each voltage. It was possible, by plotting inverse current versus inverse voltage, to use a linear extrapolation to determine the saturation current and from this the collection efficiency as a function of applied voltage. Boag's theory of general recombination in gases was also used to evaluate the collection efficiency. In order to apply Boag's theory it was necessary to estimate the separation between the electrodes, and this was done through a measurement of the capacitance, assuming a perfect plane-parallel chamber.

3. RESULTS

3.1. MicroLIC

Figure 1(a) shows the MicroLIC current as a function of applied electric field measured at the low dose rate. The dose rates were 2.93 mGy/s and 3.57 mGy/s for the 6 MV and 18 MV beams, respectively; the fit constants are shown in Table I. The normalized beam quality conversion factors of the MicroLIC, LIC 9902-mix and Exradin A12 as a function of beam quality for photon beams are shown in Fig. 1(b). Values are normalized to the response for the 6 MV beam. Table II shows the ion recombination and polarity corrections applied to the MicroLIC measurements. Note that P_{ion} is determined using the measured ionization current, not the current in the absence of recombination estimated using Johansson et al.'s [5] model. As indicated by the error bars, there was close to a 1% variation in the response of the MicroLIC from one day of measurements to the next. This could not be explained by changes in the polarity effect, which were found to be less than 0.5%. Both the reproducibility

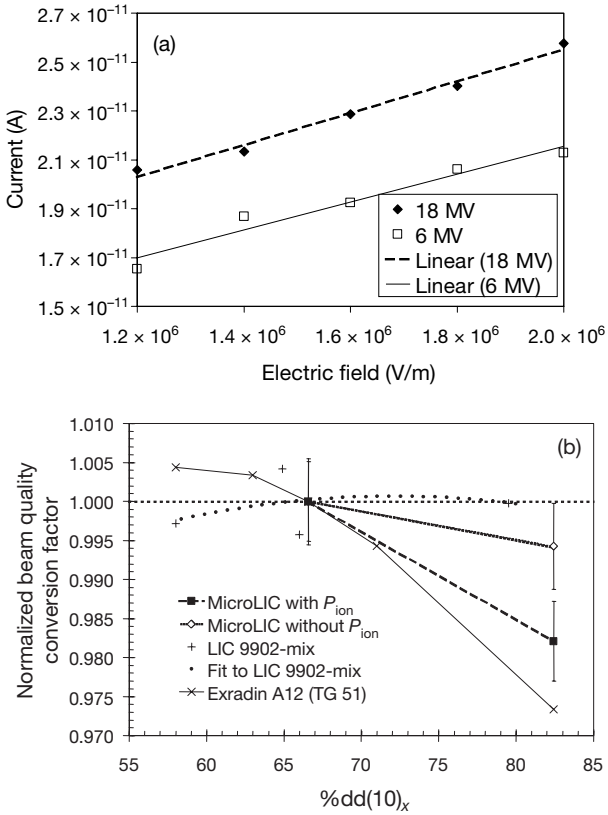

FIG. 1. (a) MicroLIC current as a function of applied electric field for 6 MV and 18 MV photon beams. (b) Normalized beam quality conversion factor as a function of beam quality for the MicroLIC, LIC 9902-mix and Exradin A12 [1] chambers normalized to the response for the 6 MV beam. MicroLIC measurements are shown with (filled symbols) and without (open symbols) the ion recombination correction applied. Polarity corrections were applied in all cases. Error bars indicate the range of variation in response from one day of measurements to the next.

issues with the MicroLIC and the problems observed regarding recombination for both the MicroLIC and the LIC 9902-mix triggered the development of the new GLIC-02.

3.2. Air filled GLIC-02

Table III shows the values of P_{ion}, P_{pol} and $N_{D,w}^{X}$ obtained for both the GLIC-02 and A14P from cross-calibration measurements. In addition, by taking

TABLE I. FIT CONSTANTS FROM MicroLIC RESPONSE AS A FUNCTION OF APPLIED ELECTRIC FIELD

	c_1 (C/Gy)	c_2 (C·m·Gy^{-1}·V^{-1})
6 MV	3.452×10^{-9}	1.953×10^{-12}
18 MV	3.493×10^{-9}	1.827×10^{-12}

TABLE II. ION RECOMBINATION AND POLARITY CORRECTIONS FOR THE MicroLIC FOR 6 MV AND 18 MV PHOTON BEAMS

	P_{ion} (day 1)	P_{ion} (day 2)	P_{pol}
6 MV	1.0091	1.0084	0.9909
18 MV	1.0219	1.0209	0.9950

TABLE III. VALUES OF P_{ion}, P_{pol} AND $N_{D,w}^{X}$ OBTAINED FOR THE GLIC-02 AND EXRADIN A14P CHAMBERS FROM THE CROSS-CALIBRATION MEASUREMENTS AGAINST THE EXRADIN A12 CHAMBER

(The ratio of absorbed dose calibration factors for the 18 MV and 6 MV beams is also shown. For the GLIC-02, values shown are averages from measurements on two different days.)

		GLIC-02	Exradin A14P
P_{ion}	18 MV	1.0000	1.0071
	6 MV	1.0002	1.0079
P_{pol}	18 MV	0.9976	1.1704
	6 MV	0.9869	1.1896
$N_{D,w}^{X}$ (cGy/nC)	18 MV	968.9	883.9
	6 MV	1002.7	907.5
Ratio of $N_{D,w}^{X}$	18 MV/6 MV	0.9663	0.9740

a ratio of absorbed dose calibration factors for the 18 MV and 6 MV beams, the energy dependence for each chamber over this energy range is shown. Differences between the values obtained on two separate days were less than 0.2% in all cases, indicating good reproducibility. The GLIC-02 has a significantly smaller polarity correction than the A14P (17% and 18% less for the 18 MV and 6 MV beams, respectively). The calibration factor of the GLIC-02 was 10% greater than that of the A14P, indicating a 10% smaller sensitive volume for the GLIC-02. In terms of the P_{ion} correction and energy dependence, the two chambers are very similar, with differences of less than 1%. In all measurements, for both chambers the leakage current was less than 0.2% of the measured signal and was corrected for.

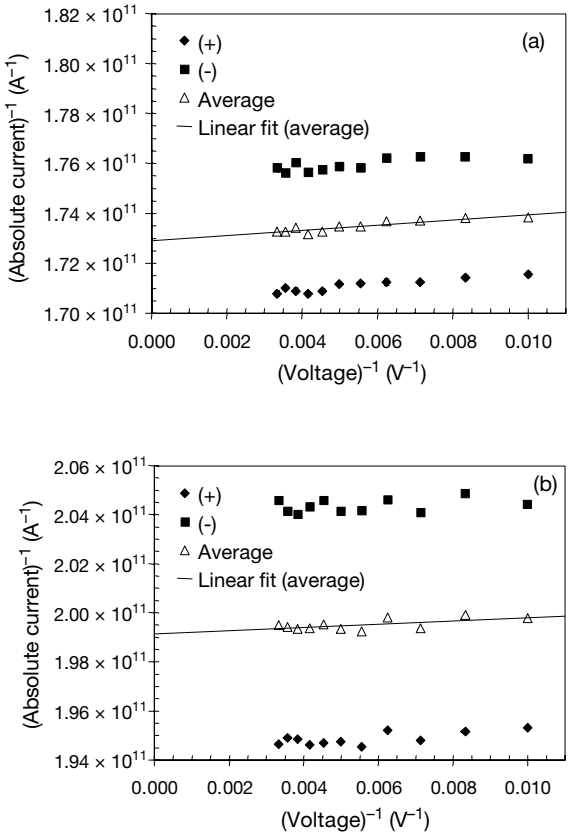

FIG. 2. Absolute value of the inverse current versus inverse voltage for the GLIC-02 chamber for the (a) 18 MV and (b) 6 MV beam. Both the positive (filled diamonds) and negative (filled squares) polarities as well as the average (open triangles) are shown. A fit to the average was used to determine the saturation current for calculating P_{ion}.

Figures 2(a) and (b) show the inverse current versus inverse voltage for the GLIC-02 for the 18 MV and 6 MV beams, respectively. A linear fit to the average of both polarities was used to determine the saturation charge by extrapolating to the intercept ($V \rightarrow \infty$). Values of P_{ion} calculated from this extrapolation are shown in Fig. 3(a). The gap between the electrodes was estimated from the capacitance measurements to be 0.7 mm, and using this in Boag's theory for general recombination the theoretical values of P_{ion} were obtained (shown in Fig. 3(a)). Given the relatively large uncertainty in the P_{ion} values determined using the extrapolation, there is reasonable agreement

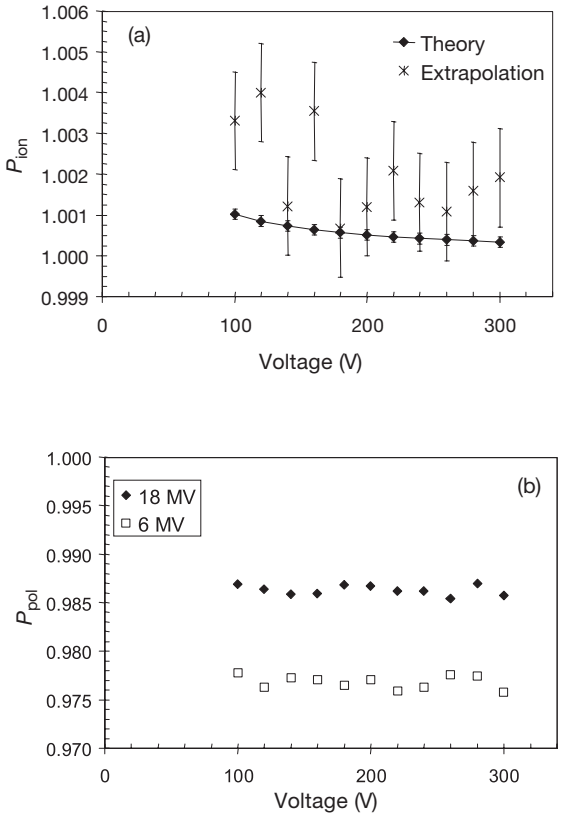

FIG. 3. (a) P_{ion} as a funcion of voltage for the 6 MV beam found using Boag's theory (filled symbols) and the extrapolated saturation current (crosses). The error bars represent the combined 1σ type A uncertainty resulting from both the measurements and the extrapolation procedure. (b) P_{pol} as a function of applied voltage for the 6 MV (open symbols) and 18 MV (filled symbols) beams.

between the values obtained from each method. The P_{ion} values at 300 V also agree to within 0.2% with those determined during cross-calibration by using the two voltage technique recommended in TG 51. Figure 3(b) shows the polarity effect for both 6 MV and 18 MV beams as a function of applied voltage. P_{pol} is independent of applied voltage and is less than 3% for both energies. Values for P_{pol} from this test agree to within 1% with the values found during the cross-calibration.

4. CONCLUSIONS

The ratios of the average beam quality conversion factors from 18 MV to 6 MV were 0.982 ± 0.004 for the MicroLIC and 1.000 ± 0.003 for the LIC 9902-mix. Comparing these results with the ratio for the air filled A14P chamber (0.973) indicates that liquid filled chambers, consistent with expectations, have superior energy dependence characteristics. The tests of the GLIC-02 as an air filled chamber indicate that it is a well behaved ionization chamber with characteristics equivalent to or, in the case of polarity effect, superior to those of the Exradin A14P, an air filled chamber of similar volume. We can now proceed to the next stage in the development of this chamber, which is to fill the sensitive volume of the GLIC-02 with insulating liquid and investigate its properties as a liquid filled chamber.

ACKNOWLEDGEMENTS

The authors would like to acknowledge the work of R. Van Gils in the construction of the GLIC-02 and the assistance of W. Abdel-Rahman with saturation and capacitance measurements for the GLIC-02. We would also like to thank the National Research Council of Canada and Standard Imaging, Inc., for providing on loan the modified Exradin A14P and Exradin A12 (SN310) chambers, respectively. Funding was provided by the American Association of Physicists in Medicine and the Radiological Society of North America through a pre-doctoral fellowship, and by the Natural Sciences and Engineering Research Council of Canada through research grant RG 227800. J.P. Seuntjens is a research scientist of the National Cancer Institute of Canada, with funds provided by the Canadian Cancer Society.

REFERENCES

[1] AMERICAN ASSOCIATION OF PHYSICISTS IN MEDICINE, AAPM's TG-51 protocol for clinical reference dosimetry of high-energy photon and electron beams, Med. Phys. **26** (1999) 1847–1870.

[2] INTERNATIONAL ATOMIC ENERGY AGENCY, Absorbed Dose Determination in External Beam Radiotherapy, Technical Reports Series No. 398, IAEA, Vienna (2000).

[3] SEUNTJENS, J., OLIVARES, M., EVANS, M., PODGORSAK, E., Dose transfer methods for QA procedures used in the clinical implementation of TG-51, Med. Phys. **28** (2001) 1289.

[4] STEWART, K.J., SEUNTJENS, J.P., ROSS, C.K., WICKMAN, G., Investigating a liquid ionization chamber as a beam quality independent dosimeter, Med. Phys. **28** (2001) 1244.

[5] JOHANSSON, B., WICKMAN, G., BAHAR-GOGANI, J., General collection efficiency for liquid isooctane and tetramethylsilane in pulsed radiation, Phys. Med. Biol. **42** (1997) 1929–1938.

CORRECTING FOR ION RECOMBINATION EFFECTS IN IONIZATION CHAMBERS CONSISTENTLY IN CONTINUOUS AND PULSED RADIATION

K. DERIKUM
Physikalisch-Technische Bundesanstalt,
Braunschweig, Germany
E-mail: klaus.derikum@ptb.de

Abstract

Incomplete charge collection in ionization chambers used in external beam radiotherapy is investigated. In ^{60}Co beams the relative charge loss due to volume recombination is of the order of 10^{-4} at dose rates below a few Gy/min. Depending on the chamber type and on the magnitude of the polarizing voltage, the relative charge loss due to initial recombination is up to 0.2%. Neglecting the effect of initial recombination when calibrating ionization chambers in ^{60}Co beams is a potential source of error for dose measurements in pulsed beams, for which the effects of volume recombination and initial recombination cannot be separated experimentally.

1. INTRODUCTION

Incomplete charge collection in an ionization chamber cavity requires the use of a correction factor, k_s. Different methods for deriving k_s are recommended in the IAEA code of practice in Technical Reports Series No. 398 [1], depending on whether the radiation is continuous or pulsed.

In pulsed beams the recombination correction factor is obtained experimentally by extrapolating the inverse of the chamber reading, M, as a function of the inverse of the polarizing voltage, U, to $1/U = 0$. This method accounts for initial and volume recombination and also for the charge loss by diffusion, since all effects depend linearly on $1/U$ in pulsed beams.

In continuous radiation, notably ^{60}Co beams, the recommended correction procedures are based on the linear dependence of $1/M$ on $1/U^2$. This accounts for the volume recombination only, neglecting the initial recombination and diffusion. These procedures are hence applicable only if the volume recombination is significantly more pronounced than the initial recombination. Furthermore, neglecting the initial recombination and the diffusion at the calibration is a potential source of inconsistencies if these effects are corrected in pulsed beams.

In this paper the magnitude of the two effects of charge recombination is studied for two types of ionization chamber commonly used in dosimetry for external beam radiotherapy. The readings of NE 2561 and NE 2571 ionization chambers were measured as a function of the polarizing voltage in ^{60}Co beams at various dose rates. The procedures for deriving recombination correction factors consistently in pulsed and continuous beams are discussed.

2. METHODS AND MATERIALS

2.1. Theory

The main mechanisms of charge loss are diffusion loss, initial recombination and volume recombination [2]. Close to saturation, the respective collection efficiencies may be calculated from:

$$f_d = 1 - 2kT/(Ue)$$

for diffusion loss [3] and:

$$f_i = 1 - E_i d/U$$

for initial recombination [4].

The volume recombination depends on the dose rate, whereas the diffusion loss and initial recombination do not [5]. The respective collection efficiency in pulsed beams is:

$$f_v(\text{pulsed}) = 1 - \tfrac{1}{2}\mu q d^2/U$$

if the pulse duration is shorter than the ion collection time and the ions produced by each pulse are collected before the next pulse occurs. In continuous radiation, the respective collection efficiency is:

$$f_v(\text{cont}) = 1 - \beta j d^4/U^2$$

where

e is the electron charge (1.6022×10^{-19} C);
k is the Boltzmann constant (1.3807×10^{-23} J/K);
T is the air temperature;

U is the polarizing voltage;
d is the effective electrode separation;
j is the current generated per volume;
q is the charge generated per volume and per pulse;
E_i, μ, β are constants.

The resulting total collection efficiency is the product of the three factors $f = f_i f_d f_v$. In pulsed beams it is a linear function of the reciprocal of the polarizing voltage:

$$f(\text{pulsed}) = 1 - a/U$$

where $a = 2kT/\text{e} + E_i d + ½\mu q d^2$.

In typical radiotherapy beams the relative charge loss due to volume recombination is about 0.4–0.7%. It can be concluded from previously published data [6] that the sum of the diffusion and initial recombination can be up to 0.2%, depending on the polarizing voltage applied.

In continuous radiation the total collection efficiency depends both linearly and quadratically on the polarizing voltage:

$$f(\text{cont}) = 1 - b/U - \beta j d^4/U^2$$

where $b = 2kT/e + E_i d$. The shape of the function depends on the magnitude of the coefficients b and β.

The charge loss due to diffusion and initial recombination is expected to be the same as in pulsed beams. Using $\beta = 6.73 \times 10^{13}$ V^2/(A·m) from Ref. [5], the relative charge loss due to the volume recombination can be expressed in terms of the absorbed dose rate to water, $\dot{D}_w$, at ^{60}Co:

$$\beta j d^4/U^2 = 2.1 \dot{D}_w d^4/U^2$$

where $\dot{D}_w$ is in Gy/s, d is in millimetres and U is in volts.

At 1 Gy/min, a dose rate typical for radiotherapy, the relative charge loss due to volume recombination is 7×10^{-5} for the chambers investigated (d = 3 mm, U = 200 V). The value of 0.1%, which is the magnitude of the relative charge loss due to the initial recombination, is reached at a dose rate above 14 Gy/min.

In typical ^{60}Co beams the reciprocal of the reading is expected to be an almost linear function of the reciprocal of the polarizing voltage, with deviations at low polarizing voltages that become more pronounced with increasing dose rates.

2.2. Experiment

The charge collected at a constant dose in ^{60}Co beams for NE 2561 and NE 2571 ionization chambers was measured as a function of the polarizing voltage at various dose rates.

The measurements were performed in a water phantom. The chambers were kept in close fitting polymethylmethacrylate (PMMA) sheaths with a wall thickness of 1 mm. The dose rate was varied from 0.03 Gy/min to 1.6 Gy/min using two ^{60}Co sources and varying the depth in the phantom and the source to phantom surface distance. The readings, *M,* were corrected for air density and ^{60}Co decay. Each value is the mean charge collected at the two polarities of the polarizing voltage.

3. RESULTS

Figure 1 shows $1/M$ versus $1/U$ for an NE 2561 ionization chamber for various dose rates. The curves are normalized to the readings at 100 V (M_{100V}). Figure 2 shows the corresponding curves for an NE 2571 ionization chamber.

In accordance with the expression for f(cont) described in Section 2.1, a second degree polynomial was fitted simultaneously on all the curves for one chamber type. The formula applied was:

$$M(U) = f(U)/f(U = 100\ \mathrm{V})$$

where $f(U) = 1 - b/U - \beta j d^4/U^2$.

For the chamber volumes (0.69 cm^3 for the NE 2571, 0.325 cm^3 for the NE 2561) and the effective electrode separations (d = 3 mm for both chamber types), the nominal values were used. The parameters fitted were b and β. The results were: NE 2561, b = 0.27 V, $\beta = 6.0 \times 10^{13}$ V^2/(A·m); NE 2571, b = 0.22 V, $\beta = 7.6 \times 10^{13}$ V^2/(A·m).

The results for the constant β describing the magnitude of the volume recombination deviate in both cases from the literature value by about 10%. This is consistent with theory, since only nominal values for the chamber geometries were used. The relative statistical standard uncertainties derived from the fit were 3% (1 standard deviation) for both constants.

At the largest dose rate investigated, 1.6 Gy/min, the charge collection efficiencies were:

$$f(\mathrm{NE\ 2561}) = 1 - 0.27U^{-1}\ \mathrm{V} - 3.8U^{-2}\ \mathrm{V}^2$$
$$f(\mathrm{NE\ 2571}) = 1 - 0.22U^{-1}\ \mathrm{V} - 5.2U^{-2}\ \mathrm{V}^2$$

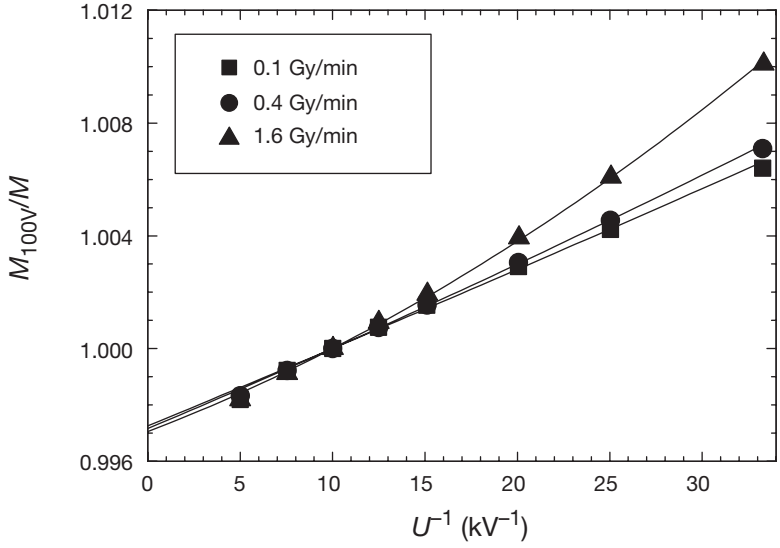

FIG. 1. Reciprocal of reading M (normalized to 1 at 100 V) as a function of the reciprocal of the polarizing voltage U for an NE 2561 ionization chamber in ^{60}Co radiation at different dose rates. The lines are a fit to the measured data.

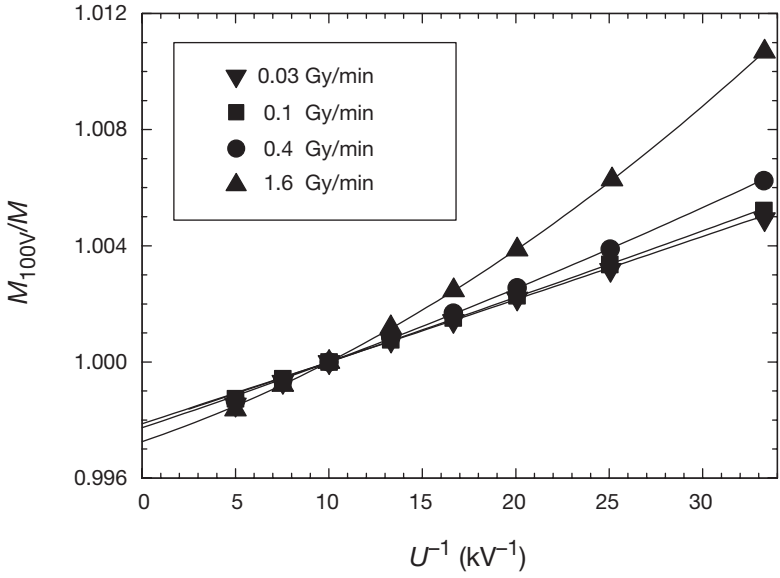

FIG. 2. Reciprocal of reading M (normalized to 1 at 100 V) as a function of the reciprocal of the polarizing voltage U for an NE 2571 ionization chamber in ^{60}Co radiation at different dose rates. The lines are a fit to the measured data.

For the NE 2561 chamber, when operated at 200 V, the correction for complete saturation was 0.15% and the portion of volume recombination was 0.01%. For the NE 2571 chamber, when operated at 300 V, the correction for complete saturation was 0.08% and the portion of volume recombination was less than 0.01%.

4. CONCLUSION

The effect of volume recombination in ^{60}Co beams can be neglected at dose rates below a few Gy/min. Correction procedures based on a linear dependence of $1/M$ on $1/U^2$ are not appropriate at such dose rates.

Neglecting the effect of initial recombination when calibrating ionization chambers in ^{60}Co beams is a potential source of error of up to 0.2% for dose measurements in pulsed beams, since the correction procedures applied in pulsed beams do not separate the effects of diffusion, initial recombination and volume recombination.

The relative charge loss due to initial recombination and diffusion can be determined experimentally by extrapolating the inverse of the chamber reading, M, as a function of the inverse of the polarizing voltage, U, to $1/U = 0$ in ^{60}Co beams at dose rates of less than 0.5 Gy/min.

For the ionization chambers most commonly used in external beam radiotherapy, a relative charge loss of 0.1% due to the initial recombination and diffusion is a good estimate for typical operating conditions.

REFERENCES

[1] INTERNATIONAL ATOMIC ENERGY AGENCY, Absorbed Dose Determination in External Beam Radiotherapy, Technical Reports Series No. 398, IAEA, Vienna (2000).

[2] BÖHM, J., Saturation corrections for plane parallel ionization chambers, Phys. Med. Biol. **21** (1976) 754–759.

[3] LANGEVIN, P., Mesure de la valence des ions dans les gaz, Le Radium **10** (1913) 113–118.

[4] KARA-MICHAILOVA, E., LEA, D.E., The interpretation of ionization measurements in gases at high pressures, Proc. Camb. Phil. Soc. **36** (1940) 101–126.

[5] BOAG, J.W., "Ionization chambers", The Dosimetry of Ionizing Radiation, Vol. 11 (KASE, K.R., BJARNGARD, B.E., ATTIX, F.H., Eds), Academic Press, London (1987) 169–243.

[6] DERIKUM, K., ROOS, M., Measurement of saturation correction factors of thimble-type ionization chambers in pulsed photon beams, Phys. Med. Biol. **38** (1993) 755–763.

BLANK

DEVELOPMENT OF CALIBRATION PROCEDURES FOR THE ELECTRON BEAM CALIBRATION OF PLANE-PARALLEL IONIZATION CHAMBERS

R. PARKKINEN, A. KOSUNEN, P. SIPILÄ, H. JÄRVINEN
Radiation and Nuclear Safety Authority (STUK),
Helsinki, Finland
E-mail: ritva.parkkinen@stuk.fi

Abstract

The change from ^{60}Co beam calibration to electron beam cross-calibration of plane-parallel chambers in Finland has improved the accuracy of dose measurements in hospitals. In comparative measurements at STUK and in Finnish hospitals the average difference decreased from 0.8% to negligible. The calibration procedure used until now has been the Technical Reports Series No. 381 (TRS 381) cross-calibration procedure. The first cross-calibrations based on TRS 398 have been carried out using the same high precision jig set-up developed for the calibrations carried out previously.

1. INTRODUCTION

Plane-parallel ionization chambers have been used in Finland for more than 20 years for absolute dose measurements in electron beams of radiation therapy accelerators for energies below 15 MeV. Before 1997 plane-parallel chambers were calibrated in a ^{60}Co gamma beam at the Finnish secondary standards dosimetry laboratory (STUK) for air kerma. Since 1999 all plane-parallel chambers have been calibrated by STUK in accelerator electron beams, and plane-parallel chambers have been used for measuring all electron energies.

The local absolute dose measurements (beam calibrations) at hospitals are verified every second year by independent dose measurements carried out by STUK using ionization chambers during a site visit. All absolute dose measurements are carried out in a water phantom. The acceptable conditions of the beam for the calibration are always verified by the measurement of beam profiles and depth doses.

Results in early comparisons revealed large discrepancies in comparative dose measurements, which led to the need for further investigations and to the development of calibration procedures in parallel with the development of international recommendations.

2. DEVELOPMENT OF CALIBRATION PROCEDURES

2.1. From ^{60}Co gamma beam calibrations to cross-calibrations in electron beams

The Nordic Association of Clinical Physics (NACP) recommendations for the calibration of plane-parallel chambers for air kerma in a ^{60}Co gamma beam were followed in Finland until 1997 [1]. On account of the results of studies by other groups and the large discrepancies in the comparative dose measurements observed in Finland, the individual behaviour of NACP plane-parallel chambers in a ^{60}Co gamma beam was studied in 1993 [2]. The results of this study indicated large (up to 3%) deviations between individual NACP plane-parallel chambers in the assumed chamber type specific factors (k_m and k_{att}). After a development period the cross-calibration procedure in electron beams was fully implemented in 1997, when Technical Reports Series No. 381 (TRS 381) [3] was published. All the plane-parallel chambers used in Finland were calibrated by the end of 1999 in accordance with the TRS 381 cross-calibration procedure.

2.2. Electron beam calibration with TRS 381

The first electron beam cross-calibrations were made with a manual set-up of the chambers, but it was uncertain whether repeatability was good enough. A high precision jig for plane-parallel chamber calibration (see Fig. 1) was therefore constructed during 1998. In the precision jig all the chambers are in fixed positions and the only movement in the calibration process is to slide a sledge to replace the reference cylindrical chamber (0.6 cm^3) with the plane-parallel chamber to be calibrated. In Fig. 1 the plane-parallel chamber is in the calibration position and the cylindrical reference chamber is out of the beam. When the sledge is moved left to its extreme position the cylindrical chamber is then in the calibration position and the plane-parallel chamber is out of the beam. Measurements are taken sequentially. The depths of the chambers in water are adjusted beforehand so that in the calibration process the chambers themselves remain in a fixed position. The effective points of the two chambers were adjusted to the same depth, z_{ref}, which is R_{100} or at least 2 cm, as recommended in TRS 381. Two monitoring chambers with a volume of 0.1 cm^3 were used to compensate for the beam output variations. The field size used was 20 cm × 20 cm. The reference chamber was a PTW 30002, with a graphite central electrode.

During 1999 TRS 381 was implemented in Finland and all 16 NACP type parallel-plate ionization chambers were calibrated both in the ^{60}Co beam at

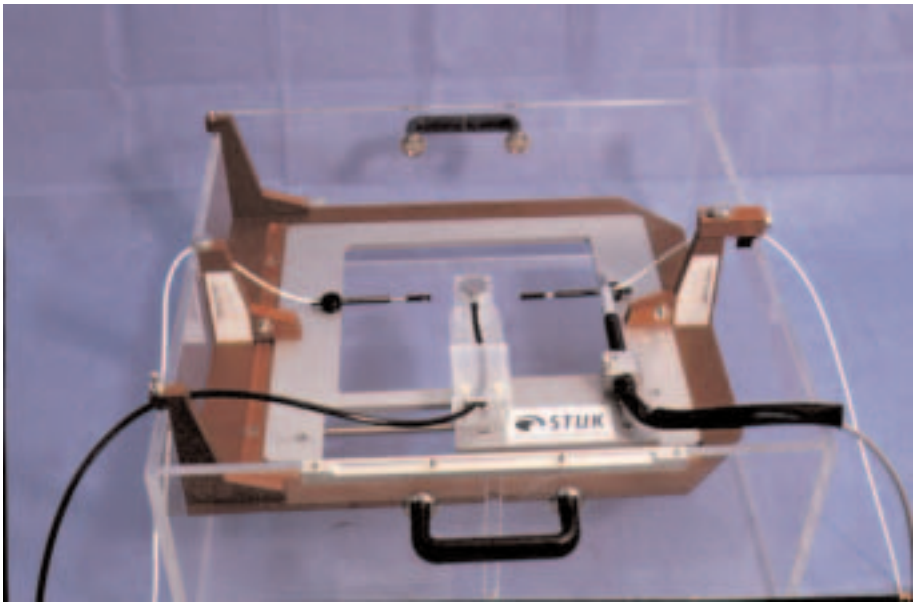

FIG. 1. The precision jig for plane-parallel chamber calibration.

STUK and in electron beams in hospitals. The calibration results are given in Fig. 2. The polarization effect of each chamber was determined during the electron beam calibration and the recombination effect was measured with several voltages. The results showed that none of the chambers had difficulties with the polarization effect and almost all chambers were ideal with the recombination effect. Two chambers had slight problems with recombination, and they stabilized very slowly after changing the voltage; these chambers were made by two different manufacturers.

It can be seen from Fig. 2 that the difference between the ^{60}Co beam calibration and the electron beam cross-calibration is due to the individual characteristics of the chamber and is not dependent on the chamber type. After calibration, comparative absolute dose measurements were continued during regular site visits by STUK staff. Absorbed dose to water was measured at the depth of dose maximum in water, as recommended in TRS 277 [4] and in TRS 381. The results of comparative absolute dose measurements with plane-parallel chambers are shown in Fig. 3. Results from 1995 to 1999 with the ^{60}Co calibration (No. = 136) showed a 0.8% average difference (1.4% standard deviation), and from 1999 to 2001 with electron beam calibration (No. = 126) a 0.0% average difference (0.7% standard deviation).

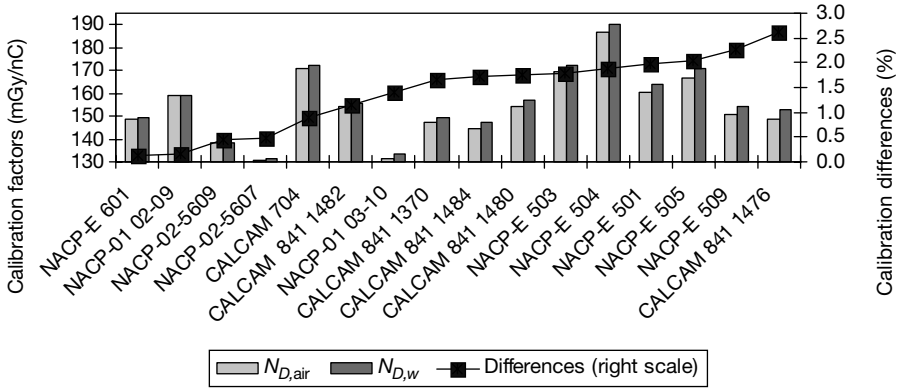

FIG. 2. Differences in calibration factors between calibration in a ^{60}Co beam and in a user's electron beam in accordance with TRS 381.

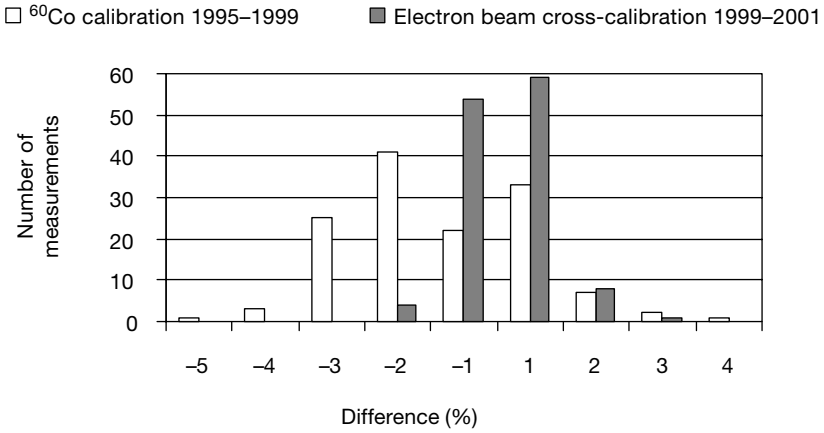

FIG. 3. Differences between absolute dose values in electron beams measured by STUK and by Finnish hospitals. Measurements are carried out with NACP type plane-parallel chambers during site visits to the hospitals. The average dose difference was 0.8% with ^{60}Co beam calibrations and 0.0% with electron beam cross-calibrations.

2.3. Preparation for electron beam cross-calibration based on the recommendations of TRS 398

TRS 398 [5] will be implemented in Finland from the beginning of 2003. In August 2002 the first plane-parallel chambers were calibrated following the

new protocol with the high precision jig. The only change in the calibration procedure is the use of z_{ref}, as recommended by TRS 398, instead of the depth of dose maximum recommended in TRS 381. As previously, the depth ionization curve is measured with a plane-parallel chamber before the calibration set-up. The beam profiles are also checked with a small ionization chamber.

At the preliminary stage (before August 2002), absorbed doses at all electron energies above 15 MeV were determined during on-site visits from measurements at the depth of dose maximum and additionally at depths of z_{ref}, as required by TRS 398. Absorbed dose to water values at both depths were calculated in accordance with the recommendations of TRS 277. The absorbed dose to water values obtained at depths of z_{ref} were then recalculated to the depth of dose maximum using depth dose data, and the possible dose differences at a depth of dose maximum were analysed. Preliminary results showed slight differences between the measured and recalculated data, of about 0.3%. This difference can mostly be attributed to the effect of positioning the chamber at the reference depth. The accurate positioning of the chamber at the depth of dose maximum for higher electron energies is not critical, as the area of the dose maximum is quite large. However, if the measurement is made at the descending part of the depth dose curve, as is required by TRS 398, accurate positioning becomes much more important.

3. CONCLUSIONS

Discrepancies of 3% or more in comparative electron dose measurements in Finnish hospitals initiated investigations and the development of new calibration procedures. Cobalt-60 beam calibration was replaced with electron beam cross-calibration, and the repeatability of the procedure was improved with the use of a high precision jig. TRS 398 recommends using the reference depth in dose measurements, which for energies above 15 MeV is deeper than the dose maximum, and the set-up accuracy has become more critical in dose measurements. This is especially important if a proper computerized water phantom is not available.

REFERENCES

[1] NORDIC ASSOCIATION OF CLINICAL PHYSICS, Electron beams with mean energies at the phantom surface below 15 MeV: Supplement to the recommendations by the NACP (1980), Acta Radiol. Oncol. **20** (1981) 401–415.

[2] KOSUNEN, A., JÄRVINEN, H., SIPILÄ, P., "Optimum calibration of NACP type plane parallel ionization chambers for absorbed dose determination in low energy electron beams", Measurement Assurance in Dosimetry (Proc. Symp. Vienna, 1993), IAEA, Vienna (1994) 505–513.

[3] INTERNATIONAL ATOMIC ENERGY AGENCY, The Use of Plane Parallel Ionization Chambers in High Energy Electron and Photon Beams, Technical Reports Series No. 381, IAEA, Vienna (1997).

[4] INTERNATIONAL ATOMIC ENERGY AGENCY, Absorbed Dose Determination in Photon and Electron Beams, 2nd edn, Technical Reports Series No. 277, IAEA, Vienna (1997).

[5] INTERNATIONAL ATOMIC ENERGY AGENCY, Absorbed Dose Determination in External Beam Radiotherapy, Technical Reports Series No. 398, IAEA, Vienna (2000).

ACCURATE CHARACTERIZATION OF KILOVOLTAGE X RAY UNITS FOR DOSIMETRY USING MONTE CARLO SIMULATIONS

L. BEN OMRANE*, F. VERHAEGEN**, A.E. NAHUM***,
N. CHAHED*, S. MTIMET*

* Centre national de radioprotection,
Tunis, Tunisia
E-mail: sadok.mtimet@rns.tn

** Montreal General Hospital, McGill University,
Montreal, Canada

*** Fox Chase Cancer Center,
Philadelphia, Pennsylvania,
United States of America

Abstract

The aim of the work was to determine the phase space from a kilovoltage X ray unit for use in dose calculations. The BEAM/EGS4 Monte Carlo radiation transport code was used to model a calibration X ray unit by incorporating the primary electron beam, the tungsten target, the beryllium window, the collimating devices, the additional filters, the diaphragm, the monitor chamber and the water phantom. Spectra were calculated by Monte Carlo simulation for six X ray beam qualities (kVp: 70–150 kV, half-value layer (HVL): 3.3 mm Al–2.2 mm Cu). The calculated HVLs and air kerma show agreement with experimental values to within 3.5% and 2.8%, respectively. Percentage depth dose data in a water phantom were derived using the modelled phase space and show very good agreement with measured values. It is concluded that, in the dosimetry of kilovoltage X ray beams, the use of Monte Carlo derived phase space data for phantom and in vivo dosimetric calculations is an excellent substitute for the often technically demanding experimental investigations.

1. INTRODUCTION

Knowledge of beam characteristics is important for accurate dose calculations and is essential for calibrating units. This includes the precise determination of the energy and angular and spatial distributions of particles in the beam. Monte Carlo simulation is currently the most accurate method to provide complete phase space data to characterize a radiation beam.

In this work the calibration X ray unit at the Centre national de radioprotection secondary standards dosimetry laboratory (SSDL) was modelled using the Monte Carlo code BEAM/EGS4 [1]. A full simulation of the transport of the particles was performed from the head of the machine and through the different components of its geometry. The phase space was investigated to provide X ray energy spectra in air for the existing beam qualities. To validate our model, first half-value layers (HVLs), second HVLs and air kerma were calculated and compared with measurements. The resulting phase space was then used to compute relative dose distributions in water.

2. METHODS AND MATERIALS

2.1. Measurements

The measurements were performed in the SSDL using an X ray machine (Pantak hf160) with a tube potential varying between 40 kV and 160 kV. The tube had a tungsten target angled at 20° and a focus size of 3 mm × 3 mm. The exit window was 1 mm of beryllium. Two collimators, additional filters, a diaphragm, a monitor chamber and a water phantom were in place.

First and second HVLs were measured for the beam qualities described in Table I using a Farmer NE 2571 ionization chamber and high purity

TABLE I. RADIATION QUALITIES FOR THE PANTAK hf160 X RAY UNIT

(First HVLs and second HVLs were measured (in either mm Al or mm Cu). The homogeneity coefficients (HCs) for the measured (aluminium or copper) HVLs are given.)

Tube potential (kV)	Added filtration (mm)	First HVL (mm)	Second HVL (mm)	Measured HC
70	0.1 Cu + 1 Al	3.3 Al	4.3 Al	0.76
80	0.1 Cu + 1 Al	3.75 Al	5.00 Al	0.75
100	0.1 Cu + 1 Al	4.70 Al–0.17 Cu	6.45 Al–0.3088 Cu	0.73 (Al)–0.55 (Cu)
120	0.1 Cu + 1 Al	5.50 Al–0.2225 Cu	7.60 Al–0.4475 Cu	0.72 (Al)–0.50 (Cu)
135	0.25 Cu + 1 Al	8.35 Al–0.435 Cu	10.15 Al–0.765 Cu	0.82 (Al)–0.57 (Cu)
150	2.5 Sn + 1 Al	2.2 Cu	2.35 Cu	0.94

aluminium and copper sheets, in accordance with the procedure outlined by various dosimetry protocols [2–5]. The air kerma was measured at a 100 cm focus to surface distance (FSD) with the same (NE 2571) chamber that was calibrated at the IAEA Laboratory. The corresponding uncertainty was 1.5% (95% confidence level).

This chamber was also used to measure the percentage depth dose (PDD) distribution in a water phantom of 30 cm × 30 cm × 30 cm. It can be noted that the first measurement depth in our phantom was limited to 2.5 cm. All the data were therefore normalized to this depth.

2.2. Monte Carlo simulations

The BEAM/EGS4 [1] Monte Carlo code was used to model the X ray unit. The code performs coupled electron–photon transport. All the interactions were considered except Rayleigh (i.e. coherent) scattering. The following values of the EGS4 [6] (Electron Gamma Shower Version 4) parameters were chosen: AE = ECUT = 0.521 MeV, AP = PCUT = 0.010 MeV.

Using the resulting phase space data, the BEAMDP code [7] was used to calculate photon fluence spectra in air and the mean photon energy, with a standard deviation of 0.3%. The first and second HVLs were derived from these spectral distributions using an iterative method. For each modelled photon fluence spectrum at an FSD of 100 cm, the air kerma was calculated from:

$$K_{\text{air}} = \sum_{i=1}^{N} \varphi(E_i) E_i \frac{\mu_{\text{en}}(E_i)}{\rho} \Delta E_i$$

where $\varphi(E_i)$ is the photon fluence in the bin with energy E_i and $(\mu_{\text{en}}/\rho)(E_i)$ is the mass energy absorption coefficient for air at energy E_i, interpolated from the Hubbell and Seltzer data [8].

The unit of the calculated air kerma was given in mGy/mAs, if it is assumed that the current is obtained from equating one electron with 1.6×10^{-16} mAs.

The dose distribution was calculated in a water phantom of 17 cm radius and 30 cm length. The phantom resolution was 0.2 cm along the z axis up to a depth of 10 cm. Then, for the final 20 cm, the resolution was 1 cm. The uncertainty in depth dose calculations was 0.3% (1 standard deviation) at the normalization depth and reached 2% at a depth of 25 cm.

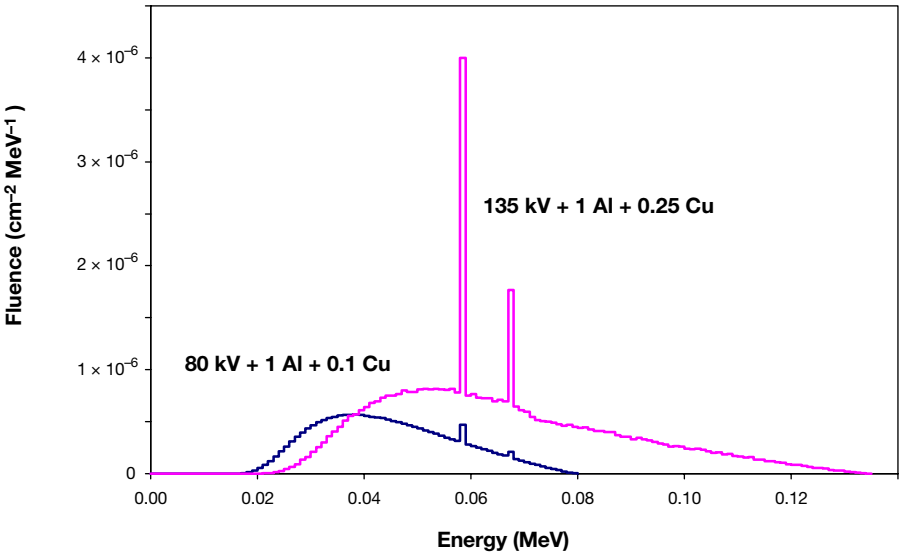

FIG. 1. Photon energy fluence spectra in air calculated by the BEAM/EGS4 Monte Carlo code for two X ray beam qualities with different kVp and added filtration.

3. RESULTS AND DISCUSSION

Figure 1 shows calculated photon fluence spectra in air for the modelled X ray unit for two of the radiation qualities given in Table I. It was noticed [9] that in this code the four characteristic photon peaks were assigned to only two energy bins: the $K\alpha_1$ (59 keV) and $K\alpha_2$ (58 keV) lines were grouped together and the $K\beta_1$ (67 keV) and $K\beta_2$ (69 keV) lines were grouped together. Furthermore, it was shown in Ref. [9] that the contribution to the characteristic peak was too low, owing to the electron impact ionization process not being modelled in EGS4.

Table II shows the mean photon energy, the first and second HVLs and the homogeneity coefficient (HC) calculated for each predicted spectrum. The overall agreement between calculated to measured HVLs was within 3.5%, except for the 100 kV and 120 kV qualities, for which the deviation was up to 5.3% for aluminium but in good agreement for copper. Also, good results for air kerma were shown, with a maximum deviation of 2.8% between the measured and calculated values. In a similar study, Verhaegen et al. [9] found good agreement between measured and calculated spectra and HVLs for two kilovoltage X ray units.

The relative dose distribution in water is shown in Fig. 2. Generally, good agreement was found between the calculated and measured PDDs: for 120 kV the deviation was less than 1.5% for up to 12.5 cm deep in the water phantom and reached 4% maximum at some depths. For the qualities less than 120 kV the deviation was up to 3% for up to 12.5 cm and reached 5%. It is known that accurate measurements of relative depth dose curves for low and medium energy X rays are very difficult, owing to the rapid decrease of the dose rate and the energy dependence of most practical detectors. However, the NE 2571 ionization chamber has a fairly flat energy response in this energy range and allows accurate measurements of doses in regions in which the dose rate does not change rapidly [10, 11]. Consequently, the normalization depth in this work (2.5 cm), which is very close to the reference point (2 cm) recommended for medium energies in the recent codes of practice for kilovoltage X ray beams, seems to give accurate results.

4. CONCLUSIONS

The phase space of the Pantak kilovoltage unit was modelled using the BEAM/EGS4 Monte Carlo code. Good agreement was found between simulations and experimental results, either for HVLs or for absolute dosimetric quantities such as air kerma.

TABLE II. VALUES OF THE MEAN ENERGY OF THE PHOTON FLUENCE SPECTRA, THE FIRST AND SECOND HVLs IN ALUMINIUM AND COPPER CALCULATED FROM THE MODELLED PHASE SPACE
(The HCs are given for the calculated HVLs. The last column gives the difference between the calculated and the measured air kerma.)

Tube potential (kV)	Mean photon energy (keV)	First HVL (mm)	Second HVL (mm)	HC (calculated)	Air kerma (calculated/ measured) (%)
70	41	3.18 Al	4.16 Al	0.76	2.8
80	45	3.63 Al	4.87 Al	0.75	2.1
100	50	4.45 Al–0.1714 Cu	6.21 Al–0.3067 Cu	0.72 (Al)–0.56 (Cu)	1.7
120	56	5.26 Al–0.2212 Cu	7.40 Al–0.4338 Cu	0.71 (Al)–0.51 (Cu)	1.6
135	65	8.08 Al–0.4359 Cu	9.84 Al–0.7458 Cu	0.82 (Al)–0.58 (Cu)	0.1
150	117	2.2789 Cu	2.3881 Cu	0.95	1.6

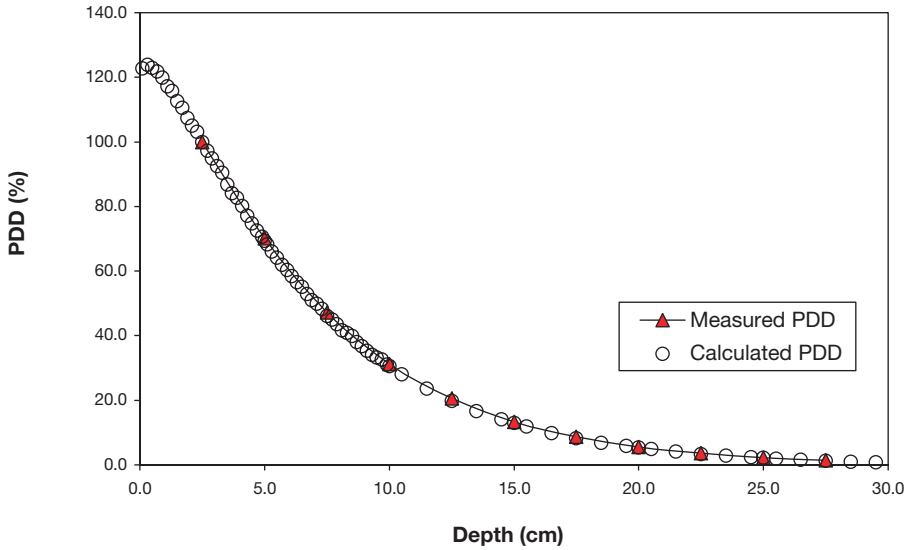

FIG. 2. Percentage depth doses calculated by the BEAM/EGS4 Monte Carlo code and measured in a water phantom, with a field of 10 cm radius at a source to surface distance of 100 cm. The beam quality is 100 kV, 1 mm Al + 0.1 mm Cu added filtration (HVL: 4.7 mm Al).

Simulations performed with the modelled phase space gave good results for PDDs in water, especially for low energy kilovoltage X ray beam (up to 160 kV, HVL of up to 8 mm Al) photons. Monte Carlo simulation is the only simple method of obtaining absorbed dose distributions and photon energy and angular distributions in water. Furthermore, the modelled phase space accurately characterizes the X ray beam and is clearly acceptable for use in dose calculations for kilovoltage X ray dosimetry.

REFERENCES

[1] ROGERS, D.W.O., et al., BEAM: A Monte Carlo code to simulate radiotherapy treatment units, Med. Phys. **22** (1995) 503–524.

[2] INTERNATIONAL ATOMIC ENERGY AGENCY, Calibration of Dosimeters Used in Radiotherapy, Technical Reports Series No. 374, IAEA, Vienna (1994).

[3] INSTITUTION OF PHYSICS AND ENGINEERING IN MEDICINE AND BIOLOGY, Code of practice for the determination of absorbed dose for x-rays below 300 kV generating potential, Phys. Med. Biol. **41** (1996) 2605–2625.

[4] NEDERLANDSE COMMISSIE VOOR STRALINGSDOSIMETRIE, Dosimetry of Low and Medium Energy X-rays, a Code of Practice for Use in Radiotherapy and Radiobiology, Rep. 10, NCS, Delft (1997).
[5] MA, C.M., et al., AAPM protocol for 40–300 kV x-ray beam dosimetry in radiotherapy and radiobiology, Med. Phys. **28** (2001) 868–893.
[6] NELSON, W.R., HIRAYAMA, H., ROGERS, D.W.O., The EGS4 Code System, Rep. SLAC-265, Stanford Linear Accelerator Center, Stanford, CA (1985).
[7] MA, C.M., ROGERS, D.W.O., BEAMDP Users Manual, Rep. PIRS-0509(C), National Research Council, Ottawa (1995).
[8] HUBBELL, J., SELTZER, S., Tables of X-ray Mass-attenuation Coefficients and Mass-energy-absorption Coefficients 1 keV to 20 MeV for Elements Z = 1 to Z = 92 and 48 Additional Substances of Dosimetric Interest, Rep. NISTIR 5632, International Institute for Standards and Technology, Gaithersburg, MD (1995).
[9] VERHAEGEN, F., NAHUM, A.E., VAN DE PUTTE, S., NAMITO, Y., Monte Carlo modelling of kV x-ray units, Phys. Med. Biol. **44** (1999) 1767–1789.
[10] SEUNTJENS, J.P., VERHAEGEN, F., Dependence of overall correction factor of a cylindrical ionization chamber on field size and depth in medium energy x-ray beams, Med. Phys. **23** (1996) 1789–1796.
[11] MA, C.M., NAHUM, A.E., Calculations of ion chamber displacement effect corrections for medium-energy X-ray dosimetry, Phys. Med. Biol. **40** (1995) 45–62.

BLANK

COMPARISON OF CALIBRATION COEFFICIENTS IN THE IAEA/WHO NETWORK OF SECONDARY STANDARDS DOSIMETRY LABORATORIES

A. MEGHZIFENE, L. CZAP, K.R. SHORTT
Division of Human Health, International Atomic Energy Agency, Vienna
E-mail: a.meghzifene@iaea.org

P. ANDREO
Medical Radiation Physics,
University of Stockholm–Karolinska Institute,
Stockholm, Sweden

Abstract

The paper describes the methodology, measurements, evaluation and analysis of the results of the IAEA programme for the comparison of calibration coefficients for radiotherapy dosimetry in the IAEA/World Health Organization network of secondary standards dosimetry laboratories (SSDLs). A pilot study was initiated in 1995 and the comparison programme started in 1997. In this programme ionization chambers that belong to the SSDLs are calibrated sequentially at the SSDL, at the IAEA and again at the SSDL. Since 1997, 42 SSDLs have participated in this comparison programme, although only 34 laboratories have effectively completed the process. The results from six participants were outside the acceptance limit set by the IAEA, but the follow-up process has improved the calibration procedures at these SSDLs. The results of the comparison, grouped according to the traceability of the SSDL measurements, are presented and discussed. As part of its own quality assurance programme, the IAEA participated in a regional comparison organized by the Sistema Interamericano de Metrología (SIM, the regional metrology organization for the Americas) from 2000 to 2002, in which four SSDLs from Latin America also participated. Taking into account the differences in the primary standards to which the various SSDLs are traceable, the results of the IAEA–SIM comparison show good consistency and demonstrate the robustness of the international measurement system in radiotherapy dosimetry.

1. INTRODUCTION

The IAEA and the World Health Organization (WHO) established a network of secondary standards dosimetry laboratories (the IAEA/WHO SSDL network) in 1976. Through SSDLs designated by Member States, this network provides a direct link of national dosimetry standards to the international

measurement system of standards traceable to the Bureau international des poids et mesures (BIPM). In this way, through the proper calibration of field instruments, the SSDLs [1] disseminate SI quantities and units. During the decade that followed the establishment of the network, the activities of the IAEA towards the SSDLs aimed mainly at the establishment of the necessary laboratory infrastructures and training of staff in calibration techniques, especially in developing countries. Since then, many laboratories have joined the network, and the scope of their work is expanding continuously. To ensure that the services provided by SSDL members to end users follow internationally accepted standards, the IAEA has set up two different comparison programmes. One programme relies on the IAEA/WHO postal thermoluminescence dosimetry service [2] and the other uses ionization chambers to help the SSDLs verify the integrity of their national standards and the procedures used for the transfer of the standards to the end users. An initial programme, based on a 'travelling set' consisting of an electrometer and an ionization chamber, was introduced in 1986, but it was discontinued for reasons of cost and reliability. In 1995 a new programme was initiated using ionization chambers that belong to the SSDLs. The results of the trial comparisons were published in the SSDL Newsletter [3].

Today the IAEA comparisons include ^{60}Co air kerma (N_K) and absorbed dose to water ($N_{D,w}$) coefficients. Prior to the publication of the IAEA code of practice in Technical Reports Series No. 398 [4], which is based on $N_{D,w}$ standards, the SSDLs were explicitly requested to disseminate only N_K coefficients to hospitals. The IAEA supplied the SSDLs $N_{D,w}$ coefficients, but only for their own development of the absorbed dose to water calibration technique. This request was published in the SSDL Newsletter [5]. When the IAEA introduced the comparison programme in 1995, less than 20% of the SSDLs had an ionization chamber calibrated in terms of $N_{D,w}$. SSDLs that were involved in radiotherapy dosimetry quality assurance programmes, and that did not have a traceable $N_{D,w}$ coefficient, determined a calculated $N_{D,w}$ using a code of practice based on N_K, such as that in Technical Reports Series No. 277 [6]. Participation of the SSDLs in the comparison programme is encouraged by the IAEA, and the laboratories are requested to provide details on the type of absorbed dose to water coefficient used. During the past two years about 75% of the SSDLs that have participated in the comparison programme have used $N_{D,w}$ calibrations traceable to the BIPM or to another primary standards dosimetry laboratory (PSDL). There is a clear trend in the dissemination of absorbed dose to water calibration coefficients by the SSDL members of the IAEA/WHO network. In this study only the results of $N_{D,w}$ comparisons based on absorbed dose to water standards are reported. The results of SSDLs that used a calculated $N_{D,w}$ are not included.

Following an invitation by the Comité international des poids et mesures (CIPM), the IAEA signed the Mutual Recognition of National Measurement Standards and of the Calibration and Measurement Certificates Issued by National Metrology Institutes (the mutual recognition arrangement, or MRA) [7] for the IAEA/WHO network of SSDLs. When the IAEA organizes dosimetry comparisons with the SSDLs it is effectively functioning as an international metrology organization. By including in such comparisons laboratories that have taken part in other CIPM comparisons, the IAEA provides a strong link to the MRA for its Member States that are not members of the Metre Convention, since they would otherwise be excluded. This action should bring benefits to those SSDLs in terms of strengthening their position as the dosimetry reference for their country [8].

The results of the comparisons are confidential and are communicated only to the participants. This is to encourage participation of the laboratories and their full co-operation in the reconciliation of any discrepancy. Because the anonymous results are presented as ratios of SSDL stated coefficients to IAEA determined coefficients, these cannot be used to support the calibration and measurement capabilities (CMCs) of the participating laboratories. This is one of the points that need to be addressed in the near future, as a result of the signing of the MRA by the IAEA.

Following its activities within the MRA, the IAEA has developed its own CMCs. These have been accepted and appear on the BIPM key comparison database. For air kerma and absorbed dose to water calibrations, the IAEA CMCs are supported by comparisons with the regional metrology organization for the Americas (Sistema Interamericano de Metrología (SIM)). The results of the SIM comparison have been published elsewhere [9], and this paper focuses on their consistency with the IAEA comparisons.

2. IAEA COMPARISON PROCEDURE

Prior to sending the selected transfer ionization chamber to the IAEA, the SSDLs are requested to make a check source measurement and calibrate the chamber in terms of N_K and $N_{D,w}$. The calibrations at the SSDLs and the IAEA are carried out under identical reference conditions [10].

The ionization chamber is sent to the IAEA for calibration along with a data sheet that includes information from the SSDL about the chamber and its traceability, the results of the check source measurements and the results of the calibrations, including their estimated uncertainties. After the chamber is calibrated at the IAEA, it is returned to the SSDL for a redundant check source measurement and recalibration. The SSDL reports the results of the

redundant checks and calibrations to the IAEA. To some extent the redundant calibrations provide an indication of the reproducibility of the SSDLs' measurement techniques and the stability of the chamber. The results are analysed at the IAEA and transmitted to the participants individually. Taking into account a previous analysis by the IAEA [11], which showed that a combined standard uncertainty of about 0.8% was achievable at the SSDLs for the calibration of dosimeters used in radiotherapy, the IAEA has set up an acceptance level of 1.5% for the results of comparisons. The additional uncertainty due to the calibration at the IAEA of the SSDL's chamber is not expected to increase the uncertainty of the ratio significantly. SSDLs with results outside the acceptance limit are advised to review their calibration procedures, although they are not informed of the magnitude and sign of the discrepancy; an additional comparison is organized to help resolve the discrepancy.

Some SSDL members of the IAEA/WHO network do not establish their traceability to the BIPM, neither directly nor through the IAEA, and instead are traceable to another PSDL. Consequently it is necessary to account for any difference between the particular standard at the PSDL used by the SSDL and the corresponding standard of the IAEA. Only six SSDLs were found to be in this category.

In the IAEA–SIM comparison the IAEA calibrated three Exradin A12 ionization chambers in September 2000 and in March 2002. The same chambers were calibrated by five other laboratories (the National Institute of Standards and Technology (NIST) in the United States of America and four SSDLs in Latin America), in addition to the National Research Council (NRC) of Canada, which was the organizing laboratory.

3. RESULTS AND DISCUSSION

From 1997 to 2002, 34 laboratories completed the IAEA comparison programme. For the purpose of this work the laboratories are grouped according to their traceability:

(a) Group 1: Laboratories traceable to the BIPM through the IAEA (22 SSDLs).
(b) Group 2: Laboratories traceable directly to the BIPM (six).
(c) Group 3: Laboratories traceable to other PSDLs (six[1]).

[1] Among these six laboratories, one SSDL provides only air kerma calibrations.

The results of the comparison are given as ratios of the calibration coefficients (N_K or $N_{D,w}$) obtained by the SSDL to those determined by the IAEA. The SSDLs are requested to report the uncertainty of their calibrations in the comparison data sheet. Unfortunately, very few SSDLs report their uncertainty values, as the majority have not yet determined their uncertainty budget. The uncertainty of the mean value of the two SSDL calibrations (pre- and post-IAEA calibration) is determined at the IAEA by analysing the results reported by the SSDL. The component of this uncertainty due to the statistical variation of the results is combined with the statistical uncertainty of the calibration coefficient determined at the IAEA and with the statistical uncertainty arising when the SSDL standards are traceable to a PSDL other than the BIPM. These three components are added in quadrature and yield the combined statistical uncertainty of the ratio of the calibration coefficients of the SSDL and the IAEA. If the dosimetry standards of the SSDL are traceable to the BIPM directly, the combined statistical uncertainty will have only two components. In addition to the statistical uncertainty, the uncertainty of the long term stability of the standards, both at the IAEA and the SSDL, is also included and combined in quadrature to determine the overall uncertainty of the ratio. These overall uncertainties are included in Figs 1–4.

Figures 1(a) and (b) show the results for SSDLs that are traceable to the BIPM through the IAEA. These results were obtained following the resolution of discrepancies with some of the participants. It can be seen that, although all participants were within the 1.5% acceptance limit set by the IAEA, only 50% of the SSDLs' coefficients agreed with those of the IAEA within the overall uncertainty of the calibrations, as determined by the IAEA. The results for absorbed dose to water (Fig. 1(b)) were comparable with those of air kerma (Fig. 1(a)). The spread of the results and the percentage of SSDLs whose calibrations agree with those of the IAEA are not significantly different in the two cases, for $N_{D,w}$ and N_K.

The results of the comparisons with SSDLs of group 2 (directly traceable to the BIPM) are shown in Figs 2(a) and (b). Although the number of SSDLs in this group is significantly smaller than those of group 1, the percentage of SSDLs whose calibrations agree with those of the IAEA, within the uncertainty of measurements, is about the same.

The results of the comparisons with SSDLs of group 3 (traceable to PSDLs other than the BIPM) are shown in Figs 3(a) and (b). For these SSDLs it is necessary to account for any difference between the particular standard at the PSDL used by the SSDL and the corresponding standard of the IAEA. It is possible to define a factor, $k_{BIPM/PSDL}$, that is the ratio of the value of a radiation quantity measured by the BIPM divided by that measured by the PSDL. In the case in which the comparison was carried out by transfer ionization

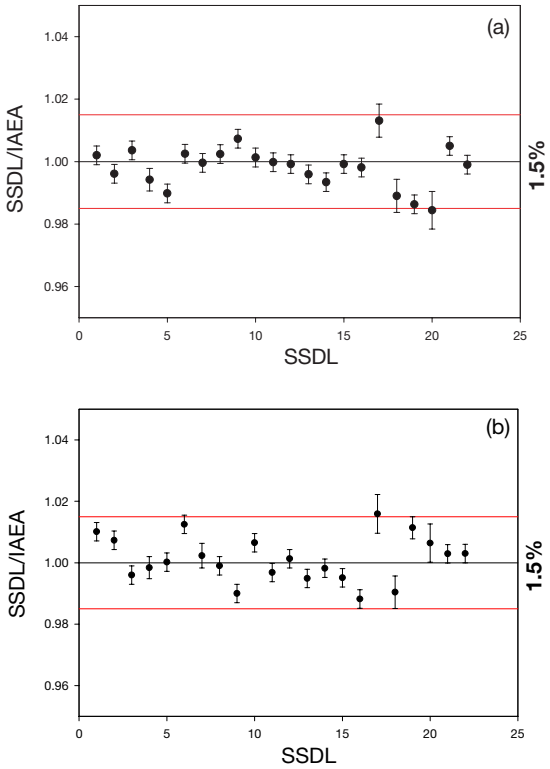

FIG. 1. (a) Air kerma comparisons of IAEA SSDLs (traceable to the BIPM through the IAEA). (b) Absorbed dose to water comparisons of IAEA SSDLs (traceable to the IAEA).

chambers, this correction factor is the ratio of the calibration coefficients determined at the BIPM and at the PSDL. The results of the comparison between the SSDLs of group 3 and the IAEA were multiplied by $k_{BIPM/PSDL}$. These factors were derived from Ref. [12]. In this case there is an additional uncertainty because of the statistical fluctuations expected in the results of the comparison involving the PSDL and the BIPM. This statistical uncertainty of the correction factor is about 0.14% (since measurements have to be made at both the PSDL and the BIPM [13, 14]). This amount must be added to the uncertainty of the ratio of the comparison between the IAEA and an SSDL whose calibration is traceable to a PSDL other than the BIPM.

The results for this group of SSDLs, shown in Figs 3(a) and (b) (see footnote 1), do not exhibit any significant difference from those of the other two groups.

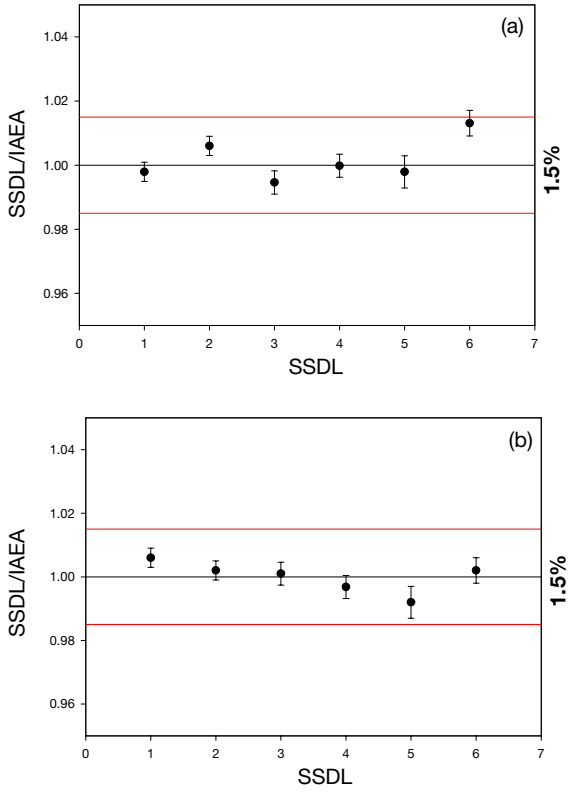

FIG. 2. (a) Air kerma comparisons of IAEA SSDLs (traceable directly to the BIPM). (b) Absorbed dose to water comparisons of IAEA SSDLs (traceable directly to the BIPM).

The IAEA has also participated in a comparison organized by SIM. Seven laboratories, including four SSDL members of the IAEA/WHO network from Latin America, the PSDLs of Canada (NRC) and the United States of America (NIST), and the IAEA, participated in the comparison. Three ionization chambers were calibrated in terms of both air kerma and absorbed dose to water at all the participant laboratories. The NRC acted as the pilot laboratory. These results have been published [9] and show that all the calibrations for both quantities fall within an interval of 0.8%. It was hence concluded that the results of this comparison could be used to support the uncertainty claims for the CMCs of all the participating laboratories.

The SIM comparison results, expressed as the ratio NRC/SSDL and NRC/IAEA for N_K and $N_{D,w}$, can be used to derive an expected SSDL/IAEA ratio for the four SSDLs in the Latin America region. The expected ratio derived from the SIM comparison and the ratio obtained from the IAEA comparisons are plotted in Figs 4(a) and (b).

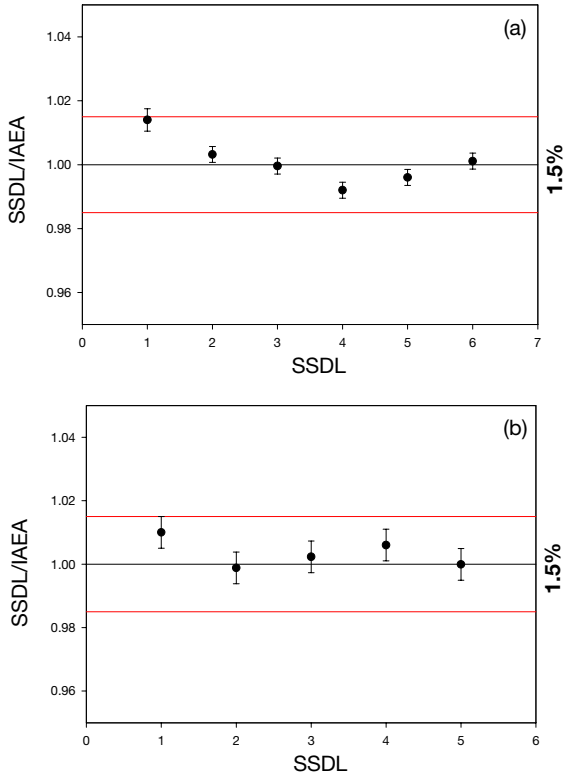

FIG. 3. (a) Air kerma comparisons of IAEA SSDLs (traceable to other PSDLs). (b) Absorbed dose to water comparisons of IAEA SSDLs (traceable to other PSDLs).

4. CONCLUSIONS

The IAEA comparison programme for calibrations in terms of N_K and $N_{D,w}$ has been designed to help the SSDLs to verify the integrity of their standards and calibration procedures and facilitate their integration into the MRA for national measurement standards and for calibration and measurement certificates.

The results of the IAEA programme show that, irrespective of the type of traceability to primary standards (the BIPM through the IAEA, directly to the BIPM or directly to another PSDL), and both for N_K and $N_{D,w}$ coefficients, all the SSDLs provide calibrations that fall inside the acceptance level of 1.5% compared with the IAEA. However, only approximately 50% of the calibrations agree within the estimated overall uncertainty of the calibrations as determined by the IAEA. Corrective actions are thus required by almost half of the SSDLs prior to achieving the status that will allow them to play a full role in

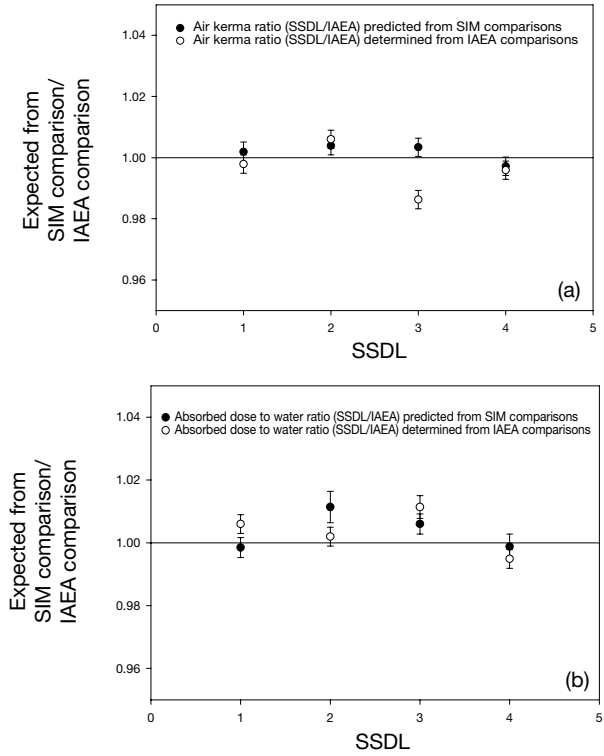

FIG. 4. (a) Air kerma ratios (SSDL/IAEA) determined from IAEA SSDL comparisons and derived from SIM comparisons. (b) Absorbed dose to water ratios (SSDL/IAEA) determined from IAEA SSDL comparisons and derived from SIM comparisons.

the MRA. These conclusions are also supported by the results of the IAEA–SIM comparison.

The results of the IAEA–SIM comparison also confirm the robustness of the international system of measurements and suggest the need for the IAEA to participate in comparisons with other regional metrology organizations.

ACKNOWLEDGEMENTS

The authors are grateful to the SSDL members of the IAEA/WHO network that participated in the IAEA comparison programme.

REFERENCES

[1] INTERNATIONAL ATOMIC ENERGY AGENCY, SSDL Network Charter, IAEA, Vienna (2000).
[2] IZEWSKA, J., ANDREO, P., The IAEA/WHO TLD postal programme for radiotherapy hospitals, Radiother. Oncol. **54** (2000) 65–72.
[3] CZAP, L., MATSCHEKO, G., ANDREO, P., Intercomparison of ionization chamber calibration factors in the IAEA/WHO Network of SSDLs, SSDL Newsletter No. 35 (1996) 17–25.
[4] INTERNATIONAL ATOMIC ENERGY AGENCY, Absorbed Dose Determination in External Beam Radiotherapy, Technical Reports Series No. 398, IAEA, Vienna (2000).
[5] INTERNATIONAL ATOMIC ENERGY AGENCY, Recommendations on the use and dissemination of calibration factors in terms of absorbed dose to water, SSDL Newsletter No. 34 (1995) 5–6.
[6] INTERNATIONAL ATOMIC ENERGY AGENCY, Absorbed Dose Determination in Photon and Electron Beams, 2nd edn, Technical Reports Series No. 277, IAEA, Vienna (1997).
[7] Mutual Recognition of National Measurement Standards and of Calibration and Measurement Certificates Issued by National Metrology Institutes, Comité international des poids et mesures, Sèvres (1999).
[8] ALLISY-ROBERTS, P.J., THOMAS, C., SHORTT, K.R., MEGHZIFENE, A., The operation of the CIPM mutual recognition arrangement and its relevance to the SSDL members of the IAEA/WHO Network, SSDL Newsletter No. 47 (2003) 25–37.
[9] SHORTT, K.R., ROSS, C.K., SEUNTJENS, J.P., "The role of comparisons in confirming the accuracy of dosimetric standards", Recent Developments in Accurate Radiation Dosimetry (Proc. Int. Workshop Montreal, 2001) (SEUNTJENS, J.P., MOBIT, P.N., Eds), Medical Physics Publishing, Madison, WI (2002).
[10] MEGHZIFENE, A., CZAP, L., ANDREO, P., Intercomparison of ionization chamber calibration factors in the IAEA/WHO Network of SSDLs, SSDL Newsletter No. 38 (1998).
[11] INTERNATIONAL ATOMIC ENERGY AGENCY, Calibration of Dosimeters Used in Radiotherapy, Technical Reports Series No. 374, IAEA, Vienna (1994).
[12] ALLISY-ROBERTS, P.J., BURNS, D.T., Comparisons and Calibrations at the BIPM, Rep. CCRI(I)/99-1, Bureau international des poids et mesures, Sèvres (1999).
[13] ALLISY-ROBERTS, P.J., Comparison of the Standards of Air Kerma of the NRC-Canada and the BIPM for ^{60}Co Gamma Rays, Rep. BIPM-99/12, Bureau international des poids et mesures, Sèvres (1999).
[14] ALLISY-ROBERTS, P.J., Comparison of the Standards of Absorbed Dose to Water of the NRC-Canada and the BIPM for ^{60}Co Gamma Rays, Rep. BIPM-99/13, Bureau international des poids et mesures, Sèvres (1999).

DOSIMETRY ISSUES FOR DIAGNOSTIC RADIOLOGY

(Session 7)

Chair

F. PERNIČKA
IAEA

Co-Chair

J. ZOETELIEF
Netherlands

Rapporteur

H.-M. KRAMER
Germany

BLANK

DOSIMETRY IN DIAGNOSTIC AND INTERVENTIONAL RADIOLOGY: INTERNATIONAL COMMISSION ON RADIATION UNITS AND MEASUREMENTS AND IAEA ACTIVITIES

J. ZOETELIEF
Interfaculty Reactor Institute, Delft University of Technology,
Delft, Netherlands
E-mail: j.zoetelief@iri.tudelft.nl

F. PERNIČKA
Division of Human Health, International Atomic Energy Agency, Vienna

G. ALM CARLSSON
University of Linköping, Linköping, Sweden

D.R. DANCE
Royal Marsden NHS Trust, London, United Kingdom

L.A. DeWERD
University of Wisconsin, Madison,
Wisconsin, United States of America

G. DREXLER
GSF – Forschungszentrum, Institut für Strahlenschutz,
Neuherberg, Germany
and Rio de Janeiro State University, Rio de Janeiro, Brazil

H. JÄRVINEN
Finnish Centre for Radiation and Nuclear Safety, Helsinki, Finland

H.-M. KRAMER
Physikalisch-Technische Bundesanstalt, Braunschweig, Germany

K.-H. NG
University of Malaya, Kuala Lumpur, Malaysia

Abstract

Dosimetric quantities are used in diagnostic and interventional radiology for the establishment of guidance or diagnostic reference levels and for the assessment of comparative risk; only a limited number of measurements serve for the assessment of potential risk. An additional objective of dosimetry in medical imaging is the assessment of equipment performance. The present situation in dosimetry for medical X ray imaging clearly indicates the need for international recommendations on appropriate radiation quantities and units. In addition, guidance on the calibration of instruments and measurements in hospitals is also needed. This has been recognized by the International Commission on Radiation Units and Measurements (ICRU) and resulted in the establishment of an ICRU report committee on patient dosimetry in medical imaging. The ICRU proposes a harmonized system of quantities and units for patient dosimetry in medical X ray imaging. New symbols are proposed for various quantities. General information is provided on measurement methods, the calibration of dosimeters and methods of determining organ and tissue doses. The IAEA is developing an international code of practice for dosimetry in X ray diagnostic radiology. The main objective is to help to achieve and maintain a high level of quality in dosimetry, to improve the implementation of traceable standards at the national level and to ensure the control of dose in X ray medical imaging worldwide. Compared with the ICRU, the IAEA puts more emphasis on the practical aspects of establishing proper calibration facilities, for example at the secondary standards dosimetry laboratories, and provides more detailed recommendations for clinical dosimetry. Co-ordination between ICRU and IAEA activities is considered important by both organizations. This has been taken into account in part by having a person who is a member of both committees. The intention is to have a restricted overlap between both documents and to harmonize them as much as possible. The paper summarizes ICRU and IAEA activities.

1. INTRODUCTION

Medical X ray examinations contribute greatly to the population dose from human-made radiation sources. There is a requirement to control this dose and, therefore, to optimize the design and use of X ray imaging systems. The main aims of patient dosimetry for X rays used in medical imaging are the establishment, use and assessment of guidance levels [1] or diagnostic reference levels [2] and the measurement of the dosimetric parameters of the performance of the equipment. An additional objective is the assessment of risk related quantities.

The dosimetric approaches in general diagnostic radiology, mammography and computed tomography (CT) differ slightly, which results in different, application specific dosimetric quantities. In general radiology various quantities and

terminologies have been used (sometimes incorrectly) for the specification of dose on the central beam axis at the point at which the X ray beam enters the patient or a phantom representing the patient. These include exposure at skin entrance (ESE), input radiation exposure, entrance surface air kerma (ESAK), entrance air kerma, air kerma, entrance surface dose (ESD), entrance skin dose (ESD) and integral skin dose. Different names are used for the same quantity, for example entrance surface air kerma, air kerma and entrance air kerma. The same abbreviation, ESD, is used for both entrance surface dose (absorbed dose most likely expressed in air) and entrance skin dose (absorbed dose most likely expressed in skin tissue). Similar problems exist for dosimetry in mammography and CT. A particular problem has been the use of absorbed dose in situations in which this quantity is inappropriate and cannot be measured because of the lack of a secondary electron equilibrium (e.g. at or close to air–tissue interfaces). The present situation in dosimetry for medical X ray imaging clearly indicates the need for international recommendations on appropriate radiation quantities and units. This has been recognized by the International Commission on Radiation Units and Measurements (ICRU) and resulted in the establishment of an ICRU report committee on patient dosimetry in medical imaging. The draft report proposes a harmonized system of quantities and units for patient dosimetry in medical imaging using X rays. New symbols are proposed for various quantities. General information is provided in the report on measurement methods, including various aspects of the calibration of dosimeters, and methods of determining organ and tissue doses.

The uncertainty of dose measurements in medical X ray imaging, as discussed in Ref. [3], should not exceed about 10% in terms of the expanded uncertainty using a coverage factor of $k = 3$. This uncertainty is more difficult to achieve with thermoluminescence dosimetry than with ionization chamber measurements. The IAEA is developing an international code of practice for dosimetry in X ray diagnostic radiology [4]. The main objectives of this code of practice are to help to achieve and maintain a high level of quality in dosimetry, to improve the implementation of traceable standards at the national level and to ensure the control of radiation dose in X ray medical imaging worldwide. Compared with the ICRU, IAEA activities put more emphasis on the practical aspects of the establishment of proper calibration facilities, for example at a secondary standards dosimetry laboratory (SSDL), and provide more detailed recommendations on clinical dosimetry.

Co-ordination between ICRU and IAEA activities is considered important by both organizations. This has been partly taken into account by having a person who is a member of both committees. The intention is to have a restricted overlap between both documents and to harmonize them as much as possible. This paper gives information on ICRU and IAEA activities.

2. QUANTITIES AND UNITS FOR MEASUREMENT AND CALCULATION IN MEDICAL X RAY IMAGING

The basic dosimetric quantities relevant for medical X ray imaging are introduced in the ICRU draft report as defined in Ref. [5]. The quantities used for specific applications such as radiography, fluoroscopy and CT are presented in some detail below. Risk related quantities and dose conversion coefficients relating mean organ doses (or the absorbed dose to a localized region of tissue) to readily measurable dosimetric quantities are presented. Quantities recommended for the establishment and use of diagnostic reference levels are given. A similar approach was selected by the group drafting the IAEA document.

2.1. Application specific quantities

Several practical dosimetric quantities have been found useful for measurements in medical X ray imaging. However, ambiguity exists in the names of the quantities and in their use. Owing to the equivalence of numerical values of absorbed dose and kerma in the same material for the X ray energies used in medical imaging and under conditions of secondary electron equilibrium, quantities have often been alternatively referred to in terms of absorbed dose (usually abbreviated to dose) or in terms of kerma. Historical names for these quantities are:

(a) Exposure (rate) at skin entrance (free in air);
(b) Entrance surface kerma (or dose) (rate) (free in air);
(c) Entrance surface dose (or kerma) (rate) (with backscatter);
(d) Kerma (or dose) area product (rate) (free in air);
(e) CT dose index (free in air or in a phantom).

It is necessary to specify the position of the points of measurement or calculation of the quantities with respect to the X ray tube focus and the patient or phantom. Since diverging radiation beams are invariably used in medical imaging, the kerma and dose will decrease with distance from the X ray tube focus approximately in accordance with the inverse square law. Radiation backscattered from within the patient or phantom will make a significant contribution (backscatter factors range from 1.25 to 1.60 for general radiology [6]) to the kerma or dose at the entrance surface.

The first three (pairs of) quantities listed above refer to the same position (the point at which the central axis of the X ray beam intercepts the plane

corresponding to the entrance surface of the patient or phantom). However, the first two pairs are to be determined free in air (i.e. in the absence of the patient or phantom) and the third pair is to be determined in the presence of the patient or phantom. In the latter case, because of the air–tissue interface, the numerical equivalence between air kerma and absorbed dose to air does not hold. It is impractical to measure absorbed dose to air in this situation, and it is proposed that air kerma be measured instead. This choice is also desirable because air kerma is the primary dosimetric quantity for the diagnostic energy range. All calibrations at national laboratories are provided in terms of air kerma. In order to specify the conditions of the air kerma measurement, qualifying words are used. These indicate the position of the measurement and whether backscattered radiation from the patient is included.

A subscript is added to the symbol for air kerma to indicate the measurement condition (i.e. incident or entrance surface air kerma, indicated by *i* or *e*). Thus incident air kerma and entrance surface air kerma are denoted by K_i and K_e, respectively.

The air kerma area product is the integral of the air kerma over the area of the X ray beam in a plane perpendicular to the beam axis. If the air kerma is constant over the beam area, the integral becomes equal to the product of the air kerma and the area, hence the name air kerma area product. The symbol recommended for the air kerma area product is P_{KA}. The symbol P indicates that the quantity is a product and the subscript KA indicates that the factors in the product are the air kerma and area. The air kerma area product rate is defined as the quotient of the increment in the air kerma area product and the time interval dt.

Similar to the air kerma area product, the air kerma length product can be defined as the integral of the air kerma along a line. This quantity is useful in CT, in which the line is chosen to be parallel to the axis of rotation of the CT scanner. If the air kerma is constant over a length, L, and equal to zero elsewhere along the line, the integral becomes equal to the product of the air kerma and the length, hence the name air kerma length product. The symbol recommended for the air kerma length product is P_{KL}. Also for dosimetry in CT, the CT air kerma index (symbol C_K) for measurements free in air for a single rotation can be defined as the air kerma length product, P_{KL}, divided by the nominal slice thickness, T. As the nominal slice thickness is used (rather than the real slice thickness), the symbol C_K is used instead of air kerma, with a relevant subscript. Air kerma measurements in CT are often made in special head and body dosimetry phantoms [7, 8]. A number of recommended names, symbols and fields of application specific quantities are given in Table I. More detailed definitions are given in the ICRU report.

TABLE I. RECOMMENDED APPLICATION SPECIFIC QUANTITIES FOR DOSIMETRY IN MEDICAL X RAY IMAGING

Quantity name	Symbol	Field of application
Incident air kerma (rate)	K_i ($\dot{K}_i$)	Radiography, including mammography and fluoroscopy
Entrance surface air kerma (rate)	K_e ($\dot{K}_e$)	Radiography, including mammography and fluoroscopy
Air kerma area product	P_{KA} ($\dot{P}_{KA}$)	Radiography and fluoroscopy
Air kerma length product	P_{KL}	CT
CT air kerma index	C_K	CT

Note: All quantities are used to assess stochastic effects. K_i and K_e are also useful for monitoring the maximum cumulative skin dose for deterministic effects in interventional radiology.

3. SPECIFICATION OF X RAY BEAMS

The radiation quality of an X ray beam can be characterized by the X ray spectrum, dealt with in a separate section of the ICRU report. X ray spectra can be measured, but the techniques used require considerable expertise and are time consuming to perform. It is therefore recommended that the radiation quality of X ray beams used for medical imaging be characterized by a combination of various parameters. These include the first half-value layer (HVL_1), the second half-value layer (HVL_2), the ratio of HVL_1 and HVL_2, referred to as the homogeneity coefficient, the tube voltage and the total filtration. In most cases the quality of an X ray beam can be adequately specified by means of the combined information on tube voltage, HVL_1 and HVL_2 (or equivalently the tube voltage, HVL_1 and homogeneity coefficient), or the tube voltage, HVL_1 and total filtration. The radiation intensity is also an important characteristic of an X ray tube (including filtration); for this purpose the X ray tube output is defined.

The practical determination of the X ray beam quality routinely relies on simple attenuation measurements, usually in aluminium, to determine the half-value layer (HVL). The HVL_1 is the thickness of a specified material that attenuates the beam of radiation to an extent such that the radiation quantity is reduced to half its initial value [9]. The use of different quantities will lead to different HVL_1 values. The air kerma or the air kerma rate is recommended for the characterization of X ray beams used for medical imaging. In the definition of HVL_1, the contribution of all scattered radiation, other than any that might

be present initially in the beam concerned, is to be excluded. The HVL alone is often not an adequate specification of the X ray beam quality, since markedly different spectra can sometimes result in the same value of HVL_1, as illustrated in Fig. 1. It should be noted that two of the spectra shown have very low filtration, and should not be used. Spectral distributions are shown in Fig. 1 for four X ray qualities having similar values of HVL_1 but generated at different tube voltages and having different filtration. When the X ray spectra are rather different, they may cause different dosimeter responses and different dose distributions in an irradiated medium (e.g. a phantom or a patient).

The recommendations of the ICRU [5] should be followed for the measurement of HVL_1. It has been shown that a narrow beam and a large distance between the absorber and the measuring device should be used to obtain the correct HVL_1. The instrument used for attenuation measurements should have a weak energy dependence over the range concerned. The use of a monitor is advisable to facilitate a correction for variations in the output of the X ray tube. The monitor should be positioned such that its readings are independent of the

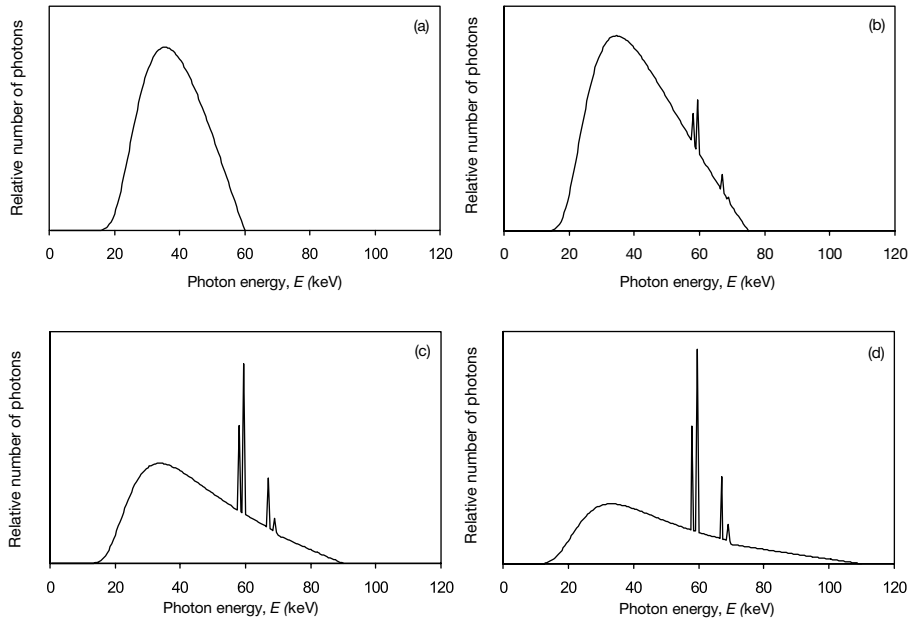

FIG. 1. Calculated spectra [10] of filtered X ray beams with almost the same HVL_1 but generated at different tube voltages (constant potential, anode angle 16°). (a) Tube voltage: 60 kV, filtration: 4.3 mm Al, HVL_1: 2.74 mm Al. (b) Tube voltage: 75 kV, filtration: 2.9 mm Al, HVL_1: 2.74 mm Al. (c) Tube voltage: 90 kV, filtration: 2.0 mm Al, HVL_1: 2.72 mm Al. (d) Tube voltage: 110 kV, filtration: 1.2 mm Al, HVL_1: 2.68 mm Al.

thickness of the absorber. By limiting the field diameter, the amount of scattered radiation recorded will be reduced, but the field dimensions must be larger than the sensitive volume of the measuring device. The diaphragm must be of sufficient thickness to absorb the primary beam. A radiographic method may be used to check the alignment.

The X ray tube output may be used in conjunction with the inverse square law to calculate the air kerma incident on a patient or a phantom if the tube current exposure time product is known. The magnitude of the X ray tube output will depend upon the design of the tube, tube voltage and filtration, and may change as the tube ages.

4. SELECTION OF INSTRUMENTS

Ionization chambers are the main devices used for dosimetry in diagnostic and interventional radiology [11]. The primary advantage of the ionization chamber as a dosimetric device is that it is a precise instrument with little energy dependence and few other complicating factors. An ionization chamber should be calibrated over the energy region of use, since different chambers can show some variations in energy dependence. The design and performance of ionization chambers must be matched to the needs of the clinical measurement. Parallel-plate ionization chambers are mainly used, but cylindrical chambers are also used. Air kerma area product meters are special types of parallel-plate ionization chamber used to measure the integral of air kerma over the area of an X ray field. The reading of a kerma area product meter can be directly converted into the energy imparted to the patient during the examination [12]. A stretched out version of a cylindrical chamber results in a unique design for a CT chamber. The unique use of the CT chamber requires that the response of the active volume be uniform along its entire axial length, a restriction that is not required of other cylindrical chambers.

Other devices with special properties, for example thermoluminescent detectors and semiconductor detectors, are also used. Some of the electronic detectors may have an energy dependence that is compensated for electronically. This electronic compensation needs quality assurance techniques to be performed in order to ensure that it remains stable.

5. CALIBRATION FACILITIES

All instruments used for dosimetry in X ray diagnostic and interventional radiology must be calibrated, having a valid calibration certificate from an

accredited calibration laboratory, typically an SSDL. Calibrations directly traceable to primary standards are currently available for most radiation qualities employed in radiology. Comparisons between several primary standards dosimetry laboratories (PSDLs) have demonstrated the mutual equivalence of the primary standards for radiation qualities developed in order to meet clinical requirements. Some SSDLs have attempted to establish diagnostic calibration services, but more efforts are needed.

5.1. Requirements for equipment used for calibration

All measuring equipment used for calibration at an SSDL shall be of a reference class and be available in duplicate at the SSDL. This includes ionization chambers, electrometers, thermometers, barometers and a device to measure the relative humidity of air. For calibration purposes, the only detector that is considered by the code of practice to be a reference class dosimeter is an ionization chamber. Table II gives the recommendations on the upper limit of the variation in response with radiation energy for chambers, for different applications. The time interval between the periodic calibrations of the standard instrument should be within the acceptable period defined by national regulations. Where no such regulations exist, the time interval should not exceed three years. Monthly measurements shall be made to check the stability of the reference chambers.

For conventional radiography, fluoroscopy, CT and dental applications, a tungsten anode tube and X ray machine operating at an X ray tube voltage ranging from 50 kV to 150 kV should be used. For the calibration of mammography dosimeters, a molybdenum anode tube with molybdenum filtration is recommended. If the SSDL has only a tungsten tube, at least two radiation qualities in the range of 20 kV to 35 kV shall be established for mammography

TABLE II. LIMITS FOR THE VARIATION IN RESPONSE FOR DOSIMETERS USED AT SSDLs

Application	Tube voltage range (kV)	Maximum variation of response (%)
General radiography	60–150	±3
Fluoroscopy	50–100	±2
Mammography	22–35	±1
CT	100–150	±1
Dental radiography	50–90	±2

calibrations. The availability of only a tungsten tube will limit the types of dosimeter that can be calibrated by the SSDL.

5.2. Radiation qualities for calibration

Radiation qualities shall be established in accordance with recommendations given elsewhere [13]. The qualities used for the calibration of dosimeters for different applications are shown in Table III. There will be an International Electrotechnical Commission (IEC) document in the future with modifications of these beams.

5.3. Calibration of instruments

The general principles for the calibration of dosimeters used in diagnostic and interventional radiology do not differ from those for instrument calibration in radiotherapy and radiation protection [14, 15]. The SSDL shall provide a calibration coefficient in terms of air kerma or air kerma length product, where appropriate. Air kerma area product meters require great care in their calibration, as their performance depends on the actual set-up in the hospital. They may be calibrated in situ. The calibration of dosimeters shall be done by the substitution method, using a transmission monitor. The cross-sectional area of the reference radiation beam should be sufficient to irradiate the standard chamber or the device to be calibrated, whichever is the larger. The variation of kerma rate over the useful beam area shall be less than 5%, and the contribution of scattered radiation to the total kerma rate shall be less than 5%

TABLE III. RADIATION QUALITIES FOR THE CALIBRATION OF DIAGNOSTIC DOSIMETERS

Application		Range of HVL_1 (mm Al)	Reference code [13]
General radiography	Unattenuated	2.11–5.62	RQR 4 to RQR 10
	Attenuated	5.38–13.3	RQA 4 to RQA 10
Fluoroscopy	Unattenuated	1.78–5.62	RQR 3 to RQR 10
	Attenuated	3.78–13.3	RQA 3 to RQA 10
CT		7.00–10.0	—
Mammography	Unattenuated	0.28–0.36	—
	Attenuated	0.56–0.58	—
Dental radiography		1.78–3.20	RQR 3 to RQR 7

[16]. An SSDL shall determine its calibration uncertainty, which has to include the uncertainty stated by the PSDL for the transfer chamber calibration, although this may be itemized separately. The procedure of establishing the uncertainty budget is described in the code of practice. The expanded uncertainty ($k = 2$) for different types of instrument shall fall within the values given in Table IV. The IEC [17] requires that the detector and measuring device be calibrated as a system, but the code of practice allows for their separate calibration and using the system calibration coefficient as a product of the detector and measuring device calibration coefficient.

For carrying out calibrations of non-invasive high voltage measuring devices, an SSDL needs to be equipped with a suitable means for calibrating the voltage delivered by the generator connected to the X ray tube. This shall be done under operating conditions (i.e. with the tube current usually used). The best method employs an appropriately calibrated and frequency compensated resistor chain connected parallel to the generator and the X ray tube. The practical peak voltage [17] shall be calculated from the readings of this device.

6. DOSIMETRY FOR DIAGNOSTIC AND INTERVENTIONAL RADIOLOGY

Measurements can be made either with a patient or using phantoms. The use of phantoms is particularly suitable for the assessment of the performance of equipment.

TABLE IV. UNCERTAINTIES FOR TYPES OF INSTRUMENT FOR AN SSDL

Type of instrument	Expanded uncertainty ($k = 2$) (%)
Reference class instruments suitable for the calibration of other instruments in general diagnostic applications	3.5
Reference class instruments suitable for the calibration of other instruments in the mammography category	2
Field class dosimeters (50–150 kV)	5
Field class mammography dosimeters (20–50 kV)	3
Electrometers	1

6.1. Measurements with phantoms

For the assessment of equipment performance, it is preferable to make dose measurements using a phantom simulating a patient. When a phantom is used, the measured dose will depend upon the phantom shape and size, and it is essential that the phantom be standardized so that such variations are avoided. Phantoms must be defined so that they offer the same primary attenuation and scatter production as a representative patient over the whole range of X ray energies used in practice. It is desirable that such phantoms be inexpensive and constructed from readily available materials.

6.1.1. General radiography and fluoroscopy

Slab phantoms made of polymethylmethacrylate (PMMA) or polystyrene containers (wall thickness of about 6 mm) filled with water are recommended by the ICRU [7] for radiology. Phantoms consisting of PMMA and aluminium have been developed at the United States Center for Devices and Radiological Health (CDRH) for chest (posteroanterior), abdomen (anteroposterior) and lumbosacral (anteroposterior) examinations for average sized US patients [18]. Servomaa and Tapiovaara [19] modified the CDRH chest phantom to phantoms suitable for skull (lateral) and thoracic spine (anteroposterior) examinations and compared them with an Alderson Rando male phantom. Scatter matching was obtained by adjusting the relative positions of PMMA and aluminium so that the air kerma values behind the phantoms were the same for both the anatomic and the homogeneous phantoms at defined positions.

The IAEA has taken a similar approach to the ICRU in recommending a suitable phantom for radiography–fluoroscopy. The draft code of practice recommends using a rectangular phantom of tissue equivalent material with a cross-sectional area of 30 cm × 30 cm and a thickness of 20 cm to simulate the trunk in anteroposterior–posteroanterior views. Two polycarbonate containers, each 10 cm thick filled with water, are recommended. A third similar container may be added to simulate a heavier patient. The water phantom is recommended because the backscatter from the two component CDRH phantoms has not been tested and may not give a good measure of the backscatter from a patient.

6.1.2. Mammography

The value of the mean glandular dose per mammographic exposure will depend upon the thickness of the compressed breast and the breast glandularity. Tissue equivalent materials are available that simulate the adipose and

glandular tissues within the breast [20], and it is possible to combine them in appropriate proportions to simulate a breast of any glandularity. A glandularity of 50% may be regarded as typical for breasts of average thickness and is generally used as a standard composition in breast dosimetry protocols. For example, the American College of Radiology (ACR) dosimetry protocol uses a standard breast 42 mm thick and of 50% glandularity that is simulated by a PMMA–dental wax composite with the same total thickness [21]. The European protocol on dosimetry in mammography [22] uses a standard breast 50 mm thick and of 50% glandularity that is simulated by a PMMA phantom 45 mm thick. For practical purposes, the use of PMMA has important advantages: it is cheaper than specially manufactured tissue substitutes and is more readily available. Dance et al. [23] provide a table of equivalent PMMA thicknesses for a breast thickness range of 20 mm to 110 mm and appropriate to women aged 50 to 64. The European protocol summarizes the various (national) recommendations for dosimetry in mammography.

A survey has shown a more extensive use of the ACR protocol for mammography dosimetry than of other protocols. For this reason, for mammographic dosimetry with a phantom, the draft version of the code of practice uses the ACR phantom and ACR conversion coefficients to relate the incident air kerma measurement to mean glandular dose.

6.1.3. CT

The CT air kerma index is measured in a standard phantom using a CT ionization chamber. The experimental configuration is in accordance with the European guidelines on quality criteria in CT [8]. The American Association of Physicists in Medicine head and body CT phantoms constructed from PMMA are used [22].

6.2. Patient dosimetry

The objective of measurements on patients is generally to obtain an indication of the typical dose being delivered to an average sized patient by the procedures and equipment used in a particular facility. For example, such measurements may be used for the establishment of diagnostic reference levels.

Direct dose measurements during the course of real examinations provide the best indication of actual clinical practice. Patients, however, vary in physique and hence in the thickness and density of the part of the body being examined. For the dose measurements to be indicative of the routine practice in a particular facility and to be comparable with those from another facility, a

careful selection of the measurement sample is required. At least ten patients should be measured per type of radiograph. Generally, thermoluminescent dosimeters (TLDs) attached to the skin of the patient are recommended for the direct measurement of the entrance surface air kerma. Alternatively, the incident air kerma can be calculated with knowledge of the machine output and exposure factors. Specific procedures for monitoring patient doses in different types of examination are recommended, as given below.

6.2.1. General radiography and fluoroscopy

The patient sample should be selected so that the mean value of the patient mass lies within 5 kg of 70 kg (or within 5 kg of 60 kg in some geographical regions). TLDs are recommended for measurements of entrance surface air kerma in examinations with fixed projections. In examinations using fluoroscopy, the irradiation geometry and irradiation times vary individually. In this case, a kerma area product meter is recommended for the measurement of the air kerma area product. In interventional procedures carried out under fluoroscopic guidance, high absorbed doses may occur, owing to long fluoroscopic times. TLDs placed on the skin may underestimate the maximum absorbed doses if they are not placed at the right position. P_{KA} measurements may be used to give an indication of the maximum skin dose by dividing the P_{KA} value by the entrance area of the field on the patient. Alternatively, devices may be employed that allow the simultaneous measurement of the air kerma area product and of the entrance surface kerma. In such a combination the risk for stochastic effects may be assessed by means of the air kerma area product, and that for deterministic effects by means of the entrance surface kerma.

6.2.2. Mammography

The European protocol [24] describes a method of determining the incident air kerma (K_i) from actual examinations. This method has been adopted in the draft code of practice. It is based on the calibration of the radiation output of the X ray machine and the recording of exposure parameters during the examination. It is suitable for machines with a manual exposure control or units with an automatic exposure control and a post-exposure display of tube loading. Patients should be selected with a compressed breast thickness in the range of 4 cm to 6 cm. For reasons of consistency, the conversion coefficients for the estimation of mean glandular dose are based on the breast model used for the ACR mammographic protocol rather than that used for the European protocol. The overall uncertainty ($k = 2$) of K_i is estimated as ±30%, mainly due to sample size.

6.2.3. CT

A weighted computed tomography dose index [25] has proved useful for dose estimation for patient dosimetry, and can be compared with a diagnostic reference level. In the IAEA code of practice, for the same purpose, it is proposed to use a weighted CT air kerma index.

6.2.4. Dental radiography

Entrance surface air kerma in intra-oral radiography may be calculated from measurements of incident air kerma at the end of the spacer–direction cone using the exposure settings in the clinical practice. Backscatter factors are subsequently applied to obtain the entrance surface air kerma. In panoramic examinations, the air kerma area product may be calculated from a measurement of the incident air kerma using TLDs positioned at the front of the secondary collimator. The measurements must be integrated over a standard exposure cycle and multiplied by the field size at the position of the TLD.

7. APPLICATION OF PATIENT DOSE MEASUREMENTS

Reference levels should be seen as a practical aid to increase awareness of the significance of observed levels of patient dose and hence to promote the optimization of imaging procedures. The adoption of the third quartile values for the establishment of reference levels is a purely pragmatic approach to help identify those radiology departments in most urgent need of better quality control.

The new code of practice briefly discusses the concept and gives guidance on the calculation of organ doses.

8. CONCLUSIONS

The present situation in dosimetry for medical X ray imaging indicates clearly the need for international recommendations on appropriate radiation quantities and units. The ICRU has established a report committee for this purpose. The draft ICRU report defines application specific quantities for dosimetry in medical X ray imaging and new symbols for these units. Recommendations are also given for the specification of X ray beams both in terms of radiation quality and in terms of radiation intensity.

The need for the standardization and traceability of dosimetry measurements in X ray diagnostic radiology stimulated the IAEA to start developing international guidance in this area. The IAEA code of practice places an emphasis on the selection of appropriate equipment for dosimetry in X ray diagnostic and interventional radiology, recommendations for establishing calibration facilities and guidance for dosimetry in clinical practice.

Close co-operation between the ICRU and the IAEA is considered essential by both organizations.

ACKNOWLEDGEMENTS

The contribution of M. Rosenstein on the ICRU report committee is gratefully acknowledged.

REFERENCES

[1] FOOD AND AGRICULTURE ORGANIZATION OF THE UNITED NATIONS, INTERNATIONAL ATOMIC ENERGY AGENCY, INTERNATIONAL LABOUR ORGANISATION, OECD NUCLEAR ENERGY AGENCY, PAN AMERICAN HEALTH ORGANIZATION, WORLD HEALTH ORGANIZATION, International Basic Safety Standards for Protection against Ionizing Radiation and for the Safety of Radiation Sources, Safety Series No. 115, IAEA, Vienna (1996).

[2] INTERNATIONAL COMMISSION ON RADIOLOGICAL PROTECTION, Protection and Safety in Medicine, Publication 73, Pergamon Press, Oxford and New York (1996).

[3] AMERICAN ASSOCIATION OF PHYSICISTS IN MEDICINE, Recommendations on performance characteristics of diagnostic exposure meters, Med. Phys. **19** (1992) 231–241.

[4] PERNICKA, F., et al., "Development of an international code of practice for dosimetry in x-ray diagnostic radiology", poster presented at IAEA Int. Conf. on Radiological Protection of Patients in Diagnostic and Interventional Radiology, Nuclear Medicine and Radiotherapy, Malaga, 2001.

[5] INTERNATIONAL COMMISSION ON RADIATION UNITS AND MEASUREMENTS, Physical Aspects of Irradiation, Rep. 10b, National Bureau of Standards Handbook 85, US Government Printing Office, Washington, DC (1964).

[6] PETOUSSI-HENSS, N., ZANKL, M., DREXLER, G., PANZER, W., REGULLA, D., Calculation of backscatter factors for diagnostic radiology using Monte Carlo methods, Phys. Med. Biol. **43** (1998) 2237–2250.

[7] INTERNATIONAL COMMISSION ON RADIATION UNITS AND MEASUREMENTS, Phantoms and Computational Models in Therapy, Diagnosis and Protection, Rep. 48, ICRU, Bethesda, MD (1992).
[8] EUROPEAN COMMISSION, Quality Criteria for Computed Tomography, EUR 16262, Office for Official Publications of the European Communities, Luxembourg (1999).
[9] INTERNATIONAL COMMISSION ON RADIATION UNITS AND MEASUREMENTS, Radiation Dosimetry: X-rays Generated at Potentials of 5 to 150 kV, Rep. 17, ICRU, Bethesda, MD (1970).
[10] INSTITUTE OF PHYSICS AND ENGINEERING IN MEDICINE, Catalogue of Diagnostic X-ray Spectra and Other Data, Rep. 78, IPEM, York, UK (1997).
[11] DeWERD, L.A., WAGNER, L.K., Characteristics of radiation detectors for diagnostic radiology, Appl. Radiat. Isot. **50** (1999) 125–136.
[12] ALM CARLSSON, G., DANCE, D.R., PERSLIDEN, J., SANDBORG, M., Use of the concept of energy imparted in diagnostic radiology, Appl. Radiat. Isot. **50** (1999) 39–62.
[13] INTERNATIONAL ELECTROTECHNICAL COMMISSION, Radiation Conditions for Use in the Determination of Characteristics of Diagnostic X-ray Equipment, Publication 61267, IEC, Geneva (1994).
[14] INTERNATIONAL ATOMIC ENERGY AGENCY, Calibration of Dosimeters Used in Radiotherapy, Technical Reports Series No. 374, IAEA, Vienna (1994).
[15] INTERNATIONAL ATOMIC ENERGY AGENCY, Calibration of Radiation Protection Monitoring Instruments, Safety Reports Series No. 16, IAEA, Vienna (1999).
[16] INTERNATIONAL ORGANIZATION FOR STANDARDIZATION, X and Gamma Reference Radiations for Calibrating Dosemeters and Doserate Meters and for Determining their Response as a Function of Photon Energy — Part 1: Radiation Characteristics and Production Methods, ISO 4037-1979, Part 1, ISO, Geneva (1996).
[17] INTERNATIONAL ELECTROTECHNICAL COMMISSION, Medical Electrical Equipment — Dosimeters With Ionization Chambers and/or Semiconductor Detectors as Used in X-ray Diagnostic Imaging, Publication 61674, IEC, Geneva (1994).
[18] CONWAY, B.J., et al., Beam quality independent attenuation phantom for estimating patient exposure from x-ray automatic controlled chest examinations, Med. Phys. **11** (1984) 827.
[19] SERVOMAA, A., TAPIOVAARA, M., Two new patient equivalent phantoms in diagnostic radiology, Radiat. Prot. Dosim. **43** (1992) 229–231.
[20] WHITE, D.R., Tissue substitutes in experimental radiation physics, Med. Phys. **5** (1978) 467–479.
[21] AMERICAN COLLEGE OF RADIOLOGY, Mammography Quality Control Manual, ACR, Reston, VA (1999).
[22] EUROPEAN COMMISSION, European Protocol on Dosimetry in Mammography, EUR 16263 EN, Office for Official Publications of the European Communities, Luxembourg (1996).

[23] DANCE, D.R., SKINNER, C.L., YOUNG, K.C., BECKETT, J.R., KOTRE, C.J., Additional factors for the estimation of mean glandular breast dose using the UK mammography dosimetry protocol, Phys. Med. Biol. **45** (2000) 3225–3240.
[24] AMERICAN ASSOCIATION OF PHYSICISTS IN MEDICINE, Standardized Methods for Measuring Diagnostic X-ray Exposures, Rep. 31, American Institute of Physics, New York (1990).
[25] LEITZ, W., AXELSSON, B., SZENDRO, G., Computed tomography dose assessment — A practical approach, Radiat. Prot. Dosim. **57** (1995) 377–380.

THE DOSE LENGTH PRODUCT IS THE BASIC DOSIMETRIC QUANTITY IN COMPUTED TOMOGRAPHY

J. KARPPINEN, M. TAPIOVAARA, H. JÄRVINEN
Radiation and Nuclear Safety Authority (STUK),
Helsinki, Finland
E-mail: juhani.karppinen@stuk.fi

Abstract

There is currently much confusion on the proper use and definitions of dosimetric quantities for computed tomography (CT), which has mainly been caused by the rapid development of CT techniques. Some of the shortcomings of using the computed tomography dose index (CTDI), one of the oldest and most widely used quantities, are presented in the paper. Instead of the weighted computed tomography dose index ($CTDI_w$), the weighted dose length product (DLP_w) and the weighted multiple scan average dose ($MSAD_w$) are proposed for use as more basic dosimetric quantities. The latter two quantities are adequate in practice for setting reference dose levels and for the determination of patient doses in CT examinations, while they are also simple to understand and easy to use by the operators of CT equipment. National guidance for CT dosimetry in Finland has been prepared based on the use of DLP_w and $MSAD_w$ only.

1. INTRODUCTION

There is currently much confusion on the proper use and definitions of dosimetric quantities in computed tomography (CT). This is partly because of the rapid development of CT equipment, including the introduction of multi-slice techniques that use increasing numbers of slices, helical scanning and automatic dose displays. The computed tomography dose index (CTDI) [1] is one of the oldest and most widely used quantities for CT dosimetry. Owing to the development of CT techniques, several new modifications of this quantity have been introduced, adding unnecessary confusion and uncertainty.

The aim of this paper is to present some of the shortcomings of using the CTDI and to suggest instead using the dose length product (DLP) and the multiple scan average dose (MSAD), which are more basic dosimetric quantities [1]. Based on these considerations, the recommendation on the quantities for CT dosimetry prepared by STUK for the users of CT equipment in Finland is briefly summarized.

2. DEFINITIONS OF THE CTDI

The CTDI has been defined [1, 2] as:

$$\mathrm{CTDI}=\frac{1}{NT}\int_{-\infty}^{+\infty} D_1(z)\mathrm{d}z \tag{1}$$

where

$D_1(z)$ is the dose along a line normal to the scan plane from one scan;
T is the nominal slice thickness;
N is the number of slices produced in a single scan.

Later modifications of this quantity include changing the limits of the integration from infinity to $\pm 7T$ (United States Food and Drug Administration (FDA) definition [2]) or to ±50 mm (the International Electrotechnical Commission (IEC) [3] and European Commission (EC) [4] definitions). The dose is commonly measured in standardized, cylindrical CT dose phantoms made of polymethylmethacrylate (PMMA) and refers either to the dose in air (the IEC and EC definitions) or in PMMA (the FDA definition). The CTDI of the IEC and EC definitions is often denoted as CTDI_{100}, where the sub-index refers to the integration range of 100 mm. Along with this quantity a weighted CTDI, denoted as CTDI_w, has been introduced as:

$$\mathrm{CTDI}_w = \frac{1}{3}\mathrm{CTDI}_{100}(\text{centre}) + \frac{2}{3}\mathrm{CTDI}_{100}(\text{periphery}) \tag{2}$$

where

CTDI_{100}(centre) is the CTDI at the central axis of the CT dosimetry phantom;
CTDI_{100}(periphery) is the CTDI at a depth of 1 cm below the surface of the CT dosimetry phantom.

The size of the phantom (diameter 16 cm in head examinations and 32 cm in body examinations) is not referred to in the notation or name of the quantity, but should be inferred from the examination in question. Further confusion has arisen from suggestions of using the smaller phantom also for body examinations of children.

If the total thickness of slices produced in a single scan is not equal to the patient support travel between scans in axial scanning, or to the patient support travel per rotation in helical scanning, this should be corrected for to show the average dose in the scanned volume. According to the IEC definition [3, 5] $CTDI_w$ in this case is corrected for by dividing by a factor $\Delta d/NT$, where Δd is the patient support travel between scans or per rotation and N and T are the same as in Eq. (1). For helical scanning the correction factor is called a CT pitch factor. The corrected $CTDI_w$ is called the volume $CTDI_w$ and is denoted by $CTDI_{vol}$ [5].

The IEC standard on the safety of CT equipment [3, 5] requires that $CTDI_{vol}$ be displayed at the operator's console. In the EC quality criteria [4] for CT examinations it is recommended that reference doses (reference levels) be specified in terms of $CTDI_w$ and DLP. The IEC standard specifically defines that the pitch correction be included, while in the EC definition it is not (or at least not explicitly) taken into account.

In addition to the various definitions mentioned above, there are other unsatisfactory aspects of the CTDI:

(a) The CTDI relates to neither the patient's radiation risk nor the noise level in the image. Rather, the CTDI expresses the average dose at the central parts of the scanned region only when the slices are nominally contiguous.
(b) The basic definition of the CTDI (Eq. (1)) does not allow corrections for non-contiguous slices: the table feed is not specified in the definition. (It is noted, however, that the case of non-contiguous slices was considered in the paper that introduced the concept of the CTDI [1].)
(c) All definitions of the CTDI involve a non-measurable quantity, the nominal slice thickness, T. No reference to the actual slice thickness is made.

3. CTDI VERSUS DLP

It can be noted from Eq. (1) that the actual measured datum for the determination of the CTDI is the integral of the one scan (or one rotation in helical scanning) dose profile. This integral is the DLP for one scan (or rotation), DLP_1:

$$DLP_1 = \int_{-\infty}^{+\infty} D_1(z)\mathrm{d}z \tag{3}$$

When the integration limits are changed to finite values, the integral can be measured easily by using a stack of thermoluminescent dosimeters or a pencil

shaped ionization chamber with a uniform response along its length. For the latter, the dosimeter reading (in mGy) corresponds to the average dose in the ionization chamber volume, and DLP_1 is obtained by multiplying the dosimeter reading by the length of the active part of the dosimeter (alternatively, it is also possible to design the instrument to express the DLP (in mGy·cm) directly). In fact, this is how the measurement is usually made and has implications for the proper calibration of ionization chambers for CT dose measurements.

DLP_1 appropriately describes the amount of radiation involved in making one scan, because, in contrast to the CTDI, the slice thickness is properly taken into account. Thus both the radiation risk to the patient and the image noise from one scan are better described in terms of DLP_1 than CTDI.

Similarly to the CTDI, the DLP of the examination can be used for evaluating the dose to the patient: reference values have been recommended for a weighted DLP quantity analogous to Eq. (2) [4]. Regrettably, notational confusion has been introduced by not clearly indicating that the quantity is a weighted quantity measured in the standard dosimetry phantom. For clarity and in analogy to $CTDI_w$ we suggest denoting the weighted DLP as DLP_w.

The weighted DLP from the whole examination can be easily measured, either directly by using a phantom and radiation monitor that is fixed at a static position during the whole scan series, or by measuring the weighted DLP of one scan (or one rotation in helical scanning) and multiplying this by the number of scans (or rotations) in the examination, n:

$$\mathrm{DLP}_{w,\mathrm{tot}} = \int D_{w,\mathrm{tot}}(z)\mathrm{d}z = n\int D_{w,1}(z)\mathrm{d}z = n\mathrm{DLP}_{w,1} \tag{4}$$

4. MULTIPLE SCAN AVERAGE DOSE

The multiple scan average dose (MSAD) [1] can be described with quantities analogous to those for the CTDI, but without the need to refer to the nominal slice thickness. The weighted multiple scan average dose ($MSAD_w$) can be simply defined as:

$$\mathrm{MSAD}_w = \frac{\mathrm{DLP}_{w,\mathrm{tot}}}{d} \tag{5}$$

where

$\mathrm{DLP}_{w,\mathrm{tot}}$ is the weighted DLP for the total CT examination;
d is the total axial length of the scanned volume.

Using Eq. (4) we obtain:

$$\begin{aligned} \mathrm{MSAD}_w &= \frac{n\,\mathrm{DLP}_{w,1}}{n\,\Delta d} = \frac{\mathrm{DLP}_{w,1}}{\Delta d} \\ &= \frac{1}{\Delta d}\left(\frac{1}{3}\int_{-a}^{+a} D_{\mathrm{centre,1}}(z)\mathrm{d}z + \frac{2}{3}\int_{-a}^{+a} D_{\mathrm{periphery,1}}(z)\mathrm{d}z \right) \end{aligned} \tag{6}$$

where

$D_{\mathrm{centre,1}}(z)$ is the dose from one scan or rotation along the central axis of the CT dosimetry phantom;

$D_{\mathrm{periphery,1}}(z)$ is the dose from one scan or rotation along a line parallel to the central axis of the CT dosimetry phantom and at a depth of 1 cm below the phantom surface;

Δd is the patient support travel between scans in axial scanning or per rotation in helical scanning.

The integration limits can be chosen to be, for example, a = 50 mm.

From Eq. (1) and Eq. (6) it can be seen that:

$$\mathrm{MSAD}_w = \frac{NT}{\Delta d}\mathrm{CTDI}_w \tag{7}$$

that is, MSAD_w is equal to the pitch corrected CTDI_w. Thus for a CT pitch factor equal to unity, $\mathrm{MSAD}_w = \mathrm{CTDI}_w$.

The DLP_w and MSAD_w are useful and user friendly quantities, as the user of the CT equipment can simply determine their values. When the pitch corrected CTDI_w (MSAD_w) is displayed on the operator's console, as required by the IEC standard [3], the DLP_w can be easily calculated from Eq. (5), as the length, d, of the examination is easily determined:

$$\mathrm{DLP}_{w,\mathrm{tot}} = d\ \mathrm{MSAD}_w \tag{8}$$

5. CONCLUSIONS: RECOMMENDED QUANTITIES FOR CT

As can be seen from the above, the most fundamental quantity for CT dose determination is the DLP (in practice the DLP_w), since it is the only quantity that can be directly measured and is the basis of the determination of other quantities defined above. In principle, DLP_w would be sufficient for setting the

reference levels and for indicating the dose to the patient. However, for the comparison of different CT techniques and equipment, the weighted multiple scan average dose, $MSAD_w$, is also a useful quantity. In contrast with these two quantities, the CTDI, with its various definitions and the need for corrections, is an unnecessarily complicated quantity and not needed in practice.

Practical guidance to the users of radiation for the determination of patient doses in diagnostic radiology, for comparison with the given national reference levels, has been prepared in Finland by STUK. For CT examinations only DLP_w and $MSAD_w$ have been introduced as the quantities to be determined. Recommendations include descriptions of the phantoms to be used for the determination of these weighted quantities. The CTDI has been mentioned only in a footnote of the recommendations, giving some explanation of this quantity and the problems related to its definition, and its relation to the recommended quantities.

REFERENCES

[1] SHOPE, T.B., GAGNE, R.M., JOHNSON, G.C., A method for describing the doses delivered by transmission x-ray computed tomography, Med. Phys. **8** (1981) 488–495.

[2] FOOD AND DRUG ADMINISTRATION, Diagnostic X-ray systems and their major component; amendment to performance standard; final rule, 21 CFR part 1020, Fed. Regist. **49** (1984) 171.

[3] INTERNATIONAL ELECTROTECHNICAL COMMISSION, Medical Electrical Equipment, Part 2-44: Particular Requirements for the Safety of X-ray Equipment for Computed Tomography, IEC 60601-2-44, 2nd edn, IEC, Geneva (2001).

[4] EUROPEAN COMMISSION, European Guidelines on Quality Criteria for Computed Tomography, EUR 16262 EN, Office for Official Publications of the European Communities, Luxembourg (2000).

[5] INTERNATIONAL ELECTROTECHNICAL COMMISSION, Amendment 1 to IEC 60601-2-44 (2001): Medical Electrical Equipment, Part 2-44: Particular Requirements for the Safety of X-ray Equipment for Computed Tomography, IEC, Geneva (2002).

DETERMINATION OF THE EQUIVALENT COPPER THICKNESS OF PATIENT EQUIVALENT PHANTOMS IN TERMS OF ATTENUATION FOR USE IN RADIOLOGY

J.T.M. JANSEN, I.I. SULIMAN, J. ZOETELIEF
Radiation Technology/Medical Physics, Interfaculty Reactor Institute,
Delft University of Technology,
Delft, Netherlands
E-mail: jtjansen@iri.tudelft.nl

Abstract

Constancy check protocols for fluoroscopic systems have been developed in the radiation protection research programme of the European Commission, as part of the DIMOND multipartner project. For practical reasons copper filters are preferred to patients or tissue equivalent phantoms of water or polymethylmethacrylate (PMMA). The objectives of the use of the filters are to obtain appropriate conditions to derive patient entrance surface dose rates and the dose rates at the image intensifier input. The DIMOND protocol states that copper sheets of either 1 mm or 1.5 mm thickness may be used. The paper investigates the equivalent thickness of copper filters compared with PMMA phantoms in terms of attenuation, for several geometries and different tube voltage–filter combinations. Calculated equivalent copper thicknesses, ranging from 0.42 mm to 14.9 mm, result in different exposure conditions being met in practice.

1. INTRODUCTION

In its Fifth Framework Programme for radiation protection research, the European Commission is supporting a multipartner project entitled Measures for Optimising Radiological Information and Dose in Digital Imaging and Interventional Radiology (DIMOND). Constancy check protocols [1] for fluoroscopic systems have been developed as a part of the work. In these protocols copper filters are preferred to patients or tissue equivalent phantoms made of water or polymethylmethacrylate (PMMA), because of practical reasons such as handling and reduction in mass and size. The objectives are to derive patient entrance surface dose rates and the dose rates at the image intensifier input with the help of filters simulating the presence of a patient. The patient entrance surface dose rate is important, as deterministic effects, for example skin necrosis, have been encountered in interventional radiology procedures

using unoptimized radiological equipment. For a typical adult patient the IAEA [2] recommends dose rate guidance levels for fluoroscopy of 25 mGy/min in the 'normal' operational mode and 100 mGy/min in an optional 'high level' operational mode. The dose rate at the image intensifier determines the sensitivity of the fluoroscopic system.

The DIMOND protocol states that copper sheets of either 1 mm or 1.5 mm thickness may be used. Furthermore, the DIMOND protocol defines two measurement geometries. In the first geometry, used to determine the patient entrance surface dose, the copper filter is placed close to the image intensifier. The ionization chamber is placed on the side of the copper sheet facing the X ray tube. The second geometry, used to determine the air kerma rate at the image intensifier, has the copper filter attached to the X ray tube diaphragm. The ionization chamber is placed on the surface of the image intensifier housing. In both cases the inverse square law is used to correct for differences in position, if necessary. Measurements are performed with different settings of the X ray unit and both with and without the use of an antiscatter grid.

This paper investigates what thickness of copper filter is equivalent to appropriate PMMA phantoms in terms of attenuation, for different geometries and several tube voltage and filter combinations.

2. METHOD AND MATERIALS

The method of Monte Carlo simulation of radiation transport was employed for the calculations. The Monte Carlo N-Particle (MCNP) code version 4C [3] was used, which was developed at the Los Alamos National Laboratory and includes the production of K shell fluorescence photons. The MCNP code runs on a Compaq XP900 Alpha Workstation with the Unix operating system Tru64 and is compiled with the DEC Fortran-77 compiler. The MCNP code was applied to calculate the attenuation in the different geometries with PMMA, copper or no filters applied. In all these cases the detector was placed 1.0005 m from the focus, on the central beam axis, with all the filters between the detector and the focus. The fluence was calculated with the MCNP code using cell or point detectors, and the fluence to air kerma free in air function was calculated in accordance with Ref. [4]. The cell detector was a cylinder with a radius of 1 cm and a thickness of 1 mm. No antiscatter grid was used in the calculations.

Two different radiation beam sizes were used: a small beam with a diameter of 0.10 m at a distance of 1.00 m from the focus and a large beam with a diameter of 0.23 m at a distance of 1.00 m from the focus. The applied combinations of tube voltage and PMMA phantom thickness were: 60 kV, 13 cm;

80 kV, 14 cm; 100 kV, 16 cm; 120 kV, 17 cm; 150 kV, 18 cm; 150 kV, 20 cm; and 150 kV, 30 cm. The spectra for the different tube voltages were generated with Institute of Physics and Engineering in Medicine software [5] at an anode angle of 16°, 0% ripple (constant potential) and 2.5 mm added aluminium filtration.

The PMMA phantoms, with a density of 1.17 g/cm^3 and an elemental composition by mass of 8% hydrogen, 60% carbon and 32% oxygen [6], had a surface area of 30 cm × 30 cm, with a variable thickness, depending on the applied tube voltage. The thickness of the copper filter, density 8.96 g/cm^3, was adjusted to get the same attenuation as obtained with the relevant PMMA phantoms. This match was made for the PMMA phantom in front of the image intensifier and the copper filter in front of the image intensifier (back–back) or attached to the X ray tube diaphragm (back–front). In addition, a match was made with both the PMMA and copper filter attached to the X ray tube diaphragm (front–front). A caesium iodide plate 0.5 mm thick, mass density 4.51 g/cm^3, simulated the image intensifier, with its front at 1.001 m from the focus. All the back filters had their exit plane at 1.00 m from the focus. The PMMA front filters had their entrance plane at 0.15 m from the focus and the copper front filters had their exit plane at 0.15 m from the focus. All materials were surrounded by dry air with a density of 1.205 mg/cm^3 and an elemental composition of 0.0124% carbon, 75.5268% nitrogen, 23.1781% oxygen and 1.2827% argon.

The results are presented as the copper equivalent filter thickness for each of the PMMA phantom thicknesses mentioned above, at the appropriate tube voltages and for the three front–back combinations and two beam sizes.

The back–back situation, with both the PMMA phantom and the copper sheet in the back position (i.e. near the image intensifier), was used to estimate patient entrance surface dose rates. The equivalent copper filter calculation was based on the detector being placed behind the attenuators to simulate the performance of an automatic exposure control (AEC). In addition, a detector was placed 1 cm in front of the PMMA phantom or the copper sheet to simulate the ionization chamber for the determination of the patient entrance surface dose rate. This detector was a cylinder with a radius of 1 cm and a thickness of 2 cm. In the DIMOND constancy check protocol the ionization chamber measurements are converted to a focus detector distance of 0.50 m [1] by applying the inverse square law with the distance to the dose measurement of the ionization chamber. The calculated ionization chamber readings in the presence of either the PMMA phantom or the copper filter were compared to assess the uncertainty in the patient entrance dose when using a copper filter.

The front–front situation, with both the PMMA phantom and the copper sheet attached to the X ray tube diaphragm, was used to estimate the dose rate at the image intensifier input. In this case only one detector was simulated for both the AEC and ionization chamber measurements.

3. RESULTS AND DISCUSSION

In Table I the equivalent copper filter thicknesses are shown for various tube voltages and PMMA phantom thicknesses, for both the small and large beam diameter and for the three filter position combinations. The equivalent copper thickness ranges from 0.42 mm to 14.9 mm, the smallest value holding true for the lowest tube voltage and smallest PMMA thickness. The values increase with increasing tube voltage and phantom thickness.

The equivalent copper thickness was increased by a factor of between 1.03 and 1.78 for the small beam diameter compared with the large beam diameter.

TABLE I. EQUIVALENT COPPER FILTER THICKNESS (mm) YIELDING THE SAME ATTENUATION AS THE PMMA PHANTOM, AS CALCULATED BEFORE THE IMAGE INTENSIFIER PLATE

(Various tube voltage and PMMA phantom thickness combinations are shown for both the small and large beam diameters. Three situations are shown, namely with the PMMA filter in the back position near the image intensifier and the copper filter either in the back or front position, and with the PMMA phantom in the front position, attached to the X ray tube diaphragm and the copper filter also in the front position.)

Tube voltage (kV)		60	80	100	120	150	150	150
PMMA thickness (cm)		13	14	16	17	18	20	30
Beam diameter at 1 m (cm)		10						
		Equivalent copper thickness (mm Cu)						
Position								
PMMA	Copper filter							
Back	Back	0.64	1.01	1.68	2.4	3.7	4.7	11.3
Back	Front	0.54	0.82	1.37	1.9	2.8	3.7	9.9
Front	Front	0.95	1.65	2.8	4.1	6.6	7.9	14.9
Beam diameter at 1 m (cm)		23						
		Equivalent copper thickness (mm Cu)						
Position								
PMMA	Copper filter							
Back	Back	0.51	0.69	1.07	1.41	2.1	2.7	7.4
Back	Front	0.42	0.56	0.86	1.12	1.60	2.1	5.9
Front	Front	0.92	1.58	2.7	4.0	6.4	7.5	13.5

The smallest differences occur with both filters in the front position. The small beam diameter and both filters in the front position reduce the contribution of scatter to the AEC detector. This is shown in Table I by the highest equivalent copper thickness. It should be remembered that the effective atomic number for PMMA is less than that for copper, so PMMA will produce more scattered radiation than copper. If the PMMA phantom is changed from the front position to the back position the scatter contribution to the AEC detector increases. This results in less attenuation for the PMMA phantom, and therefore the equivalent copper thickness decreases by a factor of between 0.25 and 0.66. This factor is smaller (more deviating from 1) for the large beam compared with the small beam and for the high tube voltage compared with the low tube voltage because scatter is more important in the large beam and for high tube voltages. If the copper filter is changed from the front position to the back position the scatter contribution to the detector increases. More copper is therefore needed to achieve the same attenuation, resulting in an increase by a factor of between 1.15 and 1.31 in equivalent copper thickness. This factor is much closer to 1 than the factor for the change in the PMMA phantom, indicating that scatter is more important for the PMMA phantom than for the copper filter.

Measurement of the patient entrance surface dose rate, according to the DIMOND protocol, involves the situation with both the PMMA phantom and the copper filter in the back position. The equivalent copper filter thickness is calculated for a constant signal of the AEC detector behind the attenuators. The detector reading in front of the attenuators may, however, differ for the two situations. In Table II is shown the ratio of the reading with the PMMA phantom and with the equivalent copper filter. For the small beam diameter the ratio is between 0.98 and 1.08 and for the large beam it is between 1.06 and 1.23.

The main reason for the deviation of this ratio from 1 is the backscatter of the PMMA phantom being larger than the backscatter of the copper filter. The backscatter of the PMMA phantom increases with increasing beam diameter and increasing tube voltage (not shown). For 150 kV tube voltage and increasing PMMA phantom thickness two effects play an opposite role. As the phantom thickness increases with the front face fixed, the backscatter factor increases, although at greater thickness it reaches a plateau. As the phantom is positioned closer to the focus, with a fixed thickness, the backscatter factor decreases, due to an increasing inhomogeneous irradiation of the phantom and because the detector remains at 1 cm in front of the phantom. It should be remembered that the detector position is at the central beam axis. Petoussi-Henss et al. [7] calculated the backscatter factor for a PMMA phantom of 30 cm × 30 cm × 15 cm with a fixed focus to surface distance of 100 cm. They used a

square field of 10 cm × 10 cm instead of a circular field with a diameter of 23 cm, a slightly higher density of 1.19 g/cm^3 instead of 1.17 g/cm^3 for PMMA, a vacuum instead of air as the surrounding material and 0 versus 1 cm distance between the detector and the entrance surface of the PMMA phantom. The backscatter factors calculated in this study are between 1% and 4% lower. Considering all the differences in the calculation, the agreement is good. Petoussi-Henss et al. [7] also calculated the backscatter factor for International Commission on Radiation Units and Measurements (ICRU) tissue, which is tissue equivalent. For the spectra used in this study, the backscatter factor of PMMA is 6% larger than for ICRU tissue, resulting in an overestimation of the patient entrance surface dose rate of 6% for the large beam diameter. In general, the reading with a copper filter is lower than with the PMMA phantom. To estimate the ICRU tissue result, for the large beam diameter, with the backscatter factor as supplied by Petoussi-Henss [7], the correction factor is 0% to +17% and quite dependent on the photon energy.

4. CONCLUSIONS

Instead of the 1 mm or 1.5 mm thick copper sheets recommended in the DIMOND protocol, copper sheets with thicknesses ranging from 0.4 mm to 7.5 mm are needed to achieve the same attenuation as the PMMA phantom (in the back position), without an antiscatter grid, for the large beam diameter. For the small beam diameter the equivalent copper thickness ranges from 0.5 mm

TABLE II. CALCULATED RATIO OF DETECTOR RESPONSES FOR THE PMMA PHANTOM OR THE COPPER FILTER

(Both attenuators are in the back position. The detector is positioned 1 cm in front of the attenuator and corrected for distance differences with the inverse square law. The copper filter thickness is adjusted to give an equal response at the AEC detector position as the PMMA phantom.)

Tube voltage (kV)	60	80	100	120	150	150	150
PMMA thickness (cm)	13	14	16	17	18	20	30
Beam diameter at 1 m (cm)	Detector reading with PMMA phantom divided by reading with copper filter (Gy/Gy)						
10	0.98	1.02	1.04	1.06	1.08	1.07	1.05
23	1.06	1.12	1.17	1.20	1.23	1.23	1.20

to 11 mm. For measurement of the patient entrance surface dose rates with the equivalent copper thickness in the back position, in accordance with the DIMOND protocol, it is expected that the dose will be underestimated by between –2% to +23%, compared with the situation with the PMMA phantom, depending on the actual situation used. For the large beam the PMMA measurement will overestimate the ICRU tissue situation described by Petoussi-Henss et al. [7] by a factor of 6%, resulting in an overall correction factor of 0% to +17%.

ACKNOWLEDGEMENT

This study received funding from the European Commission 5th Framework Programme (1998–2002), Nuclear Fission and Radiation Protection, Contract DIMOND III, Number FIGM-CT-2000-00061.

REFERENCES

[1] FAULKNER, K., Introduction to constancy check protocols in fluoroscopic systems, Radiat. Prot. Dosim. **94** (2001) 65–68.

[2] INTERNATIONAL ATOMIC ENERGY AGENCY, Radiological Protection for Medical Exposure to Ionizing Radiation, Safety Standards Series No. RS-G-1.5, IAEA, Vienna (2002).

[3] BRIESMEISTER, J.F., MCNP — A General Monte Carlo N-particle Transport Code, Version 4C, Manual LA-13709-M, Los Alamos Natl Lab., Los Alamos, NM (2000).

[4] INTERNATIONAL COMMISSION ON RADIATION UNITS AND MEASUREMENTS, Measurement of Dose Equivalents from External Photon and Electron Radiations, Rep. 47, ICRU, Bethesda, MD (1992).

[5] CRANLEY, K., GILMORE, B.J., FOGARTY, G.W.A., DESPONDS, L., Catalogue of Diagnostic X-ray Spectra and Other Data, Institute of Physics and Engineering in Medicine, Rep. 78, York, UK (1997).

[6] INTERNATIONAL COMMISSION ON RADIATION UNITS AND MEASUREMENTS, Tissue Substitutes in Radiation Dosimetry and Measurement, Rep. 44, ICRU, Bethesda, MD (1989).

[7] PETOUSSI-HENSS, N., ZANKL, M., DREXLER, G., PANZER, W., REGULLA, D., Calculation of backscatter factors for diagnostic radiology using Monte Carlo methods, Phys. Med. Biol. **43** (1998) 2237–2250.

BLANK

POSTERS ON DIAGNOSTIC RADIOLOGY

(Session 8a)

Chair

H.-M KRAMER
Germany

Co-Chair

F. PERNIČKA
IAEA

Rapporteur

C. BORRÁS
Pan American Health Organization

BLANK

PROPOSED AMENDMENTS TO EQUIPMENT STANDARDS FOR DOSIMETRY INSTRUMENTATION IN INTERVENTIONAL RADIOLOGY

A.D. MEADE*, A. DOWLING, C.L. WALSH, J.F. MALONE
Department of Medical Physics and Bioengineering, St. James's Hospital, Dublin, Ireland
E-mail: aidan.meade@dit.ie

Abstract

As part of the DIMOND III European Commission project, a number of European partners are currently involved in preparing proposals for standards for imaging and dosimetry equipment used in interventional radiology. The project aims to devise methods for the optimization of dose and image quality in digital and interventional radiology. Proposals are currently being drawn up for additions or amendments to existing standards. These proposals will be put to the relevant standards bodies for inclusion in future standards publications and are described here. The issues covered include the use of dose area product measurements to provide information relating to stochastic effects and from which an upper bound of the maximum surface dose may be estimated if certain other parameters are known. In addition, issues regarding the display and recording of this information and the connectivity of the dose area product meter to the radiological equipment are addressed. These proposals will significantly enhance the protection of the patient from stochastic and deterministic injury in interventional radiology.

1. INTRODUCTION

The European Commission DIMOND III (Measures for Optimising Radiological Information and Dose in Digital Imaging and Interventional Radiology) project is a European project consisting of 60 interlinked sub-projects concerned with providing measures to ensure optimal protection and image quality in digital and interventional radiology (IR). The project aims to optimize the dose versus image quality relationship through developing radiological image quality criteria, equipment requirements and specifications, and patient and staff dosimetry approaches. Both digital and interventional radiology have undergone significant developments over the past decade and con-

* Present address: School of Physics, Faculty of Science, Dublin Institute of Technology, Dublin, Ireland.

tinue to advance. In particular, in interventional radiology the present technology provides the user with the potential to administer very long exposure times, which are not restricted by the engineering of the technology and can result in large patient doses. Interventional radiology has increased in popularity, owing to the opportunity to provide previously costly, invasive and difficult surgical procedures on an outpatient basis. There remains a legislative requirement that developments in new equipment or procedures must be subject to radiation protection measures [1, 2]. Often developments in this area have exceeded advances in protective measures and optimization requirements, as exemplified by evidence of injury [3–6]. Existing standards [7–9] have successfully enhanced the radiation protection provided to patients and staff in interventional procedures, and have standardized the requirements for the dosimetry equipment used in diagnostic radiology. However, a realization exists that further amendments to these standards are desirable [10]; this paper proposes some amendments or additions to these standards, which should further enhance protection in IR.

2. BASIS FOR THE AMENDMENT OF EQUIPMENT STANDARDS

A potential for stochastic and deterministic effects exists in interventional radiology. Dosimetry information is required to make the interventionalist aware of the potential for such effects [3, 9, 10]. Also, for the purposes of tracking doses to patients after IR procedures, it is necessary for details of the patient's dosimetry to be available within the patient's records [9–11]. The estimation of dose from interventional procedures requires the estimation of the cumulative dose from a number of radiographic and fluoroscopic imaging exposures taken with different projections [12–14]. Dosimetry is therefore complex and many computation procedures have been developed for the computation of dose [12–15].

A review of the existing literature and standards has indicated that a number of additions to the current standards for equipment used in dosimetry, and also imaging equipment standards and protocols, are possible in the area of IR. They are:

(a) Two quantities should be made available to the clinician in order to give a comprehensive view of the potential for both radiation induced effects from IR procedures [12–14]:
    (i) The entrance surface dose (ESD) at the most exposed area (maximum ESD).
    (ii) The dose area product (DAP) for the examination as a whole.

Neither of these quantities individually describes both the potential for stochastic and deterministic effects in IR. In practice, the ESD (or the maximum entrance surface dose (MSD)) is related to the potential for local deterministic effects as a result of ionizing radiation exposure in interventional procedures [12, 13, 15]. The DAP, however, supplies an indication of the potential for late onset stochastic effects from such procedures [12–14]. Unfortunately, although standards for DAP meters and interventional equipment exist [7–9], no standard exists that defines the automatic recording and computation of the DAP and ESD for use in an interventional procedure. Indeed, many techniques for the measurement of both quantities in diagnostic radiology exist, but as yet there is insufficient scientific consensus in this area [4, 16–18]. Scope thus exists for the definition of standard measurement protocols and requirements for the display of dose in IR.

(b) In order for real time displays of the ESD and MSD to be provided to the clinician, and for dosimetry information to be recorded, certain additions are required in the area of standards for on-line dosimetry systems in IR [7, 9]. The most common facility for on-line dose measurements on modern X ray systems is the DAP meter [8]. To allow the estimation of the ESD in IR procedures certain additional requirements are proposed for the measurement capabilities of transmission ionization chambers or DAP meters over and above those specified in the existing international standards. The existing standards for interventional equipment [7] and DAP meters [8] do not take into account the requirement for connectivity between the DAP meter, the radiological equipment and radiological information systems, which is necessary for the generation of displays and the recording of the DAP and ESD. It is therefore clear that there is scope for the stipulation of equipment requirements in this area.

(c) For the purposes of the estimation of the ESD and DAP with sufficient accuracy during IR, a set of exposure and administrative data must be recorded [11]. This data set will be required to allow the estimation of the ESD and true DAP from on-line DAP measurements made under both fluoroscopy and digital radiography. In addition, complex IR procedures can cause overirradiation of a given site, which can contribute to the exceeding of deterministic levels for skin. The MSD depends on a large number of variables that change during the procedure (e.g. angulation, field size and exposure factors) and is not well correlated with the DAP [9, 10, 13, 14]. This dose is only known if the variation in the DAP and field size is known, together with exposure geometry and exposure parameters, throughout a given procedure [10]. This must be known for both individual fluoroscopic runs and radiographic projections. This therefore

exemplifies the need for a standard set of patient exposure data to be included in the patient's records for storage and use in the calculation of patient dose.

3. PROPOSED AMENDMENTS TO EQUIPMENT STANDARDS

The DIMOND project has highlighted a need for extra amendments or provisions in equipment standards. Three new items for investigation have therefore been proposed to the International Electrotechnical Commission as outcomes from this project:

(a) The first defines routines for the computation of the DAP and MSD. It will also define the necessary equipment features that will allow the determination, display and recording of the DAP and MSD during interventional procedures. It will specify a requirement for devices for on-line MSD determination, in addition to specifying standard requirements for their display and recording. A significant body of literature exists in this area that is sufficient to direct the standard.

(b) It is essential that DAP meters be capable of communicating in a standard manner with external equipment. It is therefore proposed to add a requirement to the existing standard that will provide a means for the device to communicate with other equipment and networks. Several international communication standards for use in medicine exist (e.g. the National Electrical Manufacturers Association Digital Imaging and Communication in Medicine (DICOM) standard) or are in development (the European Health Care Record Support Action (EHCR SupA)) with which the DAP connectivity should be compliant. The addendum to this standard would define the necessary communication structure and protocols that would be present in the DAP meter instrument to facilitate its communication with external devices and networks.

(c) It is proposed to generate a minimum patient data set for use in IR that allows both the real time and retrospective dosimetry of patients. It is envisaged that this data set will both be used in the estimation of dose for display and be recorded as a resource for use in the follow-up of patients. A standard will be developed that specifies the parameters that are to be included in the data set, and the requirements for recording such parameters. The data set in Table I is proposed as a list of these parameters. It is envisaged that this data set would exist in the background storage of the system, to be called upon if necessary, possibly, for example, for use in retrospective dosimetry or for the validation of the performance of the

device that calculates and displays the MSD. The user would simply view a measurement of the ESD and MSD, the calculation of which would involve the use of the data in Table I. The data set has been expanded from one proposed previously by DIMOND partners to incorporate additional information for dose estimation in IR [17]. This data set may serve as the basis for that to be used in the standard. It is also proposed

TABLE I. PROPOSED PATIENT DOSE RECORD FOR USE IN IR DOSIMETRY AND IN THE VALIDATION OF MSD DEVICES

Centre:	Date:
Room:	X ray equipment:
Physician:	Chamber/electrometer:
Patient:	Hospital number:
Date of birth:	Sex (M/F):
Examination:	Height and weight:
Maximum DAP:	
Maximum DAP rate:	
Total irradiated area (cm^2):	Mean field size (cm^2):
Digital mode:	
Dose area product per series:	Filtration:
Tube kVp:	mAs (per digital exposure):
Number of images:	Frame rate (frame/s):
Image intensifier size (cm):	Matrix size:
FSD (focus to entrance surface distance) for each exposure (or quantities allowing calculation of FSD):	Angulation/rotation for each exposure:
	Pulse rate, pulse width, mA (max., av.), pulse frequency/width:
Field size (collimation, if different from image intensifier size):	
Anatomical region for each exposure:	
Fluoroscopy mode:	
Mean kVp per fluoroscopy run:	Field size (collimation, if different from image intensifier size):
Fluoroscopy time (min):	
Pulsed fluoroscopy (yes/no):	Dose area product:
Pulse rate:	Mean tube current (mA):
FSD for each exposure (or quantities allowing calculation of the FSD):	Mean II (image intensifier) size (cm):
	Pulse width (ms):
Anatomical region for each exposure:	Angulation/rotation for each exposure:

that a requirement for the validation of the MSD device, and tolerances on the operation of the MSD device, be included in the standard.

4. CONCLUSION

Significant advances have occurred in digital and interventional radiology over the past decade, and similar developments may be expected to occur in the next. It is imperative that radiation protection standards and research keep pace with these developments for the purposes of the protection of patients and staff. In this paper the need for several international standards in the area of dosimetry in IR has been highlighted, and proposals for the direction of these standards have been made.

ACKNOWLEDGEMENTS

This work was performed under the framework of the European Commission's programme on nuclear fission and radiation protection research, project title DIMOND III: Measures for Optimising Radiological Information and Dose in Digital Imaging and Interventional Radiology. Contract FIGM-CT2000-00061. See www.dimond3.org

REFERENCES

[1] EUROPEAN UNION, Council Directive 97/43/Euratom of 30 June 1997, Health Protection of Individuals against the Dangers of Ionizing Radiation in Relation to Medical Exposure (Repealing Directive 84/466/Euratom, O.J. No. L 265/1, 5.10.1984), Official Journal of the European Communities No. L 180/22–27, Luxembourg (1997).

[2] INTERNATIONAL COMMISSION ON RADIOLOGICAL PROTECTION, Avoidance of Radiation Injuries from Interventional Procedures, Publication 85, Pergamon Press, Oxford and New York (2000).

[3] WAGNER, L.K., EIFEL, P.J., GEISE, R.A., Potential biological effects following high X-ray dose interventional procedures, J. Vasc. Interven. Radiol. **5** (1994) 71–84.

[4] RUIZ CRUCES, R., GARCIA-GRANADOS, J., DIAZ ROMERO, F.J., HERNANDEZ ARMAS, J., Estimation of effective dose in some digital angiographic and interventional procedures, Br. J. Radiol. **71** (1998) 42–47.

[5] VANO, E., GONZALEZ, L., FERNANDEZ, L., GUIBELALDE, E., Patient dose values in interventional radiology, Br. J. Radiol. **68** (1995) 1215–1220.

[6] VANO, E., et al., Dosimetric and radiation protection considerations based on some cases of patient skin injuries in interventional cardiology, Br. J. Radiol. **71** (1998) 510–516.
[7] INTERNATIONAL ELECTROTECHNICAL COMMISSION, Particular Requirements for the Safety of X-ray Equipment for Interventional Procedures, IEC 60601-2-43, IEC, Geneva (2000).
[8] INTERNATIONAL ELECTROTECHNICAL COMMISSION, Medical Electrical Equipment: Dose Area Product Meters, IEC 60580, IEC, Geneva (2000).
[9] FOOD AND DRUG ADMINISTRATION, Performance Standards for Ionizing Radiation Emitting Products, 21 CFR 1020.32, Fluoroscopic Equipment, Code of Federal Regulations, 2002.
[10] GAGNE, R.M., SHOPE, T.B., Regulatory initiatives and framework in the USA: Interventional radiology, Radiat. Prot. Dosim. **94** (2001) 13–18.
[11] FAULKNER, K., Dose displays and record keeping, Radiat. Prot. Dosim. **94** (2001) 143–145.
[12] VANO, E., et al., Skin dose and dose–area product values for interventional cardiology procedures, Br. J. Radiol. **74** (2001) 48–55.
[13] VANO, E., GUIBELALDE, E., FERNANDEZ, J.M., GONZALEZ, L., TEN, J.I., Patient dosimetry in interventional radiology using slow films, Br. J. Radiol. **70** (1997) 195–200.
[14] VAN DE PUTTE, S., VERHAEGEN, F., TAEYMANS, Y., THIERENS, H., Correlation of patient skin doses in cardiac interventional radiology with dose–area product, Br. J. Radiol. **73** (2000) 504–513.
[15] VANO, E., et al., Skin radiation injuries in patients following repeated coronary angioplasty procedures, Br. J. Radiol. **74** (2001) 1023–1031.
[16] CASTELLANO, A., McNEILL, J.G., THORP, N.C., DANCE, D.R., RAPHAEL, M.J., Assessment of organ radiation doses and associated risk for digital bifemoral arteriography, Br. J. Radiol. **68** (1995) 502–507.
[17] CHU, R.Y.L., et al., Patient doses in abdominal aortogram and aorta femoral runoff examinations, Health Phys. **75** (1998) 487–491.
[18] THWAITES, J.H., RAFFERTY, M.W., GRAY, N., BLACK, J., STOCK, B., A patient dose survey for femoral arteriogram diagnostic radiographic examinations using a dose–area product meter, Phys. Med. Biol. **41** (1996) 899–907.

BLANK

VERIFICATION OF DIAGNOSTIC RADIOLOGY CONTROL INSTRUMENTS IN SWITZERLAND

F.O. BOCHUD, T. BUCHILLIER, J.-F. VALLEY
Institut universitaire de radiophysique appliquée,
Lausanne, Switzerland
E-mail: francois.bochud@inst.hospvd.ch

Abstract

Instruments used to perform official quality controls of diagnostic radiology facilities in Switzerland have to be verified by an accredited laboratory every three years. The kinds of instrument tested, the method used and the metrological traceability are briefly presented in the paper. The distribution of the results regarding tolerance values is shown for each type of instrument. The majority of the instruments tested have been within the tolerance limits. However, two kinds of instrument are still unclearly defined from the metrological point of view: kilovoltage meters and light sensitometers.

1. INTRODUCTION

The importance of metrological traceability and of comparing tools between measuring facilities has grown for a decade. While national metrology institutes (NMIs) are building up the mutual recognition arrangement [1], diagnostic radiology facilities are pressed to assess their methods through the European directive on reference dose levels [2].

In this context, most industrialized countries have to guarantee some metrological traceability in the measurements performed in diagnostic radiology. This is performed in Switzerland through a verification process, which first started for dosimeters used in radiation therapy [3] and, since 1997, has been extended to diagnostic radiology instruments: dosimeters, kilovoltage meters (kV meters), exposure chronometers, milliampere second meters (mAs meters), optic densitometers, sensitometers and luxmeters [4]. The purpose of this paper is to present the Swiss experience and to assess the results obtained so far.

2. MATERIALS AND METHODS

The Institut universitaire de radiophysique appliquée (University Institute for Applied Radiation Physics) works as an accredited verification

laboratory in Switzerland for diagnostic radiology instruments. The facility provides several beam qualities with W anode continuous as well as W and Mo anode pulsed X ray tubes. Together with a film processing machine, these instruments allow the laboratory to verify all types of instrument at one location.

Table I lists the types of instrument subject to verification, and also the present NMI traceability, the verification tolerance and the global results. Not every instrument used in Swiss hospitals is subject to verification: only those

TABLE I. TYPE OF INSTRUMENT VERIFIED, TRACEABILITY, TOLERANCES AND GLOBAL RESULTS FROM 1 JUNE 1999 TO 31 JULY 2002

Type of instrument	NMI traceability	Tolerance[a]	Number of measurements	
			Total	Outside tolerance
Diagnostic dosimeter	NPL[b]	10%	710	12
Dental dosimeter	NPL	10%	28	1
Mammography dosimeter	METAS[c]	10%	25	4
Kerma length product dosimeter [6]	NPL	10%	1	—
Kerma area product dosimeter	NPL	10%	—	—
Diagnostic kV meter	NPL	3%	281	6
Dental kV meter	NPL	3%	117	3
Mammography kV meter	NPL	3%	24	—
Exposure chronometer	METAS	1 ms below 20 ms, 5% above 20 ms	280	8
mAs meter	METAS	5%	114	5
Optic densitometer	PTB[d]	0.025 below OD[e] = 1.00, 2.5% above OD = 1.00	142	2
Sensitometer	PTB	0.05 below OD = 1.00, 0.10 above OD = 1.00	82	19
Luxmeter	METAS	10%	56	4

[a] The uncertainty ($k = 2$) of the reference instrument is added to this tolerance value.
[b] NPL: National Physical Laboratory.
[c] METAS: Swiss Federal Office of Metrology and Accreditation.
[d] PTB: Physikalisch-Technische Bundesanstalt.
[e] OD: optical density.

used to perform official quality controls [5] of X ray and processing facilities have this legal obligation.

Since the purpose of these controls is to ensure the compliance of X ray instrumentation within some given tolerances, it is essential that the tolerances of the verification process be sufficiently small. As a guide, the verification tolerances are equal to one third of the control tolerances. In practice, owing to the very tough requirements of diagnostic radiology instrumentation, the actually applied tolerance is the verification tolerance, on to which the laboratory uncertainty ($k = 2$) is added.

The validity of a verification certificate is a maximum of three years. Three two-week verification campaigns are organized each year. The instruments are sent to the laboratory and generally returned to the customer within a week.

3. RESULTS

3.1. Dosimeters

The dose quantity used in diagnostic radiology is the air kerma. The verification laboratory owns two secondary standards traceable to the United Kingdom and Swiss NMIs (the NPL and METAS). These standards allow the calibration of transfer instruments used in the verification process for beam qualities RQR 5, RQR 7, RQR 9, RQA 5 and RQA 7 (diagnostic dosimeters), RQR 5 and RQA 5 (dental dosimeters) and RQN M (mammography dosimeters) [7]. Figure 1(a) shows the histogram of all the measurements performed in the period of interest for each type of air kerma dosimeter. It can be seen that most of the instruments are within the tolerances.

3.2. kV meters

The kV meters used in diagnostic radiology do not have a proper primary standard traceability. In Switzerland the verification of such instruments is performed by a comparison with a non-invasive instrument calibrated in terms of kV (peak) and traceable to the primary standards of voltage at the NPL. The kV meters are tested in beam qualities RQR 5, RQR 7 and RQR 9 (diagnostic kV meters), RQR 3, RQR 5 and RQR 6 (dental meters) and RQN M (mammography meters). As for the dosimeters, most of the instruments are within the tolerances, and only about 2% of the measurements fall outside (see Fig. 1(b)).

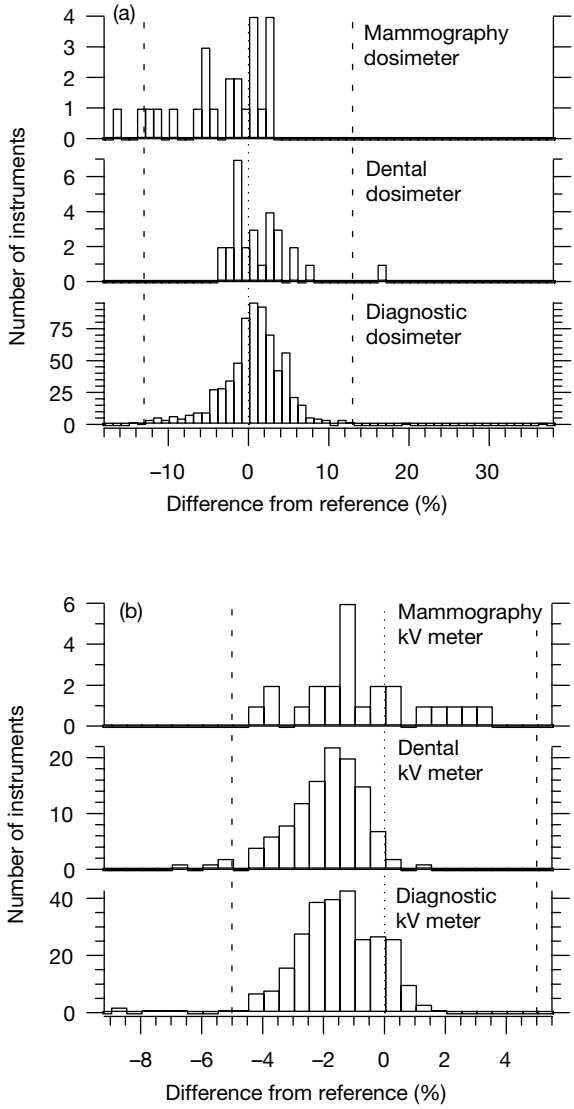

FIG. 1. Global results of dosimeters (a) and kV meters (b). Tolerances are shown by the vertical dotted lines. As for the other figures, the tolerances shown are the verification tolerance plus the laboratory uncertainty.

3.3. mAs meters and exposure chronometers

The mAs meters and exposure chronometers are electrical instruments that are straightforwardly traceable to national standards. The Swiss reference

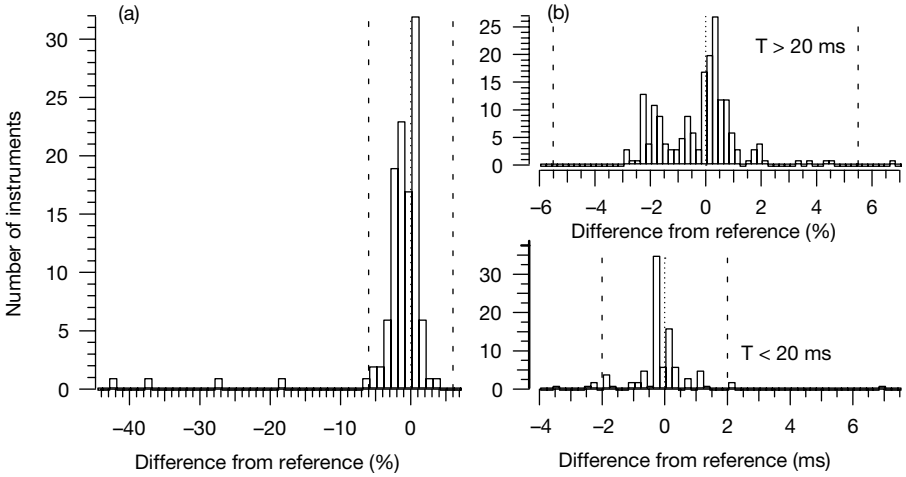

FIG. 2. Global results of mAs meters (a) and exposure chronometers (b). Tolerances are shown by the vertical dotted lines.

instruments are invasive instruments connected in series to a high voltage generator. As shown in Fig. 2, the great majority of the measurements are close to the reference value: only about 3% of the controlled instruments are outside the tolerance values.

3.4. Optical densitometers

The Swiss reference for diffuse optical density is a film strip calibrated at the German primary standards dosimetry laboratory (the PTB). The test consists of comparing the measured and reference values. Figure 3 shows the distributions of the 21 measured steps. It can be seen that the few points outside the tolerances concern only two of the 142 instruments tested and imply a slight overestimation of optical densities around 1.00.

3.5. Sensitometers

The case of film sensitometers is by far the most unclearly defined quantity dealt with in this study. As shown in Table I, the tolerances applied to such instruments are defined in terms of optical density for each of the 21 steps. Each film is exposed with a reference and the customer's sensitometer. Two films are exposed, one with green and another with blue light, processed and read by a calibrated densitometer. The principle of the method is the fact that, ideally, two sensitometers should produce the same illumination on a given

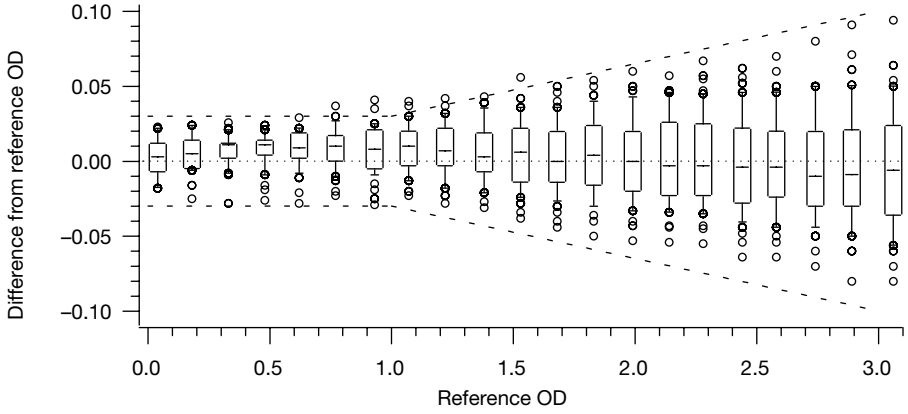

FIG. 3. Global results of the optical densitometers. The median is shown by the horizontal middle line, the boxes are the central quartiles (25% and 75%) and the whiskers show the 95% and 5% extent of the data. Values outside the 5–95% interval are shown by dots. Dotted lines show the tolerances.

film, and therefore each step should lead to the same optical density. The problem is the lack of sensitometer primary standards.

Currently only Germany (the PTB and some manufacturers) has proposed a method to standardize sensitometers, through the Deutsches Institut für Normung (DIN) [8] with LE and LK parameters, where LE is the film light sensitivity and LK is the light contrast measured on a film exposed with a light sensitometer, for a given processing condition. A comparison of the current Swiss and DIN requirements for all the instruments tested up to the present is presented in Fig. 4. Measurements are shown with crosses if they comply with the requirements defined in Table I or with dots if they do not comply for at least one light colour. For each film strip, LE and LK have also been computed in order to compare the Swiss and DIN requirements. Figure 4 is presented in terms of difference from the reference instrument in LE (Fig. 4(a)) and LK (Fig. 4(b)). It can be seen that the present Swiss tolerances are essentially equivalent to a tolerance expressed in terms of LE.

3.6. Luxmeters

Luxmeters are tested in a given light field by comparison with a reference luxmeter calibrated at the Swiss NMI (METAS). Figure 5 shows that the luminescence spread of the instruments is relatively wide and close to the tolerance values. Some 7% of the instruments do not comply with the requirements.

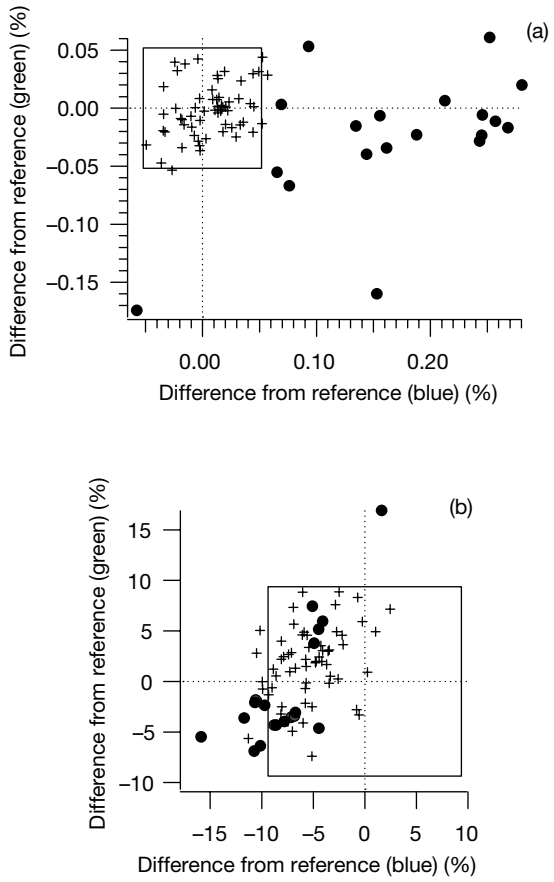

FIG. 4. Difference between measured and reference LE (a) and LK (b) obtained in green and blue light. Crosses show the instruments that were within the tolerances and round dots show the instruments outside the tolerances. Squares show possible tolerances expressed in terms of LE (±0.05%) and LK (±9.5%).

4. DISCUSSION

With a reference instrument relative uncertainty ($k = 2$) of 3%, the almost perfectly centred distributions observed for the dosimeters can be considered to be good. The spread of the values (standard deviation of more than 4%) could surely be improved, but clearly fits within the tolerance values.

The kV meter distributions are significantly shifted towards negative values. The root of the problem lies in the fact that the measured quantity (the kV peak) is not directly measured by NMIs and is not yet sufficiently clearly defined. An informal ring comparison realized by the authors of this paper with

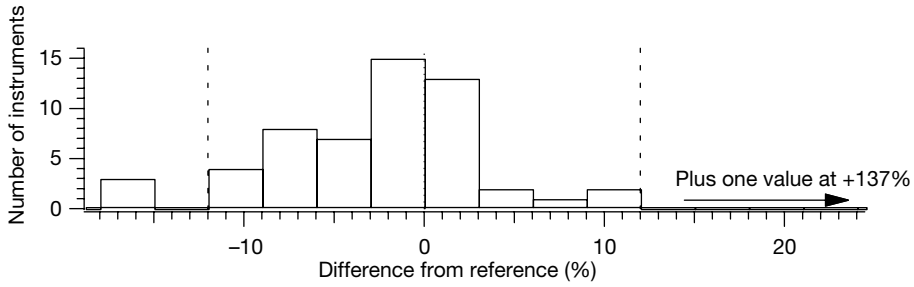

FIG. 5. Global results of the luxmeters. Tolerances are shown by the vertical dotted lines.

one instrument in 2000 between laboratories in Germany, Sweden and the UK showed differences of up to 3%. It is hoped that the solution of the problem lies in a new International Electrotechnical Commission standard [9], which defines a new quantity of interest, the practical tube voltage.

As is apparent from Table I, the worst situation arises with the sensitometers, for which about 23% of the instruments checked were outside the tolerance. A close look at failing instruments shows that almost all failures came from one model produced by a United States manufacturer that used to have a different reference from that of the German manufacturer's model. This has been corrected for the more recent models. Even more than for kV meters, the metrological situation would clearly be improved with a better primary measurement of this quantity.

5. CONCLUSION

Verification periodically performed by an independent institution can guarantee a good metrological quality of field instruments. The Swiss experience with diagnostic radiology instruments used to perform official quality controls shows that the great majority are within acceptable tolerance values.

The weakest aspects of the verification performed on these instruments lie in the need for proper primary standards for kV meters and sensitometers. The introduction of a new standard for kV meters [8] should solve the problem. The lack of an international consensus on sensitometers could be an insurmountable obstacle.

REFERENCES

[1] Mutual Recognition of National Measurement Standards and of Calibration and Measurement Certificates Issued by National Metrology Institutes, Comité international des poids et mesures, Sèvres (1999).

[2] EUROPEAN UNION, Council Directive 97/43/Euratom of 30 June 1997, Health Protection of Individuals Against the Dangers of Ionizing Radiation in Relation to Medical Exposure (Repealing Directive 84/466/Euratom, O.J. No. L 265/1, 5.10.1984), Official Journal of the European Communities No. L 180/22–27, Luxembourg (1997).

[3] MUNCH, W., STUCKI, G., MONING, R., VAUCHER, B., Standardization of a reference dosimeter system for radiotherapy in Switzerland, Z. Med. Phys. **11** (2001) 269–278.

[4] METAS directives on radiation diagnostic instruments from 30 June 1997, http://www.metas.ch/fr/calib/dod/w5014_f.pdf

[5] SWISS FEDERAL DEPARTMENT OF THE INTERIOR, Ordonnance sur les installations radiologiques à usage medical, Ord. 814.542.1, 20 January 1998, http://www.admin.ch/ch/f/rs/8/814.542.1.fr.pdf

[6] BOCHUD, F.O., GRECESCU, M., VALLEY, J.-F., Calibration of ionization chambers in air kerma length, Phys. Med. Biol. **46** (2001) 2477–2487.

[7] INTERNATIONAL ELECTROTECHNICAL COMMISSION, Medical Diagnostic X-ray Equipment — Radiation Conditions for Use in the Determination of Characteristics, IEC 61267, IEC, Geneva (1994).

[8] DEUTSCHES INSTITUT FÜR NORMUNG, Image Quality Assurance in Diagnostic X-ray Departments — Part 55: Acceptance Testing of Direct Medical Radiographic X-ray Systems; Acceptance System or Film Processing, DIN V 6868-55, DIN, Berlin (1996).

[9] INTERNATIONAL ELECTROTECHNICAL COMMISSION, Medical Electrical Equipment — Dosimetric Instruments Used for Non-invasive Measurement of X-ray Voltage in Diagnostic Radiology, IEC 61676, IEC, Geneva (2002).

BLANK

RECOMMENDATIONS FOR PATIENT DOSIMETRY IN DIAGNOSTIC RADIOLOGY USING THERMOLUMINESCENCE DOSIMETRY

J. ZOETELIEF
Interfaculty Reactor Institute, Delft University of Technology,
Delft, Netherlands
E-mail: j.zoetelief@iri.tudelft.nl

H.W. JULIUS
Putten, Netherlands

P. CHRISTENSEN
Risø National Laboratory, Roskilde, Denmark

Abstract

According to the Medical Exposure Directive, member States of the European Union shall promote the establishment and use of diagnostic reference levels for radiodiagnostic examinations; similarly, the IAEA Basic Safety Standards introduced guidance levels. Information on patient dose is consequently becoming increasingly important. Thermoluminescent dosimeters are often applied for patient dosimetry in radiology. Laboratories specialized in thermoluminescence dosimetry (TLD) usually provide services in personal dosimetry, but may lack expertise in patient dosimetry in diagnostic radiology. Conversely, experts on dosimetry in diagnostic radiology may not have sufficient expertise in TLD. Recommendations for patient dosimetry in diagnostic radiology using TLD have therefore been made within the framework of the European Commission's Programme on Radiation Protection.

1. INTRODUCTION

In the Medical Exposure Directive (MED) [1] it is stated that member States of the European Union shall promote the establishment and use of diagnostic reference levels (DRLs) [2] for radiodiagnostic examinations, and the availability of guidance for this purpose having regard to European DRLs where available. Similarly, the Basic Safety Standards [3] introduced the term 'guidance level' as a level of a specified quantity above which appropriate actions should be considered. More recently this has been reformulated by the IAEA to provide guidance on what is achievable with current good practice.

Consequently, information on patient dose is becoming increasingly important. Thermoluminescent dosimeters are often used for patient dosimetry in diagnostic and interventional radiology.

Although expertise in patient dosimetry and appropriate technical facilities should preferably be available locally, in order that dose measurements can be made in-house, it is recognized that dosimetric resources, such as well trained specialists, high quality equipment and calibration facilities, are not always present. However, appropriate assistance and dosimetric services can often be obtained from third parties. Laboratories specialized in thermoluminescence dosimetry (TLD) may provide services for individual monitoring for radiation protection purposes, but may lack expertise in patient dosimetry in diagnostic radiology. Conversely, experts on patient dosimetry in radiology may need additional information on the use of thermoluminescent dosimeters for this purpose. It therefore seemed useful to make recommendations for patient dosimetry in diagnostic radiology using TLD. These recommendations have been made for European Union member States [4].

2. DOSIMETRIC CONCEPTS AND DOSE QUANTITIES

Three objectives have been formulated for dosimetry in diagnostic radiology: (1) the measurement of patient dose for comparison with DRLs (involving patients); (2) the assessment of equipment performance (using phantoms); and (3) patient dose measurements for the assessment of risk (involving patients). Since the dosimetric approaches in general diagnostic radiology, mammography and computed tomography (CT) are slightly different, they are treated separately. The range of applications, objectives, dose quantities and measurement methods is given in Table I. The dosimetric quantities are the entrance surface dose in the presence of a patient or a phantom (ESD_{pp}), the entrance surface dose in the absence of a patient or a phantom (ESD_{pa})[1], the dose area product (DAP), the effective dose (E), the average glandular dose (AGD), the CT dose index free in air ($CTDI_{air}$), the weighted CTDI ($CTDI_{w}$) and the dose length product (DLP). Definitions of the dosimetric quantities used in CT are given elsewhere [5].

[1] It should be noted that ESD_{pp} and ESD_{pa} in today's nomenclature would be replaced by entrance surface air kerma and incident air kerma, respectively.

TABLE I. DOSE QUANTITIES FOR VARIOUS APPLICATIONS IN DIAGNOSTIC RADIOLOGY

Field of application	Objective	Dose quantity	Measurement method	Performed in	Best method	Present procedure
General diagnostic radiology	2	ESD_{pp}	TLD, IC	Phantom	TLD	TLD
	1	ESD_{pp}	TLD, IC	Patients	TLD	TLD
	1	DAP	IC	Patients	IC	—
	3	E	TLD, IC and DCF	Patients	IC and DCF	—
Mammography	2	ESD_{pa}	TLD, IC	Phantom	IC	TLD
	2	AGD	TLD, IC and DCF	Phantom	IC	TLD
	1	ESD_{pp}	TLD	Patients	IC	TLD
	3	AGD		Patients	IC	TLD
CT	2	$CTDI_{air}$	TLD, IC	Free in air	IC	TLD
	2	$CTDI_{w}$	TLD, IC	Phantom	IC	—
	1	DLP	TLD, IC	Phantom	IC	—
	3	E	TLD, IC and DCF	Phantom	IC	—

Note: The ionization chambers (IC) can be the thimble or parallel-plate type (for the measurement of ESD_{pa} and the calibration of output, respectively), transmission type (DAP) or CT type. Dose conversion factors (DCFs) can be employed to derive the organ and effective doses from the measured dose quantities.

2.1. Measurements on patients

Dose measurements on patients in general diagnostic radiology or mammography to meet objectives 1 and 3 generally refer to the assessment of ESD or DAP. Measurements for typical common diagnostic radiology procedures should be performed for a sufficient number of patients to obtain a reliable average value. At least ten patients of average size are recommended. Such measurements provide insight into the dose variation among individual patients and of actual clinical practice. It is recommended that ESD_{pp} for adult patients be measured using thermoluminescent dosimeters provided by an issuing laboratory. Information on the examination conditions is obtained through questionnaires. Local staff should select at least ten patients for the application of the thermoluminescent dosimeters and complete the questionnaire for each patient. The issuing laboratory should process the thermoluminescent dosimeters and derive the mean value of ESD_{pp}.

2.2. Measurements using phantoms

Phantoms can be used for the measurement of, for example, ESD_{pp} when a comparison is to be made between different installations and for the assessment of equipment performance (objective 2). To meet objective 3, the assessment of organ and effective doses, measurements can be made inside phantoms. This approach has been used by various authors, using thermoluminescent dosimeters and RANDO phantoms. The method is too laborious for routine use, but is valuable for the verification of calculated DCFs. Measurements of ESD_{pp} on phantoms, using thermoluminescent dosimeters provided by an issuing laboratory, to meet objective 2, are described in Ref. [4].

There are various types of phantom for dosimetry in diagnostic radiology (i.e. anthropomorphic, reference and standard phantoms). An anthropomorphic (or body) phantom has the shape of a human body, or part of it. It may consist of various tissue substitutes simulating the human body with respect to size, shape, position, mass density and radiation interactions. Reference phantoms are used to mimic attenuation in a certain part of the body, and often consist of polymethylmethacrylate (PMMA) and aluminium. A standard phantom consists of one material only, with a clearly defined geometry, elemental composition and mass density [6]. Some characteristics of the recommended phantoms are shown in Table II. It should be borne in mind that the phantoms represent average sized adult patients, and, therefore, do not allow accurate dose assessments for individuals of variable size and/or body composition.

3. DOSIMETRY USING TLD

TLD is widely used for dose measurements in diagnostic radiology. The availability of thermoluminescent dosimeters in a variety of physical forms makes them particularly suitable for measurements of the entrance surface dose. Properly encapsulated, small sized dosimeters can be attached directly and unobtrusively to the patient's skin, with very little interference with patient mobility and comfort. By choosing thermoluminescent detectors made from nearly air equivalent materials, corrections due to energy and angular dependencies of the dosimeters for the measurement of air kerma can be minimized, resulting in a simple measurement procedure with satisfactory accuracy. The energy and angular response, fading and environmental factors, and annealing and readout parameters are discussed in some detail in Ref. [4].

The advantages and drawbacks of different thermoluminescent detectors are summarized below. Preferably, near air equivalent detector materials should be used to measure the air kerma accurately (Z_{eff} = 7.64). Thus errors

TABLE II. SOME CHARACTERISTICS OF THE PHANTOMS RECOMMENDED FOR DOSIMETRY [4]

Phantom	Cross-section (cm × cm)	Thickness (cm)	Depth	Material
STUK (skull)	25.4 × 25.4	4.3	—	PMMA
	25.4 × 25.4	0.5	—	Aluminium
CDRH (chest)	25.4 × 25.4	2 × 0.93 + 5.40	—	PMMA
	25.4 × 25.4	0.25 + 0.16	—	Aluminium
	25.4 × 25.4	19	—	Air gap
CDRH (abdomen)	25.4 × 25.4	17 (outside spinal region)	—	PMMA
	25.4 × 7	16.9 + 1 + 1 (spinal region)	—	PMMA
	25.4 × 7	0.2 + 0.2 (spinal region)	—	Aluminium
Standard breast	15 × 10 or semicircular (radius ≥ 10)	4.5 (beam direction)	Surface, various depths	PMMA
CT (head)	Circular: radius 8	14 (perpendicular to beam direction)	At centre and four equally spaced at radii of 5 cm and 7 cm	PMMA
CT (body)	Circular: radius 16	14 (perpendicular to beam direction)	At centre and four equally spaced at radii of 5, 10 and 15 cm	PMMA

due to differences in response as a function of photon energy will be avoided. From calculated and experimental energy response curves it can be seen that LiF (Z_{eff} = 8.2), $Li_2B_4O_7$ (Z_{eff} = 7.4) and BeO (Z_{eff} = 7.1) all show energy response curves close to that of air. BeO has attracted less attention as an air and tissue equivalent phosphor, mainly because of its extreme light sensitivity, pyroelectric properties and high toxicity in powder form [7]. Although $Li_2B_4O_7$ shows the best air and tissue equivalence, it has some drawbacks compared with LiF: the fading is higher and can be influenced significantly by humidity. Furthermore, the thermoluminescence spectrum is close to infrared, which may be confused with the black body radiation from the heater. LiF:Mg,Ti and LiF:Mg,Cu,P both show excellent fading properties [8], satisfactory sensitivity for dose measurements in the μGy range [9] and light emission in the blue

wavelength region. The sensitivity of LiF:Mg,Cu,P is about a factor of 25 higher than that of LiF:Mg,Ti and therefore is particularly interesting for the measurement of very low doses. A problem of LiF:Mg,Cu,P is that it shows glow peaks above the required limit of the maximal readout and annealing temperature of 240°C. A short annealing process at this temperature using the thermoluminescent reader itself is not sufficient for the complete release of all electrons from the high temperature traps, and the residual thermoluminescence will increase the background for the next reading. A 30 min, 240°C oven annealing is satisfactory for an almost complete removal of the residual thermoluminescence. However, it should be mentioned that a small decrease of thermoluminescence sensitivity occurs during prolonged annealing at this temperature (i.e. approximately 1% per 30 min of annealing [10]). The problem of residual thermoluminescence can be avoided by using computerized glow curve analysis, in which the net thermoluminescent signal due to the dose to be measured can be identified. Normal reader annealing can be used with this feature [11]. For the reading of LiF:Mg,Cu,P using hot gas it may be possible to apply heating temperatures above 240°C, as no change of sensitivity of LiF:Mg,Cu,P was found for a series of 50 successive readings using gas temperatures of up to 275°C [12].

3.1. Standard uncertainty of estimated air kerma, *K*

Detailed information is given on the uncertainty analysis for air kerma measurements using thermoluminescent dosimeters, following the concept of combined standard uncertainty [4]. The air kerma, K, can be estimated from:

$$K = (C_{\text{meas}} - C_{\text{BG}})K_{\text{cal}}K_E K_F \tag{1}$$

where

C_{meas} is the corrected (for reading without a detector (TL_{instr}) and individual response factor (S_i)) measurement value: $(TL_{\text{meas}} - TL_{\text{instr}})/S_i$.
C_{BG} is the background contribution, corrected for individual sensitivity.
K_{cal} is the air kerma calibration factor.
K_E is the energy correction factor.
K_F is the fading correction factor.

The combined standard uncertainty in K, $u(K)$, can be obtained from the individual uncertainties associated with K, $u_K(i)$:

$$u(K) = [u_k^2(C_{\text{meas}}) + u_k^2(C_{\text{BG}}) + u_k^2(K_{\text{cal}}) + u_k^2(K_E) + u_k^2(K_F)]^{½} \tag{2}$$

where $u_K(i)$ is the product of the standard uncertainty, $u(i)$, and the sensitivity coefficient, $c(i)$ [13]. The sensitivity coefficient describes the extent to which the output estimate, K, is influenced by variations of the input parameter, and can be obtained from: $c(i) = \partial K/\partial X_i$, where X_i are the parameters presented in Eq. (2), for example $c(C_{meas}) = \partial K/\partial C_{meas} = K_{cal}K_EK_F$. Table III contains the different components involved in the estimation of the standard uncertainty $u(K) = 0.10$ mGy.

4. PROCEDURES AND QUESTIONNAIRES

Protocols and questionnaires are provided for laboratories that offer dosimetric services to the staff of radiological facilities [4]. They can also be applied to other types of dosimeter provided and read by issuing laboratories, or when dosimetric facilities are available locally. Table IV shows the types of examination included in general diagnostic radiology covered in Ref. [4].

TABLE III. EXAMPLE OF AN UNCERTAINTY BUDGET [13] FOR THE ESTIMATED AIR KERMA, K

Quantity	Estimate	Standard uncertainty ($u(i)$)	Sensitivity coefficient ($c(i)$)	Uncertainty contribution ($u_K(i)$)	Additional comments
C_{meas}	1040 counts	32 counts	0.002 mGy/count	0.064 mGy	[a]
C_{BG}	10 counts	9 counts	–0.002 mGy/count	–0.018 mGy	[b]
K_{cal}	0.0025 mGy/count	7.5×10^{-5} mGy/count	840 counts	0.063 mGy	[c]
K_E	0.80	0.015	2.63 mGy	0.040 mGy	[d]
K_F	1.02	0.012	2.06 mGy	0.025 mGy	[d]
K	2.10 mGy	—	—	0.10 mGy	—

[a] $C_{meas} = (TL_{meas} - TL_{instr})/S_i$. Analogously with the uncertainty budget presented for K, a new uncertainty budget can be set up for C_{meas}, resulting in $u(C_{meas}) = 32$ counts.

[b] $C_{BG} = (TL_{BG} - TL_{instr})/S_{BG}$. As in footnote a, an uncertainty budget can be used to make an estimate of $u(C_{BG}) = 9$ counts.

[c] $u(K_{cal})$ is a combined type A (estimated from the measurement) and type B uncertainty (from the calibration at the reference radiation).

[d] $u(K_E)$ and $u(K_F)$ are obtained by assuming a rectangular probability distribution [13].

TABLE IV. TYPES OF EXAMINATION IN GENERAL DIAGNOSTIC RADIOLOGY COVERED IN REF. [4]

Type of examination	Projection[a]
Chest	PA and LAT
Skull	PA and LAT
Lumbar spine	AP, PA, LAT and LSJ (possibly when the LSJ is not adequately visualized on the lateral projection)
Pelvis	AP
Urinary tract	AP (before and after the administration of contrast medium)

[a] AP: anteroposterior. LAT: lateral. LSJ: lumbosacral joint. PA: posteroanterior.

5. EVALUATION, INTERPRETATION AND REPORTING OF RESULTS AND FOLLOW-UP ACTIONS

Information is presented on the evaluation of doses measured by thermoluminescent dosimeters exposed in accordance with the procedures provided. The completed questionnaires provide information on the exposure conditions of the thermoluminescent dosimeters. Furthermore, information is given on the interpretation and reporting of results. In addition, some suggestions for follow-up actions are given.

6. CONCLUSION

The recommendations given for patient dosimetry in diagnostic radiology can be adopted by laboratories providing dosimetry services using TLD but lacking expertise in patient dosimetry in diagnostic and interventional radiology. Conversely, the recommendations can be applied by experts on patient dosimetry in radiology to develop an in-house dosimetry system based on the use of thermoluminescent dosimeters. The recommendations are aimed at the harmonization of patient dosimetry throughout the European Union.

ACKNOWLEDGEMENTS

This work was performed within the framework of the European Commission's Programme on Radiation Protection.

REFERENCES

[1] EUROPEAN UNION, Council Directive 97/43/Euratom of 30 June 1997, Health Protection of Individuals against the Dangers of Ionizing Radiation in Relation to Medical Exposure (Repealing Directive 84/466/Euratom, O.J. No. L 265/1, 5.10.1984), Official Journal of the European Communities No. L 180/22–27, Luxembourg (1997).

[2] INTERNATIONAL COMMISSION ON RADIOLOGICAL PROTECTION, Radiological Protection and Safety in Medicine, Publication 73, Pergamon Press, Oxford and New York (1996).

[3] FOOD AND AGRICULTURE ORGANIZATION OF THE UNITED NATIONS, INTERNATIONAL ATOMIC ENERGY AGENCY, INTERNATIONAL LABOUR ORGANISATION, OECD NUCLEAR ENERGY AGENCY, PAN AMERICAN HEALTH ORGANIZATION, WORLD HEALTH ORGANIZATION, International Basic Safety Standards for Protection against Ionizing Radiation and for the Safety of Radiation Sources, Safety Series No. 115, IAEA, Vienna (1996).

[4] ZOETELIEF, J., JULIUS, H.W., CHRISTENSEN, P., Recommendations for Patient Dosimetry in Diagnostic Radiology using TLD, EUR 19604, Office for Official Publications of the European Communities, Luxembourg (2000).

[5] EUROPEAN COMMISSION, Quality Criteria for Computed Tomography, EUR 16262, Office for Official Publications of the European Communities, Luxembourg (1999).

[6] INTERNATIONAL COMMISSION ON RADIATION UNITS AND MEASUREMENTS, Phantoms and Computational Models in Therapy, Diagnosis and Protection, Rep. 48, ICRU, Bethesda, MD (1992).

[7] HOROWITZ, Y.S., Thermoluminescence and Thermoluminescent Dosimetry, CRC Press, Boca Raton, FL (1984).

[8] WANG, S., WANG, Y., CAI, G., WANG, S.H., ZHA, Z., A new TL detector developed for multiple applications, Radiat. Prot. Dosim. **47** (1993) 223–225.

[9] BILSKI, P., BUDZANOWSKI, M., OLKO, P., CHRISTENSEN, P., Properties of different thin-layer LiF:Mg,Cu,P TL detectors for beta dosimetry, Radiat. Prot. Dosim. **66** (1996) 101–104.

[10] CHRISTENSEN, P., Study of LiF:Mg,Cu,P TL detectors for individual monitoring for weakly penetrating radiations, Radiat. Prot. Dosim. **47** (1993) 425–430.

[11] DELGADO, A., GÓMEZ ROS, J.M., MUÑIZ, J.L., Computerised analyses of LiF Gr-200 TL signals: Application to dose measurements in μGy range, Radiat. Prot. Dosim. **60** (1995) 147–153.

[12] SÁEZ-VERGARA, J.C., ROMERO, A.M., The influence of the heating system on the hypersensitive thermoluminescent material LiF:Mg,Cu, P (GR-200), Radiat. Prot. Dosim. **66** (1996) 431–436.

[13] EUROPEAN CO-OPERATION FOR ACCREDITATION, Expression of the Uncertainty of Measurements in Calibration, EAL-R2, 1st edn, European Co-operation for Accreditation, Paris (1997).

BLANK

COMPARISON OF AIR KERMA MEASUREMENTS IN MAMMOGRAPHY USING THERMOLUMINESCENT DOSIMETERS

F. PERNIČKA*, J. DANEŠ**, F. GICZI***, C. MILU+, D. NIKODEMOVÁ++, M.A. STANISZEWSKA+++, M. ORESEGUN*, C. MACCIA§, R. PADOVANI§§, E. VANO§§§

* Division of Human Health, International Atomic Energy Agency, Vienna
E-mail: f.pernicka@iaea.org

** Charles University, Prague, Czech Republic

*** National Research Institute for Radiobiology and Radiohygiene, Budapest, Hungary

\+ Institute of Hygiene and Public Health, Bucharest, Romania

++ Institute of Preventive and Clinical Medicine, Bratislava, Slovakia

+++ Nofer Institute of Occupational Medicine, Łódź, Poland

§ Centre d'assurance de qualité des applications technologiques dans le domaine de la santé, Bourg-la-Reine, France

§§ Istituto di Fisica Sanitaria, Udine, Italy

§§§ Complutense University, Madrid, Spain

Abstract

A co-ordinated research project, Image Quality and Patient Dose Optimization in Mammography in Eastern European Countries, was conducted by the IAEA, which aimed at defining a methodology for the implementation of a quality assurance programme in mammography and at exercising the assessment of image quality and patient doses in a sample of hospitals in eastern European countries. A comparison of dosimetry systems has been organized to ensure that dose measurements carried out within the framework of the project are comparable. Selected mammography units from the Czech Republic, Hungary, Poland, Romania, Slovakia and Spain participated in the exercise. The thermoluminescence method was selected for the comparison. The

dosimeters were irradiated free in air to values of air kerma in the range of 5 mGy to 9 mGy and mailed to the participants for evaluation. Deviations of measured values from the true values of less than 10% were considered a measure of good dosimetry performance. The results of the comparison showed that about 70% of reported values of air kerma were outside the 10% acceptance limit. Two follow-up exercises were organized. The first follow-up resulted in only 20% of reported values exceeding the limit, and during the second follow-up all results were within the acceptance limit.

1. INTRODUCTION

Screening by mammography is frequently carried out for asymptomatic women, and hence a favourable ratio between the benefits and undesirable effects of the procedure is important. During the past few decades there have been significant advances in the equipment used for mammography. However, even when the latest equipment and imaging systems are used, there is considerable variation from centre to centre in the choice of imaging parameters and techniques. There may be quite large variations in image quality and breast dose among the centres.

A co-ordinated research project, Image Quality and Patient Dose Optimization in Mammography in Eastern European Countries, was conducted by the IAEA, which aimed at defining a methodology for the implementation of a quality assurance (QA) programme in mammography and at exercising the assessment of image quality and patient doses in a sample of hospitals in eastern European countries. Selected mammography units from the Czech Republic, Hungary, Poland, Romania and Slovakia participated in this project. The teams consisted of experienced clinicians and physicists. They were supported by a group of experts (clinicians and medical physicists) from France, Italy and Spain. As an outcome of the project, improvements in the indicators for image quality and patient dose after the implementation of the QA programme are expected. A comparison of dosimetry systems has been organized to ensure that dose measurements carried out within the framework of the project are comparable. All five eastern European countries plus Spain took part in the exercise. The thermoluminescence method was selected for the comparison.

2. MATERIALS AND METHODS

To be meaningful, each measurement has to be traceable to the International System of Units (SI), and its uncertainty needs to be minimized. An uncertainty of 10% in measurement is sufficient in order to enable comparisons

between various mammography units [1]. The European Protocol on Dosimetry in Mammography [2] requires that the accuracy and precision of thermoluminescence measurements of entrance surface air kerma on patients and phantoms have an uncertainty better than 10%. This criterion was selected as a measure of good dosimetry performance. The participants were asked to send four sets of non-irradiated dosimeters to the IAEA for the reference irradiation. One set consisted of three thermoluminescent chips or pellets enclosed in a sachet of a low attenuation material such as aluminized foil, which was heat sealed and coded. Three dosimeter sets were irradiated at the IAEA Dosimetry Laboratory at radiation qualities representing the mammography beams used in clinical practice [3]. One dosimeter set was used to assess the contribution of various environmental factors to the measured signal.

2.1. Reference irradiation

A General Electric Senographe DMR unit is used to generate X ray beams at the IAEA Dosimetry Laboratory. A Radcal 10X5-6M ionization chamber connected to a Keithley 617 electrometer serves as a laboratory standard. It was calibrated at the Physikalisch-Technische Bundesanstalt (Germany) and the National Institute of Standards and Technology (United States of America). The X ray machine output is monitored using a PTW 30 363 transmission ionization chamber. A laser and a telescope are used to ensure the positioning of the dosimeters on a calibration bench. The uncertainty in measured air kerma for the reference beams is 1.6% (coverage factor $k = 2$). In total, 17 mammography beam qualities were established at the laboratory [3]. They are mainly used for the calibration of national standards from secondary standards dosimetry laboratories. The qualities selected for the irradiation of thermoluminescent dosimeters, together with their parameters, are listed in Table I.

TABLE I. MAMMOGRAPHY X RAY BEAMS USED DURING THERMOLUMINESCENCE DOSIMETRY COMPARISONS

Radiation quality[a]	Tube potential (kV)	Added filtration (mm)	First half-value layer (mm Al)	Homogeneity coefficient[b]
MoMo-25	25	0.03 Mo	0.297	0.77
MoMo-28	28	0.03 Mo	0.328	0.78
MoMo-35	35	0.03 Mo	0.382	0.80

[a] The beam codes are a combination of the chemical symbol of the anode and the filter material, followed by the potential of the tube in kilovolts.

[b] The homogeneity coefficient is defined as the ratio of the first half-value layer to the second half-value layer.

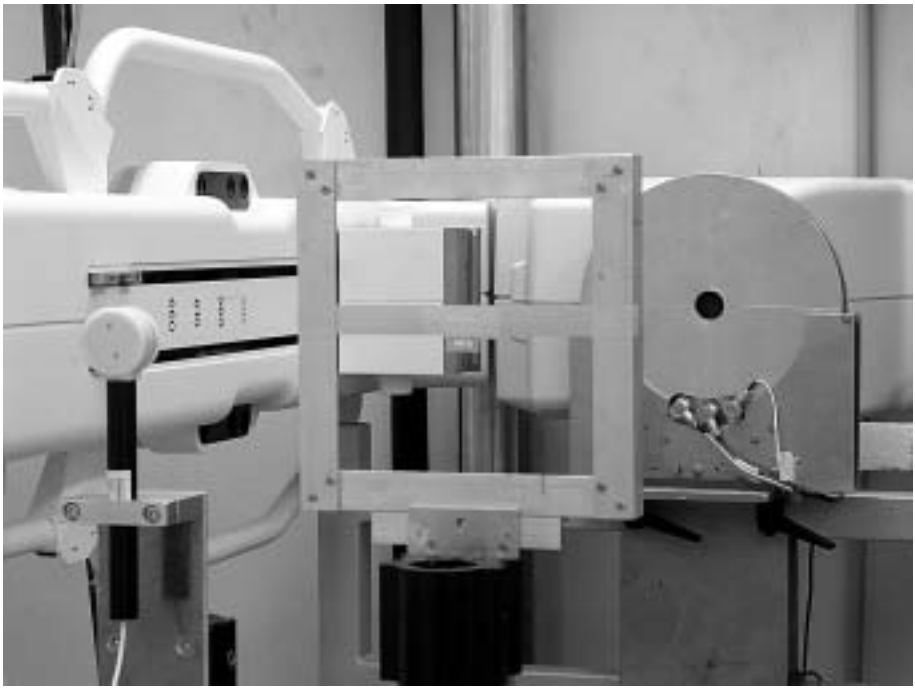

FIG. 1. Irradiation set-up at the IAEA Dosimetry Laboratory.

The air kerma at 1 m distance from the X ray focus was measured for selected loadings of the tube. The values of air kerma per monitor unit were established for each radiation quality. The irradiation set-up is shown in Fig. 1. The dosimeters were irradiated free in air using a substitution method. They were positioned in the middle of an aluminium frame and fixed by tape. The dimensions of the frame were sufficiently large to prevent the X rays from scattering significantly from the metal. The thermoluminescent dosimeter holder replaced the standard ionization chamber, and the dosimeters were exposed. The value of air kerma used to expose the dosimeters (range: 5–9 mGy) was calculated from the measured signal of the monitor chamber corrected for ambient air pressure and temperature.

2.2. Evaluation of dosimeter responses

The irradiated dosimeters were mailed to the participants for their evaluation together with data sheets and information about irradiation conditions (i.e. date of irradiation, X ray target, filtration, tube potential, half-value layer, irradiation geometry) but excluding values of the reference air kerma

actually delivered (blind test). The participants were asked to follow the European Protocol [2] and calibrate their thermoluminescence dosimetry systems in terms of air kerma free in air. The beam from a molybdenum anode with a molybdenum filter generated at 28 kV was specifically recommended for the calibration. The participants were asked to apply all necessary corrections (energy dependence of dosimeter response, fading, linearity of the system, individual sensitivity of detectors) to their readings and report the measured values of air kerma to the IAEA.

The results of measurements were evaluated at the IAEA. Participants were informed about the results and they were given recommendations on how to improve their dosimetry.

3. RESULTS

The results of the first run of the comparison[1] are given in Fig. 2. The results show that about 70% of the reported values of air kerma were outside the acceptance limit of 10%.

The analysis of the initial comparison showed that the main sources of discrepancies were: (a) poor irradiation geometry during local calibration (backscatter from a phantom and scattering from surrounding materials); (b) the application of inadequate methods for local calibration (tungsten anode, comparison with a response to various other radiations); and (c) a lack of traceability of the local calibration (expired calibration, not traceable to a primary standard). The participants were given instructions on how to improve their dosimetry, and a follow-up exercise was organized[2].

The first follow-up resulted in about 20% of the reported values of air kerma lying outside the 10% margin (Fig. 3). This is a considerable improvement compared with the first run, but it was clear that the measurement problems were not completely corrected. The participants were individually consulted, with the aim of resolving the discrepancies. Their procedures were carefully checked and adjusted. A second follow-up (Fig. 3) was organized, which resulted in all measurements lying within the acceptance limit of 10%. The dosimetric results of the co-ordinated research project were then duly corrected.

---

[1] Participant No. 1 joined the comparison during the first follow-up, but as that was their initial test the measurements are included in this group of data.

[2] Participant No. 2 withdrew from the exercise due to serious problems with its thermoluminescence dosimetry system.

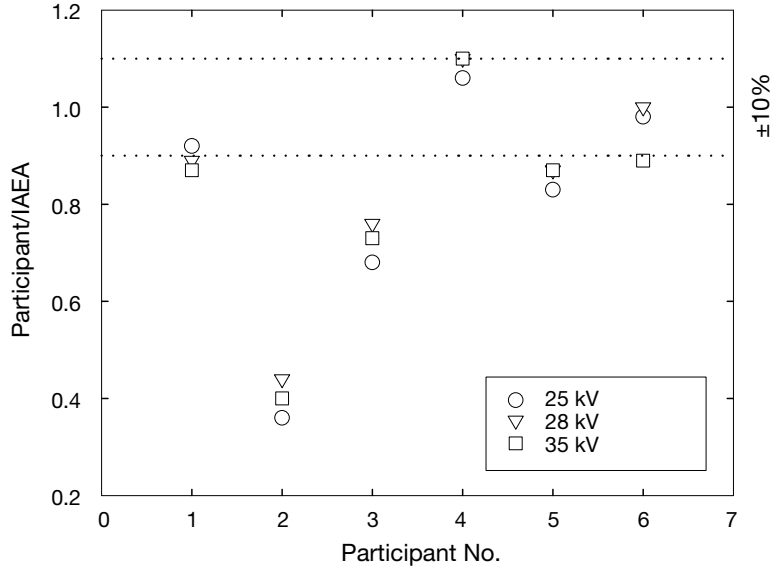

FIG. 2. Initial test results: ratios of the air kerma stated by the participant to the reference value provided by the IAEA Dosimetry Laboratory for the irradiation of thermoluminescent dosimeters in beams generated by a molybdenum anode with a molybdenum filter.

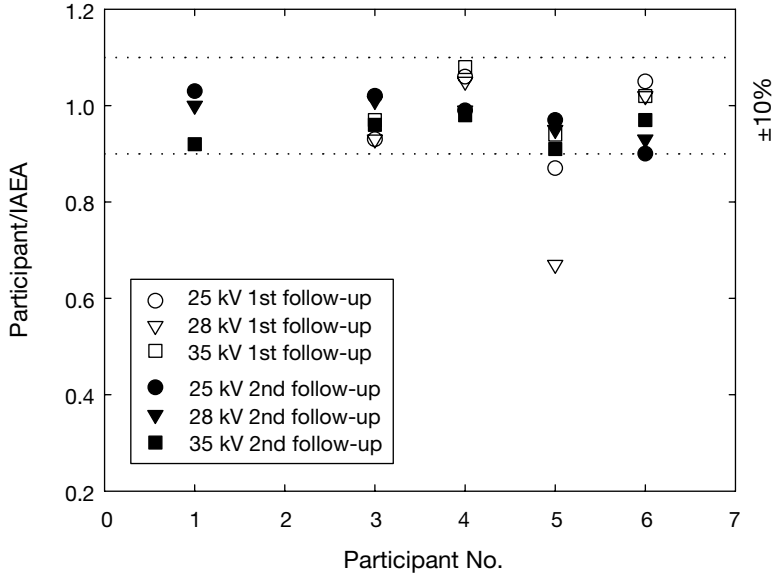

FIG. 3. Follow-up test results: ratios of the air kerma stated by the participant to the reference value provided by the IAEA Dosimetry Laboratory for the irradiation of thermoluminescent dosimeters in beams generated by a molybdenum anode with a molybdenum filter.

The individual results of the thermoluminescence dosimetry comparison are confidential and will not be disseminated without the permission of the participating institution.

4. CONCLUSIONS

The exercise shows that achieving the required 10% accuracy in mammography dose measurements is not an easy task; of course, this may also be true for other measurements in X ray diagnostics. The difficulty is mainly due to a lack of expertise in the measurement of these radiations and the poor traceability of calibrations. Many countries do not possess suitable measurement standards. In some cases the measuring instruments are calibrated only by manufacturers, which is not sufficient. A number of studies aim at establishing diagnostic reference levels (or guidance levels). These may have important implications for diagnostic practice. It is important that the measurements that are a basis for the establishment of diagnostic reference levels be accurate.

ACKNOWLEDGEMENTS

The authors would like to thank R. Girzikowski of the IAEA for his assistance with reference irradiations of thermoluminescent dosimeters. This work has been made possible by the participation of and stimulating discussion with: L. Gonzalez from the Complutense University in Madrid; J. Jankowski from the Nofer Institute of Occupational Medicine in Łódź; D. Kroutiliková from the National Radiation Protection Institute in Prague; and P. Ortiz Lopez and M. Rehani from the IAEA.

REFERENCES

[1] WAGNER, L.K., et al., Recommendations on the performance characteristics of diagnostic exposure meters, Report of AAPM Diagnostic X-ray Imaging Task Group No. 6, Med. Phys. **19** (1992) 231–241.

[2] EUROPEAN COMMISSION, European Protocol on Dosimetry in Mammography, EUR 16263 EN, Office for Official Publications of the European Communities, Luxembourg (1996).

[3] PERNIČKA, F., ANDREO, P., MEGHZIFENE, A., CZAP, L., GIRZIKOWSKI, R., Standards for radiation protection and diagnostic radiology at the IAEA Dosimetry Laboratory, SSDL Newsletter No. 41 (1999) 12–23.

BLANK

CLINICAL DIAGNOSTIC COMPTON SCATTERING X RAY SPECTROMETRY USING SIMULATED HIGH PURITY GERMANIUM DETECTOR RESPONSES

Y. PICARD
Consumer and Clinical Radiation Protection Bureau, Health Canada, Ottawa, Ontario, Canada
E-mail: yani_picard@hc-sc.gc.ca

Abstract

The distributions of the energy deposition in a Compton spectrometer system using a high purity germanium (HPGe) detector were calculated using a Monte Carlo simulation code. Each distribution was computed using a quasi-monoenergetic primary beam of photons (windows of 0.1 keV, uniformly distributed) for energies ranging from 5 keV to 150 keV in 0.1 keV steps, covering the range used in diagnostic radiology. These allow the reconstruction of the energy spectrum of primary beams of photons of X ray tubes used clinically from the measured pulse height distribution of the spectrometer–detector system through an iterative maximum likelihood expectation maximization algorithm. The probability matrix used for the iterative reconstruction was calculated by convolving the energy resolution of the HPGe detector with the simulated energy deposition distributions. A mammography X ray tube with a molybdenum target operated at a potential of 28 kV was used to assess the technique.

1. INTRODUCTION

The superior energy resolution of high purity germanium (HPGe) detectors offers an advantage for accurate X ray spectrometry. However, the photon fluence rates of clinical X ray tubes are usually much higher than the count rates that can be handled by the detector without a pulse pile-up. The use of a Compton scattering method is very efficient in reducing the fluence rate [1]. A Compton scattering device, the Spectro-X (RTI Electronics) [2], is now commercially available. The photon beam is scattered by a Lucite rod placed in the Spectro-X. Shielding is provided to ensure that only the photons scattered at 90º enter the detector. The primary spectrum is reconstructed, using an algorithm [3], from the resulting pulse height distribution (PHD).

A new method to reconstruct the energy spectrum of primary beams from the PHDs obtained with this spectrometer is presented in this paper. The method consists of determining the energy deposition of the system for a set of narrow energy windows covering the entire energy spectrum used in diagnostic

radiology (up to 150 kV peak) using Monte Carlo simulations. The primary beam is obtained from the measured PHD using an iterative maximum likelihood expectation maximization (ML-EM) reconstruction algorithm [4].

2. MATERIALS AND METHODS

2.1. Monte Carlo simulation of the energy deposition distributions

The energy deposition distributions of an HPGe detector model GLP-10180/07 (EG&G Ortec) used within a Spectro-X were computed for a set of 1450 narrow energy windows (0.1 keV, uniformly distributed) of primary beams covering the useful range of diagnostic radiology (up to 150 kV peak) using a Monte Carlo simulation code, the EGSnrc code system [5]. The specifications of the detector are given in Table I. The primary beams simulated were parallel photon beams covering a rectangular field of 4 mm × 40 mm originating 1 m from the axis of the Lucite rod of the spectrometer and going towards it. The Lucite rod used had a diameter of 4 mm. To reduce simulation times, only the photon transport was simulated and energies transferred to electrons were deposited locally. This does not affect the accuracy of the simulation significantly since the electron track is relatively short at these energies. The simulations were run on personal computers running Linux, either a personal computer (PC) having a 1.4 GHz AMD Athlon processor or one of three IBM eServers xSeries 330 with dual 1.266 GHz Intel Pentium III processors. Since the Compton spectrometer scatters the primary beam to reduce the fluence rate, most of the photons from the primary beam are never detected. The Monte Carlo simulations are therefore very computer intensive, since most of the tracked photons will never end up in the detector. Thus the determination of statistically significant energy deposition distributions takes a long time. Fortunately, the geometry of the spectrometer and HPGe detector system is always the same; therefore, the energy depositions may be computed only once, stored and reused. For each of the 1450 energy windows, 10^{10} photons were simulated. Each energy deposition was stored in an array having a bin width of 0.1 keV.

2.2. Compton spectrometry

A constant DC potential X ray tube (Pantak) was used to assess the technique. Table II shows the tube specifications. The tube has a non-rotating anode and is water cooled. This type of tube has been developed for use as an accurate stable source for radiation calibration. The anode potential was set

TABLE I. HPGe DETECTOR SPECIFICATIONS

Crystal shape	Cylindrical
Crystal diameter	10 mm
Crystal length	10 mm
Thickness of beryllium window	0.127 mm
Resolution (FWHM[a]) at 5.9 keV, ^{55}Fe peak	0.18 keV
Resolution (FWHM) at 14.41 keV, ^{57}Co peak	0.24 keV
Resolution (FWHM) at 122.07 keV, ^{57}Co peak	0.48 keV

[a] FWHM: full width at half maximum.

TABLE II. X RAY TUBE SPECIFICATIONS

Target	Mo
Focal spot size, optical	2 mm × 2 mm
Anode angle	21º
Inherent filtration	1 mm Be

to 28 kV, a commonly used potential in mammography. The anode current was set to 5 mA for 50 000 s of detector live time to get a PHD with very good statistics. The spectrometer was placed such that there was a 1 m distance between the scattering rod of the spectrometer and the X ray tube focal spot. A 4 mm Lucite rod was used for scattering and was placed orthogonally to the X ray beam. Primary collimation was done using lead plates. Additional collimation of the primary beam to a rectangular field of 4 mm × 40 mm was provided by the Spectro-X. A lead cylinder was designed to provide extra radiation shielding around the detector end cap, as recommended in the Spectro-X manual. Inside the Spectro-X most of the photons that did not interact with the Lucite rod escape, and the photons scattered at an angle of about 90º are collimated to a 2 mm diameter circle at the detector window. The detector PHD was recorded using a DSPEC digital gamma ray spectrometer (EG&G Ortec).

The PHD was calibrated before the experiment using a ^{57}Co source placed simply in front of the detector until a minimum of 30 000 counts was recorded in the main channel of the 14.41 keV peak. The response of the detec-

tor was assumed to be linear[1] up to 150 keV, thus only the 14.41 keV and the 122.07 keV peaks were used for the calibration of the channel energy. To get the same bin width as for the Monte Carlo simulated response function, the amplifier gain was adjusted so that the 14.41 keV peak would appear in channel 144 and the 122.07 keV peak would appear in channel 1220. Pulses lower than channel 32 (corresponding to an energy of 3.2 keV) were not stored in the measured PHD.

2.3. Reconstruction of the primary beam

The energy spectrum of the X ray tube was reconstructed with the simulated energy deposition distributions using an iterative ML-EM reconstruction algorithm [4] inspired by Ref. [6]. It consists of solving the equation:

$$\left(\frac{\Delta N}{\Delta E}\right)_E^{k+1} = \left(\frac{\Delta N}{\Delta E}\right)_E^{k} \sum_i \left[\frac{p(E,i)\mathrm{PHD}(i)}{\sum_E \left[p(E,i) \left(\frac{\Delta N}{\Delta E}\right)_E^{k} \right]} \right] \tag{1}$$

for each iteration k, where $(\Delta N/\Delta E)_E^k$ is the number of photons in the primary beam having an energy E (bin width ΔE = 0.1 keV), PHD(i) is the number of counts from the measured PHD in channel i and $p(E,i)$ is an element of the probability matrix giving the probability that a detected photon of energy E will be detected in channel i. This matrix was calculated by first calculating the response function matrix of the whole system by convolving the energy resolution of the detector at the ^{57}Co 14.41 keV peak (a Gaussian with FWHM = 0.24 keV) with the energy deposition distributions. The probability matrix is the response function matrix but normalized such that $\sum_E p(E,i) = 1$. The initial guess for $(\Delta N/\Delta E)_E^0$ was taken as a uniformly distributed spectrum from 5 keV to 28 keV, with a total number of counts corresponding to the integral of the measured PHD, except for the two bins corresponding to the characteristic energy of molybdenum (K edges of 17.48 keV and 19.61 keV), where it was increased by one order of magnitude. Equation (1) converges rapidly for this particular probability matrix (see Fig. 1(b)), so about ten iterations were

[1] The linearity of the detector response was confirmed by finding the 136.43 keV peak of the ^{57}Co source and the 2 K edge peaks of Mo (17.48 keV and 19.61 keV) exactly within the expected channels, that is channels 1364, 174 and 196, respectively.

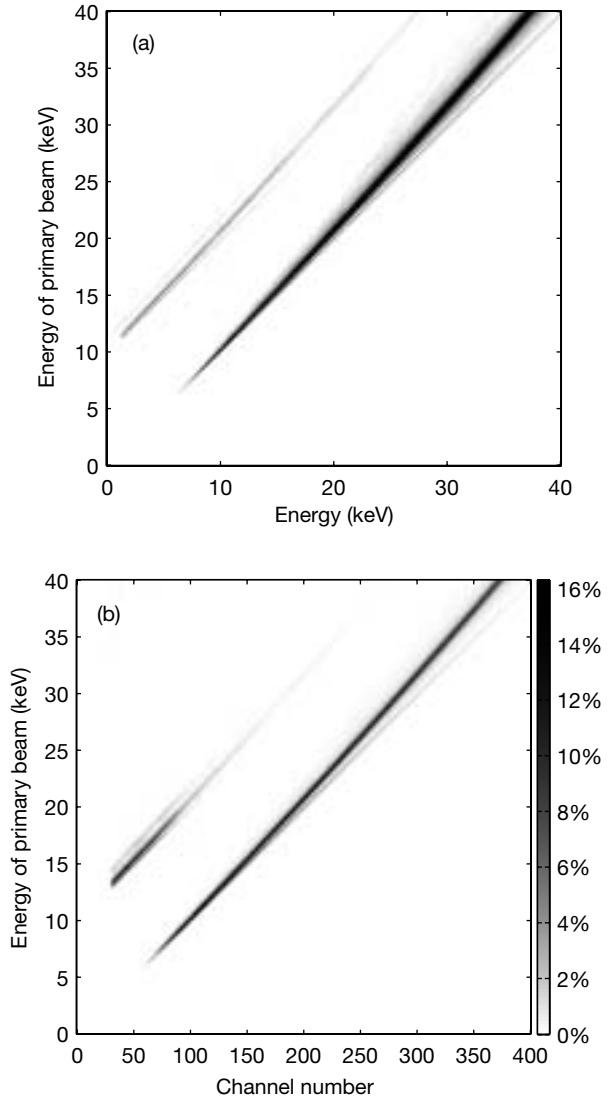

FIG. 1. (a) Qualitative representation of the energy deposition distributions. (b) Probability matrix derived from the energy deposition distributions (grey scale with white = 0% and black = 16%). Probabilities for channels below the PHD lower level discriminator (32) are nil.

sufficient. After the reconstruction iterative process the energy spectrum was corrected for the efficiency of the whole spectrometer system.

3. RESULTS AND DISCUSSION

3.1. Monte Carlo simulation of the energy deposition distributions

Figure 1(a) is a three dimensional qualitative representation of the energy deposition distributions obtained by Monte Carlo simulations. The vertical axis corresponds to the energy window of the primary beam. A profile along the horizontal line would give the energy deposition distribution for that particular energy window. Only the primary beams with energies less than 40 keV are plotted, which correspond to the energy ranges used in mammography[2]. The darker the colour the more counts the energy bin contains. The graph shows a peak with a slope of 1, corresponding to the Rayleigh scattering of the primary beam. As the energy of the primary beam increases, the peak corresponding to the Compton scattering curves towards lower energies, as expected from the Compton scattering effect. Ghost images of the Compton and Rayleigh scattering peaks, corresponding to the germanium escape peaks, can be seen in the figure, especially for the K_α edge of germanium, which is at 9.89 keV (K_β is at 10.98 keV). The intensity of the escape peaks is reduced as the energy of the primary photon increases, since the photoelectric interactions occur deeper within the germanium crystal and reduce the chance of the germanium characteristic X rays escaping the crystal. There are no Compton edges present in the energy depositions, since the incoming photons strike the detector more or less along its cylindrical axis, and their energy is so low that photoelectric interactions are more likely to occur, and the few Compton scattered photons that are produced within the detector do not escape the crystal because of its diameter. Low numbers of photons were detected, considering that it took on average 12.5 h to simulate the 10^{10} photons in the primary beam to produce each response function. The maximum number of counts in the energy deposition distributions was 530 at the primary beam energy window 19.5–19.6 keV and in the energy deposition interval 18.9–19.0 keV. The efficiency of the whole spectrometer system (data not presented as such in this paper) at different energies was obtained by integrating each energy deposition distribution and dividing the result by the number of photons generated (10^{10} photons). Figure 1(b) shows the probability matrix $p(E,i)$.

---

[2] Because the simulation is very computer intensive and due to the limit on the number of processors available for the computation, these are all the results available at the time of submitting this paper. Primary beams of energies ranging from 40 keV to 150 keV are currently being simulated.

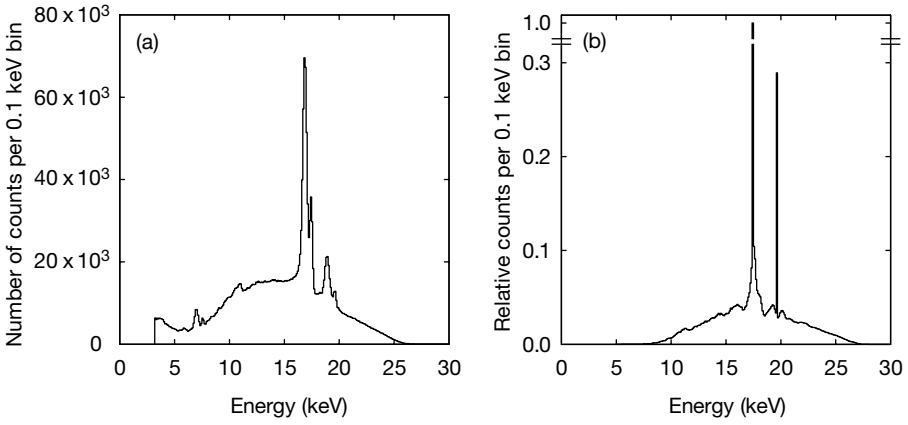

FIG. 2. (a) Measured PHD with the Compton spectrometer system. (b) Reconstructed primary beam with counts normalized to the 17.48 keV characteristic X ray peak.

3.2. Compton spectrometry and reconstruction of the primary beam

Figure 2(a) shows the PHD obtained. The detector dead time was 1.45%. The two characteristic X ray peaks of molybdenum are split in the PHD into a Rayleigh peak at the K edge energy and a more intense Compton peak at a lower energy. Figure 2(b) shows the reconstructed primary beam obtained for ten iterations, computed in a fraction of a second. The convergence of the process is fast and a good estimate of the spectrum can be obtained with just a few iterations. Characteristic X ray peaks were found at the expected energies.

4. CONCLUSION

Once the simulated energy deposition distributions are calculated, the reconstruction of the primary beam measured with a Compton spectrometer is fast and easy. This method can be applied to any other type of spectrometry. Better accuracy could be obtained by simulating even more photons for each primary energy window. Spectra from more tubes should be measured to test the robustness of the technique. Uncertainty analysis and a comparison with the Spectro-X software will be carried out soon.

REFERENCES

[1] YAFFE, M., TAYLOR, K.W., JOHNS, H.E., Spectroscopy of diagnostic x rays by a Compton-scatter method, Med. Phys. **3** (1976) 328–334.

[2] MATSCHEKO, G., RIBBERFORS, R., A Compton scattering spectrometer for determining x-ray photon energy spectra, Phys. Med. Biol. **32** (1987) 577–594.

[3] MATSCHEKO, G., RIBBERFORS, R., A generalized algorithm for spectral reconstruction in Compton spectroscopy with corrections for coherent scattering, Phys. Med. Biol. **34** (1989) 835–841.

[4] DEMPSTER, A.P., LAIRD, N.M., RUBIN, D.B., Maximum likelihood from incomplete data via the EM algorithm, J. R. Stat. Soc. Ser. B **39** (1977) 1–38.

[5] KAWRAKOW, I., ROGERS, D.W.O., The EGSnrc Code System: Monte Carlo Simulation of Electron and Photon Transport, Rep. PIRS-701, National Research Council, Ottawa (2000).

[6] SHEPP, L.A., VARDI, Y., Maximum likelihood reconstruction for emission tomography, IEEE Trans. Med. Imaging **1** (1982) 113–122.

POSTERS ON DOSIMETRY PROTOCOLS AND COMPARISONS

(Session 8b)

Chair

A. MEGHZIFENE
IAEA

Co-Chair

P. ANDREO
Sweden

Rapporteur

K.E. ROSSER
United Kingdom

BLANK

TESTING OF N_K AND $N_{D,w}$ BASED IAEA CODES OF PRACTICE FOR CLINICAL PHOTON BEAMS

K.N. GOVINDA RAJAN, S. VANDANA, M. VIJAYAM, J.B. SHIGWAN
Bhabha Atomic Research Centre,
Mumbai, India
E-mail: grajanmpss@vsnl.com

M.R. McEWEN*, S. DUANE
National Physical Laboratory,
Teddington, United Kingdom

Abstract

Over recent years there has been a move internationally to switch to $N_{D,w}$ based protocols. This is due to a number of reasons, including: (a) the absorbed dose to water calibration factor, $N_{D,w}$, is less likely to be affected by type B uncertainty compared with the air kerma calibration factor, N_K; (b) it provides a more robust international basis for dose dissemination, since all air kerma standards require the same input data, whereas there are a number of different techniques used to determine absorbed dose (water calorimetry, graphite calorimetry, ionometry, etc.); and (c) theory predicts that the ratio $N_{D,w}/N_K$ is a constant for a given type of chamber (e.g. an NE 2571), while experimental investigations have clearly shown that this is not the case and that intrinsic differences between chambers of the same type can have a significant effect on the dose realized via air kerma standards. However, when switching from an air kerma (e.g. Technical Reports Series No. 277) to an absorbed dose (e.g. Technical Reports Series No. 398) formalism, there is a concern as to the magnitude of the change in the measured dose. It is important that this change be accurately estimated and that medical physicists in the radiotherapy clinic be aware of the expected difference in order to reliably make the switch without introducing procedural errors. In this study, as part of an IAEA co-ordinated research project, results for three chamber types (NE 2571, NE 2577 and NE 2581) for ^{60}Co and higher photon beam qualities, comparing the IAEA protocols mentioned above, are reported. All three chamber types gave similar results, with the absorbed dose method giving a dose around 0.9% higher than air kerma, which is consistent with other studies.

---

* Present address: National Research Council, Ottawa, Canada.

1. INTRODUCTION

The IAEA code of practice in Technical Reports Series No. 277 (TRS 277) [1] makes use of the following equation for determining the absorbed dose to water at the point of interest (i.e. at the effective point of measurement of the chamber, P_{eff}):

$$D_w(P_{\text{eff}}, 10 \times 10, \text{SSD}) = M_u N_D (S_{w,\text{air}})_u p_u \quad (1)$$

TRS 277 recommends that the effective point of measurement of the chamber, P_{eff}, be placed at the reference depth (5 cm for $\text{TPR}_{20,10} \leq 0.70$ and 10 cm for $\text{TPR}_{20,10} > 0.70$). For photon beams, at the reference depth, $p_u = p_{\text{wall}}$, the factor that corrects for the non-water equivalence of the chamber wall material. This factor is given in graphic form in TRS 277, for chambers of different wall materials, as a function of beam quality. N_D is given by:

$$N_D = N_K(1 - g)k_{\text{att}}k_m \quad (2)$$

where N_K gives the air kerma calibration of the ionization chamber at ^{60}Co energy, k_{att} and k_m correct for the wall absorption and non-air equivalence of the chamber, respectively, and g is the fraction of energy lost to bremsstrahlung.

For ionization chambers with an aluminium central electrode, the over-response of the electrode compared with a wall equivalent central electrode must be corrected for both at the calibration quality and at the user's beam quality. Both corrections are incorporated into a global correction factor, $p_{\text{cel-gbl}}$, and applied to Eq. (1) as:

$$D_w(P_{\text{eff}}, 10 \times 10, \text{SSD}) = M_u N_D (S_{w,\text{air}})_u p_u p_{\text{cel-gbl}} \quad (3)$$

where k_{att}, k_m and $p_{\text{cel-gbl}}$ values are given in TRS 277 (tables XVIII and XIX). From this brief description it is clear that TRS 277 is based on the air kerma calibration of an ionization chamber.

The IAEA code of practice in TRS 398 [2] makes use of the following equation for determining the absorbed dose to water at the point of interest (i.e. at the geometric centre of the chamber, P_{gc}):

$$D_w(d_{\text{ref}}, 10 \times 10, \text{SSD}) = (N_{D,Qo})M_c k_Q \quad (4)$$

It can be seen from Eq. (4) that TRS 398 is based on an absorbed dose to water calibration factor of an ionization chamber, provided by a secondary standards dosimetry laboratory (SSDL) or an accredited calibration laboratory,

at the calibration quality Q_o. The most common reference quality Q_o offered by the standards laboratories is for ^{60}Co gamma radiation. The factor k_Q gives the energy dependence of $N_{D,w}$:

$$k_Q = (N_{D,w})_Q / (N_{D,w})_{Qo} \tag{5}$$

When comparing TRS 398 with TRS 277 account must be taken of the different effective point of measurements defined for the chambers. For TRS 398 the geometric centre of the chamber is used, as any fluence perturbation is taken into account during the calibration procedure. For TRS 277 an effective point of measurement in front of the geometric centre (towards the beam) is used ($P_{\text{eff}} = 0.5r$ for ^{60}Co beams and $P_{\text{eff}} = 0.75r$ for higher energy photon beams, r being the radius of the chamber cavity). In order to compare the dose at the same depth, namely at d_{ref} (5 cm for $\text{TPR}_{20,10} \leq 0.70$ and 10 cm for $\text{TPR}_{20,10} > 0.70$), a gradient or displacement correction, p_{dis}, is applied to the TRS 277 equation (i.e. Eq. (3)) above:

$$D_w(d_{\text{ref}}, 10 \times 10, \text{SSD}) = M_c N_D (S_{w,\text{air}})_u \, p_u p_{\text{cel-gbl}} p_{\text{dis}} \tag{6}$$

The objective of this paper is to compare values of $D_w(d_{\text{ref}}, 10 \times 10, \text{SSD})$, as predicted by Eqs (6) and (4), for a given number of monitor units or for a given time of integration. As part of this work, absorbed dose to water calibration factors were also determined experimentally for a range of linac energies in order to compare experimental k_Q factors with those given in TRS 398.

2. MATERIALS AND METHODS

2.1. ^{60}Co measurements

Two NE 2571 reference chambers were used to determine $N_{D,w}$ factors experimentally. A chamber (serial number 2303) was brought to the Bhabha Atomic Research Centre (BARC) SSDL from the National Physical Laboratory (NPL) in the United Kingdom; this chamber has $(N_{D,w})_Q$ factors for a set of NPL photon beam qualities traceable to the NPL primary standard calorimeter [3]. A second chamber (serial number 1692), maintained as a reference chamber at BARC, has a ^{60}Co calibration factor traceable to the ionometric standard of absorbed dose at the Bureau international des poids et mesures (BIPM). Since the bases for the two chamber calibrations are quite different, a comparison of doses measured via the two chambers has few common correlated uncertainties. This first step provided a secondary comparison of the

NPL and BIPM absorbed dose standards and a validation of the subsequent steps in order to obtain calibration factors for other chambers.

The calibration geometry is the same as stated in Eqs (4) or (6); that is, the water phantom was kept at a standard source to surface distance (SSD) (80 cm for ^{60}Co beams) and the field size at the phantom surface was 10 cm × 10 cm. The geometric centre of the chamber was placed at a reference depth of 5 cm; a water phantom of dimensions 30 cm × 30 cm × 30 cm was used for this purpose. An integration time of about 90 s was used, instead of controlling the exposure using the machine timer, in order to avoid any possible shutter timer error. The effect of using different electrometers was investigated and found to be insignificant at the 0.05% level. Absorbed dose to water calibration factors obtained for NE 2571, NE 2577 and NE 2581 type chambers are tabulated in Table I.

The comparison of the codes of practice for the BARC ^{60}Co beam was carried out using four NE 2571 chambers, one NE 2581 chamber and one NE 2577 chamber, with the same geometry as described above. The ratios of the reference doses, as predicted by the two codes of practice, are given in Table II.

TABLE I. $N_{D,w}$ FACTORS DETERMINED AT THE BARC SSDL

Chamber type	Serial number	$(N_{D,w})_{\text{expl,cal}}$ × 10^{-3} Gy/nC	$(N_{D,w})_{\text{expl,ion}}$ × 10^{-3} Gy/nC	$(N_{D,w})_{\text{NPL,BIPM}}$
NE 2571	2303	45.30[a]	—	—
NE 2571	2304	45.23	—	—
NE 2571	1692	45.63	45.78[b]	1.0033
NE 2571	3157	45.31	45.33	1.0004
NE 2571	3161	45.39	45.41	1.0004
NE 2577	—	—	139.3	—
NE 2581	—	—	58.66	—

[a] This value was determined at the NPL.

[b] This value was determined at the BIPM.

Note: The calibration factors in the third column are traceable to the calorimetric standard of absorbed dose maintained at the NPL (via chamber serial number 2303). The calibration factors in the fourth column are traceable to the ionometric standard of absorbed dose maintained at the BIPM (via chamber serial number 1692).

TABLE II. RATIO OF DOSES AT REFERENCE DEPTH AS PER TRS 398 AND TRS 277 FOR A ^{60}Co BEAM

(expressed as $[D_w(10, 10 \times 10, 80)]_{TRS398}/[D_w(10, 10 \times 10, 80)]_{TRS277}$, where the parameters refer to depth, field size and SSD, respectively, in cm)

Chamber type	Identifier	Dose ratio
NE 2571	No. 1	1.006
NE 2571	No. 2	1.004
NE 2571	No. 3	1.007
NE 2571	No. 4	1.004
NE 2581	No. 1	1.009
NE 2577	No. 1	1.010

2.2. Accelerator photon beam measurements

Three accelerators (a Varian 2100C, Varian 2100D and Siemens Primus) were used for the comparison of the high energy photon sections of the codes. The measurement geometry was 100 cm SSD, 10 cm depth and a field size of 10 cm × 10 cm at the surface. The same water phantom as described above was used. In the first step one of the BARC NE 2571 chambers was calibrated in terms of $(N_{D,w})_Q$ using the NPL reference chamber (serial number 2303). The k_Q factors of the NPL chamber, for the accelerator beam qualities used in this study, were obtained by fitting a polynomial to the k_Q factors for the NPL beam qualities. The deviation in the polynomial fit was 0.25% in the worst case and generally less than 0.1%. Calculated $(k_Q)_{\mathrm{TRS398}}$ values for the NE 2571 chamber were obtained in the same manner using the k_Q data from TRS 398 for $\mathrm{TPR}_{20,10}$ values in the range of 0.65 to 0.76. The ratios of calculated and experimental k_Q values for the two NE 2571 chambers are shown in Table III.

The comparison of the codes of practice for accelerator beams was carried out for three NE 2571 chambers, one NE 2581 chamber and one NE 2577 chamber, using the same geometry described above. The ratios of the reference doses, as predicted by the two codes of practice, for these chambers are given in Table IV.

TABLE III. RATIO OF THEORETICAL TO EXPERIMENTAL k_Q FACTORS

Beam quality ($TPR_{20,10}$)	$(k_Q)_{TRS398}/(k_Q)_{expl}$ (NPL NE 2571)	$(k_Q)_{TRS398}/(k_Q)_{expl}$ (BARC NE 2571)
0.665	1.001	0.998
0.677	1.001	0.998
0.737	1.005	1.002
0.752	1.006	1.003

TABLE IV. RATIO OF DOSES AT REFERENCE DEPTH AS PER TRS 398 AND TRS 277 FOR ACCELERATOR PHOTON BEAMS
(expressed as $[D_w(10, 10 \times 10, 100)]_{TRS398}/[D_w(10, 10 \times 10, 100)]_{TRS277}$, where the parameters refer to depth, field size and SSD, respectively, in cm)

Linac	Energy (MV)	$TPR_{20,10}$	NE 2571			NE 2577	NE 2581
			Chamber 1	Chamber 2	Chamber 3		
2100D	6	0.665	1.008	1.006	—	—	—
2100C	6	0.677	1.009	1.006	—	—	—
Primus	6	0.688	—	1.006	1.004	1.008	1.008
2100C	10	0.737	1.011	1.008	—	—	—
2100D	15	0.752	1.011	1.009	—	—	—
Primus	15	0.772	—	1.013	1.011	1.015	1.012

3. DISCUSSION

The comparison of standards (Table I) gave a difference in the dose between the ionometric standard (BIPM) and the calorimetric standard (NPL) of 0.33% in the worst case. This level of agreement is within the measurement uncertainties (estimated to be ±0.6%) and is similar to that obtained in a direct comparison between the BIPM and NPL. The results of the comparison of the two IAEA codes at the ^{60}Co beam quality showed a variation of about 0.9% and 1.0% for the NE 2581 and NE 2577 type chambers, respectively, while the NE 2571 chambers showed a difference ranging between 0.4% and 0.7% (mean

value 1.0053). TRS 398 gives the higher doses, which is consistent with other comparisons of absorbed dose and air kerma based protocols [4, 5].

Calculated k_Q factors as given in TRS 398 (and also in the American Association of Physicists in Medicine TG 51 protocol [6]) do not take into account intrinsic differences between chambers of the same make. The experimental k_Q factors and the TRS 398 k_Q factors for two NE 2571 chambers were compared and found to differ by about 0.6%, for a 15 MV beam, and the difference was found to be less for lower beam qualities. These results indicate that there is a difference in the shapes of the calculated and experimental curves. A summary of all the experimental data obtained to date for the NE 2571 chamber [7] seems to confirm the NPL experimental values, although the difference between calculation and experiment is within the measurement uncertainties.

Ratios of $[D_w(10, 10 \times 10, 100)]_{\mathrm{TRS398}}/[D_w(10, 10 \times 10, 100)]_{\mathrm{TRS277}}$, determined for NE 2571, NE 2577 and NE 2581 chambers for six photon beam qualities, showed a maximum difference of 1.3%. As can be seen in Table IV, there is a slight energy dependence of the ratio but no significant difference between chamber type. The difference between the absorbed dose and air kerma protocols is similar to that obtained for the ^{60}Co beam, as is to be expected, since the same underlying energy dependent data are used in both codes of practice [4].

4. CONCLUSIONS

Experimentally based absorbed dose calibration factors for three types of cylindrical chamber were obtained and compared with calculated factors. The level of agreement was similar to previous measurements and was within the measurement uncertainties. A comparison of high energy photon doses measured using TRS 277 and TRS 398 gave a difference of around 0.9%, which is consistent with other studies and indicates the change to be expected when moving from a protocol based on air kerma to one based on absorbed dose standards.

REFERENCES

[1] INTERNATIONAL ATOMIC ENERGY AGENCY, Absorbed Dose Determination in Photon and Electron Beams, Technical Reports Series No. 277, IAEA, Vienna (1997).

[2] INTERNATIONAL ATOMIC ENERGY AGENCY, Absorbed Dose Determination in External Beam Radiotherapy, Technical Reports Series No. 398, IAEA, Vienna (2000).
[3] DuSAUTOY, A.R., The UK primary standard calorimeter for photon-beam absorbed dose measurement, Phys. Med. Biol. **41** (1996) 137–151.
[4] ANDREO, P., et al., Protocols for the dosimetry of high-energy photon and electron beams: A comparison of the IAEA TRS-398 and previous international Codes of Practice, Phys. Med. Biol. **47** (2002) 3033–3053.
[5] ARAKI, F., KUBO, H.D., Comparison of high-energy photon and electron dosimetry for various dosimetry protocols, Med. Phys. **29** (2002) 857–868.
[6] AMERICAN ASSOCIATION OF PHYSICISTS IN MEDICINE, AAPM's TG-51 protocol for clinical reference dosimetry of high-energy photon and electron beams, Med. Phys. **26** (1999) 1847–1870.
[7] ANDREO, P., A comparison between calculated and experimental k_Q photon beam quality correction factors, Phys. Med. Biol. **45** (1995) L25–L38.

COMPARISON OF IAEA PROTOCOLS FOR CLINICAL ELECTRON BEAM DOSIMETRY

M. SOUKUP
Faculty of Nuclear Sciences and Physical Engineering,
Czech Technical University in Prague

J. NOVOTNÝ
Medical Physics Department, Hospital Na Homolce
E-mail: josef.novotny@homolka.cz

Prague, Czech Republic

Abstract

The comparison of absorbed dose to water in reference conditions for electron beams was carried out using Czech and IAEA protocols. A plane-parallel Roos ionization chamber and a PTW 30002 cylindrical chamber calibrated at the national secondary standards dosimetry laboratory were used for the direct calibration of a plane-parallel ionization chamber in electron beams and for dose determination. In addition, the stability of the reference point of measurement was investigated for clinically used beams. Maximum deviations between protocols were found to be within 2.5%, with the exception of 20 MeV energy. Combined standard uncertainties for different determination methods were also estimated.

1. INTRODUCTION

The American Association of Physicists in Medicine and the IAEA recently published new protocols, for the clinical reference dosimetry of external beams in radiation therapy using high energy photon and electron beams (TG 51 [1]) and for absorbed dose determination in external beams used in radiotherapy (Technical Reports Series No. 398 (TRS 398) [2]), respectively. The formalism and dosimetry procedures in both protocols are based on the use of an ionization chamber having an absorbed dose to water calibration factor, $N_{D,w}$, and a beam quality conversion factor, k_{Q,Q_o}, for the user's beam. Previous protocols [3–6], including the Czech dosimetry protocol [7], were based on using a ^{60}Co exposure calibration factor, N_X, or air kerma calibration factor, N_K.

For electron beams the beam quality for TG 51 [1] and TRS 398 [2] is specified by the depth of 50% absorbed dose in water, R_{50}, instead of the mean

incident energy, E_o, used in previous protocols. The clinical reference dosimetry is performed at the depth $d_{ref} = 0.6R_{50} - 0.1$ (g/cm^2). For electron beams below 10 MeV, z_{ref} is very close to R_{100}; for high energy electron beams it becomes deeper than R_{100}. A new set of stopping power ratios calculated using realistic electron beams by Monte Carlo simulation [8] is also used in the new protocols.

The purpose of this work was to compare the determination of absorbed dose to water (D_w) in electron beams in accordance with the new TRS 398 [2] protocol with the previously used TRS 277, TRS 381 and Czech dosimetry protocol (CZ) [7] in clinical practice. The comparison was performed by direct measurements in a water phantom using calibrated ionization chambers and high energy electron beams produced by a Varian Clinac 2100C linac.

2. GENERAL FORMALISM

2.1. Czech dosimetry protocol

In the Czech dosimetry protocol [7] the absorbed dose to water, $D_{w,e}(E_o, z)$, for electron beams with the quality E_o at the depth z is given by:

$$D_{w,e}(E_o, z) = M_u N_K K_{w,e}(E_o, z) \tag{1}$$

where

M_u is the electrometer reading corrected for pressure, temperature, humidity, polarity and saturation effect;
N_K is the air kerma calibration factor of the ionization chamber;
$K_{w,e}(E_o, z)$ is a conversion factor defined as:

$$K_{w,e}(E_o, z) = (1 - g)s_{w,a}(E_o, z)k_m k_{att} p_u(E_o, z)p_{cel}$$

where

g is the fraction of radiation lost by bremsstrahlung;
$s_{w,a}(E_o, z)$ is the stopping power ratio for mean electron energy, E_o, and depth, z;
k_m is the correction factor to account for the non-air equivalence of the ionization chamber wall and cap material;
k_{att} is the factor to allow for attenuation in the wall of an ionization chamber;

$p_u(E_o, z)$ is the total perturbation factor.

A factor for the central electrode correction, p_{cel}, was proposed to be equal to 1 for all chambers used.

The values necessary for the calculation of $K_{w,e}(E_o, z)$ were taken from TRS 277 [4] and, later, updated from TRS 381 [3]. The $K_{w,e}(E_o, z)$ values were calculated and tabulated for commonly used plane-parallel ionization chambers (NACP, Markus and Roos) and for standard cylindrical ionization chambers (PTW 30002 and NE 2571) and published in the Czech dosimetry protocol [7].

2.2. TRS 277 and TRS 381

The absorbed dose to water, D_w, at the effective point of measurement is, according to TRS 277 [4], given by:

$$D_w = M_u N_D (s_{w,\text{air}}) p_u \tag{2}$$

where $N_D = N_K(1 - g)k_m k_{\text{att}}$ and the symbols for all parameters are the same as above. The stopping power ratio and perturbation factor depend on the mean energy of the electron beam at the surface of the phantom and on the depth.

The formalism given in TRS 277 [4] has also been adopted in TRS 381 [3]. The absorbed dose to water, $D_{w,Q}$, in the user's beam of quality Q at the effective point of measurement is given by:

$$D_{w,Q} = M_Q N_{D,\text{air}} (s_{w,\text{air}})_Q p_Q \tag{3}$$

where

M_Q is the corrected reading;
$N_{D,\text{air}}$ is the absorbed dose to air chamber calibration factor;
$(s_{w,\text{air}})_Q$ is the stopping power ratio (water to air);
p_Q is an overall perturbation factor for the ionization chamber, which replaces p_u in Eq. (2).

The p_Q is the product of the various correction factors for the ionization chamber at a quality Q, namely p_{wall}, p_{cav} and p_{cel}. The two factors correct for electron fluence due to differences in the scattering properties between the air cavity and the phantom. The factor p_{cel} corrects for the effect of the central electrode of the ionization chamber in-phantom measurements; that is, it is not a global factor, as in TRS 277 [4]. The difference between the Czech dosimetry

protocol [7] for electron beam reference dosimetry and TRS 381 [3] is only in their formal expression; that is, the values of all correction factors and parameters are the same, but for a particular ionization chamber they are merged into one conversion factor to make the determination of absorbed dose to water as simple as possible in practice.

2.3. TRS 398

According to TRS 398 [2], the absorbed dose to water, $D_{w,Q}$, for an arbitrary electron beam with a quality Q is given by:

$$D_{w,Q} = M_Q N_{D,w,Qo} k_{Q,Qo} \tag{4}$$

where

M_Q is the electrometer reading corrected for pressure, temperature, humidity, polarity and saturation effect;

$k_{Q,Qo}$ corrects for the difference between the reference beam quality, Q_o, and the actual quality being used, Q;

$N_{D,w,Qo}$ is a calibration factor obtained either by using the cross-calibration procedure or from the secondary standards dosimetry laboratory (SSDL).

Details of formalism and correction factors can be found in Refs [2–4].

3. MATERIALS AND METHODS

Two ionization chambers were used for this study: a plane-parallel Roos type (PTW 34001) ionization chamber calibrated in terms of absorbed dose to water in ^{60}Co (in the PTW dosimetric laboratory) and in terms of air kerma, and a cylindrical Farmer type ionization chamber (PTW 30002), calibrated also in terms of air kerma at the Czech SSDL. Both chambers were connected to a PTW Unidos electrometer. A Wellhöfer WP7000 scanning phantom equipped with a Scanditronix electron beam semiconductor detector was used for percentage depth dose measurements and ionization chamber positioning. High energy electron beams in the energy range of 6 MeV to 20 MeV were produced by a Varian Clinac 2100C linac. Polarity and saturation effects for all ionization chambers were measured and evaluated for a standard linac setting (dose rate 240 MU/min).

4. RESULTS

4.1. Estimation of reference point of measurement

Absorbed depth dose curves (field size of 15 cm × 15 cm, source to surface distance (SSD) of 100 cm) recorded during the regular quality control procedures for the past four years were analysed and the stability of the reference point of measurement was evaluated using both protocols (i.e. values of R_{100} and z_{ref} were determined from the same depth dose curves). Figure 1 shows the time dependence of these two values for a 20 MeV electron beam and Table I gives an overview of the estimated basic average values of the parameters for all electron beams used. The scattered values for R_{100} indicate a lack of consistency of measurements, even though maximum care was taken during the measurements from the bottom to the top of the phantom. Finally, the choice of stopping power ratio for different depths of R_{100} influences the dose determination. The dependence of R_{50} on collimator size was measured for different collimator sizes (cones), and it was found that the difference is a maximum of 0.04 g/cm^2 for field sizes between 20 cm × 20 cm and 10 cm × 10 cm. Fields larger than 10 cm × 10 cm can therefore be used for the determination of R_{50} and also for $R_{50} > 7$ g/cm^2 (a requirement of TRS 398 [2]) under reference conditions.

4.2. Absorbed dose measurements

Absorbed dose to water was determined in a water phantom with a field size of 15 cm × 15 cm at an SSD of 100 cm with a plane-parallel ionization chamber, by various methods; average values are summarized in Table II. All

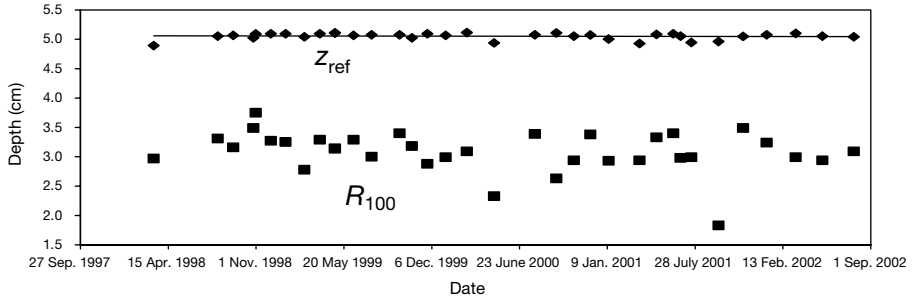

FIG. 1. Measurements of reference depths with time.

TABLE I. BASIC PARAMETERS OF MEASURED ELECTRON BEAMS
(The standard deviations of the mean are given in brackets. D_{zref}/D_{R100} are the average values calculated from all measurements.)

	Energy (MeV)				
	6	9	12	16	20
R_{50} (cm)	2.30 (±0.4)	3.62 (±0.3)	5.08 (±0.2)	6.79 (±0.2)	8.62 (±0.2)
R_{100} (cm)	1.38 (±0.7)	2.28 (±0.7)	3.20 (±0.6)	3.90 (±1.1)	3.13 (±2.3)
z_{ref} (cm)	1.28 (±0.4)	2.07 (±0.2)	2.95 (±0.2)	3.98 (±0.2)	5.07 (±0.2)
D_{zref}/D_{R100}	0.994 (±0.1)	0.989 (±0.1)	0.994 (±0.1)	1.000 (±0.1)	0.979 (±0.1)

TABLE II. SUMMARY OF METHODS FOR ABSORBED DOSE DETERMINATION IN HIGH ENERGY ELECTRON BEAMS BY PLANE-PARALLEL IONIZATION CHAMBERS

Determination method	Calibration method of plane-parallel ionization chamber	Reference depth	Code of practice used	Combined standard uncertainty[a] (%)
A	Against cylindrical ionization chamber, 20 MeV electron beam, $N_{D,w}$	R_{100}	TRS 381, CZ	2.5
B		z_{ref}	TRS 398	1.9
C	Absorbed dose to water SSDL, $N_{D,w}$	R_{100}	TRS 381, CZ	3.6
D		z_{ref}	TRS 398	2.8
E	Cobalt-60 beam SSDL, N_K	R_{100}	TRS 381, CZ	3.3

[a] Combined standard uncertainties were calculated for each method using the methodology described in TRS 398 [2] based on measured standard deviations for type A uncertainties and estimated values for type B uncertainties.

measured doses were recalculated to doses at R_{100} in order that they could be compared.

Combined relative standard uncertainties expressed at the level of one standard deviation were calculated according to the methodology described in TRS 398 (appendix IV) [2]. The results of the comparative measurements are presented in Fig. 2.

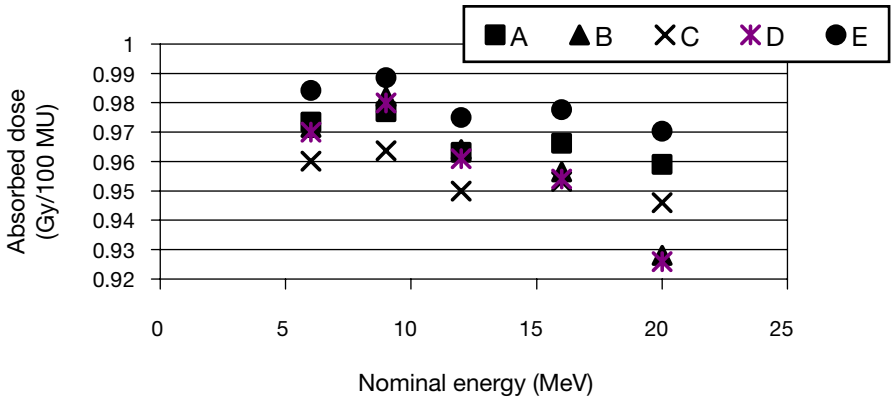

FIG. 2. Dependence of measured absorbed dose in reference conditions for electron beams for protocols used for the determination of absorbed dose.

5. DISCUSSION AND CONCLUSIONS

From Fig. 1 and Table I it can be concluded that the measurement of the R_{50} value in clinical practice, and the estimation of z_{ref} from it, is a much more precise procedure than the measurement of R_{100}. This is particularly true for high energy electron beams (above 12 MeV), for which the maximum of the depth dose curve becomes flatter with increasing energy, and it is difficult to determine a real position of R_{100} on measured depth dose curves, while R_{50} is more easy to determine and more precise. Since no dependence of R_{50} values was found on collimator size for a field size above 10 cm × 10 cm, the quality factor R_{50} and the absorbed dose at reference conditions can be estimated for any collimator equal to or larger than 10 cm × 10 cm. The conditions for field size definition, stated in TRS 398 [2], are completely fulfilled for measured electron beams. From Fig. 1 it can be also concluded that the electron beam energy is quite stable over time.

The relative difference between all measured doses, given in Fig. 2, is within 2.5%, with the exception of the 20 MeV electron beam. This difference is less than the calculated combined standard uncertainties at the level of one standard deviation. This indicates that the real value of the absorbed dose lies within this interval. However, the results suggest that the highest dose for all energies is obtained systematically from measurements using a plane-parallel ionization chamber with an air kerma calibration factor determined in a ^{60}Co beam at the national SSDL (procedure E in Fig. 2). This might be connected directly with the calibration procedure of both plane-parallel and cylindrical ionization chambers in a ^{60}Co beam. It is well known that the direct air kerma

calibration of plane-parallel ionization chambers in a ^{60}Co beam is not recommended, because of the comparatively large error connected with this procedure (see TRS 381 [3]). The absorbed dose to water calibration factor was also obtained from another dosimetry laboratory, and agreed very well (within 0.2%) with the one obtained from the cross-calibration procedure with a cylindrical ionization chamber in a 20 MeV electron beam. It is therefore very difficult to compare the dose to water calibration factor obtained from the recalculation of the air kerma calibration factor for the plane-parallel ionization chamber obtained at the national SSDL with the one determined directly. A systematic difference between these two calibrations can also be the main cause of a large difference between the determination methods. Since the comparison was performed for real clinical situations, with the main intention being to evaluate possible errors during absorbed dose determination with the help of different protocols, it was not surprising to find such a large deviation. It can be expected that under strictly controlled conditions the differences between protocols would be much smaller. The large difference for determination methods B and D for a 20 MeV electron beam is unexplained to date and is to be further investigated.

Method D is the simplest and most accurate method but, unfortunately, not all SSDLs provided calibration factors in terms of absorbed dose to water, $N_{D,w,Qo}$, for plane-parallel ionization chambers. Therefore, from the analysis of combined standard uncertainties, it can be concluded that currently the best method is procedure B; that is, the cross-calibration of a plane-parallel ionization chamber against a cylindrical chamber in a high energy electron beam and the calculation of absorbed dose using TRS 398 [2]. This method uses a simplified procedure, in which the beam quality is estimated from R_{50}, and a single conversion factor for the beam quality Q, $k_{Q,Qo}$, can be used for transferring corrected readings into absorbed dose to water. This method will therefore be adopted in our clinical practice.

REFERENCES

[1] AMERICAN ASSOCIATION OF PHYSICISTS IN MEDICINE, AAPM's TG-51 protocol for clinical reference dosimetry of high-energy photon and electron beams, Med. Phys. **26** (1999) 1847–1870.

[2] INTERNATIONAL ATOMIC ENERGY AGENCY, Absorbed Dose Determination in External Beam Radiotherapy, Technical Reports Series No. 398, IAEA, Vienna (2000).

[3] INTERNATIONAL ATOMIC ENERGY AGENCY, The Use of Plane Parallel Ionization Chambers in High Energy Electron and Photon Beams, Technical Reports Series No. 381, IAEA, Vienna (1997).

[4] INTERNATIONAL ATOMIC ENERGY AGENCY, Absorbed Dose Determination in Photon and Electron Beams, 2nd edn, Technical Reports Series No. 277, IAEA, Vienna (1997).
[5] NORDIC ASSOCIATION OF CLINICAL PHYSICS, Electron beams with mean energies at the phantom surface below 15 MeV, Acta Radiol. Oncol. **20** (1981) 402–415.
[6] NEDERLANDSE COMMISSIE VOOR STRALINGSDOSIMETRIE, Code of Practice for the Dosimetry of High-energy Electron Beams, Rep. 5, NCS, Delft (1989) 1–30.
[7] SPOLEČNOST RADIAČNÍ ONKOLOGIE BIOLOGIE A FYZIKY, Stanovení absorbované dávky v referenčním bodě, Rep. 1011-3, SROBF, Prague (1994).
[8] DING, G.X., ROGERS, D.W.O., MACKIE, T.R., Calculation of stopping power ratios using realistic electron beams, Med. Phys. **22** (1995) 489–501.